Stratigraphy and detrital zircon U-Pb-Hf isotope provenance of the Faro Peak formation, central Yukon: Implications for the Early Jurassic evolution of the northern Canadian Cordillera

By Adam Wiest

Thesis submitted to the School of Graduate studies

in partial fulfillment of the requirements for the degree of

Master of Science, Geology

Department of Earth Sciences

Memorial University of Newfoundland

November, 2021

St. John's, Newfoundland and Labrador

ABSTRACT

Late Triassic to Early Jurassic plate convergence and crustal thickening along the Cordilleran margin led to exhumation of the Intermontane terranes and subsequent deposition of multiple syn-tectonic stratigraphic assemblages in northwestern Canada. The Faro Peak formation is exposed in central Yukon along the Vangorda fault, the local suture between the Yukon-Tanana and Slide Mountain terranes, and constrains the timing and spatial extent of Early Jurassic tectonic exhumation. The Faro Peak formation unconformably overlies Yukon-Tanana terrane basement rocks (Snowcap assemblage) and unnamed Triassic strata (formerly lower member of the Faro Peak formation) and consists of Sinemurian to Toarcian massive sandstone and pebble to boulder conglomerate units. Field stratigraphic and detrital zircon U-Pb-Hf isotope studies indicate that the Faro Peak formation was locally sourced from Late Triassic to Early Jurassic arc- to syn-collisional intrusive rocks and mid- to upper Paleozoic arc and marine sedimentary successions. Snowcap assemblage rocks were recycled into the overlying Faro Peak formation and mostly consist of quartz-mica schist and quartzite units with Cryogenian and older maximum depositional ages and Precambrian detrital zircon grains that indicate northwestern Laurentian provenance. The Faro Peak formation was deposited in an isolated, structural basin by sediment gravity flows along the proto-Vangorda fault and separated from coeval, syn-tectonic deposition in the Whitehorse trough of southern Yukon by a regional drainage divide.

GENERAL SUMMARY

The Late Triassic and Early Jurassic periods were a time of tectonic activity along the northwestern Canadian margin and included plate convergence, crustal thickening, and the intrusion of plutons at mid- to lower crustal levels. Subsequent collapse of thickened crust resulted in regional subsidence and the deposition of multiple sedimentary rock units that record the timing and spatial extent of tectonic exhumation. The Faro Peak formation of central Yukon was purportedly one of these sedimentary rock units, however, the age and significance of this enigmatic assemblage was poorly understood. New field stratigraphic and sediment provenance results indicate an Early Jurassic age and rapid depositional origin for the Faro Peak formation with local sources from underlying and adjacent units and actively exhuming basement and magmatic rocks. Deposition of the Faro Peak formation was isolated along a major fault zone separated from coeval subsidence in the Whitehorse tough in southern Yukon by a regional drainage divide.

ACKNOWLEDGEMENTS

This research was funded by the Geo-mapping for Energy and Minerals (GEM) program at Natural Resources Canada. Field logistics and helicopter support were provided by the Yukon Geological Survey (YGS). Thank you to YGS staff Maurice Colpron, Donald Murphy (retired), and Lee Pigage (retired) for their expertise and for providing a safe and exciting research experience. Thank you to Markus Wälle and Rebecca Lam of the CREAIT Micro Analysis Facility at Memorial University of Newfoundland for mentorship during the laser ablation analysis, data reduction, and quality assurance and control.

I would like to thank my supervisor Dr. Luke Beranek for providing me with this opportunity and for his thoughtful and constructive mentoring throughout this entire experience. Thank you to my supervisory committee member Dr. Stephen Piercey for his review of this thesis and research publications. Thank you to fellow Beranek Research Group members Emily Johns-Buss and Maya Soukup for stimulating discussions and keeping me sane while working from home during the coronavirus. Thank you to my officemate and good friend Gabe Sindol for keeping the coffee hot and the scientific discussions even hotter. I would like to thank Matthew Manor for assistance in the field during the 2019 field season and for being a close friend ever since. Finally, I would also like to thank my roommate, friend, and fellow UW-Eau Claire alum (B.Sc.) Carly Mueller for living with me for two years during the ebb and flow of emotions completing this thesis.

CO-AUTHORSHIP STATEMENT

The identification and development of this research project is credited to Dr. Luke Beranek. The author conducted all field work including bedrock mapping, stratigraphic analysis, and sample collection with the assistance of Dr. Luke Beranek in 2018 (e.g., Wiest and Beranek, 2019) and fellow Memorial University of Newfoundland graduate student Matthew Manor (PhD candidate) in 2019 (e.g., Wiest et al., 2020). All samples were crushed, milled, and density separated at Memorial University of Newfoundland by the author in CREAIT labs run by Matthew Crocker. Detrital zircon grains were picked and mounted in Dr. John Hanchar's lab under his supervision and the supervision of Dr. Luke Beranek. Laser ablation split-stream analysis was performed by the author with the assistance of Dr. Rebecca Lam and Dr. Markus Wälle. The primary editor of this manuscript was Dr. Luke Beranek with secondary editing by committee member Dr. Stephen Piercey. Matthew Manor contributed to a research publication with the Yukon Geological Survey (e.g., Wiest et al., 2020).

TABLE OF CONTENTS

LIST OF FIGURES AND TABLES

Chapter 1

Figures

Tables

Chapter 2

Figures

Tables

Chapter 3

Figures

Tables

Chapter 4

Figures

Tables

LIST OF APPENDICES

CHAPTER 1

Introduction

1.1 INTRODUCTION

The provenance of sedimentary rock units is controlled by bedrock source, climate, and tectonic setting, and is further modified by processes related to weathering, transport, deposition, and diagenesis (Einsele, 1992; Johnsson, 1993; Boggs, 2001; Ingersoll, 1988, 2012). Detrital zircon grains have long been recognized in the sedimentary record and used to assist in provenance determination (e.g., Tyler et al., 1940), but their utility in geological studies has exponentially increased because of their abundance in siliciclastic rocks, chemical and physical stability, and among other things, ability to be accurately and efficiently dated with U-Pb geochronology (e.g., Gehrels, 2012, 2014). Detrital zircon are commonly used in provenance studies by comparing their U-Pb crystallization ages with the ages of igneous rocks in source regions (e.g., DeGraaff-Surpless et al., 2002, 2003), to determine the depositional tectonic environment (e.g., Cawood et al., 2012), and to constrain the age of a sedimentary unit using maximum depositional age statistical routines (e.g., Dickinson and Gehrels, 2009; Coutts et al., 2019; Herriott et al., 2019) especially in strata that do not contain fossils or tuffaceous beds that could otherwise provide a depositional age. Hafnium substitutes for Zr in the zircon crystal lattice making it a robust tool for identifying the Hf isotope composition of their crystalizing magmas and the combination of zircon U-Pb geochronology and Hf isotope geochemistry has become increasingly popular to better constrain sediment provenance and understand the crustal evolution of source regions (e.g., Kemp et al., 2006; Beranek et al., 2016, 2020; Brennan et al., 2021). Combining field stratigraphic studies with high-*n* U-Pb-Hf isotope laser ablation split-stream (LASS) detrital zircon techniques can determine the timing, depositional environment, provenance, and regional correlation of a sedimentary unit to clarify the ancient sedimentary record and add constraints to tectonic evolution models.

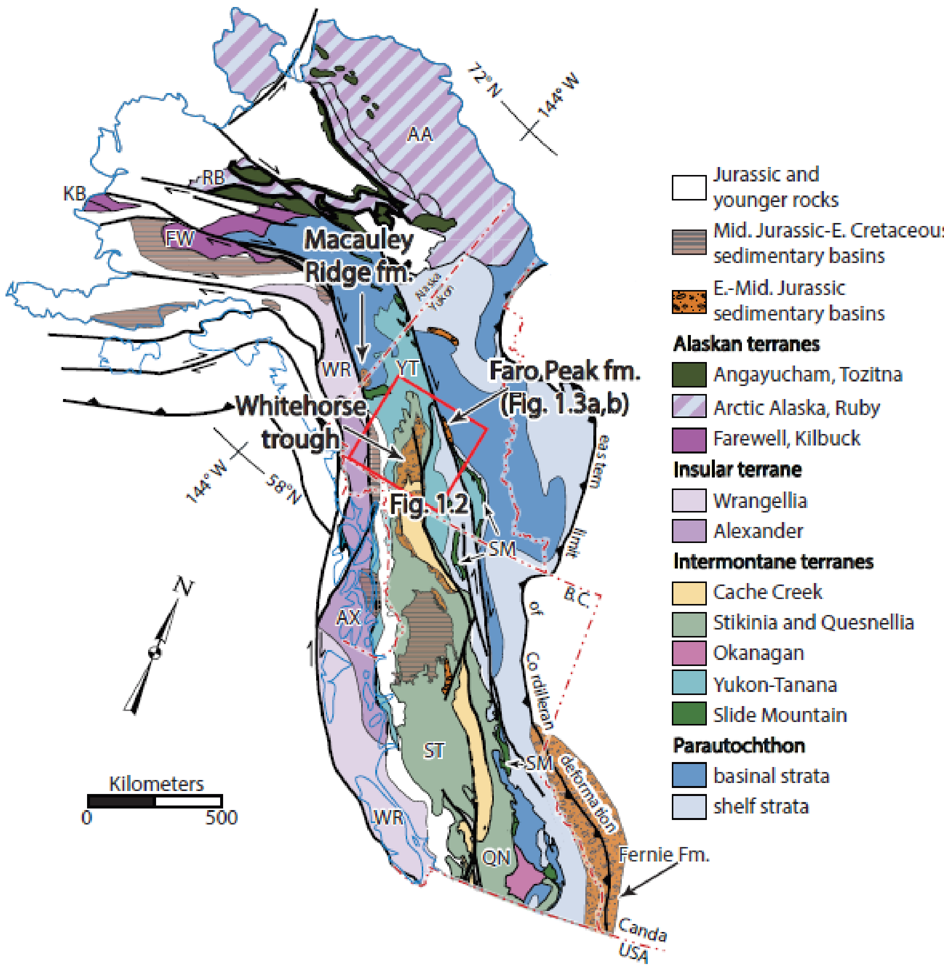

Figure 1.1 - Paleozoic to early Mesozoic terranes and Jurassic sedimentary basins of the Canadian Cordillera after Colpron et al. (2015). Terrane abbreviations: AA—Arctic Alaska; AX—Alexander; FW—Farewell; KB—Kilbuck; QN—Quesnellia; RB—Ruby; SM—Slide Mountain; ST—Stikinia; YT—Yukon-Tanana; WR—Wrangellia.

The northern Canadian Cordillera is comprised of parautochthonous North American continental margin rocks and the accreted Alaskan, Insular, and Intermontane terranes (Fig. 1.1; Monger and Price, 2002; Nelson et al., 2006; Colpron et al., 2006, 2007). The Intermontane arc terranes – Yukon-Tanana, Stikinia, and Quesnellia – and the adjacent Slide Mountain terrane of oceanic affinity, evolved during the mid- to late Paleozoic as a continental margin arc-backarc pair similar to the modern Japanese arc and Sea of Japan backarc basin (e.g., Creaser et al., 1997; Colpron et al., 2006). Mid-Permian collapse of the Slide Mountain ocean basin resulted in the accretion of Yukon-Tanana and Quesnellia (Fig. 1.1) along northwestern Pangea (Nelson et al., 2006; Colpron et al. 2006, 2007; Beranek and Mortensen, 2011). Subsequent plate convergence and arc magmatism along the composite northern Cordilleran margin resulted in Late Triassic to Early Jurassic crustal thickening, entrapment of Cache Creek ocean lithosphere, and emplacement of collision-related plutons at mid- to upper crustal depths within the Yukon-Tanana terrane, Stikinia, and Quesnellia (e.g., Mihalynuk et al., 1994; Johnston et al., 1996; Symons et al., 2000; McCausland et al., 2002; Colpron et al., 2015; Topham et al., 2016; Clark, 2017; Bickerton et al., 2020; Sack et al., 2020). The deposition of Lower Jurassic syn-tectonic sedimentary successions in Yukon and northern British Columbia (Fig. 1.1) constrain the timing and stratigraphic responses to known (e.g., Knight et al., 2013) and inferred (e.g., Colpron et al., 2015) processes that exhumed Intermontane basement infrastructure and enclosed Late Triassic to Early Jurassic arc- to collision-related plutons in the northern Canadian Cordillera.

The Faro Peak formation (informal nomenclature, Pigage, 2004) is exposed in the Faro region of central Yukon (Figs. 1.1) where it unconformably overlies pre-Late Devonian metamorphic basement units (Snowcap assemblage) and unnamed Triassic rocks of the Yukon-Tanana terrane (Wiest et al., 2020). The Faro Peak formation purportedly records syn-tectonic deposition along the Vangorda fault, the local suture between the Yukon-Tanana and Slide Mountain terranes in the easternmost Intermontane realm (Colpron et al., 2015). The Faro Peak formation is mostly composed of lithic sandstone and pebble to boulder conglomerate units with felsic intrusive rock

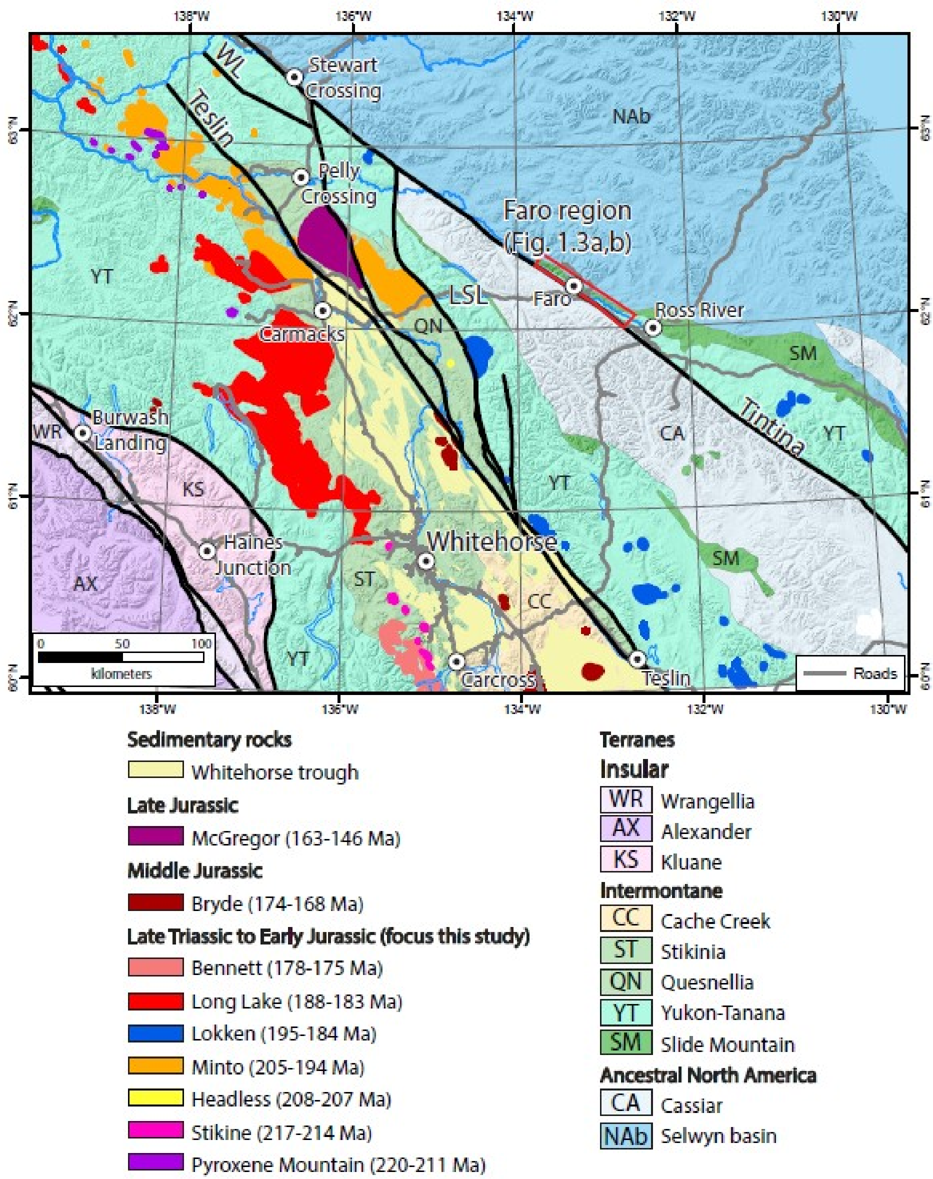

Figure 1.2 - Distribution of Late Triassic to Late Jurassic plutons in central Yukon after Sack et al. (2020). Red box outlines the focus area of this study. Abbreviations: LSL—Little Salmon Lake; WL—Willow Lake Fault.

clasts that are elsewhere diagnostic of Lower to Middle Jurassic syn-tectonic strata of the Laberge Group in the Whitehorse trough, a large marine basin that overlaps the northern Intermontane terranes of southern Yukon and northern British Columbia (Dickie and Hein, 1995; Lowey, 2004, 2008; Colpron et al., 2015; van Drecht, 2019). Detrital zircon U-Pb results for two samples (n = 75) suggested an Early Jurassic depositional age for Faro Peak formation conglomerate facies, with a dominant population of 220-180 Ma grains indicating derivation from arc- to collision-related plutonic rocks that currently flank the Whitehorse trough (Fig. 1.2; Colpron et al., 2015, 2021; Sack et al., 2020), however, the exact provenance and timing of Faro Peak basin subsidence are uncertain. Similar-aged Late Triassic to Early Jurassic detrital zircon grains characterize Laberge Group strata (Colpron et al., 2015; van Drecht, 2019) and pose the question of whether the Faro Peak formation strata accumulated in the northern reaches of the Whitehorse trough and are correlative with the Laberge Group or instead represent deposition in a coeval, but geographically isolated depocenter along the eastern edge of the Intermontane terranes.

1.2 GEOLOGICAL BACKGROUND

Late Devonian east-dipping subduction along the western Laurentian margin led to backarc extension, opening of the Slide Mountain marginal ocean basin, and outboard development of a pericratonic or continental margin-fringing arc chain recorded by the Intermontane arc terranes – Yukon-Tanana, Stikinia, and Quesnellia (Creaser et al., 1997; Colpron et al., 2007). Snowcap assemblage rock units comprise the exposed pre-Late Devonian basement of the Yukon-Tanana arc terrane and was probably part of a Neoproterozoic to lower Paleozoic passive margin succession along northwestern Laurentia (e.g., Mortensen, 1992; Colpron et al., 2006; Piercey and Colpron, 2009). The provenance of Snowcap assemblage metasedimentary rocks is based on one quartzite unit near Little Salmon Lake in central Yukon (LSL on Fig. 1.2) that yields ca. 1870, 2080, 2380, and 2720 Ma detrital zircon age peaks and suggests northwest Laurentian craton linkages (Piercey and Colpron, 2009), including unique-aged 2100-2000 Ma rocks of the Buffalo Head and Chinchaga terranes in the Peace River Arch region of northwestern Alberta and northeastern British Columbia.

The Intermontane arc terranes that flourished during the mid-Paleozoic as a west-facing arc system became proximal to the North American margin after an arc polarity shift to an east-facing arc led to the closure of the Slide Mountain ocean. Subsequent accretion of the Yukon-Tanana terrane and Quesnellia to the North American margin occurred by the late Permian (Beranek and Mortensen, 2011; Golding et al., 2016) or later (Parsons et al., 2019) while Stikinia remained partially outboard as an Aleutian arc-style festoon (Mihalynuk et al. 1994) until the return of east-dipping subduction along the western margin of the Intermontane belt by the Middle Triassic. Renewed subduction ultimately resulted in strike-slip duplication of Stikinia and Quesnellia (Wernicke and Klepacki 1988; Dostal et al. 2009) or oroclinal bending and counter-clockwise rotation of Stikinia and Yukon-Tanana around the Cache Creek terrane (e.g., Mihalynuk et al. 1994, 2004). Early Jurassic plate convergence and arc collision led to crustal thickening in the "hinge zone" of the orocline model and greenschist to amphibolite grade metamorphism of Yukon-Tanana basement rocks from central Yukon to eastern Alaska (Dusel-Bacon et al., 1992, 1995; Berman et al., 2007; Knight et al., 2013; Clark, 2017) and emplacement of plutons in the Yukon-Tanana terrane, Stikinia, and Quesnellia.

Late Triassic magmatism in central Yukon is characterized by the Pyroxene Mountain (220-211 Ma), Stikine (217-214 Ma), and Headless (208-207 Ma) suites that intrude basement units of the Yukon-Tanana, Stikinia, and Quesnellia terranes (Fig. 1.2, Table 1.1). Aluminum-in-hornblende geobarometric results indicate that the Stikine suite crystallized at ~9-17 km depth and yields zircon Hf isotope values ($\varepsilon_{Hf(t)}$: +9.7 to +11.5; $\bar{X}$ = +10.5) consistent with minor to no crustal contamination (Table 1.1; Sack et al., 2020). In eastern Alaska, ca. 216-208 Ma plutons were emplaced into Mississippian to Permian Nasina and Fortymile River assemblages of the Yukon-

Location	Source	Age (Ma)	εNd(t) whole rock	εHf(t) zircon or *	$^{207}Pb/^{204}Pb$	$^{206}Pb/^{204}Pb$	Reference
central Yukon	Pyroxene Mtn. suite	220-211	-	-	-	-	Sack et al., 2020
	Stikine suite	217-214	+5.2 to +5.3	+9.7 to +11.5	15.59	18.75	
	Headless suite	208-207	-	-	-	-	
	Minto suite	205-194	-3.6 to +1.3	+0.5 to +10.9	15.63	18.76	
	Lokken suite	195-184	-4.3 to -0.6	-2.9 to +9.3	15.67	19	
	Long Lake suite	188-183	-5.9 to +1.5	-5.8 to +6.4	15.68	19.05	
	Bennett	178-175	-2.5	-	15.64	19.13	
eastern Alaska	Taylor Mountain batholith, Kechumstuk Mountain intrusion, and others	216-208	-	-	15.62	18.73	Dusel-Bacon et al., 2015
	Mount Veta intrusion, Diamond Mountain	201-181	-	-	15.66	19.06	

Table 1.1 - Summary of ages and isotope compositions for Late Triassic to Early Jurassic plutonic rocks in eastern Alaska and central Yukon. (*) indicates ε_{Nd} converted ε_{Hf} values following Vervoort et al. (1999).

Tanana terrane and yield feldspar Pb isotope values (Dusel-Bacon et al., 2015) consistent with the Stikine suite (Table 1.1). Late Triassic (217-204 Ma) hornblende and mica $^{40}Ar/^{39}Ar$ cooling ages of Stikine suite rocks (Sack et al., 2020) and the Taylor Mountain batholith and Kechumstuk Mountain intrusion in eastern Alaska (Cushing, 1984; Newberry et al., 1998; Werdon et al., 2001) indicate rapid cooling of these plutons following crystallization.

Late Triassic to Early Jurassic granodiorite batholiths of the Minto suite (205-194 Ma) are exposed at the northern apex of the Whitehorse trough along the trace of the northern Teslin fault (Fig. 1.2). The Minto suite was emplaced into mid- to lower crustal (~16-27 km) basement rocks of the Yukon-Tanana terrane, Quesnellia, and Stikinia (McCausland et al., 2002; Tafti, 2005; Sack et al., 2020) and yield zircon Hf isotope ($\varepsilon_{Hf(t)}$: +0.5 to +10.9; $\bar{X}$ = +3.4) values indicative of minor crustal input (Table 1.1; Sack et al., 2020). Early Jurassic (194-182 Ma) mica $^{40}Ar/^{39}Ar$ ages combined with Al-in-hornblende constraints on the Minto suite intrusions suggest moderate to rapid exhumation rates of ~0.7-1.3 mm/yr to the west and ~2.1-7.5 mm/yr to the east of the Teslin fault (Sack et al., 2020).

Pliensbachian to Toarcian plutons are represented by the Long Lake (188-183 Ma) and Bennett (178-175 Ma) suites in central Yukon, respectively, and intruded the Yukon-Tanana—Stikinia terrane boundary west of the Teslin fault at mid-crustal and upper-crustal crystallization depths (McCausland et al., 2002; Sack et al., 2020). Zircon in the Long Lake suite have Hf isotope ($\varepsilon_{Hf(t)}$: -5.8 to +6.4; $\bar{X}$ = -0.9) compositions that show evidence of crustal contamination (Table 1.1; Sack et al., 2020). Early Jurassic (189-178 Ma) mica and hornblende cooling ages (Hunt and Roddick, 1991; Sack et al., 2020) combined with crystallization depths yielded from Al-in-hornblende values indicate exhumation rates for Long Lake suite that ranges from ~0.5-2.8 mm/yr (Sack et al., 2020).

The Lokken suite (195-184 Ma) crops out to the east of the Teslin fault and intrudes Permian and older units exclusively of the Yukon-Tanana terrane. The Lokken suite yields zircon Hf isotope ($\varepsilon_{Hf(t)}$: -2.9 to +9.3; $\bar{X}$ = +3.5) compositions that are more superchondritic than those of the Long Lake suite and indicate only minor crustal contamination (Table 1.1; Sack et al., 2020). Aluminum-in-hornblende values indicate mid- to upper crustal emplacement depths (~10-11.5 km; Sack et al., 2020) and Early Jurassic (194-179 Ma) hornblende and mica K-Ar and ^{40}Ar-^{39}Ar cooling ages (Stevens et al., 1982; Hunt and Roddick, 1987, 1992; Gordey et al., 1998; Joyce et al., 2015; Sack et al., 2020) suggest rapid cooling following crystallization.

Early Jurassic (201-181 Ma) granodiorite, quartz monzonite, and granite plutons in eastern Alaska intrude the Mississippian to lower Permian Nasina and Fortymile River assemblages of the Yukon-Tanana terrane and overlap in age with the Minto, Long Lake, and Lokken suites. Feldspar Pb isotope values indicate crustal contamination (Table 1.1; Dusel-Bacon et al., 2015) and magmatic epidote in some plutons suggest crystallization depths >15 km (Werdon et al., 2001; Day et al., 2002; Dusel-Bacon et al., 2009) similar to Early Jurassic plutonic suites in central Yukon (e.g., Sack et al., 2020). Early Jurassic (196-181 Ma) hornblende and mica cooling ages (Cushing, 1984, Hansen et al., 1991; Newberry et al., 1998; Szumigala et al., 2000; Dusel-Bacon et al., 2002) from these plutons and the surrounding Nasina and Fortymile River assemblages imply rapid cooling after crystallization.

Following Late Triassic to Early Jurassic (ca. 220-180 Ma) crustal thickening and pluton emplacement at mid- to upper crustal depths, the northern Intermontane terrane infrastructure from central Yukon to eastern Alaska was rapidly exhumed to upper crustal levels by the Pliensbachian (ca. 191 – 183 Ma) (e.g., Dusel-Bacon et al., 2002; Knight et al., 2013; Kellett et al., 2018; Sack et al., 2020). Early Jurassic tectonic exhumation in central Yukon was structurally controlled and documented by the different cooling ages of the Minto, Long Lake, and Lokken suite rocks along the Teslin fault (Sack et al., 2020) and cooling ages of Yukon-Tanana terrane basement rocks along the ~100 km-long, northwest-trending, low-angle Willow Lake fault (WL on Fig. 1.2; Knight et al. 2013). In eastern Alaska, the exhumation of plutons and surrounding rocks was originally interpreted to indicate thrust-related uplift and erosion (Hansen and Dusel-Bacon, 1998; Dusel-Bacon et al., 1995, 2002), however, Late Triassic to Early Jurassic plutons typically have equigranular textures and cut metamorphic fabrics (e.g. Day et al., 2002) and suggest alternate models of pluton emplacement at mid-crustal depths at or near peak metamorphic conditions and subsequent regional exhumation due to gravitational collapse and/or transtensional faulting (Berman et al., 2007; Dusel-Bacon et al., 2015).

Rapid and widespread Early Jurassic subsidence processes resulted in the deposition of multiple syn-tectonic units in the northern Cordillera, including the Faro Peak formation of central Yukon, Macauley Ridge formation of western Yukon and eastern Alaska, and Laberge Group and equivalents in the Whitehorse trough of central Yukon and northern British Columbia (Fig. 1.1; e.g., Colpron et al., 2015). Laberge Group strata in Yukon mostly consist of Sinemurian and younger terrestrial to marginal-marine strata of the Tanglefoot formation and deep-marine slope and mass-flow units of the Richthofen formation (Tempelman-Kluit, 1984, 2009; Hart, 1997; Lowey, 2004, 2008). Conglomerate units within the Laberge Group contain clasts of siliciclastic and carbonate rocks, chert, metamorphic rocks, and characteristic extrusive and intrusive igneous rocks. The Laberge Group was locally sourced with clasts primarily derived from exhumed plutons that presently flank the Whitehorse trough (Fig. 1.2) and contains basal units dominated by volcanic and sedimentary rock clasts and younger units with a higher proportion of intrusive rock clasts (Dickie and Hein, 1995; Hart et al., 1995; Johannson et al., 1997; Shirmohammad et al., 2011). Detrital zircon from the Tanglefoot and Richthofen formations are dominated by Late Triassic to Early Jurassic (~220-180 Ma) grains that yield $\varepsilon_{Hf(t)}$ values of -4.7 to +12.1 and confirm derivation from well-characterized plutons along the Whitehorse trough (van Drecht, 2019).

1.2.2 Southern Tay River map area

The Faro Peak formation is exposed intermittently for ~30 km at the eastern edge of the Intermontane belt and parallel to the northwest-trending Vangorda fault, the local suture between the Yukon-Tanana and Slide Mountain terranes in the southern Tay River map area near Faro, Yukon. The Intermontane terranes are separated from parautochthonous North American strata along the Inconnu thrust to the northeast and the Cassiar terrane along the Tintina fault to the southwest (Fig. 1.3b). The Faro area restores near the town of Eagle in eastern Alaska after ~430 km of post-Cretaceous dextral displacement on the Tintina fault (Gabrielse et al., 2006).

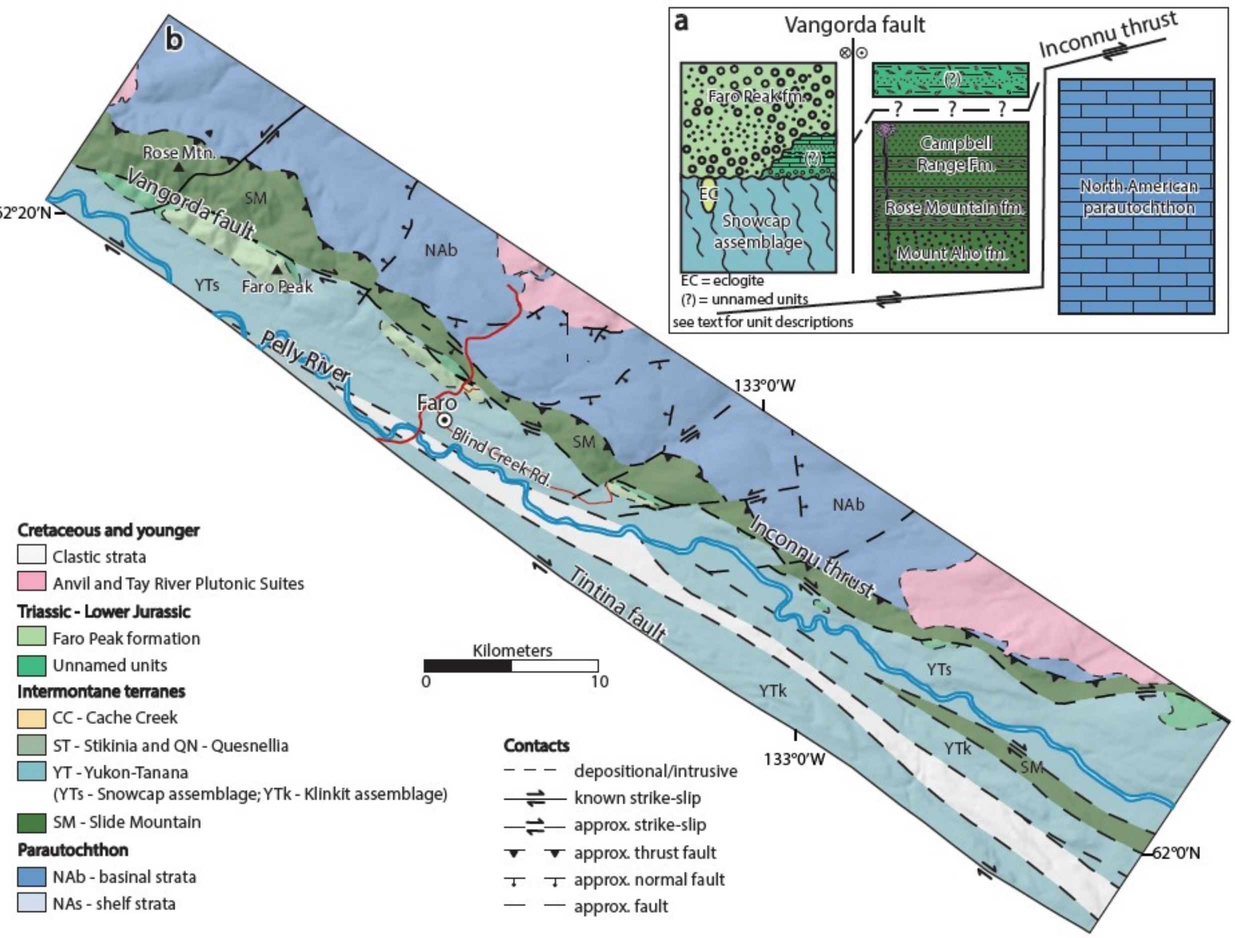

Figure 1.3 - (a) Generalized stratigraphy of the southern Tay River map area after Pigage (2004); (b) Simplified bedrock geology of the southern Tay River map area after Pigage (2004).

Micaceous quartzite, quartz-mica schist, and marble units of the Snowcap assemblage are exposed in the Faro township and along the Blind Creek Road southeast of Faro (Pigage, 2004). Mafic lenses in the Snowcap assemblage are locally metamorphosed to eclogite facies and yield 264-252 Ma Lu-Hf garnet and omphacite ages and 261-256 Ma white mica ^{40}Ar-^{39}Ar cooling ages (Erdmer et al., 1998; Philippot et al., 2001) that suggest their upper-crustal position since the late Permian.

The Slide Mountain terrane is exposed near Rose Mountain ~20 km northwest of Faro and includes Carboniferous to lower Permian argillite, sandstone, conglomerate, and multicolored chert units of the Mount Aho and Rose Mountain formations and green chert and basalt units of the Campbell Range formation (Pigage, 2004). Harzburgite, gabbro, diabase, and serpentinite units associated with Campbell Range formation have an unconstrained Permian(?) age near Faro (Pigage, 2004), however, ~150 km southeast in the Finlayson Lake area, leucogabbro and plagiogranite that intrude the Campbell Range formation yield U-Pb zircon ages of 274-273 Ma (Mortensen, 1992; Murphy et al., 2006).

The Faro Peak formation was originally assigned a Late Triassic depositional age based on Carnian to Rhaetian conodont elements from limestone beds in a fine-grained lower member unit and limestone clasts in a coarse-grained upper member unit (Templeman-Kluit, 1972; Pigage, 2004). Detrital zircon U-Pb results instead suggested an Early Jurassic depositional age for the Faro Peak formation based on the presence of 220-180 Ma grains in the coarse-grained upper member (Colpron et al., 2015).

Recent field stratigraphic studies have observed that lower member strata sit unconformably on Snowcap assemblage rocks near Rose Mountain and are unconformably overlain by coarse-grained units of the upper member (Wiest et al., 2020). The lower member consists of a locally exposed basal quartz altered conglomerate unit (Fig. 1.4a) and micaceous and calcareous argillite (Fig. 1.4b), limestone that yields Late Triassic conodonts (Fig. 1.4c; Templeman-Kluit, 1972; Pigage, 2004), basalt, and lithic to feldspathic wacke (Fig. 1.4d) to arenite units likely deposited by concentrated turbidity flows (Wiest and Beranek, 2019). The lower member is lithologically

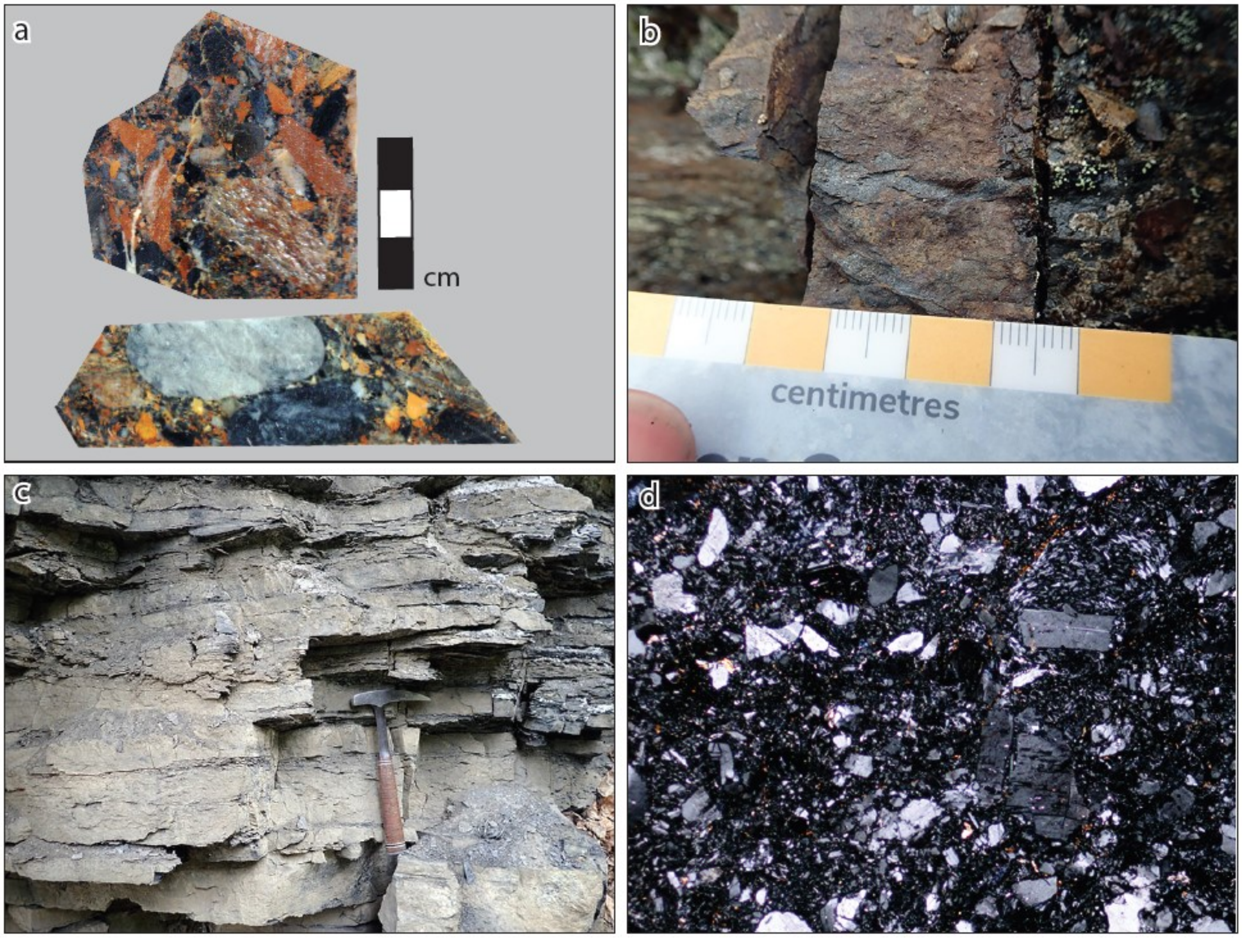

Figure 1.4 - Field photographs and photomicrograph of unnamed Triassic units. (a) Cut slab of basal conglomerate unit (3 cm scale) (b) Micaceous argillite; (c) thin bedded limestone; (d) photomicrograph of feldspathic lithic wacke (4x magnification).

distinct, of mappable extent, has unconformable lower and upper contacts, and was assigned to a new unnamed Triassic unit (Wiest et al., 2020). Some rocks formerly assigned to the lower member are probably equivalent to Upper Triassic overlap assemblages that extend from northern British Columbia to eastern Alaska (Wiest et al., 2020). Capitanian to Carnian maximum depositional ages calculated for some of these units indicate Klondike assemblage sources in the Yukon-Tanana terrane (Chapter 3) and stratigraphic links to pre-Norian units proximal to Slide Mountain terrane (c.f., Beranek and Mortensen, 2011).

Figure 1.5 - Field photographs of the Faro Peak formation. (a) Graded bedding in coarse-grained lithic arenite; (b) coarse-grained lithic feldspathic arenite; (c) limestone clast in conglomerate unit; (d) wavy laminated argillite rip-up clasts in very coarse-grained lithic arenite.

The Faro Peak formation (formerly the upper member of the Faro Peak formation) consists of a locally exposed, normally-graded, basal sandstone succession (Fig. 1.5a) and >800 m of massively bedded, coarse-grained lithic sandstone (Fig. 1.5b) and matrix- to clast-supported, granule to boulder conglomerate units consistent with deposition by submarine sedimentary gravity flows (Wiest and Beranek, 2019; Wiest et al., 2020). The Faro Peak formation unconformably overlies the Snowcap assemblage and in some locations unnamed Triassic units with clast types that reflect underlying rocks including limestone (Fig. 1.5c), sandstone, and wavy-laminated argillite (Fig. 1.5d), quartzite, and quartz mica schist (Fig. 1.6a). Other typical clast types include chert, basalt, and gabbro (Fig. 1.6b) from the adjacent Slide Mountain terrane and up to boulder-sized clasts of intermediate to felsic volcanic and intrusive rocks (Fig. 1.6c,d) with uncertain provenance. Late Triassic to Early Jurassic detrital zircon grains (200-180 Ma) suggest that igneous rock clasts were from arc- and collision-related plutonic assemblages characterized by Sack et al. (2020). Volcanic and sedimentary rock clasts are more abundant in basal successions with hypabyssal and intrusive rock clasts becoming more prevalent upsection (Wiest et al., 2020) and indicates an unroofing trend observed in the units of the Whitehorse trough (Dickie and Hein, 1995; Hart et al., 1995; Johannson et al., 1997; Shirmohammad et al., 2011).

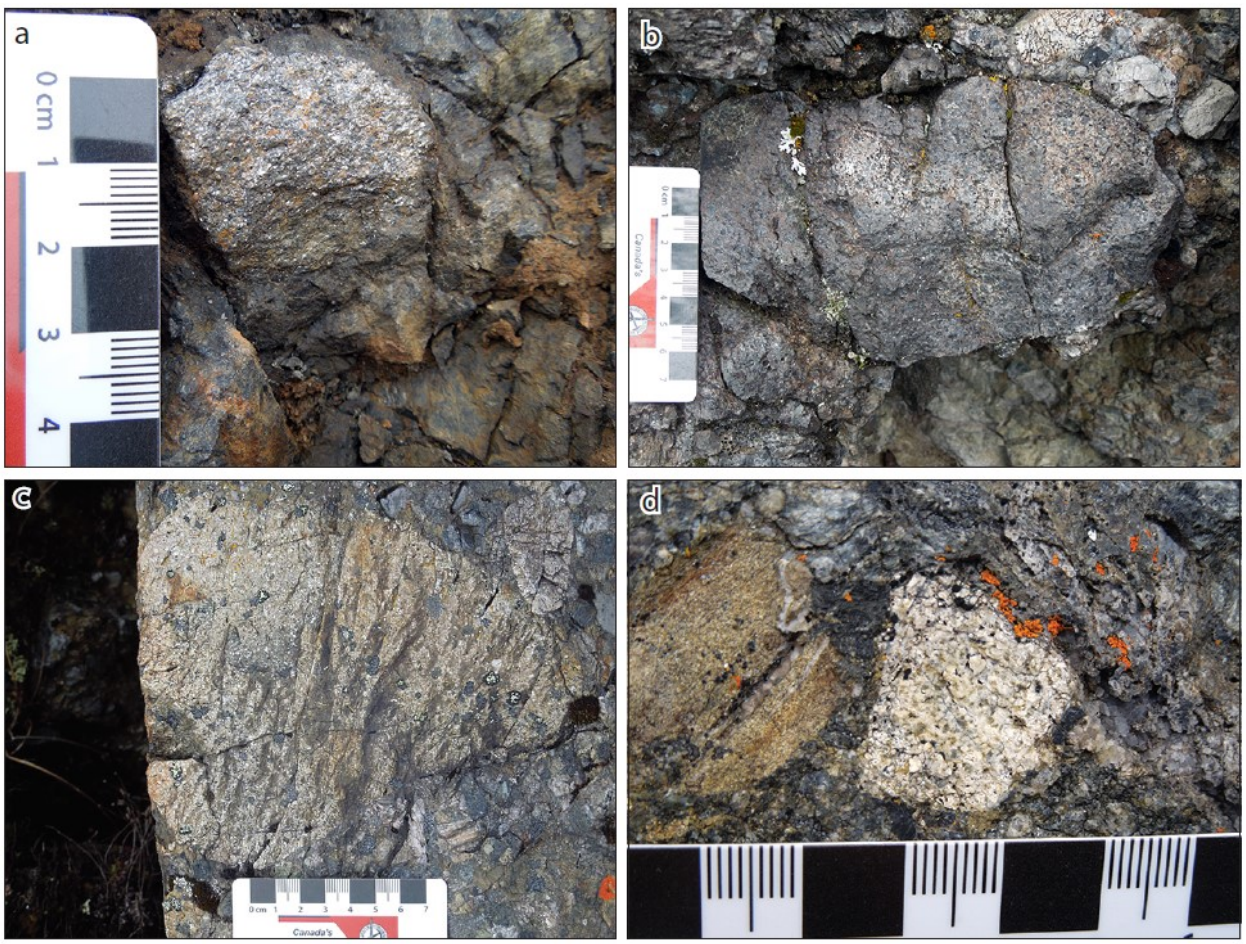

Figure 1.6 - Field photographs of clasts in conglomerate units of the Faro Peak formation. (a) Schist clast; (b) augite gabbro clast; (c) feldspar porphyry clast; (d) felsic intrusive clast.

1.3 OBJECTIVES

This thesis combines field stratigraphic studies in the Faro region (Wiest and Beranek, 2019; Wiest et al., 2020) and high-*n* (>100 analyses per sample) laser ablation split-stream (LASS) detrital zircon U-Pb geochronology and Hf isotope geochemistry to:

1) Describe the physical stratigraphy and interpret the depositional setting of the Faro Peak formation;
2) Determine the contact relationships between unnamed Triassic units and the Faro Peak formation (formerly the lower and upper members of the Faro Peak formation);
3) Investigate the contact relationships between the Faro Peak formation and the underlying and adjacent Yukon-Tanana and Slide Mountain terrane rock assemblages, respectively;
4) Determine the significance of the Vangorda fault with respect to Early Jurassic tectonics and deposition of the Faro Peak formation;
5) Use detrital zircon U-Pb geochronology to constrain the maximum depositional ages of the Faro Peak formation strata;
6) Use detrital zircon U-Pb geochronology and Hf isotope geochemistry to constrain the provenance of the Faro Peak formation;
7) Use detrital zircon U-Pb geochronology and Hf isotope geochemistry to establish a reference frame for the Snowcap assemblage and compare with published reference frames for the pre-Late Devonian Cordilleran margin;
8) Compare detrital zircon U-Pb-Hf isotope data from the Faro Peak formation to similar datasets from Laberge Group rocks in the Whitehorse trough to establish

their age equivalence, compare provenance, and assess their stratigraphic correlation;

9) Determine the significance of the Faro Peak formation with respect to its depositional setting and relation to regional Early Jurassic tectonics and paleogeography.

1.4 METHODS

1.4.1 Field studies and sample collection

Two seasons of fieldwork that included stratigraphic analysis, 1: 24,000 scale bedrock mapping, and sample collection were used to complete the thesis objectives. The 2018 field season focused on investigating adjacent units and potential sources of the Faro Peak formation (i.e., Snowcap assemblage, Campbell Range formation), general stratigraphic observations, and detrital zircon sample collection. The 2019 field season focused on targeted bedrock mapping and stratigraphic investigations of the Faro Peak formation as originally defined (e.g., Templeman-Kluit, 1972; Pigage 2004) to assess if the two members represented separate units. Sample collection focused on the base of the Faro Peak formation and underlying unnamed Triassic units.

1.4.2 Analytical methods

Rock samples were crushed and milled, sieved between 63 and 250 µm, and placed into methylene iodide for heavy liquid density separation. Heavy mineral separates from the Faro Peak formation samples were run through a Frantz magnetic separator at 0.5, 0.7, and 1.0 amperes with an inclination of 17° and tilt of 10° (Sircombe and Stern, 2002). Detrital zircon grains were handpicked, mounted in epoxy, polished, and imaged with backscatter electron (BSE) and cathodoluminescence (CL) to identify areas with complex zoning, fractures, and inherited cores.

Detrital zircon grains were ablated with a 40 µm spot size using a GeoLas 193 nm excimer laser with a frequency of 10 Hz and fluence of 5 J/cm^2. Ablated material was carried with Ar gas from the laser chamber and split to simultaneously collect U-Pb isotopes with ThermoFinnigan Element XR single-collector ICP-MS and Hf isotopes with a ThermoFinnigan Neptune multi-collector ICP-MS using the laser ablation split-stream (LASS) method at Memorial University of Newfoundland (Fisher et al., 2014; Beranek et al., 2020). The U-Pb age data were calibrated with the 91500 zircon reference material with a published ID-TIMS age of 1062.4 ± 1.3 Ma (Wiedenbeck et al. 1995) and Hf isotope data were compared with the Plešovice zircon reference material with a published weighted mean value of 0.282482 ± 0.000013 (Sláma et al. 2008).

Raw U-Pb isotopic values were reduced offline using Iolite 1.4 software (Paton et al., 2011) and ages were calculated with the VizualAge data reduction scheme (Petrus and Kamber, 2012). “Best Ages” were determined for each analysis with >1000 Ma grains reporting the $^{207}Pb/^{206}Pb$ age and <1000 Ma grains reporting the $^{206}Pb/^{238}U$ ages. Concordance was calculated using the $^{207}Pb/^{206}Pb$ and $^{206}Pb/^{238}U$ ages for grains >1000 Ma and analyses with >10% discordance were removed. Reverse discordance of >5% was negated manually when possible during data reduction with VizualAge. Grains <500 Ma were assessed for accuracy on a grain-by-grain basis in Iolite using an evaluation of the $^{207}Pb/^{206}Pb$, $^{207}Pb/^{235}U$, and $^{206}Pb/^{238}U$ ages. Hafnium isotope data are reported in epsilon notation and are corrected for time = t based on the “Best Age”.

1.4.3 Maximum depositional age

Maximum depositional age (MDA) estimations rely on the law of detrital zircon that states a sedimentary unit can be no older than its youngest detrital zircon grain (Gehrels, 2014; Herriott et al., 2019). Complicating analytical factors for LA-ICP-MS techniques include matrix effects and Pb-loss can yield detrital zircon U-Pb ages younger than the true depositional age. This study uses three multi-grain statistical methods to determine MDA estimations and mitigate these effects:

YSP—(youngest statistical peak): weighted mean of the youngest population of 2 or more grains that yields a MSWD ≈ 1 (Coutts et al., 2019);

YSC—(youngest cluster at two sigma): weighted mean of the youngest three or more grains that overlap at 2σ (Dickinson and Gehrels, 2009);

YPA—(youngest graphical peak): youngest peak age of a probability density plot (Dickinson and Gehrels, 2009) and was determined from the "AgePick" Excel macro program from the Arizona Laserchron Center.

Maximum depositional ages for this thesis are assigned from the range of YSP to YSC values using the time scale of Cohen et al. (2013).

1.4.4 Provenance

Sediment provenance was constrained by field stratigraphic observations (e.g., clast compositions) and detrital zircon U-Pb-Hf isotope results. Field studies during summer 2018 and 2019 included investigations of potential sources that are adjacent to and underlie the Faro Peak formation, including Snowcap assemblage metamorphic rocks and Slide Mountain terrane sedimentary and igneous rocks. Detrital zircon U-Pb-Hf isotope results were compared with established reference frames from central Yukon and eastern Alaska (e.g., Piercey et al., 2003; Dusel-Bacon et al., 2015; Sack et al., 2020). When applicable, whole-rock Nd isotope compositions from potential source rocks were converted to Hf isotope values ($\varepsilon_{Hf} = 1.36\ \varepsilon_{Nd} + 2.95$) following Vervoort et al. (1999).

Multidimensional scaling techniques were employed to quantitatively compare detrital zircon U-Pb results of this study with other published datasets (e.g., Sauer et al., 2017; Matthews et al., 2018; Pettit et al., 2019; Thomas et al., 2020). Multidimensional scaling is a superset of principal component analysis, a method commonly used in geochemistry (e.g., Grunsky, 2010), and groups similar samples together on an xy-plane (Vermeesch, 2013) based on the relative similarity of their cumulative distribution plots through an R package "`provenance`" (Vermeesch et al., 2016).

1.5 THESIS OUTLINE

This thesis is written in a manuscript format and consists of four chapters and supplementary appendices. Chapter one is an introduction to the thesis including previous work, outstanding questions, objectives, and methods used to complete the objectives. Chapter two is a manuscript focusing on the main conclusions of the study and is intended for submission to a peer reviewed journal. Chapter three reports data from unnamed Triassic units formerly known as the lower member of the Faro Peak formation. Chapter four provides a summary of the thesis and discussion about future work built off the data presented here that will enhance our understanding of the early tectonic evolution of the Canadian Cordillera. The supplementary appendices include a sample list from the two field seasons, thin section images from select samples, raw U-Pb-Hf isotope results, weighted mean plots for maximum depositional age calculations, weighted mean plots for results from primary U-Pb and Hf standards, and fieldwork reports published in Yukon Geology and Exploration 2018 and 2019 (Wiest and Beranek, 2019; Wiest et al., 2020).

1.6 REFERENCES

Beranek, L.P., and Mortensen, J.K., 2011, The timing and provenance record of the Late Permian Klondike orogeny in northwestern Canada and arc-continent collision along western North America: Tectonics, v. 30, 23 p, doi: 10.1029/2010TC002849.

Beranek, L.P., Gee, D.G., and Fisher, C.M., 2020, Detrital zircon U-Pb-Hf isotope signatures of Old Red Sandstone strata constrain the Silurian to Devonian paleogeography, tectonics, and crustal evolution of the Svalbard Caledonides: Geological Society of America Bulletin, v. 132, no. 9-10, p. 1987-2003, doi: 10.1130/B35318.1.

Beranek, L.P., Link, P.K., and Fanning, C.M., 2016, Detrital zircon record of mid-Paleozoic convergent margin activity in the northern U.S. Rocky Mountains: Implications for the Antler orogeny and early evolution of the North American Cordillera: Lithosphere, v. 8, no. 5, p. 553-550, doi: 10.1130/L557.1.

Berman, R.G., Ryan, J.J., Gordey, S.P., and Villeneuve, M., 2007, Permian to Cretaceous polymetamorphic evolution of the Stewart River region, Yukon-Tanana terrane, Yukon, Canada: P-T evolution linked with in situ SHRIMP monazite geochronology: Journal of Metamorphic Geology, v. 25, p. 803-827, doi: 10.1111/j.1525-1314.2007.00729.x.

Bickerton, L., Colpron, M., Gibson, H.D., Thorkelson, D., and Crowley, J.L., 2020, The northern termination of the Cache Creek terrane in Yukon: Middle Triassic arc activity and Jurassic-

Cretaceous structural imbrication: Canadian Journal of Earth Sciences, v. 57, no. 2, p. 227-248, doi: 10.1139/cjes-2018-0262.

Boggs, S.Jr., 2001, Principles of sedimentology and stratigraphy, 3rd edition: Prentice Hall, Englewood Cliffs, NJ, 726 p.

Brennan, D.T., Li, Z.-X., Rankenburg, K., Evans, N., Link, P.K., Nordsvan, A.R., Kirkland, C.L., Mahoney, J.B., Johnson, T., and McDonald, B.J., 2021, Recalibrating Rodinian rifting in the northwestern United States: Geology, v. 49, doi: 10.1130/G48435.1.

Cawood, P.A., Hawkesworth, C.J., and Dhuime, B., 2012, Detrital zircon record and tectonic setting: Geology, v. 40, p. 875-878, doi: 10.1130/G32945.1.

Clark, A.D., 2017, Tectonometamorphic history of mid-crustal rocks at Aishihik Lake, southwest Yukon: Unpublished MSc thesis, Simon Fraser University, British Columbia, Canada, p. 153.

Cohen, K.M., Finney, S.C., Gibbard, P.L., and Fran, J.-X., 2013;updated, The ICS International Chronostratigraphic Chart, ep. 36: 199-204, http://www.stratigraphy.org/ICSchart/ChronostratChart2021-07.pdf.

Colpron, M., Crowley, J.L., Gehrels, G., Long, D.G.F., Murphy, D.C., Beranek, L., and Bickerton, L., 2015, Birth of the northern Cordilleran orogeny, as recorded by detrital zircons in Jurassic synorogenic strata and regional exhumation in Yukon: Lithosphere, v. 7, p. 541-562, doi: 10.1130/L451.1.

Colpron, M., Nelson, J.L., and Murphy, D.C., 2006, A tectonostratigraphic framework for the pericratonic terranes of the northern Cordillera, *in* Colpron, M. and Nelson, J.L., eds., Paleozoic Evolution and Metallogeny of Pericratonic Terranes at the Ancient Pacific

Margin of North America, Canadian and Alaskan Cordillera: Geological Association of Canada, Special Paper 45, p. 1-23.

Colpron, M., Nelson, J.L., and Murphy, D.C., 2007, Northern Cordilleran terranes and their interactions through time: Geological Society of America Today, v. 17, no. 4/5, doi: 10.1130/GSAT01704-5A.1.

Coutts, D.S., Matthews, W.A., and Hubbard, S.M., 2019, Assessment of widely used methods to derive depositional ages from detrital zircon populations: Geoscience Frontiers, v. 10, no. 4, p. 1421-1435, doi: 10.1016/j.gsf.2018.11.002.

Cushing, G.W., 1984, The tectonic evolution of the eastern Yukon-Tanana Upland [M.S. thesis]: Albany, State University of New York, 235 p.

Day, W.C., Aleinikoff, J.N., and Gamble, B., 2002, Geochemistry and age constraints on metamorphism and deformation in the Fortymile River area, eastern Yukon-Tanana Upland, Alaska, *in* Wilson, F.H., and Galloway, J.P., eds., Studies by the U.S. Geological Survey in Alaska, 2000: U.S. Geological Survey Professional Paper 1662, p. 5–18.

DeGraff-Surpless, K., Graham, S.A., Wooden, J.L., and McWilliams, M.O., 2002, Detrital zircon provenance analysis of the Great Valley group, California: Evolution of an arc-forearc system: Geological Society of America Bulletin, v. 114, no. 12, p. 1564-1580, doi: 10.1130/0016-7606(2002)114<1564:DZPAOT>2.0.CO;2.

DeGraff-Surpless, K., Mahoney, J.B., Wooden, J.L., and McWilliams, M.O., 2003, Lithofacies control in detrital zircon provenance studies: Insights from the Cretaceous Methow basin, southern Canadian Cordillera: Geological Society of America Bulletin, v. 115, no. 8, p. 899-915, doi: 10.1130/B25267.1.

Dickie, J.R., and Hein, F.J., 1995, Conglomeratic fan deltas and submarine fans of the Jurassic Laberge Group, Whitehorse trough, Yukon Territory, Canada: fore-arc sedimentation and unroofing of a volcanic island-arc complex: Sedimentary Geology, v. 98, p. 263–292, doi:10.1016/0037-0738(95)00036-8.

Dickinson, W.R., and Gehrels, G.E., 2009, Use of U-Pb ages of detrital zircons to infer maximum depositional ages of strata: A test against a Colorado Plateau Mesozoic database: Earth and Planetary Science Letters, v. 288, p. 115-125, doi: 10.1016/j.epsl.2009.09.013.

Dostal, J., Keppie, J.D., and Ferri, F., 2009, Extrusion of high-pressure Cache Creek rocks into the Triassic Stikinia-Quesnellia arc of the Canadian Cordillera: Implications for terrane analysis of ancient orogens and palaeogeography, *in* Murphy, J.B., Keppie, J.D., and Hynes, A.J., eds., Ancient Orogens and Modern Analogues: Geological Society of London Special Publication 327, p.71-87.

Dusel-Bacon, C., Aleinikoff, J.N., Day, W.C., and Mortensen, J.K., 2015, Mesozoic magmatism and timing of epigenetic Pb-Zn-Ag mineralization in the western Fortymile mining district, east-central Alaska: Zircon U-Pb geochronology, whole-rock geo-chemistry, and Pb isotopes: Geosphere, v. 11, no. 3, p. 786-822, doi:10.1130/GES01092.

Dusel-Bacon, C., Hansen, V.L., 1992, High-pressure amphibolite-facies metamorphism and deformation within the Yukon-Tanana and Taylor Mountain terranes, eastern Alaska, *in* Geologic Studies in Alaska, US Geological Survey, 1991, Bradley, D.C. and Dusel-Bacon, C. (eds), US Geological Survey Bulletin 2041, p. 140-159.

Dusel-Bacon, C., Hansen, V.L., and Scala, J.A., 1995, High-pressure amphibolite facies dynamic metamorphism and the Mesozoic tectonic evolution of an ancient continental margin, east-central Alaska: Journal of Metamorphic Geology, v.13, p. 9-24, doi:10.1111/j.1525-1314.1995.tb00202.x.

Dusel-Bacon, C., Lanphere, M.A., Sharp, W.D., Layer, P.W., and Hanson, V.L., 2002, Mesozoic thermal history and timing of structural events for the Yukon-Tanana Upland, east-central Alaska—$^{40}Ar/^{39}Ar$ data from metamorphic and plutonic rocks: Canadian Journal of Earth Sciences, v.39, p. 1013-1051, doi:10.1139/e02-018.

Dusel-Bacon, C., Slack, J.F., Aleinikoff, J.N., and Mortensen, J.K., 2009, Mesozoic magmatism and basemetal mineralization in the Fortymile mining district, eastern Alaska—Initial results of petrographic, geochemical, and isotopic studies in the Mount Veta area, *in* Haeussler, P.J., and Galloway, J.P., eds., Studies by the U.S. Geological Survey in Alaska, 2007: U.S. Geological Survey Professional Paper 1760-A, 42 p.

Erdmer, P., Ghent, E.D., Archibald, D.A., and Stout, M.Z., 1998, Paleozoic and Mesozoic high-pressure metamorphism at the margin of ancestral North America in central Yukon: Geological Society of America Bulletin, v. 110, no. 5, p. 615-629.

Fisher C.M., Vervoort, J.D., and DuFrane, S.A., 2014, Accurate Hf isotopic determinations of complex zircons using the "laser ablation split stream" method: Geochemistry, Geophysics, Geosystems, v. 15, p. 121-139, doi: 10.1002/2013GC004962.

Gabrielse, H., Murphy, D.C., and Mortensen, J.K., 2006, Cretaceous and Cenozoic dextral orogeny-parallel displacements, magmatism, and paleogeography, north-central Canadian Cordillera, *in* Haggart, J.W., Enkin, R.J. and Monger, J.W.H., eds., Paleogeography of the North American Cordillera: Evidence for and Against Large-Scale Displacements: Geological Association of Canada Special Paper 46, p. 255-276.

Gehrels, G., 2012, Detrital zircon U-Pb geochronology: Current methods and new opportunities, *in* Busby, C. and Azor Pérez, A., eds., Tectonics of sedimentary basins: Recent advances, p. 45-62, doi: 10.1002/9781444347166.ch2

Gehrels, G., 2014, Detrital zircon U-Pb geochronology applied to tectonics: Annual Review of Earth and Planetary Sciences, v. 42, p. 127-149.

Golding, M.L., Mortensen, J.K., Ferri, F., Zonneveld, J.-P., and Orchard, M.J., 2016, Determining the provenance of Triassic sedimentary rocks in northeastern British Columbia and western Alberta using detrital zircon geochronology, with implications for regional tectonics. Canadian Journal of Earth Sciences, vol. 53, p. 140-155, doi: 10.1139/cjes-2015-0082.

Gordey, S.P., McNicoll, V.J., and Mortensen, J.K., 1998, New U-Pb ages from the Teslin area, southern Yukon, and their bearing on terrane evolution in the northern Cordillera, *in* Current Research 1998-F: Geological Survey of Canada, p.129-148.

Grunsky, E.C., 2010, The interpretation of geochemical survey data: Geochemistry, Exploration, Environmental Analysis, v. 10, no. 1 p. 27-74, doi: 10.1144/1467-7873/09-210.

Hansen, V.L., and Dusel-Bacon, C., 1998, Structural and kinematic evolution of the Yukon-Tanana Upland tectonites, east-central Alaska: A record of late Paleozoic to Mesozoic crustal assembly: Geological Society of America Bulletin, v. 110, p. 211–230, doi:10.1130/0016-7606(1998)110<0211 :SAKEOT >2.3.CO;2.

Hansen, V.L., Heizler, M.T., and Harrison, T.M., 1991, Mesozoic thermal evolution of the Yukon-Tanana composite terrane—New evidence from $^{40}Ar/^{39}Ar$ data: Tectonics, v. 10, p. 51–76, doi:10.1029/90TC01930.

Hart, C.J.R., 1997, A Transect across Northern Stikinia: Geology of the Northern Whitehorse Map Area, Southern Yukon Territory (105D/13–16): Exploration and Geological Services Division, Yukon Region, Indian and Northern Affairs Canada, Bulletin 8, p. 112.

Hart, C.J.R., Dickie, J.R., Ghosh, D.K., and Armstrong, R.L., 1995, Provenance constraints for Whitehorse trough conglomerate: U-Pb zircon dates and initial Sr ratios of granitic clasts in Jurassic Laberge Group, Yukon Territory, *in* Miller, D.M., and Busby, C., eds., Jurassic Magmatism and Tectonics of the North American Cordillera: Geological Society of America Special Paper 299, p. 47–63.

Herriott, T.M., Crowley, J.L., Schmitz, M.D., Wartes, M.A., and Gillis, R.J., 2019, Exploring the law of detrital zircon: LA-ICP-MS and CA-TIMS geochronology of Jurassic forearc strata, Cook Inlet, Alaska, USA: Geology, v. 47, no. 11, p. 1044-1048, doi: 10.1130/G46312.1.

Hunt, P.A. and Roddick, J.C., 1987, A compilation of K-Ar ages, report 17, *in* Radiogenic age and isotopic studies: Report 1, Geological Survey of Canada Paper 87-2, p. 203.

Hunt, P.A. and Roddick, J.C., 1991, A compilation of K-Ar ages: report 20, *in* Radiogenic age and isotopic studies: Report 4, Geological Survey of Canada Paper no. 90-2, p.113-143, doi: 10.4095/131943.

Hunt, P.A. and Roddick, J.C., 1992, A compilation of K-Ar and ^{40}Ar-^{39}Ar ages, report 22, *in* Radiogenic age and isotopic studies: Report 6, Geological Survey of Canada Paper 92-2, p. 179–226.

Ingersoll, R.V., 1988, Tectonics of sedimentary basins: Geological Society of America Bulletin, b. 100, p. 1704-1719, doi: 10.1130/0016-7606(1988)100<1704:TOSB>2.3.CO;2

Ingersoll, R.V., 2012, Tectonics of sedimentary basins, with revised nomenclature, *in* Busby, C. and Azor Pérez, A., eds., Tectonics of sedimentary basins: Recent advances: Blackwell Publishing Ltd., 656 p.

Johannson, G.G., Smith, P.L., and Gordey, S.P., 1997, Early Jurassic evolution of the northern Stikinian arc: evidence from the Laberge Group, northwestern British Columbia: Canadian Journal of Earth Science, v. 34, p. 1030-1057.

Johnsson, M. J., 1993, The system controlling the composition of clastic sediments, *in* Johnsson, M J., and Basu, A., eds., Processes Controlling the Composition of Clastic Sediments: Geological Society of America Special Paper 284, p. 1-19.

Johnston, S.T., Mortensen, J.K., and Erdmer, P., 1996, Igneous and metaigneous age constraints for the Aishihik metamorphic suite, southwest Yukon: Canadian Journal of Earth Sciences, v. 33, p. 1543-1555.

Joyce, N.L., Ryan, J.J., Colpron, M., Hart, C.J.R., and Murphy, D.C., 2015, A compilation of 40Ar/39Ar age determinations for igneous and metamorphic rocks, and mineral occurrences from central and southeast Yukon: Geological Survey of Canada Open-File 7924, 229 p., doi: 10.4095/297446.

Kellett, D.A., Weller, O.M., Zagorevski, A., and Regis, D., 2018, A petrochronological approach for the detrital record: Tracking mm-sized eclogite clasts in the northern Canadian Cordillera: Earth and Planetary Science Letters, v. 494, p. 23-31, doi:10.1016/j.epsl.2018.04.036.

Kemp, A.I.S., Hawkesworth, C.J., Paterson, B.A., and Kinny, P.D., 2006, Episodic growth of the Gondwana supercontinent from hafnium and oxygen isotopes in zircon: Nature, v. 439, p. 580-583.

Knight, E., Schneider, D.A., and Ryan, J., 2013, Thermochronology of the Yukon-Tanana Terrane, West-Central Yukon: Evidence for Jurassic Extension and Exhumation in the Northern Canadian Cordillera: The Journal of Geology, v. 121, p. 371-400, doi: 10.1086/670721.

Lowey, G.W., 2004, Preliminary lithostratigraphy of the Laberge Group (Jurassic), south-central Yukon: Implications concerning the petroleum potential of the Whitehorse trough, *in* Emond, D.S., and Lewis, L.L., eds., Yukon Exploration and Geology 2003: Whitehorse, Yukon, Canada, Yukon Geological Survey, p.129–142.

Lowey, G.W., 2008, Summary of the stratigraphy, sedimentology, and hydrocarbon potential of the Laberge Group (Lower–Middle Jurassic), Whitehorse trough, Yukon, *in* Emond, D.S., Blackburn, L.R., Hill, R.P., and Weston, L.H., eds., Yukon Exploration and Geology 2007: Whitehorse, Yukon, Canada, Yukon Geological Survey, p.179–197.

Matthews, W., Guest, B., and Madronich, L., 2018, Latest Neoproterozoic to Cambrian detrital zircon facies of western Laurentia: Geosphere, v. 14, no. 1, p. 243-264, doi: 10.1130/GES01544.1.

McCausland, P.J.A., Symons, D.T.A., Hart, C.J.R., and Blackburn, W.H., 2002, Paleomagnetism and geobarometry of the Granite Mountain batholith, Yukon: Minimal geotectonic motion of the Yukon-Tanana Terrane relative to North America, *in* Yukon Exploration and Geology, 2001, D.S. Emond, L.H. Weston and L.L. Lewis (eds.), Exploration and Geological Services Division, Yukon, Indian and Northern Affairs Canada, p. 163-177.

Mihalynuk, M.G., Erdmer, P., Ghent, E.D., Cordey, F., Archibald, D.A., Friedman, R.M., and Johannson, G.G., 2004, Coherent French Range blueschist: Subduction to exhumation in<2.5m.y.?: Geological Society of America Bulletin, v.116, p.910–922, doi: 10.1130/B25393.1.

Mihalynuk, M.G., Nelson, J.A., and Diakow, L.J., 1994, Cache Creek terrane entrapment: Oroclinal paradox within the Canadian Cordillera: Tectonics, v. 13, p. 575-595.

Monger, J., and Price, R., 2002, The Canadian Cordillera: Geology and Tectonic Evolution: Canadian Society of Exploration Geophysicists Recorder, v. 27, p. 17-36.

Mortensen, J.K., 1992, Pre–mid-Mesozoic tectonic evolution of the Yukon-Tanana terrane, Yukon and Alaska: Tectonics, v. 11, p. 836–853, doi: 10.1029/91TC01169.

Murphy, D.C., Mortensen, J.K., Piercey, S.J., Orchard, M.J., and Gehrels, G.E., 2006, Mid-Paleozoic to early Mesozoic tectonostratigraphy evolution of Yukon-Tanana and Slide Mountain terranes and affiliated overlap assemblages, Finlayson Lake massive sulphide district, southeastern Yukon, *in* Colpron, M. and Nelson, J.L., eds., Paleozoic Evolution and Metallogeny of Pericratonic Terranes at the Ancient Pacific Margin of North America, Canadian and Alaskan Cordillera: Geological Association of Canada, Special Paper 45, p. 75-105.

Nelson, J.L., Colpron, M., Piercey, S.J., Dusel-Bacon, C., Murphy, D.C., and Root, C.F., 2006, Paleozoic tectonic and metallogenic evolution of the pericrationic terranes in Yukon, northern British Columbia and eastern Alaska, *in* Colpron, M. and Nelson, J.L., eds., Paleozoic Evolution and Metallogeny of Pericratonic Terranes at the Ancient Pacific Margin of North America, Canadian and Alaskan Cordillera: Geological Association of Canada, Special Paper 45, p. 323-360.

Newberry, R.J., Layer, P.W., Burleigh, R.E., and Solie, D.N., 1998, New $^{40}Ar/^{39}Ar$ dates for intrusions and mineral prospects in the eastern Yukon-Tanana terrane—Regional patterns and significance, Alaska, *in* Gray, J.E., and Riehle, J.R., eds., Geologic studies in Alaska by the United States Geological Survey, 1996: U.S. Geological Survey Professional Paper 1595, p.131–159.

Parsons, A.J., Zagorevski, A., Ryan, J.J., McClelland, W.C., van Staal, C.R., Coleman, M.J., and Golding, M.L., 2019, Petrogenesis of the Dunite Peak ophiolite, south-central Yukon, and the distinction between upper-plate and lower-plate setting: A new hypothesis for the late Paleozoic—early Mesozoic tectonic evolution of the Northern Cordillera: Geological Society of America Bulletin, v. 131, no. 1/2, p. 74-298, doi: 10.1130/B31964.1.

Paton, C., Hellstrom, J., Paul, B., Woodhead, J., and Hergt, J., 2011, Iolite: Freeware for the visualization and processing of mass spectrometric data: Journal of Analytical Atomic Spectrometry, v. 26, p. 2508-2518, doi:10.1039/C1JA10172B.

Petrus, J., and Kamber, B.S., 2012, VizualAge: A Novel Approach to Laser Ablation ICP-MS U-Pb Geochronology Data Reduction: Geostandards and Geoanalytical Research, v. 36, 24 p., doi:10.1111/j.1751-908X.2012.00158.x.

Pettit, B.S., Blum, M., Pecha, M., McLean, N., Bartschi, N.C., and Saylor, J.E., 2019, Detrital-zircon U-Pb paleodrainage reconstruction and geochronology of the Campanian Blackhawk-Castlegate succession, Wasatch plateau and Brooks Cliffs, Utah, U.S.A.: Journal of Sedimentary Research, v. 89, p. 273-292, doi: 10.2110/jsr.2019.18.

Philippot, P., Blichert-Toft, J., Perchuk, A., Costa, S., Gerasimov, V., 2001, Lu-Hf and Ar-Ar chronometry supports extreme rate of subduction zone metamorphism deduced from geospeedometry: Tectonophysics, v. 342, p. 23-38.

Piercey, S.J., and Colpron, M., 2009, Composition and provenance of the Snowcap assemblage, basement to the Yukon-Tanana terrane, northern Cordillera: Implications for Cordilleran crustal growth: Geosphere, v. 5, no. 5, p. 439-464, doi: 10.1130/GS00505.1.

Piercey, S.J., Mortensen, J.K. and Creaser, R.A., 2003, Neodymium isotope geochemistry of felsic volcanic and intrusive rocks from the Yukon-Tanana terrane in the Finlayson Lake region, Yukon, Canada: Canadian Journal of Earth Sciences, v. 40, p. 77-97.

Pigage, L.C., 2004, Bedrock geology compilation of the Anvil District (parts of NTS 105K/2, 3, 5, 6, 7, and11), central Yukon: Yukon Geological Survey, Bulletin, v.15, p. 103.

Sack, P.J., Colpron, M., Crowley, J.L., Ryan, J.J., Allan, M.M. Beranek, L.P., Joyce, N.L., 2020, Atlas of Late Triassic to Jurassic plutons in the Intermontane terranes of Yukon: Yukon Geological Survey, Open File 2020-1, p. 365.

Sauer, K.B., Gordon, S.M., Miller, R.B., Vervoort, J.D., and Fisher, C.M., 2017, Evolution of the Jura-Cretaceous North American Cordilleran margin: Insights from detrital-zircon U-Pb and Hf isotopes of sedimentary units of the North Cascades Range, Washington: Geosphere, v. 13, no. 6, p. 2094-2118, doi: 10.1130/GES01501.1.

Shirmohammad, F., Smith, P.L., Anderson, R.G., and McNicoll, V.J., 2011, The Jurassic succession at Lisadale Lake (Tulsequah map area, British Columbia, Canada) and its bearing on the tectonic evolution of the Stikine terrane: Volumnia Jurassica, v. 9, p. 43-60.

Sircombe, K.N. and Stern, R.A., 2002, An investigation of artificial biasing in detrital zircon U-Pb geochronology due to magnetic separation in sample preparation: Geochemica et Cosmochimica Acta, v. 66, no. 13, p. 2379-2397, doi: 10.1016/S0016-7037(02)00839-6.

Sláma, J., Kosler, J., Condon, D., Crowley, J.L., Gerdes, A., Hanchar, J.M, Horstwood, S.A., Morris, G.A., Nasdala, L., Norberg, N., Schaltegger, U., Schoene, B., Tubrett, M., and Whitehouse, M.J., 2008, Plešovice zircon – A new natural reference material for U-Pb and Hf isotopic microanalysis: Chemical Geology, v. 249, p. 1-35, doi: 10.1016/j.chemgeo.2007.11.005.

Stevens, R.D., DeLabio, R.N., and LaChance, G.R., 1982, Age determinations and geological studies, K-Ar isotopic ages: Geological Survey of Canada, Report 15, p. 74.

Symons, D.T.A., Williams, P.R., McCausland, P.J.A., Harris, M.J., Hart, C.J.R., and Blackburn, W.H., 2000, Paleomagnetism and geobarometry of the Big Creek Batholith suggests that Yukon-Tanana Terrane has been a parautochthon since Early Jurassic: Tectonophysics, v. 326, p. 57-72.

Szumigala, D.J., Newberry, R.J., Werdon, M.B., Finseth, B.A., Pinney, D.S., and Flynn, R.L., 2000, Major-oxide, minor-oxide, trace-element, and geochemical data from rocks collected in a portion of the Fortymile Mining District, Alaska: State of Alaska Division of Geological and Geophysical Surveys Raw-Data File 2000-1, 24 p., scale 1:63,360.

Tafti, R., 2005, Nature and Origin of the Early Jurassic Copper (-Gold) Deposits at Minto and Williams Creek, Carmacks Copper Belt, Western Yukon: Examples of Deformed Porphyry Deposits [M.Sc. thesis]: Vancouver, British Columbia, Canada, University of British Columbia, 213 p.

Tempelman-Kluit, D.J., 1972, Geology and origin of the Faro, Vangorda, and Swim concordant zinc-lead deposits, central Yukon Territory: Geological Survey of Canada, Bulletin 208, 73 p.

Tempelman-Kluit, D.J., 1984, Geology, Laberge (105E) and Carmacks (105I), Yukon Territory: Geological Survey of Canada Open-File 1101, scale 1:250,000.

Tempelman-Kluit, D.J., 2009, Geology of Carmacks and Laberge Map Areas, Central Yukon: Incomplete Draft Manuscript on Stratigraphy, Structure and its Early Interpretation(ca.1986): Geological Survey of Canada Open-File 5982, 399 p.

Thomas, W.A., Gehrels, G.E., Sundell, K.E., Greb, S.F., Finzel, E.Z., Clark, R.J., Malone, D.H., Hampton, B.A., and Romero, M.C., 2020, Detrital zircons and sediment dispersal in the eastern Midcontinent of North America: Geosphere, v. 16, doi: 10.1130/GES02152.1.

Topham, M.J., Allan, M.M., Mortensen, J.K., Hart, C.J.R., Colpron, M., and Sack, P.J., 2016, Crustal depth of emplacement of the Early Jurassic Aishihik and Tatchun batholiths, west-central Yukon, *in* Yukon Exploration and Geology 2015, K.E. MacFarlane (ed.), Yukon Geological Survey, p. 233–251.

Tyler, S.A., Marsden, R.W., Grout, F.F., and Thiel, G.A., 1940, Studies of the Lake Superior Precambrian by accessory-mineral methods: Geological Society of America Bulletin, v. 51, p. 1429-1538.

University of Minnesota, 2018, Polar Geospatial Center, https://www.pgc.umn.edu, [accessed November, 2019].

Vermeesch, P., 2013, Multi-sample comparison of detrital age distributions: Chemical Geology, v. 341, p. 140-146, doi: 10.1016/j.chemgeo.2013.01.010.

Vermeesch, P., Resentini, A., and Garzanti, E., 2016, An R package for statistical provenance analysis: Sedimentary Geology, v. 336, no. 1, p. 14-25, doi: 10.1016/j.sedgeo.2016.01.009.

Vervoort, J.D., Patchett, P.J., Blichert-Toft, J., and Albarède, F., 1999, Relationships between Lu-Hf and Sm-Nd isotopic systems in the global sedimentary system: Earth and Planetary Science Letters, v. 168, p. 79-99, doi: 10.1016/S0012-821X(99)00047-3.

Werdon, M.B., Newberry, R.J., and Szumigala, D.J., 2001, Bedrock geologic map of the Eagle A-2 quadrangle, Fortymile mining district, Alaska: Alaska Division of Geological and Geophysical Surveys Preliminary Interpretive Report 2001–3b, scale: 1:63,360.

Wernicke, B., and Klepacki, D.W., 1988, Escape hypothesis for the Stikine block: Geology, v. 16, p. 461-464, doi:10.1130/0091-7613(1988)016<0461:EHFTSB>2.3.CO;2.

Wiedenbeck, M., Allé, P., Corfu, F., Griffin, W.L., Meier, M., Oberli, F., Quadt, A.V., Roddick, J.C., and Spiegel, W., 1995, Three natural zircon standards for U-Th-Pb, Lu-Hf, trace element and REE analyses: Geostandards Newsletter, v. 19, p. 1-23.

Wiest, A.C. and Beranek, L.P., 2019, Stratigraphy of the Faro Peak formation, central Yukon: New field observations of Jurassic synorogenic sedimentation along the Yukon-Tanana–Slide Mountain terrane boundary, *in* Yukon Exploration and Geology 2018, K.E. MacFarlane (ed.), Yukon Geological Survey, p.127–142.

Wiest, A.C., Beranek, L.P., and Manor, M.J., 2020, Upper Triassic to Lower Jurassic stratigraphy of the Faro Peak formation, southern Tay River map area, central Yukon (NTS 105K), *in* Yukon Exploration and Geology 2019, K.E. MacFarlane (ed.), Yukon Geological Survey, p. 121-139.

APPENDIX 1.A.1

Stratigraphy of the Faro Peak formation, central Yukon: New field observations of Jurassic synorogenic sedimentation along the Yukon-Tanana–Slide Mountain terrane boundary

A.C. Wiest* and L.P. Beranek**
Department of Earth Sciences, Memorial University of Newfoundland

Wiest, A.C. and Beranek, L.P., 2019. Stratigraphy of the Faro Peak formation, central Yukon: New field observations of Jurassic synorogenic sedimentation along the Yukon-Tanana–Slide Mountain terrane boundary. *In:* Yukon Exploration and Geology 2018, K.E. MacFarlane (ed.), Yukon Geological Survey, p. 127–142.

Abstract

The Faro Peak formation is a Lower Jurassic(?) unit assigned to the Yukon-Tanana terrane in the southern Tay River map area (NTS 105K). A two-year project was initiated in 2018 to investigate the Faro Peak formation and constrain its stratigraphy, age, and significance to Cordilleran tectonic evolution. The exposed base of the Faro Peak formation includes argillite and organized to disorganized sandstone units that crop out southwest of the Yukon-Tanana–Slide Mountain terrane boundary near Faro. Lower Faro Peak formation units have mafic-intermediate volcanic provenance and were deposited by concentrated density flows or turbidity currents. The upper Faro Peak formation contains massive, disorganized conglomerate and sandstone units that were sourced from the Yukon-Tanana and Slide Mountain terranes and deposited by non-turbulent debris or density flows. The Faro Peak formation is likely the remnant of a synorogenic basin that formed as a result of Intermontane belt exhumation in central Yukon.

* acwiest@mun.ca
** lberanek@mun.ca

Introduction

Late Triassic–Early Jurassic plate convergence and collision along the northern Cordilleran margin resulted in the exhumation of the Intermontane terranes—Yukon-Tanana, Slide Mountain, Stikinia, Quesnellia, and Cache Creek—and subsequent generation of overlapping synorogenic basins (Mihalynuk et *al*., 1994; Johnston et *al*., 1996; Evenchick et *al*., 2007; Knight et *al*., 2013; Nelson et *al*., 2013). In central Yukon, synorogenic Lower to Middle Jurassic strata assigned to the Laberge Group record the timing and spatial extent of Intermontane belt exhumation and represent a regional basin known as the Whitehorse trough (Fig. 1; *e.g*., Tempelman-Kluit, 1984; Dickie and Hein, 1995; Hart et *al*., 1995; Colpron et *al*., 2015; van Drecht and Beranek, 2018). Colpron et *al*. (2015) recently proposed that Laberge Group deposition was coincident with the onset of foreland basin subsidence in southern Canadian Rockies (see Fernie Formation in Fig. 1), suggesting that the Whitehorse trough and related synorogenic basins in Yukon and northern British Columbia are critical to understanding the early growth of the Cordilleran orogen.

Isolated occurrences of Lower Jurassic(?) strata known informally as the Faro Peak formation crop out near the Yukon-Tanana–Slide Mountain terrane boundary in the Faro region of central Yukon and are presumably correlative with synorogenic rock units of the Whitehorse trough (Fig. 1; *e.g*., Pigage, 2004; Colpron et *al*., 2015). A two-year project was initiated to test this hypothesis and constrain the role of Intermontane belt tectonics on Faro Peak formation deposition. In this article, we summarize the field geology of Faro Peak formation outcrops visited during summer 2018. These field observations will be integrated with future detrital zircon U-Pb-Hf studies to confirm the depositional age and provenance of Faro Peak formation rock units and determine the spatial extent of Jurassic exhumation and synorogenic sedimentation in the northern Cordillera.

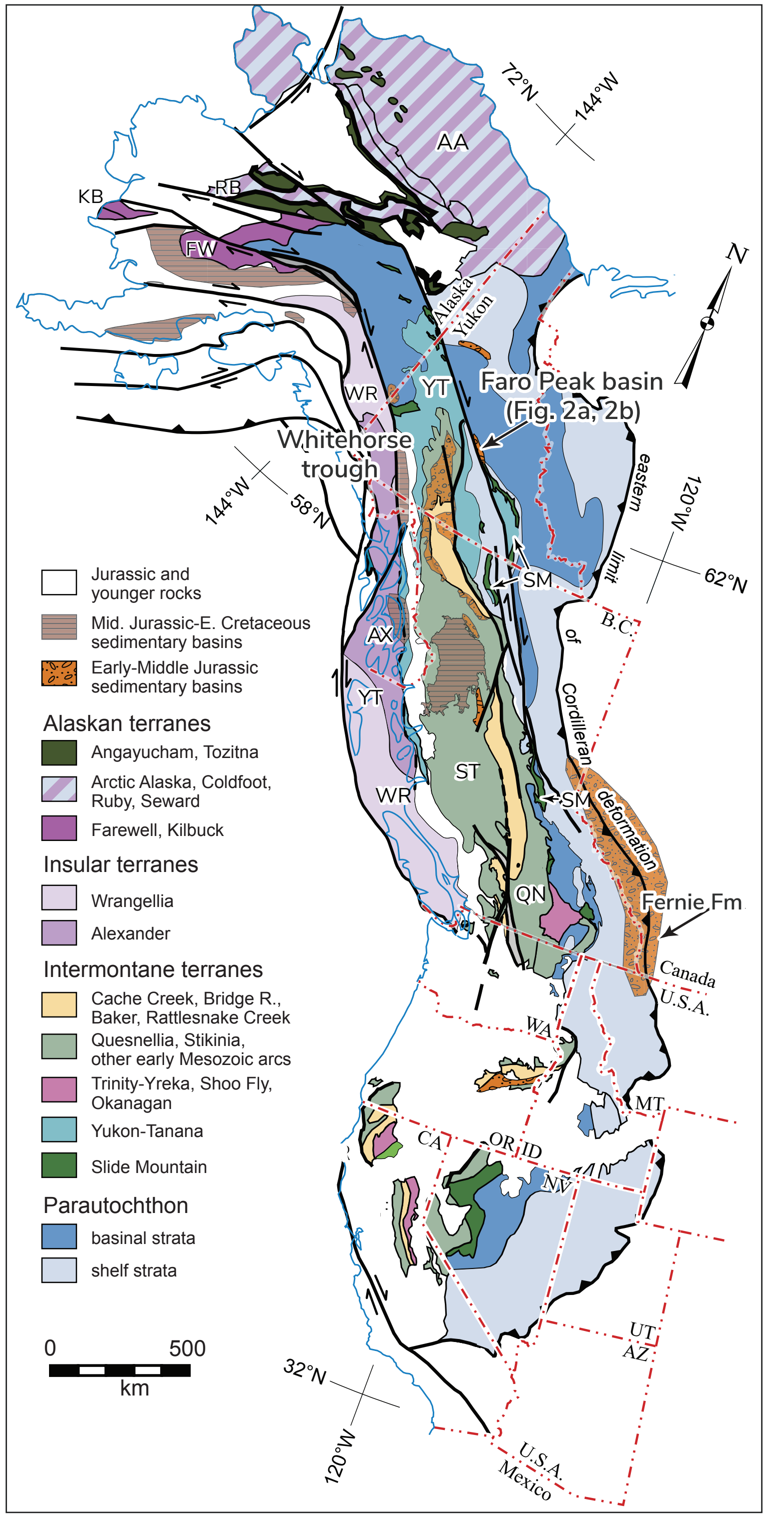

Figure 1. *Paleozoic to early Mesozoic terrane map of the North American Cordillera and associated Jurassic basins modified from Colpron et al. (2015). Terrane abbreviations: AA–Arctic Alaska; AX–Alexander; FW–Farewell; KB–Kilbuck; QN–Quesnellia; RB–Ruby; SM–Slide Mountain; ST–Stikinia; WR–Wrangellia; YT–Yukon-Tanana.*

Geological Background

The Faro townsite is located along the eastern edge of the Intermontane belt in the southern Tay River map area (NTS 105K). In this region, the Intermontane terranes are juxtaposed against North American continental margin strata of Selwyn basin along the Inconnu thrust to the northeast and Cassiar terrane across the Tintina fault to the southwest (Fig. 2a; Pigage, 2004). The Yukon-Tanana and Slide Mountain terranes are separated by the northwest-trending Vangorda fault in the Faro region (Fig. 2b). Pigage (2004) concluded that the Vangorda fault had normal displacement, whereas Colpron et *al.* (2015) interpreted a strike-slip history based on its correlation with the Jules Creek fault (Murphy et *al.*, 2006) in southeastern Yukon.

The Faro Peak formation sits unconformably on quartzite, schist, and other metasedimentary rock units of the pre-Late Devonian Snowcap assemblage, which forms the exposed base of the Yukon-Tanana terrane in central Yukon (Fig. 2b; Colpron et *al.*, 2006). Rocks that comprise the Faro Peak formation were first described by Tempelman-Kluit (1972, 1979) and informally named by Pigage (2004). The Faro Peak formation is generally divided into two members (e.g., Pigage, 2004): a lower member of interbedded basalt, argillite, chert, greywacke, limestone, and conglomerate, and an upper member of massive, polymictic conglomerate with pebble to boulder-sized clasts that are dominated by local Yukon-Tanana and Slide Mountain rocks. The Faro Peak formation has an erosional top and maximum thickness estimates range from >560 m (Pigage, 2004) to >840 m (Tempelman-Kluit, 1979).

Pigage (2004) assigned a Late Triassic depositional age to the Faro Peak formation based on Carnian to Rhaetian conodont elements retrieved from limestone clasts and beds in the lower and upper members. Beranek (2009) collected samples of upper member sandstone at two fossil localities and reported 220–190 Ma detrital zircon populations that instead support an Early Jurassic maximum depositional age for the upper Faro Peak formation. Analogous detrital zircon populations have been recognized in Laberge Group strata of the Whitehorse trough (Colpron et *al.*, 2015;

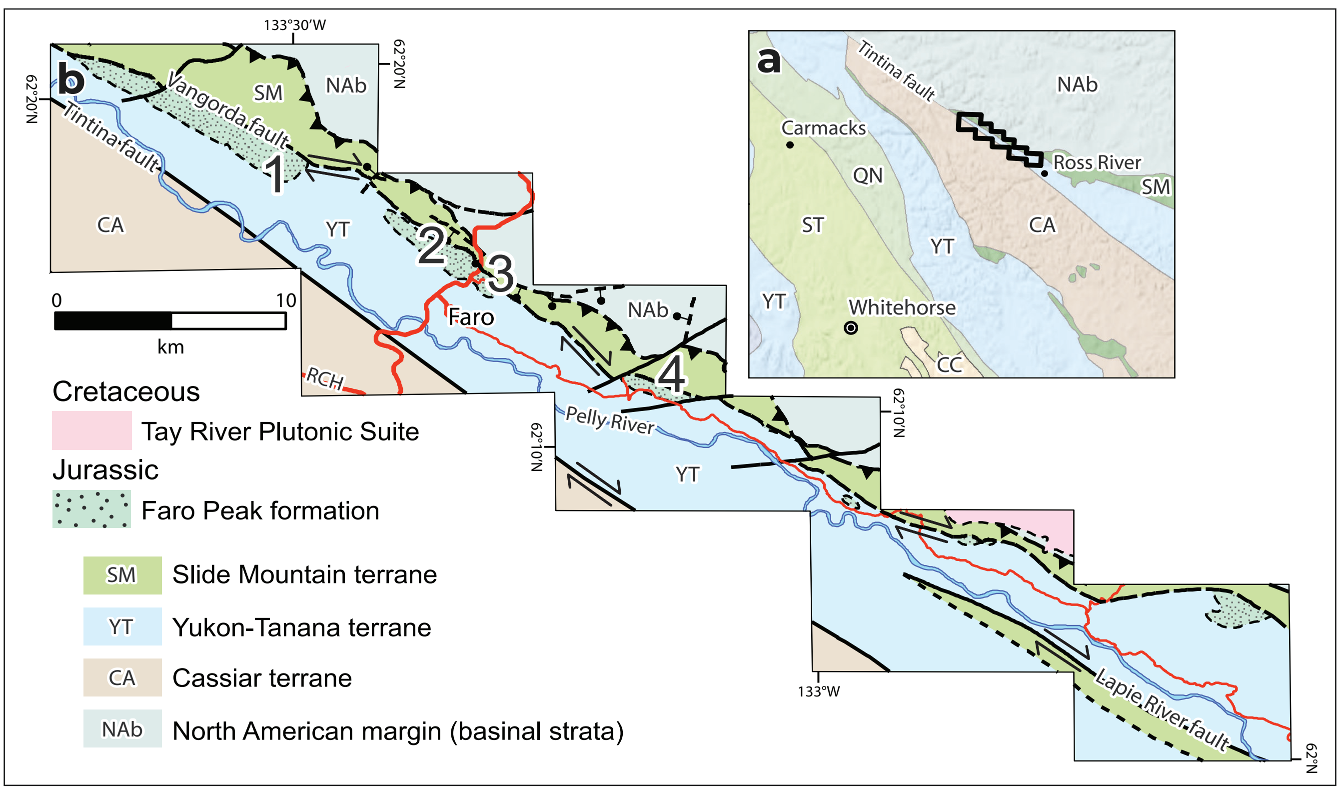

Figure 2. ***(a)*** *Terrane map of central Yukon modified from Yukon Geological Survey (2018).* ***(b)*** *Simplified bedrock geology of the southern Tay River map area modified from Pigage (2004). The numbers 1–4 denote the field localities described in this article.*

van Drecht and Beranek, 2017), suggesting that the Faro Peak formation comprises the remnants of a much larger synorogenic basin system related to Jurassic exhumation across central and southern Yukon.

2018 Field Studies

Locality 1–Faro Peak

Faro Peak and adjacent alpine ridges ~15 km northwest of Faro likely represent the thickest exposures of the Faro Peak formation (locality 1 in Fig. 2b). Lower member rock units observed during summer 2018 crop out along the northeastern flank of Faro Peak (Fig. 3), immediately southwest of the Vangorda fault, and comprise poorly exposed sections of argillite, siltstone, and fine-grained micaceous lithic arenite (Fig. 4a). Pigage (2004) reported that potentially correlative basalt and fine-grained siliciclastic rocks are exposed in the lower Faro Peak formation south and west of Rose Mountain, ~3 km northwest of Faro Peak (Fig. 3). If correct, these lower Faro Peak formation rocks may be coeval with Permian basalt and chert northeast of the Vangorda fault (Campbell Range formation) and represent an overlap assemblage that covers the Yukon-Tanana and Slide Mountain terranes. However, it is possible that these basalt and siliciclastic rock units are instead part of the Slide Mountain terrane and not Faro Peak formation, which may call for a reassessment of the Vangorda fault and location of the Yukon-Tanana–Slide Mountain terrane boundary in this region.

The upper member of the Faro Peak formation near Faro Peak mostly consists of brown weathering, granule to cobble, matrix to clast-supported, polymictic conglomerate intercalated with feldspathic lithic to lithic arenite (Fig. 4b,c). The gravelly and sandy lithofacies are generally massive and lack sedimentary structures, which make stratigraphic younging and bedding determinations difficult. Clast types in the gravelly lithofacies are dominated by quartzite and mica schist with subordinate populations of limestone, grey

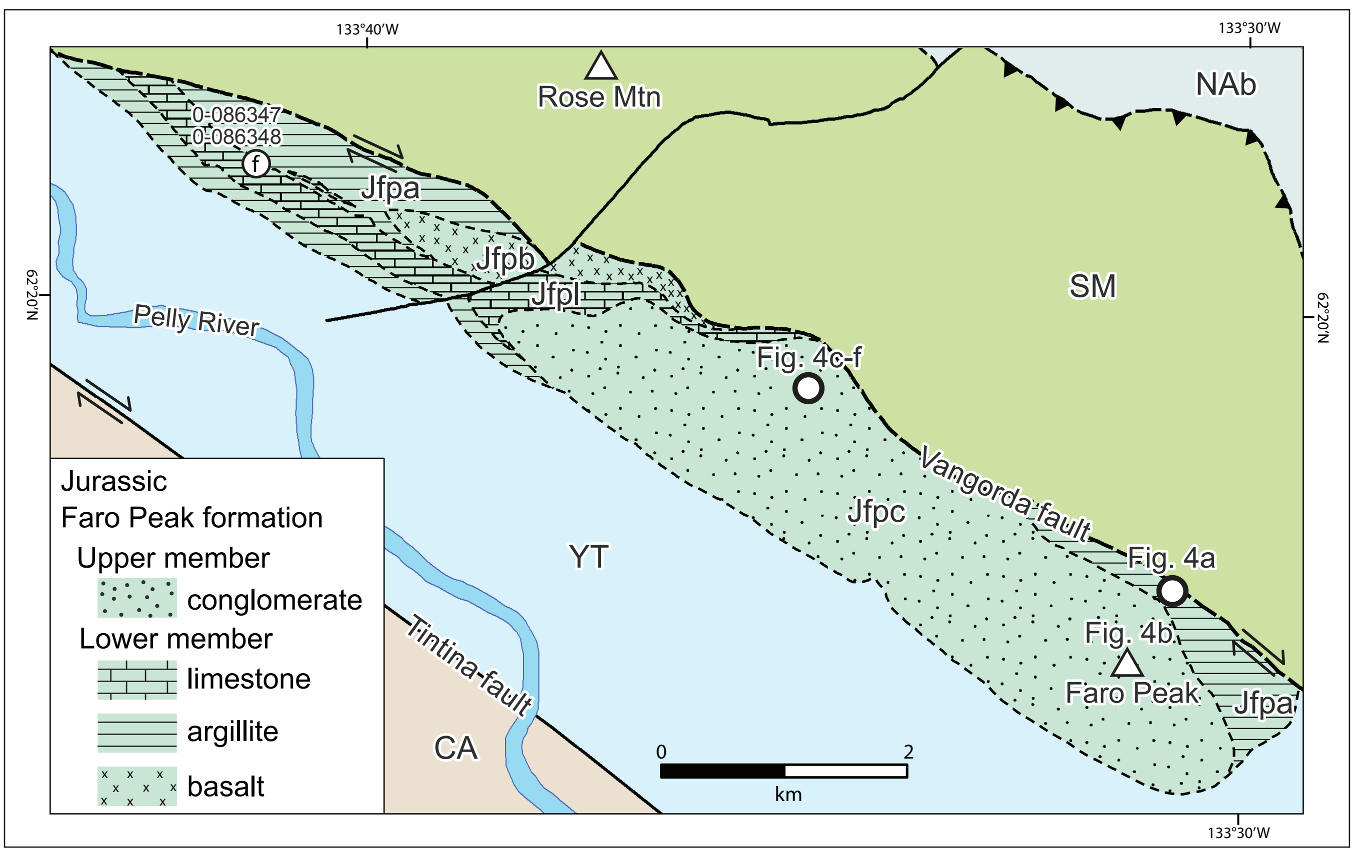

Figure 3. *Simplified bedrock geology of the Faro Peak area (locality 1) modified from Pigage (2004). Faro Peak formation units: Jfpc–upper member conglomerate and sandstone; Jfpl–lower member limestone; Jfpa–lower member argillite, chert, siltstone, and sandstone; Jfpb–lower member basalt. Terrane abbreviations as in Fig. 2b.*

Figure 4. *Field photographs of the Faro Peak area (locality 1).* ***(a)*** *Lower member argillite, siltstone, and fine-grained micaceous lithic arenite along northeastern flank of Faro Peak;* ***(b)*** *upper member lithic sandstone at Faro Peak;* ***(c)*** *upper member clast-supported polymictic conglomerate;* ***(d)*** *upper member grey chert clast;* ***(e)*** *upper member quartz-feldspar porphyry clast; and* ***(f)*** *upper member felsic intrusive clast. Scale bar has 1 cm solid divisions.*

to green to pink chert (Fig. 4d), argillite, and aphanitic to porphyritic basalt. Vein quartz, quartz-feldspar porphyry (Fig. 4e), and felsic intrusive rocks (Fig. 4f) occur as minor clast components.

Abundant quartzite and schist rock fragments in the Faro Peak area successions imply provenance from the underlying Snowcap assemblage, which suggests that gravel and coarse-grained sand deposition were coincident with the exhumation of Yukon-Tanana basement. Subordinate basalt, chert, and argillite clasts are furthermore consistent with derivation from the adjacent Campbell Range formation and older rock units of the Slide Mountain terrane near Rose Mountain. Limestone and intermediate-felsic intrusive rocks have uncertain provenance, but our working hypothesis calls for these clasts to have origins from Yukon-Tanana and/or Stikinia rock assemblages that similarly flank the Whitehorse trough in the Carmacks area of central Yukon (*e.g.*, Colpron et al., 2015).

Locality 2–Whiskey Mountain

The Faro Peak formation underlies the region ~3 km north of Faro, including Whiskey Mountain to the west of the Faro Mine Access Road (locality 2 in Fig. 2b; Figs. 5 and 6a). Some of the oldest lower member strata in this region, <500 m south of the Vangorda fault, consist of grey to green, fine to medium-grained, feldspathic lithic arenite (Fig. 6b). Preliminary petrographic observations show evidence of angular plagioclase crystals and volcanic rock fragments that

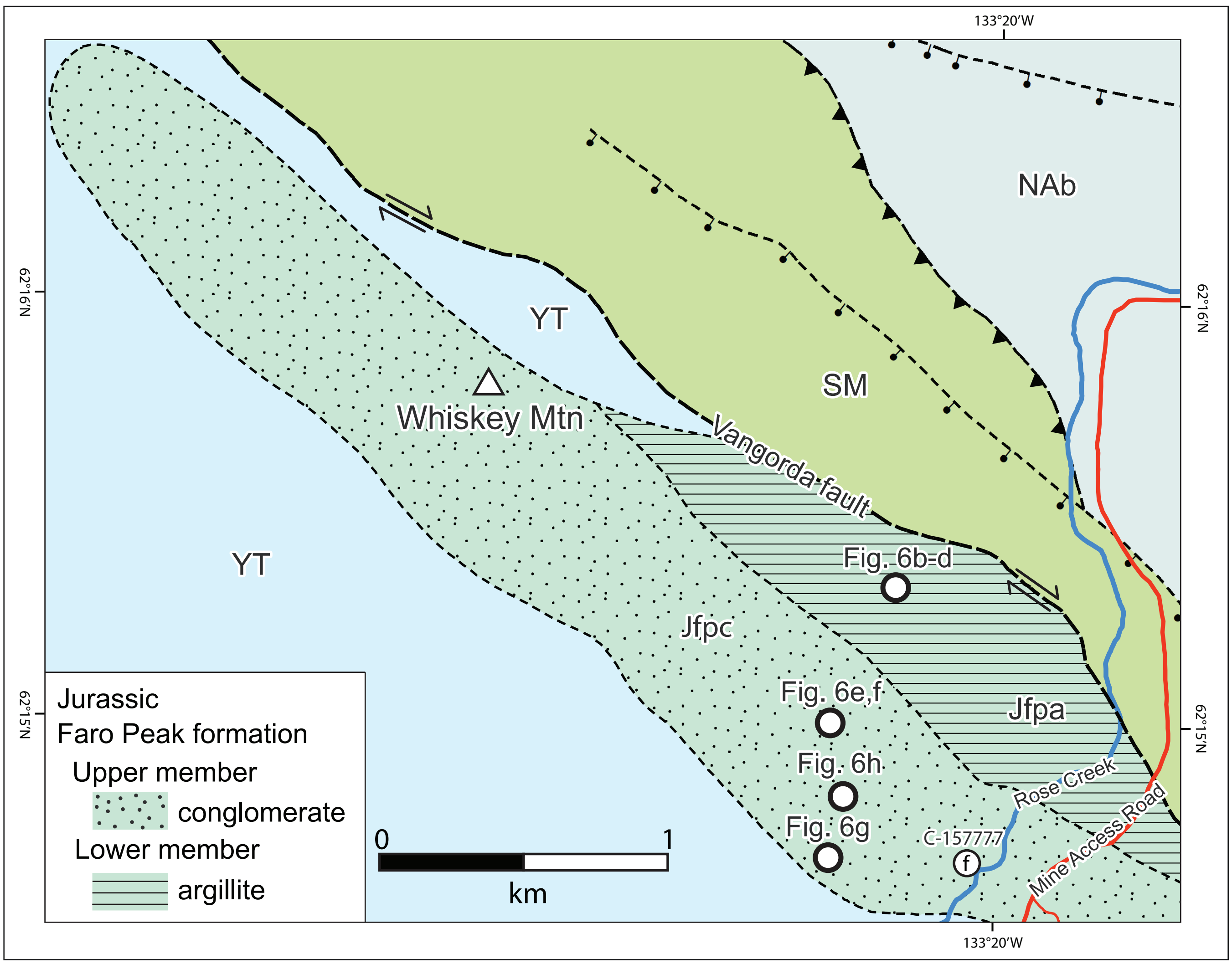

Figure 5. Simplified bedrock geology of the Whiskey Mountain area (locality 2) modified from Pigage (2004). Faro Peak formation units: Jfpc–upper member conglomerate and sandstone; Jfpa–lower member argillite, siltstone, and sandstone. Terrane abbreviations as in Fig. 2b.

suggest a proximal igneous source (Fig. 6c). Mud–sand couplets affected by isoclinal folding (Fig. 6d), interpreted in the field as convolute bedding, overlie these strata. Massive, tabular beds of coarse to very coarse grained feldspathic arenite units occur stratigraphically above the convolute beds.

The depositional contact between the lower and upper members is not well exposed in the Whiskey Mountain area. Near the cliffs along Rose Creek, immediately west of the Faro Mine Access Road, this contact may be evident where interbeds of argillite and sandstone of the lower member are overlain by sandstone and conglomerate of the upper member. More broadly, our field observations indicate that interfingered relationships may occur between some lower and upper member rock units. At other Whiskey Mountain locations, upper member rock units show both lateral and vertical fining trends, which may also indicate that sandstone layers form erosional channels within conglomerate units rather than the two having conformable, interbedded relationships. Graded bedding and channelized sandstone features are rarely observed because of vegetation and massive nature of the outcrop, but evident within some of the lower parts of the upper member at Whiskey Mountain (Fig. 6e,f). Regionally, upper member conglomerate

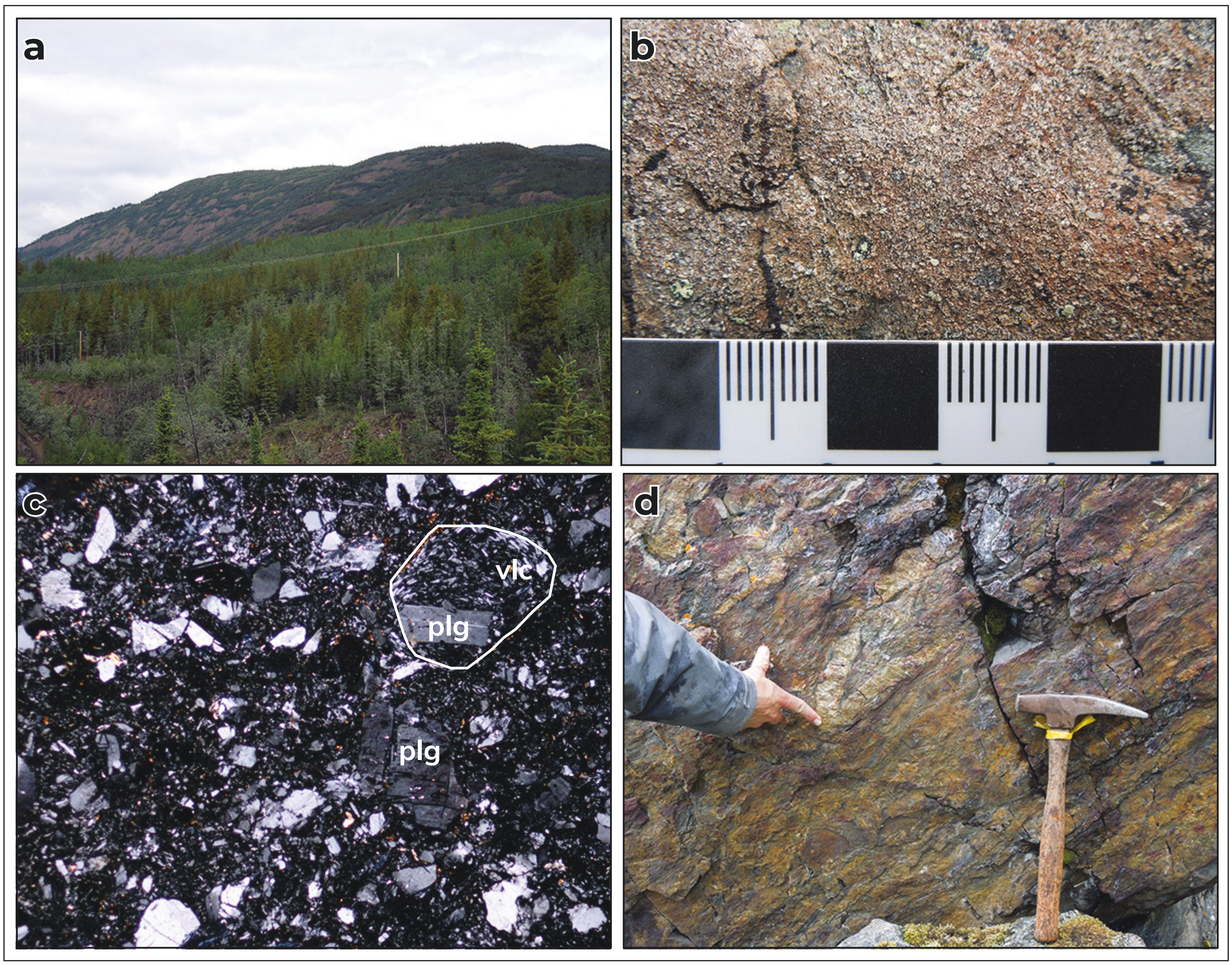

Figure 6. *Field photographs of the Whiskey Mountain area (locality 2).* ***(a)*** *North-directed view of Whiskey Mountain area and Faro Peak formation exposures from Faro townsite;* ***(b)*** *lower member feldspathic lithic arenite;* ***(c)*** *photomicrograph of lower member feldspathic lithic arenite showing angular plagioclase (plag), quartz, and volcanic lithic fragments (vlc) at 4x magnification;* ***(d)*** *isoclinal fold in convoluted beds of lower member;* ***(e)*** *through* ***(h)*** *on next page.*

units are recognized to directly overlie Snowcap assemblage basement (Pigage, 2004), suggesting that the lower member was completely removed by erosion in some areas.

Upper member units in the Whiskey Mountain area generally consist of massive, brown weathering, granule to boulder, clast-supported, polymictic conglomerate and interbedded micaceous feldspathic lithic arenite (Fig. 6g). The dominant clast types are micaceous quartzite, mica schist, chert, and limestone with Carnian conodont elements (C-157777; Pigage, 2004). Some of the micaceous quartzite and mica schist clasts are up to 50 cm in size, suggesting local derivation from the underlying Snowcap assemblage. Other clast types include basalt, argillite, vein quartz, quartz-feldspar porphyry, hornblende granodiorite, and augite-phyric basalt (Fig. 6h). Upper member sandstone adjacent to the Carnian fossil collection at Whiskey Mountain correspondingly shows a mixture of detrital zircon U-Pb ages that indicate recycled Precambrian contributions from Snowcap assemblage quartzite and schist and Late Triassic–Early Jurassic contributions presumably from igneous sources (Colpron et al., 2015).

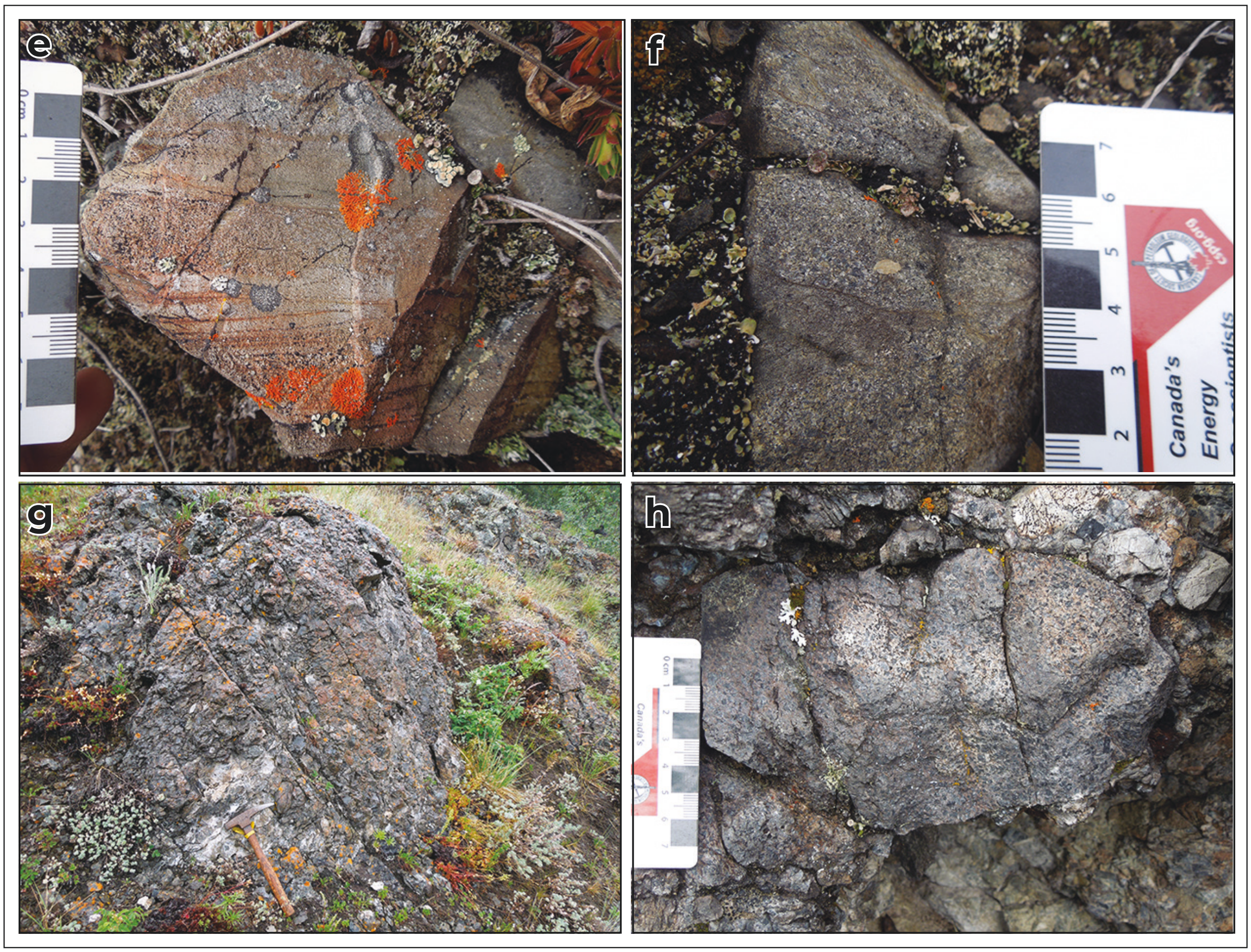

***Figure 6** continued. **(e)** graded bedding in upper member sandstone; **(f)** channelized sandstone lens in upper member conglomerate; **(g)** upper member clast-supported conglomerate; and **(h)** upper member augite-phyric basalt clast.*

Locality 3–Repeater Hill

Lower and upper member exposures of the Faro Peak formation crop out along the access road and flanks of the informally named Repeater Hill (site of the NorthwesTel repeater), ~2.5 km northeast of the Faro townsite (locality 3 in Fig. 2b; Fig. 7). The contact between lower and upper members is observed along the southeastern flank of Repeater Hill where dark grey, fine to medium-grained micaceous sandstone interfingers with, or pinches out, into matrix-supported conglomerate with pebble-sized clasts of schist, chert, argillite, micaceous quartzite, and limestone (Fig. 8a–c). This section reappears on the west side of Repeater Hill and may be analogous to the interfingered relationships observed in the adjacent Whiskey Mountain area. Grey limestone to silty limestone subcrop exposures at the top of Repeater Hill (Fig. 8d) contain early Carnian conodont elements (C-304121; Pigage, 2004) and have unclear contact relationships with upper member conglomerate.

Upper member rock units that are exposed along Repeater Road are dominated by massive, brown to grey weathering, matrix to clast-supported, pebble to cobble conglomerate (Fig. 8e) and lithic feldspathic arenite (Fig. 8f). Most clast types along the road consist of quartzite, mica schist (Fig. 8g), limestone, and chert; clasts of quartz-feldspar porphyry and other igneous rocks were observed along southwestern flank of Repeater Hill.

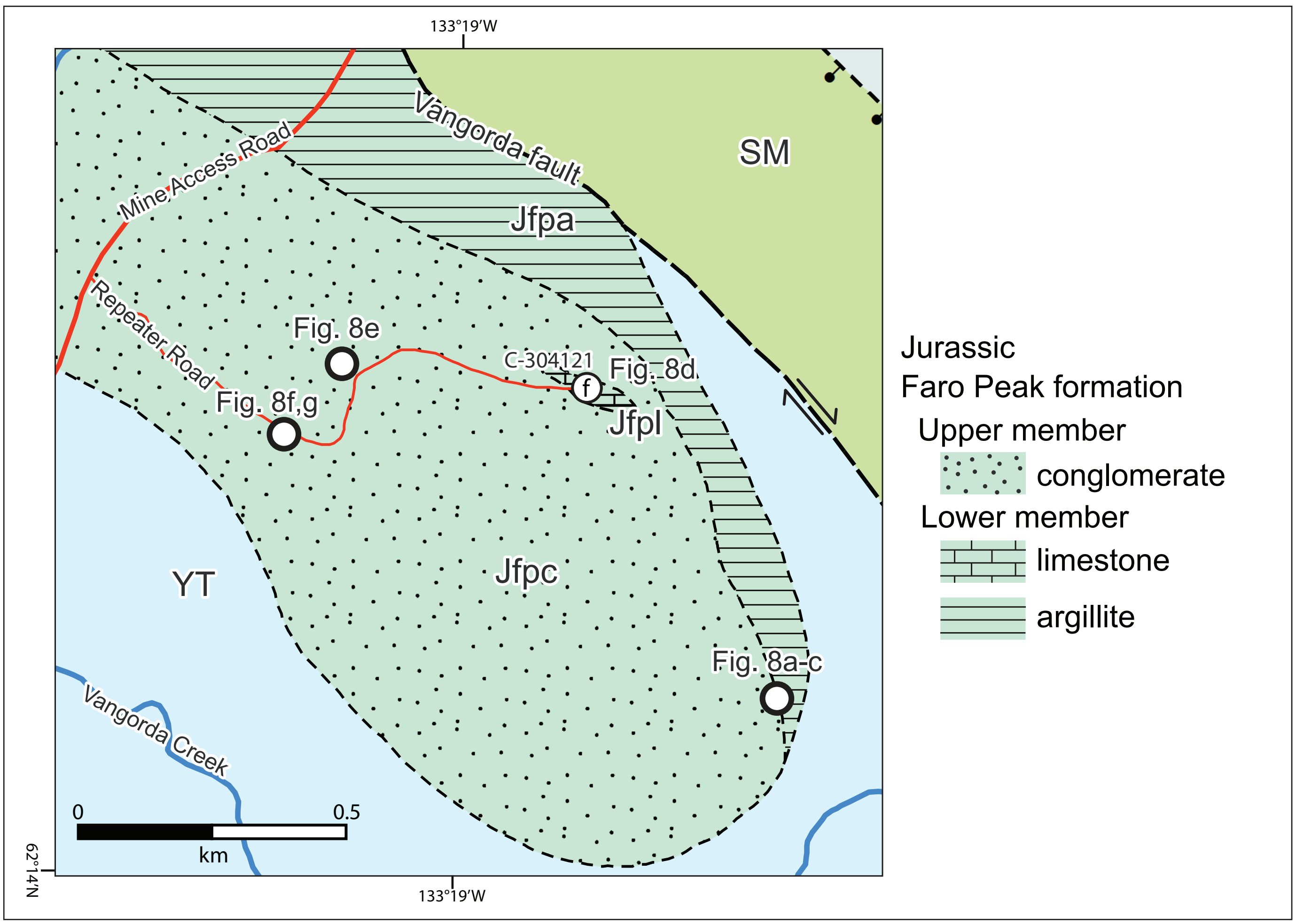

Figure 7. Simplified bedrock geology map of the Repeater Hill area (locality 3) modified from Pigage (2004). Faro Peak formation units: Jfpc–upper member conglomerate and sandstone; Jfpl–lower member limestone; Jfpa–lower member argillite, chert, siltstone, and sandstone. Terrane abbreviations as in Fig. 2b.

*Figure 8. Field photographs Repeater Hill area (locality 3). **(a)** Contact between lower and upper members along southeastern flank of Repeater Hill; **(b)** upper member basal conglomerate; **(c)** top of lower member argillite unit; **(d)** lower member limestone to silty limestone near repeater; **(e)** upper member matrix to clast-supported conglomerate on Repeater Road; **(f)** and **(g)** on next page.*

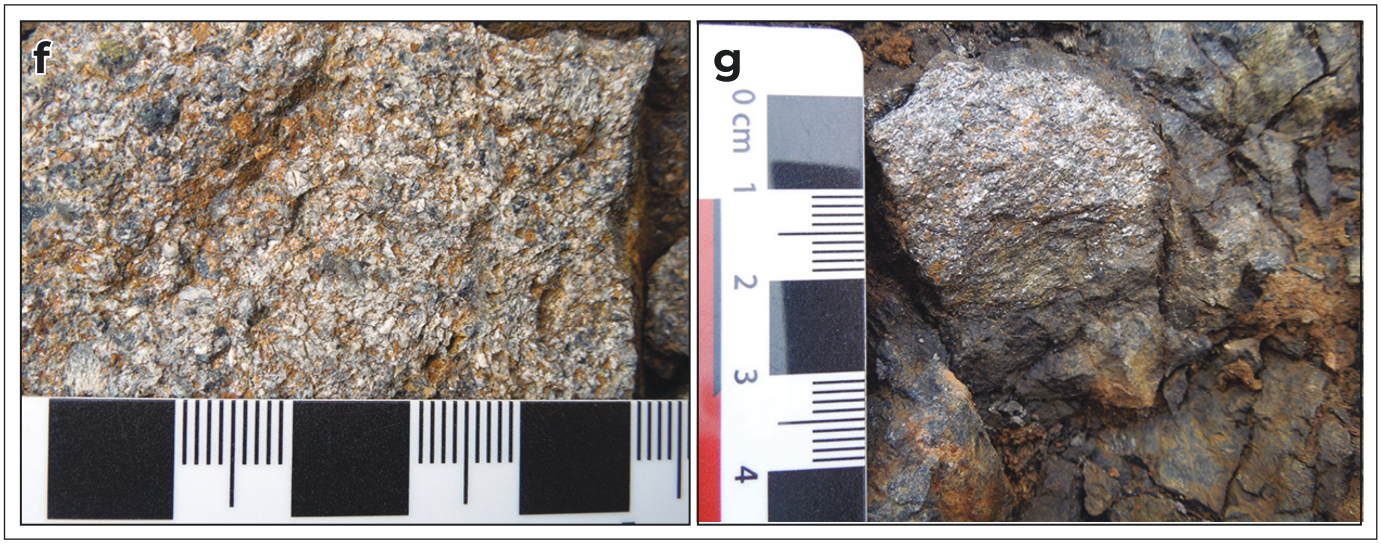

***Figure 8** continued. **(f)** upper member lithic feldspathic sandstone; and **(g)** upper member mica schist clast.*

Locality 4–Blind Creek Road and Dena Cho Trail

Upper member strata were accessed by foot traverse along the Blind Creek Road and western end of the Deno Cho Trail ~11 km east of Faro (locality 4 in Fig. 2b; Fig. 9). Near Blind Creek, Faro Peak formation outcrops mostly consist of massive, matrix to clast-supported, granule to pebble conglomerate units with quartzite, schist, chert, limestone, and minor felsic igneous and basalt clasts that resemble other upper member exposures across the southern Tay River map area (Fig. 10a–c). Sandstone matrix from a Blind Creek conglomerate layer with late Carnian limestone clasts (C-103825; Pigage, 2004) yielded Late Triassic–Early Jurassic and older detrital zircon populations that suggest mixed Mesozoic igneous and Snowcap assemblage provenance (Colpron et al., 2015).

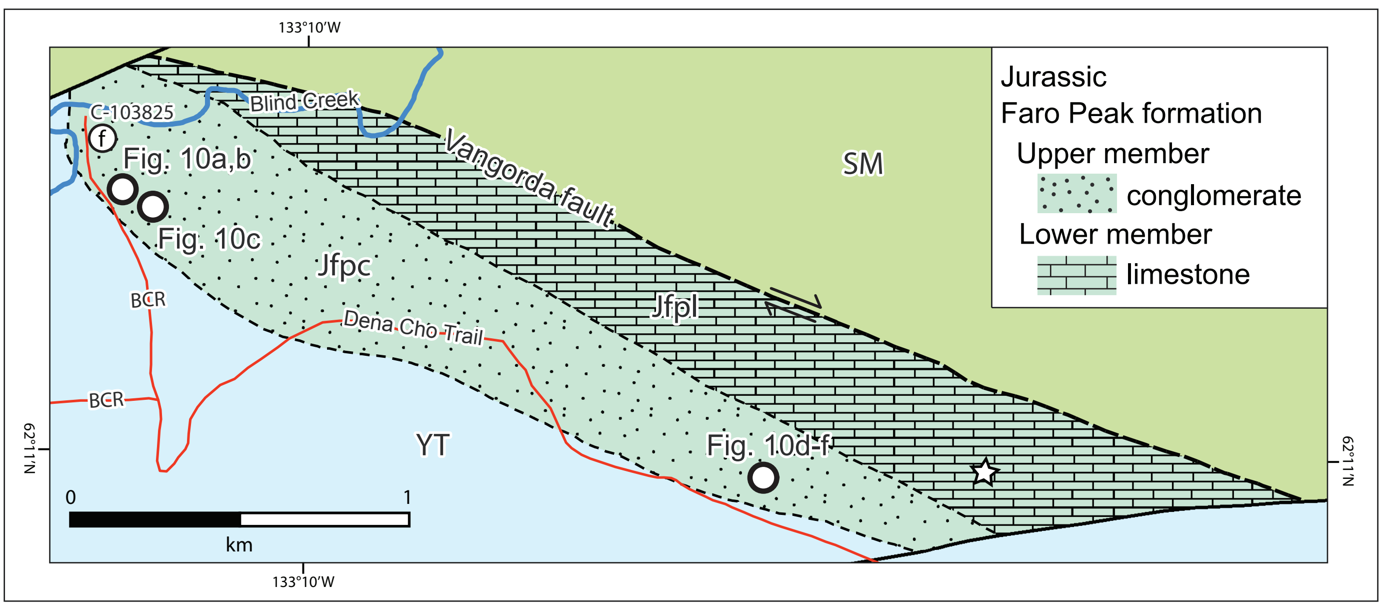

***Figure 9.** Simplified bedrock geology of the Blind Creek Road and western Dena Cho Trail areas (locality 4). Star denotes location of chloritized basalt outcrop with possible Slide Mountain terrane (Campbell Range formation) affinities. Faro Peak formation units: Jfpc–upper member conglomerate and sandstone; Jfpl–lower member limestone. BCR–Blind Creek Road. Terrane abbreviations as in Fig. 2b.*

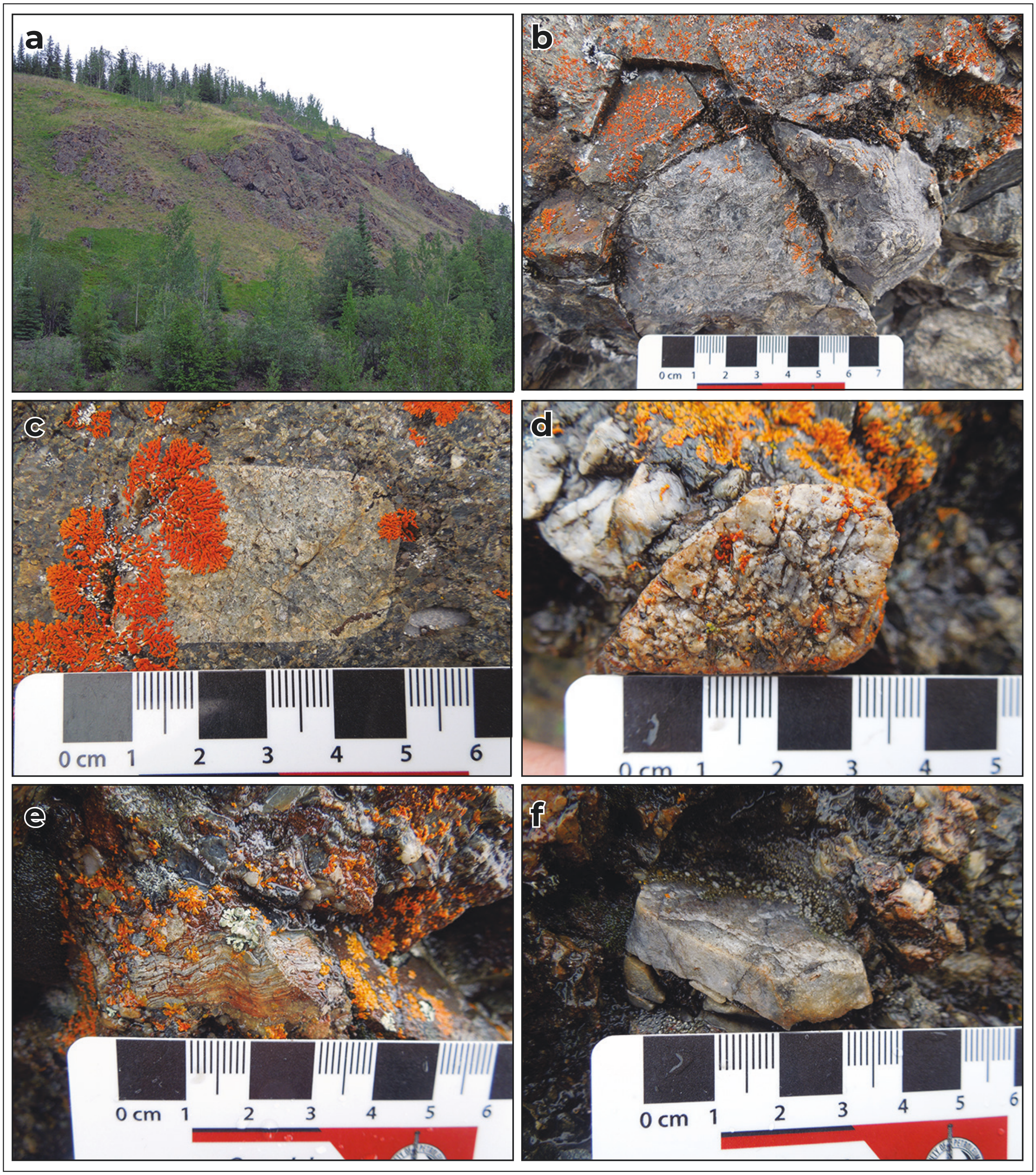

Figure 10. *Field photographs of Blind Creek Road and western Dena Cho Trail areas (locality 4).* ***(a)*** *Northeast-directed view of upper member conglomerate outcrops east of Blind Creek;* ***(b)*** *upper member limestone clast;* ***(c)*** *upper member quartz porphyry clast;* ***(d)*** *upper member felsic intrusive clast;* ***(e)*** *upper member bedded chert clast; and* ***(f)*** *upper member quartzite clast.*

Rounded and discontinuous exposures of the upper member occur along the Dena Cho Trail to the southeast of Blind Creek (Fig. 9) and generally comprise pebble to cobble conglomerate with interlayers of coarse-grained to pebbly sandstone. Clasts consist of quartzite, bedded chert, limestone, and schist with minor amounts of quartz-feldspar porphyry and felsic intrusive rocks (Fig. 10d–f). At one location along the Dena Cho Trail, a brown weathering outcrop assigned to the Faro Peak formation consists of chloritized basalt that resembles the adjacent Campbell Range formation (see Fig. 9). This outcrop is either an unmapped basalt unit within the Faro Peak formation or represents an outlier or fault sliver of Slide Mountain terrane.

Preliminary Conclusions and Future Research

The Faro Peak formation is characterized by an upper member of massive, disorganized conglomerate and sandstone units and a lower member of argillite, siltstone, and sandstone units that contain massive to graded to convolute bedding features. The depositional setting and emplacement mechanisms of these Faro Peak formation facies are the topics of current research and will continue to be a focus during the second field season in summer 2019. Tempelman-Kluit (1972) interpreted the massive and coarse-grained nature of the upper member conglomerate to indicate deposition adjacent to a fault scarp complex, presumably linked to displacement along the Vangorda fault or its predecessor. The lower member contains feldspathic and volcanic lithic sandstone strata, which further implies proximity to a mafic-intermediate igneous source. Our working hypothesis calls for massive clast to matrix-supported conglomerate and sandstone units of the upper member to represent non-turbulent, concentrated debris or density flow deposits that most likely accumulated in a subaqueous environment. Stratigraphic features in some lower member units include disorganized sand, organized sand–mud couplets, and graded bedding, which are generally consistent with concentrated density flow or turbidity current deposition.

The abundance of coarse-grained (up to boulder-sized) rock fragments in the upper member, including those derived from Yukon-Tanana basement, suggests that Faro Peak formation deposition was coincident with regional exhumation and tectonic erosion. For example, Knight *et al.* (2013) concluded that Early Jurassic extension along the Willow Lake fault of central Yukon resulted in the exhumation of Yukon-Tanana basement rocks from mid-crustal depths during the time of Faro Peak formation deposition. The recent plate tectonic model for the Whitehorse trough by Colpron *et al.* (2015) is broadly compatible with a strike-slip/transtensional setting for the Faro Peak basin along the Intermontane belt–ancient North American margin boundary. It follows that crustal-scale faults in the Faro region could have accommodated regional exhumation of Yukon-Tanana basement and adjacent Slide Mountain terrane. Although the Faro Peak formation was deposited along a convergent margin, we are investigating transtensional origins for the Faro Peak basin, including modern analogues in southern California (e.g., Ridge basin; Link, 2003) and Jamaica (e.g., Wagwater basin; Wescott and Etheridge, 1983).

Faro Peak formation rock units were sampled for petrographic and detrital zircon U-Pb-Hf studies at more than 20 locations during summer 2018. Petrographic data will constrain the framework composition of lower and upper member strata and document lateral or vertical changes in provenance. The youngest population of detrital zircon U-Pb ages will be used to constrain the maximum depositional age of lower and upper member rock units (e.g., Dickinson and Gehrels, 2009), whereas combined U-Pb-Hf data will identify specific provenance areas and regional crustal evolution of the Intermontane terranes. These results will be integrated with existing (Colpron *et al.*, 2015) and forthcoming (e.g., van Drecht and Beranek, 2017) detrital zircon U-Pb(± Hf) data from Lower to Middle Jurassic strata of the Whitehorse trough and Lower Jurassic foreland basin strata in the southern Canadian Rockies (Pană *et al.*, 2018) to better constrain Cordilleran tectonic evolution.

Field studies in summer 2019 will focus on the northwestern and southeastern extents of the Faro Peak formation in the southern Tay River map area.

Near Rose Mountain, we will investigate the contact relationships and stratigraphic architecture of lower member units that include basalt, chert, and mafic greywacke adjacent to the Vangorda fault (Fig. 3). The goal of this research is to ascertain if the lower Faro Peak formation in this location: (1) represents a Permian overlap assemblage between Yukon-Tanana and Slide Mountain terranes; (2) represents a fault sliver of Slide Mountain terrane (Campbell Range formation); or (3) represents a Late Triassic–Early Jurassic succession of basalt and related sedimentary rocks assigned to Yukon-Tanana terrane. Three isolated occurrences of Faro Peak formation occur in proximity to the Deno Cho Trail ~25, 30, and 45 km to the southeast of Faro (Fig. 2b), respectively, and include chert, mafic greywacke, and other rock units that may be similar to lower member strata near Rose Mountain. Field studies of these Faro Peak formation strata will therefore provide information about the timing and nature of stratigraphic units along the length of the Vangorda fault and their significance to understanding the Yukon-Tanana–Slide Mountain terrane boundary.

Acknowledgements

This is a product of the Geo-mapping for Energy and Minerals (GEM) program at Natural Resources Canada. The Yukon Geological Survey supported field logistics and helicopter transport to alpine exposures. Maurice Colpron provided helpful field discussions about Yukon-Tanana rock units and regional geology. Reviewer Lee Pigage provided thoughtful and constructive comments that improved this manuscript.

References

Beranek, L.P., 2009. Provenance and paleotectonic setting of North American Triassic strata in Yukon: the sedimentary record of pericratonic terrane accretion in the northern Canadian Cordillera. Unpublished PhD thesis, University of British Columbia, British Columbia, Canada, 324 p.

Colpron, M., Crowley, J.L., Gehrels, G.E., Long, D.G.F., Murphy, D.C., Beranek, L.P. and Bickerton, L., 2015. Birth of the northern Cordilleran orogen, as recorded by detrital zircons in Jurassic synorogenic strata and regional exhumation in Yukon. Lithosphere, vol. 7, p. 541–562.

Colpron, M., Nelson, J.L. and Murphy, D.C., 2006. A tectonostratigraphic framework for the pericratonic terranes of the northern Canadian Cordillera. *In*: Paleozoic Evolution and Metallogeny of Pericratonic Terranes at the Ancient Pacific Margin of North America, Canadian and Alaskan Cordillera, M. Colpron and J.L. Nelson (eds.), Geological Association of Canada Special Paper 45, p. 1–23.

Dickie, J.R. and Hein, F.J., 1995. Conglomeratic fan deltas and submarine fans of the Jurassic Laberge Group, Whitehorse Trough, Yukon Territory, Canada: fore-arc sedimentation and unroofing of a volcanic island arc complex. Sedimentary Geology, vol. 98, p. 263–282.

Dickinson, W.R. and Gehrels, G.E., 2009. Use of U-Pb ages of detrital zircons to infer maximum depositional ages of strata: A test against a Colorado Plateau Mesozoic database. Earth and Planetary Science Letters, vol. 288, p. 115–125.

Evenchick, C.A., McMechan, M.E., McNicoll, V.J. and Carr, S.D., 2007. A synthesis of the Jurassic-Cretaceous tectonic evolution of the central and southeastern Canadian Cordillera: Exploring links across the orogeny. *In*: Whence the Mountains? Inquiries into the Evolution of Orogenic Systems: A Volume in Honor of Raymond A. Price, J.W. Sears, T.A. Harms, and C.A. Evenchick (eds.), Geological Society of America Special Paper 433, p. 117–145.

Hart, C.J.R., Dickie, J.R., Ghosh, D.K. and Armstrong, R.L., 1995. Provenance constraints for Whitehorse Trough conglomerate: U-Pb zircon dates and initial Sr ratios of granitic clasts in Jurassic Laberge Group, Yukon Territory. *In*: Jurassic Magmatism and Tectonics of the North American Cordillera, D.M Miller and C. Busby (eds.), Geological Society of America Special Paper 299, p. 47–63.

Johnston, S.T., Mortensen, J.K. and Erdmer, P., 1996. Igneous and metaigneous age constraints for the Aishihik metamorphic suite, southwest Yukon. Canadian Journal of Earth Sciences, vol. 33, p. 1543–1555.

Knight, E., Schneider, D.A. and Ryan, J.J., 2013. Thermochronology of the Yukon-Tanana terrane, west-central Yukon: Evidence for Jurassic extension and exhumation in the northern Canadian Cordillera. Journal of Geology, vol. 121, p. 371–400.

Link, M.H., 2003. Depositional systems and sedimentary facies of the Miocene-Pliocene Ridge basin, southern California. *In*: Evolution of Ridge basin, southern California: An interplay of sedimentation and tectonics, J.C. Crowell (ed.), Geological Society of America Special Paper 367, p. 17–87.

Mihalynuk, M.G., Nelson, J.A. and Diakow, L.J., 1994. Cache Creek terrane entrapment: Oroclinal paradox within the Canadian Cordillera. Tectonics, vol. 13, p. 575–595.

Murphy, D.C., Mortensen, J.K., Piercey, S.J., Orchard, M.J. and Gehrels, G.E., 2006. Mid-Paleozoic to early Mesozoic tectonostratigraphic evolution of the Yukon-Tanana and Slide Mountain terranes and affiliated overlap assemblages, Finlayson Lake massive sulphide district, southeastern Yukon. *In*: Paleozoic Evolution and Metallogeny of Pericratonic Terranes at the Ancient Pacific Margin of North America, Canadian and Alaskan Cordillera, M. Colpron and J.L. Nelson (eds.), Geological Association of Canada Special Paper 45, p. 75–105.

Nelson, J.L., Colpron, M. and Israel, S. 2013. The Cordillera of British Columbia, Yukon, and Alaska: Tectonics and Metallogeny. *In*: Tectonics, Metallogeny and Discovery: The North American Cordillera and Similar Accretionary Settings, M. Colpron, T. Bissig, B.G. Rusk and J.F.H. Thompson (eds.), Society of Economic Geologists, Special Publication 17, p. 53–109.

Pană, D.I., Poulton, T.P. and DuFrane, S.A., 2018 (*in press*). U-Pb detrital zircon dating supports Early Jurassic initiation of the Cordilleran foreland basin in southwestern Canada. Geological Society of America Bulletin, doi:10.1130/B31862.1.

Pigage, L.C., 2004. Bedrock geology compilation of the Anvil District (parts of NTS 105K/2, 3, 5, 6, 7, and 11), central Yukon. Yukon Geological Survey, Bulletin 15, 103 p.

Tempelman-Kluit, D.J., 1972. Geology and origin of the Faro, Vangorda, and Swim concordant zinc-lead deposits, central Yukon Territory. Geological Survey of Canada, Bulletin 208, 73 p.

Tempelman-Kluit, D.J., 1979. Five occurrences of transported synorogenic clastic rocks in Yukon Territory. Geological Survey of Canada, Paper 79-1A, p. 1–12.

Tempelman-Kluit, D.J., 1984. Geology, Laberge (105E) and Carmacks (115I), Yukon Territory. Geological Survey of Canada, Open File 1101, 10 p.

van Drecht, L.H. and Beranek, L.P., 2017. Jurassic stratigraphy and tectonic evolution of the Whitehorse trough, central Yukon: new insights from laser ablation split stream (LASS) detrital zircon U-Pb geochronology and Hf isotope geochemistry. Geological Society of America, Abstracts with Programs, vol. 49, no. 6.

van Drecht, L.H. and Beranek, L.P., 2018. New investigations of basal Laberge Group stratigraphy, Whitehorse trough, central Yukon. *In*: Yukon Exploration and Geology 2017, K.E. MacFarlane (ed.), Yukon Geological Survey, p. 151–163.

Wescott, W.A. and Ethridge, F.G., 1983. Eocene fan delta/submarine fan deposition in the Wagwater Trough, east-central Jamaica. Sedimentology, vol. 30, p. 235–247.

Yukon Geological Survey, 2018. Yukon Digital Bedrock Geology. Yukon Geological Survey, http://www.geology.gov.yk.ca/update_yukon_bedrock_geology_map.html [accessed November, 2018].

APPENDIX 1.A.2

Upper Triassic to Lower Jurassic stratigraphy of the Faro Peak formation, southern Tay River map area, central Yukon (NTS 105K)

A.C. Wiest, L.P. Beranek* and M.J. Manor
Department of Earth Sciences, Memorial University of Newfoundland

Wiest, A.C., Beranek, L.P. and Manor, M.J., 2020. Upper Triassic to Lower Jurassic stratigraphy of the Faro Peak formation, southern Tay River map area, central Yukon (NTS 105K). *In:* Yukon Exploration and Geology 2019, K.E. MacFarlane (ed.), Yukon Geological Survey, p. 121–139.

Abstract

The lower and upper members of the Faro Peak formation comprise Upper Triassic and Lower Jurassic successions, respectively, that are assigned to the Yukon-Tanana terrane in the southern Tay River map area (NTS 105K). The lower member is ~650 m-thick and contains a basal conglomerate overlain by argillite, limestone, basalt, and lithic feldspathic wacke to arenite that represents part of an overlap assemblage and regionally covers Paleozoic rocks of the Yukon-Tanana terrane, Slide Mountain terrane, and ancestral Cordilleran margin. The upper member has >800 m of massive conglomerate and sandstone that overlies different stratigraphic levels of the lower member and locally sits on Yukon-Tanana basement. The upper member is coeval with Whitehorse trough strata of central Yukon and similarly records Early Jurassic exhumation of the northern Intermontane terranes. The two members are lithologically distinct, of mappable extent, and have unconformable contacts, and therefore should be separated into two new formations.

* lberanek@mun.ca

Introduction

The late Permian to Early Jurassic was a time of significant change along the northwestern margin of North America. The deposition of multiple syn to post-orogenic sedimentary successions from eastern Alaska to northern British Columbia (Fig. 1; Mihalynuk et *al.*, 1994; Beranek and Mortensen, 2011; Colpron et *al.*, 2015; Golding et *al.*, 2016) was related to arc accretion, outward stepping of the continental margin, new arc development, and crustal thickening and exhumation of the Intermontane terranes (*e.g.*, Yukon-Tanana, Slide Mountain, Stikinia, Quesnellia, Cache Creek). Middle to Upper Triassic overlap assemblages were deposited across the Yukon-Tanana and Slide Mountain terranes and former Cordilleran margin after late Permian closure of a marginal ocean basin (Beranek and Mortensen, 2011). Yukon-Tanana terrane basement rocks were locally metamorphosed to eclogite facies during this ocean closure and contain late Permian white mica cooling ages in the Faro area of central Yukon (Erdmer et *al.*, 1998). Subsequent Late Triassic to Early Jurassic arc collision and intra-arc shortening along the composite margin resulted in regional crustal thickening and burial of Stikinia and Yukon-Tanana basement to mid-crustal depths (Johnston et *al.* 1996; Topham et *al.*, 2016; Clark, 2017). This crustal thickening in central Yukon was followed by ~15-20 km of tectonic exhumation (Knight et *al.*, 2013) and resulted in Sinemurian and later deposition of Laberge Group strata in the Whitehorse trough (Fig. 1; Colpron et *al.*, 2015; Staples et *al.*, 2016). Dusel-Bacon et *al.* (2002) similarly documented Early Jurassic exhumation in the Yukon-Tanana terrane of eastern Alaska after regional crustal thickening. Constraining the timing and depositional setting of Late Triassic to Early Jurassic basin-filling events is critical to investigate these existing models and further constrain the tectonic evolution and growth of the Canadian Cordillera.

Isolated exposures of Upper Triassic to Lower Jurassic rocks assigned to the Faro Peak formation by Pigage (2004) crop out along the Yukon-Tanana–Slide Mountain terrane boundary near the town of Faro (Fig. 2a,b) in the southern Tay River map area (NTS 105K). Colpron et *al.* (2015) reported 200–180 Ma detrital zircon grains in conglomerate units of the Faro Peak formation and correlated these rock units with synorogenic strata of the Laberge Group in central Yukon and northern British Columbia. A two-year project was initiated in 2018 to test these hypotheses (Wiest and Beranek, 2019) and investigate the depositional age, regional correlation, and tectonic setting of the Faro Peak formation.

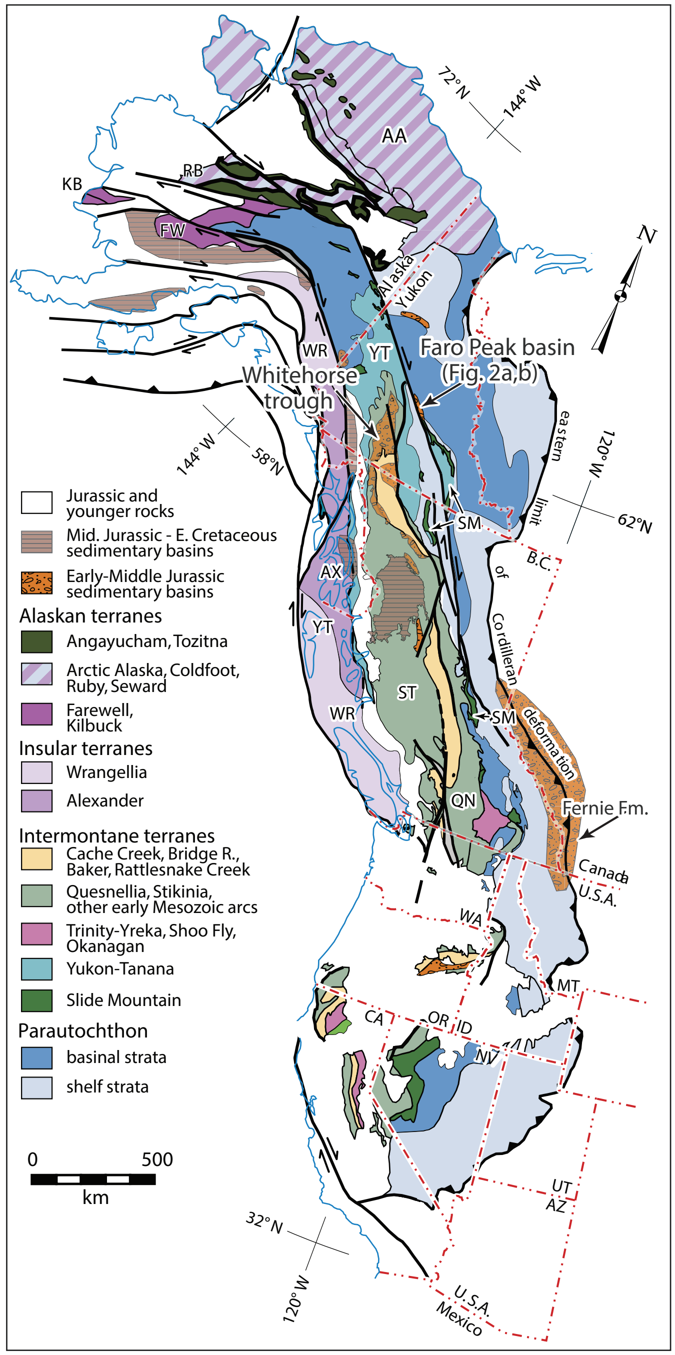

Figure 1. *Paleozoic to early Mesozoic terrane map of the North American Cordillera and associated Jurassic basins modified from Colpron et al. (2015). Terrane abbreviations: AA–Arctic Alaska; AX–Alexander; FW–Farewell; KB–Kilbuck; QN–Quesnellia; RB–Ruby; SM–Slide Mountain; ST–Stikinia; YT–Yukon-Tanana.*

In this article, we summarize our 2019 field studies and current understanding of the Faro Peak formation as originally defined by Pigage (2004). The internal character of the lower member of the Faro Peak formation is documented in a new stratigraphic section west of Rose Mountain. The contact between the upper and lower members of the Faro Peak formation appears to be transitional in at least two localities. The observation that upper member conglomerate overlies multiple units of the lower member and quartzite and schist units of the Yukon-Tanana terrane suggests, however, that the base of the upper member is an unconformity. Finally, we speculate on the basis of lithological differences and unconformable contacts that some or all rocks previously included in the lower Faro Peak formation should be re-assigned to a new formation. It is currently uncertain if all lower member units of Pigage (2004) should be included in this new formation. Ongoing detrital zircon U-Pb-Hf isotope and petrographic investigations of Faro Peak formation rock units will assist in future stratigraphic correlations and help guide a new formation designation.

Geological background

The town of Faro is located at the eastern edge of the Intermontane belt near the suture between the Yukon-Tanana and Slide Mountain terranes (Fig. 2a,b). In this area, the Intermontane terranes are separated from parautochthonous North American continental margin strata along the Inconnu thrust to the northeast and Cassiar terrane along the Tintina fault to the southwest (Fig. 2a,b; Pigage, 2004). Dextral movement along the Tintina fault accommodated at least 430 km of

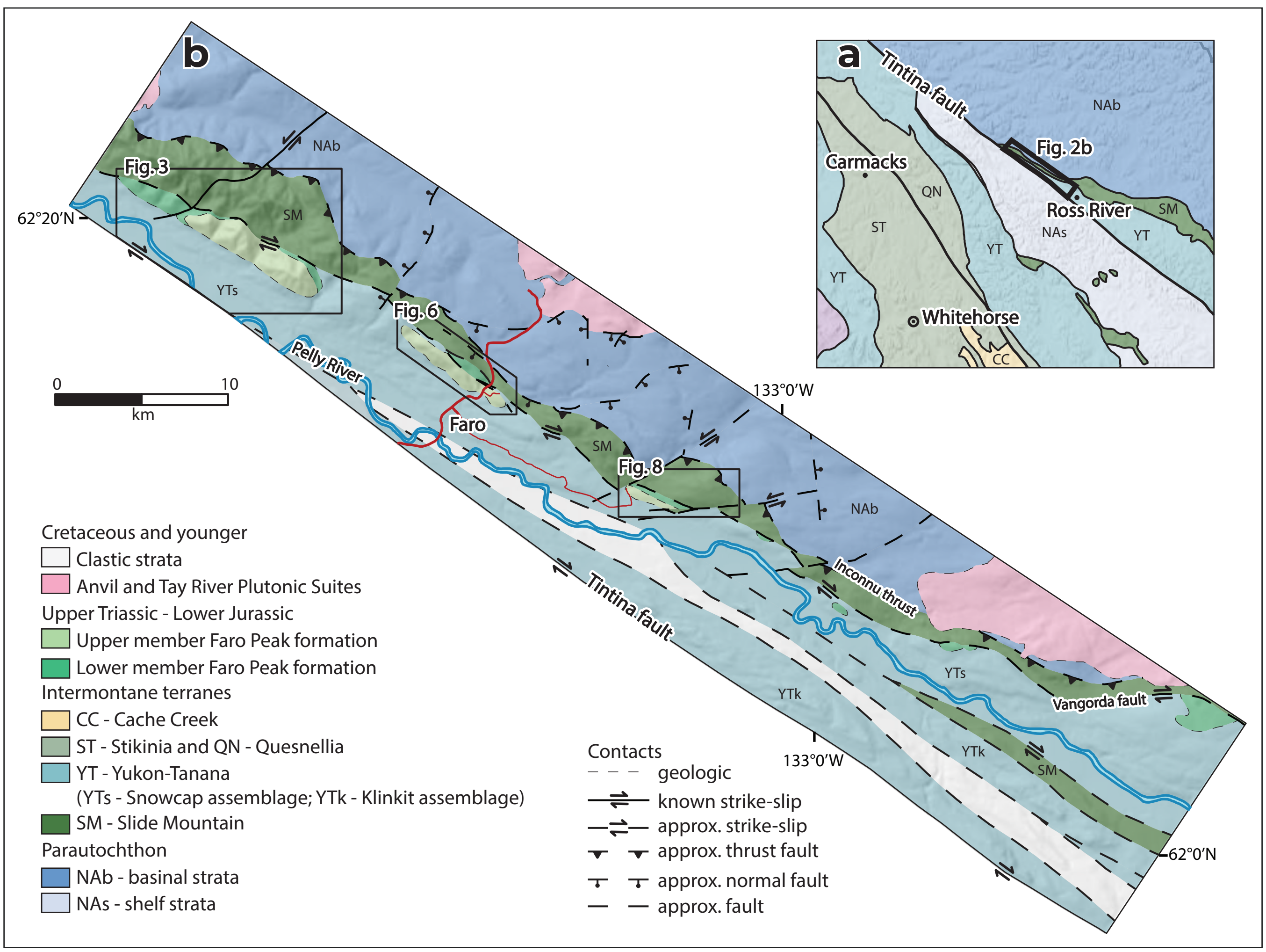

Figure 2. (a) *Terrane map of central Yukon modified from Yukon Geological Survey (2019).* **(b)** *Simplified bedrock geology of the southern Tay River map area modified from Pigage (2004).*

post-Cretaceous displacement (Gabrielse et *al.*, 2006). Restoration of the Tintina fault places Faro near the present day region of Eagle, Alaska. In the Faro area, the Yukon-Tanana and Slide Mountain terranes are separated by the Vangorda fault (Fig. 2b), a northern equivalent to the Jules Creek fault in the Finlayson Lake map area (Murphy et *al.*, 2006).

The Faro Peak formation crops out along a northwest-trending belt that parallels the Tintina Trench near Faro. Faro Peak formation strata were first described by Tempelman-Kluit (1972, 1979) as argillaceous limestone, silty slate, and polymictic conglomerate that unconformably overlies quartzite, schist, and other metasedimentary rocks of what is now called the Snowcap assemblage (*e.g.* Colpron et *al.*, 2006) of the Yukon-Tanana terrane. Pigage (2004) informally named the Faro Peak formation and defined a lower member of basal basalt overlain by interbedded argillite, chert, greywacke, limestone, and conglomerate, and an upper member of massive, polymictic conglomerate. Wiest and Beranek (2019) documented that these lower and upper member units were deposited in contrasting environments. Lower member units ~3 km northeast of the Faro township exhibit normally graded, tabular, and convolute bedding characteristics that are generally consistent with deposition by turbulent, concentrated density flows. Petrographic results indicate that some lower member sandstone units have mafic to intermediate volcanic provenance (Wiest and Beranek, 2019). Massive, upper member conglomerate and channelized sandstone units from Faro Peak and adjacent ridges are consistent with deposition by non-concentrated debris flows. Typical clasts in the upper member conglomerate units include schist, quartzite, chert, and mafic to felsic intrusive rocks, which suggests that the upper Faro Peak formation has provenance from Intermontane terrane basement assemblages and may be linked to depositional events along the Vangorda fault or its predecessor (*c.f.* Tempelman-Kluit, 1972).

2019 field observations

Lower member of the Faro Peak formation

Rose Mountain

The lower member of the Faro Peak formation near Rose Mountain, ~20 km northwest of Faro, is ~650 m-thick and generally undeformed (Figs. 3 and 4). Lower member units at this location unconformably overlie micaceous quartzite and schist of the Snowcap assemblage (Fig. 5a). The basal unconformity is defined by well-silicified, pebble to cobble conglomerate that contains clasts of schist, quartzite, black to grey chert, and tan volcanic rocks (Fig. 5b). This basal conglomerate is overlain by interbedded graphitic to calcareous shale and tan weathering, dark grey micrite (Fig. 5c). Limestone from this succession yields Late Triassic conodont elements (Late Norian to Rhaetian *M. ex gr. Polygnathiformis*, Late Carnian *Epigondolella cf. mosheri* and *Norigondolella steinbergensis*; Pigage, 2004; Orchard, 2006). Conformably above this limestone is an ~4 m-thick exposure of grey basalt and green lithic feldspathic wacke units that become sheared upsection (Fig. 5d,e). Shearing at this locality is interpreted to be intraformational bedding plane movement that occurred along the resistant basalt-wacke contact (cf., Tempelman-Kluit, 1979). Poorly exposed argillaceous to silty micrite beds that show cross-stratification overlie this sheared section (Fig. 5f). Along strike ~1 to 2 km to the southeast, limestone units are mapped as being interbedded with basalt and wacke units (Jennings et *al.*, 1978; Pigage, 2004). Exposures above the cross-stratified limestone units are rare. Small outcrop of thinly laminated, dark grey micrite and micaceous siltstone were observed directly against the Vangorda fault, which separates the lower member from foliated serpentinite and gabbro of the Slide Mountain terrane (Fig. 3).

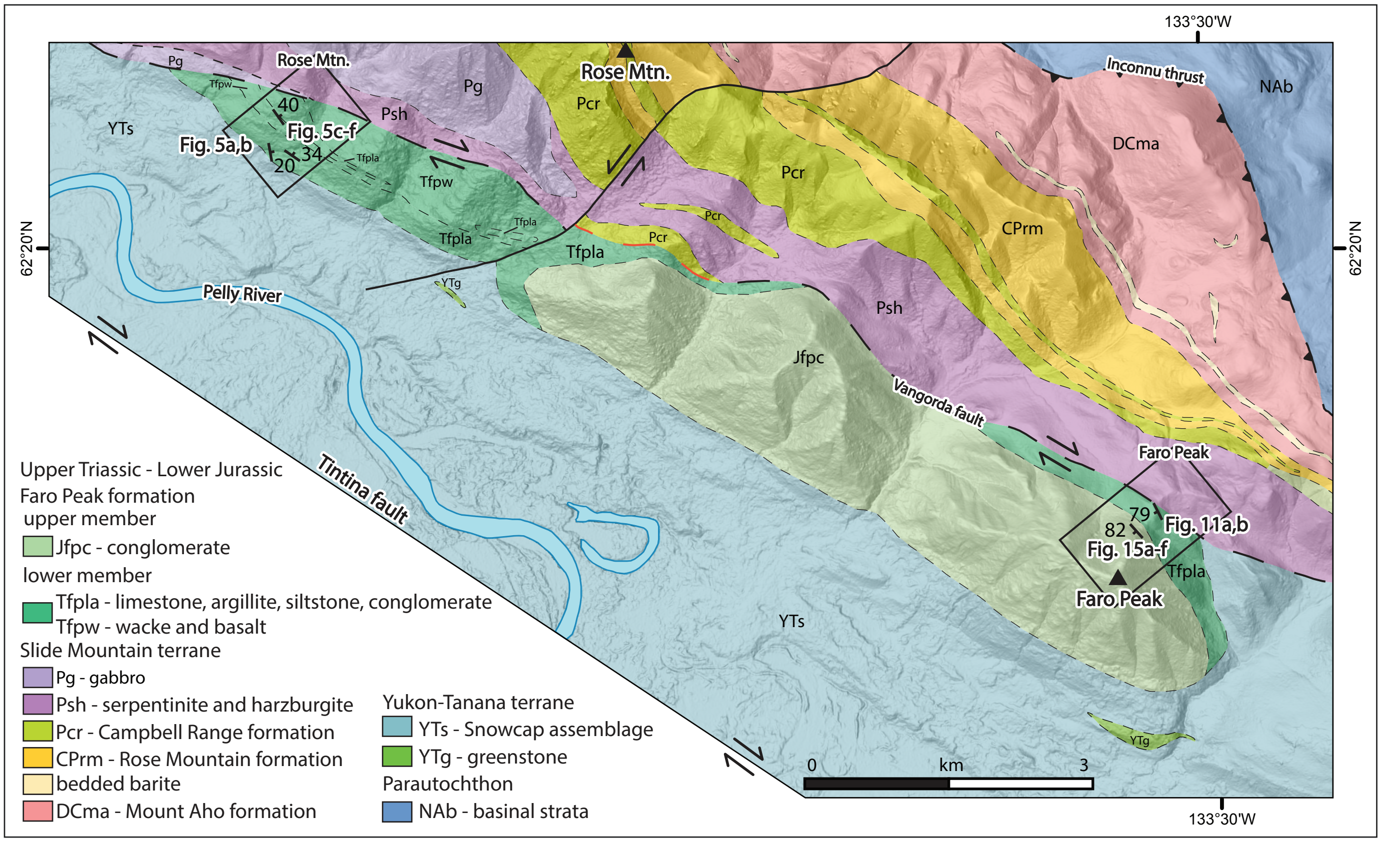

Figure 3. *Simplified bedrock geology map of the Rose Mountain and Faro Peak areas discussed in the text (modified from Pigage, 2004 and Jennings et al., 1978). Red dashed line indicates modified Vangorda fault location due to reassignment of basalt unit to Campbell Range formation. Contact symbols same as Figure 2. Basemap DEM (digital elevation model) obtained from the University of Minnesota Polar Geospatial Center (2018) and Porter et al. (2018).*

Repeater Hill

Late Triassic conodont elements (late Norian; *Epigondolella quadrata*; Orchard, 2006) are reported in dark grey micrite to wackestone units below the NorthwesTel repeater at the top of Repeater Hill, ~22 km to the southeast of Rose Mountain and ~2.5 km northwest of Faro (Fig. 6). Upper Triassic limestone units are interbedded with siltstone and argillite units similar to those at Rose Mountain, however, at Repeater Hill these fine-grained strata are strongly foliated along a fault that cuts out the basal conglomerate and juxtaposes younger lower member rocks with the Snowcap assemblage (Fig. 7a,b).

Blind Creek–Dena Cho Trail

The Blind Creek–Dena Cho Trail localities are ~10 km southeast of the Faro townsite (Fig. 8). Near the trace of the Vangorda fault, mineral exploration trenches provide access to lower member outcrops in otherwise unexposed areas. The lower member typically consists of foliated, thin-bedded, dark grey micrite, siltstone, and argillite units (Fig. 9a,b). There are no reported fossil constraints on the limestone units in this area.

Eastern Whiskey Mountain

Lower member strata exposed along the eastern ridge of Whiskey Mountain, ~3 km northeast of Faro (Fig. 6), are generally more coarse-grained than the argillite and limestone-dominated units at the Rose Mountain and Repeater Hill localities. Stratigraphic relationships along the eastern ridge of Whiskey Mountain are uncertain because of poor exposure and variable bedding. Rock units along the north fork of Vangorda Creek appear highly deformed and contain east-verging folds and small-scale west-dipping faults (Fig. 10a,b).

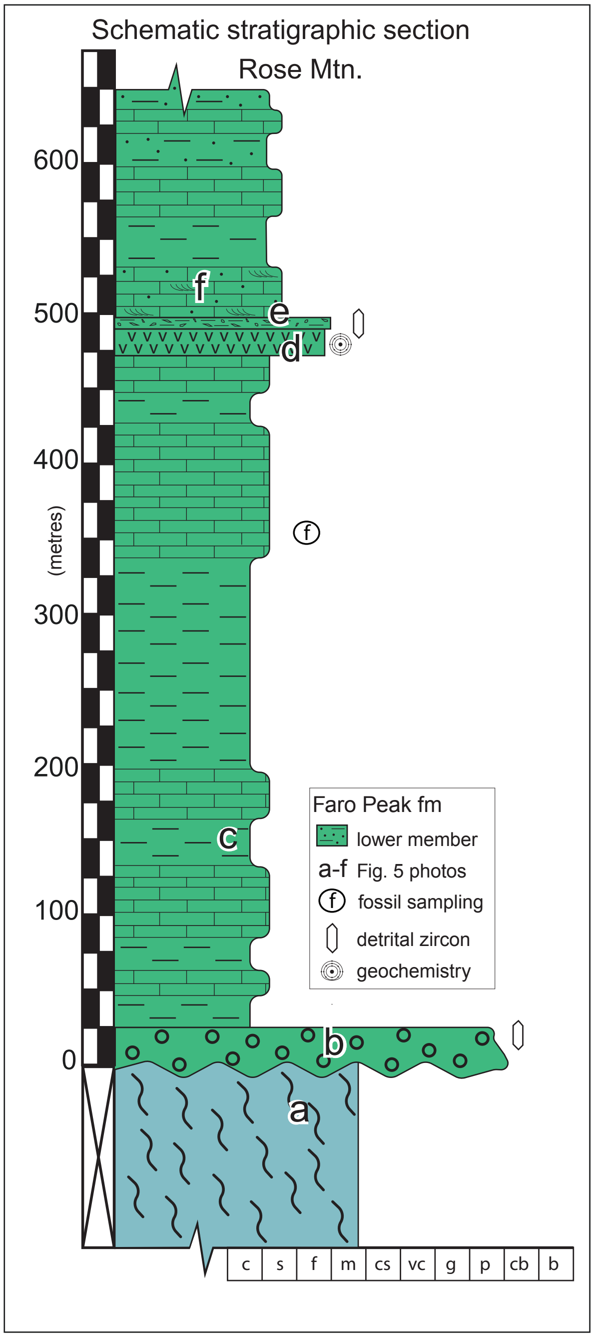

***Figure 4.** Schematic stratigraphic section of the lower member of the Faro Peak formation at Rose Mountain. The fossil location is approximate. Samples are from the 2019 field season. Abbreviations: c–clay; s–silt; f–fine sand; m–medium sand; cs–coarse sand; vc–very coarse sand; g–gravel; p–pebble; cb–cobble; b–boulder.*

Green to grey volcanic lithic feldspathic wacke and feldspathic arenite units characterize this locality. Along the north fork of Vangorda Creek, thin to medium beds of orange to tan, fine to medium-grained, feldspathic arenite are interbedded with siltstone and argillite (Fig. 10c). Slightly coarser sandstone layers show evidence of slump structures or convolute bedding (Fig. 10d). Argillite is green to grey, thin bedded to massive, and locally contains minor white mica (Fig. 10e). A unit of green lithic feldspathic wacke reported by Wiest and Beranek (2019) is interpreted to be a sheet sand above isoclinally folded beds that are the result of soft sediment deformation. This same sheet sand was observed during this field season to overlie tabular to slightly undulatory, thin-bedded argillite and siltstone indicating that soft sediment deformation was local (Fig. 10f). The highest elevation exposures along the eastern ridge of Whiskey Mountain consist of tabular, medium to thick-bedded sheets of steeply dipping, medium to very coarse grained, feldspathic to lithic feldspathic arenite and siltstone interbeds (Fig. 10g,h).

Faro Peak

Northeast of Faro Peak, ~10 km northeast of Faro, the Vangorda fault separates serpentinite and harzburgite units of the Slide Mountain terrane from the lower member Faro Peak formation (Fig. 3). Lower member units at this locality consist of subvertical, grey to brown, thin-bedded, locally wavy laminated, micaceous argillite, siltstone, and feldspathic arenite units (Fig. 11a). These siliciclastic rock units grade upwards into resistant, tabular siltstone (Fig. 11b).

Interpretation

The lower member consists of three lithological groups: (1) interbedded shale/argillite and limestone units from Rose Mountain, Repeater Hill, and Blind Creek–Dena Cho Trail; (2) basalt, wacke, and lithic feldspathic arenite units from Rose Mountain and eastern Whiskey Mountain; and (3) micaceous siltstone, argillite, and feldspathic to lithic feldspathic arenite units from Faro Peak.

Figure 5. *Field photographs of the Snowcap assemblage (Sa) and lower member of the Faro Peak formation (FPf) at Rose Mountain.* ***(a)*** *Highly deformed micaceous schist and quartzite (Sa);* ***(b)*** *cut section of basal conglomerate unit (FPf);* ***(c)*** *interbedded shale and limestone (FPf);* ***(d)*** *grey basalt overlain by green wacke (FPf);* ***(e)*** *sheared green wacke; and* ***(f)*** *cross-stratified silty limestone. Yellow-handled hammer (55 cm) and brown-handled hammer (33 cm) for scale.*

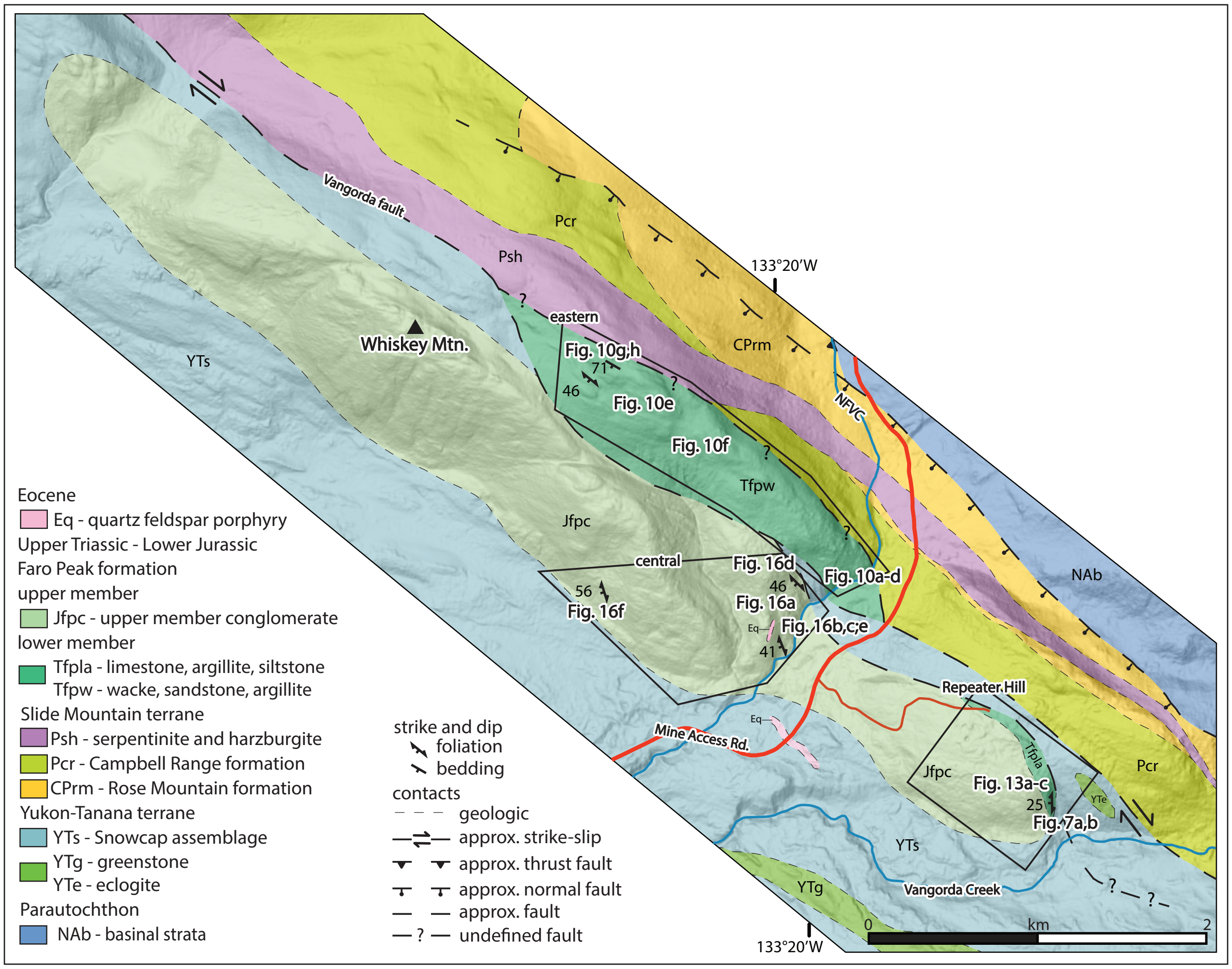

Figure 6. *Simplified bedrock geology of the eastern and central Whiskey Mountain and Repeater Hill areas (modified from Pigage, 2004). Abbreviations: NFVC–north fork Vangorda Creek. Basemap DEM (digital elevation model) obtained from the University of Minnesota Polar Geospatial Center (2018) and Porter et al. (2018).*

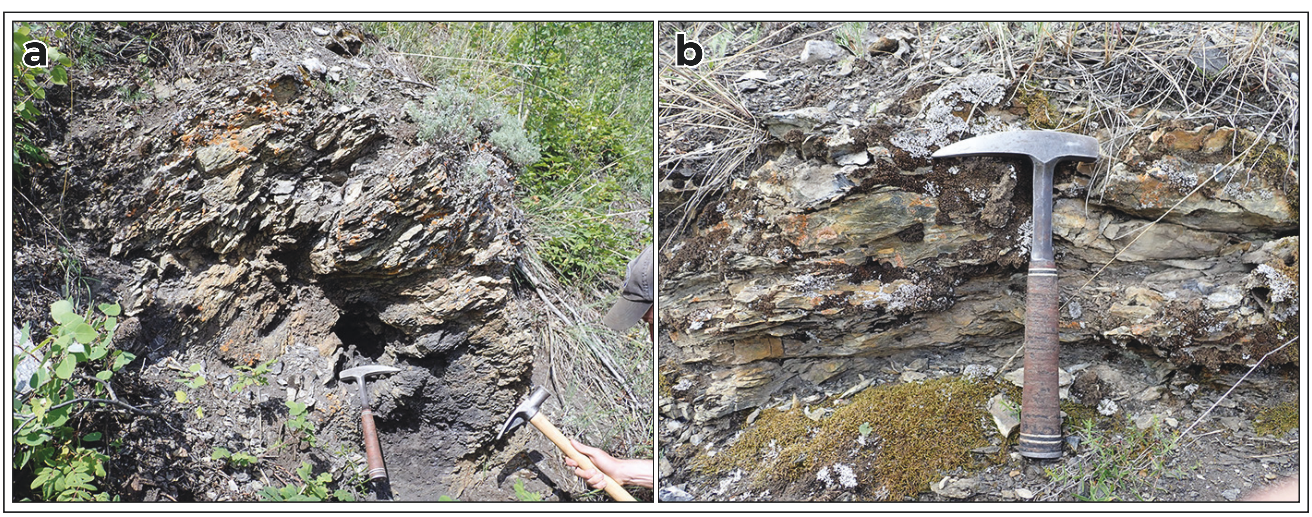

Figure 7. *Field photographs of the lower member of the Faro Peak formation at Repeater Hill.* ***(a)*** *Strongly foliated argillite and siltstone; and* ***(b)*** *thin-bedded, tan weathered, dark grey micrite. Yellow-handled hammer (55 cm) and brown-handled hammer (33 cm) for scale.*

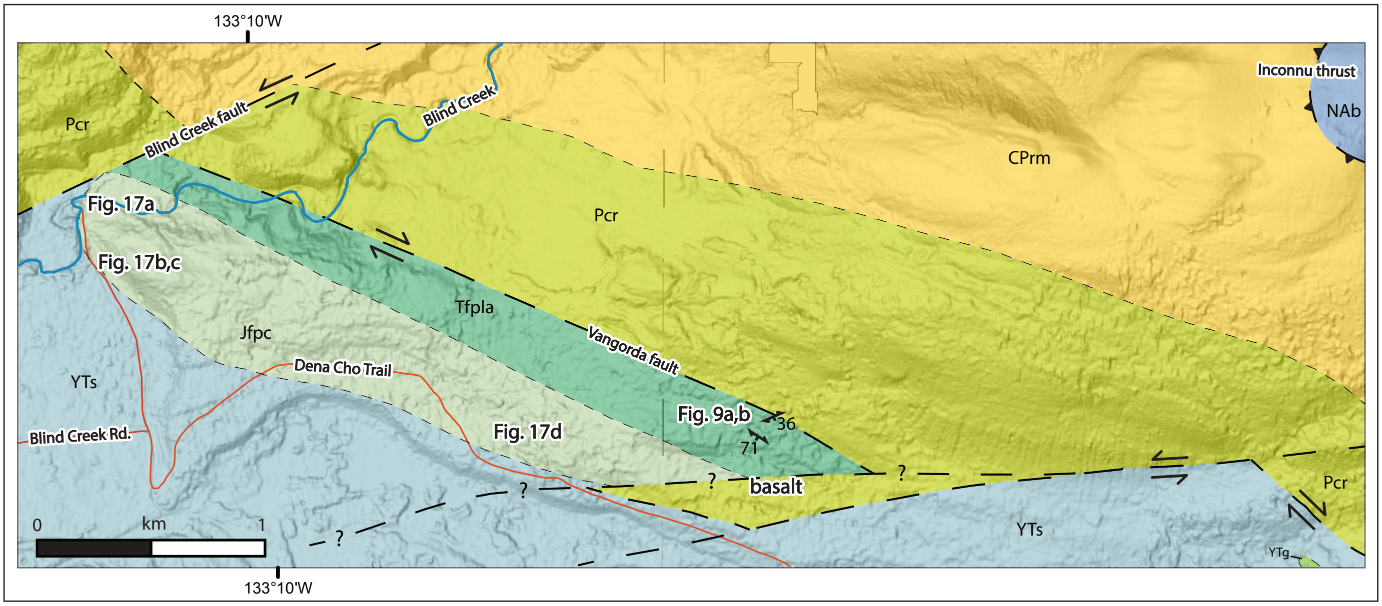

Figure 8. *Simplified bedrock geology of the Blind Creek and Dena Cho Trail area (modified from Pigage, 2004). Symbols same as Figure 6. Basemap DEM obtained from the University of Minnesota Polar Geospatial Center (2018) and Porter et al. (2018).*

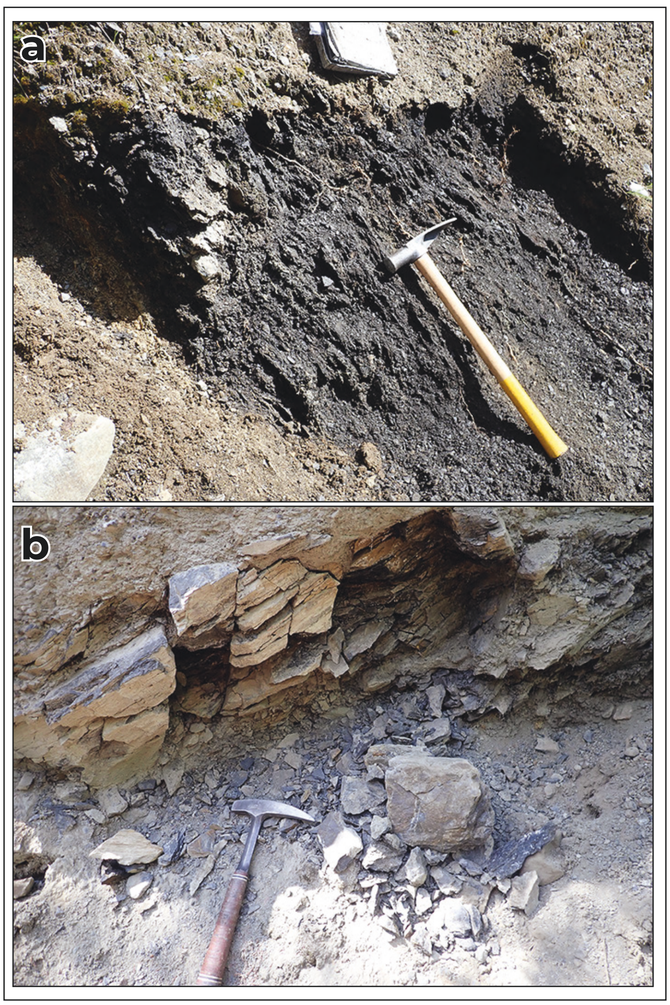

Upper Triassic limestone and shale units are age-constrained by conodont fossils in the lower part of the Rose Mountain section and sit unconformably on metasedimentary rocks of the Snowcap assemblage. These basal units are interpreted to correlate with Upper Triassic argillite and fossil-bearing limestone units that crop out at the Repeater Hill locality. The overlying basalt-wacke succession at Rose Mountain is likely correlative with green wacke and arenite units along the eastern ridge of Whiskey Mountain (Fig. 12), suggesting that the latter comprise the upper portion of the lower member. The basalt-wacke succession at Rose Mountain apparently indicates a shift from earlier, argillite-limestone deposition to proximal derivation from mafic to intermediate volcanic rocks. For example, Wiest and Beranek (2019) reported that lithic feldspathic arenite units along the eastern ridge of Whiskey Mountain contain angular mafic to intermediate volcanic rock fragments and suggest local, first-cycle sources. The uppermost parts of the lower member at Rose Mountain include micrite and micaceous siltstone that potentially correlate with micaceous argillite,

Figure 9. *Field photographs of the lower member of the Faro Peak formation near the Dena Cho Trail and Vangorda fault.* ***(a)*** *Trenched outcrop of foliated argillite; and* ***(b)*** *trenched outcrop of tan weathered, dark grey micrite.*

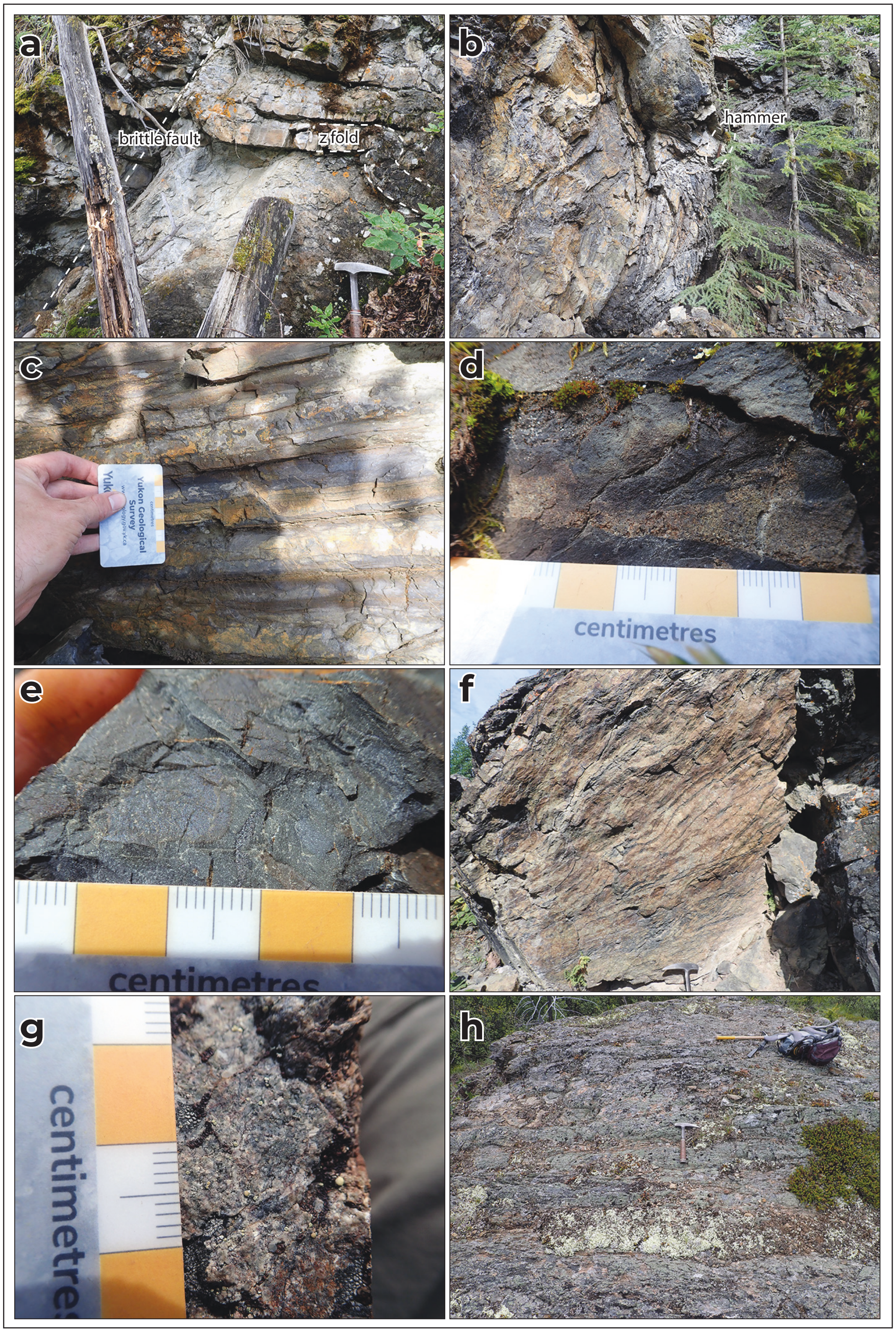

Figure 10. *Field photographs of the lower member of the Faro Peak formation at eastern Whiskey Mountain.* **(a)** *West-dipping brittle fault in argillite and medium-grained tabular sandstone with z-fold;* **(b)** *west-dipping brittle fracture in thin-bedded siltstone and fine-sandstone with east-vergent box-fold;* **(c)** *tabular bedded siltstone and argillite with local scouring* **(d)** *slump structure in coarse sandstone and argillite;* **(e)** *massive green argillite;* **(f)** *tabular, undulatory-bedded argillite and siltstone;* **(g)** *immature coarse-grained feldspathic arenite; and* **(h)** *steeply-dipping, tabular-bedded sandstone and siltstone. Brown-handled hammer (33 cm) for scale.*

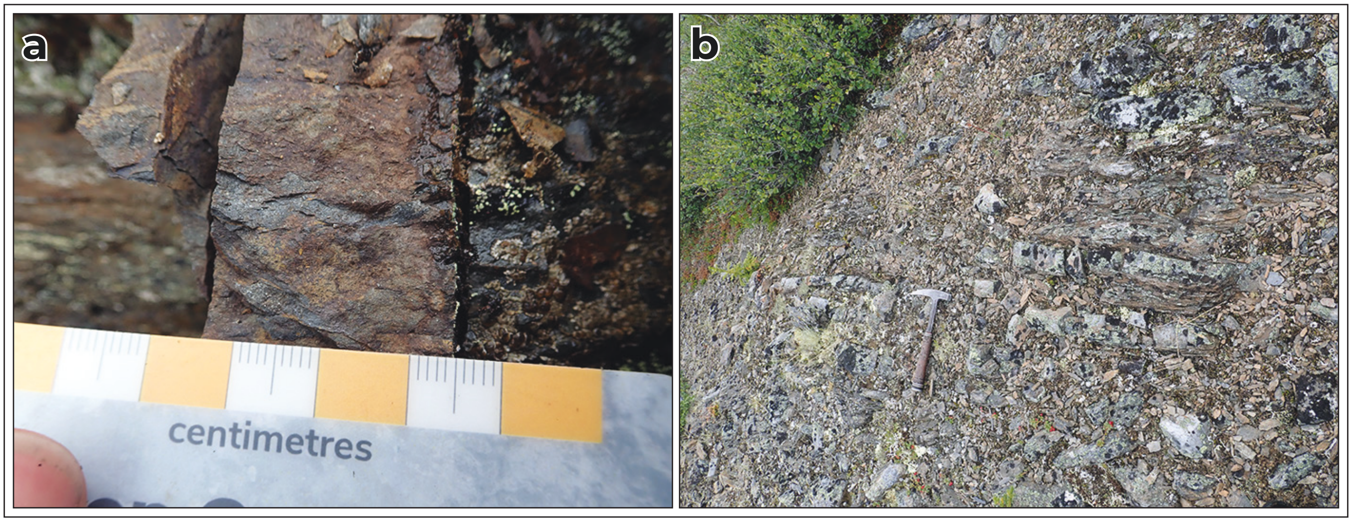

Figure 11. *Field photographs of the lower member of the Faro Peak formation at Faro Peak.* ***(a)*** *Micaceous siltstone; and* ***(b)*** *tabular-bedded micaceous siltstone. Brown-handled hammer (33 cm) for scale.*

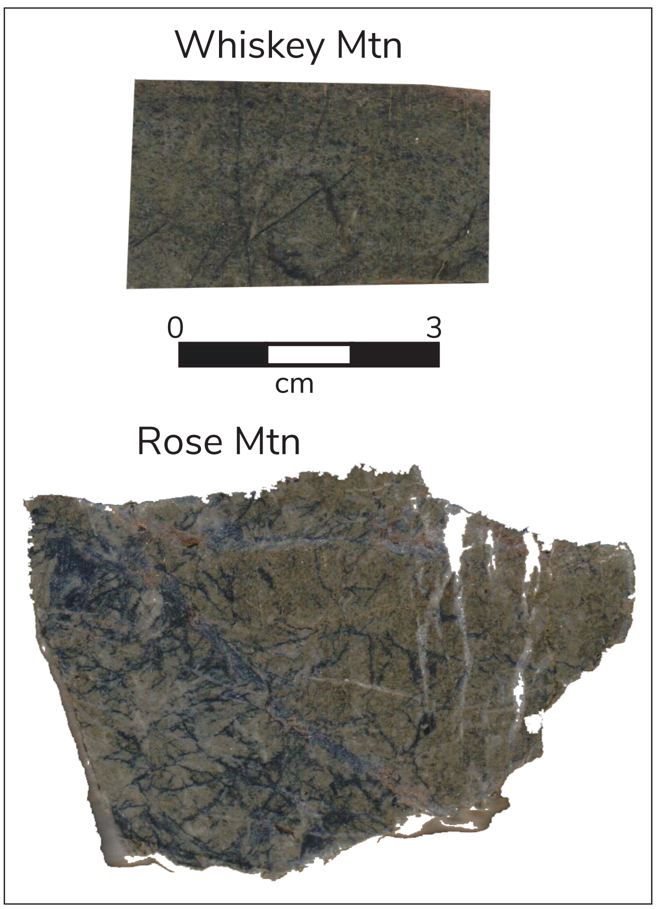

Figure 12. *Comparison between green wacke at eastern Whiskey Mountain area* ***(upper)*** *and unsheared green wacke overlying basalt at Rose Mountain area* ***(lower)****.*

siltstone, and feldspathic arenite at the Faro Peak locality. Micaceous strata are characteristic of Upper Triassic overlap assemblage units in association with Yukon-Tanana terrane, Slide Mountain terrane, and ancestral Cordilleran margin from eastern Alaska to northern British Columbia (Beranek and Mortensen, 2011).

Lower member basalt from Rose Mountain is lithologically distinct from that of the Permian Campbell Range formation to the northeast of the Vangorda fault and its apparent conformable nature above Carnian to Rhaetian limestone units indicates a Late Triassic depositional age. The lack of epidote streaking and green chlorite-alteration also suggests it is distinct from basalt mapped as basal Faro Peak formation by Pigage (2004) and Jennings *et al.* (1978) south of Rose Mountain (Fig. 3). Pigage (2004) speculated that this 'basal basalt' is unrecognized Campbell Range formation as the N-MORB (normal mid-ocean ridge basalt) whole-rock geochemical compositions of this unit are indistinguishable from Permian units in the Faro area. The geochemical signatures of Campbell Range formation rocks in the Finlayson Lake area are also similar (e.g., Piercey *et al.*, 2012). Therefore, based on the mineralogical and geochemical similarities between the 'basal basalt' of Faro Peak formation and Campbell Range formation from the Faro and Finlayson Lake areas, the 'basal basalt' locality south of Rose Mountain outlined in Pigage (2004) is herein reassigned to Campbell Range formation.

An outcrop of green basalt reported by Wiest and Beranek (2019) near the Dena Cho Trail was investigated in summer 2019 to understand its relationship with the Faro Peak and Campbell Range formations (Fig. 8). This green basalt contains epidote streaking and local to pervasive chlorite-carbonate alteration suggesting an affiliation with the Permian Campbell Range formation. Its location near lower and upper member units of the Faro Peak formation suggests it may be the result of an east-northeast trending fault splay in the area (Fig. 8).

Lower member–upper member contact relationships

Repeater Hill

The contact between lower member and upper member units at Repeater Hill is well constrained (Fig. 6). Upper Triassic limestone and argillite units of the lower member crop out directly below a bed of pebble to cobble, matrix-supported, polymictic conglomerate that contains clasts of micaceous quartzite, schist, grey and black chert, green to tan volcanic rocks, and sedimentary rocks (Fig. 13a). This conglomerate marks the base of the upper member and is consistent with the map interpretations of Pigage (2004). Above this conglomerate, micaceous argillite separates these units from massive, matrix to clast-supported conglomerate that comprises the bulk of Repeater Hill and locally contains porphyry and intrusive rock clasts (Fig. 13b,c; Wiest and Beranek, 2019).

Faro Peak

At least 800 m of upper member stratigraphy is exposed above the lower member–upper member contact at Faro Peak (Fig. 14). Subvertical, tan to brown, massive to thin-bedded, medium to very coarse grained arenite units scour into, and are interbedded with, wavy laminated, micaceous siltstone to argillite (Fig. 15a–d) above the saddle ~600 m northeast of Faro Peak. This saddle separates these upper member units from tabular, lower member micaceous siltstone. The contact between the lower and upper members is drawn at the first occurrence of coarse-grained sandstone (Fig. 3) and is consistent with the map interpretations of Pigage (2004).

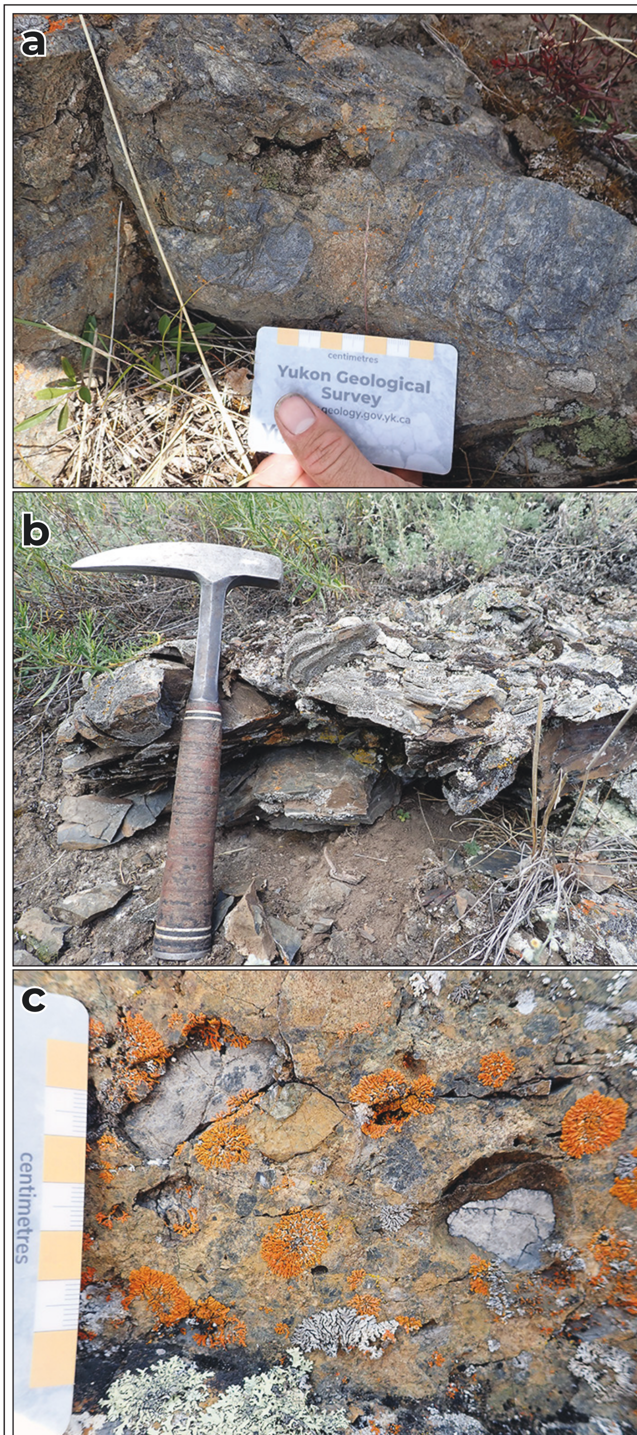

Figure 13. *Field photographs of upper member of the Faro Peak formation at Repeater Hill.* ***(a)*** *Matrix-supported conglomerate with quartzite, volcanic, and sedimentary clasts;* ***(b)*** *weakly folded micaceous argillite; and* ***(c)*** *normally graded bed in matrix-supported conglomerate. Brown-handled hammer (33 cm).*

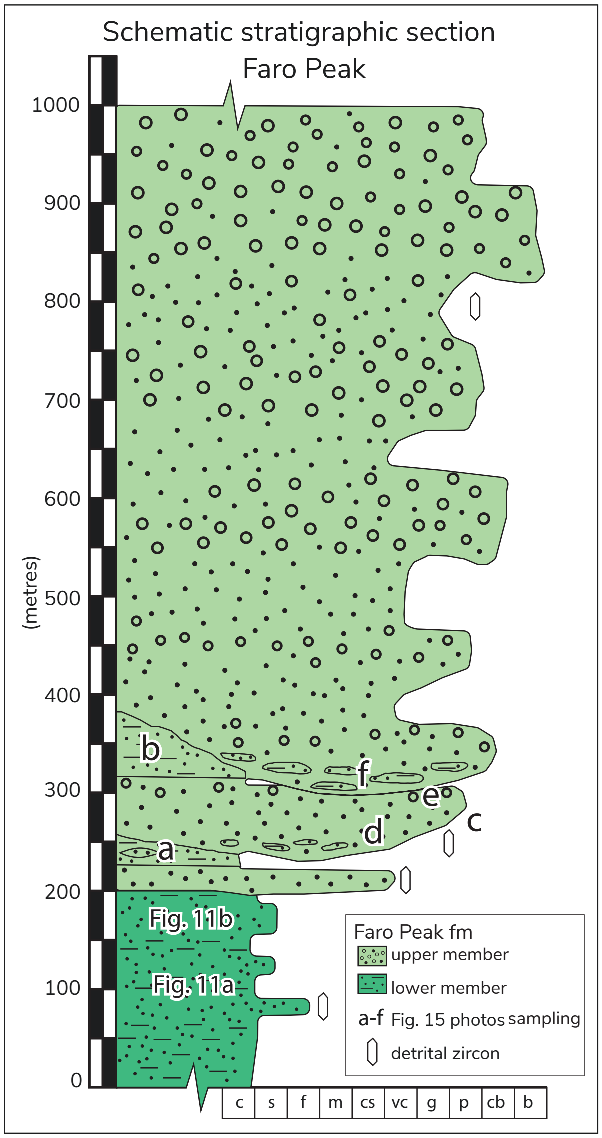

***Figure 14.** Schematic stratigraphic section of the lower and upper members of the Faro Peak formation at Faro Peak. Samples are from the 2018 and 2019 field seasons. Abbreviations same as Figure 4.*

Coarse-grained beds of feldspathic to lithic feldspathic arenite at the Faro Peak locality contain wavy laminated, micaceous argillite rip-up clasts and are locally overlain by conglomerate with clasts of grey and black chert, grey quartzite, tan volcanic rocks, and limestone (Fig. 15e). Upsection, these rip-up clasts become coarser (>10 cm) and suggest more intense scouring of argillaceous interbeds (Fig. 15f). The increase in coarse-grained sandstone, conglomerate, and rip-up clast size suggests an overall coarsening-upward sequence that continues to the summit of Faro Peak. Wiest and Beranek (2019) reported granule to cobble, matrix to clast-supported, polymictic conglomerate units containing clasts of porphyry and felsic intrusive rocks that are intercalated with very coarse grained to granule feldspathic and lithic arenite units upsection at the summit of Faro Peak and an adjacent peak ~4 km to the northwest.

Central Whiskey Mountain

The upper member of the Faro Peak formation consists of tightly folded, thin to medium-bedded, locally calcareous, micaceous feldspathic to lithic feldspathic arenite and micaceous siltstone units near the center of Whiskey Mountain, ~2.5 km northeast of Faro (Fig. 16a,b). These units occur both above and below matrix-supported conglomerate that dips gently to moderately towards the Tintina Trench and shows normally graded bedding (Fig. 16c). Conglomerate clasts include quartzite, schist, limestone, tan volcanic rocks, and pyroxenite. Below the conglomerate beds, fine-grained rocks are pervasively sheared by a fault that juxtaposes the upper member with the Snowcap assemblage (Fig. 16d). Locally, polymictic conglomerate was observed in faulted contact with these finer-grained units (Fig. 16e). It appears that fine-grained strata accommodated the majority of strain at this locality, whereas conglomerate facies are more resistant, generally appear less deformed, and contain a slight to moderate foliation (Fig. 16f) and local brittle fracturing and faulting.

Blind Creek–Dena Cho Trail

The contact between the lower and upper members is not exposed near the Blind Creek–Dena Cho Trail locality (Fig. 8). Outcrops along the southern bank of Blind Creek consist of matrix-supported conglomerate that overlies limestone and/or calcareous argillite, possibly indicating its stratigraphic position in the upper member, similar to calcareous units near central Whiskey Mountain (Fig. 17a). Upper member exposures at this locality mostly consist of matrix to clast-supported polymictic conglomerate. Clast components include green to grey quartzite, schist, black and grey chert, intermediate to mafic volcanic and intrusive rocks, and subordinate limestone, basalt, and sedimentary rocks that resemble the lower member of the Faro Peak formation (Fig. 17c,d).

Figure 15. *Field photographs of the upper member of the Faro Peak formation at Faro Peak.* ***(a)*** *Sandstone channel in interbedded micaceous argillite and siltstone;* ***(b)*** *wavy laminated argillite;* ***(c)*** *outcrop of sheet sandstone (s) and conglomerate (c) interbeds;* ***(d)*** *coarse-grained lithic feldspathic arenite (s bed from Fig. 15c);* ***(e)*** *matrix-supported conglomerate (c bed from Fig. 15c); and* ***(f)*** *disk-shaped rip-up clasts of wavy laminated argillite in very-coarse sandstone. Brown-handled hammer (33 cm) and geologist (180 cm) for scale.*

Figure 16. *Field photographs of the upper member of the Faro Peak formation at central Whiskey Mountain.* ***(a)*** *Recumbent fold in fine-grained, micaceous sandstone and siltstone;* ***(b)*** *calcareous sandstone;* ***(c)*** *Normally graded bedding in coarse-grained sandstone and matrix-supported conglomerate;* ***(d)*** *uniformly sheared fine-grained, micaceous sandstone and siltstone;* ***(e)*** *west-dipping fault separating conglomerate and fine-grained units; and* ***(f)*** *well foliated, clast-supported conglomerate. Brown-handled hammer (33 cm) for scale.*

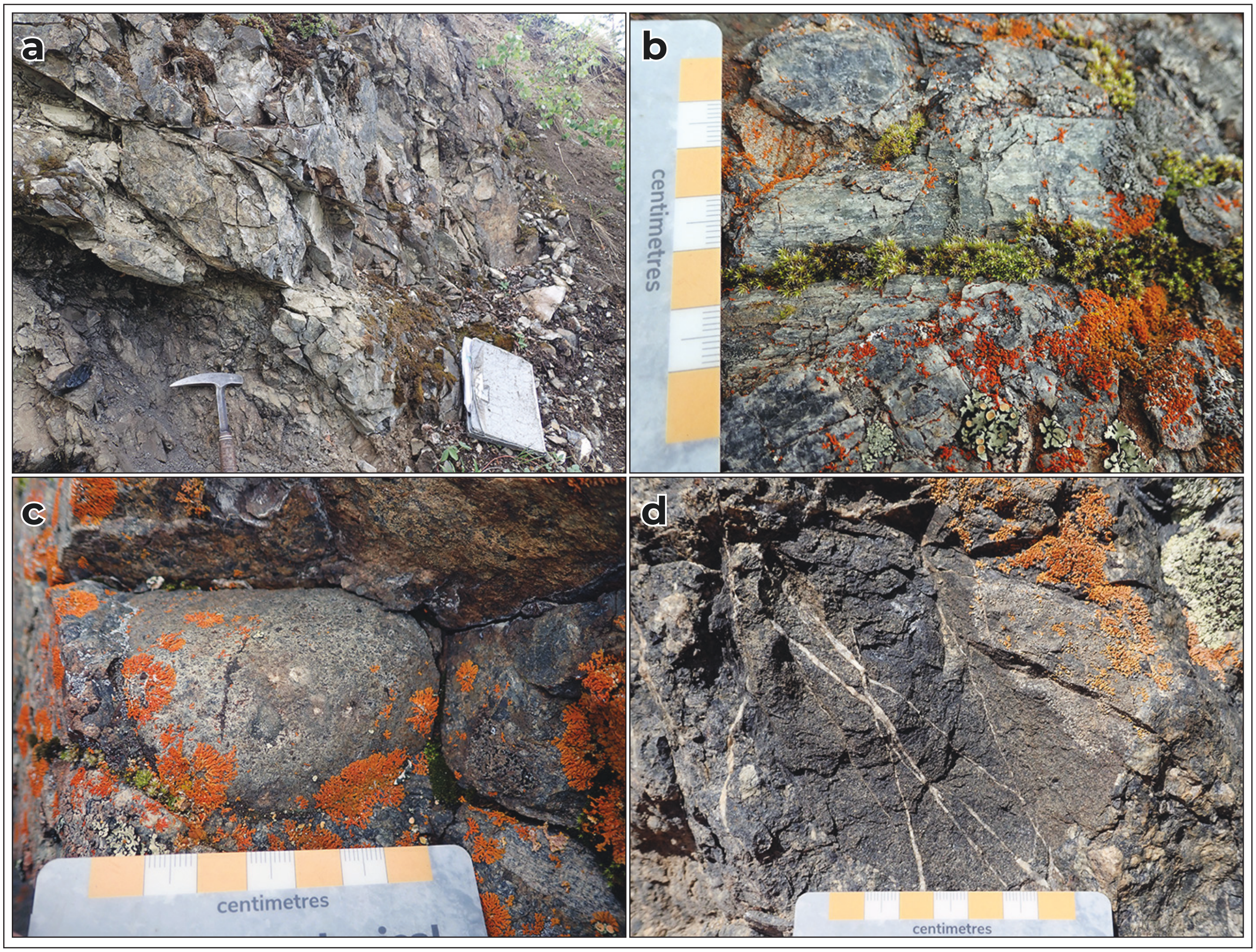

Figure 17. *Field photographs of the upper member of the Faro Peak formation at Blind Creek and Dena Cho Trail.* ***(a)*** *Calcareous unit overlain by normally graded, matrix-supported conglomerate;* ***(b)*** *green quartzite clast;* ***(c)*** *equigranular gabbro clast; and* ***(d)*** *dark grey sandstone clast. Brown-handled hammer (33 cm) for scale.*

Interpretation

The upper member of the Faro Peak formation overlies Upper Triassic limestone units that correlate with the base of the Rose Mountain section, micaceous siltstone and feldspathic arenite units that are potentially the upper part of the lower member, and Snowcap assemblage metasedimentary and eclogitic rocks that crop out below the lower member. These observations suggest that the basal contact of the upper member is an unconformity, however, the interbedded micaceous argillite and conglomerate at Repeater Hill, and interbedded micaceous siltstone, argillite, and coarse-grained sandstone to conglomerate at Faro Peak, suggest a transitional contact between the lower and upper members. A potential third occurrence of a transitional contact is located at central Whiskey Mountain where locally calcareous micaceous siltstone and feldspathic arenite units of the upper member (e.g., Pigage, 2004) are interbedded with upper member conglomerate facies.

There are a few working hypotheses that explain the transitional and unconformable contact relationships between the lower and upper members: (1) micaceous units at Faro Peak and Repeater Hill are fine-grained parts of the upper member and do not belong to the lower member. This compares well with central Whiskey Mountain where micaceous siltstone and feldspathic arenite units have previously been mapped as the upper member (Pigage, 2004); (2) lower and upper member units comprise part of a syndepositional synform. Bedding is moderately to steeply dipping and the contact with lower member and upper member units appears transitional only near the trace of the Vangorda fault. Towards the Tintina Trench, lower member units are not exposed and massive, polymictic conglomerate units of the upper member sit unconformably on Snowcap assemblage; and (3) lower member units are not laterally continuous and Upper Triassic limestone and argillite beds are correlative with micaceous siltstone and feldspathic arenite units. This last hypothesis requires that micaceous sedimentary rocks in the Faro area are not laterally continuous, suggesting that different units contain a different provenance and became interfingered in the Faro Peak basin(s).

Discussion and future work

The lower member of the Faro Peak formation should be reassigned to a new formation because it is lithologically distinct and its lower and upper contacts are defined by unconformities. This new formation likely consists of a lower, limestone-argillite unit and an upper, basalt-wacke-feldspathic arenite unit. It is uncertain if micaceous units currently mapped as the lower member of the Faro Peak formation at central Whiskey Mountain, Repeater Hill, and the base of the Faro Peak section are part of this new formation, or, if they instead represent fine-grained parts of the upper member of the Faro Peak formation. It is also uncertain if basalt and wacke units at Rose Mountain correlate with the wacke and feldspathic arenite units along the eastern ridge of Whiskey Mountain. Future detrital zircon U-Pb-Hf studies will assist in identifying the stratigraphic position of these units and determine if some, or all, of the lower member of the Faro Peak formation should be assigned to a new formation.

Preliminary conclusions

Field investigations of Upper Triassic to Lower Jurassic rock units near Faro have uncovered new details about the regional stratigraphy of the southern Tay River map area. The lower member of the Faro Peak formation likely represents part of an Upper Triassic overlap assemblage that covered the Yukon-Tanana and Slide Mountain terranes and ancestral North American margin, similar to other Upper Triassic strata that crop out along the eastern edge of the Intermontane terranes from eastern Alaska to northern British Columbia (Beranek and Mortensen, 2011; Golding *et al.* 2016). Basal conglomerate units of the lower member near Rose Mountain sit unconformably on the Snowcap assemblage and indicate that Yukon-Tanana terrane basement was locally exhumed to the surface by Late Triassic time. Black and grey chert clasts furthermore indicate that lower member sand and gravel were also partially sourced from Paleozoic rock units of the adjacent Slide Mountain terrane. These observations suggest that the suture between the Yukon-Tanana and Slide Mountain terranes accommodated early Late Triassic subsidence during regional plate convergence, initiation of a new east-dipping subduction zone, and collisional processes along the outboard edge of northwestern North America (*e.g.*, Nelson *et al.*, 2013).

The lithology and stratigraphic character of upper member strata are consistent with synorogenic deposition related to Early Jurassic exhumation of the northern Intermontane terranes in central Yukon (Colpron *et al.* 2015). The upper member is massively bedded, >800 m-thick, and its basal units are dominated by pebble to cobble-sized clasts of limestone, argillite, and volcanic rocks, whereas the exposed top also contains up to boulder-sized clasts of mafic to felsic intrusive rocks. These observations are consistent with progressive unroofing and suggest proximity to a basin-bounding structure, such as the proto-Vangorda fault (cf. Tempelman-Kluit, 1972). Faro Peak basin subsidence and exhumation of the Snowcap assemblage was likely controlled by major extensional to transcurrent structures (*e.g.*, Colpron *et al.*, 2015) similar to the Willow Lake fault in central Yukon (Knight *et al.*, 2013) that accommodated the Early Jurassic exhumation of Yukon-Tanana basement. Clasts in upper member conglomerate (Wiest and Beranek, 2019) also suggest that basin-filling along the Yukon-Tanana and Slide Mountain suture that initiated during the early Late Triassic persisted until or became active again during the Early Jurassic. Lower and upper member strata of the Faro Peak formation are cut by the Vangorda fault (see Fig. 8) and confirm that this terrane-bounding fault underwent post-Early Jurassic motion. The Jules Creek fault in the Finlayson Lake area is the southern equivalent to the Vangorda fault and is similarly suggested to have accommodated subsidence and strike-slip motion that occurred until early Mesozoic time (Murphy *et al.*, 2006). Future studies of the Faro Peak formation will further assess the potential correlations between clastic units in the Finlayson Lake and southern Tay River map areas. These results combined with continued investigations into the stratigraphic relationships between lower and upper member units will provide new insights into the evolution of the Yukon-Tanana–Slide Mountain terrane boundary and further constrain plate tectonic models for the early growth of the Canadian Cordillera.

Acknowledgements

This is a product of the Geo-mapping for Energy and Minerals (GEM) program at Natural Resources Canada. A special thanks to the Yukon Geological Survey for field logistics and helicopter support to the Rose Mountain area. Thank you to reviewer Don Murphy for thoughtful and constructive comments that significantly improved this manuscript.

References

Beranek, L.P. and Mortensen, J.K., 2011. The timing and provenance record of the Late Permian Klondike orogeny in northwestern Canada and arc-continent collision along western North America. Tectonics, vol. 30, TC5017.

Clark, A.D., 2017. Tectonometamorphic history of mid-crustal rocks at Aishihik Lake, southwest Yukon. Unpublished MSc thesis, Simon Fraser University, British Columbia, Canada, 153 p.

Colpron, M., Crowley, J.L., Gehrels, G.E., Long, D.G.F., Murphy, D.C., Beranek, L.P. and Bickerton, L., 2015. Birth of the northern Cordilleran orogen, as recorded by detrital zircons in Jurassic synorogenic strata and regional exhumation in Yukon. Lithosphere, vol. 7, p. 541–562.

Colpron, M., Nelson, J.L. and Murphy, D.C., 2006. A tectonostratigraphic framework for the pericratonic terranes of the northern Canadian Cordillera. In: Paleozoic Evolution and Metallogeny of Pericratonic Terranes at the Ancient Pacific Margin of North America, Canadian and Alaskan Cordillera, M. Colpron and J.L. Nelson (eds.), Geological Association of Canada Special Paper 45, p. 1–23.

Dusel-Bacon, C., Lanphere, M.A., Sharp, W.D., Layer, P.W. and Hansen, V.L., 2002. Mesozoic thermal history and timing of structural events for the Yukon-Tanana Upland, east-central Alaska: $^{40}Ar/^{39}Ar$ data from metamorphic and plutonic rocks. Canadian Journal of Earth Sciences, vol. 39, p. 1013–1051.

Gabrielse, H., Murphy, D.C. and Mortensen, J.K., 2006. Cretaceous and Cenozoic dextral orogen-parallel displacements, magmatism, and paleogeography, north-central Canadian Cordillera. In: Paleogeography of the North American Cordillera: Evidence For and Against Large-Scale Displacements, Haggard, J.W., Enkin, R.J. and Monger, J.W.H. (eds.), Geological Association of Canada, Special Paper 46, p. 255–276.

Golding, M.L., Mortensen, J.K., Ferri, F., Zonneveld, J.-P. and Orchard, M.J., 2016. Determining the provenance of Triassic sedimentary rocks in northeastern British Columbia and western Alberta using detrital zircon geochronology, with implications for regional tectonics. Canadian Journal of Earth Sciences, vol. 53, p. 140–155.

Jennings, D.S., Jilson, G.A., Hanson, D.J. and Franzen, J.P., 1978. Geology Anvil District map area, Unpublished Cyprus Anvil Mining Corporation internal company report 1:50 000 scale.

Johnston, S.T., Mortensen, J.K. and Erdmer, P., 1996. Igneous and metaigneous age constraints for the Aishihik metamorphic suite, southwest Yukon. Canadian Journal of Earth Sciences, vol. 33, p. 1543–1555.

Knight, E., Schneider, D.A. and Ryan, J.J., 2013. Thermochronology of the Yukon-Tanana terrane, west-central Yukon: Evidence for Jurassic extension and exhumation in the northern Canadian Cordillera. Journal of Geology, vol. 121, p. 371–400.

Mihalynuk, M.G., Nelson, J.A. and Diakow, L.J., 1994. Cache Creek terrane entrapment: Oroclinal paradox within the Canadian Cordillera. Tectonics, vol. 13, p. 575–595.

Murphy, D.C., Mortensen, J.K., Piercey, S.J., Orchard, M.J. and Gehrels, G.E., 2006. Mid-Paleozoic to early Mesozoic tectonostratigraphic evolution of the Yukon-Tanana and Slide Mountain terranes and affiliated overlap assemblages, Finlayson Lake massive sulphide district, southeastern Yukon. In: Paleozoic Evolution and Metallogeny of Pericratonic Terranes at the Ancient Pacific Margin of North America, Canadian and Alaskan Cordillera, M. Colpron and J.L. Nelson (eds.), Geological Association of Canada Special Paper 45, p. 75–105.

Nelson, J.L., Colpron, M. and Israel, S. 2013. The Cordillera of British Columbia, Yukon, and Alaska: Tectonics and Metallogeny. In: Tectonics, Metallogeny and Discovery: The North American Cordillera and Similar Accretionary Settings, M. Colpron, T. Bissig, B.G. Rusk and J.F.H. Thompson (eds.), Society of Economic Geologists, Special Publication 17, p. 53–109.

Orchard, M.J., 2006. Late Paleozoic and Triassic conodont faunas of Yukon and northern British Columbia and implications for the evolution of the Yukon-Tanana terrane. In: Paleozoic Evolution and Metallogeny of Pericratonic Terranes at the Ancient Pacific Margin of North America, Canadian and Alaskan Cordillera, M. Colpron and J.L. Nelson (eds.), Geological Association of Canada Special Paper 45, p. 229–260.

Piercey, S.J., Murphy, D.C. and Creaser, R.A., 2012. Lithosphere-asthenosphere mixing in a transform-dominated late Paleozoic backarc basin: Implications for northern Cordilleran crustal growth and assembly. Geosphere, vol. 8, no. 3, p. 716–739.

Pigage, L.C., 2004. Bedrock geology compilation of the Anvil District (parts of NTS 105K/2, 3, 5, 6, 7, and 11), central Yukon. Yukon Geological Survey, Bulletin 15, 103 p.

Porter, C., Morin, P., Howat, I., Noh, M-J., Bates, B., Peterman, K., Keesey, S., Schlenk, M., Gardiner, J., Tomko, K., Willis, M., Kelleher, C., Cloutier, M., Husby, E., Foga, S., Nakamura, H., Platson, M., Wethington, M. Jr., Williamson, C., Bauer, G., Enos, J., Arnold, G., Kramer, W., Becker, P., Doshi, A., D'Souza, C., Cummens, P., Laurier, F. and Bojesen, M., 2018. ArcticDEM, https://doi.org/10.7910/DVN/OHHUKH, Harvard Dataverse, vol. 1 [accessed November, 2019].

Staples, R.D., Gibson, H.D., Colpron, M. and Ryan, J.J., 2016. An orogenic wedge model for diachronous deformation, metamorphism, and exhumation in the hinterland of the northern Canadian Cordillera. Lithosphere, vol. 8, no. 2, p. 165–184.

Tempelman-Kluit, D.J., 1972. Geology and origin of the Faro, Vangorda, and Swim concordant zinc-lead deposits, central Yukon Territory. Geological Survey of Canada, Bulletin 208, 73 p.

Tempelman-Kluit, D.J., 1979. Five occurrences of transported synorogenic clastic rocks in Yukon Territory. Geological Survey of Canada, Paper 79-1A, p. 1–12.

Topham, M.J., Allan, M.M., Mortensen, J.K., Hart, C.J.R., Colpron, M. and Sack, P.J., 2016. Crustal depth of emplacement of the Early Jurassic Aishihik and Tatchun batholiths, west-central Yukon. *In:* Yukon Exploration and Geology 2015, K.E. MacFarlane (ed.), Yukon Geological Survey, p. 233–251.

University of Minnesota, 2018. Polar Geospatial Center, https://www.pgc.umn.edu [accessed November, 2019].

Wiest, A.C., Beranek, L.P., 2019. Stratigraphy of the Faro Peak formation, central Yukon: New field observations of Jurassic synorogenic sedimentation along the Yukon-Tanana–Slide Mountain terrane boundary. In: Yukon Exploration and Geology 2019, K.E. MacFarlane (ed.), Yukon Geological Survey, p. 127–142.

Yukon Geological Survey, 2019. Yukon Digital Bedrock Geology. Yukon Geological Survey, http://data.geology.gov.yk.ca/Compilation/3, [accessed November, 2019].

APPENDIX 1.B.1

Sample ID	Easting	Northing	Formation	Locality	Description	Method
2018 field season						
01AW18	587397	6902255	Upper member FP	Repeater Road	coarse-grained sandstone	
02AW18	587242	6902256	Upper member FP	Repeater Road	medium-grained sandstone	
03AW18	587139	6902122	Upper member FP	Repeater Road	medium to coarse-grained sandstone	dz, t
04AW18	591960	6896800	Snowcap assemblage	Blind Creek Rd.	quartz mica schist	dz, t
05AW18	594793	6896814	Upper member FP	Blind Creek/Dena Cho	coarse-grained sandstone	dz, t
06AW18	594897	6896760	Upper member FP	Blind Creek/Dena Cho	pebble conglomerate	
07AW18	596895	6895885	Upper member FP	Blind Creek/Dena Cho	coarse-grained sandstone	
08AW18	596985	6895923	Upper member FP (clast)	Blind Creek/Dena Cho	gravel-pebble conglomerate	
09AW18	585839	6902482	Upper member FP (clast)	Whiskey Mtn.	dark grey quartzite	dz, t
10AW18	586039	6902746	Upper member FP	Whiskey Mtn.	coarse-grained to gravel sandstone	
11AW18	586445	6903521	Lower member FP	Whiskey Mtn.	fine to medium-grained sandstone	dz, t
12AW18	586118	6903737	Lower member FP	Whiskey Mtn.	wackestone	dz, t
13AW18	586118	6903732	Lower member FP	Whiskey Mtn.	medium-grained sandstone-wackestone	
14AW18	585849	6903136	Upper member FP	Whiskey Mtn.	medium-grained sandstone	
15AW18	585922	6902816	Upper member FP (clast)	Whiskey Mtn.	augite gabbro	t
16AW18	586278	6901597	Snowcap assemblage	Van Gorder Falls	micaceous quartzite	t
17AW18	586142	6901437	Snowcap assemblage	Van Gorder Falls	graphitic schist	t
18AW18	586129	6901021	Snowcap assemblage	Far-O-Way	quartz mica schist	dz, t
19AW18	586523	6902507	Upper member FP (clast)	Whiskey Mtn.	fine-grained sandstone	t
20AW18	586523	6902507	Upper member FP(?)	Whiskey Mtn.	green sandstone(?)	
21AW18	586462	6902531	Upper member FP	Whiskey Mtn.	medium-grained to gravel sandstone	dz, t
22AW18	599286	6895394	Snowcap assemblage	Blind Creek/Dena Cho	micaceous quartzite	t
23AW18	588084	6901667	Lower member FP	Repeater Hill	micaceous argillite	t
24AW18	588075	6901667	Upper member FP	Repeater Hill	medium-grained to gravel sanstone	t
25AW18	587857	6901613	Upper member FP(?)	Repeater Hill	argillite to fine-grained sandstone	t
26AW18	587203	6902013	Upper member FP	Repeater Hill	gravel-pebble conglomerate	
27AW18	586129	6901025	Snowcap assemblage	Far-O-Way	albite chlorite schist or phyllite(?)	
28AW18	576677	6908762	Upper member FP	Faro Peak	medium-grained to gravel sandstone	dz, t
29AW18	573446	6911305	Upper member FP(clast)	Faro Peak	quartz feldspar prophyry	t
30AW18	573476	6911376	Upper member FP	Faro Peak	coarse-grained to pebble sandstone	
31AW18	577103	6909497	Lower member FP	Faro Peak	argillite to fine-grained sandstone	t
2019 field season						
01AW19	567771	6913700	Lower member FP(?)	Rose Mtn.	coarse-grained to pebble conglomerate (float?)	
02AW19	567822	6913666	Lower member FP	Rose Mtn.	green basalt (field call: green wackestone)	t
03AW19	567822	6913666	Lower member FP	Rose Mtn.	dark grey basalt	
04AW19	567690	6913286	Lower member FP	Rose Mtn.	coarse-grained to pebble conglomerate	dz, t
05AW19	568036	6913439	Lower member FP	Rose Mtn.	dark grey basalt	
06AW19	568378	6914926	Slide Mountain	Rose Mtn.	pegmatitic gabbro intruding mafic-ultramafic SMT	
07AW19	586466	6902404	Upper member FP	Whiskey Mtn.	medium-grained locally calcarous sandstone	
08AW19	586542	6902621	Lower member FP(?)	Whiskey Mtn.	siltstone to fine-grained sandstone	
09AW19	586700	6902837	Snowcap assemblage	Whiskey Mtn.	quartz mica schist	t
10AW19	586638	6903008	Lower member FP(?)	Whiskey Mtn.	fine-grained sandstone	dz, t
11AW19	586585	6902958	Upper member FP	Whiskey Mtn.	coarse-grained to gravel sandstone	
12AW19	586545	6902942	Upper member FP(?)	Whiskey Mtn.	fine to medium-grained sandstone	
13AW19	587959	6902142	Snowcap assemblage	Repeater Hill	micaceous quartzite to schist	
14AW19	588059	6902176	Campbell Range	Repeater Hill	dark green basalt	
15AW19	588066	6901681	Upper member FP	Repeater Hill	coarse-grained to cobble sandstone to conglomerate	dz, t
16AW19	577144	6909525	Lower member FP	Faro Peak	siltstone to fine-grained sandstone	dz, t
17AW19	576964	6909264	Upper member FP	Faro Peak	medium to coarse-grained sandstone	
18AW19	576900	6909232	Upper member FP	Faro Peak	medium to coarse-grained sandstone	dz, t
18AW19b	597514	6896218	Campbell Range	Blind Creek/Dena Cho	green basalt	
19AW19	597764	6895906	Campbell Range	Blind Creek/Dena Cho	green basalt	
20AW19	586136	6903728	Lower member FP	Whiskey Mtn.	green wackestone	
21AW19	585892	6903954	Lower member FP	Whiskey Mtn.	green argillite or basalt(?)	
22AW19	585830	6904076	Lower member FP	Whiskey Mtn.	medium to very coarse-grained sandstone	dz, t
23AW19	585362	6903651	Upper member FP	Whiskey Mtn.	medium-grained calcarous sandstone	
24AW19	585110	6903091	Dike	Whiskey Mtn.	pyrite andesite-basalt	
25AW19	586848	6902900	Lower member FP	Whiskey Mtn.	fine to medium-grained sandstone	
26AW19	587058	6902987	Lower member FP	Whiskey Mtn.	fine to medium-grained sandstone	t
27AW19	587065	6902996	Lower member FP	Whiskey Mtn.	argillite	
Clast 01	585402	6903215	Upper member FP (clast)	Whiskey Mtn.	micaceous quartzite	
Clast 02	585461	6903147	Upper member FP (clast)	Whiskey Mtn.	silty limestone	

dz = detrital zircon U-Pb-Hf
t = thin section
UTM locations in NAD 83 zone 08V

APPENDIX 1.B.2

2018 sampling

2018 sampling cont.

12AW18

billet

ppl

xpl

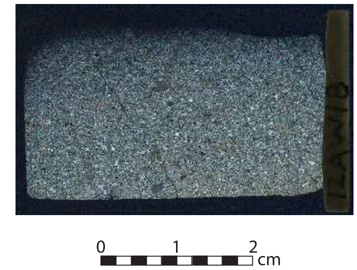

15AW18

billet

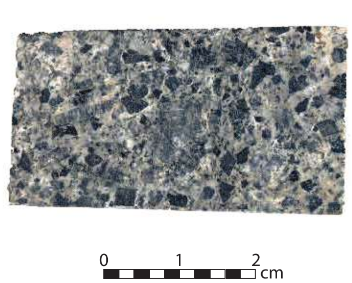

ppl

xpl

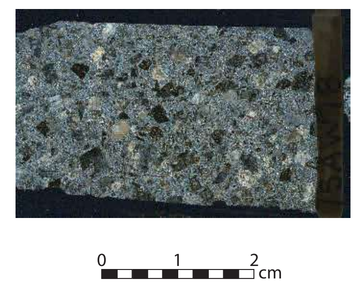

16AW18

billet

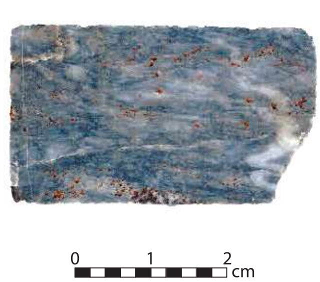

ppl

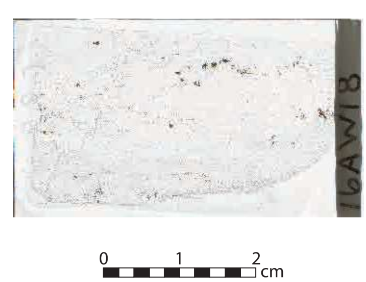

xpl

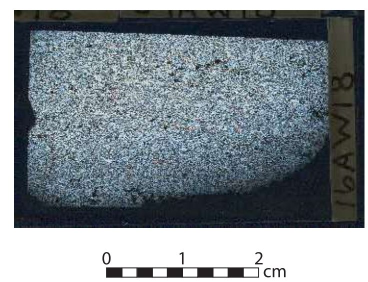

17AW18

billet

ppl

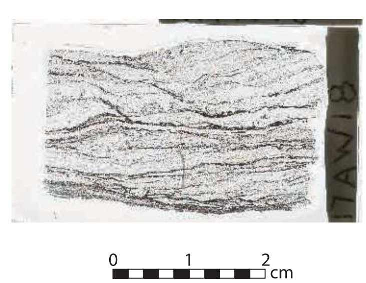

xpl

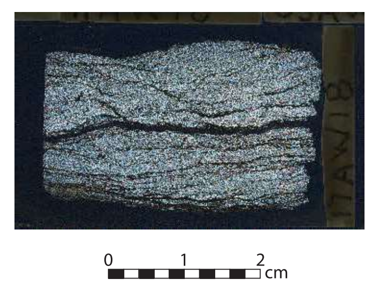

18AW18

billet

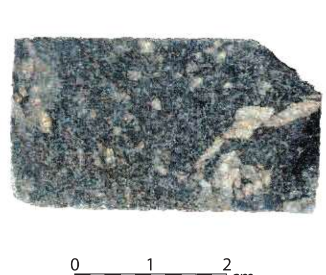

ppl

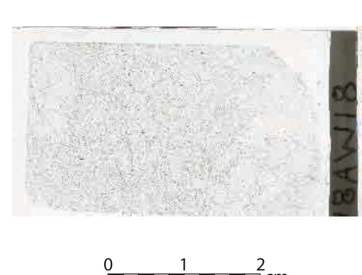

xpl

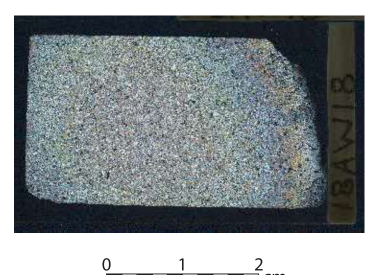

2018 sampling cont.

2018 sampling cont.

25AW18

billet

ppl

xpl

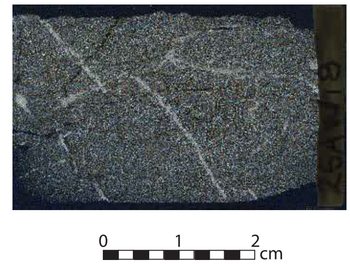

28AW18

billet

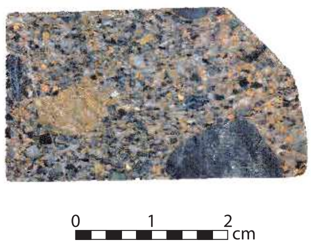

ppl

xpl

29AW18

billet

ppl

xpl

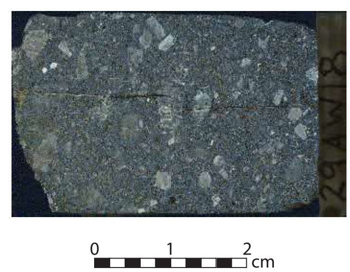

31AW18

billet

ppl

xpl

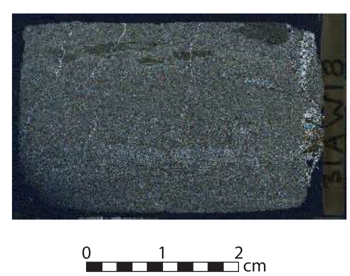

2019 sampling

02AW19

billet

ppl

xpl

04AW19

billet

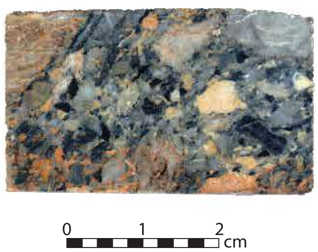

ppl

xpl

09AW19

billet

ppl

xpl

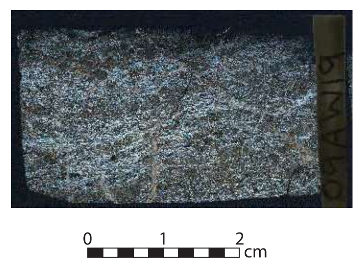

10AW19

billet

ppl

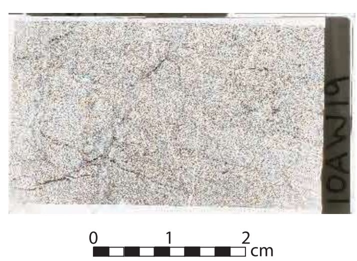

xpl

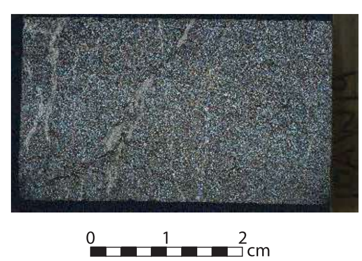

15AW19

billet

ppl

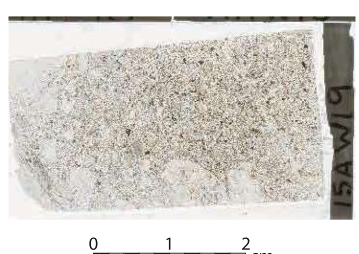

xpl

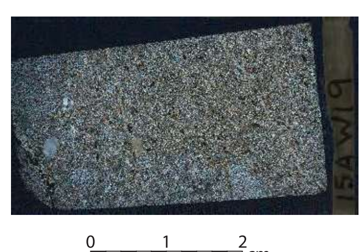

2019 sampling cont.

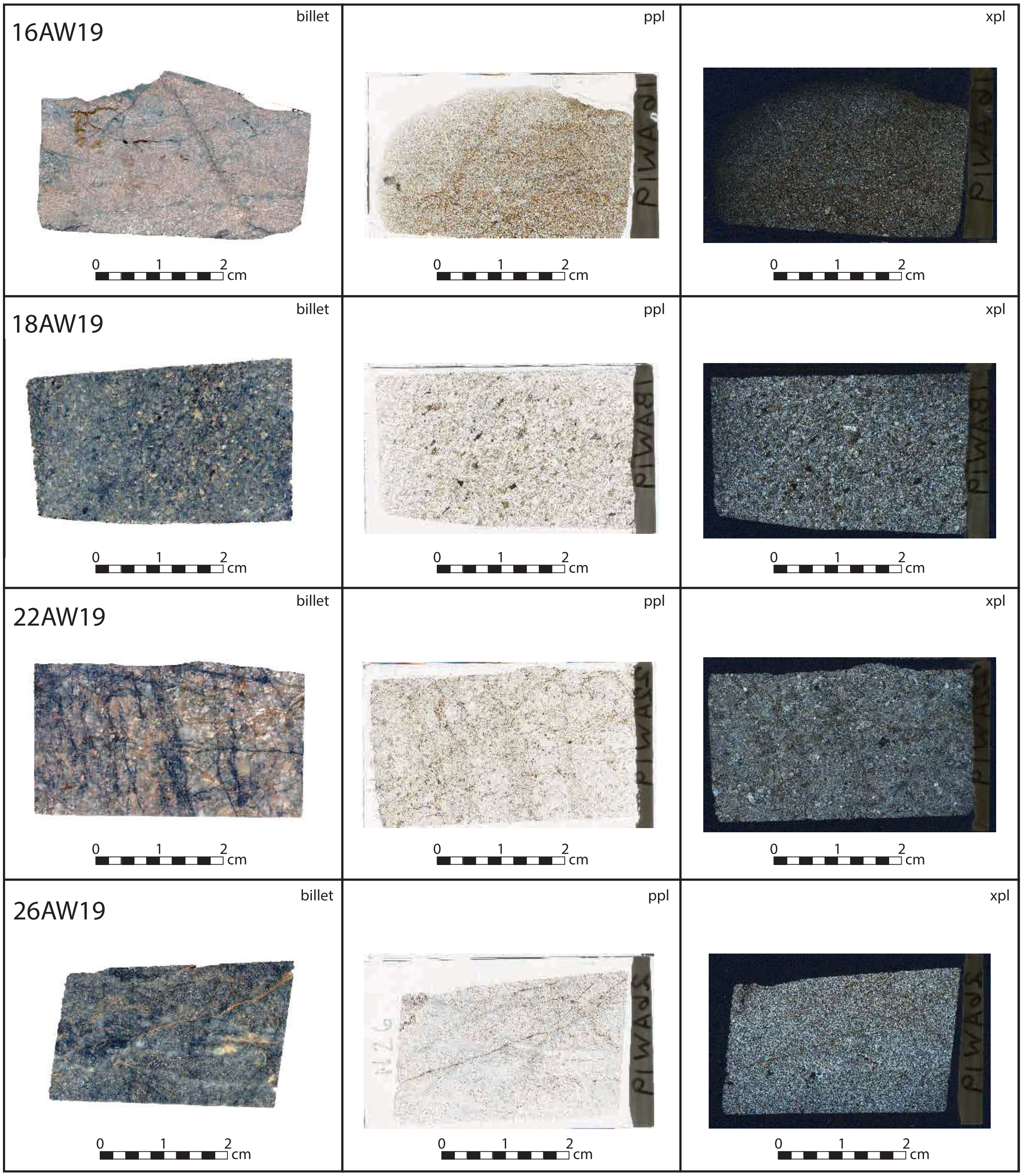

CHAPTER 2

Early Jurassic basin development and exhumation in the northern Canadian Cordillera: Detrital zircon U-Pb-Hf isotope results from the Faro Peak formation and underlying Snowcap assemblage, Yukon-Tanana terrane, central Yukon

A version of this chapter will be submitted for publication in a peer-reviewed journal

2.1 ABSTRACT

Late Triassic to Early Jurassic collisional tectonism along the Cordilleran margin resulted in the exhumation of the Intermontane terranes and generation of syn-tectonic rock assemblages in northwestern Canada. The enigmatic Faro Peak formation of central Yukon overlies pre-Late Devonian basement rocks of the Yukon-Tanana terrane (Snowcap assemblage) and records syn-tectonic deposition adjacent to the Vangorda fault, which represents the local suture with the Slide Mountain terrane. Massive sandstone and pebble to boulder conglomerate strata yield Sinemurian to Toarcian detrital zircon maximum depositional ages and indicate that the Faro Peak formation consists of Lower Jurassic debris flow units. Field stratigraphic and detrital zircon provenance results show that the Faro Peak formation was sourced from Triassic to Jurassic (220-180 Ma) intrusive rocks, Permian sedimentary and intrusive rocks of the Slide Mountain terrane, mid- to late Paleozoic (360-298 Ma) Intermontane terrane arc successions, and pre-mid-Paleozoic metasedimentary basement units assigned to the Snowcap assemblage. The Faro Peak basin is interpreted to be a local, isolated, strike-slip basin along the proto-Vangorda fault

that was separated from the coeval Whitehorse trough of southern Yukon by a ~450 km-long, northwest-trending drainage divide. Snowcap assemblage rocks that underlie and are recycled into the Faro Peak formation yield Cryogenian and older maximum depositional ages and exhibit Paleoproterozoic to Archean detrital zircon U-Pb populations and Hf isotope compositions which indicate provenance from the northwest Laurentian craton. Snowcap assemblage rocks have detrital zircon populations analogous to some Neoproterozoic to Lower Devonian strata in the northern Canadian Cordillera and strengthen original stratigraphic links between the northwestern Laurentian margin and Yukon-Tanana basement.

2.2 INTRODUCTION

The late Paleozoic to early Mesozoic growth of the North American Cordillera is in part recorded by the collapse of a marginal ocean basin (Slide Mountain) and subsequent accretion of the northern Intermontane arc terranes – Yukon-Tanana, Stikinia, and Quesnellia (Fig. 2.1) – along northwestern Pangea (Nelson et al., 2006; Colpron et al. 2006, 2007; Beranek and Mortensen, 2011). Plate convergence and arc magmatism along the composite northern Cordilleran margin was renewed by the Middle Triassic and eventually resulted in Late Triassic to Early Jurassic crustal thickening and emplacement of collision-related plutons at mid- to upper crustal depths within the Yukon-Tanana terrane, Stikinia, and Quesnellia in central Yukon (e.g., Mihalynuk et al., 1994; Johnston et al., 1996; Symons et al., 2000; McCausland et al., 2002; Colpron et al., 2015; Topham et al., 2016; Clark, 2017; Parsons et al., 2018; Bickerton et al., 2020; Sack et al., 2020). Lower Jurassic synorogenic sedimentary successions (Fig. 2.1) record the timing and stratigraphic response to known (e.g., Knight et al., 2013) and inferred (Colpron et al., 2015) syn- to post-collisional exhumation of Intermontane basement infrastructure and Late Triassic to Early Jurassic intrusive rocks in the northern Cordillera.

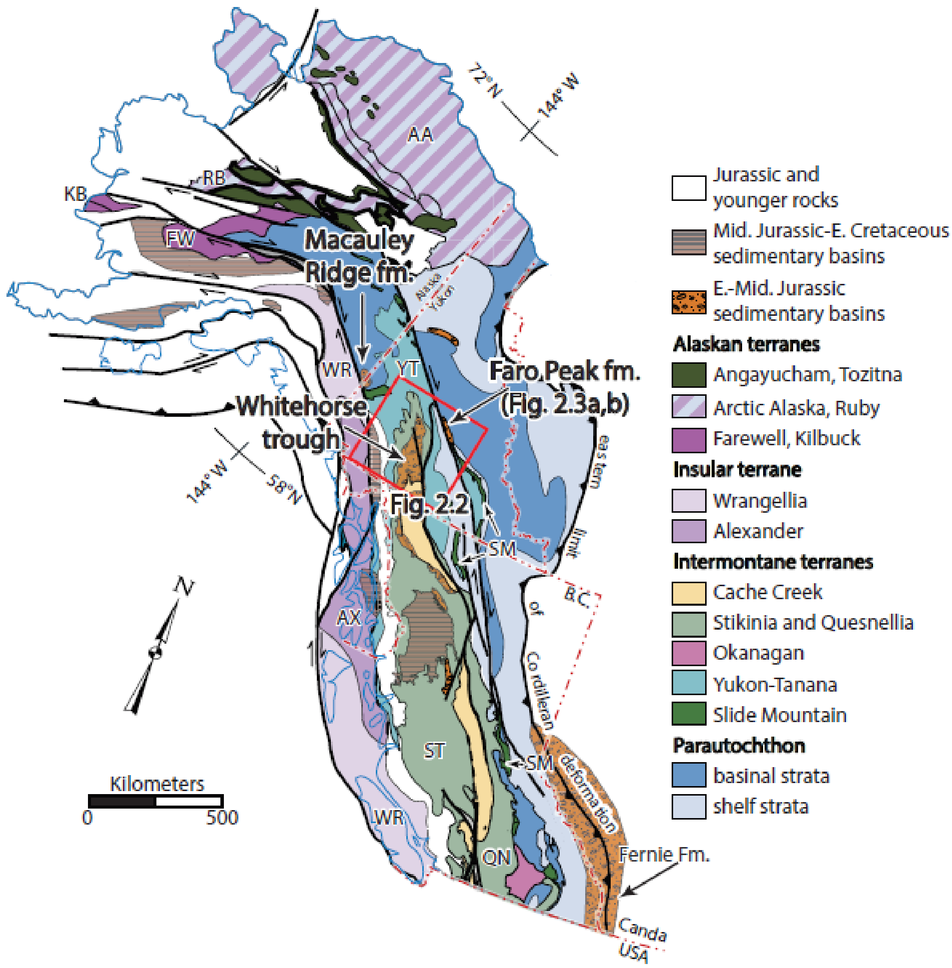

Figure 2.1 - Paleozoic to early Mesozoic terranes and Jurassic sedimentary basins of the Canadian Cordillera after Colpron et al. (2015). Terrane abbreviations: AA—Arctic Alaska; AX—Alexander; FW—Farewell; KB—Kilbuck; QN—Quesnellia; RB—Ruby; SM—Slide Mountain; ST—Stikinia; YT—Yukon-Tanana; WR—Wrangellia.

The Faro Peak formation (informal nomenclature, Pigage, 2004) unconformably overlies metasedimentary and metaigneous basement rocks of the Yukon-Tanana terrane (Snowcap assemblage) in the Faro region of central Yukon, ~200 km northeast of Whitehorse (Figs.

2.1, 2.2), and purportedly records syn-tectonic subsidence in the easternmost Intermontane realm (Colpron et al., 2015). The Faro Peak formation mostly consists of lithic sandstone and polymictic conglomerate units with felsic intrusive rock clasts that are elsewhere the hallmarks of Lower to Middle Jurassic syn-tectonic strata assigned to the Laberge Group (e.g., Dickie and Hein, 1995; Colpron et al., 2015, van Drecht, 2019) in the much larger Whitehorse trough of southern Yukon and northern British Columbia (Figs. 2.1, 2.2). Published detrital zircon U-Pb dates (2 samples, 75 grains) imply Early Jurassic depositional ages for Faro Peak formation conglomerate facies and derivation from Triassic to Jurassic plutonic rocks that flank the Whitehorse trough (Fig. 2.2) and metasedimentary rocks of the underlying Snowcap assemblage (Colpron et al., 2015), but the exact provenance and timing of basin subsidence are uncertain. It is also unclear if Faro Peak formation strata accumulated in the northern reaches of the Whitehorse trough and are correlative with the syn-tectonic Laberge Group or instead represent deposition in a coeval, but geographically isolated, fault-bounded depocenter.

In this article, we build on field stratigraphic studies of the Faro region (Wiest and Beranek, 2019; Wiest et al., 2020) and use high-*n* laser ablation split-stream (LASS) detrital zircon U-Pb geochronology and Hf isotope geochemistry methods to constrain the maximum depositional age, provenance, regional correlation, and significance of the Faro Peak formation to northern Cordilleran tectonics and paleogeography. The results establish Sinemurian to Toarcian (196 – 182 Ma) depositional ages for the Faro Peak formation and allow us to develop a new testable model for Early Jurassic strike-slip basin development in central Yukon that was coeval with, but separate from, the sinistral fault system that controlled Whitehorse trough deposition. New detrital zircon U-Pb-Hf isotope results from the underlying Snowcap assemblage strengthen the provenance reference frame for Yukon-Tanana terrane basement rocks and confirm Neoproterozoic to Devonian stratigraphic connections with the northern Cordilleran passive margin.

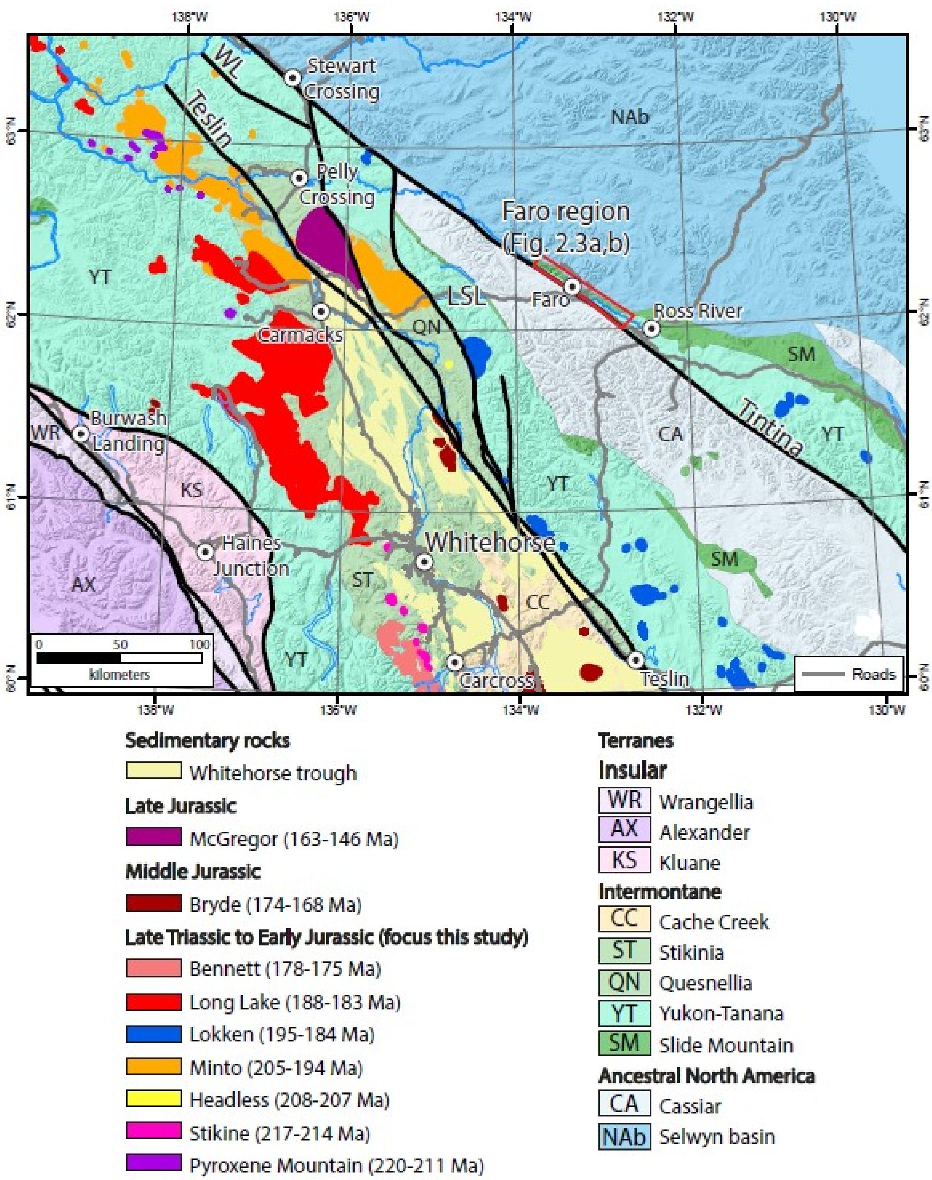

Figure 2.2 - Distribution of Late Triassic to Late Jurassic plutons in central Yukon after Sack et al. (2020). Red box outlines the focus area of this study. Abbreviations: LSL—Little Salmon Lake; WL—Willow Lake Fault.

2.3 GEOLOGICAL BACKGROUND

Late Devonian east-dipping subduction, slab rollback, and backarc extension along western Laurentia resulted in the opening of the Slide Mountain marginal ocean basin and outboard development of a pericratonic or continental margin-fringing arc chain analogous to the modern Japanese arc – Sea of Japan backarc system (e.g., Creaser et al., 1997; Colpron et al., 2007; Nelson et al., 2013). Snowcap assemblage rock units comprise the exposed basement of the Yukon-Tanana terrane and represent pre-Late Devonian rocks that were probably part of a Neoproterozoic to lower Paleozoic passive margin succession originally deposited along northwestern Laurentia (e.g., Mortensen, 1992; Colpron et al., 2006a; Piercey and Colpron, 2009). Snowcap assemblage metaigneous rocks are undated, but geochemically similar to Neoproterozoic to early Paleozoic mafic lava flows and intrusive rocks observed within the rift and passive margin successions of western Laurentia (e.g., Goodfellow et al., 1995; Campbell et al., 2019). Snowcap assemblage metasedimentary rocks generally have uncertain provenance, but one quartzite unit near Little Salmon Lake in central Yukon (LSL on Fig. 2.2) yields detrital zircon grains with ca. 1870, 2080, 2380, and 2720 Ma age peaks that indicate northwestern Laurentian craton linkages (Piercey and Colpron, 2009), including unique-aged 2100-2000 Ma rocks of the Buffalo Head and Chinchaga terranes in the Peace River Arch region of northwestern Alberta and northeastern British Columbia.

The Intermontane terranes grew as a continuous, single, west-facing arc system during the mid-Paleozoic until a polarity shift to west-dipping subduction resulted in the collapse of the Slide Mountain ocean and subsequent accretion of the Yukon-Tanana terrane and

Quesnellia to the North American margin by late Permian (Beranek and Mortensen, 2011; Golding et al., 2016) or post-Middle Triassic time (Parsons et al., 2019). Stikinia remained partially outboard as an Aleutian arc-style festoon (Mihalynuk et al. 1994) until the return of east-dipping subduction along the western margin of the Intermontane belt by the Middle Triassic. Renewed subduction ultimately resulted in strike-slip duplication of Stikinia and Quesnellia (Wernicke and Klepacki 1988; Dostal et al. 2009) or oroclinal bending and counter-clockwise rotation of Stikinia and Yukon-Tanana around the Cache Creek terrane (e.g., Mihalynuk et al. 1994, 2004) that in part formed the "hair-pin" or inverted v-shape geometry of the exposed Intermontane terranes (Figs 2.1, 2.2). Plate convergence and arc collision, required by the orocline model, led to latest Triassic to earliest Jurassic crustal thickening and greenschist to amphibolite grade metamorphism of Yukon-Tanana basement rocks in the "hinge zone" (Dusel-Bacon and Hansen 1992, Dusel-Bacon et al., 1995; Berman et al., 2007; Knight et al., 2013; Clark, 2017) and emplacement of southward-younging, syn-collisional plutons that intruded the Yukon-Tanana terrane, Stikinia, and Quesnellia.

Granodiorite, diorite, and gabbro plutons of the Pyroxene Mountain (220-211 Ma), Stikine (217-214 Ma), and Headless (208-207 Ma) suites characterize pre-collisional, Late Triassic arc magmatism in central Yukon and intrude basement units of the Yukon-Tanana terrane, Stikinia, and Quesnellia (Fig. 2.2, Table 2.1). These plutons extend along a northwest-trending belt to eastern Alaska where ca. 216-208 Ma monzodiorite, quartz diorite, leucotonalite, and granodiorite intrusions were emplaced into Mississippian to Permian Nasina and Fortymile River assemblages of the Yukon-Tanana terrane (Table 2.1). Stikine suite rocks crystallized at a depth of ~9-17 km (Sack et al., 2020) and yield whole-rock Nd-Sr isotope, zircon Hf isotope ($\varepsilon_{Hf(t)}$: +9.7 to +11.5; $\bar{X}$ = +10.5), and feldspar Pb isotope values (Sack et al., 2020) consistent with Late Triassic plutons in eastern Alaska (Table 2.1; Dusel-Bacon et al., 2015) and demonstrate minor to no crustal contamination. Late Triassic (217-204 Ma) hornblende and mica $^{40}Ar/^{39}Ar$ cooling ages of Stikine suite rocks (Sack et al., 2020) and the Taylor Mountain batholith and Kechumstuk Mountain intrusion in eastern Alaska (Cushing, 1984; Newberry et al., 1998; Werdon et al., 2001) indicate rapid cooling of these plutons following crystallization.

Faro Peak formation		Potential provenance								
Age (Ma)	εHf	Location	Source	Age (Ma)	$\varepsilon_{Nd(t)}$ (whole rock)	$\varepsilon_{Hf(t)}$ (zircon or *)	$^{207}Pb/^{204}Pb$	$^{206}Pb/^{204}Pb$	$^{87}Sr/^{86}Sr$	Reference
365-353	-13.9 to -9.6	Finlayson Lake area	Grass Lakes Grp.	365-357	-9.5	-10*	-	-	-	Piercey et al., 2003
365-353	-13.9 to -9.6	Finlayson Lake area	Simpson Range suite	357-342	-12.9	-14.6*	-	-	-	Piercey et al., 2003
365-353	-13.9 to -9.6	Finlayson Lake area	Wolverine Lake Grp.	357-342	-8.2 to -7.1	-8.2 to -6.7*	-	-	-	Piercey et al., 2003
346-286	-9.5 to +12.5	Finlayson Lake area	Klinkit Grp.	314-269	+6.7 to +7.4	+12.1 to +13.0*	-	-	-	Simard et al., 2003
271-260	-3.9 to 11.4	Finlayson Lake area	Campbell Range Fm.	274-273	+3.3 to +8.6	+7.4 to +14.7*	-	-	-	Piercey et al., 2012
271-260	-3.9 to 11.4	Dunite Peak	Gabbro (Slide Mountain)	265	+7.2 to +9.0	+12.7 to +15.2*	-	-	-	Parsons et al., 2019
271-260	-3.9 to 11.4	Stewart River	Augen granitoids	262-253	-15.3 to -2.0	-17.9 to +0.2*	-	-	-	Ruks et al., 2006
271-260	-3.9 to 11.4	Klondike region	Klondike Schist	262-253	-9.9 to -1.5	-10.5 to +0.9*	-	-	-	Metcalfe, 1981; Ruks et al., 2006
223-181	-13.1 to +12.1	central Yukon	Pyroxene Mtn. suite	220-211	-	-	-	-	-	Sack et al., 2020
223-181	-13.1 to +12.1	central Yukon	Stikine suite	217-214	+5.2 to +5.3	+9.7 to +11.5	15.59	18.75	0.704	Sack et al., 2020
223-181	-13.1 to +12.1	central Yukon	Headless suite	208-207	-	-	-	-	-	Sack et al., 2020
223-181	-13.1 to +12.1	central Yukon	Minto suite	205-194	-3.6 to +1.3	+0.5 to +10.9	15.63	18.76	0.705	Sack et al., 2020
223-181	-13.1 to +12.1	central Yukon	Lokken suite	195-184	-4.3 to -0.6	-2.9 to +9.3	15.67	19	0.705	Sack et al., 2020
223-181	-13.1 to +12.1	central Yukon	Long Lake suite	188-183	-5.9 to +1.5	-5.8 to +6.4	15.68	19.05	0.706	Sack et al., 2020
-	-	central Yukon	Bennett suite	178-175	-2.5	-	15.64	19.13	0.705	Sack et al., 2020
223-181	-13.1 to +12.1	eastern Alaska	Taylor Mountain batholith, Kechumstuk Mountain intrusion, and others	216-208	-	-	15.62	18.73	-	Dusel-Bacon et al., 2015; Foster et al., 1978; Newberry et al., 1998; Werdon et al., 2001
223-181	-13.1 to +12.1	eastern Alaska	Mount Veta intrusion, Diamond Mountain	201-181	-	-	15.66	19.06	-	Dusel-Bacon et al., 2015

* = $\varepsilon_{Nd(t)}$ converted to $\varepsilon_{Hf(t)}$ values (Vervoort et al., 1999; Vervoort and Blichert-Toft, 1999)

Table 2.1 - Summary of ages and isotopic compositions for potential source rocks for the Faro Peak formation strata. (*) indicates ε_{Nd} converted ε_{Hf} values following Vervoort et al. (1999).

Late Triassic to Early Jurassic granodiorite batholiths of the Minto suite (205-194 Ma) are exposed at the northern apex of the Whitehorse trough along the trace of the northern Teslin fault (Fig. 2.2) and were emplaced into mid- to lower crustal (~16-27 km) basement rocks of the Yukon-Tanana terrane, Quesnellia, and Stikinia during collision (McCausland et al., 2002; Tafti, 2005; Colpron et al., 2015; Sack et al., 2020). Whole-rock Nd-Sr isotope, zircon Hf isotope ($\varepsilon_{Hf(t)}$: +0.5 to +10.9; $\bar{X}$ = +3.4), and feldspar Pb isotope values are consistent with minor crustal input (Sack et al., 2020). Early Jurassic (194-182 Ma) mica

$^{40}Ar/^{39}Ar$ and Al-in-hornblende constraints on Minto suite intrusions indicate moderate to rapid exhumation rates partitioned to the west (~0.7-1.3 mm/yr) and east (~2.1-7.5 mm/yr) of the Teslin fault (Sack et al., 2020).

Early Jurassic plutons of the Long Lake (188-183 Ma) and Bennett (178-175 Ma) suites are mainly composed of granodiorite and intrude the Yukon-Tanana—Stikinia terrane. Aluminum-in-hornblende results indicate mostly mid-crustal and upper-crustal crystallization depths for the Long Lake suite (~9-23 km) and Bennett suite (~6-13 km), respectively (McCausland et al., 2002; Sack et al., 2020). Whole-rock Nd-Sr isotope, zircon Hf isotope (Long Lake, $\varepsilon_{Hf(t)}$: -5.8 to +6.4; $\bar{X}$ = -0.9), and feldspar Pb values show evidence of crustal contamination (Sack et al., 2020). Early Jurassic (189-178 Ma) mica and hornblende cooling ages (Hunt and Roddick, 1991; Sack et al., 2020) suggest exhumation rates for Long Lake suite rocks that range from ~0.5-2.8 mm/yr (Sack et al., 2020).

The Lokken suite (195-184 Ma) consists of monzonite, monzodiorite, and granodiorite units that are exposed east of the Teslin fault and intrude Permian and older units of the Yukon-Tanana terrane. Whole-rock Nd-Sr isotope, zircon Hf isotope ($\varepsilon_{Hf(t)}$: -2.9 to +9.3; $\bar{X}$ = +3.5), and feldspar Pb isotope values indicate minor crustal contamination (Sack et al., 2020). Lokken suite rocks yield Al-in-hornblende values that indicate mid- to upper crustal emplacement depths (~10-11.5 km; Sack et al,. 2020) and Early Jurassic (194-179 Ma) hornblende and mica K-Ar and ^{40}Ar-^{39}Ar cooling ages (Stevens et al., 1982; Hunt and

Roddick, 1987, 1992; Gordey et al., 1998; Joyce et al., 2015; Sack et al., 2020) that suggest rapid cooling following crystallization.

Early Jurassic (201-181 Ma) granodiorite, quartz monzonite, and granite plutons in eastern Alaska intrude the Mississippian to lower Permian Nasina and Fortymile River assemblages of the Yukon-Tanana terrane (Foster, 1992; Foster et al., 1994; Dusel-Bacon et al., 2002) and overlap in age with the Minto, Long Lake, and Lokken suites defined by Sack et al. (2020). Crustal feldspar Pb isotope values (Table 2.1; Dusel-Bacon et al., 2015) and magmatic epidote in some plutons that indicate crystallization depths >15 km (Werdon et al., 2001; Day et al., 2002; Dusel-Bacon et al., 2009) are similar to Early Jurassic plutonic suites in central Yukon (e.g., Sack et al., 2020). Early Jurassic (196-181 Ma) hornblende and mica cooling ages (Cushing, 1984, Hansen et al., 1991; Newberry et al., 1998; Szumigala et al., 2000; Dusel-Bacon et al., 2002) from these plutons and surrounding Nasina and Fortymile River assemblages imply rapid cooling after mid-crustal emplacement.

The northern Intermontane terrane infrastructure from central Yukon to eastern Alaska was exhumed to upper crustal levels by the Pliensbachian (Dusel-Bacon et al., 2002; Knight et al., 2013; Kellett et al., 2018; Sack et al., 2020). In central Yukon, structural controls on tectonic exhumation are indicated by the Early Jurassic cooling ages of the Minto suite rocks along the Teslin fault (Sack et al., 2020) and Yukon-Tanana terrane basement rocks in the footwall of the ~100 km-long, northwest-trending, low-angle Willow Lake extensional fault (WL on Fig. 2.2; Knight et al. 2013). Exhumation-related cooling in eastern Alaska was originally interpreted to indicate thrust-related uplift and erosion (Hansen and Dusel-Bacon, 1998; Dusel-Bacon et al., 1995, 2002), however, Late Triassic to Early Jurassic plutons typically have equigranular textures and cut metamorphic fabrics (e.g. Day et al., 2002) and support alternate models that involve pluton emplacement at mid-crustal depths at or near peak metamorphic conditions, and subsequent regional exhumation due to gravitational collapse and/or transtensional faulting (Berman et al., 2007; Dusel-Bacon et al., 2015).

Early Jurassic subsidence and basin-filling that resulted from rapid, widespread tectonic exhumation processes are presumably recorded by the Faro Peak formation of central Yukon, Macauley Ridge formation of western Yukon and eastern Alaska, and Laberge Group and equivalents in the Whitehorse trough of central Yukon and northern British Columbia (Fig. 2.1; e.g., Colpron et al., 2015; Kellett and Zagorevski, 2021). Sinemurian and younger Laberge Group strata mostly consist of terrestrial to marginal-marine strata of the Tanglefoot formation that transition southwards into deep-marine slope and mass-flow units of the Richthofen formation (Tempelman-Kluit, 1984, 2009; Hart, 1997; Lowey, 2004, 2008). Laberge Group conglomerate units contain clasts of siliciclastic and carbonate rocks, chert, extrusive and intrusive igneous rocks, and metamorphic rocks. Basal units tend to be dominated by volcanic and sedimentary rock clasts and younger units contain a higher proportion of intrusive rock clasts (Dickie and Hein, 1995; Hart et al., 1995; Johannson et al., 1997; Shirmohammad et al., 2011) principally derived from exhumed plutons that presently flank the Whitehorse trough (Fig. 2.2). Late Triassic to Early Jurassic (~220-180 Ma) detrital zircon grains in Laberge Group strata of southern Yukon yield $\varepsilon_{Hf(t)}$

values of -4.7 to +12.1 and confirm derivation from well-characterized plutons along the Whitehorse trough (van Drecht, 2019).

2.4 GEOLOGY OF THE FARO REGION AND STRATIGRAPHY OF THE FARO PEAK FORMATION

The Faro Peak formation crops out intermittently for ~30 km along the southwest side of the Vangorda fault, which marks the suture between the Yukon-Tanana and Slide Mountain terranes in the Faro region of central Yukon (Figs. 2.3a and b). The Intermontane terranes are separated from parautochthonous North American strata along the Inconnu thrust to the northeast and the Cassiar terrane along the Tintina fault to the southwest (Fig. 2.3b). The Tintina fault accommodated >430 km of post-Cretaceous dextral displacement (Gabrielse et al., 2006) and restoration of this fault places the Faro area near the town of Eagle, Alaska.

Snowcap assemblage rock units are exposed in the town of Faro and along the Blind Creek Road (Fig. 2.3b) and generally consist of micaceous quartzite, mica schist, and marble (Pigage, 2004). Mafic lenses in the Snowcap assemblge that were locally metamorphosed to eclogite facies have alkaline basalt, mid-ocean ridge basalt (MORB), and back-arc basin basalt (BABB) geochemical signatures (Pigage, 2004). Eclogite units yield Lu-Hf garnet and omphacite ages of 264-252 Ma and white mica ^{40}Ar-^{39}Ar cooling ages of 261-256 Ma (Erdmer et al., 1998; Philippot et al., 2001) indicating their upper-crustal position since the late Permian.

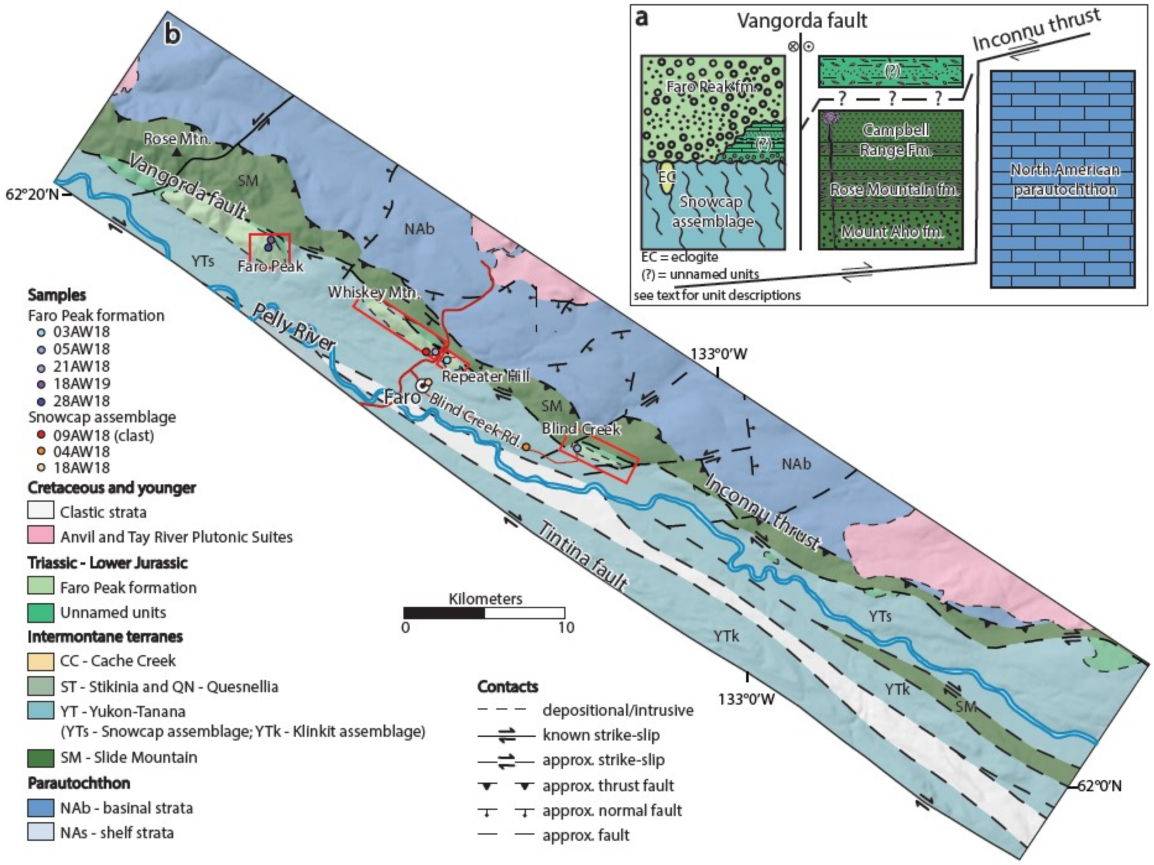

Figure 2.3 - (a) Generalized stratigraphy of the southern Tay River map area after Pigage (2004); (b) Simplified bedrock geology of the southern Tay River map area after Pigage (2004) showing the distribution of detrital zircon sample locations. Localities outlined in red discussed in the text.

Carboniferous to lower Permian rock units of the Slide Mountain terrane are up to 2300 m thick and consist of green to maroon to grey to black chert, argillite, sandstone, and conglomerate of the Mount Aho and Rose Mountain formations and green chert and basalt of the Campbell Range formation (Pigage 2004) that crop out north of the Vangorda fault. In the Finlayson Lake area, ~150 km southeast of Faro, leucogabbro and plagiogranite that intrude the Campbell Range formation yield U-Pb zircon ages of 274-273 Ma (Mortensen, 1992; Murphy et al., 2006).

The Faro Peak formation was originally assigned a Late Triassic depositional age based on Carnian to Rhaetian conodont elements from limestone beds in a fine-grained, lower member unit and limestone clasts in a coarse-grained, upper member unit (Templeman-Kluit, 1972; Pigage, 2004). The Faro Peak formation was subsequently reassigned an Early Jurassic depositional age based on the presence of 220-180 Ma detrital zircon grains in the upper member conglomerate unit (Colpron et al., 2015).

Recent field stratigraphic investigations have discovered that the lower member of the Faro Peak formation (unnamed units in Fig. 2.3a and b) sits unconformably on the Snowcap assemblage and dip towards the northwest at approximately 20-40° near Rose Mountain, ~20 km northwest of Faro (Fig. 2.3b; Wiest et al., 2020). This unconformity is defined by a quartz altered pebble to cobble conglomerate unit that contains clasts of schist, quartzite, chert, and tan volcanic rocks (Wiest et al., 2020). Above this basal conglomerate, and at several other localities in the Faro region (Faro Peak, Whiskey Mountain, Repeater Hill, and Blind Creek; Fig. 2.3b) the lower member consists of minor basalt and micaceous and calcareous argillite (Fig. 2.4a), limestone that yields Late Triassic conodonts (Fig. 2.4b; Templeman-Kluit, 1972; Pigage, 2004), and lithic to feldspathic wacke to arenite units likely deposited by turbidity flows (Wiest and Beranek, 2019). The lower member is lithologically distinct, of mappable extent, and has unconformable lower and upper contacts, and was assigned to a new unnamed unit that is likely related to Upper Triassic overlap assemblages from northern British Columbia to eastern Alaska (Wiest et al., 2020).

Figure 2.4 - Field photographs of unnamed Triassic units (Tu) and the Faro Peak formation (FPf). (a) Interbedded shale and limestone (Tu); (b) thin bedded limestone (Tu); (c) graded bedding in lithic sandstone (FPf); (d) channelized sandstone lens (FPf); (e) coarse-grained lithic feldspathic sandstone (FPf); (f) clast-supported polymictic pebble conglomerate (FPf).

The Faro Peak formation (formerly the upper member of the Faro Peak formation) tends to dip moderately to steeply to the west-southwest and unconformably overlies the Snowcap assemblage and unnamed units in the Faro area. The Faro Peak formation contains locally exposed, normal-graded basal sandstone successions (Fig. 2.4c) and >800 m of massively bedded, coarse-grained lithic sandstone (Fig. 2.4d,e) and polymictic,

Figure 2.5 - Field photographs of the Faro Peak formation. (a) Matrix-supported pebble conglomerate; (b) clast-supported cobble conglomerate; (c) limestone clast in conglomerate unit; (d) wavy laminated argillite rip-up clasts in very coarse-grained lithic arenite; (e) quartzite clast in conglomerate unit; (f) green basalt clast in conglomerate unit.

matrix- to clast-supported, granule to boulder conglomerate units (Figs. 2.4f, and 2.5a,b) that are consistent with deposition by mass sediment gravity flows (Wiest and Beranek, 2019; Wiest et al., 2020). Conglomerate clast types in the Faro Peak formation include limestone (Fig. 2.5c), sandstone, and wavy-laminated argillite (Fig. 2.5d) likely recycled from underlying unnamed strata, quartzite and quartz mica schist (Fig. 2.5e) from underlying Snowcap assemblage, and chert, basalt (Fig. 2.5f), and gabbro from the adjacent Slide Mountain terrane. Up to boulder-sized clasts of intermediate to felsic volcanic and intrusive rocks (Fig. 2.6a-d) in the Faro Peak formation have uncertain provenance, but 200-180 Ma detrital zircon grains suggest derivation from Late Triassic to Jurassic plutonic assemblages that intrude the northern Intermontane terranes (Colpron et al., 2015). Volcanic and sedimentary rock clasts dominate basal successions, whereas hypabyssal and intrusive rock clasts become more abundant upsection (Wiest et al., 2020) are similar to unroofing trends observed in Whitehorse trough units (Dickie and Hein, 1995).

Figure 2.6 - Field photographs of the conglomerate units of the Faro Peak formation. (a) Feldspar porphyry clast; (b-d) felsic intrusive rock clasts.

2.5 METHODS

Detrital zircon grains from five Faro Peak formation and three Snowcap assemblage rock samples (Table 2.2) were analyzed using the laser ablation split-stream (LASS) method at Memorial University of Newfoundland following the protocols of Fisher et al. (2014) and Beranek et al. (2020). Polished epoxy mounts were imaged with backscatter electron (BSE) and cathodoluminesence (CL) techniques using a JEOL JSM 7100F field emission scanning electron microscope (SEM) to determine grain areas with complex zoning, fractures, and inherited cores. A GeoLas 193 nm excimer laser was used to ablate a 40 µm spot with a frequency of 10 Hz and fluence of 5 J/cm^2. Uranium-Pb isotope ratios were acquired using a ThermoFinnigan Element XR single-collector ICP-MS (inductively coupled plasma mass spectrometer) and Hf isotope ratios were simultaneously collected from the same ablated material with a ThermoFinnigan Neptune multi-collector ICP-MS.

Samples						MDA						
Sample ID	Easting	Northing	Formation	Locality	Description	YSP	error	MSWD	YSC	error	YPA	ICS chart
05AW18	594793	6896814	Faro Peak fm.	Blind Creek	coarse-grained sandstone	183	0.6	1.03	182	3	194	Pliensbachian-Toarcian
03AW18	587139	6902122	Faro Peak fm.	Repeater Hill	medium- to coarse-grained sandstone	189	0.4	0.98	182	4	198	Pliensbachian-Toarcian
21AW18	586462	6902531	Faro Peak fm.	Whiskey Mtn.	medium-grained to pebble sandstone	184	0.4	1.07	183	3	190	Pliensbachian-Toarcian
18AW19	576900	6909232	Faro Peak fm.	Faro Peak	medium- to coarse-grained sandstone	187	0.9	1.48	186	3	201	Pliensbachian
28AW18	576677	6908762	Faro Peak fm.	Faro Peak	medium-grained to pebble sandstone	196	0.2	0.99	192	3	200	Sinemurian -Pliensbachian
09AW18	585839	6902482	Snowcap assemblage (clast)	Whiskey Mtn.	dark grey quartzite	719	3	2	719	3	718	Cryogenian
04AW18	591960	6896800	Snowcap assemblage	Blind Creek Rd.	quartz mica schist	1797	3	0.92	1739	72	1808	Statherian
18AW18	586129	6901021	Snowcap assemblage	Faro township	quartz mica schist	1806	4	1.2	1795	31	1863	Orosirian-Statherian

YSP youngest statistical peak (Coutts et al., 2019)
YSC youngest single cluster (Dickinson and Gehrels, 2009)
YPA youngest peak age (Arizona Laserchron "AgePick")

Table 2.2 - Summary of lithology, sample location, and maximum depositional ages for the Faro Peak formation and Snowcap assemblage samples.

U-Pb ages were calibrated to the 91500 zircon reference material (1062.4 ± 1.3 Ma, Wiedenbeck et al., 1995) and yielded a weighted mean $^{206}Pb/^{238}U$ age of 1062.7 ± 0.4 Ma (n = 282; Appendix 2.A.1). Hf isotope ratios were compared to the Plešovice zircon reference material (0.282482 ± 0.000013, Sláma et al. 2008) and yielded a weighted mean $^{176}Hf/^{177}Hf$ ratio of 0.282482 ± 0.000002 (n = 276; Appendix 2.A.1). Data were reduced offline using Iolite 1.4 software (Paton et al., 2011) and U-Pb ages were calculated using the VizualAge data reduction scheme (Petrus and Kamber, 2012). “Best Ages” were determined for each analysis with $^{207}Pb/^{206}Pb$ and $^{206}Pb/^{238}U$ ages preferred for >1000 Ma and <1000 Ma grains, respectively (Appendix 2.A.2). Initial $^{176}Hf/^{177}Hf$ ratios are reported in epsilon notation as $\varepsilon_{Hf(t)}$ and age-corrected based on the “Best Age” (Appendix 2.A.2). Concordance was calculated using the ratio of $^{207}Pb/^{206}Pb$ and $^{206}Pb/^{238}U$ ages for grains >1000 Ma. Analyses with >10% discordance and >5% reverse discordance are reported (Appendix 2.A.2), but not used for interpretation. Paleozoic and younger (<500 Ma) zircon grains were assessed on a grain-by-grain basis in VizualAge using the $^{206}Pb/^{207}Pb$, $^{207}Pb/^{235}U$, and $^{206}Pb/^{238}U$ ages.

Three techniques were used to estimate maximum depositional ages (MDAs): (1) the youngest statistical peak (YSP) method, which takes a weighted mean of the youngest population of two or more grains that yield a MSWD ≈ 1 (Coutts et al., 2019); (2) youngest cluster at two sigma (YSC) method, which takes the weighted mean of the youngest three or more grains that overlap at 2σ (Dickinson and Gehrels, 2009); and (3) youngest graphical peak (YPP) method, which is given for the youngest peak age of a probability density plot (Dickinson and Gehrels, 2009) and was determined with the “AgePick” Excel macro program from the Arizona Laserchron Center (https://sites.google.com /laserchron.org/arizonalaserchroncenter/home).

2.6 RESULTS

2.6.1 Snowcap assemblage

Quartz mica schist collected in the town of Faro (sample 18AW18; Fig. 2.3b) yields Paleoproterozoic to Mesoarchean detrital zircon grains with age peaks of 1808 (*n* = 28), 1872 (*n* = 37), 2011 (*n* = 20), 2124 (*n* = 9), 2329 (*n* = 14), and 2495 (*n* = 6) and 2629 (*n* = 22) Ma (Fig. 2.7). Paleoproterozoic zircon grains (73%) have $\varepsilon_{Hf(t)}$ values that range from -11.3 to +5.6 ($\bar{X}$ = -2.7). Archean grains (27%) yield $\varepsilon_{Hf(t)}$ values that range from -8.6 to +4.5 ($\bar{X}$ = +1.4).

Quartz mica schist collected along Blind Creek Road, ~8 km southeast of Faro (sample 04AW18; Fig. 2.3b), yields Neoproterozoic to Neoarchean detrital zircon grains with age peaks of 1863 (*n* = 44), 1925 (*n* = 49), 1997 (*n* = 42), 2103 (*n* = 30), 2310 (*n* = 17), 2457 (*n* = 6), 2551 (*n* = 10), 2612 (*n* = 12), and 2667 (*n* = 9) Ma (Fig. 2.7). Paleoproterozoic zircon grains (86%) have $\varepsilon_{Hf(t)}$ values that range from -8.2 to +6 ($\bar{X}$ = -1.6). Archean grains (13%) yield $\varepsilon_{Hf(t)}$ values of -10.5 to +6.2 ($\bar{X}$ = +1.0). Neoproterozoic (735 ± 22 Ma) and Mesoproterozoic (1494 ± 39 Ma) single grains yield $\varepsilon_{Hf(t)}$ values of -2.4 and +0.7, respectively.

A sub-rounded, cobble-sized clast of grey, medium-grained quartzite collected at the base of the Faro Peak formation, ~2 km northwest of Faro (sample 09AW18; Fig. 2.3b), yielded Neoproterozoic to Paleoarchean detrital zircon grains with age peaks of 718 (*n* = 4), 742 (*n* = 6), 1866 (*n* = 54), 1932 (*n* = 55), 2091 (*n* = 19), 2305 (*n* = 9), 2397 (*n* = 3), 2505 (*n* = 4), 2609 (*n* = 13), and 2693 (*n* = 5) Ma (Fig. 2.7). Neoproterozoic grains (5%) yield $\varepsilon_{Hf(t)}$

values -1.1 to +2.3 ($\bar{X}$ = +0.9). Paleoproterozoic zircon grains (77%) have $\varepsilon_{Hf(t)}$ values that range from -17.6 to +10.8 ($\bar{X}$ = -3.5). Archean grains (18%) yield $\varepsilon_{Hf(t)}$ values of -6.9 to +5.9 ($\bar{X}$ = -0.6). Mesoproterozoic single-grain ages of 1387 ± 37 Ma and 1498 ± 49 Ma yield $\varepsilon_{Hf(t)}$ values of +6.2 and +1.5, respectively.

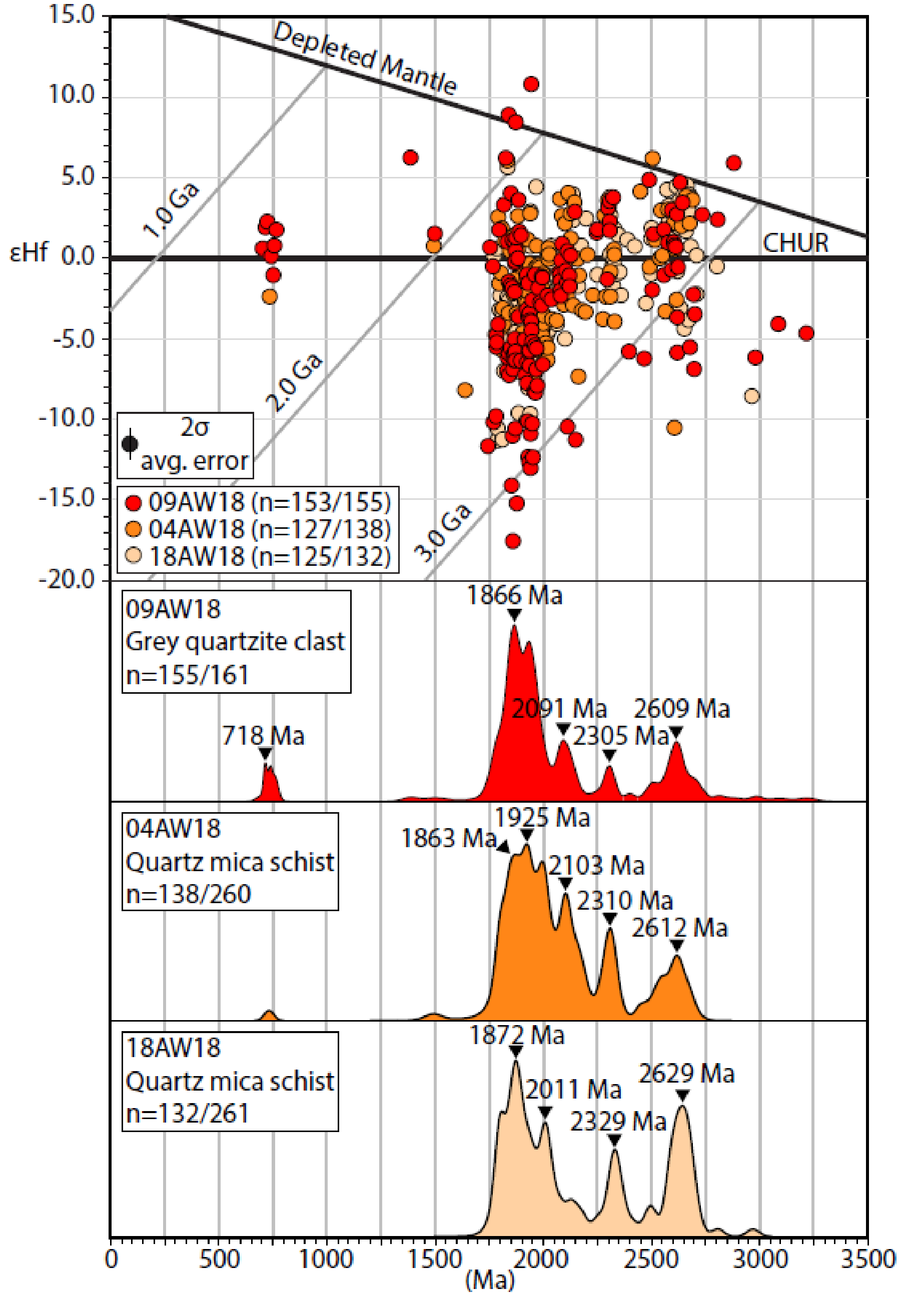

Figure 2.7 - Detrital zircon probability density U-Pb age plots versus $\varepsilon_{Hf(t)}$ values for the Snowcap assemblage.

Table 2.2 shows the maximum depositional age calculations for Snowcap assemblage samples. The YPP method consistently returned MDA estimations that were broadly consistent with, but generally older than, those of the YSP and YSC methods. The Snowcap assemblage quartzite clast in the basal Faro Peak formation (sample 09AW18) has a Cryogenian (719 ± 3 Ma) MDA using the YSP and YSC methods. Two quartz mica schist units near Faro yielded late Paleoproterozoic (ca. 1800 Ma) MDAs; however, sample 04AW18 yielded a single Tonian (735 ± 22 Ma) zircon grain, and, in combination with the quartzite clast results, are consistent with a Neoproterozoic or younger depositional age.

2.6.2 Faro Peak formation

Medium-grained to pebbly lithic arenite collected at Faro Peak, ~12 km northwest of Faro (sample 28AW18; Fig. 2.3b), yields Late Triassic to Early Jurassic zircon grains (78%) with a peak age of 200 (n = 98) Ma (Fig. 2.8a,b). Late Triassic to Early Jurassic grains have $\varepsilon_{Hf(t)}$ values of -11.3 to +11.5 ($\bar{X}$ = +2.8) with a general trend towards more subchondritic compositions with decreasing age. Carboniferous grains (10%) with peak ages of 315 (n = 7), 335 (n = 4), and 356 (n = 3) Ma give $\varepsilon_{Hf(t)}$ values that range from -10.6 to +11.2 ($\bar{X}$ = +3.7) and exhibit a trend towards superchondritic compositions with decreasing age. Proterozoic to Archean grains (11%) with peak ages of 1799 (n = 4), 1875 (n = 6), 2002 (n = 3), and 2614 (n = 3) Ma have $\varepsilon_{Hf(t)}$ values of -10.8 to +3.3 ($\bar{X}$ = -1.5) (Fig. 2.8b). Permian single grains of 288 ± 5 Ma and 271 ± 3 Ma age yield $\varepsilon_{Hf(t)}$ values of +4.8 to -0.5, respectively. A single Mesoproterozoic (1418 ± 21 Ma) grain gives an $\varepsilon_{Hf(t)}$ value of +6.1.

Medium to coarse-grained feldspathic lithic arenite collected at Faro Peak, ~12 km northwest of Faro (sample 18AW19; Fig 2.34b) yields Late Triassic to Early Jurassic zircon grains (85%) with a peak age of 201 (*n* = 76) Ma (Fig. 2.8a,b). Late Triassic to Early Jurassic grains have $\varepsilon_{Hf(t)}$ values that range from -8.4 to +11.0 ($\bar{X}$ = +2.6). Carboniferous grains (6%) with a peak age of 321 (*n* = 5) Ma yield $\varepsilon_{Hf(t)}$ values of -0.7 to +8.8 ($\bar{X}$ = +2.6). A single Middle Triassic grain of 240 ± 4 Ma age has an $\varepsilon_{Hf(t)}$ value of +1.8. Permian single grains of 260 ± 4, 268 ± 3, and 293 ± 6 Ma age give $\varepsilon_{Hf(t)}$ values of +9.8, +10.4, and +5.5, respectively. Paleozoic grains of 368 ± 6 Ma and 395 ± 6 Ma yield $\varepsilon_{Hf(t)}$ values of -8.8 and +4.0, respectively. One Neoproterozoic (688 ± 21 Ma) grain has an $\varepsilon_{Hf(t)}$ value of +8.0 and four Paleoproterozoic (2285-1835 Ma) grains give $\varepsilon_{Hf(t)}$ values of -4.8 to -5.4 ($\bar{X}$ = -4.0).

Medium to coarse-grained feldspathic arenite collected at Repeater Hill, ~2 km north of Faro (sample 03AW18; Fig. 2.3b), yields Late Triassic to Early Jurassic zircon grains (84%) with a peak ages of 198 (*n* = 92) and 217 (*n* = 14) Ma (Fig. 2.8a,b). Late Triassic to Early Jurassic grains have $\varepsilon_{Hf(t)}$ values that range from -6.2 to +12.1 ($\bar{X}$ = +3.0) and generally show increasing subchondritic compositions with decreasing age. Carboniferous grains (8%) with peak ages of 324 (*n* = 8) Ma and 341 (*n* = 5) Ma yield $\varepsilon_{Hf(t)}$ values of -15.9 to +12.5 ($\bar{X}$ = +4.7). Paleozoic single grains and age groups of 286-264, 365 ± 5, and 424 ± 5 Ma give $\varepsilon_{Hf(t)}$ values of -6.9 to +9.6 ($\bar{X}$ = -0.4), -13.9, and +9.8, respectively. Five Mesoproterozoic (1374-942 Ma) grains give $\varepsilon_{Hf(t)}$ values that range from -12.8 to +4.9 ($\bar{X}$ = +0.4) and a single Paleoproterozoic (1875 ± 17 Ma) grain has an $\varepsilon_{Hf(t)}$ value of -2.6.

Medium-grained to pebbly lithic feldspathic arenite collected at Whiskey Mountain, ~2 km north of Faro (sample 21AW18; Fig. 2.3b), yields Late Triassic to Early Jurassic zircon grains (89%) with a peak age of 190 (n = 101) Ma (Fig. 2.8a,b). Late Triassic to Early Jurassic grains have $\varepsilon_{Hf(t)}$ values of -6.0 to +11.2 ($\bar{X}$ = +2.8) with a trend towards more subchondritic compositions with decreasing age. Carboniferous grains (7%) with peak ages of 303 (n = 6), 322 (n = 8), and 337 (n = 3) Ma yield $\varepsilon_{Hf(t)}$ values of -0.7 to +10.9 ($\bar{X}$ = +5.4) and exhibit a trend towards superchondritic compositions with decreasing age. Single Middle Triassic (240 ± 4 Ma) and Permian (298 ± 4 Ma, 262 ± 5 Ma) grains give $\varepsilon_{Hf(t)}$ values of +2.2, +3.8, and +11.4, respectively. Single Mesoproterozoic (1124 ± 70 Ma, 1453 ± 4.5 Ma) and Paleoproterozoic (1650 ± 49 Ma, 1654 ± 60 Ma) grains yield $\varepsilon_{Hf(t)}$ values of +6.3, +4.5, +4.4, and +3.5, respectively.

Coarse-grained lithic arenite collected along Blind Creek, ~10 km southeast of Faro (sample 05AW18; Fig. 2.3b), yields Late Triassic to Early Jurassic zircon grains (82%) with a peak age of 194 (n = 95) Ma (Fig. 2.8a,b). Late Triassic to Early Jurassic grains have $\varepsilon_{Hf(t)}$ values of -13.1 to +10.4 ($\bar{X}$ = +2.7). Carboniferous grains (4%) with a peak age of 323 (n = 5) Ma give $\varepsilon_{Hf(t)}$ values of -9.5 to +10.8 ($\bar{X}$ = +1.8). Proterozoic grains (9%) give peak ages of 1487 (n = 4), 1748 (n = 7), 1811 (n = 8), and 1995 (n = 6) Ma have $\varepsilon_{Hf(t)}$ values of -17.0 to +7.3 ($\bar{X}$ = -2.3) (Fig. 2.8b). Single Early Triassic (248 ± 4 Ma) and Permian (263 ± 7 Ma) grains yield $\varepsilon_{Hf(t)}$ values of +6.3 and +11.0, respectively. Proterozoic single grains (670 ± 5, 1157 ± 35, 2273 ± 22, and 2477 ± 115 Ma) give $\varepsilon_{Hf(t)}$ values of -4.0, +2.4, +4.4 and +10.3, respectively. Two Archean (2557 ± 23 Ma, 2719 ± 21 Ma) grains yield $\varepsilon_{Hf(t)}$ values of -3.2 and +0.1, respectively.

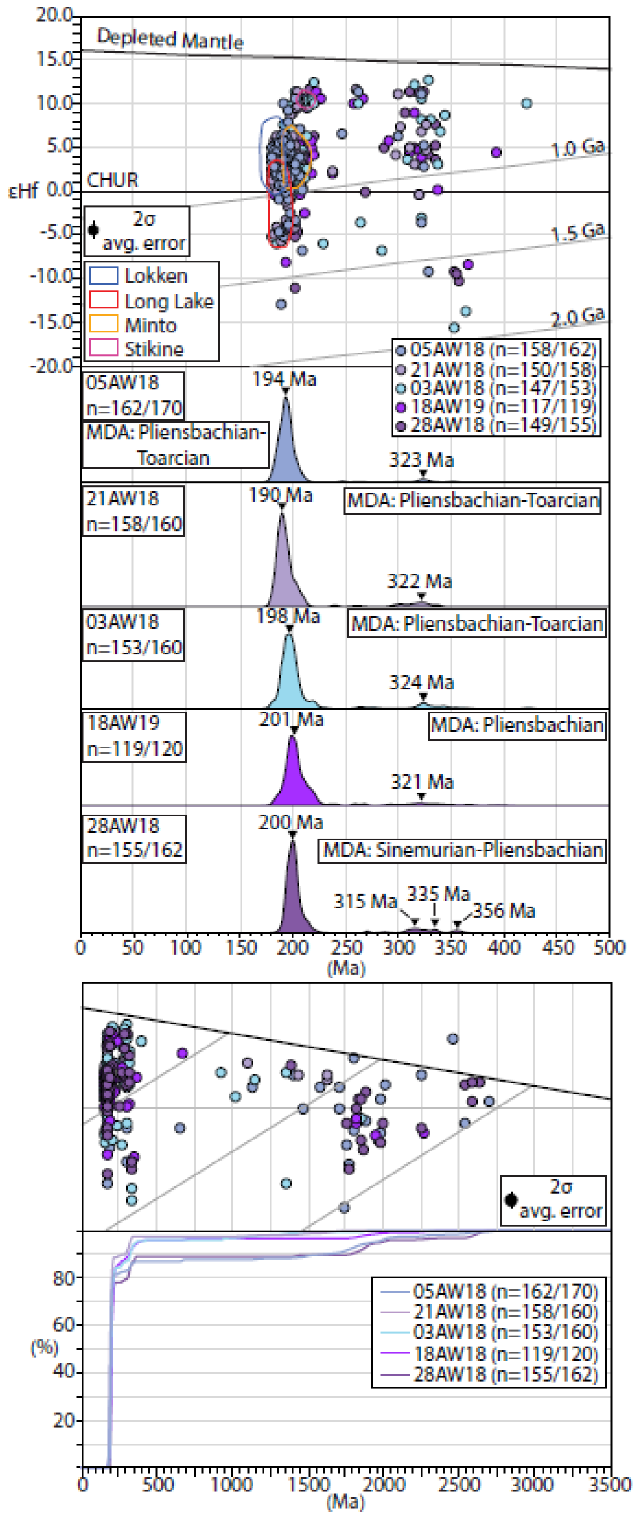

Figure 2.8 - (below) Detrital zircon cumulative distribution U-Pb age plots versus $\varepsilon_{Hf(t)}$ values showing distribution of Precambrian grains and (above) detrital zircon probability density U-Pb age plots versus $\varepsilon_{Hf(t)}$ values focused on Phanerozoic grains from the Faro Peak formation.

Table 2.2 shows the maximum depositional age calculations for Faro Peak formation samples. The YSP and YSC methods return MDA estimations that are generally similar within 1-7 Myr and the YPP age is consistently older. Medium-grained to pebbly lithic to feldspathic lithic arenite units from Faro Peak (samples 28AW18 and 18AW19) returned Sinemurian to Pliensbachian MDA estimations, which are the oldest in the sample suite. Units of similar lithology from the Repeater Hill, Blind Creek, and Whiskey Mountain localities yielded Pliensbachian to Toarcian MDA estimations.

2.7 DETRITAL ZIRCON PROVENANCE INTERPRETATION

2.7.1 Snowcap assemblage

New detrital zircon U-Pb-Hf isotope results from Snowcap assemblage micaceous quartzite and quartz mica schist units provide opportunities to assess sediment provenance and test pre-Late Devonian linkages with the Laurentian craton. Snowcap assemblage units of the Faro region are dominated by polycyclic Paleoproterozoic (73-86%) detrital zircon grains with subsidiary Archean (13-27%) and Neoproterozoic (0-5%) age populations. The Snowcap assemblage has an abundance of grains that are >1000 Myr older than the interpreted depositional age and indicate long-term sediment recycling along a passive margin (e.g., Cawood et al., 2012).

Archean grains (2881-2500 Ma) overlap in age with Laurentian sources including the Slave, Rae, Hearne, Wyoming, and Superior provinces (Table 2.3). Archean detrital zircon grains yield a mean $\varepsilon_{Hf(t)}$ value of +1.0 ($1\sigma = 3.1$, range: -10.5 to +6.2, $n = 68/72$) that suggests near-chondritic melt compositions.

Age populations	Snowcap detrital zircon ages	Snowcap detrital zircon $\varepsilon_{Hf(t)}$	Primary Source
Archean			
>2500 Ma	2881-2500 Ma	-10.5 to +6.2	Slave, Rae, Herne, Wyoming, and Superior provinces
Paleoproterozoic			
2500-1600 Ma	2396-1980 Ma	-10.5 to +4.0	Thorsby, Buffalo Head, and Chinchaga
	1950-1840 Ma	-17.6 to +10.8	Taltson, Ksituan, Kiskatinaw, Great Bear, Hottah, Nova, and Fort Simpston terranes and arc terranes of the Trans-Hudson orogen (*and younger units in the Thorsby, Buffalo Head, and Chinchaga terranes*)
Neoproterozoic			
1000-541 Ma	767-703 Ma	-2.4 to +2.3	Gunbarrel magmatic event and Franklinian large igneous province, and undated mafic igneous rocks interbedded with Snowcap assemblage

Table 2.3 - Summary of primary source regions for the Snowcap assemblage units.

Paleoproterozoic grains form a dominant peak age of ca. 1930-1860 Ma and subsidiary peak ages of ca. 2100-2000 and 2300 Ma, respectively. The older populations (2396-2205 Ma) yield a mean $\varepsilon_{Hf(t)}$ value of +0.1 (1σ = 2.3, range: -5.8 to +3.8, *n* = 35/38) and are potentially derived from the Wabamun, Buffalo Head, and Chinchaga terranes of the Peace River Arch region of northwestern Alberta and northeastern British Columbia (Table 2.3) (e.g., Ross, 1990). Younger grains (1950-1840 Ma) give variable $\varepsilon_{Hf(t)}$ values ($\bar{X}$ = -3.7, 1σ = 4.6, range: -17.6 to +10.8, *n* = 118/123) consistent with influence from the older Archean crust of the Canadian Shield (Gehrels and Pecha, 2014) and are likely derived from orogenic belts along the Coronation margin (e.g., Hoffman, 1989) including the Taltson, Great Bear, Hottah, Nova, and Fort Simpson terranes (Table 2.3) and juvenile arc rocks accreted during the Trans-Hudson orogen (e.g., Corrigan et al., 2009).

Neoproterozoic (767-703 Ma) detrital zircon grains yield near-chondritic $\varepsilon_{Hf(t)}$ values of -2.4 to +2.3 ($\bar{X}$ = +0.9, 1σ = 1.5, *n* = 8/8). Late Tonian to earliest Cryogenian igneous rocks along the northwestern Laurentian margin, including those that comprise the ca. 780 Ma and 720 Ma Gunbarrel and Franklinian events, respectively, potentially sourced these Neoproterozoic grains (Table 2.3). Mafic igneous rocks interbedded with the Snowcap assemblage in central Yukon are a potential local source, however, they have an unconstrained age and yield superchondritic whole-rock Hf isotope values (Piercey and Colpron, 2009).

2.7.2 Faro Peak formation

Polymictic conglomerate and lithic arenite units of the Faro Peak formation contain clasts of limestone, sandstone, chert, gabbro, basalt, and intermediate to felsic volcanic and intrusive rocks that suggest provenance from the underlying Snowcap assemblage basement, adjacent Slide Mountain terrane, and Triassic to Jurassic igneous suites of Yukon-Tanana terrane, Stikinia, and Quesnellia. Detrital zircon U-Pb age results demonstrate that Faro Peak formation strata are mostly composed of Late Triassic to Early Jurassic (~70-90%) detrital zircon grains that likely correspond to the intermediate to felsic volcanic and intrusive rock clasts and subsidiary populations of Carboniferous (~4-10%), Permian (~1-3%), and Precambrian (~3-13%) components. The abundance of detrital zircon ages presumably near the depositional age is characteristic of convergent margins with ongoing magmatism and deformation (Cawood et al., 2012).

Precambrian (2719-1728 Ma) detrital zircon grains (Fig. 2.8b) are ultimately derived from Archean provinces (e.g. Slave, Superior, Hearne, Rae, and Wyoming) and Proterozoic terranes (e.g. Buffalo Head, Hottah, Wopmay, Great Bear, and Fort Simpson) of the Laurentian craton. The U-Pb-Hf isotope signatures of these grains match those of the underlying Snowcap assemblage and combined with ubiquitous quartzite and quartz mica schist clasts in the Faro Peak formation, confirm that Yukon-Tanana basement was recycled into the Faro Peak basin during the Sinemurian to Toarcian. The presence of 1654-942 Ma zircon grains in Faro Peak formation units also supports recycling of Upper Devonian and younger units that cover the Intermontane terranes and adjacent regions (e.g., Beranek et al., 2010a, 2010b; Beranek and Mortensen, 2011).

Late Devonian to Early Mississippian (365-353 Ma) grains are consistent with provenance from Yukon-Tanana felsic rock units in central Yukon (Table 2.1). A composite peak age of 355 Ma from all Faro Peak formation detrital zircon grains (this study) yields an $\varepsilon_{Hf(t)}$ mean value of -11.9 ($1\sigma = 2.5$, range: -13.9 to -9.6, $n = 5/6$) and is comparable in age to crustally contaminated felsic rocks of the Grass Lakes group, Simpson Range plutonic suite, and Wolverine Lake group in central and southeastern Yukon (Piercey et al. 2003, 2006). Published $\varepsilon_{Nd(t)}$ values for these rock units converted to $\varepsilon_{Hf(t)}$ values (Vervoort et al., 1999; Vervoort and Blichert-Toft, 1999) range from -14.6 to -6.7 (Grass Lakes group: -10.0, Simpson Range plutonic suite: -14.6, Wolverine Lake group: $\bar{X} = -7.6$, $1\sigma = 0.5$), consistent with the subchondritic compositions of Late Devonian to Mississippian detrital zircon grains in the Faro Peak formation (Table 2.1, Fig. 2.8a).

Carboniferous to early Permian (346-286 Ma) grains mostly yield superchondritic $\varepsilon_{Hf(t)}$ values ($\bar{X} = +5.1$, $1\sigma = 4.7$, range: -9.5 to +12.5, $n = 47/50$) that suggest provenance from the late Paleozoic juvenile arc infrastructure of Stikinia (Takhini assemblage), Quesnellia

(Boswell assemblage), and Yukon-Tanana (Klinkit assemblage) in central Yukon (Table 2.4, Fig. 2.8a; e.g., Simard et al., 2003; Colpron et al., 2006b).

Mid-Permian (271-260 Ma) grains have subchondritic ($\bar{X}$ = -2.2, 1σ = 1.7, range: -3.9 to -0.5, *n* = 2/2) and superchondritic ($\bar{X}$ = +10.5, 1σ = 0.7, range: +9.6 to +11.4, *n* = 5/5) $\varepsilon_{Hf(t)}$ values derived from separate sources including rocks of the Slide Mountain terrane and Klondike assemblage of the Yukon-Tanana terrane. Gabbro units in suprasubduction zone ophiolite sequences assigned to the Slide Mountain terrane are ca. 265 Ma in central Yukon and yield converted $\varepsilon_{Hf(t)}$ values of +12.7 to +15.2 (van Staal et al., 2018; Parsons et al., 2019). In the Finlayson Lake area, ca. 274-273 Ma plagiogranite and gabbro intrusions (Mortensen 1992; Murphy et al. 2006) are comagmatic with Campbell Range formation basalt units that yield converted $\varepsilon_{Hf(t)}$ values of +7.4 to +15.1, consistent with the character of some Permian detrital zircon grains in the Faro Peak formation (Table 2.1, Fig. 2.8a). Subchondritic ca. 271 Ma and 266 Ma zircon grains are consistent with the petrogenesis of 262 Ma and younger Klondike assemblage rocks of the Yukon-Tanana terrane (Table 2.1; Metcalfe, 1981; Mortensen, 1990; Ruks et al., 2006; Beranek and Mortensen, 2011).

Late Triassic (229-206 Ma), Late Triassic to Early Jurassic (205-195 Ma), and Early Jurassic (194-181 Ma) grains yield mean $\varepsilon_{Hf(t)}$ values of +4.9 (1σ = 3.8, range: -7.2 to +12.1, *n* = 81/84), +2.5 (1σ = 2.6, range: -11.3 to +11.0, *n* = 308/318), and +2.4 (1σ = 2.8, range: -13.1 to +9.7, *n* = 214/220), respectively. Late Triassic to Early Jurassic plutons emplaced into the Yukon-Tanana terrane, Stikinia, and Quesnellia crop out along the flanks of the Whitehorse trough and extend northwest ~450 km into eastern Alaska. These suites overlap in age with ca. 220-180 Ma detrital zircon grains in the Faro Peak formation and combined with detrital zircon Hf isotope values indicate provenance linkages to the Stikine, Minto, Long Lake, and Lokken plutonic suites and their presumed equivalents in eastern Alaska (Sack et al., 2020; Table 2.1, Fig. 2.8). The up-to-boulder size clasts of intermediate to felsic rocks in the Faro Peak formation favor proximal sources for most Late Triassic to Early Jurassic detrital zircon grains and were likely sourced from plutons in eastern Alaska and the Finlayson Lake area based on the pre-Cretaceous location of the Faro region prior to dextral displacement along the Tintina fault.

2.8 DISCUSSION

2.8.1 Pre-Late Devonian links between the Snowcap assemblage and western Laurentian margin

New and published detrital zircon U-Pb and Hf isotope results from Snowcap assemblage metaclastic rock units provide opportunities to test ancient stratigraphic correlations between Yukon-Tanana basement and parautochthonous to autochthonous rocks of western North America. Snowcap assemblage rock units from the Little Salmon Lake (Fig. 2.2; Piercey and Colpron, 2009) and Faro (this study) areas of central Yukon are generally consistent and together yield a composite detrital zircon signature with ca. 719, 1870, 2100, 2300, and 2600 Ma age peaks (Fig. 2.9).

The comparison of large detrital zircon U-Pb datasets from the Snowcap assemblage and greater Cordilleran margin succession can be accomplished using multidimensional scaling (MDS) techniques (Vermeesch, 2013; Vermeesch and Garzanti, 2015). Detrital zircon samples with similar cumulative probability profiles using the Kolomogorov-Smirnov test cluster closely together in x-y space, whereas samples with dissimilar profiles will be separated in x-y space.

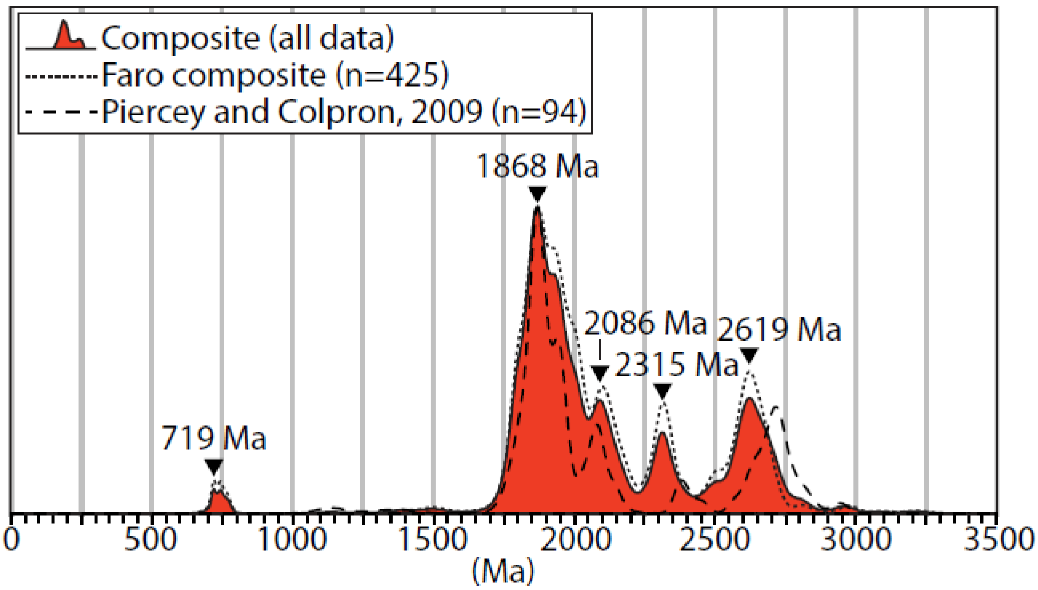

Figure 2.9 - Detrital zircon probability density U-Pb age plot comparing the Snowcap assemblage samples (this study) and Piercey and Colpron (2009).

Paleoproterozoic to Upper Devonian continental margin strata from the western U.S., Canadian, and Alaskan Cordillera show two distinct clusters on an MDS plot (Fig. 2.10). Neoproterozoic to Cambrian-Ordovician strata from central Yukon that plot in the far right contain ca. 1300-1000 Ma grains with Grenville orogen provenance (Rainbird et al., 1992, 2012) and lack ca. 2400-2000 Ma grains characteristic of the Snowcap assemblage and northwestern Laurentia (Fig. 2.10). Neoproterozoic to Cambrian strata from southern and central British Columbia plot in the lower left and similarly lack ca. 2400-2000 Ma grains, however, these rock units contain ca. 1800 Ma grains that comprise the dominant age peak in the Snowcap assemblage, hence their proximity to Yukon-Tanana basement on the MDS plot (Fig. 2.10).

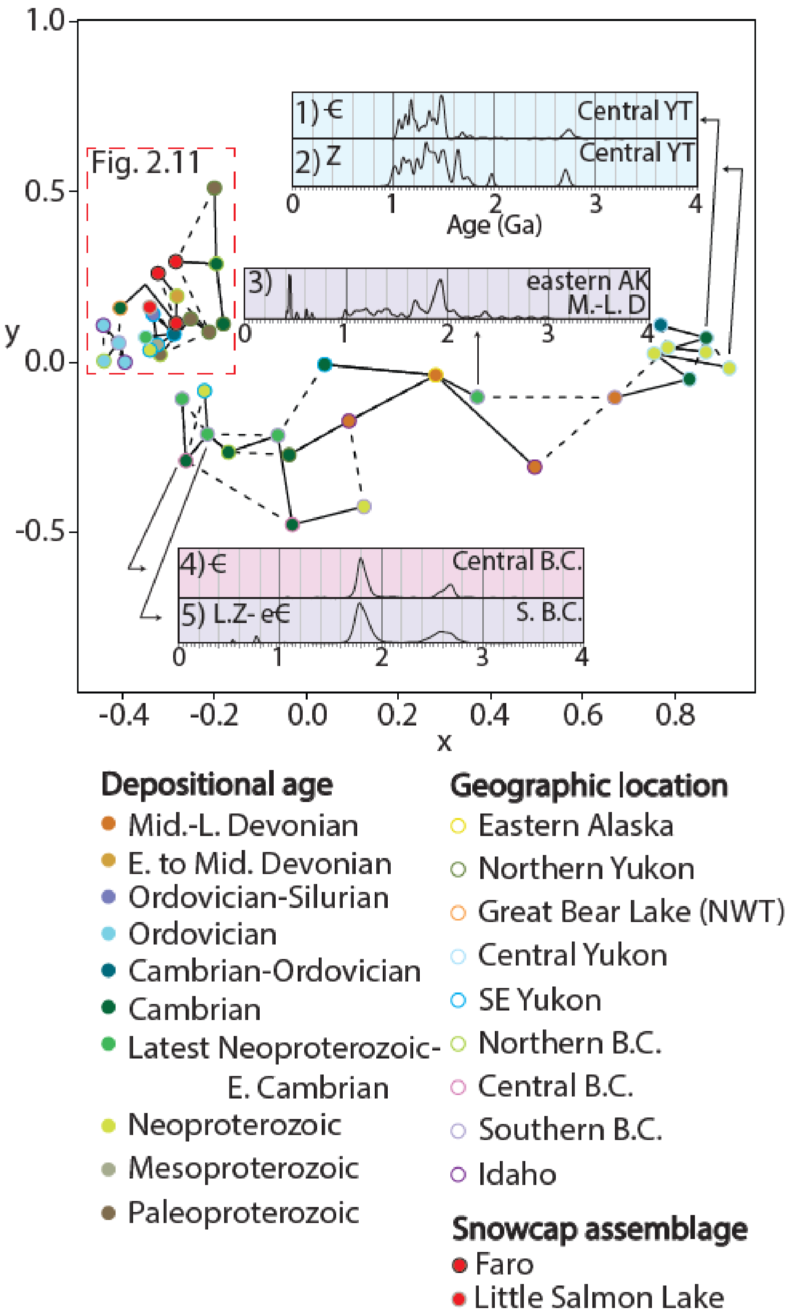

Figure 2.10 - Multidimensional scaling plot of detrital zircon U-Pb ages showing the relative dissimilarity of the Snowcap assemblage samples (this study; Piercey and Colpron, 2009) and Paleoproterozoic to Late Devonian sedimentary strata of the Cordilleran margin (Gehrels and Ross, 1998; Ross et al., 2001; Leslie, 2009; Pigage, 2009; Hadlari et al., 2012; Gehrels and Pecha, 2014; Lane and Gehrels 2014; Pigage et al., 2015; Beranek et al., 2016; Furlanetto et al., 2016; McMechan et al., 2017; Matthews et al., 2018). Note samples with similar U-Pb age spectra plot close together and dissimilar spectra plot farther apart. Inset PDPs: 1) Saline River Formation (*n* = 176); 2) Katherine Group (*n* = 33); 3) Nation River Formation (*n* = 98); 4) McNaughton Formation (*n* = 173); 5) Gog Group (*n* = 706). The red dashed indicates samples shown on Fig. 2.14 as probability density plots.

Early Paleozoic sea-level highs (e.g., Sloss, 1988) and the uplift of older strata and basement infrastructure within the Mackenzie, Ogilvie, Peace River, and Transcontinental arches resulted in widespread sediment recycling and mixing along the Cordilleran margin (Gehrels and Pecha, 2014; Lane and Gehrels, 2014; Brennan et al., 2021). Local recycling of pre-existing sedimentary rocks and their detrital zircon signatures into younger, overlying strata is reflected by the clustering of Neoproterozoic to Cambrian strata of central Yukon and southern British Columbia (Fig. 2.10). Middle to Upper Devonian strata from Idaho to eastern Alaska that plot in the middle of the MDS plot (Fig. 2.10) contain minor Neoproterozoic to Archean and <600 Ma populations that indicate recycling and mixing of Neoproterozoic to Cambrian-Ordovician strata from central Yukon and Neoproterozoic to Cambrian strata from southern and central British Columbia.

Tonian to Cryogenian detrital zircon (ca. 770-700 Ma) grains are rarely observed in northern Cordilleran margin strata. Cryogenian single-grain analyses are documented in the Cambrian Mount Roosevelt Formation (ca. 687-640 Ma; Fig. 2.11g) and Cambrian-Ordovician Crow Formation (ca. 724 Ma, 714 Ma; Fig. 2.11j) of northern British Columbia and southeast Yukon, respectively (Pigage, 2009; Gehrels and Pecha, 2014; Pigage et al., 2015; McMechan et al., 2017). Similar-aged grains are also present in the underlying Gog Group of southern British Columbia (Fig. 2.10) that does not cluster with the Snowcap assemblage; however, only the Mount Roosevelt and Crow formations yield ca. 2300 Ma and 2100 Ma grains consistent with Snowcap assemblage provenance.

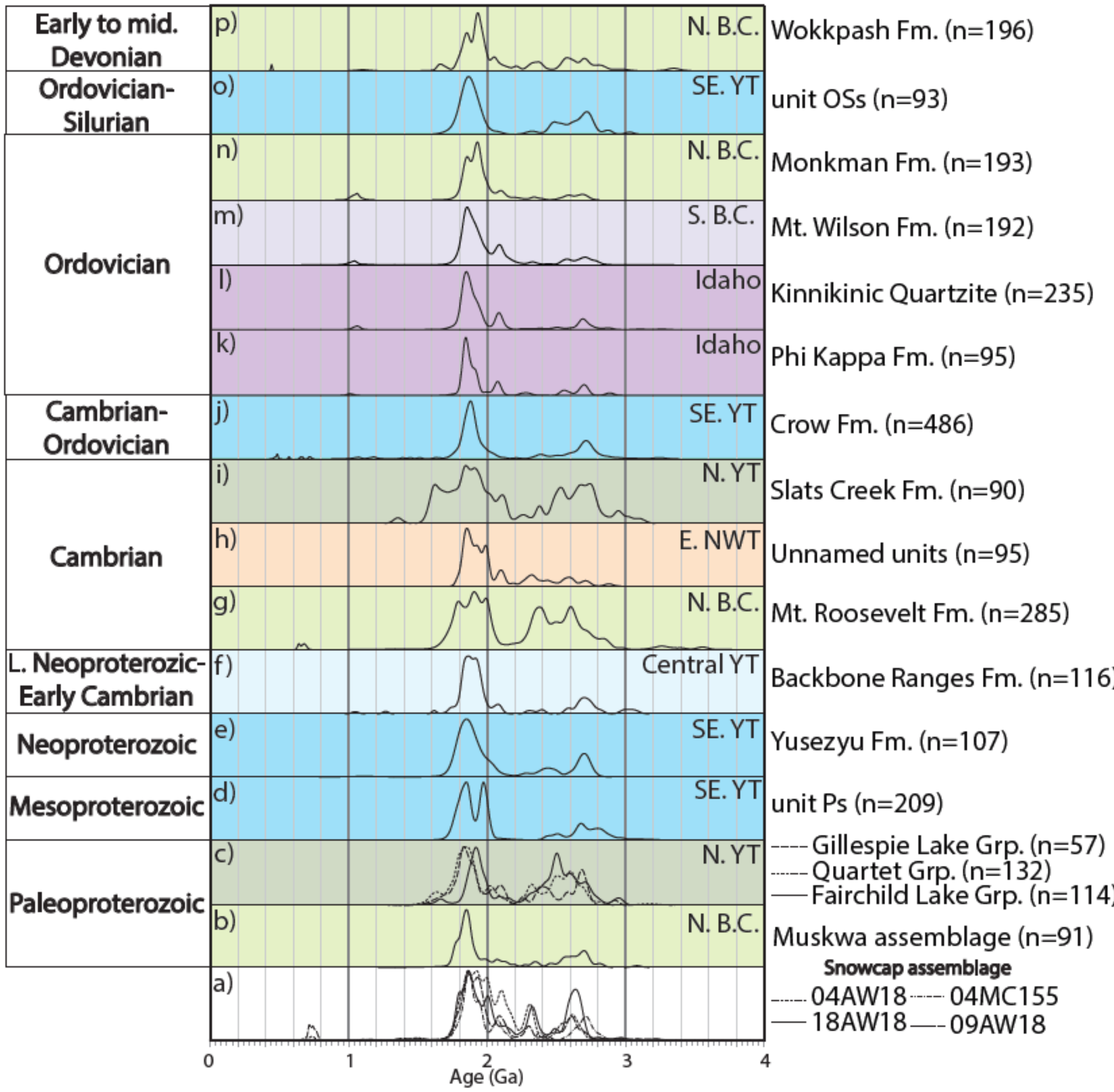

Figure 2.11 - Detrital zircon probability density U-Pb age plot of (a) the Snowcap assemblage (this study; Piercey and Colpron, 2009) and (b-p) Paleoproterozoic to Lower to Middle Devonian strata of the Cordilleran margin that cluster with Snowcap assemblage on Figure 2.10. Abbreviations: S.B.C.—Southern British Columbia; N.B.C —Northern British Columbia; SE. YT—Southeast Yukon; Central YT—Central Yukon; N. YT—Northern Yukon; E.NWT—Eastern Northwest Territory (b—Ross et al., 2001; c—Furlanetto et al., 2016; d,j,o—Pigage, 2009; e—Pigage et al., 2015; f—Leslie, 2009; g,m,n,p—Gehrels and Pecha, 2014; McMechan et al., 2017; h—Hadlari et al., 2012; i—Lane and Gehrels, 2014; k,l—Beranek et al., 2016).

Neoproterozoic to Middle Devonian strata in southeastern Yukon and northern British Columbia cluster together with Snowcap assemblage units (Fig. 2.10) and similarly contain ca. 1870, 2100, 2300, and 2600 Ma age populations (Fig. 2.11a-p) that strengthen its inferred stratigraphic links with the northwestern Laurentian margin (e.g., Mortensen, 1992; Colpron et al., 2006a; Piercey and Colpron, 2009). Subsidiary ca. 2100-2000 and

2300 Ma populations specifically suggest ties to the Peace River Arch region of northwestern Laurentia, including basement rocks and supracrustal derivatives of the Buffalo Head and Chinchaga terranes (e.g., Gehrels and Ross, 1998; Gehrels and Pecha, 2014). The Muskwa assemblage (Fig. 2.11b) and Wernecke Supergroup (Gillespie, Quartet, and Fairchild Lake Groups; Fig. 2.11c) of northern British Columbia and northern Yukon, respectively, are older than the Cryogenian MDA for the Snowcap assemblage, but yield most of the same Mesoproterozoic and older age populations and are potential recycled sources of 3000-1750 Ma zircon grains. The clustering of Paleozoic and Neoproterozoic units in similar areas on the MDS plot (Fig. 2.10), and the clustering of Muskwa assemblage and Wernecke Supergroup with the Snowcap assemblage, further indicates ancient linkages between Yukon-Tanana basement and the northwestern Laurentian margin.

2.8.2 Deposition of the Faro Peak formation and implications for Early Jurassic tectonics and basin development

Late Triassic to Early Jurassic collisional tectonism along the northern Cordilleran margin led to crustal thickening and emplacement of plutons at mid- to upper-crustal depths from central Yukon to eastern Alaska (e.g., Werdon et al., 2001; Dusel-Bacon et al., 2009; Colpron et al., 2015; Sack et al., 2020). Collision-related processes are in part recorded by Early Jurassic tectonic burial and amphibolite facies metamorphism in the Yukon-Tanana terrane (Johnston et al., 1996; Berman et al., 2007; Clark, 2017; Gaidies et al., 2021). Early to Middle Jurassic deposition of the Faro Peak formation, Laberge Group, and related syn-orogenic units resulted from subsidence adjacent to Intermontane basement domains (e.g., Knight et al., 2013; Kellett et al., 2018; van Drecht, 2019) and enclosed Late Triassic to Early Jurassic plutons that were rapidly exhumed along normal and strike-slip faults from southern Yukon ~450 km to eastern Alaska (Dusel-Bacon et al., 2002; Sack et al., 2020). Syn-tectonic units of the Faro Peak formation and Laberge Group were coeval, but differing provenance suggest they are not correlative, and likely deposited in isolated, fault-bounded basins separated by a drainage divide that resulted from the actively exhuming Intermontane terrane infrastructure.

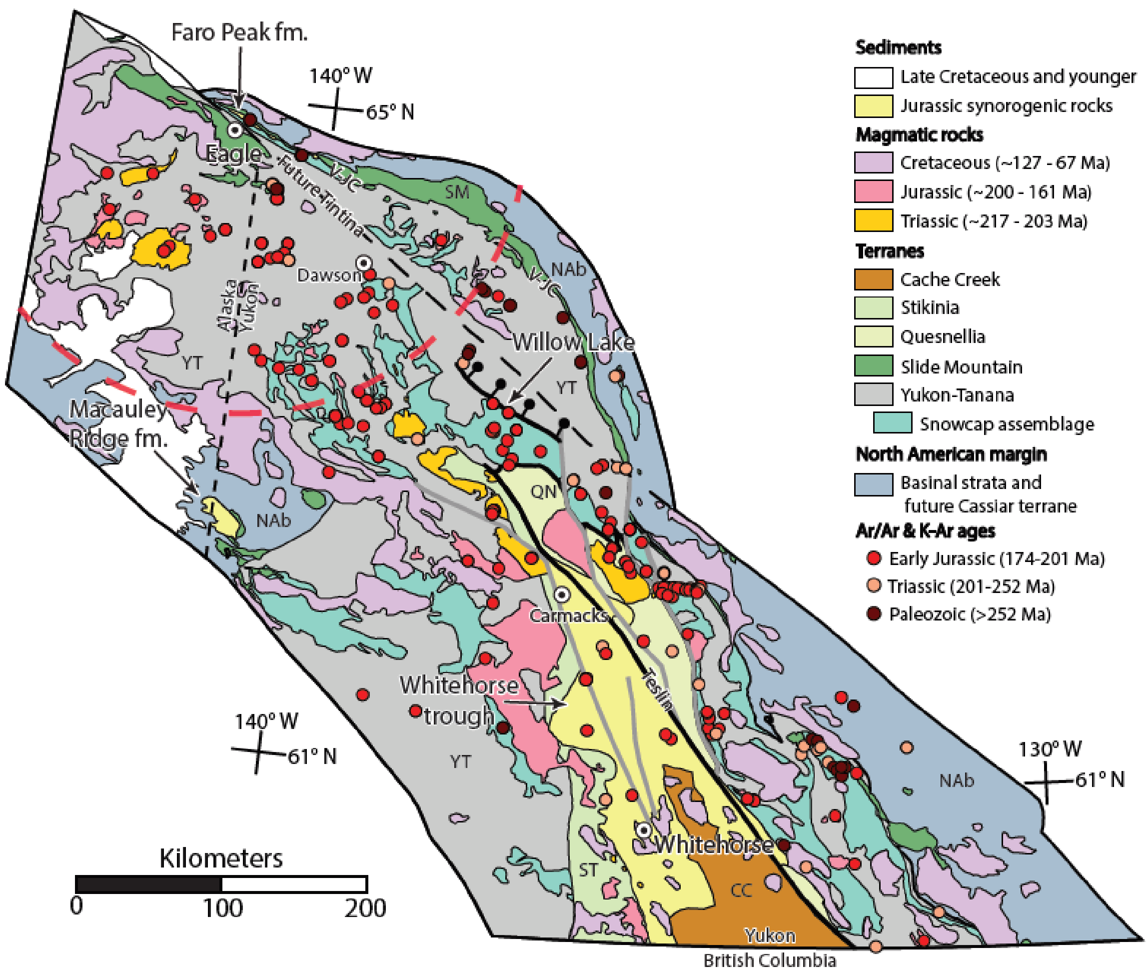

Figure 2.12 - Simplified terrane map of central Yukon with the Tinitna fault restored to a pre-Cretaceous location. Map includes a 200 km radius around the restored Faro region (red dashed line) and Ar/Ar and K-Ar cooling ages (Hansen et al., 1991; Hunt and Roddick, 1987, 1991, 1992; Erdmer et al., 1998; Newberry et al., 1998; Szumigala et al., 2000; Tafti, 2005; Dusel-Bacon et al., 2002, 2006, 2009; Knight et al., 2013; Joyce et al., 2015).

The Faro Peak formation restores to a pre-Cretaceous location near Eagle, Alaska (Fig. 2.12), along the Vangorda fault, the local name for the suture between the Yukon-Tanana and Slide Mountain terranes (e.g., Tempelman-Kluit, 1972; Pigage, 2004). The Faro Peak formation contains massively bedded, channelized sandstone and pebble to boulder conglomerate units that are consistent with syn-tectonic deposition by sediment gravity flows during Early Jurassic motion along the Vangorda fault zone (Wiest and Beranek, 2019; Wiest et al., 2020). Clast compositions and detrital zircon U-Pb-Hf isotope results (this study) indicate that the Faro Peak formation was sourced from exhumed basement rocks on both sides Vangorda fault, including the Snowcap assemblage and Paleozoic units of the Slide Mountain terrane. Locally abundant igneous rock clasts were likely derived from proximal Late Triassic to Early Jurassic intrusive complexes in eastern Alaska and Early Jurassic plutons in the Finlayson and Stewart River map areas of Yukon (red dashed line on Fig. 2.12 represents 200 km radius from depositional zone). Basal units of the Faro Peak formation are dominated by limestone, argillite, and volcanic rock clasts, whereas the exposed top contains up to boulder-sized clasts of mafic to felsic intrusive rocks consistent with progressive unroofing and minimal transportation that suggests proximity to a basin-bounding structure such as the Vangorda fault (c.f., Tempelman-Kluit, 1972).

The Faro Peak formation records rapid, coarse-grained deposition in an Early Jurassic structural basin likely controlled by normal and/or strike-slip faults (Wiest and Beranek, 2019). Although syn- to post-collisional displacements along the Vangorda and other inferred faults in the Faro region remain uncertain, there is evidence for crustal-scale, Early Jurassic low-angle normal faults in central Yukon (e.g., Willow Lake fault, Knight et al.,

2013) and sinistral strike-slip faults along the western (Llewellyn fault, Tally-ho shear zone; e.g., Dickie and Hein, 1995) and eastern (Teslin fault; de Keijzer et al., 2000) margins of the Whitehorse trough that accommodated exhumation and adjacent basin filling. Sediment accumulation rates for the Faro Peak formation range from 0.08-0.13 cm/yr assuming a 30% porosity of uncompacted sediment and a 9-14 Myr duration. These rates and the short duration of sedimentation are consistent with strike-slip basins such as the Ridge basin of southern California (0.12 cm/yr; Hempton and Dunne, 1984) and contrast with much longer-lived foreland basins (Xie and Heller, 2009) with lower sedimentation rates such as the Tremp—Jaca basin in the southern Pyrenees (0.009-0.09 cm/yr; Vinyoles et al., 2020).

Yukon-Tanana basement rocks from eastern Alaska (Lake George and Fortymile River assemblages) to the Stewart River and McQuesten map areas of central Yukon proximal to the restored Faro region underwent crustal thickening and amphibolite grade metamorphism during the Late Triassic to Early Jurassic. Mississippian to lower Permian rocks (Nasina and Fortymile River assemblages) in eastern Alaska were subsequently intruded by ca. 216-181 Ma plutons that post-date or were emplaced during peak metamorphic conditions (e.g., Hansen and Dusel-Bacon, 1998; Day et al., 2002). Early Jurassic (ca. 197-181 Ma) regional cooling in eastern Alaska (Dusel-Bacon et al., 2002) was likely a result of strike-slip faulting (Berman et al., 2007) and/or tectonic collapse concurrent with Sinemurian to Toarcian (ca. 196-182 Ma) exhumation along the Yukon-Tanana – Slide Mountain terrane suture responsible for basin subsidence and deposition of the Faro Peak formation.

Overlapping depositional ages for syn-tectonic Laberge Group and Faro Peak formation strata suggest that Faro Peak basin development was coeval with subsidence in the Whitehorse trough ~450 km to the southeast. Both the Laberge Group and Faro Peak formation units were locally sourced (e.g., Colpron et al., 2015; Wiest and Beranek, 2019; Wiest et al., 2020) and have basal sections dominated by volcanic rock clasts that transition to more abundant intrusive rock clasts upsection (e.g. Dickie and Hein, 1995; Wiest et al., 2020), which suggests similar basin evolution during Early Jurassic tectonic exhumation.

Faro Peak formation strata yield detrital zircon U-Pb-Hf isotope signatures that differ from those of the coeval Laberge Group (Tanglefoot and Richthofen formations) and indicate they were not sourced from the same plutons (Fig. 2.13a,b). The Faro Peak formation samples show a clustering of Late Triassic to Early Jurassic (ca. 205-185 Ma) grains with superchondritic $\varepsilon_{Hf(t)}$ values of ~0 to +5 (Fig. 2.13a). Tanglefoot formation strata in the northernmost Whitehorse trough have a cluster of Early Jurassic (ca. 200-180 Ma) subchondritic grains (Fig. 2.13a) consistent with its proximity to peraluminous, syn-collisional plutons of the Minto and Long Lake suites (see Fig. 2.2; Sack et al., 2020). The Richthofen formation in southern Yukon contains a Late Triassic to earliest Jurassic (~215-195 Ma) cluster that is younger and more juvenile than those of the Faro Peak formation (Fig. 2.13a,b).

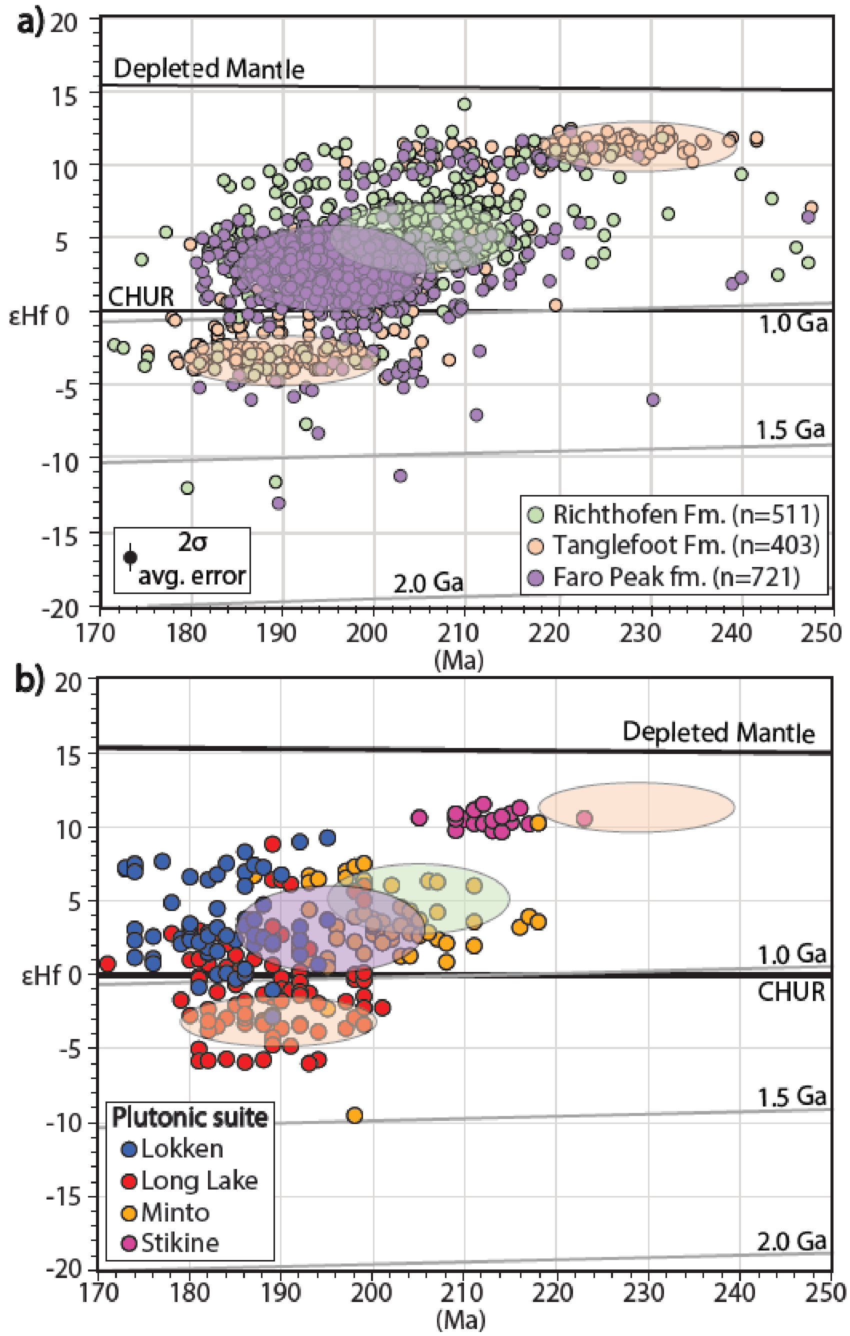

Figure 2.13 - (a) Detrital zircon U-Pb age versus $\varepsilon_{Hf(t)}$ values for the Faro Peak formation (this study) and Richthofen and Tanglefoot formations (van Drecht, 2019); (b) Detrital zircon U-Pb age versus $\varepsilon_{Hf(t)}$ values for Late Triassic to Early Jurassic plutonic suites compared with major populations of grains in the Faro Peak, Richthofen, and Tanglefoot formations, respectively.

It is unlikely that the Whitehorse trough was regionally extensive enough to span the ~500 km long, actively exhuming belt of Intermontane terrane infrastructure and accommodate deposition of the Faro Peak formation along the Yukon-Tanana—Slide Mountain suture, which restores to a position >100 km northwest of the Teslin and Willow Lake fault systems (Fig. 2.12 and Fig. 2.14). Evidence for Early Jurassic thrusting and crustal thickening to the north of the northern apex of the Whitehorse trough (e.g., Yukon River shear zone; Parsons et al., 2018), in addition to the ~450 km belt of Yukon-Tanana terrane rocks that yield Early Jurassic (ca. 197-175 Ma) cooling ages from central Yukon to eastern Alaska (Fig. 2.12), likely acted as a drainage divide that separated the Faro Peak basin and Whitehorse trough (Fig. 2.14).

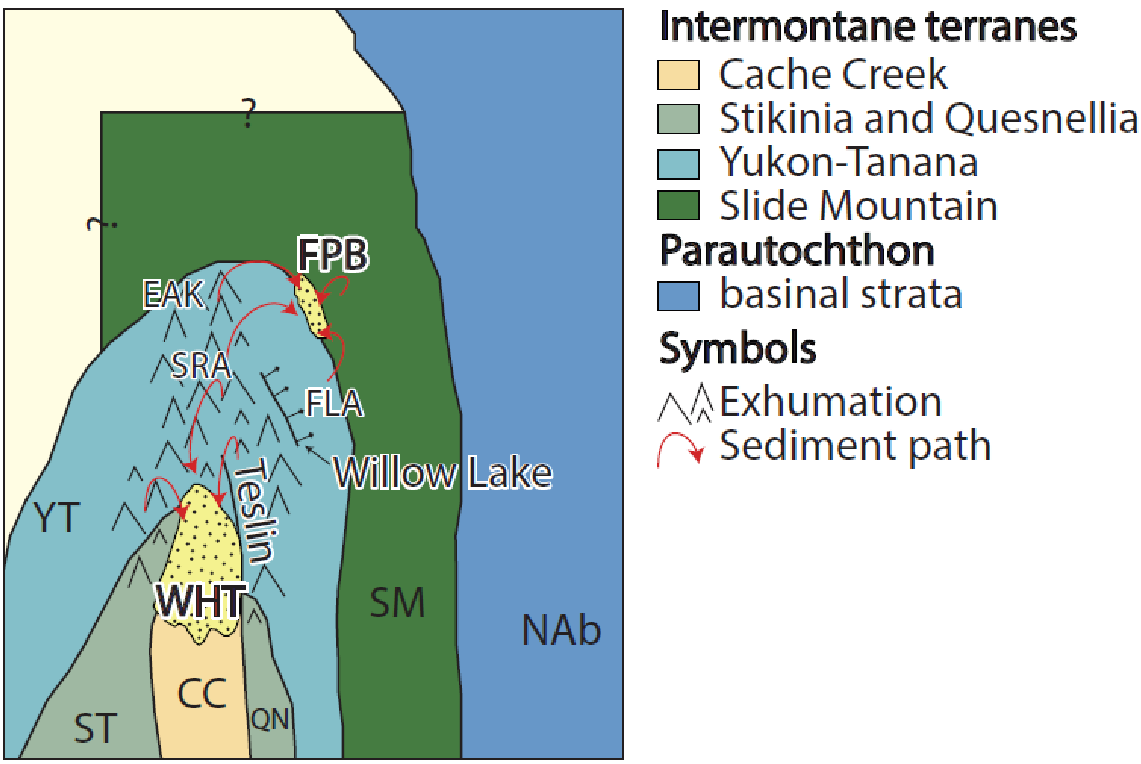

Figure 2.14 – Schematic diagram of Early Jurassic exhumation and basin development. Abbreviations: CC—Cache Creek; EAK—eastern Alaska; FLA—Finlayson Lake area; FPB—Faro Peak basin; Nab—North American basinal strata; QN—Quesnellia; SM—Slide Mountain; SRA—Stewart River area; ST—Stikinia; WHT—Whitehorse trough; YT—Yukon-Tanana terrane.

2.8.3 Implications for the Vangorda fault

The Vangorda fault cuts Upper Triassic to Lower Jurassic strata that sit on Snowcap assemblage in the Faro region (Fig. 2.3) and confirms post-Faro Peak formation displacement, mostly likely during the Jurassic to Late Cretaceous growth of the northern Cordilleran orogen (e.g., Pigage, 2004). The Jules Creek fault in the Finlayson Lake area, ~150 km to the southeast, is the southern equivalent of the Vangorda fault and interpreted to have accommodated strike-slip motion during the early Mesozoic (Murphy et al., 2006). Faro Peak formation clast lithologies and detrital zircon grains were derived from the Slide Mountain and Yukon-Tanana terranes and indicate that the Vangorda fault or its predecessor accommodated subsidence within the Faro Peak basin prior to post-Late Jurassic displacement. Approximately 60 km of currently unaccounted for dextral offset is required to match the Inconnu thrust fault across the Tintina fault in Late Cretaceous time (Gabrielse et al., 2006). The Vangorda and/or proto-Vangorda fault may have initially acted as a basin-bounding strike-slip or extensional fault that accommodated sedimentation in the Faro Peak basin followed by post- to syn-depositional dextral slip during the Early to Late Cretaceous and may account for the missing displacement in eastern Alaska required to match the Inconnu thrust across the Tintina fault.

2.9 CONCLUSIONS

Snowcap assemblage metaclastic rocks in the Faro region of central Yukon yield Cryogenian MDA estimations and detrital zircon age peaks ca. 719, 1930-1870, 2100-2000, 2300, and 2600 Ma. The oldest detrital zircon grains are likely polycyclic and consistent with ultimate derivation from the Archean core (e.g. Slave, Rae, Hearne, Wyoming, and Superior) and younger Proterozoic assemblages (e.g. Thorsby, Wabamun, Buffalo Head, Chinchaga, Taltson, Ksituan, Great Bear, Hottah, and Nova terranes and intrusions of the Trans-Hudson orogen) of the Laurentian craton. Multidimensional scaling comparisons between the Snowcap assemblage and pre-Late Devonian sedimentary units from the western North American margin indicate that Yukon-Tanana basement rocks have detrital zircon populations that match northwestern Laurentian source areas and specifically indicate stratigraphic links with Neoproterozoic to Lower Devonian rock units in northern British Columbia and southeast Yukon.

Sinemurian tectonic subsidence and deposition of the Faro Peak formation occurred along the inboard edge of the Intermontane terranes and was contemporaneous with regional exhumation of plutons and metamorphic basement rocks of the Yukon-Tanana terrane from central Yukon to eastern Alaska. The Faro Peak formation was rapidly deposited in an isolated fault-bound basin, most likely in a transtensional setting, with sediment derivation north, south, and along the modern trace of the Vangorda fault suggesting it or its predecessor (c.f. Templeman-Kluit, 1972) facilitated Early Jurassic subsidence (Fig. 2.13 or 2.14).

New detrital zircon U-Pb-Hf isotope results combined with field stratigraphic results indicate that deposition of the Faro Peak formation was coeval with the Laberge Group in the Whitehorse trough. Similarities in interpreted sedimentation style, including deposition by sediment gravity flows and unroofing provenance trends, suggests similar basin development during Early Jurassic tectonic exhumation of Intermontane terrane infrastructure. However, differences in clast lithologies, pre-Late Triassic detrital zircon populations, and Late Triassic to Early Jurassic detrital zircon Hf isotope compositions, indicates the basins were mostly derived from different source regions. Widespread Early

Jurassic cooling ages that parallel Late Triassic to Early Jurassic plutons from central Yukon to eastern Alaska likely indicate the location of a ~500 km-long, northwest-trending drainage divide along the northern Intermontane terranes that separated isolated, fault-bounded basin development and rapid, locally derived sedimentation in the Faro Peak basin and Whitehorse trough.

ACKNOWLEDGEMENTS

This research is a product of the Geo-mapping for Energy and Minerals (GEM) program at Natural Resources Canada. A special thanks to the Yukon Geological Survey and their staff for field logistics, helicopter support, and for facilitating a safe and stimulating research experience in central Yukon.

2.10 REFERENCES

Beranek L.P., Mortensen, J.K., Lane, L.S., Allen, T.L., Fraser, T.A., Hadlari, T., and Zantvoort, W.G., 2010a, Detrital zircon geochronology of the western Ellesmerian clastic wedge, northwestern Canada: Insights on Arctic tectonics and the evolution of the northern Cordilleran miogeocline: Geological Society of America Bulletin, v. 112, no. 11-12, p. 1889-1911, doi: 10.1130/B30120.1.

Beranek, L.P., and Mortensen, J.K., 2011, The timing and provenance record of the Late Permian Klondike orogeny in northwestern Canada and arc-continent collision along western North America: Tectonics, v. 30, 23 p, doi: 10.1029/2010TC002849.

Beranek, L.P., Gee, D.G., and Fisher, C.M., 2020, Detrital zircon U-Pb-Hf isotope signatures of Old Red Sandstone strata constrain the Silurian to Devonian paleogeography, tectonics, and crustal evolution of the Svalbard Caledonides: Geological Society of America Bulletin, v. 132, no. 9-10, p. 1987-2003, doi: 10.1130/B35318.1.

Beranek, L.P., Link, P.K., and Fanning, C.M., 2016, Detrital zircon record of mid-Paleozoic convergent margin activity in the northern U.S. Rocky Mountains: Implications for the Antler orogeny and early evolution of the North American Cordillera: Lithosphere, v. 8, no. 5, p. 553-550, doi: 10.1130/L557.1.

Beranek, L.P., Mortensen, J.K., Orchard, M.J., and Ullrich, T., 2010b, Provenance of North American Triassic strata from west-central and southeastern Yukon: correlations with coeval strata in the Western Canada Sedimentary Basin and Canadian Arctic Islands: Canadian Journal of Earth Sciences, v. 47(1), p. 53-73, doi: 10.1139/E09-065.

Berman, R.G., Ryan, J.J., Gordey, S.P., and Villeneuve, M., 2007, Permian to Cretaceous polymetamorphic evolution of the Stewart River region, Yukon-Tanana terrane, Yukon, Canada: P-T evolution linked with in situ SHRIMP monazite geochronology: Journal of Metamorphic Geology, v. 25, p. 803-827, doi: 10.1111/j.1525-1314.2007.00729.x.

Bickerton, L., Colpron, M., Gibson, H.D., Thorkelson, D., and Crowley, J.L., 2020, The northern termination of the Cache Creek terrane in Yukon: Middle Triassic arc activity and Jurassic-Cretaceous structural imbrication: Canadian Journal of Earth Sciences, v. 57, no. 2, p. 227-248, doi: 10.1139/cjes-2018-0262.

Brennan, D.T., Li, Z.-X., Rankenburg, K., Evans, N., Link, P.K., Nordsvan, A.R., Kirkland, C.L., Mahoney, J.B., Johnson, T., and McDonald, B.J., 2021, Recalibrating Rodinian rifting in the northwestern United States: Geology, v. 49, doi: 10.1130/G48435.1.

Campbell, R.W., Beranek, L.P., Piercey, S.J., and Friedman, R., 2019, Early Paleozoic post-breakup magmatism along the Cordilleran margin of western North America: New zircon u-Pb age and whole-rick Nd- and Hf-isotope and lithogeochemical results from the Kechika group, Yukon, Canada: Geosphere, v. 15, doi: 10.1130/GES02044.1.

Cawood, P.A., Hawkesworth, C.J., and Dhuime, B., 2012, Detrital zircon record and tectonic setting: Geology, v. 40, p. 875-878, doi: 10.1130/G32945.1.

Clark, A.D., 2017, Tectonometamorphic history of mid-crustal rocks at Aishihik Lake, southwest Yukon: Unpublished MSc thesis, Simon Fraser University, British Columbia, Canada, p. 153.

Colpron, M., Crowley, J.L., Gehrels, G., Long, D.G.F., Murphy, D.C., Beranek, L., and Bickerton, L., 2015, Birth of the northern Cordilleran orogeny, as recorded by detrital zircons in Jurassic synorogenic strata and regional exhumation in Yukon: Lithosphere, v. 7, p. 541-562, doi: 10.1130/L451.1.

Colpron, M., Mortensen, J.K., Gehrels, G.E., and Villeneuve, M., 2006b, Basement complex, Carboniferous magmatism and Paleozoic deformation in Yukon-Tanana terrane of central Yukon: Field, geochemical and geochronological constraints from Glenlyon map area, *in* Colpron, M. and Nelson, J.L., eds., Paleozoic Evolution and Metallogeny of Pericratonic Terranes at the Ancient Pacific Margin of North America, Canadian and Alaskan Cordillera: Geological Association of Canada, Special Paper 45, p. 131-151.

Colpron, M., Nelson, J.L., and Murphy, D.C., 2006a, A tectonostratigraphic framework for the pericratonic terranes of the northern Cordillera, *in* Colpron, M. and Nelson, J.L., eds., Paleozoic Evolution and Metallogeny of Pericratonic Terranes at the Ancient Pacific Margin of North America, Canadian and Alaskan Cordillera: Geological Association of Canada, Special Paper 45, p. 1-23.

Colpron, M., Nelson, J.L., and Murphy, D.C., 2007, Northern Cordilleran terranes and their interactions through time: Geological Society of America Today, v. 17, no. 4/5, doi: 10.1130/GSAT01704-5A.1.

Corrigan, D., Pehrsson, S., Wodicka, N., and de Kemp, E., 2009, The Paleoproterozoic Trans-Hudson Orogen: a prototype of modern accretionary processes: Geological Society of London, Special Publications 327, p. 457-479, doi: 10.1144/SP327.19.

Coutts, D.S., Matthews, W.A., and Hubbard, S.M., 2019, Assessment of widely used methods to derive depositional ages from detrital zircon populations: Geoscience Frontiers, v. 10, no. 4, p. 1421-1435, doi: 10.1016/j.gsf.2018.11.002.

Cushing, G.W., 1984, The tectonic evolution of the eastern Yukon-Tanana Upland [M.S. thesis]: Albany, State University of New York, 235 p.

Day, W.C., Aleinikoff, J.N., and Gamble, B., 2002, Geochemistry and age constraints on metamorphism and deformation in the Fortymile River area, eastern Yukon-Tanana Upland, Alaska, *in* Wilson, F.H., and Galloway, J.P., eds., Studies by the U.S. Geological Survey in Alaska, 2000: U.S. Geological Survey Professional Paper 1662, p. 5–18.

de Keijzer, M., Mihalynuk, M.G., and Johnston, S.T., 2000, Structural investigation of an exposure of the Teslin fault, northwestern British Columbia: Geological Survey of Canada, Current Research 2000-A5, 10 pp.

Dickie, J.R., and Hein, F.J., 1995, Conglomeratic fan deltas and submarine fans of the Jurassic Laberge Group, Whitehorse trough, Yukon Territory, Canada: fore-arc sedimentation and unroofing of a volcanic island-arc complex: Sedimentary Geology, v. 98, p. 263–292, doi:10.1016/0037-0738(95)00036-8.

Dickinson, W.R., and Gehrels, G.E., 2009, Use of U-Pb ages of detrital zircons to infer maximum depositional ages of strata: A test against a Colorado Plateau Mesozoic database: Earth and Planetary Science Letters, v. 288, p. 115-125, doi: 10.1016/j.epsl.2009.09.013.

Dostal, J., Keppie, J.D., and Ferri, F., 2009, Extrusion of high-pressure Cache Creek rocks into the Triassic Stikinia-Quesnellia arc of the Canadian Cordillera: Implications for terrane analysis of ancient orogens and palaeogeography, *in* Murphy, J.B., Keppie, J.D., and Hynes, A.J., eds., Ancient Orogens and Modern Analogues: Geological Society of London Special Publication 327, p.71-87.

Dusel-Bacon, C., Aleinikoff, J.N., Day, W.C., and Mortensen, J.K., 2015, Mesozoic magmatism and timing of epigenetic Pb-Zn-Ag mineralization in the western Fortymile mining district, east-central Alaska: Zircon U-Pb geochronology, whole-rock geo-chemistry, and Pb isotopes: Geosphere, v. 11, no. 3, p. 786-822, doi:10.1130/GES01092.

Dusel-Bacon, C., Hansen, V.L., 1992, High-pressure amphibolite-facies metamorphism and deformation within the Yukon-Tanana and Taylor Mountain terranes, eastern

Alaska, *in* Geologic Studies in Alaska, US Geological Survey, 1991, Bradley, D.C. and Dusel-Bacon, C. (eds), US Geological Survey Bulletin 2041, p. 140-159.

Dusel-Bacon, C., Hansen, V.L., and Scala, J.A., 1995, High-pressure amphibolite facies dynamic metamorphism and the Mesozoic tectonic evolution of an ancient continental margin, east-central Alaska: Journal of Metamorphic Geology, v.13, p. 9-24, doi:10.1111/j.1525-1314.1995.tb00202.x.

Dusel-Bacon, C., Lanphere, M.A., Sharp, W.D., Layer, P.W., and Hanson, V.L., 2002, Mesozoic thermal history and timing of structural events for the Yukon-Tanana Upland, east-central Alaska—$^{40}Ar/^{39}Ar$ data from metamorphic and plutonic rocks: Canadian Journal of Earth Sciences, v.39, p. 1013-1051, doi:10.1139/e02-018.

Dusel-Bacon, C., Slack, J.F., Aleinikoff, J.N., and Mortensen, J.K., 2009, Mesozoic magmatism and basemetal mineralization in the Fortymile mining district, eastern Alaska—Initial results of petrographic, geochemical, and isotopic studies in the Mount Veta area, *in* Haeussler, P.J., and Galloway, J.P., eds., Studies by the U.S. Geological Survey in Alaska, 2007: U.S. Geological Survey Professional Paper 1760-A, 42 p.

Erdmer, P., Ghent, E.D., Archibald, D.A., and Stout, M.Z., 1998, Paleozoic and Mesozoic high-pressure metamorphism at the margin of ancestral North America in central Yukon: Geological Society of America Bulletin, v. 110, no. 5, p. 615-629.

Fisher C.M., Vervoort, J.D., and DuFrane, S.A., 2014, Accurate Hf isotopic determinations of complex zircons using the “laser ablation split stream” method: Geochemistry, Geophysics, Geosystems, v. 15, p. 121-139, doi: 10.1002/2013GC004962.

Foster, H.L., 1992, Geologic map of the eastern Yukon-Tanana region, Alaska: US Geological Survey, Open-File Report 92-313, scale 1:50,000.

Foster, H.L., Donato, M.M., and Yount, M.E., 1978, Petrographic and chemical data on Mesozoic granitic rocks of the Eagle quadrangle, Alaska: U.S. Geological Survey Open-File Report 78-253, 29 p., 2 maps, scale 1:250,000.

Foster, H.L., Keith, T.E.C., and Menzie, W.D., 1994, Geology of the Yukon-Tanana area of east-central Alaska, *in* Plafker, G. and Berg, H.C., (eds.), The geology of Alaska: Geological Society of America, G-1, p. 197-217.

Furlanetto, F., Thorkelson, D.J., Rainbird, R.H., Davis, W.J., Gibson, H.D., and Marshall, D.D., 2016, The Paleoproterozoic Wernecke Supergroup of Yukon, Canada: Relationships to orogeny in northwestern Laurentia and basins in North America, East Australia, and China: Gondwana Research, v. 39, p. 14-40, doi: 10.1016/j.gr.2016.06.007.

Gabrielse, H., Murphy, D.C., and Mortensen, J.K., 2006, Cretaceous and Cenozoic dextral orogeny-parallel displacements, magmatism, and paleogeography, north-central Canadian Cordillera, *in* Haggart, J.W., Enkin, R.J. and Monger, J.W.H., eds., Paleogeography of the North American Cordillera: Evidence for and Against Large-Scale Displacements: Geological Association of Canada Special Paper 46, p. 255-276.

Gaidies, F., Morneau, Y.E., Petts, D.C., Jackson, S.E., Zagorevski, A. and Ryan, J.J., 2021, Major and trace element mapping of garnet: Unravelling the conditions, timing and rates of metamorphism of the Snowcap assemblage, west-central Yukon: Journal of metamorphic Geology, v. 39, p. 133-164, doi: 10.1111/jmg.12562.

Gehrels, G. and Pecha, M., 2014, Detrital zircon U-Pb geochronology and Hf isotope geochemistry of Paleozoic and Triassic passive margin strata of western North America: Geosphere, v. 10, no. 1, p. 49-65, doi: 10.1130/GES00889.1.

Gehrels, G.E. and Ross, G.M., 1998, Detrital zircon geochronology of Neoproterozoic to Permian miogeoclinal strata in British Columbia and Alberta: Canadian Journal of Earth Sciences, v. 35, p. 1380-1401, doi: 10.1139/e98-071.

Golding, M.L., Mortensen, J.K., Ferri, F., Zonneveld, J.-P., and Orchard, M.J., 2016, Determining the provenance of Triassic sedimentary rocks in northeastern British Columbia and western Alberta using detrital zircon geochronology, with implications for regional tectonics. Canadian Journal of Earth Sciences, vol. 53, p. 140-155, doi: 10.1139/cjes-2015-0082.

Goodfellow, W.D., Cecile, M.P., and Leybourne, M.I., 1995, Geochemistry, petrogenesis, and tec-tonic setting of lower Paleozoic alkalic and potassic volcanic rocks, Northern Canadian Cor-dilleran Miogeocline: Canadian Journal of Earth Sciences, v. 32, p. 1236-1254, doi: 10.1139/e95-101.

Gordey, S.P., McNicoll, V.J., and Mortensen, J.K., 1998, New U-Pb ages from the Teslin area, southern Yukon, and their bearing on terrane evolution in the northern Cordillera, *in* Current Research 1998-F: Geological Survey of Canada, p.129-148.

Hadlari, T., Davis, W.J., Dewing, K., Heaman, L.M., Lemieux, Y., Ootes, L., Pratt, B.R., and Pyle, L.J., 2012, Two detrital zircon signatures for the Cambrian passive margin of northern Laurentia highlighted by new U-Pb results from northern Canada: Geological Society of America Bulletin, v. 124, p. 1155–1168, doi: 10.1130 /B30530.1.

Hansen, V.L., and Dusel-Bacon, C., 1998, Structural and kinematic evolution of the Yukon-Tanana Upland tectonites, east-central Alaska: A record of late Paleozoic to Mesozoic crustal assembly: Geological Society of America Bulletin, v. 110, p. 211–230, doi:10.1130/0016-7606(1998)110<0211 :SAKEOT >2.3.CO;2.

Hansen, V.L., Heizler, M.T., and Harrison, T.M., 1991, Mesozoic thermal evolution of the Yukon-Tanana composite terrane—New evidence from ^{40}Ar/^{39}Ar data: Tectonics, v. 10, p. 51–76, doi:10.1029/90TC01930.

Hart, C.J.R., 1997, A Transect across Northern Stikinia: Geology of the Northern Whitehorse Map Area, Southern Yukon Territory (105D/13–16): Exploration and Geological Services Division, Yukon Region, Indian and Northern Affairs Canada, Bulletin 8, p. 112.

Hart, C.J.R., Dickie, J.R., Ghosh, D.K., and Armstrong, R.L., 1995, Provenance constraints for Whitehorse trough conglomerate: U-Pb zircon dates and initial Sr ratios of granitic clasts in Jurassic Laberge Group, Yukon Territory, *in* Miller, D.M., and Busby, C., eds., Jurassic Magmatism and Tectonics of the North American Cordillera: Geological Society of America Special Paper 299, p. 47–63.

Hempton, M., Dunne, L., 1984, Sedimentation in pull-apart basins: Active examples in Eastern Turkey: The Journal of Geology, v. 92, no. 5, p. 513-530.

Hoffman, P.F., 1989, Precambrian geology and tectonic history of North America, *in* Bally, A.W., and Palmer, A.R., eds., The Geology of North America: An Overview: Boulder, Colorado, Geological Society of America, The Geology of North America, v. A, p. 447–512.

Hunt, P.A. and Roddick, J.C., 1987, A compilation of K-Ar ages, report 17, *in* Radiogenic age and isotopic studies: Report 1, Geological Survey of Canada Paper 87-2, p. 203.

Hunt, P.A. and Roddick, J.C., 1991, A compilation of K-Ar ages: report 20, *in* Radiogenic age and isotopic studies: Report 4, Geological Survey of Canada Paper no. 90-2, p.113-143, doi: 10.4095/131943.

Hunt, P.A. and Roddick, J.C., 1992, A compilation of K-Ar and ^{40}Ar-^{39}Ar ages, report 22, *in* Radiogenic age and isotopic studies: Report 6, Geological Survey of Canada Paper 92-2, p. 179–226.

Johannson, G.G., Smith, P.L., and Gordey, S.P., 1997, Early Jurassic evolution of the northern Stikinian arc: evidence from the Laberge Group, northwestern British Columbia: Canadian Journal of Earth Science, v. 34, p. 1030-1057.

Johnston, S.T., Mortensen, J.K., and Erdmer, P., 1996, Igneous and metaigneous age constraints for the Aishihik metamorphic suite, southwest Yukon: Canadian Journal of Earth Sciences, v. 33, p. 1543-1555.

Joyce, N.L., Ryan, J.J., Colpron, M., Hart, C.J.R., and Murphy, D.C., 2015, A compilation of 40Ar/39Ar age determinations for igneous and metamorphic rocks, and mineral occurrences from central and southeast Yukon: Geological Survey of Canada Open-File 7924, 229 p., doi: 10.4095/297446.

Kellett, D.A. and Zagorevski, A., 2021, Overlap assemblages: Laberge Group of the Whitehorse trough, northern Canadian Cordillera, Yukon–British Columbia, *in* Ryan, J.J. and Zagorevski, A., eds., Northern Cordillera geology: a synthesis of research from the Geo-mapping for Energy and Minerals program, British Columbia and Yukon: Geological Survey of Canada, Bulletin 610, p. 1-22.

Kellett, D.A., Weller, O.M., Zagorevski, A., and Regis, D., 2018, A petrochronological approach for the detrital record: Tracking mm-sized eclogite clasts in the northern Canadian Cordillera: Earth and Planetary Science Letters, v. 494, p. 23-31, doi:10.1016/j.epsl.2018.04.036.

Knight, E., Schneider, D.A., and Ryan, J., 2013, Thermochronology of the Yukon-Tanana Terrane, West-Central Yukon: Evidence for Jurassic Extension and Exhumation in the Northern Canadian Cordillera: The Journal of Geology, v. 121, p. 371-400, doi: 10.1086/670721.

Lane, L.S. and Gehrels, G.E., 2014, Detrital zircon lineages of late Neoproterozoic and Cambrian strata, NW Laurentia: Geological Society of America Bulletin, v. 126, no. 3/4, p. 398-414, doi: 10.1130/B30848.1.

Leslie, C.D., 2009, Detrital zircon geochronology and rift-related magmatism: central Mackenzie Mountains, Northwest Territories [M.Sc. thesis]: Vancouver, British Columbia, The University of British Columbia, 224 p.

Lowey, G.W., 2004, Preliminary lithostratigraphy of the Laberge Group (Jurassic), south-central Yukon: Implications concerning the petroleum potential of the Whitehorse trough, *in* Emond, D.S., and Lewis, L.L., eds., Yukon Exploration and Geology 2003: Whitehorse, Yukon, Canada, Yukon Geological Survey, p.129–142.

Lowey, G.W., 2008, Summary of the stratigraphy, sedimentology, and hydrocarbon potential of the Laberge Group (Lower–Middle Jurassic), Whitehorse trough, Yukon, *in* Emond, D.S., Blackburn, L.R., Hill, R.P., and Weston, L.H., eds., Yukon Exploration and Geology 2007: Whitehorse, Yukon, Canada, Yukon Geological Survey, p.179–197.

Matthews, W., Guest, B., and Madronich, L., 2018, Latest Neoproterozoic to Cambrian detrital zircon facies of western Laurentia: Geosphere, v. 14, no. 1, p. 243-264, doi: 10.1130/GES01544.1.

McCausland, P.J.A., Symons, D.T.A., Hart, C.J.R., and Blackburn, W.H., 2002, Paleomagnetism and geobarometry of the Granite Mountain batholith, Yukon: Minimal geotectonic motion of the Yukon-Tanana Terrane relative to North America, *in* Yukon Exploration and Geology, 2001, D.S. Emond, L.H. Weston and L.L. Lewis (eds.), Exploration and Geological Services Division, Yukon, Indian and Northern Affairs Canada, p. 163-177.

McMechan, M., Currie, L., Ferri, F., Matthews, W., O'Sullivan, P., 2017, Cambrian detrital zircon signatures of the northern Cordillera passive margin, Liard area, Canada: evidence of sediment recycling, non-Laurentian ultimate sources, and basement denudation: Canadian Journal of Earth Sciences, v. 54, p. 609-621, doi: 10.1139/cjes-2016-0127.

Metcalfe, P., 1981, Petrogenesis of the Klondike formation, Yukon Territory [MS.c. thesis], University of Manitoba, Winnipeg, M.B., 305 p.

Mihalynuk, M.G., Erdmer, P., Ghent, E.D., Cordey, F., Archibald, D.A., Friedman, R.M., and Johannson, G.G., 2004, Coherent French Range blueschist: Subduction to exhumation in<2.5m.y.?: Geological Society of America Bulletin, v.116, p.910–922, doi: 10.1130/B25393.1.

Mihalynuk, M.G., Nelson, J.A., and Diakow, L.J., 1994, Cache Creek terrane entrapment: Oroclinal paradox within the Canadian Cordillera: Tectonics, v. 13, p. 575-595.

Mortensen, J. K., 1990, Geology and U-Pb geochronology of the Klondike District, west-central Yukon Territory, Canadian Journal of Earth Sciences, v. 27, p. 903–914, doi:10.1139/e90-093.

Mortensen, J.K., 1992, Pre–mid-Mesozoic tectonic evolution of the Yukon-Tanana terrane, Yukon and Alaska: Tectonics, v. 11, p. 836–853, doi: 10.1029/91TC01169.

Murphy, D.C., Mortensen, J.K., Piercey, S.J., Orchard, M.J., and Gehrels, G.E., 2006, Mid-Paleozoic to early Mesozoic tectonostratigraphy evolution of Yukon-Tanana and Slide Mountain terranes and affiliated overlap assemblages, Finlayson Lake massive sulphide district, southeastern Yukon, *in* Colpron, M. and Nelson, J.L., eds., Paleozoic Evolution and Metallogeny of Pericratonic Terranes at the Ancient Pacific Margin of North America, Canadian and Alaskan Cordillera: Geological Association of Canada, Special Paper 45, p. 75-105.

Nelson, J.L., Colpron, M., Piercey, S.J., Dusel-Bacon, C., Murphy, D.C., and Root, C.F., 2006, Paleozoic tectonic and metallogenic evolution of the pericrationic terranes in Yukon, northern British Columbia and eastern Alaska, *in* Colpron, M. and Nelson, J.L., eds., Paleozoic Evolution and Metallogeny of Pericratonic Terranes at the Ancient Pacific Margin of North America, Canadian and Alaskan Cordillera: Geological Association of Canada, Special Paper 45, p. 323-360.

Newberry, R.J., Layer, P.W., Burleigh, R.E., and Solie, D.N., 1998, New $^{40}Ar/^{39}Ar$ dates for intrusions and mineral prospects in the eastern Yukon-Tanana terrane—Regional patterns and significance, Alaska, *in* Gray, J.E., and Riehle, J.R., eds., Geologic studies in Alaska by the United States Geological Survey, 1996: U.S. Geological Survey Professional Paper 1595, p.131–159.

Parsons, A.J., Coleman, M.J., Ryan, J.J., Zagorevski, A., Joyce, N.L., Gibson, H.D., and Larson, K.P., 2018, Structural evolution of a crustal-scale shear zone through a decreasing temperature regime: The Yukon River shear zone, Yukon-Tanana terrane, northern Cordillera: Lithosphere, v. 10, p. 760-782, doi: 10.1130/L724.1.

Parsons, A.J., Zagorevski, A., Ryan, J.J., McClelland, W.C., van Staal, C.R., Coleman, M.J., and Golding, M.L., 2019, Petrogenesis of the Dunite Peak ophiolite, south-central Yukon, and the distinction between upper-plate and lower-plate setting: A new hypothesis for the late Paleozoic—early Mesozoic tectonic evolution of the Northern Cordillera: Geological Society of America Bulletin, v. 131, no. 1/2, p. 74-298, doi: 10.1130/B31964.1.

Paton, C., Hellstrom, J., Paul, B., Woodhead, J., and Hergt, J., 2011, Iolite: Freeware for the visualization and processing of mass spectrometric data: Journal of Analytical Atomic Spectrometry, v. 26, p. 2508-2518, doi:10.1039/C1JA10172B.

Petrus, J., and Kamber, B.S., 2012, VizualAge: A Novel Approach to Laser Ablation ICP-MS U-Pb Geochronology Data Reduction: Geostandards and Geoanalytical Research, v. 36, 24 p., doi:10.1111/j.1751-908X.2012.00158.x.

Philippot, P., Blichert-Toft, J., Perchuk, A., Costa, S., Gerasimov, V., 2001, Lu-Hf and Ar-Ar chronometry supports extreme rate of subduction zone metamorphism deduced from geospeedometry: Tectonophysics, v. 342, p. 23-38.

Piercey, S.J., and Colpron, M., 2009, Composition and provenance of the Snowcap assemblage, basement to the Yukon-Tanana terrane, northern Cordillera: Implications for Cordilleran crustal growth: Geosphere, v. 5, no. 5, p. 439-464, doi: 10.1130/GS00505.1.

Piercey, S.J., Mortensen, J.K. and Creaser, R.A., 2003, Neodymium isotope geochemistry of felsic volcanic and intrusive rocks from the Yukon-Tanana terrane in the Finlayson Lake region, Yukon, Canada: Canadian Journal of Earth Sciences, v. 40, p. 77-97.

Piercey, S.J., Nelson, J.L., Colpron, M., Dusel-Bacon, C., Simard, R-L. and Roots, C.F., 2006, Paleozoic magmatism and crustal recycling along the ancient Pacific margin of North American, northern Canadian Cordillera, *in* Colpron, M. and Nelson, J.L., eds., Paleozoic Evolution and Metallogeny of Pericratonic Terranes at the Ancient Pacific Margin of North America, Canadian and Alaskan Cordillera: Geological Association of Canada, Special Paper 45, p. 281-322.

Pigage, L.C., 2004, Bedrock geology compilation of the Anvil District (parts of NTS 105K/2, 3, 5, 6, 7, and11), central Yukon: Yukon Geological Survey, Bulletin, v.15, p. 103.

Pigage, L.C., 2009, Bedrock geology of NTS 95C/5 (Pool Creek) and NTS 95D/8 map sheets, southeast Yukon: Yukon Geological Survey, Bulletin 16, 150 p.

Pigage, L.C., Roots, C.F., and Abbott, J.G. 2015. Regional bedrock geology for Coal River map area (NTS 95D), southeast Yukon: Yukon Geological Survey, Bulletin 17, 155 p.

Rainbird, R., Cawood, P., and Gehrels, G., 2012, The great Grenvillian sedimentation episode: Record of supercontinent Rodinia’s assembly, *in* Busby, C., and Azor,A., eds., Tectonics of Sedimentary Basins: Recent Advances: Chichester, West Sussex, UK, Wiley-Black-well Publishing, p. 583-601.

Rainbird, R.H., Heaman, L.M., and Young, G., 1992, Sampling Laurentia: Detrital zircon geochronology offers evidence for an extensive Neoproterozoic river system originating from the Grenville orogen: Geology, v. 20, p. 351-354, doi: 10.1130/0091-7613(1992)020<0351:SLDZGO>2.3.CO;2.

Ross, G.M., 1990, Deep crust and basement structure of the Peace River Arch region: constraints on mechanisms of formation: Bulletin of Canadian Petroleum Geology, v. 38A, p. 25-35, doi: 10.35767/gscpgbull.38a.1.025.

Ross, G.M., Villeneuve, M.E., and Theriault, R.J., 2001, Isotopic provenance of the lower Muskwa assemblage (Mesoproterozoic, Rocky Mountains, British Columbia): new clues to correlation and source areas: Precambrian Research, v. 111, p. 57-77, doi: 10.1016/S0301-9268(01)00156-5.

Ruks, T.W., Piercey, S.J., Ryan, J.J., Villeneuve, M.E., and Creaser, R.A., 2006, Mid- to late Paleozoic K-feldspar augen granitoids of the Yukon-Tanana terrane, Yukon, Canada: Implications for crustal growth and tectonic evolution of the northern Cordillera: Geological Society of America Bulletin, v. 118, no. 9/10, doi: 10.1130/B25854.1.

Sack, P.J., Colpron, M., Crowley, J.L., Ryan, J.J., Allan, M.M. Beranek, L.P., Joyce, N.L., 2020, Atlas of Late Triassic to Jurassic plutons in the Intermontane terranes of Yukon: Yukon Geological Survey, Open File 2020-1, p. 365.

Shirmohammad, F., Smith, P.L., Anderson, R.G., and McNicoll, V.J., 2011, The Jurassic succession at Lisadale Lake (Tulsequah map area, British Columbia, Canada) and its bearing on the tectonic evolution of the Stikine terrane: Volumnia Jurassica, v. 9, p. 43-60.

Simard, R.-L., Dostal, J., and Roots, C.F., 2003, Development of late Paleozoic volcanic arcs in the Canadian Cordillera: An example from the Klinkit Group, northern British Columbia and southern Yukon: Canadian Journal of Earth Sciences, v. 40, p. 907–924, doi:10.1139/e03-025.

Sláma, J., Kosler, J., Condon, D., Crowley, J.L., Gerdes, A., Hanchar, J.M, Horstwood, S.A., Morris, G.A., Nasdala, L., Norberg, N., Schaltegger, U., Schoene, B., Tubrett, M., and Whitehouse, M.J., 2008, Plešovice zircon – A new natural reference material for U-Pb and Hf isotopic microanalysis: Chemical Geology, v. 249, p. 1-35, doi: 10.1016/j.chemgeo.2007.11.005.

Sloss, L.L., 1988, Tectonic evolution of the craton in Phanerozoic time, *in* Sloss, L.L., ed., Sedimentary Cover—North American Craton: Boulder, Colorado, Geological Society of America, The Geology of North America, v. D-2, p. 25–51.

Stevens, R.D., DeLabio, R.N., and LaChance, G.R., 1982, Age determinations and geological studies, K-Ar isotopic ages: Geological Survey of Canada, Report 15, p. 74.

Symons, D.T.A., Williams, P.R., McCausland, P.J.A., Harris, M.J., Hart, C.J.R., and Blackburn, W.H., 2000, Paleomagnetism and geobarometry of the Big Creek Batholith suggests that Yukon-Tanana Terrane has been a parautochthon since Early Jurassic: Tectonophysics, v. 326, p. 57-72.

Szumigala, D.J., Newberry, R.J., Werdon, M.B., Finseth, B.A., Pinney, D.S., and Flynn, R.L., 2000, Major-oxide, minor-oxide, trace-element, and geochemical data from rocks collected in a portion of the Fortymile Mining District, Alaska: State of

Alaska Division of Geological and Geophysical Surveys Raw-Data File 2000-1, 24 p., scale 1:63,360.

Tafti, R., 2005, Nature and Origin of the Early Jurassic Copper (-Gold) Deposits at Minto and Williams Creek, Carmacks Copper Belt, Western Yukon: Examples of Deformed Porphyry Deposits [M.Sc. thesis]: Vancouver, British Columbia, Canada, University of British Columbia, 213 p.

Tempelman-Kluit, D.J., 1972, Geology and origin of the Faro, Vangorda, and Swim concordant zinc-lead deposits, central Yukon Territory: Geological Survey of Canada, Bulletin 208, 73 p.

Tempelman-Kluit, D.J., 1984, Geology, Laberge (105E) and Carmacks (105I), Yukon Territory: Geological Survey of Canada Open-File 1101, scale 1:250,000.

Tempelman-Kluit, D.J., 2009, Geology of Carmacks and Laberge Map Areas, Central Yukon: Incomplete Draft Manuscript on Stratigraphy, Structure and its Early Interpretation(ca.1986): Geological Survey of Canada Open-File 5982, 399 p.

Topham, M.J., Allan, M.M., Mortensen, J.K., Hart, C.J.R., Colpron, M., and Sack, P.J., 2016, Crustal depth of emplacement of the Early Jurassic Aishihik and Tatchun batholiths, west-central Yukon, *in* Yukon Exploration and Geology 2015, K.E. MacFarlane (ed.), Yukon Geological Survey, p. 233–251.

van Drecht, L.H., 2019, Detrital zircon U-Pb geochronology and Hf isotope geochemistry of the Laberge Group: synorogenic siliciclastic record of early Mesozoic crustal thickening and tectonic evolution of the Whitehorse trough in the northern Canadian Cordillera [M.Sc. thesis]: St. John's, Newfoundland, Canada, Memorial University of Newfoundland, 351 p.

Vermeesch, P., 2013, Multi-sample comparison of detrital age distributions: Chemical Geology, v. 341, p. 140-146, doi: 10.1016/j.chemgeo.2013.01.010.

Vermeesch, P., Garzanti, E., 2015, Making geological sense of 'Big Data' in sedimentary provenance analysis: Chemical Geology, g. 409, p. 20-27, doi: 10.1016/j.chemgeo.2015.05.004.

Vervoort, J.D., and Blichert-Toft, J., 1999, Evolution of the depleted mantle: Hf isotope evidence from juvenile rocks through time: Geochemica et Cosmochimica Acta, v. 63, p. 533-556, doi: 10.1016/S0016-7037(98)00274-9.

Vervoort, J.D., Patchett, P.J., Blichert-Toft, J., and Albarède, F., 1999, Relationships between Lu-Hf and Sm-Nd isotopic systems in the global sedimentary system: Earth and Planetary Science Letters, v. 168, p. 79-99, doi: 10.1016/S0012-821X(99)00047-3.

Vinyoles, A., López-Blanco, M., Garcés, M., Arbués, P., Valero, L., Beamud, E., Oliva-Urcia, B., and Cabello, P., 2020, 10 Myr evolution of sedimentation rates in a deep marine to non-marine foreland basin system: Tectonic and sedimentary controls (Eocene, Tremp—Jaca Basin, Southern Pyrenees, NE Spain): Basin Research, v. 33, p. 447-477, doi: 10.1111/bre.12481.

Werdon, M.B., Newberry, R.J., and Szumigala, D.J., 2001, Bedrock geologic map of the Eagle A-2 quadrangle, Fortymile mining district, Alaska: Alaska Division of Geological and Geophysical Surveys Preliminary Interpretive Report 2001–3b, scale: 1:63,360.

Wernicke, B., and Klepacki, D.W., 1988, Escape hypothesis for the Stikine block: Geology, v. 16, p. 461-464, doi:10.1130/0091-7613(1988)016<0461:EHFTSB>2.3.CO;2.

White, D., Colpron, M., and Buffett, G., 2012, Seismic and geological constraints on the structure of the northern Whitehorse trough, Yukon, Canada: Bulletin of Canadian Petroleum Geology, v. 60, p.239-255, https://doi.org/10.2113/gscpgbull.60.4.239.

Wiedenbeck, M., Allé, P., Corfu, F., Griffin, W.L., Meier, M., Oberli, F., Quadt, A.V., Roddick, J.C., and Spiegel, W., 1995, Three natural zircon standards for U-Th-Pb, Lu-Hf, trace element and REE analyses: Geostandards Newsletter, v. 19, p. 1-23.

Wiest, A.C. and Beranek, L.P., 2019, Stratigraphy of the Faro Peak formation, central Yukon: New field observations of Jurassic synorogenic sedimentation along the Yukon-Tanana–Slide Mountain terrane boundary, *in* Yukon Exploration and Geology 2018, K.E. MacFarlane (ed.), Yukon Geological Survey, p.127–142.

Wiest, A.C., Beranek, L.P., and Manor, M.J., 2020, Upper Triassic to Lower Jurassic stratigraphy of the Faro Peak formation, southern Tay River map area, central Yukon (NTS 105K), *in* Yukon Exploration and Geology 2019, K.E. MacFarlane (ed.), Yukon Geological Survey, p. 121-139.

Xie, X., Heller, P.L., 2009, Plate tectonics and basin subsidence history: Geological Society of America Bulletin, v. 121, no. 1/2, p. 55-64, doi: 10.1130/B26398 .1.

APPENDIX 2.A.1

91500

U-Pb standard

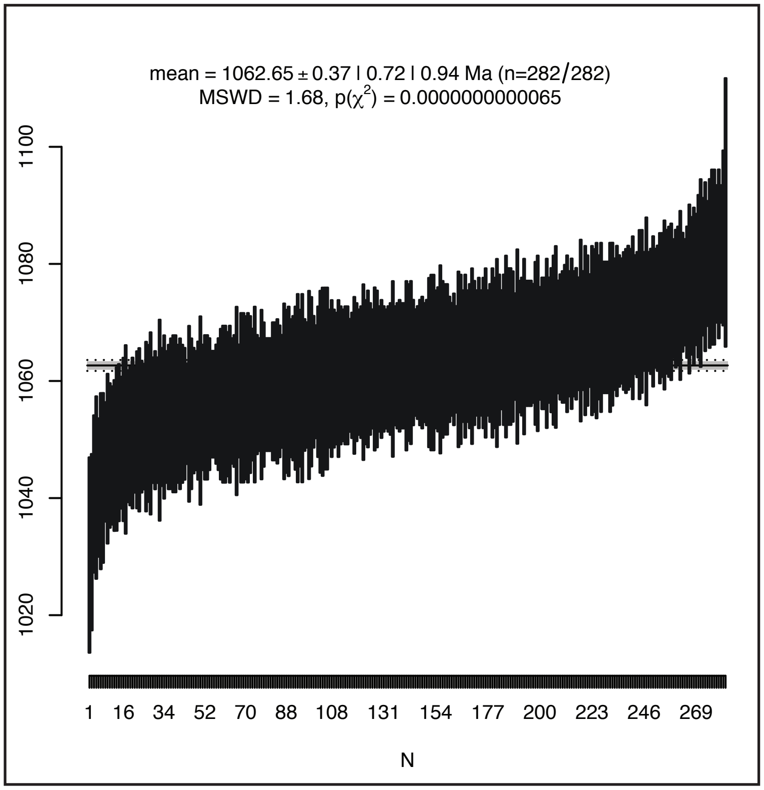

^{176}Hf/^{177}Hf

Plešovice Lu-Hf standard

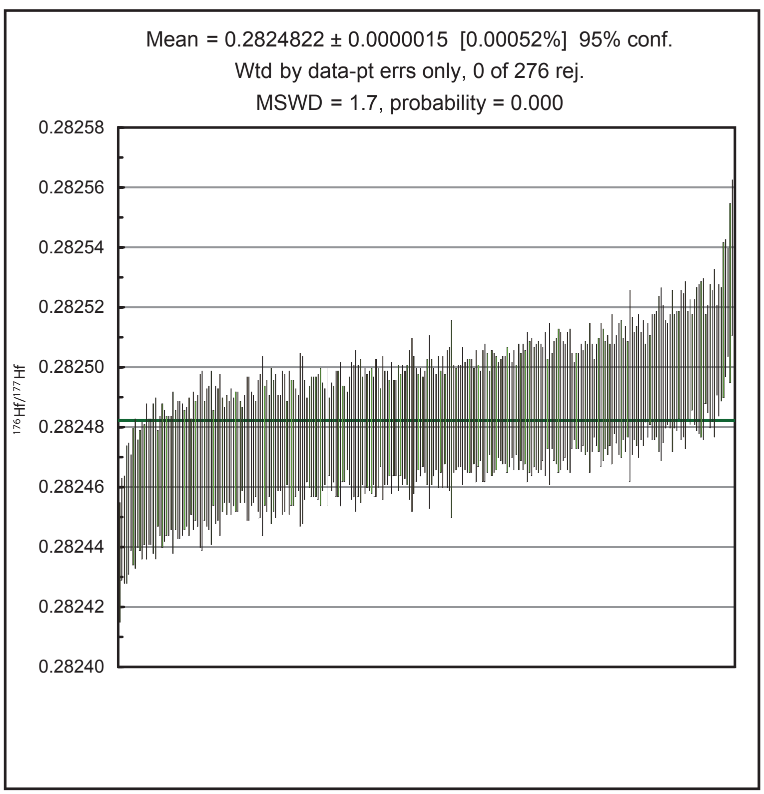

APPENDIX 2.A.2

U-Pb geochronology																	Hf isotope geochemistry								
		Isotopic ratios						Isotopic ages									Isotopic ratios						Epsilon units		
Grain #	Spot name	$^{207}Pb/^{206}Pb$	± 2SE	$^{207}Pb/^{235}U$	± 2SE	$^{206}Pb/^{238}U$	± 2SE	$^{207}Pb/^{206}Pb$	± 2SE (Ma)	$^{207}Pb/^{235}U$	± 2SE (Ma)	$^{206}Pb/^{238}U$	± 2SE (Ma)	Conc. %	Best Age	± 2SE (Ma)	$^{176}Lu/^{177}Hf$	± 2SE	$^{176}Hf/^{177}Hf$	± 2SE	$^{176}Yb/^{177}Hf$	± 2SE	εHf_0	2SE	εHf_t
09AW18--Snowcap assemblage (clast); (Zone 08V NAD 83, 586129 E, 6901021 N)																									
141	190830_534.FIN2	0.06300	0.00260	1.004	0.056	0.1153	0.0042	708	88	704	27	703	24	N/A	703	24	0.0009021	0.000009	0.282370	0.000024	0.02660	0.00030	-14.7	0.8	0.6
70	190830_433.FIN2	0.06320	0.00110	1.027	0.020	0.1175	0.0013	715	37	716	10	716	7	N/A	716	7	0.0006378	0.000004	0.282395	0.000023	0.01734	0.00012	-13.8	0.8	1.9
18	190830_350.FIN2	0.06430	0.00160	1.054	0.026	0.1192	0.0018	752	53	729	13	725	10	N/A	725	10	0.0007570	0.000013	0.282401	0.000024	0.02243	0.00043	-13.6	0.8	2.3
139	190830_532.FIN2	0.06430	0.00140	1.085	0.026	0.1220	0.0014	752	46	742	13	742	8	N/A	742	8	0.0007090	0.000006	0.282329	0.000028	0.02029	0.00018	-16.1	1.0	0.1
58	190830_415.FIN2	0.06520	0.00500	1.109	0.083	0.1238	0.0045	781	161	755	41	752	26	N/A	752	26	0.0005740	0.000006	0.282288	0.000036	0.01545	0.00020	-17.6	1.3	-1.1
41	190830_385.FIN2	0.06500	0.00190	1.118	0.036	0.1246	0.0025	774	61	760	17	757	15	N/A	757	15	0.0010870	0.000014	0.282344	0.000019	0.03123	0.00037	-15.6	0.7	0.8
20	190830_352.FIN2	0.06610	0.00260	1.150	0.049	0.1264	0.0023	810	82	771	22	767	13	N/A	767	13	0.0007280	0.000036	0.282360	0.000025	0.01970	0.00100	-15.0	0.9	1.7
128	190830_515.FIN2	0.08820	0.00170	2.893	0.064	0.2372	0.0043	1387	37	1377	17	1371	23	99	1387	37	0.0007700	0.000045	0.282099	0.000025	0.01690	0.00110	-24.3	0.9	6.2
65	190830_422.FIN2	0.09350	0.00240	3.371	0.095	0.2595	0.0046	1498	49	1488	22	1486	23	99	1498	49	0.0005840	0.000020	0.281891	0.000023	0.01426	0.00050	-31.6	0.8	1.5
39	190830_383.FIN2	0.09940	0.00600	3.780	0.220	0.2770	0.0110	1613	112	1582	45	1575	57	98	1613	112									
63	190830_420.FIN2	0.10670	0.00340	4.510	0.200	0.3062	0.0083	1744	58	1725	37	1721	41	99	1744	58	0.0004733	0.000009	0.281360	0.000025	0.01150	0.00023	-50.4	0.9	-11.7
73	190830_436.FIN2	0.10730	0.00150	4.644	0.074	0.3128	0.0033	1754	26	1753	14	1753	16	100	1754	26	0.0010280	0.000039	0.281719	0.000032	0.02604	0.00098	-37.7	1.1	0.7
149	190830_548.FIN2	0.10810	0.00170	4.658	0.097	0.3129	0.0051	1768	29	1756	17	1754	25	99	1768	29	0.0001410	0.000023	0.281648	0.000022	0.00411	0.00076	-40.2	0.8	-0.5
28	190830_366.FIN2	0.10830	0.00240	4.750	0.120	0.3159	0.0052	1771	40	1769	22	1768	26	100	1771	40	0.0004470	0.000026	0.281384	0.000032	0.01078	0.00064	-49.5	1.1	-10.2
14	190830_346.FIN2	0.10890	0.00160	4.771	0.079	0.3170	0.0038	1781	27	1777	14	1774	18	100	1781	27	0.0007560	0.000015	0.281398	0.000022	0.01919	0.00042	-49.0	0.8	-9.8
31	190830_369.FIN2	0.10900	0.00130	4.781	0.075	0.3175	0.0042	1783	22	1778	13	1776	20	100	1783	22	0.0004580	0.000011	0.281528	0.000028	0.01192	0.00030	-44.5	1.0	-4.8
124	190830_511.FIN2	0.10900	0.00270	4.760	0.160	0.3169	0.0072	1783	45	1775	28	1774	35	100	1783	45	0.0005770	0.000011	0.281512	0.000022	0.01522	0.00032	-45.0	0.8	-5.5
64	190830_421.FIN2	0.10910	0.00130	4.799	0.064	0.3183	0.0036	1784	22	1783	11	1780	17	100	1784	22	0.0005160	0.000004	0.281517	0.000024	0.01333	0.00010	-44.8	0.9	-5.2
156	190830_555.FIN2	0.10950	0.00120	4.845	0.065	0.3190	0.0035	1791	20	1789	11	1783	17	100	1791	20	0.0004887	0.000005	0.281543	0.000020	0.01271	0.00013	-43.9	0.7	-4.1
145	190830_538.FIN2	0.10980	0.00200	4.810	0.110	0.3186	0.0057	1796	33	1783	19	1782	28	99	1796	33	0.0009470	0.000043	0.281721	0.000024	0.02400	0.00120	-37.6	0.9	1.8
104	190830_479.FIN2	0.11110	0.00150	4.957	0.085	0.3243	0.0044	1817	25	1810	15	1810	22	100	1817	25	0.0005720	0.000016	0.281738	0.000022	0.01450	0.00046	-37.0	0.8	3.3
71	190830_434.FIN2	0.11170	0.00110	5.071	0.068	0.3280	0.0036	1827	18	1828	11	1827	18	100	1827	18	0.0002703	0.000003	0.281803	0.000022	0.00704	0.00009	-34.7	0.8	6.2
42	190830_386.FIN2	0.11200	0.00190	5.100	0.110	0.3275	0.0049	1832	31	1829	18	1829	24	100	1832	31	0.0004680	0.000028	0.281435	0.000027	0.01181	0.00078	-47.7	1.0	-7.0
98	190830_473.FIN2	0.11220	0.00160	5.038	0.096	0.3264	0.0053	1835	26	1825	17	1819	26	99	1835	26	0.0016690	0.000053	0.281700	0.000030	0.04300	0.00150	-38.4	1.1	1.0
138	190830_531.FIN2	0.11220	0.00220	5.150	0.120	0.3298	0.0055	1835	36	1841	20	1836	27	100	1835	36	0.0004030	0.000014	0.281454	0.000028	0.01048	0.00035	-47.1	1.0	-6.2
49	190830_399.FIN2	0.11250	0.00220	5.100	0.140	0.3284	0.0064	1840	35	1829	23	1828	31	99	1840	35	0.0003765	0.000003	0.281582	0.000017	0.00922	0.00007	-42.5	0.6	-1.5
153	190830_552.FIN2	0.11250	0.00160	5.112	0.083	0.3285	0.0042	1840	26	1835	14	1833	21	100	1840	26	0.0006710	0.000012	0.281884	0.000029	0.01730	0.00035	-31.9	1.0	8.9
158	190830_557.FIN2	0.11250	0.00130	5.097	0.071	0.3286	0.0036	1840	21	1832	12	1831	17	100	1840	21	0.0005575	0.000003	0.281464	0.000017	0.01379	0.00004	-46.7	0.6	-5.9
106	190830_487.FIN2	0.11260	0.00210	5.120	0.110	0.3281	0.0047	1842	34	1830	19	1827	23	99	1842	34	0.0004580	0.000015	0.281421	0.000022	0.01141	0.00037	-48.2	0.8	-7.3
117	190830_498.FIN2	0.11300	0.00120	5.210	0.081	0.3330	0.0041	1848	19	1853	13	1852	20	100	1848	19	0.0004450	0.000004	0.281573	0.000024	0.01113	0.00013	-42.9	0.9	-1.7
157	190830_556.FIN2	0.11300	0.00130	5.179	0.073	0.3321	0.0039	1848	21	1847	12	1847	19	100	1848	21	0.0002820	0.000018	0.281458	0.000028	0.00692	0.00055	-46.9	1.0	-5.6
123	190830_510.FIN2	0.11310	0.00150	5.150	0.130	0.3302	0.0083	1850	24	1840	23	1835	41	99	1850	24	0.0005350	0.000022	0.281736	0.000026	0.01346	0.00077	-37.1	0.9	4.0
78	190830_441.FIN2	0.11330	0.00300	5.140	0.140	0.3283	0.0053	1853	48	1827	23	1827	25	99	1853	48	0.0001684	0.000005	0.281211	0.000025	0.00441	0.00013	-55.7	0.9	-14.1
2	190830_328.FIN2	0.11350	0.00280	5.180	0.150	0.3310	0.0060	1856	45	1845	25	1842	29	99	1856	45	0.0003940	0.000017	0.281562	0.000030	0.00997	0.00046	-43.2	1.1	-1.8
30	190830_368.FIN2	0.11360	0.00170	5.222	0.089	0.3328	0.0041	1858	27	1851	15	1850	20	100	1858	27	0.0007900	0.000021	0.281658	0.000026	0.01947	0.00053	-39.9	0.9	1.1
92	190830_461.FIN2	0.11360	0.00130	5.261	0.077	0.3347	0.0040	1858	21	1860	13	1859	19	100	1858	21	0.0002143	0.000009	0.281296	0.000021	0.00518	0.00023	-52.7	0.7	-11.0
17	190830_349.FIN2	0.11370	0.00230	5.170	0.110	0.3305	0.0055	1859	37	1843	19	1839	27	99	1859	37	0.0004235	0.000007	0.281419	0.000026	0.01044	0.00016	-48.3	0.9	-6.9
80	190830_443.FIN2	0.11370	0.00250	5.270	0.180	0.3341	0.0082	1859	40	1858	28	1857	39	100	1859	40	0.0004640	0.000030	0.281120	0.000024	0.01157	0.00084	-58.9	0.9	-17.6
129	190830_516.FIN2	0.11370	0.00550	4.920	0.150	0.3220	0.0130	1859	87	1805	26	1797	61	97	1859	87	0.0006827	0.000008	0.281448	0.000030	0.01765	0.00021	-47.3	1.1	-6.2
77	190830_440.FIN2	0.11390	0.00150	5.300	0.084	0.3357	0.0038	1863	24	1864	13	1864	18	100	1863	24	0.0004875	0.000004	0.281446	0.000027	0.01231	0.00014	-47.4	1.0	-5.9
122	190830_509.FIN2	0.11400	0.00230	5.260	0.120	0.3336	0.0054	1864	36	1857	19	1854	26	99	1864	36	0.0004020	0.000028	0.281442	0.000028	0.01025	0.00088	-47.5	1.0	-5.9
99	190830_474.FIN2	0.11420	0.00160	5.312	0.082	0.3360	0.0037	1867	25	1866	13	1866	18	100	1867	25	0.0005704	0.000008	0.281472	0.000029	0.01472	0.00020	-46.4	1.0	-5.0
21	190830_359.FIN2	0.11430	0.00200	5.230	0.110	0.3329	0.0043	1869	32	1852	18	1851	21	99	1869	32	0.0004740	0.000011	0.281636	0.000033	0.01223	0.00029	-40.6	1.2	1.0
57	190830_414.FIN2	0.11430	0.00210	5.190	0.120	0.3319	0.0053	1869	33	1845	18	1845	26	99	1869	33	0.0004720	0.000012	0.281430	0.000021	0.01202	0.00033	-47.9	0.7	-6.3
125	190830_512.FIN2	0.11430	0.00330	5.380	0.200	0.3383	0.0087	1869	52	1877	31	1877	42	100	1869	52	0.0003889	0.000004	0.281546	0.000020	0.01009	0.00013	-43.8	0.7	-2.1
4	190830_330.FIN2	0.11440	0.00140	5.309	0.075	0.3357	0.0034	1870	22	1868	12	1865	16	100	1870	22	0.0006830	0.000030	0.281606	0.000031	0.01705	0.00074	-41.7	1.1	-0.3
91	190830_460.FIN2	0.11440	0.00140	5.333	0.073	0.3361	0.0038	1870	22	1870	12	1870	19	100	1870	22	0.0002700	0.000026	0.281595	0.000020	0.00629	0.00069	-42.1	0.7	-0.2
83	190830_452.FIN2	0.11450	0.00140	5.299	0.075	0.3347	0.0035	1872	22	1865	12	1860	17	99	1872	22	0.0004679	0.000001	0.281443	0.000023	0.01192	0.00004	-47.5	0.8	-5.8
134	190830_527.FIN2	0.11450	0.00150	5.293	0.079	0.3354	0.0041	1872	24	1866	13	1863	20	100	1872	24	0.0003670	0.000012	0.281305	0.000017	0.00861	0.00022	-52.3	0.6	-10.6
118	190830_499.FIN2	0.11460	0.00210	5.360	0.110	0.3377	0.0045	1874	33	1874	17	1874	22	100	1874	33	0.0004770	0.000009	0.281618	0.000031	0.01217	0.00023	-41.3	1.1	0.4
133	190830_526.FIN2	0.11460	0.00280	5.290	0.140	0.3330	0.0058	1874	44	1860	24	1855	29	99	1874	44	0.0010980	0.000058	0.281865	0.000032	0.02660	0.00130	-32.5	1.1	8.4
150	190830_549.FIN2	0.11460	0.00210	5.330	0.120	0.3358	0.0053	1874	33	1868	18	1868	26	100	1874	33	0.0004440	0.000018	0.281462	0.000029	0.01116	0.00055	-48.1	1.0	-6.3
60	190830_417.FIN2	0.11470	0.00120	5.360	0.078	0.3372	0.0038	1875	19	1874	12	1872	18	100	1875	19	0.0006640	0.000017	0.281647	0.000020	0.01686	0.00044	-40.2	0.7	1.3
131	190830_518.FIN2	0.11490	0.00250	5.370	0.150	0.3371	0.0063	1878	39	1873	24	1871	30	100	1878	39	0.0001262	0.000002	0.281162	0.000028	0.00346	0.00005	-57.4	1.0	-15.2
81	190830_450.FIN2	0.11520	0.00150	5.387	0.083	0.3390	0.0039	1883	23	1883	13	1880	19	100	1883	23	0.0004714	0.000005	0.281599	0.000023	0.01180	0.00015	-41.9	0.8	0.0
148	190830_547.FIN2	0.11530	0.00300	5.380	0.160	0.3377	0.0058	1885	47	1874	25	1873	28	99	1885	47	0.0001906	0.000003	0.281486	0.000032	0.00515	0.00009	-45.9	1.1	-3.6
32	190830_370.FIN2	0.11540	0.00360	5.380	0.160	0.3375	0.0075	1886	56	1879	26	1873	36	99	1886	56	0.0004760	0.000010	0.281699	0.000028	0.01214	0.00027	-38.4	1.0	3.6
116	190830_497.FIN2	0.11560	0.00110	5.414	0.067	0.3389	0.0036	1889	17	1884	11	1880	17	100	1889	17	0.0005414	0.000002	0.281644	0.000023	0.01334	0.00004	-40.3	0.8	1.6
96	190830_471.FIN2	0.11600	0.00240	5.380	0.120	0.3392	0.0049	1895	37	1882	20	1882	23	99	1895	37	0.0003411	0.000005	0.281408	0.000028	0.00826	0.00011	-48.7	1.0	-6.4
25	190830_363.FIN2	0.11610	0.00310	5.410	0.160	0.3387	0.0071	1897	48	1882	26	1879	34	99	1897	48	0.0005280	0.000036	0.281632	0.000026	0.01231	0.00075	-40.8	0.9	1.4
40	190830_384.FIN2	0.11720	0.00150	5.590	0.100	0.3447	0.0053	1914	23	1911	16	1907	26	100	1914	23	0.0005090	0.000011	0.281439	0.000027	0.01309	0.00028	-47.6	1.0	-5.0
159	190830_558.FIN2	0.11740	0.00220	5.530	0.120	0.3413	0.0052	1917	34	1904	18	1895	26	99	1917	34	0.0002700	0.000003	0.281366	0.000022	0.00686	0.00010	-50.2	0.8	-7.3
5	190830_331.FIN2	0.11780	0.00120	5.671	0.073	0.3480	0.0041	1923	18	1925	11	1924	19	100	1923	18	0.0003800	0.000015	0.281541	0.000018	0.01006	0.00043	-44.0	0.6	-1.1
3	190830_329.FIN2	0.11790	0.00120	5.636	0.075	0.3461	0.0042	1925	18	1920	12	1915	20	99	1925	18	0.0004670	0.000004	0.281391	0.000022	0.01200	0.00012	-49.3	0.8	-6.5
16	190830_348.FIN2	0.11790	0.00270	5.740	0.160	0.3496	0.0083	1925	41	1933	24	1931	39	100	1925	41	0.0003010	0.000034	0.281348	0.000017	0.00820	0.00100	-50.8	0.6	-7.8
135	190830_528.FIN2	0.11790	0.00250	5.600	0.140	0.3447	0.0067	1925	38	1911	22	1909	32	99	1925	38	0.0004270	0.000026	0.281482	0.000029	0.01113	0.00072	-46.1	1.0	-3.2
55	190830_405.FIN2	0.11810	0.00180	5.730	0.110	0.3495	0.0052	1928	27	1932	16	1931	25	100	1928	27	0.0003100	0.000015	0.281280	0.000023	0.00826	0.00041	-53.2	0.8	-10.1
9	190830_341.FIN2	0.11820	0.00460	5.540	0.280	0.3410	0.0110	1929	70	1892	42	1888	54	98	1929	70	0.0008717	0.000008	0.281483	0.000026	0.02348	0.00023	-46.0	0.9	-3.6
44	190830_388.FIN2	0.11820	0.00340	5.480	0.170	0.3396	0.0065	1929	52	1888	27	1881	31	98	1929	52	0.0005520	0.000012	0.281529	0.000022	0.01416	0.00028	-44.4	0.8	-1.6
53	190830_403.FIN2	0.11820	0.00150	5.705	0.095	0.3490	0.0043	1929	23	1929	15	1928	20	100	1929	23	0.0001885	0.000002	0.281212	0.000021	0.00525	0.00005	-55.6	0.7	-12.3
82	190830_451.FIN2	0.11850	0.00210	5.780	0.140	0.3511	0.0066	1934	32	1938	21	1938	31	100	1934	32	0.0003177	0.000007	0.281397	0.000024	0.00902	0.00017	-49.1	0.9	-5.8
100	190830_475.FIN2	0.11860	0.00160	5.786	0.096	0.3511	0.0043	1935	24	1939	14	1938	21	100	1935	24	0.0001529	0.000002	0.281197	0.000023	0.00414	0.00007	-56.2	0.8	-12.7
127	190830_514.FIN2	0.11860	0.00260	5.670	0.150	0.3460	0.0066	1935	39	1919	24	1918	32	99	1935	39	0.0005010	0.000025	0.281406	0.000022	0.01266	0.00067	-48.8	0.8	-5.7
76	190830_439.FIN2	0.11870	0.00150	5.771	0.079	0.3512	0.0037	1937	23	1939	12	1939	18	100	1937	23	0.0003059	0.000007	0.281371	0.000022	0.00781	0.00021	-50.0	0.8	-6.7
97	190830_472.FIN2	0.11870	0.00130	5.716	0.085	0.3488	0.0048	1937	20	1932	13	1927	23	99	1937	20	0.0003160	0.000016	0.281398	0.000015	0.00807	0.00047	-49.0	0.5	-5.7
144	190830_537.FIN2	0.11870	0.00250	5.720	0.180	0.3482	0.0078	1937	38	1929	28	1925	37	99	1937	38	0.0004600	0.000012	0.281468	0.000025	0.01112	0.00030	-46.6	0.9	-3.4
43	190830_387.FIN2	0.11890	0.00180	5.767	0.096	0.3509	0.0045	1940	27	1937	14	1937	21	100	1940	27	0.0005420	0.000011	0.281457	0.000020	0.01329	0.00036	-47.0	0.7	-3.9
101	190830_476.FIN2	0.11900	0.00190	5.700	0.110	0.3490	0.0052	1941	29	1932	17	1929	25	99	1941	29	0.0007325	0.000004	0.281205	0.000026	0.01917	0.00013	-55.9	0.9	-13.0
113	190830_494.FIN2	0.11900	0.00220	5.730	0.130	0.3486	0.0051	1941	33	1927	20	1926	24	99	1941	33	0.0001673	0.000003	0.281244	0.000022	0.00449	0.00007	-54.5	0.8	-10.9
50	190830_400.FIN2	0.11920	0.00530	5.420	0.240	0.3350	0.0110	1944	79	1897	45	1861	52	96	1944	79	0.0007450	0.000023	0.281874	0.000030	0.01728	0.00056	-32.2	1.1	10.8
142	190830_535.FIN2	0.11920	0.00150	5.805	0.091	0.3519	0.0042	1944	22	1943	14	1942	20	100	1944	22	0.0001211	0.000001	0.281436	0.000017	0.00340	0.00004	-47.7	0.6	-4.0
151	190830_550.FIN2	0.11930	0.00300	5.890	0.170	0.3539	0.0070	1946	45	1953	25	1951	33	100	1946	45	0.0004060	0.000011	0.281431	0.000028	0.01034	0.00030	-47.9	1.0	-4.5
87	190830_456.FIN2	0.11960	0.00130	5.821	0.082	0.3524	0.0045	1950	19	1948	12	1945	22	100	1950	19	0.0005350	0.000038	0.281270	0.000022	0.01450	0.00100	-53.6	0.8	-10.3
132	190830_519.FIN2	0.11960	0.00350	5.790	0.260	0.3510	0.0110	1950	52	1940	38	1936	53	99	1950	52	0.0006670	0.000060	0.281490	0.000035	0.01870	0.00200	-45.8	1.2	-2.6
146	190830_539.FIN2	0.11960	0.00240	5.750	0.160	0.3501	0.0094	1950	36	1936	23	1933	45	99	1950	36	0.0003780	0.000002	0.281407	0.000025	0.01071	0.00007	-48.7	0.9	-5.2
111	190830_492.FIN2	0.11980	0.00300	5.790	0.170	0.3506	0.0061	1953	45	1937	25	1936	29	99	1953	45	0.0003949	0.000008	0.281204	0.000021	0.01034	0.00021	-55.9	0.7	-12.4
109	190830_490.FIN2	0.12020	0.00270	5.870	0.150	0.3530	0.0052	1959	40	1947	22	1946	25	99	1959	40	0.0006483	0.000010	0.281324	0.000018	0.01683	0.00027	-51.7	0.6	-8.3
12	190830_344.FIN2	0.12030	0.00320	5.850	0.170	0.3524	0.0071	1961	47	1949	25	1943	34	99	1961	47	0.0003620	0.000033	0.281393	0.000019	0.00968	0.00091	-49.2	0.7	-5.4
110	190830_491.FIN2	0.12030	0.00400	5.760	0.200	0.3492	0.0064	1961	59	1929	32	1928	31	98	1961	59	0.0007607	0.000009	0.281531	0.000029	0.02002	0.00026	-44.3	1.0	-1.1
130	190830_517.FIN2	0.12050	0.00120	5.912	0.088	0.3555	0.0048	1964	18	1959	13	1959	23	100	1964	18	0.0004225	0.000009	0.281311	0.000019	0.01082	0.00028	-52.1	0.7	-8.4
152	190830_551.FIN2	0.12070	0.00120	5.902	0.088	0.3552	0.0048	1967	18	1958	13	1958	23	100	1967	18	0.0004330	0.000011	0.281350	0.000021	0.01134	0.00036	-50.7	0.7	-6.9
161	190830_560.FIN2	0.12090	0.00460	5.810	0.230	0.3502	0.0075	1970	68	1933	36	1933	36	98	1970	68	0.0001732	0.000004	0.281375	0.000025	0.00437	0.00010	-49.9	0.9	-5.6
61	190830_418.FIN2	0.12110	0.00160	5.915	0.095	0.3551	0.0040	1972	24	1958	13	1957	19	99	1972	24	0.0001055	0.000001	0.281306	0.000018	0.00325	0.00002	-52.3	0.6	-7.9
72	190830_435.FIN2	0.12140	0.00210	5.970	0.120	0.3566	0.0044	1977	31	1966	17	1964	21	99	1977	31	0.0002149	0.000005	0.281477	0.000021	0.00515	0.00012	-46.3	0.7	-1.9

U-Pb geochronology																	Hf isotope geochemistry								
		Isotopic ratios						Isotopic ages									Isotopic ratios						Epsilon units		
Grain #	Spot name	$^{207}Pb/^{206}Pb$	± 2SE	$^{207}Pb/^{235}U$	± 2SE	$^{206}Pb/^{238}U$	± 2SE	$^{207}Pb/^{206}Pb$	± 2SE (Ma)	$^{207}Pb/^{235}U$	± 2SE (Ma)	$^{206}Pb/^{238}U$	± 2SE (Ma)	Conc. %	Best Age	± 2SE (Ma)	$^{176}Lu/^{177}Hf$	± 2SE	$^{176}Hf/^{177}Hf$	± 2SE	$^{176}Yb/^{177}Hf$	± 2SE	εHf_0	2SE	εHf_t
79	190830_442.FIN2	0.12210	0.00150	6.082	0.099	0.3601	0.0045	1987	22	1984	14	1981	21	100	1987	22	0.0005313	0.000006	0.281458	0.000026	0.01339	0.00016	-46.9	0.9	-2.7
119	190830_506.FIN2	0.12250	0.00420	6.170	0.260	0.3610	0.0100	1993	61	1992	36	1985	49	100	1993	61	0.0005031	0.000006	0.281498	0.000029	0.01289	0.00019	-45.5	1.0	-1.1
147	190830_546.FIN2	0.12250	0.00190	6.060	0.110	0.3592	0.0052	1993	28	1981	16	1977	25	99	1993	28	0.0003275	0.000003	0.281441	0.000017	0.00824	0.00008	-47.5	0.6	-2.9
154	190830_553.FIN2	0.12270	0.00210	6.070	0.140	0.3598	0.0072	1996	30	1984	19	1980	34	99	1996	30	0.0016030	0.000050	0.281536	0.000029	0.04100	0.00130	-44.2	1.0	-1.2
13	190830_345.FIN2	0.12290	0.00790	6.730	0.450	0.3920	0.0150	1999	114	2060	63	2126	67	106	1999	114	0.0003866	0.000003	0.281336	0.000026	0.00982	0.00009	-51.2	0.9	-6.6
137	190830_530.FIN2	0.12450	0.00200	6.330	0.130	0.3674	0.0068	2022	28	2019	18	2016	32	100	2022	28	0.0005350	0.000024	0.281448	0.000025	0.01331	0.00062	-47.3	0.9	-2.3
52	190830_402.FIN2	0.12560	0.00180	6.440	0.110	0.3713	0.0048	2037	25	2034	14	2033	22	100	2037	25	0.0004332	0.000008	0.281427	0.000022	0.01118	0.00025	-48.0	0.8	-2.6
15	190830_347.FIN2	0.12820	0.00670	6.720	0.350	0.3760	0.0160	2073	92	2064	46	2053	74	99	2073	92	0.0004295	0.000003	0.281450	0.000021	0.01052	0.00007	-47.2	0.7	-0.9
11	190830_343.FIN2	0.12840	0.00180	6.650	0.180	0.3750	0.0097	2076	25	2071	22	2070	42	100	2076	25	0.0007979	0.000007	0.281459	0.000028	0.01994	0.00017	-46.9	1.0	-1.0
86	190830_455.FIN2	0.12870	0.00140	6.827	0.095	0.3825	0.0041	2080	19	2086	12	2086	19	100	2080	19	0.0006074	0.000004	0.281438	0.000021	0.01495	0.00007	-47.6	0.7	-1.4
105	190830_486.FIN2	0.12870	0.00280	6.730	0.150	0.3795	0.0069	2080	38	2072	20	2071	32	100	2080	38	0.0005410	0.000030	0.281419	0.000024	0.01331	0.00074	-48.3	0.9	-2.0
121	190830_508.FIN2	0.12880	0.00160	6.780	0.110	0.3805	0.0044	2082	22	2078	14	2077	20	100	2082	22	0.0006780	0.000045	0.281414	0.000029	0.01810	0.00130	-48.5	1.0	-2.4
66	190830_423.FIN2	0.12890	0.00150	6.801	0.093	0.3813	0.0039	2083	20	2083	12	2081	18	100	2083	20	0.0004510	0.000017	0.281466	0.000019	0.01133	0.00047	-46.6	0.7	-0.2
84	190830_453.FIN2	0.12930	0.00200	6.800	0.120	0.3813	0.0057	2088	27	2082	15	2081	27	100	2088	27	0.0006390	0.000017	0.281499	0.000020	0.01623	0.00048	-45.5	0.7	0.9
93	190830_468.FIN2	0.13040	0.00240	6.900	0.140	0.3837	0.0055	2103	32	2095	18	2091	25	99	2103	32	0.0007990	0.000043	0.281449	0.000027	0.02130	0.00120	-47.2	1.0	-0.8
35	190830_379.FIN2	0.13080	0.00170	6.980	0.110	0.3863	0.0049	2109	23	2103	15	2103	23	100	2109	23	0.0006710	0.000038	0.281420	0.000025	0.01750	0.00100	-48.3	0.9	-1.5
6	190830_332.FIN2	0.13100	0.00250	6.900	0.140	0.3828	0.0048	2111	33	2089	18	2087	22	99	2111	33	0.0003264	0.000006	0.281459	0.000018	0.00831	0.00017	-46.9	0.6	0.4
23	190830_361.FIN2	0.13110	0.00720	6.760	0.360	0.3820	0.0170	2113	96	2086	42	2082	79	99	2113	96	0.0005770	0.000060	0.281162	0.000024	0.01530	0.00180	-57.4	0.9	-10.5
26	190830_364.FIN2	0.13170	0.00160	7.040	0.100	0.3878	0.0046	2121	21	2114	13	2111	21	100	2121	21	0.0007910	0.000013	0.281429	0.000029	0.02049	0.00038	-48.0	1.0	-1.1
115	190830_496.FIN2	0.13180	0.00220	7.080	0.130	0.3893	0.0057	2122	29	2118	16	2118	27	100	2122	29	0.0005283	0.000003	0.281399	0.000017	0.01337	0.00008	-49.0	0.6	-1.8
103	190830_478.FIN2	0.13220	0.00230	7.250	0.180	0.3937	0.0092	2127	30	2139	22	2138	43	100	2127	30	0.0007450	0.000049	0.281458	0.000026	0.01890	0.00140	-46.9	0.9	0.1
33	190830_377.FIN2	0.13360	0.00190	7.320	0.120	0.3958	0.0051	2146	25	2148	15	2148	24	100	2146	25	0.0008520	0.000038	0.281527	0.000026	0.02180	0.00100	-44.5	0.9	2.9
120	190830_507.FIN2	0.13390	0.00270	7.430	0.230	0.3986	0.0094	2150	35	2161	27	2161	43	101	2150	35	0.0000361	0.000006	0.281093	0.000023	0.00122	0.00021	-59.8	0.8	-11.3
143	190830_536.FIN2	0.14160	0.00300	8.250	0.220	0.4176	0.0084	2247	37	2253	24	2247	38	100	2247	37	0.0004735	0.000008	0.281410	0.000037	0.01181	0.00027	-48.6	1.3	1.6
74	190830_437.FIN2	0.14190	0.00360	7.220	0.220	0.3700	0.0120	2251	44	2137	28	2027	59	90	2251	44	0.0014750	0.000053	0.281456	0.000030	0.03900	0.00190	-47.0	1.1	1.8
46	190830_396.FIN2	0.14570	0.00190	8.660	0.150	0.4284	0.0064	2296	22	2300	16	2297	29	100	2296	22	0.0006670	0.000021	0.281305	0.000022	0.01695	0.00057	-52.3	0.8	-1.3
27	190830_365.FIN2	0.14600	0.00150	8.630	0.120	0.4275	0.0049	2300	18	2296	12	2293	22	100	2300	18	0.0006340	0.000012	0.281426	0.000029	0.01539	0.00032	-48.1	1.0	3.1
112	190830_493.FIN2	0.14660	0.00390	9.060	0.410	0.4370	0.0140	2307	46	2338	40	2335	62	101	2307	46	0.0006808	0.000008	0.281436	0.000030	0.01632	0.00015	-47.7	1.1	3.5
36	190830_380.FIN2	0.14670	0.00170	8.790	0.140	0.4304	0.0057	2308	20	2312	15	2309	26	100	2308	20	0.0006410	0.000036	0.281398	0.000025	0.01630	0.00120	-49.0	0.9	2.3
69	190830_432.FIN2	0.14670	0.00140	8.720	0.100	0.4296	0.0040	2308	16	2307	11	2302	18	100	2308	16	0.0003898	0.000010	0.281371	0.000018	0.00898	0.00019	-50.0	0.6	1.7
37	190830_381.FIN2	0.14800	0.00180	8.900	0.180	0.4341	0.0079	2323	21	2323	18	2321	35	100	2323	21	0.0013200	0.000190	0.281460	0.000041	0.03350	0.00490	-46.9	1.5	3.8
95	190830_470.FIN2	0.15450	0.00160	9.560	0.140	0.4486	0.0057	2396	18	2391	14	2387	25	100	2396	18	0.0005990	0.000011	0.281112	0.000024	0.01590	0.00034	-59.2	0.9	-5.8
89	190830_458.FIN2	0.16100	0.00470	9.900	0.270	0.4480	0.0110	2466	49	2422	26	2385	50	97	2466	49	0.0003666	0.000003	0.281044	0.000030	0.00882	0.00010	-61.6	1.1	-6.2
56	190830_406.FIN2	0.16330	0.00310	10.660	0.290	0.4709	0.0099	2490	32	2483	24	2482	43	100	2490	32	0.0007688	0.000004	0.281359	0.000039	0.01936	0.00015	-50.4	1.4	4.9
8	190830_340.FIN2	0.16460	0.00200	10.720	0.180	0.4715	0.0057	2503	20	2495	16	2487	25	99	2503	20	0.0004732	0.000008	0.281144	0.000021	0.01198	0.00021	-58.0	0.7	-2.0
54	190830_404.FIN2	0.16510	0.00210	10.880	0.230	0.4757	0.0081	2509	21	2508	20	2506	36	100	2509	21	0.0005880	0.000021	0.281244	0.000025	0.01494	0.00052	-54.5	0.9	1.5
38	190830_382.FIN2	0.17000	0.00210	11.530	0.220	0.4875	0.0074	2558	21	2561	18	2557	32	100	2558	21	0.0005360	0.000012	0.281138	0.000026	0.01363	0.00033	-58.2	0.9	-1.1
140	190830_533.FIN2	0.17000	0.00180	11.440	0.210	0.4869	0.0089	2558	18	2557	17	2552	39	100	2558	18	0.0005280	0.000017	0.281217	0.000026	0.01316	0.00048	-55.4	0.9	1.8
45	190830_395.FIN2	0.17200	0.00210	11.670	0.180	0.4902	0.0060	2577	20	2574	15	2570	26	100	2577	20	0.0004065	0.000002	0.281176	0.000027	0.00985	0.00005	-56.9	1.0	1.0
19	190830_351.FIN2	0.17370	0.00210	11.860	0.190	0.4928	0.0059	2594	20	2588	15	2583	26	100	2594	20	0.0004141	0.000005	0.281118	0.000031	0.01010	0.00014	-58.9	1.1	-0.7
90	190830_459.FIN2	0.17380	0.00160	11.880	0.140	0.4940	0.0051	2595	15	2593	11	2586	22	100	2595	15	0.0004900	0.000014	0.281225	0.000030	0.01233	0.00035	-55.2	1.1	3.0
29	190830_367.FIN2	0.17470	0.00280	12.000	0.300	0.4970	0.0130	2603	27	2600	23	2597	54	100	2603	27	0.0004810	0.000002	0.281163	0.000028	0.01224	0.00005	-57.4	1.0	1.0
88	190830_457.FIN2	0.17520	0.00170	12.070	0.160	0.4979	0.0062	2608	16	2606	13	2603	27	100	2608	16	0.0003421	0.000004	0.281148	0.000027	0.00875	0.00010	-57.9	1.0	0.8
160	190830_559.FIN2	0.17580	0.00190	12.120	0.170	0.4986	0.0049	2614	18	2609	13	2606	21	100	2614	18	0.0005260	0.000017	0.281150	0.000026	0.01319	0.00045	-57.8	0.9	0.7
48	190830_398.FIN2	0.17620	0.00280	12.240	0.250	0.5015	0.0086	2617	26	2622	18	2618	37	100	2617	26	0.0007090	0.000032	0.281214	0.000031	0.01900	0.00100	-55.6	1.1	2.7
7	190830_333.FIN2	0.17640	0.00220	12.310	0.200	0.5023	0.0069	2619	21	2624	15	2624	30	100	2619	21	0.0004310	0.000013	0.280958	0.000022	0.01069	0.00033	-64.6	0.8	-5.9
1	190830_327.FIN2	0.17650	0.00290	12.140	0.230	0.4984	0.0073	2620	27	2608	18	2603	31	99	2620	27	0.0005600	0.000018	0.281025	0.000023	0.01407	0.00049	-62.2	0.8	-3.7
102	190830_477.FIN2	0.17680	0.00360	12.270	0.290	0.5014	0.0089	2623	34	2620	22	2618	38	100	2623	34	0.0004685	0.000001	0.281106	0.000027	0.01174	0.00002	-59.4	1.0	-0.6
47	190830_397.FIN2	0.17750	0.00260	12.450	0.310	0.5050	0.0110	2630	24	2634	23	2631	46	100	2630	24									
107	190830_488.FIN2	0.17780	0.00250	12.270	0.220	0.5016	0.0087	2632	23	2622	17	2618	37	99	2632	23	0.0017260	0.000033	0.281311	0.000027	0.04355	0.00086	-52.1	1.0	4.7
85	190830_454.FIN2	0.17900	0.00280	12.330	0.270	0.5019	0.0093	2644	26	2631	22	2618	40	99	2644	26	0.0006600	0.000036	0.281215	0.000023	0.01719	0.00096	-55.5	0.8	3.4
24	190830_362.FIN2	0.18280	0.00260	13.110	0.290	0.5163	0.0093	2678	24	2686	20	2683	40	100	2678	24	0.0004030	0.000015	0.280927	0.000019	0.01002	0.00043	-65.7	0.7	-5.5
10	190830_342.FIN2	0.18460	0.00170	13.210	0.180	0.5174	0.0062	2695	15	2691	13	2689	26	100	2695	15	0.0002799	0.000003	0.281002	0.000023	0.00602	0.00007	-63.1	0.8	-2.3
67	190830_424.FIN2	0.18500	0.00370	13.200	0.330	0.5180	0.0110	2698	33	2691	23	2690	48	100	2698	33	0.0005780	0.000017	0.280885	0.000036	0.01528	0.00068	-67.2	1.3	-6.9
136	190830_529.FIN2	0.18530	0.00230	13.430	0.250	0.5221	0.0092	2701	20	2707	17	2705	39	100	2701	20	0.0006907	0.000007	0.280985	0.000025	0.01751	0.00020	-63.7	0.9	-3.5
108	190830_489.FIN2	0.18920	0.00210	13.840	0.190	0.5289	0.0063	2735	18	2736	13	2734	27	100	2735	18	0.0004736	0.000005	0.281125	0.000034	0.01134	0.00014	-58.7	1.2	2.7
126	190830_513.FIN2	0.19770	0.00240	15.040	0.320	0.5480	0.0100	2807	20	2814	20	2812	42	100	2807	20	0.0011600	0.000140	0.281106	0.000028	0.03090	0.00380	-59.4	1.0	2.4
94	190830_469.FIN2	0.20690	0.00510	16.150	0.520	0.5612	0.0072	2881	40	2869	28	2869	30	100	2881	40	0.0006960	0.000012	0.281132	0.000028	0.01719	0.00032	-58.5	1.0	5.9
22	190830_360.FIN2	0.22010	0.00340	17.930	0.400	0.5890	0.0100	2981	25	2981	21	2981	42	100	2981	25	0.0005296	0.000009	0.280719	0.000023	0.01327	0.00026	-73.1	0.8	-6.2
155	190830_554.FIN2	0.23500	0.00700	20.050	0.760	0.6150	0.0210	3086	48	3087	36	3083	84	100	3086	48	0.0005062	0.000010	0.280707	0.000030	0.01259	0.00024	-73.5	1.1	-4.1
51	190830_401.FIN2	0.25510	0.00670	22.740	0.850	0.6440	0.0200	3217	41	3213	37	3203	78	100	3217	41	0.0010110	0.000070	0.280637	0.000030	0.02730	0.00210	-76.0	1.1	-4.7
rejected analyses																									
34	190830_378.FIN2	0.18900	0.01000	11.830	0.980	0.4510	0.0150	2733	87	2567	71	2396	68	88	N/A	N/A	0.0004590	0.000022	0.281268	0.000026	0.01079	0.00058	-53.6	0.9	N/A
59	190830_416.FIN2	0.11410	0.00300	4.660	0.150	0.2968	0.0074	1866	47	1758	27	1675	37	90	N/A	N/A	0.0021100	0.000059	0.281691	0.000035	0.05760	0.00200	-38.7	1.2	N/A
62	190830_419.FIN2	0.11570	0.00240	3.536	0.095	0.2235	0.0051	1891	37	1532	22	1300	27	69	N/A	N/A	0.0010270	0.000016	0.281743	0.000028	0.02815	0.00043	-36.8	1.0	N/A
68	190830_425.FIN2	0.18970	0.00500	8.720	0.300	0.3311	0.0077	2740	43	2302	32	1842	37	67	N/A	N/A	0.0010570	0.000092	0.281195	0.000033	0.02880	0.00270	-56.2	1.2	N/A
75	190830_438.FIN2	0.17130	0.00290	8.160	0.260	0.3451	0.0098	2570	28	2242	28	1909	47	74	N/A	N/A	0.0008390	0.000038	0.281200	0.000026	0.02050	0.00100	-56.0	0.9	N/A
114	190830_495.FIN2	0.11340	0.00390	2.730	0.110	0.1760	0.0038	1855	62	1332	31	1045	21	56	N/A	N/A	0.0005440	0.000014	0.281476	0.000029	0.01384	0.00040	-46.3	1.0	N/A
04AW18--Snowcap assemblage; (Zone 08V NAD 83 591960 E, 6896800 N)																									
107	190208_171.FIN2	0.06490	0.00300	1.087	0.062	0.1209	0.0038	771	97	745	30	735	22	N/A	735	22	0.0012440	0.000056	0.282270	0.000051	0.03840	0.00170	-18.2	1.8	-2.4
245	190830_147.FIN2	0.09330	0.00190	3.351	0.088	0.2599	0.0056	1494	39	1489	21	1488	29	100	1494	39	0.0008350	0.000037	0.281879	0.000029	0.02130	0.00100	-32.0	1.0	0.7
159	190830_016.FIN2	0.10080	0.00830	3.960	0.290	0.2850	0.0150	1639	153	1615	60	1614	75	98	1639	153	0.0012800	0.000160	0.281550	0.000026	0.03550	0.00520	-43.7	0.9	-8.2
84	190208_136.FIN2	0.10920	0.00270	4.690	0.140	0.3139	0.0087	1786	45	1763	25	1759	43	98	1786	45									
212	190830_096.FIN2	0.10950	0.00110	4.924	0.061	0.3230	0.0034	1791	18	1804	10	1803	17	101	1791	18	0.0007130	0.000014	0.281738	0.000019	0.01823	0.00037	-37.0	0.7	2.5
37	190208_065.FIN2	0.10970	0.00270	4.840	0.210	0.3180	0.0110	1794	45	1788	35	1779	54	99	1794	45									
79	190208_125.FIN2	0.10980	0.00130	4.826	0.066	0.3194	0.0037	1796	22	1787	12	1786	18	99	1796	22	0.0006680	0.000014	0.281617	0.000032	0.01907	0.00035	-41.3	1.1	-1.6
204	190830_088.FIN2	0.11030	0.00130	4.911	0.088	0.3222	0.0044	1804	21	1804	16	1800	21	100	1804	21	0.0009190	0.000010	0.281639	0.000027	0.02420	0.00037	-40.5	1.0	-0.9
22	190208_038.FIN2	0.11150	0.00110	5.064	0.068	0.3278	0.0037	1824	18	1826	11	1826	18	100	1808	56	0.0004448	0.000009	0.281476	0.000023	0.01271	0.00022	-46.3	0.8	-5.7
28	190208_050.FIN2	0.11060	0.00100	4.901	0.077	0.3216	0.0047	1809	16	1799	13	1799	22	99	1809	16	0.0008430	0.000014	0.281711	0.000022	0.02366	0.00044	-38.0	0.8	1.8
224	190830_114.FIN2	0.11080	0.00220	4.910	0.110	0.3222	0.0075	1813	36	1801	19	1798	37	99	1813	36	0.0007600	0.000100	0.281567	0.000026	0.02130	0.00310	-43.1	0.9	-3.1
67	190208_107.FIN2	0.11090	0.00230	4.870	0.140	0.3207	0.0062	1814	38	1794	24	1792	30	99	1814	38	0.0004990	0.000006	0.281525	0.000028	0.01423	0.00016	-44.6	1.0	-4.2
174	190830_038.FIN2	0.11100	0.00570	5.080	0.250	0.3280	0.0110	1816	93	1830	41	1829	53	101	1816	93	0.0009370	0.000039	0.281544	0.000027	0.02520	0.00110	-43.9	1.0	-4.1
73	190208_119.FIN2	0.11140	0.00180	4.920	0.110	0.3227	0.0067	1822	29	1803	20	1801	33	99	1822	29	0.0011300	0.000028	0.281691	0.000035	0.03243	0.00035	-38.7	1.2	1.1
248	190830_150.FIN2	0.11150	0.00640	5.040	0.440	0.3250	0.0220	1824	104	1809	75	1810	110	99	1824	104									
236	190830_132.FIN2	0.11210	0.00540	4.800	0.280	0.3100	0.0110	1834	87	1780	49	1740	56	95	1834	87	0.0009260	0.000054	0.281817	0.000030	0.02220	0.00140	-34.2	1.1	6.0
162	190830_019.FIN2	0.11250	0.00100	5.170	0.063	0.3309	0.0036	1840	16	1844	10	1843	17	100	1840	16	0.0006202	0.000010	0.281536	0.000025	0.01533	0.00024	-44.2	0.9	-3.4
190	190830_067.FIN2	0.11270	0.00220	5.330	0.150	0.3368	0.0069	1843	35	1870	24	1870	33	101	1843	35	0.0010150	0.000053	0.281679	0.000027	0.02590	0.00130	-39.1	1.0	1.2
164	190830_021.FIN2	0.11271	0.00094	5.193	0.060	0.3321	0.0035	1844	15	1848	10	1847	17	100	1844	15	0.0012316	0.000006	0.281684	0.000023	0.03138	0.00013	-38.9	0.8	1.2
114	190208_178.FIN2	0.11280	0.00230	5.070	0.170	0.3271	0.0093	1845	37	1820	29	1820	45	99	1845	37	0.0004660	0.000012	0.281637	0.000040	0.01407	0.00042	-40.6	1.4	0.5
206	190830_090.FIN2	0.11290	0.00240	5.200	0.120	0.3327	0.0062	1847	38	1853	21	1850	30	100	1847	38	0.0013500	0.000160	0.281478	0.000028	0.03760	0.00490	-46.2	1.0	-6.2
123	190208_193.FIN2	0.11330	0.00210	5.240	0.120	0.3352	0.0053	1853	34	1858	19	1862	26	100	1853	34	0.0003960	0.000012	0.281564	0.000026	0.01057	0.00030	-43.2	0.9	-1.9
205	190830_089.FIN2	0.11370	0.00240	5.150	0.140	0.3290	0.0077	1859	38	1849	26	1843	42	99	1859	38	0.0009300	0.000050	0.281669	0.000026	0.02490	0.00150	-39.5	0.9	1.4
243	190830_145.FIN2	0.11370	0.00400	5.170	0.180	0.3310	0.0130	1859	64	1845	29	1842	61	99	1859	64	0.0011940	0.000057	0.281677	0.000032	0.03070	0.00150	-39.2	1.1	1.3
18	190208_034.FIN2	0.11380	0.00110	5.217	0.069	0.3332	0.0042	1861	17	1854	11	1854	20	100	1861	17	0.0005129	0.000008	0.281553	0.000023	0.01354	0.00032	-43.6	0.8	-2.2
61	190208_101.FIN2	0.11450	0.00400	5.020	0.160	0.3193	0.0097	1872	63	1821	27	1786	47	95	1872	63	0.0009600	0.000100	0.281479	0.000032	0.02780	0.00320	-46.2	1.1	-5.2
136	190208_212.FIN2	0.11450	0.00190	5.300	0.100	0.3356	0.0050	1872	30	1865	16	1864	24	100	1872	30	0.0005800	0.000010	0.281558	0.000024	0.01565	0.00024	-43.4	0.9	-1.9
223	190830_113.FIN2	0.11450	0.00210	5.300	0.120	0.3359	0.0065	1872	33	1867	19	1866	31	100	1872	33	0.0002975	0.000009	0.281564	0.000021	0.00741	0.00025	-43.2	0.7	-1.3
137	190208_213.FIN2	0.11460	0.00250	5.250	0.150	0.3354	0.0068	1874	39	1863	23	1863	33	99	1874	39	0.0010000	0.000033	0.281643	0.000039	0.02820	0.00130	-40.4	1.4	0.7

U-Pb geochronology																	Hf isotope geochemistry								
		Isotopic ratios						Isotopic ages									Isotopic ratios						Epsilon units		
Grain #	Spot name	$^{207}Pb/^{206}Pb$	± 2SE	$^{207}Pb/^{235}U$	± 2SE	$^{206}Pb/^{238}U$	± 2SE	$^{207}Pb/^{206}Pb$	± 2SE (Ma)	$^{207}Pb/^{235}U$	± 2SE (Ma)	$^{206}Pb/^{238}U$	± 2SE (Ma)	Conc. %	Best Age	± 2SE (Ma)	$^{176}Lu/^{177}Hf$	± 2SE	$^{176}Hf/^{177}Hf$	± 2SE	$^{176}Yb/^{177}Hf$	± 2SE	$εHf_0$	2SE	$εHf_t$
125	190208_195.FIN2	0.11470	0.00230	5.260	0.170	0.3345	0.0084	1875	36	1858	26	1858	41	99	1875	36	0.0005140	0.000017	0.281435	0.000039	0.01496	0.00035	-47.7	1.4	-6.1
43	190208_071.FIN2	0.11480	0.00220	5.235	0.096	0.3331	0.0057	1877	35	1855	16	1851	28	99	1877	35	0.0006360	0.000025	0.281512	0.000028	0.01760	0.00082	-45.0	1.0	-3.5
10	190208_020.FIN2	0.11520	0.00190	5.360	0.130	0.3379	0.0067	1883	30	1875	20	1874	32	100	1883	30	0.0011820	0.000038	0.281639	0.000045	0.03410	0.00130	-40.5	1.6	0.5
97	190208_155.FIN2	0.11520	0.00130	5.359	0.080	0.3378	0.0045	1883	20	1877	12	1877	21	100	1883	20	0.0002590	0.000041	0.281665	0.000033	0.00770	0.00120	-39.6	1.2	2.6
1	190208_011.FIN2	0.11530	0.00230	5.330	0.120	0.3361	0.0052	1885	36	1868	19	1866	25	99	1885	36	0.0006730	0.000023	0.281464	0.000041	0.01812	0.00052	-46.7	1.5	-5.0
188	190830_058.FIN2	0.11530	0.00180	5.440	0.110	0.3395	0.0064	1885	28	1887	18	1887	30	100	1885	28	0.0010410	0.000081	0.281649	0.000027	0.02610	0.00190	-40.2	1.0	1.1
251	190830_159.FIN2	0.11550	0.00210	5.420	0.110	0.3395	0.0063	1888	33	1886	18	1882	30	100	1888	33	0.0004930	0.000036	0.281584	0.000020	0.01257	0.00098	-42.5	0.7	-0.5
33	190208_055.FIN2	0.11630	0.00360	5.390	0.210	0.3376	0.0092	1900	56	1879	33	1874	44	99	1900	56									
141	190208_217.FIN2	0.11660	0.00350	5.570	0.230	0.3434	0.0082	1905	54	1903	34	1901	40	100	1905	54	0.0003655	0.000006	0.281523	0.000031	0.00993	0.00021	-44.6	1.1	-2.1
147	190211_016.FIN2	0.11660	0.00140	4.902	0.076	0.3043	0.0040	1905	22	1801	13	1712	20	90	1905	22	0.0012500	0.000170	0.281484	0.000050	0.03450	0.00520	-46.0	1.8	-4.6
59	190208_099.FIN2	0.11730	0.00250	5.410	0.180	0.3350	0.0100	1915	38	1884	29	1861	50	97	1915	38	0.0000554	0.000010	0.281489	0.000023	0.00198	0.00044	-45.8	0.8	-2.7
12	190208_022.FIN2	0.11740	0.00270	5.340	0.200	0.3300	0.0120	1917	41	1870	32	1837	56	96	1917	41	0.0004491	0.000008	0.281533	0.000034	0.01237	0.00033	-44.3	1.2	-1.6
183	190830_053.FIN2	0.11760	0.00120	5.630	0.088	0.3465	0.0055	1920	18	1918	14	1915	26	100	1920	18	0.0006010	0.000045	0.281531	0.000020	0.01560	0.00120	-44.3	0.7	-1.8
196	190830_073.FIN2	0.11790	0.00280	5.710	0.180	0.3488	0.0097	1925	43	1930	28	1928	46	100	1925	43	0.0005671	0.000005	0.281498	0.000025	0.01429	0.00013	-45.5	0.9	-2.8
133	190208_209.FIN2	0.11800	0.00130	5.628	0.085	0.3465	0.0044	1926	20	1917	13	1917	21	100	1926	20	0.0006442	0.000010	0.281520	0.000036	0.01755	0.00023	-44.7	1.3	-2.1
163	190830_020.FIN2	0.11805	0.00086	5.706	0.061	0.3496	0.0034	1927	13	1933	9	1931	16	100	1927	13	0.0010150	0.000037	0.281563	0.000025	0.02690	0.00110	-43.2	0.9	-1.0
102	190208_160.FIN2	0.11810	0.00320	5.490	0.240	0.3370	0.0110	1928	49	1896	37	1873	53	97	1928	49	0.0004170	0.000023	0.281601	0.000026	0.01152	0.00074	-41.9	0.9	1.1
30	190208_052.FIN2	0.11870	0.00230	5.600	0.130	0.3454	0.0059	1937	35	1912	21	1911	28	99	1937	35	0.0001637	0.000007	0.281355	0.000029	0.00520	0.00027	-50.6	1.0	-7.1
256	190830_164.FIN2	0.11870	0.00120	5.741	0.074	0.3498	0.0037	1937	18	1934	11	1934	18	100	1937	18	0.0013240	0.000081	0.281586	0.000031	0.03520	0.00230	-42.4	1.1	-0.4
13	190208_029.FIN2	0.11890	0.00340	5.510	0.170	0.3382	0.0061	1940	51	1898	26	1877	30	97	1940	51	0.0011240	0.000034	0.281665	0.000031	0.03153	0.00094	-39.6	1.1	2.8
16	190208_032.FIN2	0.11890	0.00140	5.823	0.091	0.3530	0.0037	1940	21	1946	14	1950	18	101	1940	21	0.0007210	0.000018	0.281472	0.000030	0.02115	0.00069	-46.4	1.1	-3.6
152	190211_021.FIN2	0.11940	0.00190	5.720	0.130	0.3506	0.0070	1947	28	1929	21	1935	33	99	1947	28	0.0001674	0.000010	0.281335	0.000020	0.00494	0.00025	-51.3	0.7	-7.5
209	190830_093.FIN2	0.11980	0.00580	5.640	0.290	0.3360	0.0160	1953	86	1921	43	1867	77	96	1953	86	0.0009260	0.000044	0.281456	0.000026	0.02380	0.00120	-47.0	0.9	-4.1
225	190830_115.FIN2	0.12010	0.00550	6.240	0.430	0.3640	0.0220	1958	82	2009	62	2000	100	102	1958	82	0.0005420	0.000068	0.281339	0.000031	0.01500	0.00200	-51.1	1.1	-7.6
246	190830_148.FIN2	0.12010	0.00240	5.860	0.150	0.3523	0.0051	1958	36	1945	22	1944	24	99	1958	36	0.0005440	0.000020	0.281480	0.000024	0.01343	0.00053	-46.1	0.9	-2.6
247	190830_149.FIN2	0.12050	0.00390	5.980	0.250	0.3550	0.0130	1964	58	1971	36	1959	61	100	1964	58	0.0007420	0.000037	0.281541	0.000027	0.01890	0.00100	-44.0	1.0	-0.6
93	190208_145.FIN2	0.12090	0.00120	5.928	0.077	0.3562	0.0045	1970	18	1965	11	1963	21	100	1970	18	0.0001933	0.000003	0.281555	0.000024	0.00511	0.00004	-43.5	0.9	0.8
197	190830_074.FIN2	0.12090	0.00520	5.960	0.270	0.3550	0.0180	1970	77	1968	39	1955	84	99	1970	77	0.0010530	0.000050	0.281406	0.000016	0.02890	0.00160	-48.8	0.6	-5.7
181	190830_051.FIN2	0.12140	0.00300	5.900	0.190	0.3490	0.0120	1977	44	1959	29	1929	58	98	1977	44	0.0013200	0.000100	0.281558	0.000018	0.03490	0.00280	-43.4	0.6	-0.5
233	190830_129.FIN2	0.12170	0.00230	6.030	0.130	0.3594	0.0069	1981	34	1979	18	1978	33	100	1981	34	0.0007023	0.000006	0.281528	0.000022	0.01856	0.00015	-44.5	0.8	-0.6
124	190208_194.FIN2	0.12180	0.00310	6.120	0.170	0.3617	0.0099	1983	45	1992	24	1989	47	100	1983	45	0.0012550	0.000086	0.281528	0.000024	0.03450	0.00220	-44.5	0.9	-1.3
238	190830_140.FIN2	0.12180	0.00200	6.120	0.110	0.3621	0.0069	1983	29	1992	16	1991	32	100	1983	29	0.0006650	0.000038	0.281453	0.000022	0.01770	0.00110	-47.1	0.8	-3.2
80	190208_126.FIN2	0.12190	0.00260	6.160	0.210	0.3640	0.0120	1984	38	1993	28	1998	57	101	1984	38	0.0005380	0.000018	0.281495	0.000034	0.01605	0.00064	-45.6	1.2	-1.5
192	190830_069.FIN2	0.12240	0.00360	6.150	0.180	0.3618	0.0070	1992	52	1992	26	1989	33	100	1992	52	0.0004780	0.000011	0.281380	0.000018	0.01224	0.00025	-49.7	0.6	-5.3
98	190208_156.FIN2	0.12270	0.00300	5.870	0.170	0.3494	0.0093	1996	43	1954	25	1930	44	97	1996	43	0.0005387	0.000007	0.281403	0.000023	0.01526	0.00013	-48.9	0.8	-4.5
154	190830_011.FIN2	0.12270	0.00490	6.220	0.270	0.3640	0.0130	1996	71	2005	38	2001	59	100	1996	71	0.0005690	0.000018	0.281370	0.000024	0.01498	0.00049	-50.0	0.9	-5.7
71	190208_117.FIN2	0.12290	0.00500	5.960	0.340	0.3560	0.0170	1999	72	1957	49	1955	82	98	1999	72									
100	190208_158.FIN2	0.12290	0.00260	6.140	0.140	0.3605	0.0088	1999	38	1993	19	1983	41	99	1999	38	0.0010350	0.000023	0.281493	0.000025	0.02814	0.00083	-45.7	0.9	-1.9
175	190830_039.FIN2	0.12290	0.00160	6.230	0.110	0.3653	0.0054	1999	23	2007	16	2006	25	100	1999	23	0.0004517	0.000008	0.281388	0.000016	0.01161	0.00020	-49.4	0.6	-4.9
237	190830_133.FIN2	0.12290	0.00150	6.143	0.092	0.3620	0.0051	1999	22	1993	13	1990	24	100	1999	22	0.0007420	0.000035	0.281508	0.000024	0.01848	0.00098	-45.2	0.9	-1.0
51	190208_085.FIN2	0.12300	0.00120	6.160	0.097	0.3630	0.0052	2000	17	1994	14	1994	25	100	2000	17	0.0006010	0.000033	0.281415	0.000028	0.01666	0.00099	-48.4	1.0	-4.1
118	190208_182.FIN2	0.12330	0.00120	6.128	0.080	0.3617	0.0042	2005	17	1992	11	1989	20	99	2005	17	0.0004160	0.000021	0.281419	0.000022	0.01147	0.00051	-48.3	0.8	-3.6
9	190208_019.FIN2	0.12380	0.00280	5.920	0.130	0.3519	0.0096	2012	40	1962	19	1942	45	97	2012	40	0.0004360	0.000013	0.281367	0.000023	0.01241	0.00039	-50.1	0.8	-5.3
88	190208_140.FIN2	0.12430	0.00180	6.360	0.150	0.3698	0.0081	2019	26	2026	21	2026	38	100	2019	26	0.0006990	0.000062	0.281343	0.000021	0.01990	0.00200	-51.0	0.7	-6.3
89	190208_141.FIN2	0.12450	0.00440	6.370	0.270	0.3690	0.0120	2022	63	2022	37	2022	58	100	2022	63	0.0012640	0.000089	0.281385	0.000036	0.03400	0.00270	-49.5	1.3	-5.5
57	190208_091.FIN2	0.12470	0.00220	6.210	0.150	0.3627	0.0060	2025	31	2003	21	1994	28	98	2025	31	0.0010610	0.000028	0.281549	0.000028	0.02810	0.00093	-43.7	1.0	0.6
91	190208_143.FIN2	0.12470	0.00180	6.350	0.160	0.3692	0.0074	2025	26	2019	23	2022	35	100	2025	26	0.0004670	0.000040	0.281507	0.000033	0.01330	0.00120	-45.2	1.2	-0.1
131	190208_207.FIN2	0.12490	0.00430	6.150	0.270	0.3600	0.0110	2027	61	1991	39	1980	50	98	2027	61	0.0006240	0.000043	0.281519	0.000037	0.01790	0.00140	-44.8	1.3	0.2
216	190830_106.FIN2	0.12580	0.00450	6.140	0.450	0.3520	0.0210	2040	63	1991	60	1942	99	95	2040	63	0.0012150	0.000082	0.281421	0.000024	0.03280	0.00230	-48.2	0.9	-3.8
4	190208_014.FIN2	0.12740	0.00290	6.500	0.210	0.3705	0.0098	2062	40	2041	29	2042	46	99	2062	40	0.0007140	0.000069	0.281385	0.000030	0.02030	0.00220	-49.5	1.1	-3.9
158	190830_015.FIN2	0.12840	0.00280	6.670	0.200	0.3770	0.0110	2076	38	2065	26	2062	52	99	2076	38	0.0014070	0.000084	0.281616	0.000024	0.03860	0.00250	-41.3	0.9	3.7
228	190830_124.FIN2	0.12850	0.00290	6.520	0.220	0.3670	0.0120	2078	40	2046	31	2013	55	97	2078	40	0.0005590	0.000011	0.281448	0.000026	0.01453	0.00031	-47.3	0.9	-1.1
167	190830_031.FIN2	0.12890	0.00250	6.740	0.130	0.3800	0.0050	2083	34	2075	18	2074	24	100	2083	34	0.0002860	0.000003	0.281425	0.000020	0.00747	0.00008	-48.1	0.7	-1.4
234	190830_130.FIN2	0.12900	0.00480	6.860	0.320	0.3820	0.0130	2084	65	2085	41	2082	63	100	2084	65	0.0008030	0.000020	0.281424	0.000034	0.02076	0.00053	-48.1	1.2	-2.1
217	190830_107.FIN2	0.12910	0.00170	6.800	0.130	0.3816	0.0066	2086	23	2082	17	2082	31	100	2086	23	0.0009000	0.000064	0.281560	0.000028	0.02300	0.00170	-43.3	1.0	2.6
113	190208_177.FIN2	0.12980	0.00300	6.390	0.180	0.3600	0.0099	2095	41	2029	25	1981	47	95	2095	41	0.0013100	0.000120	0.281415	0.000042	0.03680	0.00430	-48.4	1.5	-2.9
35	190208_063.FIN2	0.13020	0.00150	6.880	0.100	0.3835	0.0048	2101	20	2095	13	2091	22	100	2101	20	0.0006401	0.000005	0.281527	0.000019	0.01776	0.00019	-44.5	0.7	2.1
179	190830_049.FIN2	0.13030	0.00190	6.940	0.130	0.3853	0.0061	2102	26	2101	17	2100	28	100	2102	26	0.0006370	0.000029	0.281477	0.000025	0.01720	0.00140	-46.3	0.9	0.4
120	190208_190.FIN2	0.13040	0.00290	6.560	0.160	0.3680	0.0110	2103	39	2053	22	2020	51	96	2103	39	0.0007650	0.000010	0.281493	0.000027	0.02162	0.00035	-45.7	1.0	0.8
218	190830_108.FIN2	0.13040	0.00120	6.932	0.082	0.3845	0.0044	2103	16	2100	11	2095	21	100	2103	16	0.0007350	0.000035	0.281463	0.000027	0.01885	0.00098	-46.7	1.0	-0.2
173	190830_037.FIN2	0.13100	0.00160	7.010	0.140	0.3868	0.0070	2111	21	2110	18	2106	32	100	2111	21	0.0009090	0.000066	0.281403	0.000024	0.02420	0.00190	-48.9	0.9	-2.4
69	190208_109.FIN2	0.13130	0.00210	6.940	0.190	0.3850	0.0085	2115	28	2100	24	2097	40	99	2115	28	0.0008720	0.000072	0.281580	0.000031	0.02530	0.00220	-42.6	1.1	4.0
90	190208_142.FIN2	0.13140	0.00220	6.960	0.150	0.3863	0.0082	2117	29	2103	19	2103	38	99	2117	29									
77	190208_123.FIN2	0.13210	0.00220	6.250	0.150	0.3436	0.0080	2126	29	2010	20	1903	38	90	2126	29	0.0003700	0.000150	0.281474	0.000035	0.01110	0.00510	-46.4	1.2	1.2
184	190830_054.FIN2	0.13220	0.00460	6.430	0.280	0.3520	0.0120	2127	61	2034	37	1944	58	91	2127	61	0.0008440	0.000038	0.281535	0.000025	0.02240	0.00100	-44.2	0.9	2.7
105	190208_163.FIN2	0.13300	0.00310	7.190	0.220	0.3922	0.0093	2138	41	2126	27	2130	43	100	2138	41	0.0009390	0.000007	0.281372	0.000030	0.02819	0.00021	-50.0	1.1	-2.9
134	190208_210.FIN2	0.13350	0.00410	6.650	0.250	0.3650	0.0140	2145	54	2064	33	2003	66	93	2145	54	0.0015510	0.000056	0.281573	0.000038	0.04590	0.00200	-42.9	1.3	3.5
15	190208_031.FIN2	0.13450	0.00250	7.260	0.160	0.3929	0.0065	2158	32	2141	20	2140	32	99	2158	32	0.0007480	0.000024	0.281433	0.000041	0.02203	0.00071	-47.8	1.5	-0.1
31	190208_053.FIN2	0.13480	0.00190	6.690	0.150	0.3604	0.0078	2161	25	2069	21	1983	37	92	2161	25									
226	190830_122.FIN2	0.13490	0.00220	7.510	0.170	0.3994	0.0056	2163	28	2165	20	2163	26	100	2163	28	0.0003613	0.000010	0.281209	0.000027	0.00904	0.00030	-55.7	1.0	-7.3
235	190830_131.FIN2	0.13510	0.00160	7.490	0.110	0.4002	0.0048	2165	21	2169	14	2168	22	100	2165	21	0.0007747	0.000006	0.281400	0.000026	0.01896	0.00018	-49.0	0.9	-1.1
8	190208_018.FIN2	0.13620	0.00740	7.000	0.430	0.3710	0.0210	2179	95	2104	58	2032	97	93	2179	95	0.0015890	0.000071	0.281364	0.000028	0.04430	0.00290	-50.3	1.0	-3.3
65	190208_105.FIN2	0.13750	0.00150	7.670	0.140	0.4042	0.0065	2196	19	2188	16	2186	30	100	2196	19	0.0002330	0.000017	0.281294	0.000019	0.00624	0.00056	-52.7	0.7	-3.4
36	190208_064.FIN2	0.13820	0.00500	7.820	0.400	0.4070	0.0170	2205	63	2203	48	2198	79	100	2205	63	0.0014320	0.000030	0.281439	0.000035	0.03881	0.00065	-47.6	1.2	0.2
199	190830_076.FIN2	0.14020	0.00600	8.150	0.360	0.4170	0.0130	2230	74	2243	40	2244	59	101	2230	74	0.0011800	0.000140	0.281342	0.000037	0.03140	0.00390	-51.0	1.3	-2.3
96	190208_154.FIN2	0.14210	0.00560	7.840	0.280	0.4010	0.0130	2253	68	2212	31	2172	61	96	2253	68									
211	190830_095.FIN2	0.14410	0.00200	8.560	0.230	0.4260	0.0110	2277	24	2290	24	2284	49	100	2277	24	0.0007750	0.000067	0.281253	0.000027	0.01980	0.00190	-54.2	1.0	-3.8
117	190208_181.FIN2	0.14460	0.00390	8.010	0.320	0.4050	0.0140	2283	46	2230	37	2193	66	96	2283	46	0.0007470	0.000083	0.281429	0.000037	0.02070	0.00250	-48.0	1.3	2.7
169	190830_033.FIN2	0.14510	0.00300	8.540	0.210	0.4255	0.0093	2289	36	2287	22	2284	42	100	2289	36	0.0007130	0.000014	0.281282	0.000028	0.01764	0.00033	-53.1	1.0	-2.4
5	190208_015.FIN2	0.14580	0.00310	8.510	0.360	0.4260	0.0160	2297	37	2285	39	2286	71	100	2297	37									
220	190830_110.FIN2	0.14590	0.00290	8.560	0.210	0.4253	0.0096	2298	34	2290	22	2283	43	99	2298	34	0.0008680	0.000028	0.281450	0.000027	0.02284	0.00084	-47.2	1.0	3.6
214	190830_104.FIN2	0.14620	0.00200	8.690	0.150	0.4292	0.0072	2302	24	2303	16	2300	33	100	2302	24	0.0018050	0.000063	0.281477	0.000025	0.04400	0.00170	-46.3	0.9	3.1
82	190208_128.FIN2	0.14650	0.00140	8.710	0.091	0.4303	0.0040	2305	16	2305	10	2305	18	100	2305	16	0.0007230	0.000036	0.281311	0.000023	0.01950	0.00110	-52.1	0.8	-1.0
78	190208_124.FIN2	0.14700	0.00180	8.860	0.160	0.4343	0.0068	2311	21	2320	17	2323	30	101	2311	21	0.0005200	0.000021	0.281259	0.000022	0.01472	0.00055	-54.0	0.8	-2.4
161	190830_018.FIN2	0.14700	0.00120	8.818	0.091	0.4328	0.0039	2311	14	2318	9	2317	18	100	2311	14	0.0004680	0.000014	0.281300	0.000023	0.01144	0.00033	-52.5	0.8	-0.9
40	190208_068.FIN2	0.14830	0.00360	8.960	0.270	0.4351	0.0095	2326	42	2330	28	2327	42	100	2326	42	0.0009832	0.000009	0.281352	0.000035	0.02559	0.00036	-50.7	1.2	0.5
94	190208_146.FIN2	0.14850	0.00140	9.040	0.130	0.4377	0.0054	2329	16	2340	13	2339	24	100	2329	16	0.0010470	0.000049	0.281344	0.000029	0.02830	0.00160	-51.0	1.0	0.2
70	190208_110.FIN2	0.14860	0.00230	8.750	0.250	0.4300	0.0100	2330	27	2308	26	2302	47	99	2330	27	0.0008460	0.000064	0.281218	0.000038	0.02290	0.00190	-55.4	1.4	-3.9
29	190208_051.FIN2	0.14880	0.00280	8.880	0.250	0.4340	0.0130	2332	32	2322	27	2322	56	100	2332	32									
26	190208_048.FIN2	0.15930	0.00190	10.000	0.210	0.4574	0.0084	2448	20	2431	19	2426	37	99	2448	20	0.0024900	0.000120	0.281446	0.000038	0.06780	0.00360	-47.4	1.4	4.1
128	190208_198.FIN2	0.16340	0.00630	10.710	0.490	0.4730	0.0180	2491	65	2491	42	2494	78	100	2491	65	0.0005160	0.000014	0.281194	0.000025	0.01471	0.00050	-56.3	0.9	-0.6
17	190208_033.FIN2	0.16490	0.00420	10.560	0.520	0.4640	0.0190	2507	43	2482	46	2454	81	98	2507	43	0.0009030	0.000058	0.281392	0.000030	0.02540	0.00200	-49.3	1.1	6.2
7	190208_017.FIN2	0.16590	0.00300	9.670	0.300	0.4249	0.0099	2517	30	2400	29	2281	45	91	2517	30	0.0006700	0.000034	0.281232	0.000030	0.01850	0.00130	-54.9	1.1	1.1
255	190830_163.FIN2	0.16830	0.00630	11.090	0.410	0.4810	0.0200	2541	63	2527	34	2527	87	99	2541	63	0.0013300	0.000120	0.281217	0.000026	0.03600	0.00330	-55.4	0.9	0.0
244	190830_146.FIN2	0.16870	0.00240	11.500	0.270	0.4870	0.0110	2545	24	2560	22	2556	50	100	2545	24	0.0006330	0.000040	0.281264	0.000028	0.01650	0.00120	-53.8	1.0	3.0
200	190830_077.FIN2	0.16940	0.00290	11.600	0.300	0.4890	0.0130	2552	29	2579	24	2576	58	101	2552	29	0.0006741	0.000006	0.281183	0.000023	0.01766	0.00014	-56.7	0.8	0.2
176	190830_040.FIN2	0.17070	0.00470	11.510	0.470	0.4880	0.0180	2565	46	2563	39	2563	80	100	2565	46	0.0006960	0.000015	0.281078	0.000025	0.01869	0.00040	-60.4	0.9	-3.3
3	190208_013.FIN2	0.17200	0.00390	10.310	0.460	0.4380	0.0190	2577	38	2459	40	2337	85	91	2577	38	0.0006220	0.000091	0.281244	0.000051	0.01830	0.00310	-54.5	1.8	3.0
56	190208_090.FIN2	0.17480	0.00320	11.850	0.380	0.4940	0.0140	2604	31	2590	30	2586	59	99	2604	31	0.0007900	0.000100	0.281211	0.000039	0.02310	0.00340	-55.7	1.4	2.2

U-Pb geochronology																	Hf isotope geochemistry								
		Isotopic ratios						Isotopic ages									Isotopic ratios						Epsilon units		
Grain #	Spot name	$^{207}Pb/^{206}Pb$	± 2SE	$^{207}Pb/^{235}U$	± 2SE	$^{206}Pb/^{238}U$	± 2SE	$^{207}Pb/^{206}Pb$	± 2SE (Ma)	$^{207}Pb/^{235}U$	± 2SE (Ma)	$^{206}Pb/^{238}U$	± 2SE (Ma)	Conc. %	Best Age	± 2SE (Ma)	$^{176}Lu/^{177}Hf$	± 2SE	$^{176}Hf/^{177}Hf$	± 2SE	$^{176}Yb/^{177}Hf$	± 2SE	εHf_0	2SE	εHf_t
23	190208_045.FIN2	0.11050	0.00340	4.570	0.190	0.2969	0.0076	1808	56	1739	35	1675	38	93	2607	87	0.0004850	0.000041	0.281352	0.000025	0.01430	0.00130	-50.7	0.9	-10.5
101	190208_159.FIN2	0.17540	0.00160	12.050	0.170	0.4987	0.0063	2610	15	2607	13	2606	27	100	2610	15	0.0006120	0.000011	0.281153	0.000033	0.01776	0.00044	-57.7	1.2	0.5
104	190208_162.FIN2	0.17610	0.00200	12.090	0.170	0.4994	0.0066	2616	19	2607	14	2611	28	100	2616	19	0.0005930	0.000011	0.281060	0.000031	0.01676	0.00021	-61.0	1.1	-2.6
168	190830_032.FIN2	0.17630	0.00270	12.200	0.260	0.5000	0.0100	2618	25	2617	20	2614	45	100	2618	25	0.0008680	0.000021	0.281232	0.000030	0.02349	0.00068	-54.9	1.1	3.1
38	190208_066.FIN2	0.17640	0.00300	11.220	0.300	0.4558	0.0095	2619	28	2537	24	2427	44	93	2619	28	0.0005950	0.000011	0.281210	0.000027	0.01521	0.00034	-55.7	1.0	2.8
66	190208_106.FIN2	0.17790	0.00330	12.250	0.490	0.5010	0.0170	2633	31	2617	38	2616	73	99	2633	31									
46	190208_074.FIN2	0.17860	0.00470	11.160	0.410	0.4510	0.0140	2640	44	2534	35	2400	61	91	2640	44	0.0006300	0.000140	0.281175	0.000031	0.01920	0.00410	-56.9	1.1	2.0
14	190208_030.FIN2	0.18080	0.00200	12.740	0.200	0.5101	0.0070	2660	18	2655	15	2654	30	100	2660	18	0.0005940	0.000005	0.281212	0.000041	0.01617	0.00027	-55.6	1.5	3.8
221	190830_111.FIN2	0.18260	0.00140	13.040	0.140	0.5151	0.0050	2677	13	2679	10	2676	21	100	2677	13	0.0006320	0.000082	0.281156	0.000030	0.01550	0.00210	-57.6	1.1	2.1
202	190830_086.FIN2	0.18410	0.00380	13.130	0.300	0.5170	0.0110	2690	34	2687	21	2687	48	100	2690	34	0.0010430	0.000093	0.281209	0.000025	0.02480	0.00230	-55.7	0.9	3.6
rejected analyses																									
2	190208_012.FIN2	0.17880	0.00280	8.240	0.200	0.3359	0.0091	2642	26	2255	22	1865	44	71	N/A	N/A	0.0013060	0.000083	0.281086	0.000031	0.03890	0.00270	-60.1	1.1	N/A
6	190208_016.FIN2	0.18040	0.00730	8.980	0.450	0.3590	0.0210	2657	67	2333	47	1974	99	74	N/A	N/A									
11	190208_021.FIN2	0.14930	0.00730	4.610	0.280	0.2247	0.0064	2338	84	1742	50	1306	34	56	N/A	N/A	0.0033200	0.000740	0.281629	0.000051	0.10200	0.02200	-40.9	1.8	N/A
19	190208_035.FIN2	0.12700	0.00170	1.996	0.046	0.1147	0.0026	2057	24	1113	16	700	15	34	N/A	N/A									
20	190208_036.FIN2	0.12350	0.00230	4.540	0.160	0.2667	0.0069	2007	33	1737	29	1523	35	76	N/A	N/A									
21	190208_037.FIN2	0.13490	0.00490	4.760	0.260	0.2530	0.0100	2163	63	1772	46	1455	51	67	N/A	N/A	0.0016500	0.000280	0.281457	0.000036	0.04690	0.00870	-47.0	1.3	N/A
24	190208_046.FIN2	0.17510	0.00910	1.950	0.130	0.0802	0.0021	2607	87	1092	43	497	12	19	N/A	N/A	0.0053600	0.000720	0.281663	0.000038	0.16900	0.02300	-39.7	1.3	N/A
25	190208_047.FIN2	0.14390	0.00440	4.550	0.300	0.2260	0.0160	2275	53	1730	54	1310	84	58	N/A	N/A	0.0026100	0.000340	0.281591	0.000033	0.08300	0.01100	-42.2	1.2	N/A
27	190208_049.FIN2	0.15210	0.00270	2.429	0.054	0.1153	0.0026	2370	30	1248	16	703	15	30	N/A	N/A	0.0020200	0.000240	0.281253	0.000042	0.06260	0.00770	-54.2	1.5	N/A
32	190208_054.FIN2	0.13480	0.00260	3.870	0.170	0.2069	0.0087	2161	34	1604	34	1212	46	56	N/A	N/A									
34	190208_056.FIN2	0.14320	0.00490	2.740	0.170	0.1400	0.0071	2266	59	1324	47	843	40	37	N/A	N/A									
39	190208_067.FIN2	0.14900	0.00550	6.290	0.300	0.3040	0.0072	2334	63	2008	40	1710	35	73	N/A	N/A	0.0007640	0.000025	0.281231	0.000030	0.02170	0.00100	-55.0	1.1	N/A
41	190208_069.FIN2	0.14380	0.00250	3.272	0.069	0.1641	0.0035	2273	30	1473	16	979	20	43	N/A	N/A	0.0024400	0.000180	0.281334	0.000031	0.07820	0.00560	-51.3	1.1	N/A
42	190208_070.FIN2	0.15200	0.00210	6.880	0.170	0.3301	0.0072	2369	24	2093	23	1838	35	78	N/A	N/A									
44	190208_072.FIN2	0.13000	0.00230	4.950	0.130	0.2761	0.0062	2098	31	1807	22	1571	31	75	N/A	N/A	0.0009120	0.000021	0.281433	0.000032	0.02534	0.00045	-47.8	1.1	N/A
45	190208_073.FIN2	0.17050	0.00280	9.710	0.210	0.4146	0.0076	2563	27	2405	20	2235	35	87	N/A	N/A	0.0005010	0.000021	0.281161	0.000028	0.01380	0.00068	-57.4	1.0	N/A
47	190208_081.FIN2	0.12710	0.00190	5.700	0.110	0.3273	0.0054	2058	26	1929	17	1825	26	89	N/A	N/A	0.0007800	0.000061	0.281504	0.000026	0.02170	0.00190	-45.3	0.9	N/A
48	190208_082.FIN2	0.11350	0.00190	3.404	0.071	0.2167	0.0037	1856	30	1503	16	1264	20	68	N/A	N/A	0.0011380	0.000066	0.281642	0.000029	0.03320	0.00180	-40.4	1.0	N/A
49	190208_083.FIN2	0.11350	0.00150	4.341	0.084	0.2784	0.0042	1856	24	1699	16	1583	21	85	N/A	N/A	0.0011010	0.000059	0.281573	0.000031	0.03250	0.00190	-42.9	1.1	N/A
50	190208_084.FIN2	0.09620	0.00270	0.716	0.031	0.0538	0.0014	1552	53	545	18	338	9	22	N/A	N/A	0.0056000	0.000410	0.281957	0.000084	0.17800	0.01100	-29.3	3.0	N/A
52	190208_086.FIN2	0.13750	0.00370	3.630	0.160	0.1879	0.0066	2196	47	1553	35	1110	35	51	N/A	N/A									
53	190208_087.FIN2	0.11070	0.00230	1.415	0.040	0.0926	0.0030	1811	38	893	17	571	17	32	N/A	N/A	0.0035000	0.000360	0.281676	0.000045	0.11000	0.01100	-39.2	1.6	N/A
54	190208_088.FIN2	0.14600	0.00290	6.720	0.200	0.3319	0.0099	2300	34	2071	26	1846	48	80	N/A	N/A	0.0008600	0.000110	0.281352	0.000038	0.02580	0.00390	-50.7	1.4	N/A
55	190208_089.FIN2	0.13930	0.00250	4.820	0.170	0.2526	0.0081	2219	31	1787	32	1449	42	65	N/A	N/A									
58	190208_092.FIN2	0.09310	0.00150	0.953	0.034	0.0735	0.0020	1490	31	678	17	457	12	31	N/A	N/A	0.0028200	0.000410	0.281752	0.000040	0.08700	0.01200	-36.5	1.4	N/A
60	190208_100.FIN2	0.12220	0.00300	4.810	0.150	0.2842	0.0079	1989	44	1784	25	1612	40	81	N/A	N/A	0.0010020	0.000051	0.281558	0.000030	0.03040	0.00180	-43.4	1.1	N/A
62	190208_102.FIN2	0.11170	0.00280	3.740	0.120	0.2444	0.0051	1827	45	1577	25	1409	26	77	N/A	N/A	0.0014100	0.000170	0.281574	0.000049	0.04140	0.00580	-42.8	1.7	N/A
63	190208_103.FIN2	0.10990	0.00150	3.230	0.063	0.2114	0.0034	1798	25	1462	15	1236	18	69	N/A	N/A	0.0012280	0.000039	0.281636	0.000028	0.03740	0.00120	-40.6	1.0	N/A
64	190208_104.FIN2	0.16670	0.00580	2.610	0.140	0.1156	0.0062	2525	58	1287	41	703	35	28	N/A	N/A	0.0029900	0.000520	0.281455	0.000049	0.09200	0.01600	-47.0	1.7	N/A
68	190208_108.FIN2	0.12470	0.00240	4.160	0.150	0.2435	0.0089	2025	34	1665	28	1404	46	69	N/A	N/A	0.0027000	0.000370	0.281633	0.000043	0.08500	0.01200	-40.7	1.5	N/A
72	190208_118.FIN2	0.08720	0.00180	0.614	0.020	0.0506	0.0012	1365	40	485	12	318	8	23	N/A	N/A	0.0042300	0.000320	0.281684	0.000045	0.12210	0.00860	-38.9	1.6	N/A
74	190208_120.FIN2	0.12390	0.00210	5.480	0.100	0.3180	0.0050	2013	30	1895	16	1779	25	88	N/A	N/A	0.0022900	0.000370	0.281605	0.000035	0.06600	0.01200	-41.7	1.2	N/A
75	190208_121.FIN2	0.13450	0.00200	4.230	0.120	0.2273	0.0056	2158	26	1673	24	1319	29	61	N/A	N/A	0.0009480	0.000046	0.281237	0.000029	0.02780	0.00130	-54.7	1.0	N/A
76	190208_122.FIN2	0.13120	0.00210	2.889	0.080	0.1622	0.0055	2114	28	1379	22	968	31	46	N/A	N/A									
81	190208_127.FIN2	0.15230	0.00240	6.340	0.210	0.3019	0.0092	2372	27	2021	30	1699	46	72	N/A	N/A	0.0015300	0.000200	0.281280	0.000033	0.04610	0.00600	-53.2	1.2	N/A
83	190208_135.FIN2	0.12430	0.00540	2.151	0.094	0.1279	0.0038	2019	77	1162	30	775	22	38	N/A	N/A									
85	190208_137.FIN2	0.11490	0.00200	1.322	0.050	0.0835	0.0026	1878	31	851	23	517	15	28	N/A	N/A	0.0048500	0.000730	0.281609	0.000041	0.14800	0.02100	-41.6	1.5	N/A
86	190208_138.FIN2	0.14390	0.00360	7.130	0.180	0.3615	0.0097	2275	43	2126	22	1988	46	87	N/A	N/A	0.0016720	0.000080	0.281244	0.000035	0.04940	0.00260	-54.5	1.2	N/A
87	190208_139.FIN2	0.12060	0.00520	4.150	0.180	0.2520	0.0085	1965	77	1661	36	1448	44	74	N/A	N/A									
92	190208_144.FIN2	0.16000	0.00740	4.200	0.310	0.1876	0.0071	2456	78	1651	61	1106	39	45	N/A	N/A	0.0016900	0.000220	0.281348	0.000047	0.05390	0.00740	-50.8	1.7	N/A
95	190208_153.FIN2	0.16960	0.00310	9.220	0.290	0.3960	0.0120	2554	31	2358	29	2147	55	84	N/A	N/A	0.0014300	0.000069	0.281255	0.000032	0.04450	0.00220	-54.1	1.1	N/A
99	190208_157.FIN2	0.15630	0.00380	0.916	0.021	0.0428	0.0011	2416	41	659	11	270	7	11	N/A	N/A									
103	190208_161.FIN2	0.11610	0.00380	4.790	0.210	0.2937	0.0078	1897	59	1778	37	1659	39	87	N/A	N/A									
106	190208_164.FIN2	0.13070	0.00210	2.169	0.046	0.1214	0.0022	2107	28	1170	15	739	13	35	N/A	N/A									
108	190208_172.FIN2	0.14550	0.00290	1.886	0.098	0.0946	0.0041	2294	34	1073	34	582	24	25	N/A	N/A									
109	190208_173.FIN2	0.18220	0.00450	10.350	0.450	0.4110	0.0170	2673	41	2462	40	2216	77	83	N/A	N/A									
110	190208_174.FIN2	0.12730	0.00250	4.270	0.130	0.2422	0.0059	2061	35	1684	25	1398	31	68	N/A	N/A									
111	190208_175.FIN2	0.11600	0.00250	2.956	0.075	0.1842	0.0035	1895	39	1394	19	1090	19	58	N/A	N/A	0.0012100	0.000130	0.281549	0.000045	0.03510	0.00460	-43.7	1.6	N/A
112	190208_176.FIN2	0.10770	0.00630	2.130	0.160	0.1429	0.0081	1761	107	1153	51	860	46	49	N/A	N/A	0.0010800	0.000320	0.281405	0.000046	0.03500	0.01100	-48.8	1.6	N/A
115	190208_179.FIN2	0.08280	0.00290	0.498	0.018	0.0440	0.0008	1265	68	409	12	278	5	22	N/A	N/A									
116	190208_180.FIN2	0.08710	0.00130	0.642	0.020	0.0535	0.0013	1363	29	502	12	336	8	25	N/A	N/A	0.0049300	0.000300	0.281748	0.000085	0.15640	0.00850	-36.7	3.0	N/A
119	190208_189.FIN2	0.09690	0.00490	1.058	0.073	0.0794	0.0048	1565	95	734	40	492	29	31	N/A	N/A									
121	190208_191.FIN2	0.18020	0.00390	10.750	0.290	0.4360	0.0120	2655	36	2500	25	2331	54	88	N/A	N/A	0.0008590	0.000070	0.281174	0.000038	0.02460	0.00200	-57.0	1.4	N/A
122	190208_192.FIN2	0.14240	0.00530	3.230	0.350	0.1610	0.0120	2257	64	1449	80	958	63	42	N/A	N/A									
126	190208_196.FIN2	0.14830	0.00240	6.130	0.140	0.3041	0.0063	2326	28	1999	22	1711	31	74	N/A	N/A	0.0010700	0.000120	0.281321	0.000029	0.03110	0.00420	-51.8	1.0	N/A
127	190208_197.FIN2	0.13180	0.00250	1.035	0.033	0.0560	0.0014	2122	33	719	16	353	9	17	N/A	N/A									
129	190208_199.FIN2	0.10480	0.00270	1.909	0.073	0.1336	0.0059	1711	47	1083	25	808	34	47	N/A	N/A	0.0013300	0.000260	0.281408	0.000038	0.04100	0.00890	-48.7	1.4	N/A
130	190208_200.FIN2	0.10840	0.00250	4.060	0.130	0.2707	0.0080	1773	42	1643	26	1543	40	87	N/A	N/A	0.0013400	0.000400	0.281598	0.000025	0.04200	0.01300	-42.0	0.9	N/A
132	190208_208.FIN2	0.17720	0.00800	2.890	0.280	0.1165	0.0078	2627	75	1354	68	709	45	27	N/A	N/A									
135	190208_211.FIN2	0.09000	0.01200	1.030	0.130	0.0851	0.0050	1426	255	707	61	526	30	37	N/A	N/A									
138	190208_214.FIN2	0.12930	0.00240	5.670	0.170	0.3201	0.0096	2088	33	1924	27	1789	47	86	N/A	N/A	0.0012600	0.000180	0.281543	0.000043	0.03870	0.00650	-43.9	1.5	N/A
139	190208_215.FIN2	0.11420	0.00160	4.540	0.074	0.2911	0.0046	1867	25	1739	14	1646	23	88	N/A	N/A	0.0010330	0.000059	0.281674	0.000026	0.02900	0.00180	-39.3	0.9	N/A
140	190208_216.FIN2	0.12830	0.00310	5.490	0.210	0.3120	0.0110	2075	43	1895	32	1751	52	84	N/A	N/A	0.0012600	0.000130	0.281419	0.000046	0.03750	0.00390	-48.3	1.6	N/A
142	190211_011.FIN2	0.11533	0.00089	4.405	0.048	0.2763	0.0028	1885	14	1713	9	1574	14	83	N/A	N/A	0.0011730	0.000081	0.281568	0.000032	0.03010	0.00180	-43.0	1.1	N/A
143	190211_012.FIN2	0.11250	0.00210	2.601	0.064	0.1638	0.0035	1840	34	1299	18	977	19	53	N/A	N/A	0.0022400	0.000260	0.281571	0.000056	0.06820	0.00750	-42.9	2.0	N/A
144	190211_013.FIN2	0.12360	0.00490	2.660	0.150	0.1606	0.0080	2009	70	1319	42	959	45	48	N/A	N/A									
145	190211_014.FIN2	0.14820	0.00180	7.740	0.120	0.3793	0.0072	2325	21	2199	15	2071	33	89	N/A	N/A	0.0007140	0.000047	0.281288	0.000027	0.02040	0.00130	-52.9	1.0	N/A
146	190211_015.FIN2	0.28520	0.00850	5.760	0.190	0.1470	0.0049	3392	46	1936	29	884	28	26	N/A	N/A	0.0012300	0.000120	0.281220	0.000037	0.03440	0.00360	-55.3	1.3	N/A
148	190211_017.FIN2	0.10120	0.00280	0.929	0.040	0.0655	0.0019	1646	51	665	20	409	11	25	N/A	N/A	0.0024600	0.000230	0.281557	0.000035	0.07030	0.00630	-43.4	1.2	N/A
149	190211_018.FIN2	0.14720	0.00110	6.790	0.084	0.3359	0.0037	2314	13	2082	11	1866	18	81	N/A	N/A	0.0007740	0.000027	0.281271	0.000033	0.02270	0.00100	-53.5	1.2	N/A
150	190211_019.FIN2	0.12980	0.00290	5.250	0.140	0.2875	0.0061	2095	39	1861	25	1628	31	78	N/A	N/A	0.0025400	0.000430	0.281553	0.000033	0.07700	0.01300	-43.6	1.2	N/A
151	190211_020.FIN2	0.15300	0.00330	5.200	0.190	0.2492	0.0062	2380	37	1846	32	1433	32	60	N/A	N/A	0.0008500	0.000049	0.281325	0.000025	0.02560	0.00180	-51.6	0.9	N/A
153	190211_022.FIN2	0.12700	0.00180	1.079	0.018	0.0613	0.0008	2057	25	742	9	384	5	19	N/A	N/A	0.0033100	0.000150	0.281530	0.000045	0.10500	0.00390	-44.4	1.6	N/A
155	190830_012.FIN2	0.15330	0.00430	1.838	0.059	0.0853	0.0014	2383	48	1055	21	527	8	22	N/A	N/A	0.0042200	0.000140	0.281548	0.000034	0.11750	0.00440	-43.7	1.2	N/A
156	190830_013.FIN2	0.07700	0.00140	0.675	0.031	0.0632	0.0021	1121	36	521	18	395	13	35	N/A	N/A	0.0025100	0.000120	0.281644	0.000024	0.07590	0.00370	-40.3	0.9	N/A
157	190830_014.FIN2	0.13230	0.00570	6.020	0.230	0.3300	0.0140	2129	75	1978	34	1839	69	86	N/A	N/A	0.0012430	0.000013	0.281613	0.000019	0.03381	0.00041	-41.4	0.7	N/A
160	190830_017.FIN2	0.12980	0.00570	1.925	0.086	0.1056	0.0024	2095	77	1085	31	647	14	31	N/A	N/A	0.0019000	0.000210	0.281504	0.000028	0.05410	0.00630	-45.3	1.0	N/A
165	190830_022.FIN2	0.21540	0.00930	3.760	0.200	0.1253	0.0045	2947	70	1569	41	760	26	26	N/A	N/A	0.0026300	0.000220	0.281332	0.000023	0.07630	0.00680	-51.4	0.8	N/A
166	190830_030.FIN2	0.10760	0.00120	1.798	0.029	0.1204	0.0016	1759	20	1043	11	733	9	42	N/A	N/A	0.0027040	0.000061	0.281587	0.000033	0.07370	0.00170	-42.4	1.2	N/A
170	190830_034.FIN2	0.17070	0.00320	9.840	0.190	0.4191	0.0082	2565	31	2423	20	2255	37	88	N/A	N/A	0.0010800	0.000100	0.281205	0.000024	0.03150	0.00330	-55.9	0.9	N/A
171	190830_035.FIN2	0.11690	0.00220	4.970	0.170	0.3020	0.0100	1909	34	1811	29	1698	51	89	N/A	N/A	0.0003810	0.000034	0.281482	0.000024	0.01004	0.00093	-46.1	0.9	N/A
172	190830_036.FIN2	0.13190	0.00210	5.200	0.130	0.2839	0.0071	2123	28	1851	22	1610	36	76	N/A	N/A	0.0011800	0.000200	0.281431	0.000022	0.03430	0.00640	-47.9	0.8	N/A
177	190830_041.FIN2	0.11030	0.00310	3.910	0.140	0.2539	0.0079	1804	51	1611	30	1457	40	81	N/A	N/A	0.0011100	0.000220	0.281601	0.000026	0.03030	0.00630	-41.9	0.9	N/A
178	190830_048.FIN2	0.11790	0.00230	5.080	0.120	0.3071	0.0059	1925	35	1828	20	1725	29	90	N/A	N/A	0.0012700	0.000300	0.281583	0.000025	0.03640	0.00950	-42.5	0.9	N/A
180	190830_050.FIN2	0.14030	0.00230	7.030	0.190	0.3589	0.0078	2231	28	2111	24	1976	37	89	N/A	N/A									
182	190830_052.FIN2	0.11280	0.00710	2.840	0.290	0.1810	0.0140	1845	114	1350	79	1069	76	58	N/A	N/A	0.0025100	0.000330	0.281565	0.000035	0.07300	0.01000	-43.1	1.2	N/A
185	190830_055.FIN2	0.13110	0.00380	2.859	0.088	0.1551	0.0051	2113	51	1370	23	929	29	44	N/A	N/A									
186	190830_056.FIN2	0.12450	0.00190	4.450	0.170	0.2536	0.0089	2022	27	1719	32	1456	46	72	N/A	N/A	0.0010790	0.000044	0.281372	0.000022	0.02780	0.00160	-50.0	0.8	N/A

U-Pb geochronology																	Hf isotope geochemistry									
		Isotopic ratios						Isotopic ages									Isotopic ratios						Epsilon units		
Grain #	Spot name	$^{207}Pb/^{206}Pb$	± 2SE	$^{207}Pb/^{235}U$	± 2SE	$^{206}Pb/^{238}U$	± 2SE	$^{207}Pb/^{206}Pb$	± 2SE (Ma)	$^{207}Pb/^{235}U$	± 2SE (Ma)	$^{206}Pb/^{238}U$	± 2SE (Ma)	Conc. %	Best Age	± 2SE (Ma)	$^{176}Lu/^{177}Hf$	± 2SE	$^{176}Hf/^{177}Hf$	± 2SE	$^{176}Yb/^{177}Hf$	± 2SE	εHf_0	2SE	εHf_t
187	190830_057.FIN2	0.12330	0.00230	2.795	0.075	0.1644	0.0048	2005	33	1353	20	981	26	49	N/A	N/A	0.0014430	0.000047	0.281448	0.000024	0.04160	0.00130	-47.3	0.9	N/A
189	190830_059.FIN2	0.12280	0.00230	4.805	0.097	0.2832	0.0050	1997	33	1784	17	1607	25	80	N/A	N/A	0.0006030	0.000032	0.281397	0.000021	0.01460	0.00084	-49.1	0.7	N/A
191	190830_068.FIN2	0.11340	0.00250	2.043	0.062	0.1277	0.0032	1855	40	1128	21	774	18	42	N/A	N/A	0.0024400	0.000180	0.281591	0.000031	0.07070	0.00520	-42.2	1.1	N/A
193	190830_070.FIN2	0.10880	0.00330	3.835	0.081	0.2554	0.0064	1779	55	1599	18	1466	33	82	N/A	N/A	0.0011200	0.000190	0.281629	0.000028	0.03230	0.00570	-40.9	1.0	N/A
194	190830_071.FIN2	0.13570	0.00190	2.520	0.089	0.1335	0.0036	2173	24	1275	26	808	21	37	N/A	N/A	0.0038000	0.000340	0.281451	0.000051	0.10600	0.00990	-47.2	1.8	N/A
195	190830_072.FIN2	0.10900	0.00320	1.349	0.061	0.0881	0.0028	1783	54	865	26	544	17	31	N/A	N/A	0.0020500	0.000029	0.281484	0.000038	0.05783	0.00078	-46.0	1.3	N/A
198	190830_075.FIN2	0.11510	0.00540	1.128	0.084	0.0695	0.0024	1881	85	758	39	433	15	23	N/A	N/A	0.0031100	0.000220	0.281510	0.000026	0.08660	0.00610	-45.1	0.9	N/A
201	190830_078.FIN2	0.07880	0.00190	0.487	0.016	0.0445	0.0013	1167	48	403	11	281	8	24	N/A	N/A	0.0066900	0.000150	0.281653	0.000037	0.19180	0.00460	-40.0	1.3	N/A
203	190830_087.FIN2	0.13130	0.00270	4.390	0.150	0.2350	0.0056	2115	36	1708	28	1360	29	64	N/A	N/A	0.0017200	0.000110	0.281402	0.000024	0.04790	0.00330	-48.9	0.9	N/A
207	190830_091.FIN2	0.11890	0.00230	2.951	0.082	0.1783	0.0039	1940	35	1393	21	1057	21	54	N/A	N/A	0.0022800	0.000320	0.281593	0.000035	0.06490	0.00950	-42.2	1.2	N/A
208	190830_092.FIN2	0.16250	0.00390	4.760	0.120	0.2122	0.0042	2482	40	1776	21	1240	22	50	N/A	N/A	0.0019140	0.000066	0.281229	0.000026	0.05200	0.00170	-55.0	0.9	N/A
210	190830_094.FIN2	0.16900	0.00570	5.530	0.220	0.2363	0.0058	2548	57	1902	34	1367	30	54	N/A	N/A	0.0024800	0.000290	0.281349	0.000036	0.06940	0.00930	-50.8	1.3	N/A
213	190830_097.FIN2	0.10970	0.00410	3.240	0.150	0.2121	0.0051	1794	68	1463	35	1239	27	69	N/A	N/A	0.0011460	0.000093	0.281523	0.000031	0.03090	0.00230	-44.6	1.1	N/A
215	190830_105.FIN2	0.13830	0.00370	5.540	0.140	0.2911	0.0073	2206	46	1904	22	1646	37	75	N/A	N/A	0.0020200	0.000130	0.281501	0.000027	0.05590	0.00330	-45.4	1.0	N/A
219	190830_109.FIN2	0.11250	0.00220	4.280	0.130	0.2721	0.0065	1840	35	1686	26	1551	33	84	N/A	N/A									
222	190830_112.FIN2	0.14630	0.00340	7.520	0.230	0.3700	0.0150	2303	40	2174	27	2028	71	88	N/A	N/A	0.0008340	0.000049	0.281279	0.000028	0.02250	0.00140	-53.3	1.0	N/A
227	190830_123.FIN2	0.11910	0.00460	3.930	0.190	0.2380	0.0100	1943	69	1614	40	1375	54	71	N/A	N/A	0.0014000	0.000140	0.281533	0.000027	0.03870	0.00390	-44.3	1.0	N/A
229	190830_125.FIN2	0.13190	0.00190	6.040	0.170	0.3251	0.0089	2123	25	1979	25	1813	43	85	N/A	N/A	0.0014080	0.000046	0.281511	0.000032	0.03750	0.00130	-45.1	1.1	N/A
230	190830_126.FIN2	0.10970	0.00230	0.929	0.024	0.0614	0.0014	1794	38	667	13	384	9	21	N/A	N/A	0.0063800	0.000250	0.281583	0.000055	0.18530	0.00790	-42.5	2.0	N/A
231	190830_127.FIN2	0.14260	0.00480	2.580	0.110	0.1307	0.0029	2259	58	1289	30	792	17	35	N/A	N/A	0.0032600	0.000200	0.281561	0.000024	0.09590	0.00580	-43.3	0.9	N/A
232	190830_128.FIN2	0.15050	0.00590	6.650	0.280	0.3210	0.0092	2352	67	2062	37	1793	45	76	N/A	N/A	0.0010850	0.000065	0.281440	0.000029	0.02830	0.00170	-47.6	1.0	N/A
239	190830_141.FIN2	0.11360	0.00200	4.020	0.100	0.2523	0.0047	1858	32	1636	21	1450	24	78	N/A	N/A	0.0016000	0.000180	0.281588	0.000039	0.04220	0.00540	-42.3	1.4	N/A
240	190830_142.FIN2	0.17900	0.01200	3.150	0.270	0.1254	0.0036	2644	111	1423	66	761	21	29	N/A	N/A	0.0030100	0.000230	0.281515	0.000033	0.08150	0.00670	-44.9	1.2	N/A
241	190830_143.FIN2	0.11720	0.00600	0.647	0.042	0.0397	0.0009	1914	92	502	25	251	6	13	N/A	N/A	0.0065700	0.000190	0.281808	0.000039	0.17160	0.00480	-34.5	1.4	N/A
242	190830_144.FIN2	0.08810	0.00180	0.551	0.016	0.0453	0.0009	1385	39	445	11	286	6	21	N/A	N/A	0.0068160	0.000089	0.281840	0.000056	0.18860	0.00270	-33.4	2.0	N/A
249	190830_151.FIN2	0.13610	0.00230	3.940	0.082	0.2111	0.0034	2178	29	1620	17	1234	18	57	N/A	N/A	0.0005330	0.000065	0.281298	0.000018	0.01420	0.00200	-52.6	0.6	N/A
250	190830_158.FIN2	0.07160	0.00120	0.425	0.011	0.0427	0.0006	975	34	359	8	269	4	28	N/A	N/A									
252	190830_160.FIN2	0.11750	0.00190	4.180	0.130	0.2557	0.0066	1919	29	1665	24	1466	34	76	N/A	N/A	0.0012500	0.000062	0.281694	0.000031	0.03090	0.00220	-38.6	1.1	N/A
253	190830_161.FIN2	0.10560	0.00230	2.096	0.057	0.1438	0.0034	1725	40	1146	18	866	19	50	N/A	N/A	0.0023000	0.000120	0.281551	0.000032	0.06550	0.00350	-43.6	1.1	N/A
254	190830_162.FIN2	0.12190	0.00210	3.276	0.082	0.1936	0.0041	1984	31	1473	20	1141	22	58	N/A	N/A	0.0017100	0.000130	0.281543	0.000028	0.04470	0.00340	-43.9	1.0	N/A
257	190830_165.FIN2	0.12690	0.00650	2.070	0.096	0.1176	0.0029	2055	90	1135	31	716	17	35	N/A	N/A									
258	190830_166.FIN2	0.12840	0.00430	5.380	0.270	0.3036	0.0099	2076	59	1877	43	1708	49	82	N/A	N/A	0.0012700	0.000130	0.281560	0.000031	0.03490	0.00390	-43.3	1.1	N/A
259	190830_167.FIN2	0.12090	0.00350	3.130	0.110	0.1878	0.0052	1970	52	1437	29	1109	28	56	N/A	N/A	0.0025400	0.000140	0.281551	0.000033	0.06890	0.00390	-43.6	1.2	N/A
260	190830_168.FIN2	0.17840	0.00320	5.260	0.190	0.2139	0.0069	2638	30	1859	32	1248	37	47	N/A	N/A	0.0040700	0.000380	0.281254	0.000039	0.11100	0.01100	-54.1	1.4	N/A
18AW18--Snowcap assemblage; (Zone 08V NAD 83, 586129 E, 6901021 N)																									
182	190830_205.FIN2	0.10840	0.00260	4.440	0.140	0.2919	0.0085	1773	44	1719	27	1651	43	93	1773	44	0.0018800	0.000180	0.281721	0.000033	0.05440	0.00580	-37.6	1.2	0.1
257	190830_322.FIN2	0.10880	0.00240	4.770	0.170	0.3171	0.0089	1779	40	1774	30	1774	44	100	1779	40	0.0018930	0.000099	0.281580	0.000030	0.05010	0.00280	-42.6	1.1	-4.8
135	190211_229.FIN2	0.10920	0.00150	4.750	0.140	0.3151	0.0088	1786	25	1771	26	1761	45	99	1786	25	0.0007240	0.000041	0.281687	0.000035	0.02150	0.00130	-38.8	1.2	0.6
127	190211_215.FIN2	0.10930	0.00150	4.808	0.077	0.3180	0.0035	1788	25	1782	13	1780	18	100	1788	25	0.0003840	0.000010	0.281339	0.000030	0.01061	0.00031	-51.1	1.1	-11.3
193	190830_222.FIN2	0.10930	0.00140	4.814	0.080	0.3188	0.0043	1788	23	1783	14	1783	21	100	1788	23	0.0004058	0.000006	0.281361	0.000020	0.01086	0.00022	-50.4	0.7	-10.6
126	190211_214.FIN2	0.10950	0.00120	4.862	0.062	0.3205	0.0027	1791	20	1795	11	1792	13	100	1791	20	0.0005500	0.000014	0.281524	0.000024	0.01538	0.00047	-44.6	0.9	-4.9
202	190830_237.FIN2	0.10990	0.00120	4.939	0.076	0.3236	0.0046	1798	20	1807	13	1806	22	100	1798	20	0.0004680	0.000011	0.281564	0.000022	0.01301	0.00028	-43.2	0.8	-3.2
254	190830_313.FIN2	0.11000	0.00110	4.869	0.079	0.3205	0.0048	1799	18	1793	14	1791	24	100	1799	18	0.0001938	0.000004	0.281497	0.000021	0.00475	0.00011	-45.5	0.7	-5.2
230	190830_277.FIN2	0.11010	0.00130	4.940	0.110	0.3227	0.0070	1801	21	1806	19	1801	34	100	1801	21	0.0005090	0.000021	0.281588	0.000032	0.01381	0.00054	-42.3	1.1	-2.3
66	190211_124.FIN2	0.11058	0.00091	4.878	0.058	0.3208	0.0034	1809	15	1797	10	1793	17	99	1809	15	0.0008240	0.000015	0.281564	0.000019	0.02232	0.00053	-43.2	0.7	-3.4
60	190211_112.FIN2	0.11070	0.00360	4.990	0.200	0.3222	0.0069	1811	59	1814	32	1799	34	99	1811	59	0.0007910	0.000013	0.281340	0.000027	0.02214	0.00038	-51.1	1.0	-11.2
201	190830_236.FIN2	0.11110	0.00370	5.010	0.250	0.3240	0.0120	1817	60	1813	41	1809	58	100	1817	60	0.0011740	0.000036	0.281469	0.000026	0.03020	0.00120	-46.5	0.9	-7.0
242	190830_295.FIN2	0.11170	0.00290	4.970	0.150	0.3231	0.0073	1827	47	1810	26	1804	35	99	1827	47	0.0016800	0.000110	0.281541	0.000036	0.04430	0.00330	-44.0	1.3	-4.8
165	190830_181.FIN2	0.11190	0.00250	5.040	0.150	0.3265	0.0059	1831	40	1822	24	1821	28	99	1831	40	0.0008400	0.000170	0.281539	0.000022	0.02350	0.00480	-44.1	0.8	-3.8
115	190211_197.FIN2	0.11200	0.00160	4.913	0.079	0.3213	0.0047	1832	26	1803	14	1795	23	98	1832	26									
222	190830_269.FIN2	0.11210	0.00260	5.220	0.150	0.3327	0.0085	1834	42	1852	25	1850	41	101	1834	42	0.0002140	0.000020	0.281553	0.000024	0.00550	0.00052	-43.6	0.9	-2.5
162	190830_178.FIN2	0.11220	0.00120	5.102	0.095	0.3288	0.0059	1835	19	1833	16	1830	29	100	1835	19	0.0003970	0.000023	0.281786	0.000024	0.01035	0.00063	-35.3	0.9	5.6
248	190830_307.FIN2	0.11260	0.00190	5.080	0.120	0.3267	0.0075	1842	31	1827	20	1825	35	99	1842	31	0.0003160	0.000011	0.281547	0.000031	0.00877	0.00038	-43.8	1.1	-2.6
40	190211_086.FIN2	0.11270	0.00190	5.140	0.100	0.3245	0.0041	1843	31	1839	17	1811	20	98	1843	31	0.0012600	0.000120	0.281489	0.000023	0.03360	0.00350	-45.8	0.8	-5.8
81	190211_145.FIN2	0.11290	0.00140	5.115	0.080	0.3298	0.0037	1847	22	1838	14	1836	18	99	1847	22	0.0006870	0.000022	0.281515	0.000032	0.01790	0.00060	-44.9	1.1	-4.1
77	190211_141.FIN2	0.11340	0.00140	4.998	0.085	0.3203	0.0046	1855	22	1816	15	1790	23	97	1855	22	0.0004740	0.000037	0.281457	0.000035	0.01230	0.00120	-47.0	1.2	-5.7
12	190211_040.FIN2	0.11380	0.00190	5.020	0.110	0.3246	0.0060	1861	30	1821	18	1811	29	97	1861	30	0.0004100	0.000082	0.281520	0.000027	0.01240	0.00270	-44.7	1.0	-3.3
57	190211_109.FIN2	0.11403	0.00094	5.338	0.059	0.3375	0.0032	1865	15	1873	9	1873	16	100	1865	15	0.0003760	0.000071	0.281489	0.000028	0.00890	0.00220	-45.8	1.0	-4.2
3	190211_031.FIN2	0.11410	0.00150	5.043	0.084	0.3134	0.0039	1866	24	1824	14	1756	19	94	1866	24	0.0003985	0.000009	0.281648	0.000025	0.01079	0.00025	-40.2	0.9	1.4
196	190830_231.FIN2	0.11410	0.00320	5.300	0.230	0.3340	0.0110	1866	51	1858	38	1856	51	99	1866	51	0.0005730	0.000036	0.281484	0.000020	0.01534	0.00096	-46.0	0.7	-4.6
113	190211_195.FIN2	0.11430	0.00170	5.116	0.087	0.3218	0.0039	1869	27	1835	14	1798	19	96	1869	27	0.0013830	0.000058	0.281574	0.000033	0.03680	0.00190	-42.8	1.2	-2.4
250	190830_309.FIN2	0.11430	0.00790	5.180	0.390	0.3290	0.0210	1869	125	1857	75	1830	100	98	1869	125	0.0011950	0.000094	0.281491	0.000028	0.03240	0.00290	-45.8	1.0	-5.1
54	190211_106.FIN2	0.11440	0.00180	5.210	0.110	0.3334	0.0047	1870	28	1852	17	1853	23	99	1870	28	0.0003830	0.000034	0.281475	0.000024	0.00974	0.00085	-46.3	0.9	-4.6
112	190211_194.FIN2	0.11459	0.00090	5.322	0.051	0.3362	0.0027	1873	14	1872	8	1868	13	100	1873	14	0.0004490	0.000036	0.281414	0.000021	0.01120	0.00100	-48.5	0.7	-6.8
50	190211_102.FIN2	0.11460	0.00140	5.191	0.087	0.3319	0.0047	1874	22	1849	14	1847	22	99	1874	22	0.0006320	0.000015	0.281437	0.000029	0.01686	0.00039	-47.7	1.0	-6.2
111	190211_193.FIN2	0.11490	0.00190	5.360	0.140	0.3376	0.0068	1878	30	1874	23	1874	33	100	1878	30									
27	190211_067.FIN2	0.11500	0.00260	5.280	0.130	0.3346	0.0063	1880	41	1859	21	1858	30	99	1880	41	0.0006340	0.000047	0.281457	0.000023	0.01680	0.00130	-47.0	0.8	-5.3
16	190211_050.FIN2	0.11510	0.00120	5.271	0.078	0.3344	0.0037	1881	19	1861	13	1859	18	99	1881	19	0.0006640	0.000023	0.281408	0.000040	0.01775	0.00067	-48.7	1.4	-7.1
218	190830_259.FIN2	0.11530	0.00260	5.330	0.150	0.3359	0.0070	1885	41	1869	23	1865	34	99	1885	41	0.0012040	0.000017	0.281532	0.000036	0.03252	0.00063	-44.3	1.3	-3.3
34	190211_074.FIN2	0.11540	0.00300	5.530	0.150	0.3401	0.0051	1886	47	1899	22	1886	25	100	1886	47	0.0002258	0.000008	0.281318	0.000025	0.00603	0.00025	-51.9	0.9	-9.6
139	190211_233.FIN2	0.11550	0.00130	5.320	0.100	0.3363	0.0052	1888	20	1868	16	1867	25	99	1888	20	0.0002516	0.000007	0.281513	0.000023	0.00652	0.00015	-45.0	0.8	-2.7
163	190830_179.FIN2	0.11590	0.00180	5.450	0.110	0.3402	0.0057	1894	28	1888	17	1886	28	100	1894	28	0.0006470	0.000059	0.281584	0.000027	0.01780	0.00170	-42.5	1.0	-0.5
35	190211_075.FIN2	0.11600	0.00310	5.340	0.120	0.3339	0.0046	1895	48	1866	19	1851	20	98	1895	48	0.0009280	0.000050	0.281515	0.000023	0.02520	0.00160	-44.9	0.8	-3.3
187	190830_216.FIN2	0.11610	0.00190	5.590	0.130	0.3458	0.0080	1897	29	1916	19	1912	38	101	1897	29									
149	190211_249.FIN2	0.11670	0.00120	5.507	0.097	0.3432	0.0062	1906	18	1897	15	1899	30	100	1906	18	0.0007760	0.000096	0.281495	0.000029	0.02080	0.00260	-45.6	1.0	-3.6
90	190211_160.FIN2	0.11680	0.00150	5.476	0.087	0.3419	0.0043	1908	23	1896	13	1895	20	99	1908	23									
11	190211_039.FIN2	0.11750	0.00240	5.450	0.100	0.3412	0.0077	1919	37	1890	16	1889	38	98	1919	37	0.0005160	0.000018	0.281463	0.000022	0.01278	0.00032	-46.7	0.8	-4.1
15	190211_049.FIN2	0.11770	0.00220	5.120	0.120	0.3189	0.0046	1922	34	1838	20	1784	23	93	1922	34									
164	190830_180.FIN2	0.11780	0.00180	5.640	0.110	0.3468	0.0061	1923	27	1921	16	1918	29	100	1923	27	0.0005170	0.000008	0.281292	0.000025	0.01342	0.00029	-52.8	0.9	-10.1
53	190211_105.FIN2	0.11800	0.00270	5.860	0.150	0.3538	0.0043	1926	41	1949	23	1952	21	101	1926	41	0.0005930	0.000017	0.281414	0.000031	0.01568	0.00053	-48.5	1.1	-5.8
108	190211_184.FIN2	0.11820	0.00160	5.720	0.130	0.3504	0.0066	1929	24	1929	20	1932	33	100	1929	24	0.0001536	0.000005	0.281332	0.000031	0.00435	0.00008	-51.4	1.1	-8.0
147	190211_247.FIN2	0.11887	0.00095	5.722	0.048	0.3493	0.0027	1939	14	1933	7	1931	13	100	1939	14	0.0000220	0.000001	0.281275	0.000017	0.00080	0.00007	-53.4	0.6	-9.7
9	190211_037.FIN2	0.11900	0.00260	5.680	0.180	0.3470	0.0075	1941	39	1930	28	1919	36	99	1941	39	0.0009400	0.000170	0.281661	0.000032	0.02400	0.00520	-39.7	1.1	2.9
58	190211_110.FIN2	0.11900	0.00110	5.709	0.068	0.3489	0.0038	1941	17	1931	10	1928	18	99	1941	17	0.0016240	0.000042	0.281625	0.000026	0.04523	0.00090	-41.0	0.9	0.7
169	190830_185.FIN2	0.11910	0.00470	5.740	0.270	0.3500	0.0130	1943	71	1933	41	1932	64	99	1943	71	0.0005000	0.000110	0.281381	0.000025	0.01470	0.00360	-49.6	0.9	-6.4
166	190830_182.FIN2	0.12030	0.00160	5.880	0.110	0.3548	0.0066	1961	24	1957	15	1953	32	100	1961	24	0.0002580	0.000018	0.281340	0.000022	0.00761	0.00057	-51.1	0.8	-7.2
146	190211_246.FIN2	0.12080	0.00120	5.899	0.077	0.3558	0.0040	1968	18	1960	12	1961	19	100	1968	18	0.0005480	0.000018	0.281672	0.000026	0.01318	0.00079	-39.4	0.9	4.4
14	190211_048.FIN2	0.12160	0.00180	5.820	0.140	0.3395	0.0070	1980	26	1947	21	1883	34	95	1980	26	0.0003540	0.000019	0.281384	0.000019	0.00987	0.00062	-49.5	0.7	-5.3
2	190211_030.FIN2	0.12240	0.00160	5.488	0.093	0.3258	0.0042	1992	23	1899	14	1817	21	91	1992	23	0.0007610	0.000046	0.281461	0.000026	0.02070	0.00150	-46.8	0.9	-2.8
170	190830_186.FIN2	0.12300	0.00140	6.207	0.098	0.3645	0.0050	2000	20	2002	14	2002	24	100	2000	20	0.0003945	0.000006	0.281450	0.000017	0.00930	0.00015	-47.2	0.6	-2.5
140	190211_234.FIN2	0.12310	0.00230	5.920	0.130	0.3531	0.0061	2002	33	1960	19	1947	29	97	2002	33	0.0005950	0.000003	0.281417	0.000028	0.01599	0.00011	-48.4	1.0	-4.0
198	190830_233.FIN2	0.12320	0.00130	6.223	0.092	0.3642	0.0047	2003	19	2006	13	2001	22	100	2003	19	0.0005028	0.000009	0.281401	0.000031	0.01279	0.00021	-48.9	1.1	-4.4
212	190830_253.FIN2	0.12330	0.00230	6.160	0.140	0.3631	0.0074	2005	33	1996	20	1995	35	100	2005	33	0.0003600	0.000015	0.281399	0.000013	0.00938	0.00046	-49.0	0.5	-4.2
137	190211_231.FIN2	0.12350	0.00150	5.991	0.094	0.3564	0.0052	2007	22	1973	14	1964	25	98	2007	22	0.0014190	0.000061	0.281396	0.000030	0.03920	0.00170	-49.1	1.1	-5.7
206	190830_241.FIN2	0.12360	0.00260	6.160	0.390	0.3620	0.0210	2009	37	1995	54	1987	99	99	2009	37	0.0006860	0.000033	0.281478	0.000024	0.01840	0.00130	-46.2	0.9	-1.7
121	190211_209.FIN2	0.12380	0.00140	5.621	0.087	0.3322	0.0041	2012	20	1918	13	1848	20	92	2012	20	0.0008090	0.000023	0.281499	0.000020	0.02315	0.00096	-45.5	0.7	-1.1
18	190211_052.FIN2	0.12412	0.00096	6.330	0.061	0.3674	0.0032	2016	14	2020	8	2016	15	100	2016	14	0.0003094	0.000009	0.281520	0.000025	0.00819	0.00022	-44.7	0.9	0.4
62	190211_120.FIN2	0.12430	0.00170	6.375	0.099	0.3692	0.0042	2019	24	2026	14	2025	20	100	2019	24	0.0003916	0.000005	0.281377	0.000020	0.01042	0.00010	-49.8	0.7	-4.7

U-Pb geochronology																	Hf isotope geochemistry								
		Isotopic ratios						Isotopic ages									Isotopic ratios						Epsilon units		
Grain #	Spot name	$^{207}Pb/^{206}Pb$	± 2SE	$^{207}Pb/^{235}U$	± 2SE	$^{206}Pb/^{238}U$	± 2SE	$^{207}Pb/^{206}Pb$	± 2SE (Ma)	$^{207}Pb/^{235}U$	± 2SE (Ma)	$^{206}Pb/^{238}U$	± 2SE (Ma)	Conc. %	Best Age	± 2SE (Ma)	$^{176}Lu/^{177}Hf$	± 2SE	$^{176}Hf/^{177}Hf$	± 2SE	$^{176}Yb/^{177}Hf$	± 2SE	$εHf_0$	2SE	$εHf_t$
157	190211_257.FIN2	0.12480	0.00210	6.500	0.130	0.3729	0.0050	2026	30	2044	17	2041	23	101	2026	30	0.0004750	0.000023	0.281382	0.000021	0.01310	0.00066	-49.6	0.7	-4.5
61	190211_119.FIN2	0.12550	0.00100	6.370	0.077	0.3705	0.0039	2036	14	2026	11	2031	19	100	2036	14	0.0005648	0.000002	0.281526	0.000025	0.01542	0.00005	-44.5	0.9	0.7
208	190830_249.FIN2	0.12560	0.00180	6.350	0.120	0.3680	0.0059	2037	25	2024	17	2018	28	99	2037	25	0.0003630	0.000054	0.281490	0.000027	0.00990	0.00150	-45.8	1.0	-0.2
200	190830_235.FIN2	0.12750	0.00190	6.680	0.140	0.3783	0.0069	2064	26	2071	18	2067	32	100	2064	26	0.0003960	0.000028	0.281425	0.000020	0.01046	0.00083	-48.1	0.7	-2.0
247	190830_306.FIN2	0.12750	0.00290	6.740	0.170	0.3798	0.0087	2064	40	2073	23	2073	41	100	2064	40	0.0007710	0.000022	0.281380	0.000029	0.01991	0.00061	-49.7	1.0	-4.1
68	190211_126.FIN2	0.12843	0.00094	6.728	0.074	0.3788	0.0039	2077	13	2074	10	2070	18	100	2077	13	0.0007020	0.000013	0.281436	0.000019	0.01903	0.00032	-47.7	0.7	-1.7
220	190830_267.FIN2	0.13020	0.00770	6.860	0.400	0.3820	0.0170	2101	104	2088	52	2086	77	99	2101	104	0.0016700	0.000089	0.281367	0.000023	0.04120	0.00170	-50.1	0.8	-5.0
31	190211_071.FIN2	0.13100	0.00110	6.995	0.080	0.3868	0.0037	2111	15	2108	10	2107	17	100	2111	15	0.0005587	0.000003	0.281456	0.000024	0.01526	0.00014	-47.0	0.9	0.0
26	190211_066.FIN2	0.13250	0.00220	6.770	0.140	0.3678	0.0054	2131	29	2077	18	2017	28	95	2131	29	0.0005355	0.000007	0.281472	0.000039	0.01402	0.00031	-46.4	1.4	1.0
24	190211_058.FIN2	0.13290	0.00120	7.158	0.089	0.3909	0.0044	2137	16	2130	11	2126	20	100	2137	16	0.0015000	0.000110	0.281590	0.000034	0.04460	0.00330	-42.3	1.2	4.0
177	190830_200.FIN2	0.13290	0.00580	7.220	0.410	0.3900	0.0140	2137	76	2135	52	2122	63	99	2137	76	0.0009490	0.000099	0.281522	0.000046	0.02610	0.00280	-44.7	1.6	2.3
238	190830_291.FIN2	0.13480	0.00340	6.640	0.190	0.3573	0.0082	2161	44	2063	26	1969	39	91	2161	44	0.0007530	0.000050	0.281383	0.000025	0.01930	0.00170	-49.6	0.9	-1.8
156	190211_256.FIN2	0.13590	0.00160	7.450	0.130	0.3996	0.0056	2176	21	2166	15	2166	26	100	2176	21	0.0008965	0.000006	0.281451	0.000020	0.02605	0.00019	-47.2	0.7	0.8
207	190830_242.FIN2	0.13770	0.00450	7.740	0.350	0.4070	0.0170	2198	57	2199	41	2198	78	100	2198	57	0.0012900	0.000150	0.281500	0.000034	0.03480	0.00460	-45.4	1.2	2.4
80	190211_144.FIN2	0.14190	0.00190	8.270	0.130	0.4209	0.0051	2251	23	2256	14	2262	23	101	2251	23	0.0008220	0.000030	0.281349	0.000023	0.02287	0.00078	-50.8	0.8	-1.0
195	190830_224.FIN2	0.14670	0.00170	8.770	0.160	0.4314	0.0079	2308	20	2312	17	2309	36	100	2308	20	0.0007018	0.000008	0.281442	0.000027	0.01878	0.00019	-47.5	1.0	3.7
236	190830_289.FIN2	0.14680	0.00350	8.690	0.320	0.4280	0.0130	2309	41	2302	34	2296	61	99	2309	41	0.0010600	0.000130	0.281358	0.000030	0.02760	0.00390	-50.5	1.1	0.2
234	190830_287.FIN2	0.14690	0.00430	8.690	0.420	0.4280	0.0130	2310	50	2301	43	2296	58	99	2310	50	0.0012790	0.000048	0.281435	0.000027	0.03370	0.00140	-47.7	1.0	2.6
153	190211_253.FIN2	0.14730	0.00260	8.090	0.160	0.3917	0.0055	2315	30	2239	18	2130	25	92	2315	30	0.0011130	0.000017	0.281324	0.000027	0.03139	0.00055	-51.7	1.0	-0.9
179	190830_202.FIN2	0.14760	0.00320	8.480	0.220	0.4180	0.0110	2318	37	2282	23	2248	49	97	2318	37	0.0006280	0.000013	0.281313	0.000023	0.01651	0.00037	-52.1	0.8	-0.5
172	190830_195.FIN2	0.14800	0.00140	8.890	0.130	0.4344	0.0058	2323	16	2324	14	2324	26	100	2323	16	0.0007220	0.000064	0.281324	0.000028	0.01860	0.00180	-51.7	1.0	-0.1
178	190830_201.FIN2	0.14800	0.00190	8.930	0.200	0.4342	0.0077	2323	22	2325	21	2320	34	100	2323	22	0.0002830	0.000019	0.281259	0.000025	0.00705	0.00058	-54.0	0.9	-1.8
124	190211_212.FIN2	0.14840	0.00150	8.630	0.170	0.4275	0.0069	2328	17	2298	18	2294	31	99	2328	17	0.0005970	0.000012	0.281297	0.000022	0.01611	0.00023	-52.6	0.8	-0.8
110	190211_192.FIN2	0.14850	0.00130	8.187	0.095	0.3994	0.0039	2329	15	2250	10	2166	18	93	2329	15	0.0007030	0.000014	0.281311	0.000019	0.01862	0.00043	-52.1	0.7	-0.4
19	190211_053.FIN2	0.14860	0.00300	8.210	0.200	0.4060	0.0094	2330	35	2253	22	2196	43	94	2330	35	0.0006850	0.000046	0.281372	0.000029	0.01830	0.00130	-50.0	1.0	1.8
226	190830_273.FIN2	0.14940	0.00960	9.050	0.760	0.4370	0.0300	2339	110	2337	78	2330	140	100	2339	110	0.0005780	0.000024	0.281283	0.000029	0.01549	0.00051	-53.1	1.0	-1.0
249	190830_308.FIN2	0.15000	0.00170	9.110	0.160	0.4389	0.0057	2346	19	2344	16	2344	26	100	2346	19	0.0006450	0.000017	0.281350	0.000021	0.01664	0.00039	-50.7	0.7	1.4
45	190211_091.FIN2	0.15060	0.00160	9.190	0.120	0.4405	0.0064	2353	18	2355	12	2352	29	100	2353	18	0.0003200	0.000011	0.281266	0.000019	0.00833	0.00026	-53.7	0.7	-0.9
102	190211_178.FIN2	0.15120	0.00140	8.960	0.140	0.4356	0.0061	2360	16	2332	14	2330	28	99	2360	16	0.0009370	0.000057	0.281249	0.000030	0.02560	0.00160	-54.3	1.1	-2.3
130	190211_218.FIN2	0.15380	0.00150	8.420	0.130	0.4026	0.0050	2389	17	2276	14	2180	23	91	2389	17	0.0004440	0.000013	0.281305	0.000019	0.01173	0.00029	-52.3	0.7	1.1
168	190830_184.FIN2	0.15690	0.00180	9.910	0.190	0.4560	0.0073	2423	19	2419	18	2418	32	100	2423	19	0.0004190	0.000031	0.281270	0.000023	0.01072	0.00087	-53.6	0.8	0.7
32	190211_072.FIN2	0.16180	0.00190	9.880	0.170	0.4488	0.0069	2475	20	2422	16	2389	30	97	2475	20	0.0003589	0.000007	0.281134	0.000026	0.00901	0.00021	-58.4	0.9	-2.8
261	190830_326.FIN2	0.16410	0.00150	10.770	0.170	0.4743	0.0076	2498	15	2501	15	2499	33	100	2498	15	0.0006540	0.000015	0.281184	0.000030	0.01635	0.00050	-56.6	1.1	-1.0
119	190211_201.FIN2	0.16420	0.00330	10.320	0.300	0.4430	0.0110	2499	34	2461	27	2361	49	94	2499	34	0.0007330	0.000038	0.281249	0.000022	0.02160	0.00120	-54.3	0.8	1.2
46	190211_092.FIN2	0.16430	0.00240	9.990	0.240	0.4468	0.0095	2500	25	2431	22	2380	42	95	2500	25	0.0006420	0.000048	0.281262	0.000032	0.01880	0.00170	-53.9	1.1	1.9
217	190830_258.FIN2	0.17150	0.00430	11.720	0.410	0.4920	0.0160	2572	42	2575	33	2574	68	100	2572	42	0.0006440	0.000037	0.281283	0.000026	0.01710	0.00130	-53.1	0.9	4.2
191	190830_220.FIN2	0.17230	0.00250	11.720	0.260	0.4910	0.0100	2580	24	2580	21	2572	45	100	2580	24	0.0008350	0.000016	0.281231	0.000032	0.02207	0.00049	-55.0	1.1	2.2
215	190830_256.FIN2	0.17230	0.00270	10.910	0.260	0.4593	0.0094	2580	26	2513	22	2435	41	94	2580	26	0.0010240	0.000024	0.281269	0.000026	0.02788	0.00088	-53.6	0.9	3.3
143	190211_237.FIN2	0.17260	0.00200	11.570	0.200	0.4887	0.0062	2583	19	2568	16	2564	27	99	2583	19	0.0006820	0.000025	0.281207	0.000029	0.01920	0.00088	-55.8	1.0	1.7
213	190830_254.FIN2	0.17280	0.00300	10.620	0.290	0.4390	0.0100	2585	29	2487	26	2344	46	91	2585	29									
228	190830_275.FIN2	0.17300	0.00270	10.760	0.280	0.4520	0.0110	2587	26	2504	25	2402	49	93	2587	26	0.0009080	0.000016	0.281197	0.000032	0.02401	0.00054	-56.2	1.1	1.1
8	190211_036.FIN2	0.17320	0.00230	11.950	0.190	0.4959	0.0060	2589	22	2597	15	2595	26	100	2589	22	0.0004550	0.000015	0.281178	0.000034	0.01217	0.00046	-56.8	1.2	1.2
65	190211_123.FIN2	0.17420	0.00210	11.830	0.270	0.4934	0.0097	2598	20	2589	21	2582	42	99	2598	20	0.0009140	0.000091	0.281238	0.000034	0.02620	0.00260	-54.7	1.2	2.8
219	190830_260.FIN2	0.17610	0.00240	12.210	0.260	0.5000	0.0100	2616	23	2616	20	2611	44	100	2616	23	0.0006750	0.000019	0.281262	0.000033	0.01744	0.00056	-53.9	1.2	4.5
151	190211_251.FIN2	0.17620	0.00200	11.840	0.210	0.4931	0.0088	2617	19	2590	17	2582	38	99	2617	19	0.0009150	0.000025	0.281207	0.000033	0.02629	0.00097	-55.8	1.2	2.1
78	190211_142.FIN2	0.17640	0.00140	12.110	0.130	0.4987	0.0048	2619	13	2611	10	2607	21	100	2619	13	0.0003034	0.000005	0.281093	0.000022	0.00751	0.00013	-59.8	0.8	-0.8
117	190211_199.FIN2	0.17640	0.00140	11.550	0.150	0.4805	0.0063	2619	13	2570	13	2528	27	97	2619	13	0.0007260	0.000049	0.281192	0.000021	0.02070	0.00150	-56.3	0.7	1.9
159	190830_169.FIN2	0.17640	0.00150	12.270	0.190	0.5006	0.0078	2619	14	2621	15	2618	33	100	2619	14	0.0007860	0.000040	0.281213	0.000022	0.02040	0.00120	-55.6	0.8	2.6
30	190211_070.FIN2	0.17730	0.00250	12.390	0.210	0.5037	0.0043	2628	23	2621	11	2628	18	100	2628	23	0.0005472	0.000009	0.281176	0.000020	0.01462	0.00020	-56.9	0.7	1.9
114	190211_196.FIN2	0.17750	0.00200	12.280	0.180	0.4967	0.0064	2630	19	2624	14	2598	27	99	2630	19	0.0007840	0.000036	0.281234	0.000023	0.02200	0.00100	-54.8	0.8	3.6
52	190211_104.FIN2	0.17810	0.00240	12.730	0.190	0.5112	0.0056	2635	22	2656	14	2660	24	101	2635	22	0.0005700	0.000017	0.281032	0.000023	0.01525	0.00052	-62.0	0.8	-3.1
64	190211_122.FIN2	0.17810	0.00120	12.210	0.140	0.5005	0.0051	2635	11	2619	11	2615	22	99	2635	11	0.0005515	0.000004	0.281201	0.000021	0.01465	0.00015	-56.0	0.7	2.9
259	190830_324.FIN2	0.17910	0.00600	11.340	0.630	0.4520	0.0300	2645	56	2546	52	2400	130	91	2645	56									
42	190211_088.FIN2	0.17940	0.00130	12.350	0.120	0.5018	0.0046	2647	12	2630	9	2620	20	99	2647	12	0.0007690	0.000052	0.281190	0.000023	0.02150	0.00150	-56.4	0.8	2.4
186	190830_215.FIN2	0.17970	0.00190	12.680	0.210	0.5094	0.0079	2650	18	2652	16	2652	34	100	2650	18	0.0011500	0.000160	0.281250	0.000027	0.03100	0.00440	-54.3	1.0	3.9
43	190211_089.FIN2	0.17990	0.00150	12.650	0.170	0.5074	0.0062	2652	14	2649	13	2643	27	100	2652	14	0.0006360	0.000054	0.281182	0.000019	0.01710	0.00150	-56.3	0.7	2.9
183	190830_206.FIN2	0.17990	0.00240	12.630	0.220	0.5064	0.0097	2652	22	2650	16	2646	44	100	2652	22	0.0009150	0.000022	0.281003	0.000026	0.02410	0.00068	-63.0	0.9	-4.4
133	190211_227.FIN2	0.18080	0.00180	11.290	0.140	0.4581	0.0055	2660	16	2546	12	2431	24	91	2660	16	0.0008480	0.000050	0.281164	0.000025	0.02320	0.00160	-57.3	0.9	1.7
205	190830_240.FIN2	0.18130	0.00150	12.900	0.210	0.5130	0.0085	2665	14	2673	15	2671	35	100	2665	14	0.0005260	0.000031	0.281224	0.000026	0.01312	0.00071	-55.2	0.9	4.5
154	190211_254.FIN2	0.18200	0.00230	12.710	0.340	0.5100	0.0110	2671	21	2659	25	2656	45	99	2671	21	0.0006810	0.000042	0.280994	0.000028	0.01830	0.00120	-63.3	1.0	-3.8
176	190830_199.FIN2	0.18220	0.00230	12.950	0.240	0.5147	0.0084	2673	21	2675	17	2673	36	100	2673	21	0.0003620	0.000017	0.281195	0.000022	0.00911	0.00041	-56.2	0.8	3.9
158	190211_258.FIN2	0.18230	0.00200	12.880	0.190	0.5126	0.0067	2674	18	2669	14	2666	28	100	2674	18	0.0005620	0.000015	0.281176	0.000024	0.01434	0.00068	-56.9	0.9	2.9
99	190211_175.FIN2	0.18290	0.00120	12.870	0.150	0.5120	0.0057	2679	11	2669	11	2667	24	100	2679	11	0.0016860	0.000018	0.281254	0.000024	0.04549	0.00059	-54.1	0.9	3.8
211	190830_252.FIN2	0.18290	0.00200	12.970	0.290	0.5147	0.0099	2679	18	2673	22	2672	42	100	2679	18	0.0006510	0.000050	0.281198	0.000028	0.01570	0.00120	-56.1	1.0	3.7
70	190211_128.FIN2	0.18310	0.00170	13.040	0.160	0.5159	0.0052	2681	15	2680	12	2680	22	100	2681	15	0.0006270	0.000011	0.281113	0.000027	0.01638	0.00033	-59.1	1.0	0.7
83	190211_147.FIN2	0.18620	0.00250	12.310	0.240	0.4871	0.0087	2709	22	2626	18	2556	38	94	2709	22	0.0007450	0.000040	0.281085	0.000045	0.02090	0.00120	-60.1	1.6	0.2
152	190211_252.FIN2	0.18630	0.00210	12.860	0.210	0.5070	0.0078	2710	19	2667	16	2642	33	97	2710	19	0.0012400	0.000130	0.281043	0.000028	0.03320	0.00410	-61.6	1.0	-2.2
246	190830_305.FIN2	0.19730	0.00270	15.710	0.420	0.5770	0.0140	2804	22	2857	26	2935	58	105	2804	22	0.0011400	0.000130	0.281026	0.000030	0.03020	0.00360	-62.2	1.1	-0.5
188	190830_217.FIN2	0.21790	0.00260	17.790	0.440	0.5870	0.0150	2965	19	2970	25	2970	60	100	2965	19	0.0005870	0.000020	0.280665	0.000030	0.01597	0.00070	-75.0	1.1	-8.6
rejected analyses																									
1	190211_029.FIN2	0.12390	0.00160	1.026	0.017	0.0588	0.0010	2013	23	716	9	370	6	18	N/A	N/A	0.0061700	0.000260	0.281628	0.000048	0.19300	0.00790	-40.9	1.7	N/A
4	190211_032.FIN2	0.11700	0.00140	1.857	0.060	0.1161	0.0033	1911	21	1061	21	707	19	37	N/A	N/A	0.0018500	0.000110	0.281580	0.000026	0.05380	0.00300	-42.6	0.9	N/A
5	190211_033.FIN2	0.11820	0.00220	2.445	0.046	0.1481	0.0025	1929	33	1255	13	890	14	46	N/A	N/A	0.0020180	0.000058	0.281435	0.000018	0.06100	0.00180	-47.7	0.6	N/A
6	190211_034.FIN2	0.11200	0.00150	3.382	0.061	0.2212	0.0033	1832	24	1499	14	1288	18	70	N/A	N/A	0.0011380	0.000066	0.281781	0.000033	0.03310	0.00220	-35.5	1.2	N/A
7	190211_035.FIN2	0.14180	0.00450	4.030	0.160	0.2087	0.0028	2249	55	1632	32	1222	15	54	N/A	N/A	0.0014710	0.000030	0.281599	0.000027	0.04095	0.00079	-41.9	1.0	N/A
10	190211_038.FIN2	0.16560	0.00190	5.740	0.120	0.2468	0.0050	2514	19	1939	16	1421	26	57	N/A	N/A	0.0022800	0.000230	0.281119	0.000042	0.06460	0.00650	-58.9	1.5	N/A
13	190211_047.FIN2	0.10820	0.00110	1.317	0.022	0.0871	0.0012	1769	19	852	10	538	7	30	N/A	N/A	0.0034400	0.000250	0.281627	0.000040	0.10260	0.00720	-40.9	1.4	N/A
17	190211_051.FIN2	0.23230	0.00310	3.334	0.054	0.1041	0.0021	3068	21	1488	13	638	13	21	N/A	N/A	0.0025900	0.000140	0.281047	0.000037	0.07890	0.00500	-61.5	1.3	N/A
20	190211_054.FIN2	0.19070	0.00260	9.470	0.170	0.3643	0.0049	2748	22	2384	16	2002	23	73	N/A	N/A	0.0013160	0.000079	0.281226	0.000020	0.04450	0.00270	-55.1	0.7	N/A
21	190211_055.FIN2	0.14780	0.00130	7.265	0.092	0.3585	0.0038	2321	15	2144	12	1974	18	85	N/A	N/A	0.0011250	0.000048	0.281421	0.000036	0.02740	0.00100	-48.2	1.3	N/A
22	190211_056.FIN2	0.12200	0.00260	3.620	0.120	0.2093	0.0062	1986	38	1553	26	1224	33	62	N/A	N/A									
23	190211_057.FIN2	0.14640	0.00270	5.950	0.160	0.2890	0.0070	2304	32	1966	24	1636	35	71	N/A	N/A	0.0019400	0.000220	0.281427	0.000029	0.05890	0.00830	-48.0	1.0	N/A
25	190211_065.FIN2	0.16810	0.00280	3.810	0.110	0.1668	0.0047	2539	28	1593	23	994	26	39	N/A	N/A	0.0023600	0.000200	0.281256	0.000051	0.07240	0.00690	-54.1	1.8	N/A
28	190211_068.FIN2	0.16680	0.00200	5.550	0.160	0.2399	0.0060	2526	20	1905	23	1392	33	55	N/A	N/A	0.0015100	0.000100	0.281303	0.000025	0.04270	0.00340	-52.4	0.9	N/A
29	190211_069.FIN2	0.17200	0.01500	9.330	0.860	0.3820	0.0190	2577	146	2349	81	2083	87	81	N/A	N/A	0.0009040	0.000037	0.281650	0.000022	0.02800	0.00130	-40.1	0.8	N/A
33	190211_073.FIN2	0.27190	0.00390	16.260	0.500	0.4330	0.0130	3317	22	2890	30	2318	60	70	N/A	N/A									
36	190211_076.FIN2	0.11740	0.00190	4.510	0.100	0.2826	0.0055	1917	29	1732	19	1604	28	84	N/A	N/A	0.0009700	0.000140	0.281634	0.000030	0.02820	0.00430	-40.7	1.1	N/A
37	190211_083.FIN2	0.11440	0.00170	4.423	0.077	0.2746	0.0037	1870	27	1714	15	1564	19	84	N/A	N/A	0.0012310	0.000049	0.281519	0.000032	0.03340	0.00160	-44.8	1.1	N/A
38	190211_084.FIN2	0.13500	0.00190	1.026	0.023	0.0558	0.0009	2164	25	716	12	350	6	16	N/A	N/A	0.0042800	0.000330	0.281469	0.000037	0.12750	0.00920	-46.5	1.3	N/A
39	190211_085.FIN2	0.12390	0.00270	5.380	0.140	0.3105	0.0065	2013	39	1879	23	1743	32	87	N/A	N/A	0.0006700	0.000050	0.281564	0.000020	0.01870	0.00170	-43.2	0.7	N/A
41	190211_087.FIN2	0.15560	0.00230	7.790	0.150	0.3597	0.0062	2408	25	2206	17	1980	29	82	N/A	N/A									
44	190211_090.FIN2	0.14410	0.00190	6.440	0.120	0.3244	0.0052	2277	23	2036	16	1810	25	79	N/A	N/A	0.0012160	0.000093	0.281413	0.000029	0.03630	0.00330	-48.5	1.0	N/A
47	190211_093.FIN2	0.21200	0.01100	12.760	0.910	0.4400	0.0120	2921	84	2649	64	2349	52	80	N/A	N/A	0.0011300	0.000140	0.281213	0.000028	0.03180	0.00470	-55.6	1.0	N/A
48	190211_094.FIN2	0.20990	0.00370	1.606	0.034	0.0543	0.0010	2905	29	972	13	341	6	12	N/A	N/A									
49	190211_101.FIN2	0.11740	0.00220	4.110	0.130	0.2422	0.0057	1917	34	1655	26	1398	30	73	N/A	N/A									
51	190211_103.FIN2	0.11680	0.00190	4.581	0.067	0.2801	0.0041	1908	29	1745	12	1591	20	83	N/A	N/A	0.0021700	0.000560	0.281467	0.000031	0.06800	0.01700	-46.6	1.1	N/A
55	190211_107.FIN2	0.17020	0.00420	8.880	0.160	0.3817	0.0083	2560	41	2325	17	2083	39	81	N/A	N/A	0.0007320	0.000028	0.281235	0.000018	0.02010	0.00110	-54.8	0.6	N/A
56	190211_108.FIN2	0.15690	0.00200	8.670	0.120	0.3985	0.0050	2423	22	2303	13	2162	23	89	N/A	N/A	0.0009400	0.000120	0.281106	0.000029	0.03080	0.00440	-59.4	1.0	N/A
59	190211_111.FIN2	0.12660	0.00180	5.280	0.130	0.2911	0.0057	2051	25	1868	20	1646	28	80	N/A	N/A	0.0006500	0.000140	0.281386	0.000024	0.02060	0.00430	-49.5	0.9	N/A

U-Pb geochronology																	Hf isotope geochemistry								
		Isotopic ratios						Isotopic ages									Isotopic ratios						Epsilon units		
Grain #	Spot name	$^{207}Pb/^{206}Pb$	± 2SE	$^{207}Pb/^{235}U$	± 2SE	$^{206}Pb/^{238}U$	± 2SE	$^{207}Pb/^{206}Pb$	± 2SE (Ma)	$^{207}Pb/^{235}U$	± 2SE (Ma)	$^{206}Pb/^{238}U$	± 2SE (Ma)	Conc. %	Best Age	± 2SE (Ma)	$^{176}Lu/^{177}Hf$	± 2SE	$^{176}Hf/^{177}Hf$	± 2SE	$^{176}Yb/^{177}Hf$	± 2SE	εHf_0	2SE	εHf_t
63	190211_121.FIN2	0.15430	0.00580	6.190	0.440	0.2890	0.0200	2394	64	1991	62	1630	98	68	N/A	N/A									
67	190211_125.FIN2	0.10780	0.00310	1.800	0.064	0.1194	0.0029	1763	53	1042	24	727	17	41	N/A	N/A	0.0052500	0.000420	0.281681	0.000048	0.15800	0.01300	-39.0	1.7	N/A
69	190211_127.FIN2	0.14310	0.00220	5.370	0.120	0.2757	0.0037	2265	27	1877	19	1569	19	69	N/A	N/A	0.0008460	0.000065	0.281228	0.000027	0.02250	0.00200	-55.1	1.0	N/A
71	190211_129.FIN2	0.18360	0.00190	9.390	0.260	0.3758	0.0094	2686	17	2374	26	2055	44	77	N/A	N/A	0.0023400	0.000160	0.281242	0.000036	0.07210	0.00620	-54.6	1.3	N/A
72	190211_130.FIN2	0.14280	0.00190	5.890	0.120	0.3014	0.0047	2261	23	1956	18	1697	23	75	N/A	N/A	0.0005250	0.000011	0.281240	0.000033	0.01446	0.00045	-54.6	1.2	N/A
73	190211_137.FIN2	0.16290	0.00390	4.200	0.130	0.1848	0.0051	2486	40	1669	24	1092	28	44	N/A	N/A	0.0027800	0.000420	0.281234	0.000036	0.08100	0.01300	-54.8	1.3	N/A
74	190211_138.FIN2	0.11960	0.00290	3.950	0.110	0.2409	0.0056	1950	43	1621	24	1391	29	71	N/A	N/A	0.0005680	0.000056	0.281669	0.000022	0.01520	0.00170	-39.5	0.8	N/A
75	190211_139.FIN2	0.21620	0.00760	2.231	0.090	0.0750	0.0011	2953	57	1188	27	466	7	16	N/A	N/A	0.0032500	0.000210	0.281552	0.000042	0.09700	0.00660	-43.6	1.5	N/A
76	190211_140.FIN2	0.15140	0.00140	7.530	0.100	0.3569	0.0059	2362	16	2175	12	1966	28	83	N/A	N/A	0.0005100	0.000030	0.281310	0.000023	0.01486	0.00093	-52.2	0.8	N/A
79	190211_143.FIN2	0.13750	0.00400	4.930	0.180	0.2546	0.0063	2196	51	1801	31	1461	33	67	N/A	N/A	0.0017800	0.000210	0.281547	0.000034	0.05060	0.00660	-43.8	1.2	N/A
82	190211_146.FIN2	0.16820	0.00240	6.740	0.160	0.2931	0.0060	2540	24	2077	21	1656	30	65	N/A	N/A	0.0003970	0.000054	0.281187	0.000029	0.01060	0.00160	-56.5	1.0	N/A
84	190211_148.FIN2	0.11850	0.00190	2.213	0.060	0.1376	0.0033	1934	29	1186	20	831	19	43	N/A	N/A	0.0022200	0.000290	0.281847	0.000025	0.06580	0.00930	-33.2	0.9	N/A
85	190211_155.FIN2	0.11420	0.00170	2.946	0.064	0.1856	0.0041	1867	27	1393	16	1097	22	59	N/A	N/A	0.0026500	0.000450	0.281642	0.000054	0.08100	0.01300	-40.4	1.9	N/A
86	190211_156.FIN2	0.12090	0.00160	3.743	0.070	0.2221	0.0027	1970	24	1578	15	1292	14	66	N/A	N/A	0.0015300	0.000170	0.281703	0.000033	0.04380	0.00560	-38.3	1.2	N/A
87	190211_157.FIN2	0.14810	0.00250	6.570	0.180	0.3265	0.0091	2324	29	2054	24	1821	44	78	N/A	N/A	0.0014000	0.000110	0.281469	0.000037	0.03460	0.00290	-46.5	1.3	N/A
88	190211_158.FIN2	0.14910	0.00230	7.360	0.200	0.3548	0.0082	2336	26	2154	24	1956	39	84	N/A	N/A	0.0012200	0.000140	0.281304	0.000032	0.03280	0.00400	-52.4	1.1	N/A
89	190211_159.FIN2	0.11700	0.00190	4.500	0.100	0.2716	0.0046	1911	29	1729	18	1548	23	81	N/A	N/A	0.0010370	0.000069	0.281692	0.000024	0.02870	0.00200	-38.7	0.9	N/A
91	190211_161.FIN2	0.11890	0.00170	4.799	0.098	0.2918	0.0042	1940	26	1783	17	1650	21	85	N/A	N/A									
92	190211_162.FIN2	0.12650	0.00240	4.530	0.094	0.2578	0.0050	2050	34	1735	17	1478	26	72	N/A	N/A	0.0009020	0.000069	0.281338	0.000028	0.02710	0.00220	-51.2	1.0	N/A
93	190211_163.FIN2	0.19450	0.00570	4.880	0.150	0.1814	0.0053	2781	48	1796	26	1074	29	39	N/A	N/A									
94	190211_164.FIN2	0.12450	0.00230	4.340	0.110	0.2550	0.0043	2022	33	1700	21	1464	22	72	N/A	N/A	0.0019200	0.000190	0.281867	0.000043	0.05480	0.00490	-32.5	1.5	N/A
95	190211_165.FIN2	0.12160	0.00140	1.120	0.025	0.0672	0.0012	1980	20	760	12	419	7	21	N/A	N/A	0.0040800	0.000150	0.281520	0.000034	0.12080	0.00430	-44.7	1.2	N/A
96	190211_166.FIN2	0.18100	0.01000	8.500	0.460	0.3405	0.0063	2662	92	2274	50	1888	30	71	N/A	N/A	0.0004820	0.000026	0.281482	0.000028	0.01278	0.00094	-46.1	1.0	N/A
97	190211_173.FIN2	0.15410	0.00200	5.143	0.099	0.2447	0.0038	2392	22	1844	16	1411	20	59	N/A	N/A									
98	190211_174.FIN2	0.11880	0.00160	3.543	0.072	0.2067	0.0042	1938	24	1536	16	1211	22	62	N/A	N/A									
100	190211_176.FIN2	0.14390	0.00340	2.139	0.064	0.1079	0.0028	2275	41	1160	21	661	16	29	N/A	N/A	0.0038300	0.000094	0.281438	0.000039	0.11580	0.00280	-47.6	1.4	N/A
101	190211_177.FIN2	0.12470	0.00350	3.440	0.130	0.1913	0.0073	2025	50	1510	30	1128	40	56	N/A	N/A									
103	190211_179.FIN2	0.24870	0.00330	1.845	0.035	0.0537	0.0010	3177	21	1061	12	337	6	11	N/A	N/A									
104	190211_180.FIN2	0.11290	0.00190	3.424	0.066	0.2199	0.0053	1847	30	1509	15	1281	28	69	N/A	N/A	0.0015700	0.000110	0.281596	0.000029	0.04550	0.00380	-42.0	1.0	N/A
105	190211_181.FIN2	0.12530	0.00280	5.180	0.150	0.3032	0.0055	2033	40	1852	22	1706	27	84	N/A	N/A	0.0006840	0.000038	0.281666	0.000023	0.01820	0.00120	-39.6	0.8	N/A
106	190211_182.FIN2	0.11620	0.00250	2.328	0.074	0.1425	0.0042	1899	39	1218	23	859	23	45	N/A	N/A	0.0040500	0.000390	0.281753	0.000037	0.11500	0.01100	-36.5	1.3	N/A
107	190211_183.FIN2	0.10960	0.00180	3.141	0.090	0.2087	0.0058	1793	30	1441	22	1221	31	68	N/A	N/A	0.0023200	0.000220	0.281451	0.000022	0.07820	0.00820	-47.2	0.8	N/A
109	190211_191.FIN2	0.11300	0.01000	1.570	0.150	0.0994	0.0032	1848	160	943	64	610	19	33	N/A	N/A	0.0052400	0.000230	0.281669	0.000051	0.16590	0.00500	-39.5	1.8	N/A
116	190211_198.FIN2	0.11440	0.00310	4.290	0.120	0.2774	0.0032	1870	49	1691	22	1581	17	85	N/A	N/A	0.0009500	0.000019	0.281513	0.000024	0.02779	0.00067	-45.0	0.9	N/A
118	190211_200.FIN2	0.11550	0.00170	4.300	0.170	0.2740	0.0110	1888	26	1688	35	1561	56	83	N/A	N/A									
120	190211_202.FIN2	0.13480	0.00120	6.434	0.096	0.3485	0.0038	2161	16	2035	13	1927	18	89	N/A	N/A	0.0005250	0.000010	0.281274	0.000035	0.01439	0.00045	-53.4	1.2	N/A
122	190211_210.FIN2	0.20240	0.00350	5.050	0.170	0.1815	0.0060	2846	28	1824	29	1075	32	38	N/A	N/A	0.0022400	0.000160	0.281166	0.000030	0.06520	0.00540	-57.3	1.1	N/A
123	190211_211.FIN2	0.23320	0.00240	1.626	0.023	0.0506	0.0005	3074	16	979	9	318	3	10	N/A	N/A	0.0059400	0.000560	0.281632	0.000047	0.18100	0.01800	-40.8	1.7	N/A
125	190211_213.FIN2	0.15800	0.00260	3.996	0.082	0.1852	0.0027	2434	28	1632	17	1095	15	45	N/A	N/A	0.0016800	0.000240	0.280756	0.000035	0.05750	0.00920	-71.8	1.2	N/A
128	190211_216.FIN2	0.11280	0.00210	1.903	0.047	0.1236	0.0022	1845	34	1081	16	751	13	41	N/A	N/A									
129	190211_217.FIN2	0.12810	0.00270	2.096	0.059	0.1136	0.0025	2072	37	1150	21	693	14	33	N/A	N/A	0.0014300	0.000200	0.281294	0.000031	0.04190	0.00610	-52.7	1.1	N/A
131	190211_219.FIN2	0.18420	0.00280	9.000	0.200	0.3601	0.0077	2691	25	2336	20	1982	37	74	N/A	N/A									
132	190211_220.FIN2	0.10090	0.00170	1.044	0.020	0.0737	0.0017	1641	31	725	10	459	10	28	N/A	N/A									
134	190211_228.FIN2	0.16080	0.00340	7.090	0.190	0.3055	0.0081	2464	36	2121	24	1718	40	70	N/A	N/A	0.0008110	0.000089	0.281238	0.000032	0.02260	0.00250	-54.7	1.1	N/A
136	190211_230.FIN2	0.15060	0.00180	7.800	0.110	0.3815	0.0044	2353	20	2208	12	2083	21	89	N/A	N/A	0.0014390	0.000090	0.281315	0.000019	0.03980	0.00270	-52.0	0.7	N/A
138	190211_232.FIN2	0.19280	0.00250	4.742	0.087	0.1765	0.0036	2766	21	1774	15	1048	20	38	N/A	N/A									
141	190211_235.FIN2	0.11150	0.00130	1.052	0.018	0.0689	0.0008	1824	21	729	9	430	5	24	N/A	N/A									
142	190211_236.FIN2	0.13180	0.00190	6.100	0.100	0.3413	0.0048	2122	25	1989	15	1893	23	89	N/A	N/A	0.0015460	0.000078	0.281551	0.000031	0.04510	0.00320	-43.6	1.1	N/A
144	190211_238.FIN2	0.20580	0.00970	9.530	0.610	0.3338	0.0081	2873	77	2360	57	1855	39	65	N/A	N/A	0.0010180	0.000055	0.281164	0.000039	0.02870	0.00180	-57.3	1.4	N/A
145	190211_245.FIN2	0.15460	0.00640	1.639	0.057	0.0784	0.0015	2397	70	982	21	487	9	20	N/A	N/A									
148	190211_248.FIN2	0.15740	0.00250	8.020	0.310	0.3530	0.0140	2428	27	2231	35	1946	68	80	N/A	N/A	0.0012900	0.000100	0.281338	0.000024	0.03590	0.00310	-51.2	0.9	N/A
150	190211_250.FIN2	0.14520	0.00160	7.180	0.110	0.3652	0.0053	2290	19	2133	14	2006	25	88	N/A	N/A	0.0009480	0.000034	0.281421	0.000024	0.02770	0.00140	-48.2	0.9	N/A
155	190211_255.FIN2	0.09390	0.00170	0.815	0.030	0.0638	0.0024	1506	34	604	17	398	14	26	N/A	N/A									
160	190830_176.FIN2	0.16070	0.00580	3.420	0.120	0.1549	0.0054	2463	61	1507	28	928	30	38	N/A	N/A	0.0011600	0.000230	0.281274	0.000028	0.02410	0.00620	-53.4	1.0	N/A
161	190830_177.FIN2	0.12480	0.00270	1.681	0.057	0.0976	0.0030	2026	38	1000	22	600	18	30	N/A	N/A	0.0024900	0.000110	0.281511	0.000029	0.07010	0.00320	-45.1	1.0	N/A
167	190830_183.FIN2	0.12610	0.00190	5.497	0.083	0.3160	0.0044	2044	27	1899	13	1769	22	87	N/A	N/A	0.0008850	0.000039	0.281419	0.000025	0.02310	0.00110	-48.3	0.9	N/A
171	190830_187.FIN2	0.15110	0.00790	1.367	0.038	0.0673	0.0026	2358	89	873	16	419	16	18	N/A	N/A	0.0036000	0.000440	0.281576	0.000046	0.10500	0.01300	-42.8	1.6	N/A
173	190830_196.FIN2	0.12530	0.00660	4.360	0.240	0.2509	0.0079	2033	93	1699	45	1442	41	71	N/A	N/A	0.0011330	0.000073	0.281529	0.000024	0.02960	0.00220	-44.4	0.9	N/A
174	190830_197.FIN2	0.13780	0.00260	3.750	0.120	0.1970	0.0050	2200	33	1579	26	1159	27	53	N/A	N/A	0.0022280	0.000088	0.281380	0.000027	0.06880	0.00280	-49.7	1.0	N/A
175	190830_198.FIN2	0.11050	0.00150	3.193	0.060	0.2075	0.0033	1808	25	1454	15	1215	17	67	N/A	N/A	0.0009700	0.000150	0.281615	0.000030	0.02770	0.00540	-41.4	1.1	N/A
180	190830_203.FIN2	0.13930	0.00580	2.970	0.110	0.1550	0.0062	2219	72	1398	27	929	35	42	N/A	N/A	0.0031000	0.000130	0.281350	0.000045	0.09240	0.00380	-50.7	1.6	N/A
181	190830_204.FIN2	0.08340	0.00220	0.698	0.021	0.0604	0.0012	1279	51	537	13	378	7	30	N/A	N/A	0.0038430	0.000094	0.281487	0.000034	0.10610	0.00260	-45.9	1.2	N/A
184	190830_213.FIN2	0.11680	0.00430	4.450	0.340	0.2680	0.0150	1908	66	1719	64	1530	78	80	N/A	N/A									
185	190830_214.FIN2	0.14900	0.00200	2.452	0.072	0.1191	0.0032	2334	23	1254	22	725	18	31	N/A	N/A	0.0029270	0.000074	0.281329	0.000032	0.08550	0.00240	-51.5	1.1	N/A
189	190830_218.FIN2	0.11540	0.00250	3.380	0.110	0.2106	0.0062	1886	39	1498	26	1231	33	65	N/A	N/A									
190	190830_219.FIN2	0.13100	0.00330	2.030	0.120	0.1098	0.0042	2111	44	1105	37	670	24	32	N/A	N/A	0.0035300	0.000320	0.281789	0.000045	0.10230	0.00970	-35.2	1.6	N/A
192	190830_221.FIN2	0.14810	0.00320	1.670	0.120	0.0844	0.0062	2324	37	989	43	519	36	22	N/A	N/A	0.0062800	0.000320	0.281571	0.000040	0.18670	0.00980	-42.9	1.4	N/A
194	190830_223.FIN2	0.13990	0.00290	3.019	0.093	0.1566	0.0042	2226	36	1410	24	937	23	42	N/A	N/A	0.0013410	0.000060	0.281479	0.000030	0.03730	0.00180	-46.2	1.1	N/A
197	190830_232.FIN2	0.11400	0.00200	3.299	0.076	0.2082	0.0037	1864	32	1477	18	1219	20	65	N/A	N/A	0.0021500	0.000240	0.281777	0.000026	0.06310	0.00740	-35.6	0.9	N/A
199	190830_234.FIN2	0.12910	0.00280	4.760	0.130	0.2655	0.0061	2086	38	1775	23	1517	31	73	N/A	N/A	0.0020700	0.000300	0.281690	0.000029	0.05780	0.00930	-38.7	1.0	N/A
203	190830_238.FIN2	0.17060	0.00260	5.640	0.120	0.2391	0.0049	2564	25	1919	19	1381	25	54	N/A	N/A	0.0010160	0.000058	0.281237	0.000028	0.02840	0.00180	-54.7	1.0	N/A
204	190830_239.FIN2	0.10710	0.00230	1.096	0.025	0.0734	0.0012	1751	39	750	12	456	7	26	N/A	N/A	0.0034500	0.000170	0.281618	0.000035	0.10140	0.00500	-41.3	1.2	N/A
209	190830_250.FIN2	0.17600	0.00420	10.000	0.270	0.4120	0.0120	2616	40	2432	25	2223	53	85	N/A	N/A	0.0006335	0.000010	0.281219	0.000025	0.01676	0.00025	-55.4	0.9	N/A
210	190830_251.FIN2	0.17290	0.00250	9.370	0.220	0.3929	0.0078	2586	24	2372	22	2135	36	83	N/A	N/A	0.0008900	0.000150	0.281232	0.000023	0.02550	0.00440	-54.9	0.8	N/A
214	190830_255.FIN2	0.14300	0.00210	2.090	0.150	0.1028	0.0061	2264	25	1111	45	628	35	28	N/A	N/A									
216	190830_257.FIN2	0.11010	0.00340	1.578	0.054	0.1040	0.0024	1801	56	959	21	637	14	35	N/A	N/A	0.0019300	0.000140	0.281890	0.000038	0.05150	0.00440	-31.6	1.3	N/A
221	190830_268.FIN2	0.12790	0.00280	5.380	0.250	0.3060	0.0130	2069	39	1879	39	1717	66	83	N/A	N/A									
223	190830_270.FIN2	0.15070	0.00300	5.280	0.130	0.2527	0.0048	2354	34	1863	21	1452	25	62	N/A	N/A	0.0006130	0.000013	0.281305	0.000024	0.01579	0.00034	-52.3	0.9	N/A
224	190830_271.FIN2	0.14460	0.00310	1.379	0.035	0.0690	0.0013	2283	37	879	15	430	8	19	N/A	N/A	0.0052200	0.000190	0.281669	0.000045	0.14750	0.00540	-39.5	1.6	N/A
225	190830_272.FIN2	0.11610	0.00420	4.750	0.160	0.2977	0.0099	1897	65	1773	29	1679	49	89	N/A	N/A	0.0008100	0.000120	0.281532	0.000029	0.02310	0.00370	-44.3	1.0	N/A
227	190830_274.FIN2	0.11460	0.00170	2.470	0.100	0.1555	0.0061	1874	27	1250	30	929	34	50	N/A	N/A	0.0026500	0.000170	0.281577	0.000031	0.07270	0.00430	-42.7	1.1	N/A
229	190830_276.FIN2	0.19980	0.00850	3.510	0.320	0.1239	0.0061	2825	69	1516	66	753	35	27	N/A	N/A	0.0023000	0.000190	0.281577	0.000048	0.06880	0.00590	-42.7	1.7	N/A
231	190830_278.FIN2	0.13380	0.00600	1.273	0.067	0.0719	0.0045	2148	78	821	28	446	26	21	N/A	N/A									
232	190830_285.FIN2	0.17300	0.04400	0.265	0.059	0.0155	0.0037	2587	424	241	52	99	24	4	N/A	N/A									
233	190830_286.FIN2	0.14700	0.00260	7.660	0.200	0.3775	0.0092	2311	30	2189	23	2063	43	89	N/A	N/A	0.0007390	0.000023	0.281327	0.000026	0.01950	0.00037	-51.6	0.9	N/A
235	190830_288.FIN2	0.13400	0.00720	3.840	0.240	0.2110	0.0130	2151	94	1599	57	1229	69	57	N/A	N/A									
237	190830_290.FIN2	0.17260	0.00450	8.310	0.270	0.3490	0.0110	2583	44	2260	29	1927	51	75	N/A	N/A	0.0005760	0.000027	0.281031	0.000027	0.01465	0.00081	-62.0	1.0	N/A
239	190830_292.FIN2	0.11710	0.00310	4.110	0.150	0.2487	0.0083	1912	48	1653	30	1431	43	75	N/A	N/A	0.0008600	0.000098	0.281412	0.000030	0.03010	0.00330	-48.6	1.1	N/A
240	190830_293.FIN2	0.22300	0.02500	6.250	0.690	0.2050	0.0120	3002	180	1972	95	1198	62	40	N/A	N/A									
241	190830_294.FIN2	0.11440	0.00190	4.090	0.100	0.2576	0.0055	1870	30	1649	20	1476	28	79	N/A	N/A	0.0015000	0.000180	0.281823	0.000035	0.04060	0.00510	-34.0	1.2	N/A
243	190830_296.FIN2	0.17950	0.00690	2.053	0.066	0.0821	0.0024	2648	64	1131	22	508	14	19	N/A	N/A									
244	190830_297.FIN2	0.11820	0.00310	3.137	0.096	0.1900	0.0062	1929	47	1438	24	1120	34	58	N/A	N/A									
245	190830_304.FIN2	0.12030	0.00270	4.570	0.150	0.2761	0.0073	1961	40	1741	27	1571	37	80	N/A	N/A	0.0012000	0.000140	0.281411	0.000029	0.03500	0.00390	-48.6	1.0	N/A
251	190830_310.FIN2	0.11310	0.00230	4.134	0.092	0.2622	0.0057	1850	37	1659	18	1500	29	81	N/A	N/A	0.0010500	0.000140	0.281595	0.000028	0.02920	0.00370	-42.1	1.0	N/A
252	190830_311.FIN2	0.17480	0.00640	3.140	0.300	0.1237	0.0080	2604	61	1371	68	747	45	29	N/A	N/A	0.0030700	0.000250	0.281416	0.000030	0.09050	0.00680	-48.4	1.1	N/A
253	190830_312.FIN2	0.11270	0.00190	4.067	0.098	0.2621	0.0069	1843	31	1646	20	1500	35	81	N/A	N/A	0.0006600	0.000140	0.281577	0.000021	0.01740	0.00390	-42.7	0.7	N/A
255	190830_314.FIN2	0.11390	0.00220	3.450	0.110	0.2173	0.0070	1863	35	1514	24	1267	37	68	N/A	N/A	0.0030500	0.000300	0.281594	0.000042	0.09800	0.01100	-42.1	1.5	N/A
256	190830_315.FIN2	0.14450	0.00420	6.970	0.250	0.3476	0.0093	2282	50	2102	32	1921	45	84	N/A	N/A	0.0011200	0.000180	0.281337	0.000032	0.03110	0.00540	-51.2	1.1	N/A
258	190830_323.FIN2	0.12720	0.00220	1.078	0.023	0.0612	0.0010	2060	31	742	11	383	6	19	N/A	N/A									

U-Pb geochronology																	Hf isotope geochemistry								
		Isotopic ratios						Isotopic ages									Isotopic ratios						Epsilon units		
Grain #	Spot name	$^{207}Pb/^{206}Pb$	± 2SE	$^{207}Pb/^{235}U$	± 2SE	$^{206}Pb/^{238}U$	± 2SE	$^{207}Pb/^{206}Pb$	± 2SE (Ma)	$^{207}Pb/^{235}U$	± 2SE (Ma)	$^{206}Pb/^{238}U$	± 2SE (Ma)	Conc. %	Best Age	± 2SE (Ma)	$^{176}Lu/^{177}Hf$	± 2SE	$^{176}Hf/^{177}Hf$	± 2SE	$^{176}Yb/^{177}Hf$	± 2SE	εHf_0	2SE	εHf_t
260	190830_325.FIN2	0.13950	0.00330	5.850	0.180	0.3003	0.0086	2221	41	1951	27	1691	42	76	N/A	N/A	0.0018800	0.000130	0.281408	0.000040	0.05190	0.00380	-48.7	1.4	N/A
05AW18--Faro Peak formation; (Zone 08V NAD 83, 594793 E, 6896814 N)																									
114	190828_280.FIN2	0.05030	0.00160	0.198	0.007	0.0285	0.0004	209	74	183	6	181	2	N/A	181	2	0.0017800	0.000100	0.282768	0.000038	0.04070	0.00230	-0.6	1.3	3.2
81	190828_230.FIN2	0.05130	0.00330	0.201	0.012	0.0286	0.0006	254	148	185	10	182	3	N/A	182	3	0.0013030	0.000046	0.282811	0.000036	0.02872	0.00093	0.9	1.3	4.8
160	190828_349.FIN2	0.05150	0.00360	0.202	0.013	0.0287	0.0006	263	160	186	11	182	4	N/A	182	4	0.0010590	0.000055	0.282777	0.000015	0.02330	0.00130	-0.3	0.5	3.6
122	190828_294.FIN2	0.05040	0.00150	0.198	0.006	0.0288	0.0004	213	69	183	5	183	3	N/A	183	3	0.0010960	0.000043	0.282801	0.000024	0.02310	0.00094	0.6	0.8	4.5
53	190828_182.FIN2	0.05010	0.00220	0.201	0.009	0.0291	0.0004	200	102	185	8	185	3	N/A	185	3	0.0010840	0.000088	0.282770	0.000025	0.02480	0.00240	-0.5	0.9	3.4
79	190828_221.FIN2	0.05080	0.00410	0.205	0.016	0.0291	0.0011	232	186	189	13	185	7	N/A	185	7									
82	190828_231.FIN2	0.05070	0.00230	0.201	0.009	0.0291	0.0004	227	105	185	7	185	3	N/A	185	3	0.0010890	0.000024	0.282777	0.000026	0.02478	0.00051	-0.3	0.9	3.7
133	190828_312.FIN2	0.05090	0.00420	0.204	0.017	0.0291	0.0008	236	190	188	14	185	5	N/A	185	5	0.0007330	0.000052	0.282773	0.000031	0.01650	0.00120	-0.4	1.1	3.6
150	190828_334.FIN2	0.05190	0.00310	0.210	0.013	0.0292	0.0007	281	137	193	11	185	5	N/A	185	5	0.0008810	0.000065	0.282743	0.000029	0.01900	0.00180	-1.5	1.0	2.5
40	190828_163.FIN2	0.05040	0.00290	0.206	0.013	0.0292	0.0006	213	133	189	11	186	4	N/A	186	4	0.0007700	0.000038	0.282737	0.000025	0.01701	0.00080	-1.7	0.9	2.3
49	190828_178.FIN2	0.05060	0.00240	0.203	0.010	0.0292	0.0005	223	110	186	8	186	3	N/A	186	3	0.0007760	0.000032	0.282761	0.000019	0.01803	0.00073	-0.8	0.7	3.2
37	190828_160.FIN2	0.05070	0.00240	0.202	0.010	0.0293	0.0007	227	109	186	8	186	4	N/A	186	4	0.0015580	0.000057	0.282791	0.000032	0.03820	0.00140	0.2	1.1	4.2
65	190828_201.FIN2	0.05110	0.00220	0.205	0.008	0.0293	0.0004	245	99	189	7	186	2	N/A	186	2	0.0008160	0.000030	0.282795	0.000022	0.01753	0.00060	0.4	0.8	4.4
129	190828_308.FIN2	0.04970	0.00250	0.202	0.010	0.0293	0.0006	181	117	186	9	186	4	N/A	186	4	0.0014600	0.000100	0.282722	0.000026	0.03120	0.00220	-2.2	0.9	1.7
38	190828_161.FIN2	0.05040	0.00370	0.204	0.017	0.0293	0.0009	213	170	188	14	186	5	N/A	186	5	0.0009670	0.000041	0.282727	0.000026	0.02290	0.00100	-2.1	0.9	2.0
131	190828_310.FIN2	0.05130	0.00400	0.206	0.015	0.0293	0.0009	254	179	190	13	186	5	N/A	186	5	0.0009990	0.000015	0.282787	0.000019	0.02131	0.00026	0.1	0.7	4.1
64	190828_200.FIN2	0.05010	0.00170	0.203	0.008	0.0293	0.0004	200	79	187	6	186	2	N/A	186	2	0.0010890	0.000092	0.282713	0.000024	0.02430	0.00200	-2.5	0.8	1.5
20	190828_131.FIN2	0.04980	0.00220	0.204	0.010	0.0294	0.0004	186	103	188	8	187	3	N/A	187	3	0.0014590	0.000026	0.282822	0.000031	0.03042	0.00054	1.3	1.1	5.3
41	190828_164.FIN2	0.05070	0.00280	0.205	0.011	0.0294	0.0004	227	128	187	10	187	3	N/A	187	3	0.0006440	0.000017	0.282757	0.000023	0.01434	0.00036	-1.0	0.8	3.1
119	190828_291.FIN2	0.04990	0.00160	0.203	0.007	0.0295	0.0004	190	75	187	6	187	3	N/A	187	3	0.0015860	0.000063	0.282797	0.000026	0.03240	0.00140	0.4	0.9	4.4
43	190828_166.FIN2	0.05020	0.00150	0.205	0.006	0.0295	0.0004	204	69	188	5	188	2	N/A	188	2	0.0011480	0.000082	0.282736	0.000026	0.02710	0.00190	-1.7	0.9	2.3
47	190828_176.FIN2	0.05060	0.00190	0.206	0.008	0.0296	0.0004	223	87	189	7	188	3	N/A	188	3	0.0017890	0.000046	0.282798	0.000023	0.03950	0.00110	0.5	0.8	4.4
21	190828_138.FIN2	0.05110	0.00330	0.208	0.013	0.0296	0.0005	245	149	190	11	188	3	N/A	188	3	0.0006390	0.000010	0.282784	0.000020	0.01515	0.00021	0.0	0.7	4.1
128	190828_300.FIN2	0.05020	0.00170	0.205	0.007	0.0296	0.0004	204	79	190	6	188	3	N/A	188	3	0.0010730	0.000055	0.282727	0.000020	0.02480	0.00130	-2.1	0.7	2.0
138	190828_317.FIN2	0.05020	0.00220	0.206	0.009	0.0297	0.0004	204	102	189	8	188	3	N/A	188	3	0.0011910	0.000034	0.282817	0.000023	0.02861	0.00082	1.1	0.8	5.2
89	190828_238.FIN2	0.04990	0.00190	0.205	0.008	0.0297	0.0004	190	89	189	7	189	2	N/A	189	2	0.0008710	0.000018	0.282800	0.000021	0.01868	0.00036	0.5	0.7	4.6
52	190828_181.FIN2	0.05100	0.00210	0.207	0.008	0.0298	0.0004	241	95	191	7	189	3	N/A	189	3	0.0005300	0.000016	0.282680	0.000021	0.01147	0.00033	-3.7	0.7	0.4
55	190828_184.FIN2	0.04980	0.00250	0.206	0.011	0.0298	0.0007	186	117	190	9	189	4	N/A	189	4	0.0013190	0.000018	0.282636	0.000028	0.02966	0.00047	-5.3	1.0	-1.2
48	190828_177.FIN2	0.05030	0.00240	0.207	0.010	0.0298	0.0004	209	111	190	9	189	3	N/A	189	3	0.0007700	0.000014	0.282802	0.000022	0.01620	0.00030	0.6	0.8	4.7
51	190828_180.FIN2	0.05110	0.00300	0.211	0.013	0.0298	0.0005	245	135	193	10	189	3	N/A	189	3	0.0007700	0.000034	0.282786	0.000022	0.01662	0.00080	0.0	0.8	4.1
115	190828_281.FIN2	0.05030	0.00250	0.207	0.010	0.0298	0.0004	209	115	191	9	190	3	N/A	190	3	0.0006030	0.000027	0.282528	0.000032	0.01279	0.00062	-9.1	1.1	-5.0
75	190828_217.FIN2	0.05060	0.00220	0.209	0.009	0.0299	0.0004	223	101	191	7	190	2	N/A	190	2	0.0006537	0.000008	0.282721	0.000032	0.01452	0.00016	-2.3	1.1	1.9
112	190828_278.FIN2	0.05040	0.00140	0.208	0.006	0.0299	0.0003	213	64	192	5	190	2	N/A	190	2	0.0014080	0.000090	0.282532	0.000028	0.03050	0.00210	-8.9	1.0	-4.9
146	190828_330.FIN2	0.05110	0.00300	0.209	0.011	0.0299	0.0007	245	135	192	9	190	4	N/A	190	4	0.0007180	0.000024	0.282297	0.000031	0.01717	0.00055	-17.3	1.1	-13.1
111	190828_277.FIN2	0.05090	0.00290	0.213	0.013	0.0300	0.0006	236	131	195	11	190	4	N/A	190	4	0.0010960	0.000027	0.282749	0.000027	0.02570	0.00073	-1.3	1.0	2.8
132	190828_311.FIN2	0.04990	0.00140	0.206	0.006	0.0300	0.0004	190	65	191	5	191	2	N/A	191	2	0.0007140	0.000058	0.282743	0.000021	0.01230	0.00110	-1.5	0.7	2.7
100	190828_255.FIN2	0.05040	0.00290	0.210	0.012	0.0301	0.0006	213	133	193	10	191	4	N/A	191	4	0.0013400	0.000012	0.282838	0.000033	0.02900	0.00028	1.9	1.2	6.0
97	190828_252.FIN2	0.05110	0.00220	0.212	0.009	0.0301	0.0004	245	99	194	8	191	3	N/A	191	3	0.0009860	0.000038	0.282775	0.000023	0.02222	0.00084	-0.4	0.8	3.8
155	190828_344.FIN2	0.05070	0.00200	0.211	0.009	0.0301	0.0004	227	91	193	7	191	3	N/A	191	3	0.0008750	0.000050	0.282708	0.000019	0.01960	0.00100	-2.7	0.7	1.4
161	190828_350.FIN2	0.05080	0.00190	0.212	0.009	0.0301	0.0005	232	86	194	7	191	3	N/A	191	3	0.0010330	0.000023	0.282764	0.000027	0.02330	0.00049	-0.7	1.0	3.4
25	190828_142.FIN2	0.05040	0.00140	0.209	0.006	0.0301	0.0004	213	64	192	5	191	2	N/A	191	2	0.0018010	0.000043	0.282767	0.000027	0.04019	0.00099	-0.6	1.0	3.4
77	190828_219.FIN2	0.05160	0.00220	0.213	0.009	0.0302	0.0006	268	98	196	7	192	4	N/A	192	4	0.0011700	0.000100	0.282785	0.000025	0.02630	0.00270	0.0	0.9	4.1
34	190828_157.FIN2	0.05050	0.00220	0.210	0.010	0.0302	0.0006	218	101	195	9	192	4	N/A	192	4	0.0007210	0.000011	0.282745	0.000026	0.01365	0.00024	-1.4	0.9	2.8
142	190828_326.FIN2	0.05230	0.00480	0.214	0.018	0.0301	0.0007	299	209	194	15	192	5	N/A	192	5	0.0006315	0.000003	0.282713	0.000025	0.01515	0.00008	-2.5	0.9	1.6
76	190828_218.FIN2	0.05060	0.00200	0.210	0.008	0.0302	0.0004	223	91	193	7	192	3	N/A	192	3	0.0006190	0.000008	0.282783	0.000022	0.01355	0.00020	-0.1	0.8	4.1
42	190828_165.FIN2	0.05060	0.00220	0.211	0.009	0.0302	0.0004	223	101	193	8	192	3	N/A	192	3	0.0007119	0.000009	0.282769	0.000027	0.01591	0.00022	-0.6	1.0	3.6
147	190828_331.FIN2	0.05060	0.00150	0.210	0.007	0.0303	0.0004	223	69	193	6	192	3	N/A	192	3	0.0012440	0.000073	0.282731	0.000021	0.02750	0.00180	-1.9	0.7	2.2
98	190828_253.FIN2	0.05110	0.00250	0.214	0.011	0.0303	0.0004	245	113	196	9	193	3	N/A	193	3	0.0008980	0.000022	0.282735	0.000028	0.01959	0.00039	-1.8	1.0	2.4
110	190828_276.FIN2	0.05150	0.00360	0.217	0.016	0.0303	0.0009	263	160	199	13	193	6	N/A	193	6	0.0013810	0.000061	0.282847	0.000031	0.02960	0.00130	2.2	1.1	6.3
159	190828_348.FIN2	0.05200	0.00730	0.217	0.032	0.0303	0.0015	285	321	198	27	193	10	N/A	193	10	0.0021600	0.000160	0.282829	0.000024	0.04700	0.00350	1.6	0.8	5.6
74	190828_216.FIN2	0.05020	0.00260	0.210	0.011	0.0303	0.0004	204	120	193	10	193	3	N/A	193	3	0.0013180	0.000026	0.282751	0.000035	0.03197	0.00063	-1.2	1.2	2.9
36	190828_159.FIN2	0.05080	0.00200	0.212	0.009	0.0304	0.0006	232	91	195	7	193	4	N/A	193	4	0.0027330	0.000092	0.282948	0.000028	0.07040	0.00280	5.8	1.0	9.7
107	190828_273.FIN2	0.04990	0.00160	0.210	0.007	0.0304	0.0004	190	75	194	6	193	2	N/A	193	2	0.0010230	0.000052	0.282699	0.000026	0.02330	0.00100	-3.0	0.9	1.1
135	190828_314.FIN2	0.05030	0.00250	0.212	0.011	0.0304	0.0005	209	115	194	9	193	3	N/A	193	3	0.0009240	0.000064	0.282808	0.000021	0.01960	0.00130	0.8	0.7	5.0
139	190828_318.FIN2	0.05130	0.00310	0.215	0.012	0.0304	0.0007	254	139	197	10	193	4	N/A	193	4	0.0011900	0.000120	0.282802	0.000023	0.02830	0.00280	0.6	0.8	4.7
163	190828_352.FIN2	0.05020	0.00200	0.211	0.009	0.0304	0.0004	204	92	193	7	193	3	N/A	193	3	0.0014520	0.000083	0.282828	0.000029	0.03610	0.00260	1.5	1.0	5.6
46	190828_175.FIN2	0.05060	0.00200	0.213	0.009	0.0304	0.0004	223	91	195	8	193	3	N/A	193	3	0.0013351	0.000006	0.282798	0.000027	0.02858	0.00021	0.5	1.0	4.6
9	190212_019.FIN2	0.05010	0.00120	0.212	0.005	0.0305	0.0003	200	56	194	4	193	2	N/A	193	2	0.0008830	0.000079	0.282730	0.000024	0.01940	0.00170	-1.9	0.8	2.2
59	190828_195.FIN2	0.05010	0.00160	0.211	0.007	0.0305	0.0004	200	74	194	6	194	2	N/A	194	2	0.0007230	0.000010	0.282510	0.000022	0.01543	0.00018	-9.7	0.8	-5.5
137	190828_316.FIN2	0.05040	0.00170	0.212	0.007	0.0305	0.0004	213	78	195	6	194	3	N/A	194	3	0.0010790	0.000041	0.282675	0.000024	0.02325	0.00093	-3.9	0.8	0.3
61	190828_197.FIN2	0.05030	0.00140	0.211	0.006	0.0305	0.0003	209	65	194	5	194	2	N/A	194	2	0.0007960	0.000067	0.282776	0.000024	0.01650	0.00140	-0.3	0.8	3.9
152	190828_336.FIN2	0.05180	0.00480	0.218	0.021	0.0305	0.0008	277	212	198	17	194	5	N/A	194	5	0.0003920	0.000023	0.282682	0.000027	0.00850	0.00055	-3.6	1.0	0.6
169	190828_364.FIN2	0.05060	0.00240	0.213	0.010	0.0305	0.0004	223	110	195	9	194	3	N/A	194	3	0.0009730	0.000038	0.282757	0.000027	0.02251	0.00094	-1.0	1.0	3.3
39	190828_162.FIN2	0.05120	0.00280	0.214	0.011	0.0306	0.0006	250	126	196	10	194	4	N/A	194	4	0.0006490	0.000010	0.282772	0.000029	0.01229	0.00012	-0.5	1.0	3.8
88	190828_237.FIN2	0.05100	0.00170	0.214	0.007	0.0306	0.0004	241	77	196	6	194	3	N/A	194	3	0.0014460	0.000066	0.282778	0.000026	0.03130	0.00150	-0.2	0.9	3.9
94	190828_249.FIN2	0.05190	0.00150	0.218	0.007	0.0306	0.0004	281	66	200	6	194	2	N/A	194	2	0.0007760	0.000054	0.282811	0.000021	0.01730	0.00120	0.9	0.7	5.1
153	190828_342.FIN2	0.05030	0.00180	0.212	0.008	0.0306	0.0004	209	83	194	7	194	3	N/A	194	3	0.0004900	0.000050	0.282699	0.000018	0.00990	0.00120	-3.0	0.6	1.2
149	190828_333.FIN2	0.05050	0.00210	0.214	0.009	0.0306	0.0004	218	96	196	8	194	2	N/A	194	2	0.0013360	0.000053	0.282803	0.000021	0.02940	0.00120	0.6	0.7	4.8
109	190828_275.FIN2	0.05150	0.00240	0.215	0.009	0.0306	0.0006	263	107	197	8	194	3	N/A	194	3	0.0014860	0.000020	0.282661	0.000037	0.03379	0.00062	-4.4	1.3	-0.3
127	190828_299.FIN2	0.05060	0.00330	0.215	0.014	0.0306	0.0006	223	151	195	12	194	4	N/A	194	4	0.0007380	0.000019	0.282754	0.000024	0.01635	0.00042	-1.1	0.8	3.1
141	190828_325.FIN2	0.05050	0.00330	0.213	0.012	0.0306	0.0005	218	151	195	10	195	3	N/A	195	3	0.0006015	0.000009	0.282800	0.000026	0.01353	0.00022	0.5	0.9	4.8
28	190828_145.FIN2	0.05060	0.00220	0.213	0.009	0.0306	0.0004	223	101	197	8	195	3	N/A	195	3	0.0006020	0.000022	0.282680	0.000017	0.01307	0.00040	-3.7	0.6	0.5
162	190828_351.FIN2	0.05050	0.00190	0.213	0.008	0.0307	0.0004	218	87	196	7	195	2	N/A	195	2	0.0006760	0.000047	0.282763	0.000027	0.01490	0.00110	-0.8	1.0	3.5
168	190828_357.FIN2	0.05110	0.00220	0.216	0.009	0.0307	0.0004	245	99	197	8	195	2	N/A	195	2	0.0005720	0.000030	0.282717	0.000023	0.01297	0.00063	-2.4	0.8	1.8
11	190212_021.FIN2	0.05200	0.00370	0.217	0.015	0.0307	0.0005	285	163	197	12	195	3	N/A	195	3	0.0004590	0.000014	0.282770	0.000024	0.00976	0.00039	-0.5	0.8	3.7
45	190828_174.FIN2	0.05060	0.00230	0.214	0.009	0.0308	0.0004	223	105	195	8	195	3	N/A	195	3	0.0010610	0.000069	0.282756	0.000022	0.02330	0.00150	-1.0	0.8	3.2
1	190212_011.FIN2	0.04970	0.00160	0.213	0.007	0.0308	0.0004	181	75	196	6	195	3	N/A	195	3	0.0013170	0.000067	0.282687	0.000038	0.03010	0.00190	-3.5	1.3	0.7
121	190828_293.FIN2	0.05070	0.00210	0.212	0.008	0.0308	0.0004	227	96	196	7	195	3	N/A	195	3	0.0012110	0.000075	0.282801	0.000024	0.02700	0.00190	0.6	0.8	4.8
123	190828_295.FIN2	0.05120	0.00310	0.216	0.013	0.0308	0.0005	250	139	199	10	196	3	N/A	196	3	0.0008120	0.000028	0.282788	0.000024	0.01698	0.00052	0.1	0.8	4.3
105	190828_271.FIN2	0.05070	0.00260	0.215	0.011	0.0308	0.0005	227	119	197	9	196	3	N/A	196	3	0.0010370	0.000014	0.282838	0.000022	0.01913	0.00035	1.9	0.8	6.1
15	190212_025.FIN2	0.05100	0.00210	0.217	0.009	0.0309	0.0004	241	95	199	8	196	2	N/A	196	2	0.0005800	0.000021	0.282772	0.000020	0.01163	0.00029	-0.5	0.7	3.8
7	190212_017.FIN2	0.05120	0.00320	0.219	0.013	0.0309	0.0008	250	144	201	11	196	5	N/A	196	5	0.0008700	0.000110	0.282713	0.000033	0.01960	0.00240	-2.5	1.2	1.7
130	190828_309.FIN2	0.05020	0.00200	0.215	0.009	0.0309	0.0005	204	92	196	7	196	3	N/A	196	3	0.0006920	0.000017	0.282729	0.000023	0.01546	0.00039	-2.0	0.8	2.3
5	190212_015.FIN2	0.05070	0.00180	0.218	0.008	0.0309	0.0004	227	82	199	6	196	2	N/A	196	2	0.0006290	0.000040	0.282789	0.000024	0.01300	0.00120	0.1	0.8	4.4
8	190212_018.FIN2	0.05010	0.00220	0.213	0.009	0.0309	0.0005	200	102	197	8	196	3	N/A	196	3	0.0011950	0.000070	0.282807	0.000022	0.02780	0.00170	0.8	0.8	5.0
91	190828_240.FIN2	0.05050	0.00150	0.216	0.007	0.0310	0.0004	218	69	198	5	197	3	N/A	197	3	0.0013680	0.000045	0.282680	0.000025	0.02821	0.00084	-3.7	0.9	0.5
154	190828_343.FIN2	0.04990	0.00180	0.214	0.008	0.0310	0.0004	190	84	197	7	197	3	N/A	197	3	0.0008230	0.000022	0.282547	0.000021	0.01782	0.00039	-8.4	0.7	-4.2
13	190212_023.FIN2	0.05120	0.00170	0.221	0.008	0.0310	0.0004	250	76	202	6	197	2	N/A	197	2	0.0010500	0.000016	0.282680	0.000033	0.02229	0.00035	-3.7	1.2	0.5
54	190828_183.FIN2	0.05060	0.00240	0.216	0.011	0.0310	0.0005	223	110	197	9	197	3	N/A	197	3	0.0006980	0.000031	0.282705	0.000020	0.01518	0.00059	-2.8	0.7	1.5
2	190212_012.FIN2	0.05100	0.00230	0.219	0.010	0.0310	0.0005	241	104	200	8	197	3	N/A	197	3	0.0006450	0.000011	0.282721	0.000033	0.01393	0.00028	-2.3	1.2	2.0
120	190828_292.FIN2	0.05090	0.00210	0.218	0.009	0.0311	0.0004	236	95	199	8	197	3	N/A	197	3	0.0005090	0.000016	0.282677	0.000022	0.01096	0.00035	-3.8	0.8	0.5
136	190828_315.FIN2	0.05160	0.00330	0.221	0.014	0.0311	0.0006	268	147	199	12	197	4	N/A	197	4	0.0005190	0.000045	0.282919	0.000022	0.01100	0.00100	4.7	0.8	9.1
14	190212_024.FIN2	0.05020	0.00170	0.215	0.007	0.0311	0.0004	204	79	198	6	197	2	N/A	197	2	0.0011760	0.000087	0.282823	0.000031	0.02380	0.00170	1.3	1.1	5.6
151	190828_335.FIN2	0.05120	0.00190	0.219	0.008	0.0311	0.0005	250	85	201	7	198	3	N/A	198	3	0.0018200	0.000230	0.282763	0.000031	0.03890	0.00510	-0.8	1.1	3.4
68	190828_204.FIN2	0.05090	0.00150	0.217	0.006	0.0312	0.0004	236	68	199	5	198	2	N/A	198	2	0.0007342	0.000006	0.282721	0.000019	0.01420	0.00017	-2.3	0.7	2.0
90	190828_239.FIN2	0.05070	0.00150	0.216	0.007	0.0312	0.0004	227	68	198	5	198	3	N/A	198	3	0.0008570	0.000030	0.282788	0.000022	0.01677	0.00074	0.1	0.8	4.4

U-Pb geochronology																	Hf isotope geochemistry								
		Isotopic ratios						Isotopic ages									Isotopic ratios						Epsilon units		
Grain #	Spot name	$^{207}Pb/^{206}Pb$	± 2SE	$^{207}Pb/^{235}U$	± 2SE	$^{206}Pb/^{238}U$	± 2SE	$^{207}Pb/^{206}Pb$	± 2SE (Ma)	$^{207}Pb/^{235}U$	± 2SE (Ma)	$^{206}Pb/^{238}U$	± 2SE (Ma)	Conc. %	Best Age	± 2SE (Ma)	$^{176}Lu/^{177}Hf$	± 2SE	$^{176}Hf/^{177}Hf$	± 2SE	$^{176}Yb/^{177}Hf$	± 2SE	εHf_0	2SE	εHf_t
70	190828_212.FIN2	0.05080	0.00180	0.219	0.008	0.0312	0.0005	232	82	200	7	198	3	N/A	198	3	0.0010320	0.000052	0.282635	0.000027	0.02260	0.00100	-5.3	1.0	-1.0
156	190828_345.FIN2	0.05080	0.00260	0.218	0.011	0.0312	0.0005	232	118	199	9	198	3	N/A	198	3	0.0009960	0.000019	0.282880	0.000029	0.02129	0.00054	3.4	1.0	7.6
157	190828_346.FIN2	0.05090	0.00140	0.218	0.006	0.0312	0.0005	236	63	200	5	198	3	N/A	198	3	0.0010130	0.000031	0.282796	0.000023	0.02064	0.00062	0.4	0.8	4.7
10	190212_020.FIN2	0.05047	0.00087	0.219	0.005	0.0313	0.0003	217	40	201	4	198	2	N/A	198	2	0.0012590	0.000049	0.282706	0.000019	0.02520	0.00097	-2.8	0.7	1.5
71	190828_213.FIN2	0.05120	0.00280	0.221	0.012	0.0313	0.0005	250	126	201	10	199	3	N/A	199	3	0.0010180	0.000012	0.282786	0.000022	0.02346	0.00033	0.0	0.8	4.3
60	190828_196.FIN2	0.04890	0.00680	0.210	0.027	0.0313	0.0010	143	326	200	28	199	6	N/A	199	6	0.0007140	0.000033	0.282665	0.000019	0.01713	0.00079	-4.2	0.7	0.1
125	190828_297.FIN2	0.05280	0.00410	0.224	0.017	0.0313	0.0007	320	176	203	14	199	5	N/A	199	5	0.0004390	0.000028	0.282777	0.000021	0.00953	0.00068	-0.3	0.7	4.1
78	190828_220.FIN2	0.05150	0.00240	0.220	0.010	0.0314	0.0005	263	107	200	8	199	3	N/A	199	3	0.0006370	0.000031	0.282657	0.000027	0.01377	0.00066	-4.5	1.0	-0.2
166	190828_355.FIN2	0.05190	0.00320	0.224	0.014	0.0314	0.0007	281	141	204	11	199	5	N/A	199	5	0.0010020	0.000038	0.282807	0.000023	0.02145	0.00084	0.8	0.8	5.1
73	190828_215.FIN2	0.05070	0.00180	0.220	0.008	0.0315	0.0005	227	82	201	7	200	3	N/A	200	3	0.0006000	0.000024	0.282682	0.000022	0.01359	0.00054	-3.6	0.8	0.7
99	190828_254.FIN2	0.05100	0.00170	0.221	0.007	0.0314	0.0005	241	77	202	6	200	3	N/A	200	3	0.0010410	0.000037	0.282559	0.000019	0.02341	0.00079	-8.0	0.7	-3.7
72	190828_214.FIN2	0.05080	0.00200	0.219	0.009	0.0315	0.0004	232	91	200	7	200	3	N/A	200	3	0.0008290	0.000049	0.282756	0.000026	0.01820	0.00100	-1.0	0.9	3.3
85	190828_234.FIN2	0.05160	0.00320	0.222	0.014	0.0315	0.0007	268	142	203	12	200	4	N/A	200	4	0.0010640	0.000037	0.282710	0.000024	0.02370	0.00087	-2.7	0.8	1.6
145	190828_329.FIN2	0.05060	0.00200	0.219	0.009	0.0315	0.0004	223	91	200	7	200	3	N/A	200	3	0.0012390	0.000020	0.282785	0.000024	0.02558	0.00069	0.0	0.8	4.3
143	190828_327.FIN2	0.05060	0.00160	0.221	0.007	0.0316	0.0004	223	73	202	6	200	2	N/A	200	2	0.0010760	0.000079	0.282700	0.000023	0.02420	0.00210	-3.0	0.8	1.3
170	190828_365.FIN2	0.05020	0.00120	0.218	0.005	0.0316	0.0004	204	55	200	4	200	2	N/A	200	2	0.0011020	0.000075	0.282703	0.000025	0.02230	0.00150	-2.9	0.9	-2.9
116	190828_282.FIN2	0.05140	0.00490	0.223	0.020	0.0316	0.0009	259	219	204	17	201	6	N/A	201	6	0.0010190	0.000084	0.282789	0.000017	0.02070	0.00180	0.1	0.6	4.5
86	190828_235.FIN2	0.05110	0.00260	0.222	0.011	0.0317	0.0004	245	117	202	9	201	3	N/A	201	3	0.0006930	0.000052	0.282765	0.000022	0.01500	0.00110	-0.7	0.8	3.7
104	190828_259.FIN2	0.05120	0.00220	0.221	0.009	0.0317	0.0005	250	99	203	8	201	3	N/A	201	3	0.0007197	0.000008	0.282750	0.000019	0.01582	0.00016	-1.2	0.7	3.1
44	190828_167.FIN2	0.05090	0.00270	0.222	0.012	0.0317	0.0006	236	122	202	10	201	4	N/A	201	4	0.0005840	0.000072	0.282758	0.000022	0.01120	0.00130	-1.0	0.8	3.4
58	190828_194.FIN2	0.05100	0.00590	0.226	0.031	0.0318	0.0011	241	267	205	25	202	7	N/A	202	7	0.0005320	0.000010	0.282758	0.000018	0.01019	0.00018	-1.0	0.6	3.5
12	190212_022.FIN2	0.05140	0.00230	0.225	0.010	0.0318	0.0004	259	103	208	8	202	3	N/A	202	3	0.0006950	0.000022	0.282727	0.000030	0.01521	0.00053	-2.1	1.1	2.3
29	190828_146.FIN2	0.05070	0.00220	0.223	0.009	0.0321	0.0005	227	100	204	8	203	3	N/A	203	3	0.0010260	0.000063	0.282549	0.000018	0.02010	0.00120	-8.3	0.6	-4.0
80	190828_222.FIN2	0.05060	0.00240	0.225	0.011	0.0321	0.0005	223	110	207	10	203	3	N/A	203	3	0.0007740	0.000030	0.282954	0.000020	0.01682	0.00074	6.0	0.7	10.4
106	190828_272.FIN2	0.05120	0.00140	0.225	0.006	0.0322	0.0004	250	63	206	5	204	2	N/A	204	2	0.0008600	0.000044	0.282716	0.000028	0.02090	0.00100	-2.4	1.0	2.0
165	190828_354.FIN2	0.05170	0.00260	0.226	0.011	0.0322	0.0005	272	115	207	10	204	3	N/A	204	3	0.0007770	0.000083	0.282737	0.000024	0.01710	0.00200	-1.7	0.8	2.7
17	190212_033.FIN2	0.05150	0.00380	0.229	0.016	0.0323	0.0007	263	169	208	13	205	4	N/A	205	4									
118	190828_290.FIN2	0.05090	0.00200	0.227	0.010	0.0323	0.0006	236	91	207	8	205	3	N/A	205	3	0.0006040	0.000021	0.282557	0.000023	0.01368	0.00058	-8.1	0.8	-3.6
6	190212_016.FIN2	0.05090	0.00240	0.229	0.011	0.0324	0.0005	236	109	208	9	205	3	N/A	205	3									
26	190828_143.FIN2	0.05130	0.00250	0.228	0.011	0.0326	0.0006	254	112	207	9	207	4	N/A	207	4	0.0023000	0.000170	0.282956	0.000033	0.05260	0.00430	6.0	1.2	10.3
96	190828_251.FIN2	0.05120	0.00630	0.229	0.027	0.0326	0.0009	250	283	207	22	207	6	N/A	207	6	0.0007040	0.000036	0.282761	0.000019	0.01646	0.00084	-0.8	0.7	3.7
102	190828_257.FIN2	0.05100	0.00180	0.229	0.008	0.0327	0.0005	241	81	210	7	207	3	N/A	207	3	0.0015590	0.000023	0.282854	0.000028	0.03504	0.00057	2.4	1.0	6.8
140	190828_319.FIN2	0.05080	0.00420	0.230	0.018	0.0328	0.0008	232	191	208	15	208	5	N/A	208	5	0.0005580	0.000025	0.282758	0.000019	0.01227	0.00052	-1.0	0.7	3.6
16	190212_032.FIN2	0.05080	0.00390	0.236	0.019	0.0330	0.0007	232	177	214	16	209	5	N/A	209	5	0.0005850	0.000043	0.282696	0.000030	0.01265	0.00084	-3.1	1.1	1.4
158	190828_347.FIN2	0.05130	0.00240	0.232	0.011	0.0331	0.0005	254	108	210	9	210	3	N/A	210	3	0.0009900	0.000110	0.282656	0.000021	0.02100	0.00240	-4.6	0.7	0.0
56	190828_185.FIN2	0.05090	0.00290	0.234	0.014	0.0333	0.0009	236	131	213	12	211	5	N/A	211	5	0.0005730	0.000031	0.282452	0.000023	0.01277	0.00064	-11.8	0.8	-7.2
35	190828_158.FIN2	0.05130	0.00150	0.278	0.008	0.0392	0.0006	254	67	248	6	248	4	N/A	248	4	0.0008710	0.000043	0.282812	0.000026	0.01860	0.00076	1.0	0.9	6.3
124	190828_296.FIN2	0.05310	0.00470	0.301	0.028	0.0417	0.0011	333	201	268	23	263	7	N/A	263	7	0.0007570	0.000014	0.282935	0.000020	0.01863	0.00039	5.3	0.7	11.0
69	190828_211.FIN2	0.05320	0.00460	0.351	0.029	0.0478	0.0017	337	196	304	22	301	10	N/A	301	10	0.0011220	0.000038	0.282772	0.000030	0.02574	0.00086	-0.5	1.1	6.0
126	190828_298.FIN2	0.05330	0.00190	0.378	0.014	0.0513	0.0007	342	81	324	10	322	4	N/A	322	4	0.0015830	0.000033	0.282897	0.000027	0.04188	0.00094	4.0	1.0	10.8
27	190828_144.FIN2	0.05280	0.00130	0.378	0.011	0.0516	0.0009	320	56	324	8	324	6	N/A	324	6	0.0015980	0.000066	0.282480	0.000032	0.03900	0.00170	-10.8	1.1	-3.9
92	190828_241.FIN2	0.05370	0.00350	0.386	0.026	0.0518	0.0014	358	147	329	19	326	9	N/A	326	9	0.0003922	0.000006	0.282720	0.000023	0.00931	0.00018	-2.3	0.8	4.9
113	190828_279.FIN2	0.05300	0.00200	0.379	0.015	0.0518	0.0009	329	86	327	12	326	6	N/A	326	6	0.0009250	0.000018	0.282660	0.000025	0.02382	0.00052	-4.4	0.9	2.6
117	190828_289.FIN2	0.05390	0.00690	0.388	0.050	0.0523	0.0023	367	289	332	37	329	14	N/A	329	14	0.0003890	0.000021	0.282313	0.000041	0.00878	0.00055	-16.7	1.5	-9.5
4	190212_014.FIN2	0.05400	0.00170	0.424	0.014	0.0562	0.0007	371	71	358	10	353	4	N/A	353	4									
164	190828_353.FIN2	0.06215	0.00082	0.938	0.014	0.1095	0.0009	679	28	670	7	670	5	N/A	670	5	0.0006870	0.000038	0.282257	0.000025	0.02040	0.00110	-18.7	0.9	-4.0
84	190828_233.FIN2	0.07840	0.00140	2.101	0.044	0.1943	0.0028	1157	35	1145	14	1144	15	99	1157	35	0.0007440	0.000024	0.282136	0.000020	0.01997	0.00071	-23.0	0.7	2.4
32	190828_149.FIN2	0.09010	0.00250	3.041	0.090	0.2454	0.0068	1428	53	1416	23	1414	35	99	1428	53	0.0004842	0.000009	0.282017	0.000028	0.01179	0.00024	-27.2	1.0	4.5
23	190828_140.FIN2	0.09300	0.00100	3.313	0.041	0.2584	0.0024	1488	20	1481	10	1481	12	100	1488	20	0.0012580	0.000068	0.281842	0.000020	0.03200	0.00170	-33.3	0.7	-1.1
22	190828_139.FIN2	0.09870	0.00370	3.800	0.160	0.2789	0.0059	1600	70	1587	33	1585	30	99	1600	70	0.0012570	0.000046	0.281872	0.000025	0.03114	0.00094	-32.3	0.9	2.4
134	190828_313.FIN2	0.10580	0.00710	4.520	0.350	0.3070	0.0100	1728	123	1719	62	1723	49	100	1728	123	0.0008270	0.000033	0.281678	0.000023	0.02165	0.00087	-39.1	0.8	-1.1
144	190828_328.FIN2	0.10640	0.00130	4.508	0.065	0.3084	0.0032	1739	22	1733	12	1731	16	100	1739	22	0.0004460	0.000013	0.281759	0.000023	0.01095	0.00040	-36.3	0.8	2.4
33	190828_156.FIN2	0.10760	0.00410	4.620	0.220	0.3110	0.0110	1759	70	1750	40	1747	53	99	1759	70	0.0007500	0.000020	0.281210	0.000019	0.02015	0.00052	-55.7	0.7	-17.0
148	190828_332.FIN2	0.10830	0.00740	4.310	0.340	0.2890	0.0180	1771	125	1690	66	1637	90	92	1771	125	0.0007320	0.000052	0.281492	0.000025	0.02050	0.00170	-45.7	0.9	-6.7
167	190828_356.FIN2	0.10960	0.00230	4.790	0.110	0.3174	0.0048	1793	38	1775	20	1775	23	99	1793	38	0.0003046	0.000004	0.281374	0.000023	0.00810	0.00013	-49.9	0.8	-9.9
63	190828_199.FIN2	0.11160	0.00240	4.980	0.130	0.3242	0.0062	1826	39	1812	22	1809	30	99	1826	39	0.0003660	0.000008	0.281839	0.000028	0.00934	0.00024	-33.5	1.0	7.3
66	190828_202.FIN2	0.11160	0.00340	5.060	0.170	0.3267	0.0073	1826	55	1821	28	1820	35	100	1826	55	0.0006460	0.000016	0.281515	0.000030	0.01645	0.00039	-44.9	1.1	-4.5
18	190828_129.FIN2	0.11640	0.00410	5.500	0.190	0.3424	0.0063	1902	63	1897	30	1896	30	100	1902	63	0.0004170	0.000012	0.281506	0.000022	0.01064	0.00029	-45.2	0.8	-2.8
108	190828_274.FIN2	0.12250	0.00170	6.080	0.110	0.3601	0.0052	1993	25	1984	16	1981	25	99	1993	25	0.0005361	0.000007	0.281366	0.000019	0.01514	0.00025	-50.2	0.7	-5.9
87	190828_236.FIN2	0.12270	0.00580	6.110	0.260	0.3600	0.0150	1996	84	1990	37	1983	69	99	1996	84	0.0005008	0.000010	0.281543	0.000024	0.01315	0.00028	-43.9	0.9	0.5
103	190828_258.FIN2	0.12290	0.00160	6.130	0.100	0.3623	0.0047	1999	23	1992	15	1991	22	100	1999	23	0.0005900	0.000010	0.281389	0.000023	0.01518	0.00027	-49.4	0.8	-5.0
95	190828_250.FIN2	0.12560	0.00830	6.360	0.430	0.3680	0.0300	2037	117	2023	62	2020	140	99	2037	117	0.0014410	0.000066	0.281621	0.000032	0.04260	0.00190	-41.2	1.1	2.9
30	190828_147.FIN2	0.14380	0.00180	8.340	0.130	0.4213	0.0054	2273	22	2267	15	2265	24	100	2273	22	0.0017500	0.000140	0.281529	0.000033	0.03970	0.00370	-44.4	1.2	4.4
101	190828_256.FIN2	0.16200	0.01100	10.400	0.980	0.4600	0.0300	2477	115	2427	88	2430	130	98	2477	115	0.0004985	0.000004	0.281509	0.000025	0.01356	0.00011	-45.1	0.9	10.3
50	190828_179.FIN2	0.16990	0.00230	11.340	0.200	0.4857	0.0081	2557	23	2549	16	2548	35	100	2557	23	0.0005370	0.000016	0.281078	0.000025	0.01380	0.00045	-60.4	0.9	-3.2
67	190828_203.FIN2	0.18730	0.00240	13.460	0.210	0.5228	0.0068	2719	21	2708	15	2708	29	100	2719	21	0.0007380	0.000017	0.281078	0.000029	0.01783	0.00042	-60.4	1.0	0.1
rejected analyses																									
3	190212_013.FIN2	0.06340	0.00650	0.267	0.027	0.0302	0.0009	722	218	239	22	192	6	N/A	N/A	N/A									
19	190828_130.FIN2	0.16900	0.00260	9.390	0.270	0.3998	0.0096	2548	26	2374	26	2167	44	85	N/A	N/A	0.0001544	0.000006	0.281188	0.000031	0.00481	0.00015	-56.5	1.1	N/A
24	190828_141.FIN2	0.09680	0.00550	0.409	0.025	0.0306	0.0006	1563	107	343	18	194	4	12	N/A	N/A	0.0011113	0.000008	0.282820	0.000029	0.02423	0.00010	1.2	1.0	N/A
31	190828_148.FIN2	0.06300	0.00570	0.433	0.038	0.0499	0.0015	708	192	363	27	314	9	N/A	N/A	N/A	0.0005740	0.000023	0.282608	0.000025	0.01429	0.00061	-6.3	0.9	N/A
57	190828_193.FIN2	0.05840	0.00720	0.252	0.037	0.0311	0.0018	545	269	227	30	197	11	N/A	N/A	N/A	0.0007650	0.000012	0.282746	0.000016	0.01668	0.00044	-1.4	0.6	N/A
62	190828_198.FIN2	0.09280	0.00650	0.395	0.028	0.0310	0.0010	1484	133	336	20	197	7	13	N/A	N/A	0.0007470	0.000006	0.282714	0.000027	0.01638	0.00016	-2.5	1.0	N/A
83	190828_232.FIN2	0.11800	0.00220	3.675	0.093	0.2279	0.0056	1926	33	1570	23	1323	30	69	N/A	N/A	0.0021600	0.000140	0.281481	0.000035	0.06540	0.00450	-46.1	1.2	N/A
93	190828_248.FIN2	0.07360	0.00420	0.331	0.025	0.0316	0.0005	1031	115	285	17	201	3	N/A	N/A	N/A	0.0020400	0.000110	0.282651	0.000033	0.04660	0.00220	-4.7	1.2	N/A
21AW18--Faro Peak formation; (Zone 08V NAD 83, 586462 E, 6902531 N)																									
39	190826_067.FIN2	0.05040	0.00240	0.198	0.009	0.0286	0.0004	213	110	183	8	182	3	N/A	182	3	0.0013350	0.000083	0.282744	0.000026	0.03240	0.00250	-1.4	0.9	2.4
27	190826_049.FIN2	0.05000	0.00270	0.199	0.011	0.0286	0.0004	195	126	182	9	182	3	N/A	182	3	0.0013810	0.000084	0.282731	0.000030	0.03290	0.00190	-1.9	1.1	2.0
28	190826_050.FIN2	0.05000	0.00200	0.197	0.008	0.0286	0.0004	195	93	182	7	182	3	N/A	182	3	0.0014010	0.000091	0.282697	0.000027	0.03200	0.00230	-3.1	1.0	0.8
146	190826_229.FIN2	0.05020	0.00270	0.198	0.011	0.0287	0.0005	204	125	183	9	182	3	N/A	182	3	0.0006240	0.000035	0.282700	0.000025	0.01364	0.00081	-3.0	0.9	1.0
135	190826_212.FIN2	0.04960	0.00240	0.200	0.011	0.0288	0.0007	176	113	184	9	183	4	N/A	183	4	0.0007560	0.000026	0.282778	0.000023	0.01562	0.00048	-0.2	0.8	3.7
129	190826_200.FIN2	0.05100	0.00440	0.203	0.018	0.0290	0.0006	241	199	187	15	184	4	N/A	184	4	0.0010570	0.000027	0.282752	0.000034	0.02490	0.00066	-1.2	1.2	2.8
134	190826_211.FIN2	0.05190	0.00300	0.201	0.011	0.0290	0.0005	281	132	185	9	184	3	N/A	184	3	0.0006540	0.000028	0.282813	0.000025	0.01413	0.00057	1.0	0.9	5.0
51	190826_085.FIN2	0.05000	0.00230	0.200	0.009	0.0290	0.0005	195	107	185	8	184	3	N/A	184	3	0.0010660	0.000090	0.282832	0.000022	0.02310	0.00200	1.7	0.8	5.6
90	190826_143.FIN2	0.05040	0.00300	0.201	0.012	0.0290	0.0005	213	138	185	10	184	3	N/A	184	3	0.0012250	0.000039	0.282795	0.000034	0.02873	0.00087	0.4	1.2	4.3
47	190826_075.FIN2	0.05080	0.00590	0.203	0.024	0.0291	0.0009	232	268	185	20	185	5	N/A	185	5	0.0007080	0.000042	0.282685	0.000026	0.01780	0.00120	-3.5	0.9	0.5
128	190826_199.FIN2	0.05010	0.00170	0.202	0.007	0.0291	0.0004	200	79	186	6	185	2	N/A	185	2	0.0016390	0.000033	0.282529	0.000030	0.03746	0.00063	-9.1	1.1	-5.1
130	190826_201.FIN2	0.05100	0.00420	0.204	0.017	0.0292	0.0005	241	190	187	14	185	3	N/A	185	3	0.0004420	0.000033	0.282748	0.000017	0.00853	0.00070	-1.3	0.6	2.8
26	190826_048.FIN2	0.04980	0.00160	0.201	0.007	0.0292	0.0005	186	75	186	6	186	3	N/A	186	3	0.0006600	0.000036	0.282529	0.000029	0.01468	0.00080	-9.1	1.0	-5.0
57	190826_091.FIN2	0.04990	0.00190	0.202	0.008	0.0292	0.0004	190	89	186	7	186	2	N/A	186	2	0.0011220	0.000010	0.282844	0.000028	0.02329	0.00015	2.1	1.0	6.1
29	190826_051.FIN2	0.05020	0.00180	0.202	0.008	0.0292	0.0004	204	83	186	6	186	3	N/A	186	3	0.0006210	0.000036	0.282545	0.000029	0.01349	0.00080	-8.5	1.0	-4.4
152	190826_235.FIN2	0.05160	0.00330	0.207	0.014	0.0293	0.0005	268	147	190	12	186	3	N/A	186	3	0.0010070	0.000067	0.282794	0.000021	0.02170	0.00140	0.3	0.7	4.3
11	190826_021.FIN2	0.05030	0.00200	0.204	0.008	0.0293	0.0005	209	92	188	7	186	3	N/A	186	3	0.0009690	0.000049	0.282772	0.000028	0.02040	0.00120	-0.5	1.0	3.6
13	190826_029.FIN2	0.05030	0.00230	0.203	0.009	0.0293	0.0005	209	106	186	8	186	3	N/A	186	3	0.0011190	0.000037	0.282761	0.000027	0.02474	0.00090	-0.8	1.0	3.2
105	190826_164.FIN2	0.05020	0.00250	0.203	0.010	0.0293	0.0005	204	116	187	8	186	3	N/A	186	3	0.0014400	0.000150	0.282762	0.000028	0.03520	0.00370	-0.8	1.0	3.2
33	190826_055.FIN2	0.05020	0.00260	0.203	0.010	0.0294	0.0006	204	120	187	9	187	3	N/A	187	3	0.0011620	0.000043	0.282801	0.000031	0.02537	0.00091	0.6	1.1	4.6
155	190826_238.FIN2	0.05100	0.00360	0.204	0.014	0.0294	0.0006	241	163	187	12	187	4	N/A	187	4	0.0008080	0.000041	0.282658	0.000027	0.02005	0.00094	-4.5	1.0	-0.4
55	190826_089.FIN2	0.05300	0.00500	0.208	0.019	0.0294	0.0009	329	214	191	16	187	6	N/A	187	6									

U-Pb geochronology																	Hf isotope geochemistry								
		Isotopic ratios						Isotopic ages									Isotopic ratios						Epsilon units		
Grain #	Spot name	$^{207}Pb/^{206}Pb$	± 2SE	$^{207}Pb/^{235}U$	± 2SE	$^{206}Pb/^{238}U$	± 2SE	$^{207}Pb/^{206}Pb$	± 2SE (Ma)	$^{207}Pb/^{235}U$	± 2SE (Ma)	$^{206}Pb/^{238}U$	± 2SE (Ma)	Conc. %	Best Age	± 2SE (Ma)	$^{176}Lu/^{177}Hf$	± 2SE	$^{176}Hf/^{177}Hf$	± 2SE	$^{176}Yb/^{177}Hf$	± 2SE	εHf_0	2SE	εHf_t
44	190826_072.FIN2	0.05020	0.00120	0.204	0.005	0.0294	0.0003	204	55	189	5	187	2	N/A	187	2	0.0012630	0.000088	0.282733	0.000031	0.02550	0.00200	-1.8	1.1	2.2
102	190826_161.FIN2	0.05040	0.00150	0.203	0.006	0.0294	0.0004	213	69	188	5	187	2	N/A	187	2	0.0015280	0.000078	0.282787	0.000032	0.03600	0.00210	0.1	1.1	4.0
5	190826_015.FIN2	0.05110	0.00260	0.204	0.010	0.0294	0.0005	245	117	187	8	187	3	N/A	187	3	0.0005000	0.000021	0.282682	0.000023	0.01088	0.00050	-3.6	0.8	0.5
107	190826_166.FIN2	0.05120	0.00380	0.206	0.015	0.0295	0.0007	250	171	187	12	187	4	N/A	187	4	0.0010470	0.000059	0.282798	0.000035	0.02520	0.00120	0.5	1.2	4.5
15	190826_031.FIN2	0.05010	0.00300	0.206	0.013	0.0295	0.0005	200	139	189	11	187	3	N/A	187	3	0.0004900	0.000013	0.282763	0.000022	0.00946	0.00016	-0.8	0.8	3.3
79	190826_126.FIN2	0.05040	0.00380	0.205	0.016	0.0295	0.0008	213	175	189	13	188	5	N/A	188	5	0.0008170	0.000041	0.282653	0.000023	0.01658	0.00079	-4.7	0.8	-0.6
10	190826_020.FIN2	0.05070	0.00220	0.207	0.009	0.0296	0.0005	227	100	190	7	188	3	N/A	188	3	0.0009110	0.000081	0.282787	0.000030	0.01890	0.00150	0.1	1.1	4.1
14	190826_030.FIN2	0.05020	0.00260	0.203	0.010	0.0296	0.0006	204	120	189	9	188	4	N/A	188	4	0.0014260	0.000073	0.282803	0.000030	0.03270	0.00180	0.6	1.1	4.6
54	190826_088.FIN2	0.05000	0.00180	0.205	0.008	0.0296	0.0004	195	84	188	6	188	3	N/A	188	3	0.0009420	0.000010	0.282771	0.000026	0.02088	0.00042	-0.5	0.9	3.6
80	190826_127.FIN2	0.05090	0.00240	0.205	0.010	0.0296	0.0005	236	109	189	8	188	3	N/A	188	3	0.0021300	0.000130	0.282693	0.000039	0.04770	0.00320	-3.3	1.4	0.7
58	190826_092.FIN2	0.05060	0.00250	0.206	0.010	0.0296	0.0004	223	114	188	9	188	3	N/A	188	3	0.0007670	0.000016	0.282734	0.000024	0.01724	0.00039	-1.8	0.8	2.3
115	190826_180.FIN2	0.05020	0.00170	0.205	0.007	0.0296	0.0003	204	79	189	6	188	2	N/A	188	2	0.0013400	0.000110	0.282781	0.000025	0.02690	0.00210	-0.1	0.9	3.9
56	190826_090.FIN2	0.05170	0.00340	0.209	0.014	0.0296	0.0005	272	151	192	12	188	3	N/A	188	3	0.0013270	0.000062	0.282795	0.000024	0.03130	0.00140	0.4	0.8	4.4
133	190826_210.FIN2	0.05060	0.00360	0.206	0.014	0.0296	0.0006	223	165	189	12	188	4	N/A	188	4	0.0004910	0.000016	0.282725	0.000017	0.01044	0.00034	-2.1	0.6	2.0
122	190826_193.FIN2	0.05070	0.00380	0.209	0.016	0.0296	0.0005	227	173	192	13	188	3	N/A	188	3	0.0009960	0.000063	0.282746	0.000029	0.02360	0.00170	-1.4	1.0	2.7
132	190826_203.FIN2	0.05050	0.00250	0.207	0.010	0.0296	0.0004	218	115	189	9	188	3	N/A	188	3	0.0006870	0.000024	0.282775	0.000025	0.01469	0.00062	-0.4	0.9	3.7
121	190826_192.FIN2	0.04970	0.00170	0.205	0.008	0.0297	0.0004	181	80	189	6	189	2	N/A	189	2	0.0008998	0.000007	0.282697	0.000023	0.02071	0.00018	-3.1	0.8	1.0
104	190826_163.FIN2	0.05030	0.00290	0.206	0.011	0.0297	0.0005	209	134	189	10	189	3	N/A	189	3	0.0007180	0.000019	0.282715	0.000021	0.01581	0.00041	-2.5	0.7	1.6
1	190826_011.FIN2	0.05080	0.00180	0.207	0.007	0.0297	0.0004	232	82	191	6	189	2	N/A	189	2	0.0013600	0.000170	0.282745	0.000024	0.02970	0.00380	-1.4	0.8	2.6
145	190826_228.FIN2	0.05040	0.00200	0.206	0.008	0.0298	0.0004	213	92	189	7	189	3	N/A	189	3	0.0006270	0.000014	0.282642	0.000029	0.01329	0.00037	-5.1	1.0	-0.9
32	190826_054.FIN2	0.05200	0.00550	0.206	0.021	0.0298	0.0007	285	242	191	18	189	4	N/A	189	4	0.0008100	0.000060	0.282753	0.000024	0.01940	0.00150	-1.1	0.8	3.0
30	190826_052.FIN2	0.05010	0.00160	0.206	0.007	0.0298	0.0004	200	74	190	6	189	2	N/A	189	2	0.0015530	0.000036	0.282767	0.000020	0.03227	0.00063	-0.6	0.7	3.4
31	190826_053.FIN2	0.05160	0.00170	0.211	0.007	0.0298	0.0004	268	76	193	6	190	3	N/A	190	3	0.0011950	0.000027	0.282767	0.000031	0.02668	0.00074	-0.6	1.1	3.4
93	190826_146.FIN2	0.05030	0.00160	0.206	0.007	0.0299	0.0004	209	74	190	6	190	2	N/A	190	2	0.0018290	0.000075	0.282735	0.000030	0.03830	0.00110	-1.8	1.1	2.2
156	190826_239.FIN2	0.05080	0.00230	0.207	0.009	0.0299	0.0005	232	105	190	8	190	3	N/A	190	3	0.0006890	0.000021	0.282757	0.000027	0.01379	0.00044	-1.0	1.0	3.1
76	190826_123.FIN2	0.05170	0.00380	0.209	0.015	0.0299	0.0008	272	168	192	12	190	5	N/A	190	5									
8	190826_018.FIN2	0.05010	0.00290	0.209	0.012	0.0299	0.0005	200	134	190	10	190	3	N/A	190	3	0.0005830	0.000033	0.282789	0.000027	0.01262	0.00063	0.1	1.0	4.3
36	190826_058.FIN2	0.05140	0.00580	0.212	0.024	0.0299	0.0008	259	259	193	20	190	5	N/A	190	5	0.0005000	0.000035	0.282760	0.000031	0.01083	0.00061	-0.9	1.1	3.3
9	190826_019.FIN2	0.05150	0.00300	0.211	0.012	0.0299	0.0007	263	134	194	10	190	4	N/A	190	4	0.0007280	0.000032	0.282688	0.000031	0.01503	0.00072	-3.4	1.1	0.7
18	190826_034.FIN2	0.05000	0.00160	0.208	0.007	0.0299	0.0004	195	74	191	6	190	2	N/A	190	2	0.0016380	0.000023	0.282732	0.000025	0.03531	0.00066	-1.9	0.9	2.1
124	190826_195.FIN2	0.05060	0.00310	0.208	0.012	0.0299	0.0005	223	142	191	10	190	3	N/A	190	3	0.0008430	0.000017	0.282741	0.000024	0.01833	0.00037	-1.6	0.8	2.6
150	190826_233.FIN2	0.05080	0.00200	0.208	0.008	0.0299	0.0005	232	91	191	7	190	3	N/A	190	3	0.0011160	0.000074	0.282775	0.000029	0.02390	0.00160	-0.4	1.0	3.7
68	190826_108.FIN2	0.05090	0.00230	0.209	0.009	0.0300	0.0005	236	104	193	8	190	3	N/A	190	3	0.0011900	0.000046	0.282765	0.000025	0.02760	0.00100	-0.7	0.9	3.4
86	190826_139.FIN2	0.05060	0.00270	0.208	0.011	0.0300	0.0006	223	123	191	9	190	4	N/A	190	4	0.0010100	0.000062	0.282809	0.000030	0.02260	0.00140	0.8	1.1	5.0
17	190826_033.FIN2	0.05140	0.00410	0.209	0.016	0.0300	0.0006	259	183	191	13	190	4	N/A	190	4	0.0004993	0.000005	0.282667	0.000028	0.01204	0.00012	-4.2	1.0	0.0
6	190826_016.FIN2	0.05070	0.00150	0.208	0.006	0.0300	0.0004	227	68	192	5	191	2	N/A	191	2	0.0011320	0.000070	0.282808	0.000026	0.02260	0.00140	0.8	0.9	4.9
95	190826_148.FIN2	0.05110	0.00390	0.210	0.016	0.0300	0.0007	245	176	192	13	191	4	N/A	191	4	0.0011040	0.000047	0.282802	0.000026	0.02620	0.00110	0.6	0.9	4.7
96	190826_149.FIN2	0.05090	0.00310	0.208	0.012	0.0300	0.0005	236	141	192	11	191	3	N/A	191	3	0.0009130	0.000048	0.282742	0.000031	0.02060	0.00120	-1.5	1.1	2.6
34	190826_056.FIN2	0.05180	0.00360	0.212	0.014	0.0300	0.0006	277	159	195	12	191	4	N/A	191	4									
40	190826_068.FIN2	0.05110	0.00250	0.208	0.010	0.0300	0.0004	245	113	191	8	191	3	N/A	191	3	0.0005075	0.000006	0.282709	0.000025	0.01201	0.00018	-2.7	0.9	1.5
71	190826_111.FIN2	0.05110	0.00220	0.209	0.009	0.0300	0.0004	245	99	192	7	191	2	N/A	191	2	0.0013000	0.000014	0.282769	0.000027	0.02919	0.00042	-0.6	1.0	3.5
42	190826_070.FIN2	0.05090	0.00170	0.210	0.007	0.0301	0.0004	236	77	194	6	191	2	N/A	191	2	0.0008450	0.000096	0.282775	0.000019	0.01790	0.00200	-0.4	0.7	3.8
126	190826_197.FIN2	0.05080	0.00250	0.209	0.010	0.0301	0.0004	232	114	191	8	191	3	N/A	191	3	0.0007700	0.000022	0.282764	0.000025	0.01612	0.00041	-0.7	0.9	3.4
19	190826_035.FIN2	0.05140	0.00340	0.212	0.013	0.0301	0.0005	259	152	193	11	191	3	N/A	191	3	0.0005930	0.000011	0.282687	0.000021	0.01439	0.00026	-3.5	0.7	0.7
141	190826_218.FIN2	0.05100	0.00380	0.210	0.015	0.0301	0.0006	241	172	193	13	191	4	N/A	191	4	0.0009920	0.000047	0.282703	0.000022	0.02330	0.00120	-2.9	0.8	1.2
23	190826_039.FIN2	0.05060	0.00210	0.209	0.008	0.0301	0.0004	223	96	192	7	191	3	N/A	191	3	0.0013110	0.000027	0.282806	0.000029	0.02943	0.00060	0.7	1.0	4.8
131	190826_202.FIN2	0.05090	0.00230	0.211	0.010	0.0301	0.0004	236	104	193	8	191	2	N/A	191	2	0.0010390	0.000025	0.282799	0.000027	0.02279	0.00053	0.5	1.0	4.6
50	190826_084.FIN2	0.05040	0.00150	0.209	0.006	0.0302	0.0003	213	69	193	5	192	2	N/A	192	2	0.0014400	0.000100	0.282769	0.000029	0.02950	0.00190	-0.6	1.0	3.5
20	190826_036.FIN2	0.05230	0.00360	0.218	0.015	0.0302	0.0004	299	157	192	8	192	3	N/A	192	3	0.0006810	0.000018	0.282791	0.000021	0.01481	0.00041	0.2	0.7	4.4
78	190826_125.FIN2	0.05030	0.00290	0.210	0.012	0.0302	0.0005	209	134	192	10	192	3	N/A	192	3	0.0008600	0.000041	0.282497	0.000022	0.02040	0.00110	-10.2	0.8	-6.0
12	190826_022.FIN2	0.05040	0.00320	0.209	0.013	0.0302	0.0006	213	147	192	11	192	4	N/A	192	4	0.0006040	0.000035	0.282739	0.000023	0.01146	0.00053	-1.6	0.8	2.6
24	190826_040.FIN2	0.05120	0.00300	0.208	0.012	0.0302	0.0005	250	135	192	10	192	3	N/A	192	3	0.0005300	0.000007	0.282720	0.000024	0.01222	0.00015	-2.3	0.8	1.9
73	190826_120.FIN2	0.05140	0.00250	0.210	0.009	0.0302	0.0005	259	112	193	8	192	3	N/A	192	3	0.0012000	0.000140	0.282703	0.000025	0.02520	0.00270	-2.9	0.9	1.2
61	190826_101.FIN2	0.05080	0.00320	0.211	0.014	0.0303	0.0006	232	145	192	11	192	4	N/A	192	4	0.0006820	0.000012	0.282689	0.000026	0.01474	0.00032	-3.4	0.9	0.8
62	190826_102.FIN2	0.05100	0.00300	0.215	0.013	0.0303	0.0005	241	136	196	11	192	3	N/A	192	3	0.0009550	0.000022	0.282767	0.000026	0.02091	0.00058	-0.6	0.9	3.5
43	190826_071.FIN2	0.05080	0.00150	0.212	0.006	0.0304	0.0003	232	68	195	5	193	2	N/A	193	2	0.0007810	0.000036	0.282517	0.000022	0.01754	0.00075	-9.5	0.8	-5.3
142	190826_219.FIN2	0.05060	0.00250	0.211	0.010	0.0304	0.0004	223	114	193	9	193	2	N/A	193	2	0.0008590	0.000050	0.282760	0.000027	0.01900	0.00110	-0.9	1.0	3.3
89	190826_142.FIN2	0.05050	0.00270	0.212	0.012	0.0304	0.0005	218	124	194	10	193	3	N/A	193	3	0.0008220	0.000048	0.282760	0.000029	0.01870	0.00110	-0.9	1.0	3.3
157	190826_246.FIN2	0.05020	0.00150	0.210	0.007	0.0304	0.0004	204	69	194	6	193	2	N/A	193	2	0.0014800	0.000033	0.282769	0.000027	0.03358	0.00083	-0.6	1.0	3.5
110	190826_175.FIN2	0.05040	0.00130	0.211	0.006	0.0304	0.0004	213	60	194	5	193	2	N/A	193	2	0.0012120	0.000084	0.282761	0.000026	0.02590	0.00200	-0.8	0.9	3.3
7	190826_017.FIN2	0.05070	0.00300	0.211	0.012	0.0305	0.0004	227	137	194	10	193	3	N/A	193	3	0.0006830	0.000075	0.282708	0.000029	0.01510	0.00150	-2.7	1.0	1.5
87	190826_140.FIN2	0.05080	0.00260	0.212	0.010	0.0305	0.0005	232	118	194	9	194	3	N/A	194	3	0.0007150	0.000039	0.282771	0.000021	0.01568	0.00078	-0.5	0.7	3.7
67	190826_107.FIN2	0.05070	0.00250	0.212	0.011	0.0305	0.0004	227	114	195	9	194	3	N/A	194	3	0.0007000	0.000017	0.282760	0.000025	0.01594	0.00046	-0.9	0.9	3.3
63	190826_103.FIN2	0.05170	0.00500	0.216	0.021	0.0305	0.0008	272	222	194	17	194	5	N/A	194	5	0.0006480	0.000012	0.282779	0.000023	0.01518	0.00035	-0.2	0.8	4.0
143	190826_220.FIN2	0.05100	0.00270	0.214	0.011	0.0306	0.0005	241	122	194	9	194	3	N/A	194	3	0.0006260	0.000030	0.282749	0.000026	0.01397	0.00084	-1.3	0.9	3.0
151	190826_234.FIN2	0.05290	0.00620	0.219	0.027	0.0306	0.0012	325	266	198	23	194	8	N/A	194	8	0.0007290	0.000036	0.282681	0.000035	0.01659	0.00080	-3.7	1.2	0.5
49	190826_083.FIN2	0.05150	0.00300	0.214	0.012	0.0306	0.0006	263	134	198	11	194	4	N/A	194	4	0.0010710	0.000073	0.282753	0.000027	0.02090	0.00170	-1.1	1.0	3.0
77	190826_124.FIN2	0.05060	0.00230	0.212	0.010	0.0306	0.0005	223	105	194	8	194	3	N/A	194	3	0.0012380	0.000067	0.282715	0.000025	0.02790	0.00150	-2.5	0.9	1.7
125	190826_196.FIN2	0.05070	0.00240	0.213	0.010	0.0306	0.0005	227	109	195	8	194	3	N/A	194	3	0.0008180	0.000024	0.282769	0.000025	0.01563	0.00048	-0.6	0.9	3.7
113	190826_178.FIN2	0.05000	0.00220	0.214	0.010	0.0307	0.0004	195	102	195	8	195	3	N/A	195	3	0.0006520	0.000026	0.282657	0.000022	0.01425	0.00057	-4.5	0.8	-0.3
81	190826_128.FIN2	0.05110	0.00320	0.216	0.014	0.0307	0.0005	245	144	196	11	195	3	N/A	195	3	0.0005400	0.000028	0.282712	0.000023	0.01173	0.00063	-2.6	0.8	1.7
85	190826_138.FIN2	0.05130	0.00460	0.216	0.020	0.0307	0.0007	254	206	196	17	195	5	N/A	195	5	0.0004810	0.000062	0.282774	0.000026	0.01120	0.00170	-0.4	0.9	3.9
117	190826_182.FIN2	0.05040	0.00160	0.213	0.007	0.0308	0.0004	213	74	196	6	195	3	N/A	195	3	0.0008200	0.000020	0.282621	0.000024	0.01829	0.00047	-5.8	0.8	-1.6
4	190826_014.FIN2	0.05140	0.00230	0.218	0.010	0.0308	0.0004	259	103	199	8	195	3	N/A	195	3	0.0006083	0.000007	0.282700	0.000024	0.01510	0.00023	-3.0	0.8	1.3
97	190826_156.FIN2	0.05100	0.00260	0.216	0.011	0.0308	0.0005	241	118	196	9	195	3	N/A	195	3	0.0010010	0.000060	0.282764	0.000026	0.02250	0.00150	-0.7	0.9	3.5
98	190826_157.FIN2	0.05130	0.00250	0.215	0.010	0.0308	0.0004	254	112	196	9	195	3	N/A	195	3	0.0008100	0.000017	0.282798	0.000024	0.01733	0.00049	0.5	0.8	4.7
70	190826_110.FIN2	0.05130	0.00370	0.215	0.015	0.0308	0.0006	254	166	196	13	196	4	N/A	196	4	0.0006950	0.000032	0.282744	0.000025	0.01693	0.00089	-1.4	0.9	2.8
149	190826_232.FIN2	0.05110	0.00270	0.217	0.012	0.0308	0.0005	245	122	197	10	196	3	N/A	196	3	0.0007920	0.000035	0.282746	0.000029	0.01739	0.00082	-1.4	1.0	2.9
120	190826_185.FIN2	0.05070	0.00210	0.214	0.009	0.0309	0.0004	227	96	196	7	196	3	N/A	196	3	0.0010050	0.000071	0.282561	0.000019	0.02220	0.00150	-7.9	0.7	-3.7
159	190826_248.FIN2	0.05300	0.00610	0.222	0.025	0.0309	0.0008	329	261	199	21	196	5	N/A	196	5	0.0011090	0.000025	0.282744	0.000026	0.02708	0.00065	-1.4	0.9	2.8
108	190826_167.FIN2	0.05120	0.00430	0.216	0.018	0.0309	0.0006	250	193	196	15	196	4	N/A	196	4	0.0008010	0.000035	0.282760	0.000026	0.01901	0.00075	-0.9	0.9	3.4
38	190826_066.FIN2	0.05050	0.00180	0.215	0.008	0.0309	0.0004	218	83	196	6	196	2	N/A	196	2	0.0006160	0.000036	0.282655	0.000025	0.01360	0.00083	-4.6	0.9	-0.3
106	190826_165.FIN2	0.05080	0.00260	0.216	0.011	0.0309	0.0005	232	118	197	9	196	3	N/A	196	3	0.0009490	0.000037	0.282753	0.000025	0.02032	0.00066	-1.1	0.9	3.1
82	190826_129.FIN2	0.05080	0.00220	0.215	0.009	0.0310	0.0005	232	100	197	8	197	3	N/A	197	3	0.0009140	0.000076	0.282790	0.000024	0.01960	0.00180	0.2	0.8	4.4
111	190826_176.FIN2	0.05060	0.00150	0.216	0.007	0.0310	0.0003	223	69	197	6	197	2	N/A	197	2	0.0009270	0.000030	0.282785	0.000029	0.02073	0.00072	0.0	1.0	4.3
16	190826_032.FIN2	0.05080	0.00300	0.216	0.013	0.0311	0.0005	232	136	198	11	197	3	N/A	197	3	0.0006690	0.000025	0.282772	0.000023	0.01578	0.00057	-0.5	0.8	3.8
116	190826_181.FIN2	0.05080	0.00210	0.217	0.009	0.0311	0.0004	232	95	198	7	198	2	N/A	198	2	0.0006380	0.000037	0.282740	0.000025	0.01220	0.00070	-1.6	0.9	2.7
112	190826_177.FIN2	0.05020	0.00110	0.216	0.005	0.0312	0.0003	204	51	199	4	198	2	N/A	198	2	0.0013700	0.000110	0.282766	0.000023	0.02930	0.00230	-0.7	0.8	3.5
109	190826_174.FIN2	0.05090	0.00160	0.217	0.007	0.0312	0.0004	236	73	199	6	198	2	N/A	198	2	0.0006750	0.000030	0.282685	0.000022	0.01489	0.00070	-3.5	0.8	0.8
139	190826_216.FIN2	0.05200	0.00380	0.218	0.016	0.0312	0.0007	285	167	201	14	198	4	N/A	198	4	0.0004580	0.000035	0.282775	0.000027	0.01051	0.00080	-0.4	1.0	4.0
2	190826_012.FIN2	0.05070	0.00170	0.219	0.007	0.0313	0.0003	227	77	200	6	198	2	N/A	198	2	0.0006140	0.000032	0.282603	0.000024	0.01254	0.00071	-6.4	0.8	-2.1
101	190826_160.FIN2	0.05080	0.00350	0.219	0.015	0.0313	0.0007	232	159	199	12	199	4	N/A	199	4	0.0004970	0.000016	0.282749	0.000027	0.01130	0.00043	-1.3	1.0	3.1
21	190826_037.FIN2	0.05160	0.00490	0.220	0.020	0.0313	0.0008	268	218	200	17	199	5	N/A	199	5									
65	190826_105.FIN2	0.05090	0.00310	0.220	0.014	0.0314	0.0005	236	141	200	11	199	3	N/A	199	3	0.0020800	0.000130	0.282907	0.000038	0.04190	0.00260	4.3	1.3	8.5
66	190826_106.FIN2	0.05190	0.00480	0.221	0.020	0.0314	0.0008	281	212	199	17	199	5	N/A	199	5	0.0005890	0.000016	0.282767	0.000019	0.01302	0.00039	-0.6	0.7	3.7
41	190826_069.FIN2	0.05150	0.00340	0.222	0.015	0.0314	0.0006	263	152	202	12	199	4	N/A	199	4	0.0005166	0.000006	0.282778	0.000023	0.01232	0.00015	-0.2	0.8	4.1
91	190826_144.FIN2	0.05080	0.00190	0.219	0.008	0.0314	0.0004	232	86	200	6	199	2	N/A	199	2	0.0009760	0.000027	0.282771	0.000021	0.01883	0.00048	-0.5	0.7	3.8
103	190826_162.FIN2	0.05050	0.00330	0.220	0.016	0.0315	0.0007	218	151	201	13	200	4	N/A	200	4	0.0007300	0.000035	0.282770	0.000022	0.01447	0.00071	-0.5	0.8	3.8
52	190826_086.FIN2	0.05110	0.00240	0.223	0.010	0.0317	0.0005	245	108	202	9	201	3	N/A	201	3	0.0012100	0.000067	0.282909	0.000029	0.02660	0.00180	4.4	1.0	8.7

U-Pb geochronology																	Hf isotope geochemistry								
		Isotopic ratios						Isotopic ages									Isotopic ratios						Epsilon units		
Grain #	Spot name	$^{207}Pb/^{206}Pb$	± 2SE	$^{207}Pb/^{235}U$	± 2SE	$^{206}Pb/^{238}U$	± 2SE	$^{207}Pb/^{206}Pb$	± 2SE (Ma)	$^{207}Pb/^{235}U$	± 2SE (Ma)	$^{206}Pb/^{238}U$	± 2SE (Ma)	Conc. %	Best Age	± 2SE (Ma)	$^{176}Lu/^{177}Hf$	± 2SE	$^{176}Hf/^{177}Hf$	± 2SE	$^{176}Yb/^{177}Hf$	± 2SE	εHf_0	2SE	εHf_t
99	190826_158.FIN2	0.05090	0.00220	0.223	0.009	0.0318	0.0005	236	100	203	8	202	3	N/A	202	3	0.0014160	0.000046	0.282755	0.000028	0.03140	0.00110	-1.1	1.0	3.2
48	190826_076.FIN2	0.05060	0.00220	0.222	0.010	0.0319	0.0007	223	101	203	9	203	4	N/A	203	4	0.0008570	0.000030	0.282831	0.000022	0.01803	0.00066	1.6	0.8	6.0
118	190826_183.FIN2	0.05070	0.00190	0.223	0.008	0.0320	0.0003	227	87	203	7	203	2	N/A	203	2	0.0010080	0.000030	0.282539	0.000023	0.02040	0.00068	-8.7	0.8	-4.3
138	190826_215.FIN2	0.05150	0.00320	0.225	0.014	0.0321	0.0006	263	143	204	11	204	4	N/A	204	4	0.0006970	0.000041	0.282757	0.000021	0.01590	0.00100	-1.0	0.7	3.4
114	190826_179.FIN2	0.05100	0.00200	0.225	0.009	0.0321	0.0004	241	90	205	7	204	2	N/A	204	2	0.0005940	0.000021	0.282781	0.000020	0.01169	0.00032	-0.1	0.7	4.3
88	190826_141.FIN2	0.05140	0.00310	0.227	0.013	0.0322	0.0006	259	139	206	11	204	4	N/A	204	4	0.0007180	0.000068	0.282779	0.000038	0.01550	0.00150	-0.2	1.3	4.2
136	190826_213.FIN2	0.05110	0.00220	0.226	0.010	0.0322	0.0005	245	99	206	8	204	3	N/A	204	3	0.0013910	0.000070	0.282800	0.000030	0.03110	0.00160	0.5	1.1	4.9
147	190826_230.FIN2	0.05110	0.00260	0.224	0.012	0.0322	0.0005	245	117	205	10	205	3	N/A	205	3	0.0007990	0.000048	0.282754	0.000030	0.01860	0.00110	-1.1	1.1	3.3
92	190826_145.FIN2	0.05070	0.00260	0.226	0.012	0.0323	0.0005	227	119	205	10	205	3	N/A	205	3	0.0010390	0.000035	0.282918	0.000022	0.02088	0.00048	4.7	0.8	9.1
123	190826_194.FIN2	0.05170	0.00390	0.228	0.016	0.0324	0.0007	272	173	206	14	206	5	N/A	206	5	0.0008240	0.000051	0.282927	0.000030	0.01810	0.00110	5.0	1.1	9.5
72	190826_112.FIN2	0.05110	0.00270	0.228	0.012	0.0325	0.0006	245	122	207	10	206	4	N/A	206	4	0.0003930	0.000020	0.282919	0.000028	0.00879	0.00074	4.7	1.0	9.3
69	190826_109.FIN2	0.05050	0.00320	0.228	0.014	0.0326	0.0006	218	147	210	11	207	4	N/A	207	4	0.0006580	0.000066	0.282762	0.000026	0.01290	0.00120	-0.8	0.9	3.7
119	190826_184.FIN2	0.05160	0.00300	0.228	0.013	0.0326	0.0006	268	133	208	11	207	4	N/A	207	4	0.0007320	0.000057	0.282974	0.000025	0.01540	0.00130	6.7	0.9	11.2
144	190826_221.FIN2	0.05180	0.00470	0.230	0.020	0.0326	0.0008	277	208	208	17	207	5	N/A	207	5									
25	190826_047.FIN2	0.05250	0.00510	0.236	0.023	0.0329	0.0009	307	221	210	19	208	5	N/A	208	5	0.0006780	0.000041	0.282939	0.000021	0.01377	0.00091	5.4	0.7	10.0
59	190826_093.FIN2	0.05060	0.00110	0.231	0.006	0.0331	0.0004	223	50	210	5	210	3	N/A	210	3	0.0018790	0.000025	0.282668	0.000026	0.04324	0.00061	-4.1	0.9	0.3
83	190826_130.FIN2	0.05090	0.00170	0.232	0.008	0.0332	0.0005	236	77	211	7	210	3	N/A	210	3	0.0010030	0.000026	0.282764	0.000030	0.02022	0.00044	-0.7	1.1	3.8
160	190826_249.FIN2	0.05010	0.00340	0.233	0.016	0.0331	0.0007	200	158	210	14	210	4	N/A	210	4	0.0010250	0.000040	0.282758	0.000022	0.02328	0.00095	-1.0	0.8	3.6
153	190826_236.FIN2	0.05130	0.00240	0.232	0.011	0.0332	0.0007	254	108	211	9	210	4	N/A	210	4	0.0011690	0.000077	0.282753	0.000021	0.02240	0.00120	-1.1	0.7	3.4
158	190826_247.FIN2	0.05110	0.00210	0.268	0.011	0.0380	0.0006	245	95	241	9	240	4	N/A	240	4	0.0011580	0.000057	0.282700	0.000029	0.02530	0.00130	-3.0	1.0	2.2
148	190826_231.FIN2	0.05320	0.00360	0.300	0.020	0.0415	0.0009	337	153	262	16	262	5	N/A	262	5	0.0006660	0.000058	0.282947	0.000026	0.01420	0.00130	5.7	0.9	11.4
127	190826_198.FIN2	0.05310	0.00170	0.344	0.011	0.0473	0.0007	333	73	298	8	298	4	N/A	298	4	0.0012090	0.000060	0.282713	0.000029	0.02980	0.00160	-2.5	1.0	3.8
64	190826_104.FIN2	0.05350	0.00240	0.348	0.015	0.0479	0.0008	350	101	302	12	302	5	N/A	302	5	0.0016580	0.000084	0.282914	0.000032	0.03920	0.00200	4.6	1.1	10.9
60	190826_094.FIN2	0.05240	0.00190	0.351	0.013	0.0484	0.0007	303	83	304	10	304	4	N/A	304	4	0.0003690	0.000041	0.282796	0.000027	0.00681	0.00078	0.4	1.0	7.1
94	190826_147.FIN2	0.05400	0.00270	0.367	0.018	0.0498	0.0009	371	113	313	13	313	5	N/A	313	5	0.0012200	0.000053	0.282726	0.000026	0.02870	0.00120	-2.1	0.9	4.6
140	190826_217.FIN2	0.05340	0.00340	0.370	0.024	0.0501	0.0014	346	144	318	18	315	9	N/A	315	9									
37	190826_065.FIN2	0.05420	0.00350	0.376	0.024	0.0504	0.0011	379	145	318	18	317	7	N/A	317	7	0.0006526	0.000009	0.282672	0.000024	0.01607	0.00026	-4.0	0.8	2.9
3	190826_013.FIN2	0.05390	0.00220	0.375	0.015	0.0511	0.0012	367	92	322	11	321	7	N/A	321	7	0.0014800	0.000130	0.282573	0.000043	0.03680	0.00370	-7.5	1.5	-0.7
100	190826_159.FIN2	0.05340	0.00140	0.374	0.011	0.0512	0.0008	346	59	322	8	322	5	N/A	322	5									
22	190826_038.FIN2	0.05300	0.00150	0.379	0.011	0.0516	0.0008	329	64	326	8	324	5	N/A	324	5	0.0013240	0.000030	0.282778	0.000027	0.03472	0.00084	-0.2	1.0	6.7
75	190826_122.FIN2	0.05310	0.00370	0.385	0.028	0.0521	0.0012	333	158	329	21	327	7	N/A	327	7	0.0012040	0.000031	0.282791	0.000028	0.03001	0.00078	0.2	1.0	7.2
45	190826_073.FIN2	0.05370	0.00240	0.387	0.018	0.0523	0.0011	358	101	331	13	329	7	N/A	329	7	0.0012020	0.000055	0.282713	0.000035	0.02990	0.00120	-2.5	1.2	4.5
46	190826_074.FIN2	0.05350	0.00110	0.396	0.008	0.0538	0.0005	350	46	339	6	338	3	N/A	338	3									
35	190826_057.FIN2	0.07710	0.00270	1.935	0.064	0.1832	0.0031	1124	70	1085	22	1083	17	96	1124	70	0.0008530	0.000012	0.282267	0.000031	0.02276	0.00034	-18.3	1.1	6.3
137	190826_214.FIN2	0.09130	0.00190	3.132	0.078	0.2491	0.0038	1453	40	1437	19	1433	20	99	1453	40	0.0008410	0.000038	0.282011	0.000021	0.02050	0.00120	-27.4	0.7	4.5
74	190826_121.FIN2	0.10140	0.00270	4.010	0.110	0.2887	0.0047	1650	49	1634	23	1634	23	99	1650	49	0.0012820	0.000020	0.281898	0.000030	0.03301	0.00047	-31.4	1.1	4.4
53	190826_087.FIN2	0.10160	0.00330	4.010	0.140	0.2872	0.0059	1654	60	1629	27	1626	29	98	1654	60	0.0018200	0.000130	0.281888	0.000033	0.04820	0.00360	-31.7	1.2	3.5
rejected analyses																									
84	190826_131.FIN2	0.08320	0.00710	0.343	0.029	0.0301	0.0009	1274	166	295	21	191	5	15	N/A	N/A									
154	190826_237.FIN2	0.13720	0.00590	0.676	0.028	0.0360	0.0006	2192	75	519	17	228	4	10	N/A	N/A	0.0014480	0.000051	0.282916	0.000026	0.03350	0.00130	4.6	0.9	N/A
03AW18-- Faro Peak formation; (Zone 08V NAD 83, 587139 E, 6902122 N)																									
131	190828_086.FIN2	0.05100	0.00280	0.198	0.010	0.0285	0.0005	241	127	183	9	181	3	N/A	181	3	0.0012000	0.000150	0.282524	0.000042	0.02570	0.00320	-9.2	1.5	-5.3
120	190828_069.FIN2	0.05040	0.00160	0.198	0.007	0.0286	0.0005	213	74	183	6	182	3	N/A	182	3	0.0011150	0.000050	0.282715	0.000018	0.02460	0.00160	-2.5	0.6	1.4
88	190828_019.FIN2	0.05060	0.00370	0.200	0.015	0.0287	0.0010	223	169	184	13	182	6	N/A	182	6	0.0007020	0.000048	0.282780	0.000027	0.01487	0.00077	-0.2	1.0	3.8
91	190828_022.FIN2	0.05070	0.00410	0.205	0.016	0.0292	0.0008	227	187	188	13	186	5	N/A	186	5	0.0008080	0.000037	0.282761	0.000021	0.01820	0.00083	-0.8	0.7	3.2
89	190828_020.FIN2	0.05050	0.00260	0.204	0.010	0.0294	0.0005	218	119	188	9	187	3	N/A	187	3	0.0011160	0.000076	0.282759	0.000024	0.02600	0.00170	-0.9	0.8	3.1
114	190828_057.FIN2	0.05120	0.00630	0.208	0.024	0.0294	0.0010	250	283	191	20	187	6	N/A	187	6	0.0012300	0.000110	0.282496	0.000031	0.02610	0.00220	-10.2	1.1	-6.2
150	190828_111.FIN2	0.05060	0.00410	0.206	0.018	0.0294	0.0007	223	187	189	15	187	4	N/A	187	4	0.0011670	0.000014	0.282777	0.000029	0.02545	0.00031	-0.3	1.0	3.7
124	190828_073.FIN2	0.05160	0.00640	0.211	0.028	0.0295	0.0009	268	285	193	23	187	6	N/A	187	6	0.0009780	0.000045	0.282737	0.000026	0.02183	0.00080	-1.7	0.9	2.3
79	190827_275.FIN2	0.04970	0.00160	0.204	0.007	0.0296	0.0004	181	75	188	6	188	2	N/A	188	2	0.0010480	0.000032	0.282772	0.000020	0.02199	0.00076	-0.5	0.7	3.6
84	190828_015.FIN2	0.05070	0.00190	0.207	0.008	0.0296	0.0008	227	87	191	7	188	5	N/A	188	5	0.0018540	0.000075	0.282792	0.000024	0.04140	0.00180	0.2	0.8	4.2
90	190828_021.FIN2	0.05000	0.00250	0.209	0.011	0.0297	0.0009	195	116	192	9	189	6	N/A	189	6	0.0012600	0.000120	0.282716	0.000027	0.02870	0.00260	-2.4	1.0	1.6
112	190828_055.FIN2	0.05010	0.00180	0.205	0.008	0.0297	0.0005	200	83	189	7	189	3	N/A	189	3	0.0009580	0.000097	0.282740	0.000024	0.02190	0.00210	-1.6	0.8	2.5
71	190827_266.FIN2	0.05020	0.00120	0.206	0.005	0.0298	0.0003	204	55	190	4	189	2	N/A	189	2	0.0010550	0.000045	0.282780	0.000020	0.02390	0.00097	-0.2	0.7	3.9
62	190827_250.FIN2	0.05020	0.00140	0.207	0.006	0.0298	0.0004	204	65	190	5	189	3	N/A	189	3	0.0008990	0.000023	0.282688	0.000025	0.01932	0.00044	-3.4	0.9	0.7
78	190827_274.FIN2	0.05000	0.00210	0.207	0.009	0.0299	0.0004	195	98	190	8	190	3	N/A	190	3	0.0009300	0.000230	0.282775	0.000026	0.02080	0.00550	-0.4	0.9	3.7
141	190828_102.FIN2	0.05020	0.00170	0.207	0.007	0.0299	0.0005	204	79	191	6	190	3	N/A	190	3	0.0010420	0.000038	0.282783	0.000020	0.02123	0.00078	-0.1	0.7	4.0
13	190212_156.FIN2	0.05060	0.00270	0.210	0.011	0.0300	0.0004	223	123	194	9	190	3	N/A	190	3									
50	190827_232.FIN2	0.05090	0.00180	0.210	0.007	0.0300	0.0004	236	82	193	6	190	3	N/A	190	3	0.0007600	0.000036	0.282714	0.000024	0.01644	0.00093	-2.5	0.8	1.6
148	190828_109.FIN2	0.05040	0.00150	0.208	0.006	0.0300	0.0004	213	69	192	5	191	3	N/A	191	3	0.0008330	0.000023	0.282687	0.000025	0.01773	0.00040	-3.5	0.9	0.7
122	190828_071.FIN2	0.05120	0.00280	0.213	0.012	0.0300	0.0007	250	126	195	10	191	4	N/A	191	4	0.0006541	0.000007	0.282690	0.000020	0.01610	0.00018	-3.4	0.7	0.8
81	190828_012.FIN2	0.04950	0.00160	0.208	0.007	0.0300	0.0004	172	75	191	6	191	3	N/A	191	3	0.0011160	0.000019	0.282681	0.000030	0.02405	0.00020	-3.7	1.1	0.4
28	190212_177.FIN2	0.05090	0.00540	0.211	0.023	0.0301	0.0008	236	245	191	19	191	5	N/A	191	5	0.0006230	0.000064	0.282711	0.000043	0.01470	0.00160	-2.6	1.5	1.6
53	190827_235.FIN2	0.05040	0.00150	0.209	0.006	0.0301	0.0004	213	69	192	5	191	2	N/A	191	2	0.0012020	0.000039	0.282693	0.000023	0.02590	0.00110	-3.3	0.8	0.8
83	190828_014.FIN2	0.05020	0.00230	0.209	0.010	0.0302	0.0005	204	106	192	8	192	3	N/A	192	3	0.0012160	0.000010	0.282679	0.000029	0.02600	0.00024	-3.7	1.0	0.4
125	190828_074.FIN2	0.05050	0.00330	0.211	0.014	0.0302	0.0006	218	151	194	11	192	4	N/A	192	4	0.0006580	0.000049	0.282766	0.000030	0.01550	0.00130	-0.7	1.1	3.5
127	190828_076.FIN2	0.05060	0.00210	0.210	0.009	0.0302	0.0004	223	96	194	7	192	3	N/A	192	3	0.0013200	0.000065	0.282719	0.000026	0.02990	0.00150	-2.3	0.9	1.8
64	190827_252.FIN2	0.05040	0.00220	0.212	0.010	0.0303	0.0004	213	101	194	8	193	3	N/A	193	3	0.0007700	0.000038	0.282796	0.000021	0.01680	0.00082	0.4	0.7	4.6
55	190827_237.FIN2	0.05020	0.00180	0.211	0.008	0.0304	0.0004	204	83	194	7	193	3	N/A	193	3	0.0016770	0.000056	0.282823	0.000022	0.03670	0.00130	1.3	0.8	5.4
129	190828_084.FIN2	0.05050	0.00170	0.211	0.007	0.0304	0.0004	218	78	194	6	193	3	N/A	193	3	0.0030400	0.000340	0.282881	0.000036	0.07800	0.01000	3.4	1.3	7.3
103	190828_040.FIN2	0.05060	0.00240	0.212	0.010	0.0304	0.0005	223	110	195	9	193	3	N/A	193	3	0.0006370	0.000085	0.282515	0.000021	0.01420	0.00190	-9.5	0.7	-5.3
76	190827_272.FIN2	0.04980	0.00170	0.210	0.007	0.0305	0.0004	186	79	194	6	193	3	N/A	193	3	0.0015070	0.000059	0.282766	0.000021	0.03430	0.00180	-0.7	0.7	3.4
80	190828_011.FIN2	0.05080	0.00290	0.212	0.012	0.0305	0.0006	232	132	195	10	193	4	N/A	193	4	0.0006410	0.000020	0.282729	0.000029	0.01424	0.00046	-2.0	1.0	2.2
130	190828_085.FIN2	0.05060	0.00180	0.211	0.007	0.0305	0.0004	223	82	194	6	193	2	N/A	193	2	0.0008820	0.000018	0.282789	0.000019	0.01989	0.00036	0.1	0.7	4.3
72	190827_267.FIN2	0.05030	0.00280	0.213	0.012	0.0305	0.0006	209	129	195	10	194	4	N/A	194	4	0.0006520	0.000021	0.282771	0.000019	0.01442	0.00044	-0.5	0.7	3.7
134	190828_089.FIN2	0.05030	0.00330	0.213	0.014	0.0305	0.0006	209	152	194	12	194	3	N/A	194	3	0.0007510	0.000028	0.282789	0.000027	0.01751	0.00069	0.1	1.0	4.4
21	190212_170.FIN2	0.05060	0.00150	0.213	0.006	0.0305	0.0003	223	69	195	5	194	2	N/A	194	2	0.0007650	0.000014	0.282699	0.000024	0.01618	0.00031	-3.0	0.8	1.2
57	190827_245.FIN2	0.05070	0.00210	0.214	0.009	0.0306	0.0005	227	96	196	8	194	3	N/A	194	3	0.0012260	0.000012	0.282814	0.000026	0.02603	0.00026	1.0	0.9	5.2
77	190827_273.FIN2	0.05030	0.00190	0.212	0.008	0.0306	0.0004	209	88	194	6	194	2	N/A	194	2	0.0006810	0.000017	0.282690	0.000019	0.01539	0.00041	-3.4	0.7	0.9
156	190828_124.FIN2	0.05010	0.00130	0.211	0.005	0.0306	0.0003	200	60	194	4	194	2	N/A	194	2	0.0007459	0.000010	0.282668	0.000024	0.01683	0.00025	-4.1	0.8	0.1
111	190828_054.FIN2	0.05060	0.00170	0.213	0.007	0.0306	0.0004	223	78	196	6	194	2	N/A	194	2	0.0015310	0.000068	0.282759	0.000028	0.03410	0.00150	-0.9	1.0	3.2
68	190827_263.FIN2	0.05050	0.00170	0.213	0.007	0.0306	0.0004	218	78	195	6	195	2	N/A	195	2	0.0009260	0.000047	0.282728	0.000022	0.02020	0.00100	-2.0	0.8	2.2
126	190828_075.FIN2	0.05030	0.00150	0.213	0.007	0.0306	0.0004	209	69	197	6	195	2	N/A	195	2	0.0016460	0.000075	0.282709	0.000026	0.03510	0.00160	-2.7	0.9	1.4
40	190212_195.FIN2	0.05010	0.00120	0.212	0.005	0.0307	0.0003	200	56	195	4	195	2	N/A	195	2	0.0014970	0.000036	0.282723	0.000023	0.02903	0.00075	-2.2	0.8	1.9
109	190828_052.FIN2	0.04900	0.00210	0.205	0.008	0.0307	0.0005	148	100	189	7	195	3	N/A	195	3	0.0009600	0.000034	0.282790	0.000023	0.02401	0.00085	0.2	0.8	4.4
118	190828_067.FIN2	0.05090	0.00270	0.216	0.011	0.0308	0.0006	236	122	198	10	195	4	N/A	195	4	0.0006840	0.000033	0.282822	0.000023	0.01401	0.00069	1.3	0.8	5.6
138	190828_093.FIN2	0.05050	0.00370	0.213	0.016	0.0308	0.0008	218	170	198	12	195	5	N/A	195	5	0.0009270	0.000040	0.282789	0.000027	0.02024	0.00084	0.1	1.0	4.4
44	190212_205.FIN2	0.05060	0.00210	0.216	0.009	0.0308	0.0004	223	96	198	8	196	3	N/A	196	3	0.0012190	0.000041	0.282683	0.000034	0.02777	0.00093	-3.6	1.2	0.6
52	190827_234.FIN2	0.05110	0.00390	0.218	0.020	0.0308	0.0012	245	176	199	17	196	8	N/A	196	8	0.0007050	0.000035	0.282760	0.000024	0.01623	0.00079	-0.9	0.8	3.4
12	190212_155.FIN2	0.05060	0.00180	0.214	0.008	0.0309	0.0005	223	82	197	7	196	3	N/A	196	3	0.0025600	0.000220	0.282780	0.000032	0.06590	0.00710	-0.2	1.1	3.9
61	190827_249.FIN2	0.05020	0.00130	0.214	0.006	0.0309	0.0003	204	60	197	5	196	2	N/A	196	2	0.0010110	0.000048	0.282674	0.000020	0.02190	0.00110	-3.9	0.7	0.3
99	190828_036.FIN2	0.05220	0.00390	0.221	0.017	0.0309	0.0007	294	171	201	14	196	4	N/A	196	4	0.0007050	0.000023	0.282755	0.000026	0.01690	0.00052	-1.1	0.9	3.2
15	190212_158.FIN2	0.05130	0.00230	0.218	0.010	0.0310	0.0005	254	103	199	8	197	3	N/A	197	3	0.0010250	0.000070	0.282734	0.000035	0.02340	0.00130	-1.8	1.2	2.4
133	190828_088.FIN2	0.05030	0.00230	0.216	0.010	0.0310	0.0005	209	106	197	8	197	3	N/A	197	3	0.0006980	0.000028	0.282734	0.000023	0.01550	0.00056	-1.8	0.8	2.5
48	190212_209.FIN2	0.05140	0.00270	0.219	0.011	0.0310	0.0005	259	121	201	10	197	3	N/A	197	3									
59	190827_247.FIN2	0.05080	0.00240	0.215	0.009	0.0310	0.0005	232	109	198	8	197	3	N/A	197	3	0.0007460	0.000017	0.282731	0.000024	0.01668	0.00036	-1.9	0.8	2.4
69	190827_264.FIN2	0.05070	0.00220	0.216	0.009	0.0310	0.0004	227	100	198	8	197	3	N/A	197	3	0.0009630	0.000024	0.282805	0.000018	0.02076	0.00051	0.7	0.6	5.0

U-Pb geochronology																	Hf isotope geochemistry								
		Isotopic ratios						Isotopic ages									Isotopic ratios						Epsilon units		
Grain #	Spot name	$^{207}Pb/^{206}Pb$	± 2SE	$^{207}Pb/^{235}U$	± 2SE	$^{206}Pb/^{238}U$	± 2SE	$^{207}Pb/^{206}Pb$	± 2SE (Ma)	$^{207}Pb/^{235}U$	± 2SE (Ma)	$^{206}Pb/^{238}U$	± 2SE (Ma)	Conc. %	Best Age	± 2SE (Ma)	$^{176}Lu/^{177}Hf$	± 2SE	$^{176}Hf/^{177}Hf$	± 2SE	$^{176}Yb/^{177}Hf$	± 2SE	εHf_0	2SE	εHf_t
25	190212_174.FIN2	0.05020	0.00170	0.214	0.007	0.0310	0.0004	204	79	197	6	197	2	N/A	197	2	0.0014860	0.000038	0.282640	0.000029	0.03380	0.00110	-5.1	1.0	-0.9
16	190212_159.FIN2	0.05130	0.00480	0.219	0.020	0.0310	0.0007	254	215	200	16	197	4	N/A	197	4	0.0013200	0.000120	0.282736	0.000038	0.02960	0.00270	-1.7	1.3	2.5
56	190827_244.FIN2	0.05050	0.00220	0.216	0.009	0.0311	0.0004	218	101	198	8	197	3	N/A	197	3	0.0005560	0.000045	0.282848	0.000022	0.01335	0.00088	2.2	0.8	6.5
128	190828_083.FIN2	0.05100	0.00200	0.216	0.008	0.0311	0.0005	241	90	197	7	197	3	N/A	197	3	0.0011430	0.000075	0.282726	0.000026	0.02650	0.00190	-2.1	0.9	2.1
70	190827_265.FIN2	0.05120	0.00390	0.219	0.015	0.0311	0.0010	250	175	201	13	197	6	N/A	197	6	0.0008300	0.000120	0.282606	0.000028	0.01750	0.00230	-6.3	1.0	-2.1
43	190212_204.FIN2	0.05060	0.00320	0.221	0.014	0.0312	0.0006	223	146	201	12	198	4	N/A	198	4									
146	190828_107.FIN2	0.05050	0.00180	0.216	0.007	0.0311	0.0005	218	83	199	7	198	3	N/A	198	3	0.0011900	0.000110	0.282795	0.000027	0.02630	0.00240	0.4	1.0	4.6
116	190828_065.FIN2	0.05040	0.00250	0.217	0.011	0.0312	0.0004	213	115	198	9	198	3	N/A	198	3	0.0008860	0.000015	0.282787	0.000022	0.01990	0.00030	0.1	0.8	4.4
113	190828_056.FIN2	0.05160	0.00330	0.219	0.014	0.0312	0.0005	268	147	199	12	198	3	N/A	198	3	0.0008600	0.000018	0.282753	0.000022	0.01870	0.00051	-1.1	0.8	3.2
29	190212_178.FIN2	0.05070	0.00220	0.219	0.009	0.0312	0.0004	227	100	201	8	198	2	N/A	198	2	0.0007770	0.000033	0.282712	0.000041	0.01707	0.00070	-2.6	1.5	1.7
41	190212_196.FIN2	0.05160	0.00350	0.221	0.015	0.0312	0.0008	268	156	202	12	198	5	N/A	198	5	0.0012850	0.000063	0.282807	0.000027	0.02680	0.00140	0.8	1.0	5.0
96	190828_033.FIN2	0.05150	0.00330	0.218	0.013	0.0312	0.0005	263	147	200	12	198	3	N/A	198	3	0.0006680	0.000020	0.282759	0.000018	0.01652	0.00054	-0.9	0.6	3.4
123	190828_072.FIN2	0.05060	0.00530	0.218	0.023	0.0312	0.0008	223	242	200	19	198	5	N/A	198	5	0.0007130	0.000032	0.282679	0.000023	0.01693	0.00064	-3.7	0.8	0.6
95	190828_032.FIN2	0.05060	0.00220	0.218	0.009	0.0312	0.0004	223	101	200	8	198	3	N/A	198	3	0.0013290	0.000051	0.282752	0.000022	0.02663	0.00097	-1.2	0.8	3.1
63	190827_251.FIN2	0.05140	0.00270	0.217	0.011	0.0313	0.0007	259	121	200	9	199	4	N/A	199	4	0.0007670	0.000064	0.282736	0.000024	0.01690	0.00140	-1.7	0.8	2.6
58	190827_246.FIN2	0.05060	0.00120	0.218	0.006	0.0313	0.0004	223	55	200	5	199	3	N/A	199	3	0.0013500	0.000110	0.282707	0.000025	0.03300	0.00290	-2.8	0.9	1.5
157	190828_125.FIN2	0.05160	0.00260	0.218	0.011	0.0313	0.0005	268	116	199	9	199	3	N/A	199	3	0.0006860	0.000058	0.282755	0.000020	0.01560	0.00130	-1.1	0.7	3.3
2	190212_139.FIN2	0.05060	0.00260	0.221	0.011	0.0313	0.0007	223	119	203	10	199	4	N/A	199	4									
104	190828_047.FIN2	0.05100	0.00200	0.219	0.009	0.0314	0.0004	241	90	201	7	199	2	N/A	199	2	0.0009870	0.000014	0.282766	0.000028	0.02168	0.00031	-0.7	1.0	3.6
82	190828_013.FIN2	0.05050	0.00210	0.218	0.009	0.0314	0.0005	218	96	199	7	199	3	N/A	199	3	0.0011850	0.000041	0.282742	0.000025	0.02810	0.00100	-1.5	0.9	2.7
110	190828_053.FIN2	0.05070	0.00190	0.218	0.008	0.0313	0.0004	227	87	200	7	199	3	N/A	199	3	0.0011060	0.000036	0.282700	0.000020	0.02761	0.00096	-3.0	0.7	1.3
17	190212_160.FIN2	0.05020	0.00320	0.218	0.015	0.0314	0.0008	204	148	200	12	199	5	N/A	199	5	0.0008900	0.000074	0.282935	0.000018	0.01930	0.00170	5.3	0.6	9.6
54	190827_236.FIN2	0.05110	0.00190	0.221	0.008	0.0314	0.0004	245	86	203	7	199	3	N/A	199	3	0.0010430	0.000035	0.282762	0.000029	0.02334	0.00075	-0.8	1.0	3.5
20	190212_169.FIN2	0.05120	0.00170	0.222	0.008	0.0314	0.0004	250	76	203	7	199	3	N/A	199	3	0.0010780	0.000049	0.282638	0.000025	0.02440	0.00110	-5.2	0.9	-0.9
74	190827_270.FIN2	0.05030	0.00230	0.221	0.011	0.0315	0.0005	209	106	202	9	200	3	N/A	200	3	0.0008930	0.000090	0.282704	0.000022	0.02110	0.00240	-2.9	0.8	1.5
100	190828_037.FIN2	0.04970	0.00220	0.219	0.010	0.0316	0.0004	181	103	201	8	200	3	N/A	200	3	0.0010100	0.000042	0.282766	0.000021	0.02530	0.00110	-0.7	0.7	3.6
51	190827_233.FIN2	0.05260	0.00410	0.224	0.017	0.0316	0.0007	312	177	202	14	200	4	N/A	200	4	0.0006160	0.000033	0.282782	0.000017	0.01451	0.00083	-0.1	0.6	4.3
65	190827_253.FIN2	0.05080	0.00180	0.220	0.008	0.0316	0.0005	232	82	201	6	200	3	N/A	200	3	0.0012810	0.000080	0.282732	0.000024	0.02890	0.00200	-1.9	0.8	2.4
153	190828_121.FIN2	0.05090	0.00140	0.221	0.006	0.0316	0.0004	236	63	202	5	201	2	N/A	201	2	0.0004800	0.000032	0.282792	0.000020	0.00972	0.00064	0.2	0.7	4.6
18	190212_161.FIN2	0.05100	0.00150	0.222	0.007	0.0316	0.0003	241	68	203	6	201	2	N/A	201	2	0.0011660	0.000056	0.282710	0.000027	0.02670	0.00150	-2.7	1.0	1.7
60	190827_248.FIN2	0.05070	0.00210	0.221	0.009	0.0316	0.0005	227	96	202	8	201	3	N/A	201	3	0.0009950	0.000062	0.282800	0.000031	0.02250	0.00140	0.5	1.1	4.9
115	190828_058.FIN2	0.05140	0.00310	0.222	0.013	0.0317	0.0005	259	139	201	11	201	3	N/A	201	3	0.0007810	0.000045	0.282776	0.000025	0.01890	0.00110	-0.3	0.9	4.0
7	190212_150.FIN2	0.05170	0.00270	0.226	0.012	0.0317	0.0006	272	120	206	10	201	4	N/A	201	4	0.0006270	0.000028	0.282706	0.000041	0.01446	0.00083	-2.8	1.5	1.6
139	190828_094.FIN2	0.05080	0.00280	0.224	0.013	0.0317	0.0005	232	127	201	10	201	3	N/A	201	3	0.0007000	0.000100	0.282770	0.000025	0.01680	0.00260	-0.5	0.9	3.8
34	190212_189.FIN2	0.05240	0.00360	0.230	0.016	0.0317	0.0007	303	157	210	13	201	4	N/A	201	4	0.0010630	0.000018	0.282841	0.000035	0.02363	0.00032	2.0	1.2	6.3
93	190828_030.FIN2	0.05090	0.00170	0.221	0.008	0.0317	0.0004	236	77	202	6	201	3	N/A	201	3	0.0010020	0.000011	0.282683	0.000027	0.02181	0.00032	-3.6	1.0	0.7
49	190212_210.FIN2	0.05080	0.00160	0.221	0.007	0.0317	0.0003	232	73	202	6	201	2	N/A	201	2	0.0010110	0.000025	0.282748	0.000026	0.02077	0.00058	-1.3	0.9	3.0
32	190212_187.FIN2	0.05120	0.00270	0.225	0.012	0.0318	0.0007	250	121	205	10	202	5	N/A	202	5	0.0007780	0.000025	0.282784	0.000032	0.01509	0.00057	0.0	1.1	4.3
38	190212_193.FIN2	0.05110	0.00140	0.224	0.006	0.0319	0.0003	245	63	205	5	202	2	N/A	202	2	0.0009650	0.000065	0.282657	0.000026	0.01980	0.00110	-4.5	0.9	-0.2
75	190827_271.FIN2	0.05040	0.00190	0.222	0.009	0.0319	0.0004	213	87	203	7	202	3	N/A	202	3	0.0006900	0.000031	0.282785	0.000022	0.01487	0.00065	0.0	0.8	4.4
105	190828_048.FIN2	0.05060	0.00250	0.223	0.011	0.0319	0.0005	223	114	203	9	202	3	N/A	202	3	0.0004310	0.000028	0.282853	0.000020	0.00976	0.00070	2.4	0.7	6.8
132	190828_087.FIN2	0.05120	0.00570	0.226	0.027	0.0319	0.0012	250	256	207	23	203	8	N/A	203	8	0.0012580	0.000028	0.282722	0.000029	0.02608	0.00052	-2.2	1.0	2.1
154	190828_122.FIN2	0.05020	0.00200	0.222	0.009	0.0320	0.0005	204	92	203	8	203	3	N/A	203	3	0.0011770	0.000067	0.282684	0.000024	0.02640	0.00170	-3.6	0.8	0.8
8	190212_151.FIN2	0.05200	0.00400	0.229	0.017	0.0320	0.0008	285	176	209	14	203	5	N/A	203	5	0.0008590	0.000029	0.282655	0.000030	0.01863	0.00069	-4.6	1.1	-0.2
1	190212_138.FIN2	0.05040	0.00250	0.225	0.012	0.0320	0.0006	213	115	205	10	203	4	N/A	203	4									
160	190828_128.FIN2	0.05120	0.00240	0.226	0.011	0.0320	0.0005	250	108	207	9	203	3	N/A	203	3	0.0005243	0.000006	0.282720	0.000021	0.01184	0.00014	-2.3	0.7	2.2
4	190212_141.FIN2	0.05300	0.00390	0.233	0.017	0.0321	0.0006	329	167	210	14	204	4	N/A	204	4	0.0004860	0.000016	0.282661	0.000027	0.01155	0.00035	-4.4	1.0	0.1
155	190828_123.FIN2	0.05050	0.00210	0.222	0.009	0.0321	0.0005	218	96	204	8	204	3	N/A	204	3	0.0011010	0.000056	0.282753	0.000026	0.02460	0.00120	-1.1	0.9	3.2
26	190212_175.FIN2	0.05070	0.00210	0.222	0.009	0.0321	0.0004	227	96	204	8	204	2	N/A	204	2	0.0008030	0.000019	0.282740	0.000022	0.01732	0.00029	-1.6	0.8	2.8
143	190828_104.FIN2	0.05110	0.00270	0.225	0.011	0.0321	0.0005	245	122	206	10	204	3	N/A	204	3	0.0014120	0.000081	0.282973	0.000026	0.03080	0.00180	6.6	0.9	11.0
66	190827_254.FIN2	0.05140	0.00220	0.226	0.010	0.0322	0.0005	259	98	206	8	204	3	N/A	204	3	0.0005868	0.000009	0.282730	0.000028	0.01318	0.00021	-1.9	1.0	2.5
152	190828_120.FIN2	0.05140	0.00270	0.221	0.010	0.0322	0.0005	259	121	204	9	204	3	N/A	204	3	0.0005250	0.000043	0.282684	0.000024	0.01180	0.00100	-3.6	0.8	0.9
11	190212_154.FIN2	0.05080	0.00220	0.225	0.010	0.0322	0.0005	232	100	205	8	205	3	N/A	205	3	0.0006200	0.000018	0.282677	0.000030	0.01463	0.00037	-3.8	1.1	0.6
117	190828_066.FIN2	0.05110	0.00320	0.227	0.014	0.0323	0.0009	245	144	208	12	205	6	N/A	205	6	0.0007350	0.000041	0.282799	0.000025	0.01555	0.00081	0.5	0.9	5.0
46	190212_207.FIN2	0.05070	0.00210	0.226	0.009	0.0324	0.0004	227	96	206	8	205	3	N/A	205	3	0.0006050	0.000019	0.282678	0.000035	0.01403	0.00035	-3.8	1.2	0.7
9	190212_152.FIN2	0.05040	0.00190	0.227	0.009	0.0325	0.0004	213	87	207	7	206	3	N/A	206	3	0.0014010	0.000072	0.282753	0.000029	0.02760	0.00140	-1.1	1.0	3.3
33	190212_188.FIN2	0.05240	0.00340	0.235	0.016	0.0326	0.0006	303	148	212	13	207	4	N/A	207	4	0.0008890	0.000049	0.282688	0.000036	0.02200	0.00130	-3.4	1.3	1.0
24	190212_173.FIN2	0.05090	0.00180	0.228	0.008	0.0327	0.0004	236	82	208	7	207	2	N/A	207	2	0.0010540	0.000083	0.282761	0.000027	0.02380	0.00210	-0.8	1.0	3.6
98	190828_035.FIN2	0.05080	0.00200	0.229	0.009	0.0327	0.0005	232	91	208	7	208	3	N/A	208	3	0.0009390	0.000092	0.282760	0.000021	0.01790	0.00190	-0.9	0.7	3.6
10	190212_153.FIN2	0.05060	0.00260	0.228	0.011	0.0330	0.0005	223	119	210	10	209	3	N/A	209	3	0.0009680	0.000046	0.282741	0.000031	0.02190	0.00140	-1.6	1.1	3.0
92	190828_029.FIN2	0.05060	0.00520	0.230	0.024	0.0331	0.0009	223	238	210	21	210	6	N/A	210	6	0.0004850	0.000011	0.282652	0.000023	0.01173	0.00028	-4.7	0.8	-0.1
3	190212_140.FIN2	0.05050	0.00300	0.233	0.015	0.0333	0.0006	218	138	212	12	211	3	N/A	211	3	0.0012280	0.000079	0.282786	0.000026	0.02820	0.00190	0.0	0.9	4.6
30	190212_179.FIN2	0.05090	0.00300	0.234	0.014	0.0333	0.0005	236	136	213	11	211	3	N/A	211	3	0.0009340	0.000014	0.282932	0.000025	0.02300	0.00035	5.2	0.9	9.8
106	190828_049.FIN2	0.05030	0.00400	0.236	0.020	0.0335	0.0011	209	184	214	16	212	7	N/A	212	7	0.0009540	0.000039	0.282691	0.000022	0.02052	0.00090	-3.3	0.8	1.3
35	190212_190.FIN2	0.05170	0.00300	0.238	0.013	0.0337	0.0005	272	133	214	11	214	3	N/A	214	3	0.0010320	0.000053	0.282936	0.000027	0.02180	0.00110	5.3	1.0	10.0
108	190828_051.FIN2	0.05290	0.00980	0.241	0.042	0.0340	0.0016	325	421	215	34	215	10	N/A	215	10	0.0005470	0.000039	0.282718	0.000024	0.01294	0.00099	-2.4	0.8	2.3
27	190212_176.FIN2	0.05180	0.00490	0.242	0.022	0.0340	0.0012	277	217	219	18	216	8	N/A	216	8	0.0008150	0.000079	0.282823	0.000029	0.01680	0.00210	1.3	1.0	6.0
6	190212_143.FIN2	0.05110	0.00360	0.241	0.017	0.0342	0.0007	245	162	217	13	217	4	N/A	217	4	0.0004140	0.000012	0.282921	0.000026	0.00904	0.00022	4.8	0.9	9.6
5	190212_142.FIN2	0.05130	0.00140	0.242	0.006	0.0345	0.0004	254	63	220	5	219	2	N/A	219	2	0.0008730	0.000045	0.282941	0.000025	0.01820	0.00130	5.5	0.9	10.3
47	190212_208.FIN2	0.05160	0.00380	0.246	0.017	0.0347	0.0006	268	169	220	14	220	4	N/A	220	4	0.0006200	0.000040	0.282931	0.000029	0.01438	0.00085	5.2	1.0	10.0
14	190212_157.FIN2	0.05130	0.00260	0.248	0.013	0.0350	0.0004	254	117	223	10	222	3	N/A	222	3	0.0009650	0.000078	0.282991	0.000031	0.02000	0.00110	7.3	1.1	12.1
97	190828_034.FIN2	0.05130	0.00100	0.245	0.005	0.0352	0.0006	254	45	223	4	223	4	N/A	223	4	0.0005620	0.000066	0.282922	0.000022	0.01200	0.00140	4.8	0.8	9.7
119	190828_068.FIN2	0.05160	0.00330	0.259	0.017	0.0365	0.0008	268	147	232	13	231	5	N/A	231	5	0.0006330	0.000068	0.282469	0.000020	0.01550	0.00150	-11.2	0.7	-6.1
86	190828_017.FIN2	0.05150	0.00250	0.299	0.014	0.0418	0.0007	263	111	264	11	264	4	N/A	264	4	0.0009330	0.000017	0.282896	0.000026	0.02212	0.00048	3.9	0.9	9.6
151	190828_112.FIN2	0.05190	0.00250	0.303	0.016	0.0421	0.0009	281	110	268	13	266	6	N/A	266	6	0.0006820	0.000063	0.282512	0.000023	0.01570	0.00170	-9.7	0.8	-3.9
36	190212_191.FIN2	0.05290	0.00190	0.319	0.010	0.0439	0.0008	325	82	281	7	277	5	N/A	277	5									
137	190828_092.FIN2	0.05310	0.00310	0.331	0.017	0.0453	0.0013	333	132	289	13	286	8	N/A	286	8	0.0006800	0.000052	0.282413	0.000026	0.01630	0.00120	-13.2	0.9	-6.9
23	190212_172.FIN2	0.05400	0.00380	0.367	0.030	0.0492	0.0014	371	158	317	22	310	9	N/A	310	9	0.0005900	0.000011	0.282690	0.000022	0.01280	0.00032	-3.4	0.8	3.4
102	190828_039.FIN2	0.05310	0.00180	0.369	0.014	0.0504	0.0007	333	77	319	10	317	5	N/A	317	5	0.0019340	0.000037	0.282930	0.000021	0.05252	0.00083	5.1	0.7	11.8
101	190828_038.FIN2	0.05300	0.00120	0.377	0.009	0.0514	0.0005	329	51	323	7	323	3	N/A	323	3	0.0011950	0.000056	0.282880	0.000026	0.03000	0.00150	3.4	0.9	10.3
121	190828_070.FIN2	0.05320	0.00140	0.379	0.012	0.0515	0.0008	337	60	325	9	324	5	N/A	324	5	0.0018460	0.000052	0.282500	0.000026	0.04740	0.00120	-10.1	0.9	-3.3
149	190828_110.FIN2	0.05350	0.00130	0.381	0.010	0.0516	0.0007	350	55	328	8	324	4	N/A	324	4	0.0024800	0.000560	0.282818	0.000039	0.06000	0.01400	1.2	1.4	7.9
94	190828_031.FIN2	0.05295	0.00097	0.378	0.008	0.0517	0.0005	327	42	325	6	325	3	N/A	325	3	0.0021500	0.000140	0.282716	0.000026	0.04700	0.00310	-2.4	0.9	4.3
39	190212_194.FIN2	0.05390	0.00190	0.392	0.013	0.0526	0.0008	367	79	335	10	331	5	N/A	331	5	0.0014750	0.000049	0.282938	0.000030	0.03780	0.00130	5.4	1.1	12.5
73	190827_269.FIN2	0.05420	0.00250	0.394	0.019	0.0529	0.0008	379	104	336	14	332	5	N/A	332	5	0.0013200	0.000061	0.282809	0.000026	0.03000	0.00160	0.8	0.9	8.0
19	190212_168.FIN2	0.05510	0.00220	0.406	0.017	0.0540	0.0010	416	89	344	12	339	6	N/A	339	6	0.0004871	0.000008	0.282655	0.000024	0.01085	0.00023	-4.6	0.8	2.8
31	190212_186.FIN2	0.05370	0.00230	0.403	0.018	0.0543	0.0007	358	97	342	13	341	5	N/A	341	5	0.0009700	0.000034	0.282759	0.000027	0.02159	0.00042	-0.9	1.0	6.4
158	190828_126.FIN2	0.05360	0.00120	0.406	0.010	0.0551	0.0006	354	51	346	7	346	4	N/A	346	4	0.0016370	0.000020	0.282817	0.000022	0.03480	0.00034	1.1	0.8	8.5
37	190212_192.FIN2	0.05360	0.00150	0.420	0.011	0.0566	0.0007	354	63	355	8	355	4	N/A	355	4	0.0005167	0.000006	0.282116	0.000027	0.01296	0.00015	-23.7	1.0	-15.9
42	190212_197.FIN2	0.05510	0.00180	0.436	0.015	0.0582	0.0008	416	73	366	10	365	5	N/A	365	5	0.0008060	0.000048	0.282168	0.000029	0.02030	0.00130	-21.8	1.0	-13.9
159	190828_127.FIN2	0.05600	0.00160	0.526	0.016	0.0680	0.0008	452	63	426	10	424	5	N/A	424	5	0.0010545	0.000006	0.282802	0.000018	0.02865	0.00012	0.6	0.6	9.8
67	190827_255.FIN2	0.07093	0.00091	1.537	0.022	0.1574	0.0017	955	26	943	9	942	10	N/A	942	10	0.0013250	0.000028	0.282350	0.000027	0.03157	0.00070	-15.4	1.0	4.9
147	190828_108.FIN2	0.07400	0.00120	1.694	0.081	0.1671	0.0077	1041	33	985	23	982	37	94	1041	33	0.0011580	0.000050	0.282179	0.000027	0.03030	0.00160	-21.4	1.0	1.1
107	190828_050.FIN2	0.07930	0.00180	2.173	0.062	0.1991	0.0040	1180	45	1173	21	1170	21	99	1180	45	0.0005420	0.000024	0.282158	0.000019	0.01432	0.00084	-22.2	0.7	3.9
144	190828_105.FIN2	0.08760	0.00730	2.440	0.190	0.2030	0.0120	1374	160	1252	57	1193	63	87	1374	160	0.0009050	0.000084	0.281574	0.000030	0.02490	0.00240	-42.8	1.1	-12.8
145	190828_106.FIN2	0.08760	0.00180	2.804	0.062	0.2326	0.0034	1374	40	1348	17	1348	18	98	1374	40	0.0008070	0.000052	0.282068	0.000029	0.02220	0.00150	-25.4	1.0	4.8
22	190212_171.FIN2	0.11470	0.00110	5.333	0.065	0.3370	0.0031	1875	17	1873	10	1872	15	100	1875	17	0.0019180	0.000059	0.281583	0.000044	0.05000	0.00200	-42.5	1.6	-2.6
rejected analyses																									
45	190212_206.FIN2	0.06860	0.00170	0.536	0.015	0.0567	0.0008	887	51	435	10	356	5	N/A	N/A	N/A	0.0020300	0.000190	0.282874	0.000035	0.04520	0.00440	3.1	1.2	N/A

U-Pb geochronology																	Hf isotope geochemistry								
		Isotopic ratios						Isotopic ages									Isotopic ratios						Epsilon units		
Grain #	Spot name	^{207}Pb/ ^{206}Pb	± 2SE	^{207}Pb/ ^{235}U	± 2SE	^{206}Pb/ ^{238}U	± 2SE	^{207}Pb/ ^{206}Pb	± 2SE (Ma)	^{207}Pb/ ^{235}U	± 2SE (Ma)	^{206}Pb/ ^{238}U	± 2SE (Ma)	Conc. %	Best Age	± 2SE (Ma)	^{176}Lu/ ^{177}Hf	± 2SE	^{176}Hf/ ^{177}Hf	± 2SE	^{176}Yb/ ^{177}Hf	± 2SE	εHf_0	2SE	εHf_t
85	190828_016.FIN2	0.06420	0.00200	0.424	0.013	0.0477	0.0009	748	66	358	9	301	6	N/A	N/A	N/A	0.0015100	0.000110	0.282273	0.000032	0.04020	0.00370	-18.1	1.1	N/A
87	190828_018.FIN2	0.06710	0.00400	0.273	0.015	0.0296	0.0005	841	124	244	12	188	3	N/A	N/A	N/A	0.0007080	0.000031	0.282769	0.000029	0.01636	0.00071	-0.6	1.0	N/A
135	190828_090.FIN2	0.06510	0.00290	0.275	0.012	0.0306	0.0006	778	94	246	10	195	4	N/A	N/A	N/A	0.0011040	0.000054	0.282519	0.000024	0.02440	0.00120	-9.4	0.8	N/A
140	190828_101.FIN2	0.05420	0.00210	0.231	0.010	0.0301	0.0004	379	87	210	8	191	3	N/A	N/A	N/A	0.0007710	0.000023	0.282700	0.000029	0.01630	0.00044	-3.0	1.0	N/A
28AW18--Faro Peak formation; (Zone 08V NAD 83, 576677 E; 6908762 N)																									
13	190826_252.FIN2	0.05150	0.00340	0.209	0.013	0.0297	0.0007	263	152	192	11	188	4	N/A	188	4	0.0007380	0.000022	0.282777	0.000029	0.01731	0.00055	-0.3	1.0	3.8
78	190827_094.FIN2	0.05010	0.00350	0.211	0.016	0.0303	0.0007	200	162	194	13	192	4	N/A	192	4	0.0009558	0.000009	0.282696	0.000023	0.01992	0.00013	-3.1	0.8	1.0
136	190827_191.FIN2	0.05030	0.00170	0.211	0.008	0.0303	0.0006	209	78	194	6	193	3	N/A	193	3	0.0013180	0.000060	0.282711	0.000023	0.03010	0.00200	-2.6	0.8	1.5
68	190827_084.FIN2	0.05010	0.00240	0.211	0.010	0.0304	0.0004	200	111	193	8	193	3	N/A	193	3	0.0007770	0.000017	0.282702	0.000024	0.01865	0.00053	-2.9	0.8	1.3
48	190827_052.FIN2	0.05010	0.00160	0.209	0.007	0.0304	0.0004	200	74	194	6	193	3	N/A	193	3	0.0022100	0.000270	0.282797	0.000033	0.05340	0.00680	0.4	1.2	4.4
50	190827_054.FIN2	0.05200	0.00620	0.218	0.027	0.0306	0.0008	285	273	198	23	194	5	N/A	194	5	0.0006984	0.000007	0.282763	0.000029	0.01642	0.00015	-0.8	1.0	3.4
81	190827_103.FIN2	0.05050	0.00330	0.214	0.013	0.0306	0.0006	218	151	197	11	194	4	N/A	194	4	0.0013520	0.000035	0.282751	0.000029	0.03077	0.00092	-1.2	1.0	2.9
84	190827_106.FIN2	0.04970	0.00140	0.213	0.007	0.0306	0.0004	181	66	195	6	195	3	N/A	195	3	0.0013280	0.000031	0.282553	0.000030	0.02879	0.00060	-8.2	1.1	-4.1
95	190827_123.FIN2	0.05040	0.00140	0.212	0.006	0.0307	0.0004	213	64	195	5	195	2	N/A	195	2	0.0012600	0.000033	0.282797	0.000018	0.02732	0.00055	0.4	0.6	4.6
94	190827_122.FIN2	0.05010	0.00100	0.212	0.005	0.0307	0.0003	200	46	195	4	195	2	N/A	195	2	0.0012000	0.000110	0.282782	0.000014	0.02460	0.00210	-0.1	0.5	4.1
28	190827_020.FIN2	0.05050	0.00140	0.213	0.006	0.0307	0.0003	218	64	195	5	195	2	N/A	195	2	0.0009510	0.000020	0.282692	0.000022	0.02136	0.00048	-3.3	0.8	0.9
87	190827_109.FIN2	0.05020	0.00150	0.213	0.006	0.0307	0.0003	204	69	196	5	195	2	N/A	195	2	0.0009170	0.000026	0.282692	0.000023	0.01850	0.00049	-3.3	0.8	0.9
74	190827_090.FIN2	0.04930	0.00230	0.214	0.011	0.0308	0.0004	162	109	196	9	195	3	N/A	195	3	0.0009550	0.000064	0.282745	0.000030	0.02220	0.00150	-1.4	1.1	2.8
129	190827_176.FIN2	0.05020	0.00120	0.213	0.005	0.0307	0.0004	204	55	196	4	195	2	N/A	195	2	0.0015740	0.000066	0.282750	0.000025	0.03670	0.00160	-1.2	0.9	2.9
52	190827_056.FIN2	0.05080	0.00250	0.214	0.010	0.0308	0.0005	232	114	196	9	195	3	N/A	195	3	0.0012970	0.000053	0.282715	0.000028	0.03200	0.00130	-2.5	1.0	1.7
57	190827_067.FIN2	0.05080	0.00230	0.216	0.010	0.0308	0.0004	232	105	197	8	196	2	N/A	196	2	0.0009640	0.000013	0.282775	0.000025	0.02363	0.00030	-0.4	0.9	3.9
11	190826_250.FIN2	0.05150	0.00370	0.218	0.016	0.0309	0.0006	263	165	197	13	196	4	N/A	196	4	0.0008270	0.000026	0.282684	0.000032	0.02086	0.00055	-3.6	1.1	0.7
71	190827_087.FIN2	0.05000	0.00220	0.216	0.010	0.0308	0.0004	195	102	198	9	196	2	N/A	196	2	0.0007134	0.000005	0.282745	0.000022	0.01746	0.00008	-1.4	0.8	2.8
6	190212_039.FIN2	0.05040	0.00260	0.219	0.013	0.0309	0.0008	213	120	200	11	196	5	N/A	196	5	0.0006730	0.000030	0.282763	0.000023	0.01434	0.00079	-0.8	0.8	3.5
90	190827_112.FIN2	0.05020	0.00140	0.214	0.006	0.0309	0.0005	204	65	197	5	196	3	N/A	196	3	0.0015800	0.000130	0.282732	0.000023	0.03370	0.00280	-1.9	0.8	2.3
63	190827_073.FIN2	0.04950	0.00340	0.216	0.016	0.0309	0.0007	172	160	198	13	196	4	N/A	196	4	0.0015040	0.000047	0.282818	0.000026	0.03570	0.00100	1.2	0.9	5.3
141	190827_196.FIN2	0.05040	0.00160	0.214	0.007	0.0309	0.0004	213	74	198	6	196	3	N/A	196	3	0.0010700	0.000060	0.282761	0.000025	0.02400	0.00140	-0.8	0.9	3.4
55	190827_065.FIN2	0.05030	0.00220	0.215	0.009	0.0309	0.0004	209	101	197	8	196	2	N/A	196	2	0.0007990	0.000018	0.282731	0.000019	0.01853	0.00042	-1.9	0.7	2.4
120	190827_160.FIN2	0.05050	0.00270	0.216	0.011	0.0310	0.0007	218	124	198	9	197	4	N/A	197	4	0.0009090	0.000031	0.282715	0.000020	0.01785	0.00073	-2.5	0.7	1.8
9	190212_042.FIN2	0.05260	0.00410	0.226	0.017	0.0310	0.0008	312	177	205	14	197	5	N/A	197	5									
101	190827_129.FIN2	0.05120	0.00240	0.216	0.010	0.0310	0.0005	250	108	197	8	197	3	N/A	197	3	0.0010800	0.000043	0.282702	0.000016	0.02710	0.00120	-2.9	0.6	1.3
12	190826_251.FIN2	0.05150	0.00330	0.219	0.014	0.0311	0.0005	263	147	197	11	197	3	N/A	197	3	0.0005570	0.000012	0.282692	0.000024	0.01432	0.00025	-3.3	0.8	1.0
27	190827_019.FIN2	0.05090	0.00190	0.217	0.008	0.0311	0.0005	236	86	199	7	197	3	N/A	197	3	0.0011190	0.000072	0.282735	0.000024	0.02420	0.00140	-1.8	0.8	2.5
40	190827_038.FIN2	0.05059	0.00090	0.215	0.004	0.0311	0.0003	222	41	198	3	197	2	N/A	197	2	0.0017600	0.000110	0.282727	0.000022	0.03670	0.00230	-2.1	0.8	2.1
66	190827_076.FIN2	0.05010	0.00210	0.216	0.009	0.0311	0.0005	200	97	198	7	197	3	N/A	197	3	0.0010290	0.000068	0.282754	0.000020	0.02370	0.00140	-1.1	0.7	3.2
79	190827_101.FIN2	0.05000	0.00300	0.216	0.013	0.0311	0.0005	195	139	197	11	197	3	N/A	197	3	0.0006360	0.000018	0.282647	0.000027	0.01382	0.00037	-4.9	1.0	-0.6
67	190827_083.FIN2	0.05050	0.00420	0.218	0.019	0.0311	0.0007	218	193	199	16	197	4	N/A	197	4	0.0011710	0.000039	0.282764	0.000027	0.02634	0.00073	-0.7	1.0	3.5
111	190827_144.FIN2	0.05130	0.00270	0.217	0.011	0.0311	0.0010	254	121	200	9	198	6	N/A	198	6	0.0025710	0.000080	0.282774	0.000031	0.06130	0.00230	-0.4	1.1	3.7
77	190827_093.FIN2	0.05040	0.00160	0.217	0.007	0.0311	0.0004	213	74	199	6	198	2	N/A	198	2	0.0007220	0.000041	0.282788	0.000021	0.01500	0.00070	0.1	0.7	4.4
61	190827_071.FIN2	0.05180	0.00480	0.223	0.020	0.0312	0.0010	277	212	203	16	198	7	N/A	198	7	0.0010900	0.000110	0.282816	0.000024	0.02650	0.00290	1.1	0.8	5.4
145	190827_207.FIN2	0.05080	0.00170	0.218	0.007	0.0312	0.0004	232	77	200	6	198	3	N/A	198	3	0.0016200	0.000130	0.282754	0.000034	0.03720	0.00370	-1.1	1.2	3.1
80	190827_102.FIN2	0.04980	0.00250	0.219	0.011	0.0313	0.0005	186	117	199	9	199	3	N/A	199	3	0.0005610	0.000033	0.282680	0.000031	0.01277	0.00087	-3.7	1.1	0.6
142	190827_197.FIN2	0.05060	0.00190	0.218	0.008	0.0313	0.0006	223	87	200	7	199	4	N/A	199	4	0.0010560	0.000020	0.282789	0.000024	0.02337	0.00045	0.1	0.8	4.4
154	190827_216.FIN2	0.05110	0.00300	0.221	0.014	0.0313	0.0006	245	135	201	12	199	4	N/A	199	4	0.0007869	0.000010	0.282693	0.000021	0.01752	0.00032	-3.3	0.7	1.1
25	190827_017.FIN2	0.05200	0.00280	0.222	0.012	0.0313	0.0006	285	123	203	10	199	4	N/A	199	4	0.0008710	0.000025	0.282775	0.000024	0.01999	0.00065	-0.4	0.8	3.9
56	190827_066.FIN2	0.05060	0.00170	0.219	0.008	0.0313	0.0004	223	78	201	6	199	2	N/A	199	2	0.0004570	0.000031	0.282775	0.000016	0.00816	0.00056	-0.4	0.6	4.0
133	190827_188.FIN2	0.04970	0.00170	0.217	0.008	0.0314	0.0004	181	80	199	7	199	2	N/A	199	2	0.0004758	0.000005	0.282758	0.000018	0.01046	0.00007	-1.0	0.6	3.4
29	190827_021.FIN2	0.05060	0.00120	0.218	0.005	0.0314	0.0003	223	55	200	4	199	2	N/A	199	2	0.0012520	0.000089	0.282794	0.000024	0.02840	0.00210	0.3	0.8	4.6
72	190827_088.FIN2	0.04990	0.00240	0.220	0.011	0.0314	0.0006	190	112	201	10	199	4	N/A	199	4	0.0012410	0.000047	0.282734	0.000029	0.02980	0.00140	-1.8	1.0	2.5
73	190827_089.FIN2	0.05140	0.00420	0.222	0.016	0.0314	0.0008	259	188	203	13	199	5	N/A	199	5	0.0017990	0.000039	0.282778	0.000035	0.03913	0.00096	-0.2	1.2	3.9
123	190827_164.FIN2	0.05100	0.00180	0.219	0.007	0.0314	0.0004	241	81	200	6	199	2	N/A	199	2	0.0006760	0.000026	0.282727	0.000016	0.01579	0.00053	-2.1	0.6	2.3
49	190827_053.FIN2	0.05030	0.00230	0.217	0.010	0.0314	0.0005	209	106	200	9	200	3	N/A	200	3	0.0010280	0.000016	0.282758	0.000029	0.02339	0.00046	-1.0	1.0	3.3
69	190827_085.FIN2	0.05030	0.00220	0.219	0.009	0.0314	0.0004	209	101	201	7	200	2	N/A	200	2	0.0004860	0.000047	0.282694	0.000020	0.00951	0.00090	-3.2	0.7	1.2
148	190827_210.FIN2	0.05110	0.00320	0.220	0.014	0.0315	0.0006	245	144	201	12	200	4	N/A	200	4	0.0008500	0.000056	0.282754	0.000022	0.01900	0.00110	-1.1	0.8	3.2
10	190212_043.FIN2	0.05030	0.00220	0.220	0.010	0.0315	0.0005	209	101	201	8	200	3	N/A	200	3									
58	190827_068.FIN2	0.05020	0.00130	0.218	0.006	0.0315	0.0003	204	60	200	5	200	2	N/A	200	2	0.0011530	0.000019	0.282716	0.000021	0.02621	0.00041	-2.4	0.7	1.9
153	190827_215.FIN2	0.05160	0.00590	0.224	0.026	0.0315	0.0011	268	262	204	21	200	7	N/A	200	7	0.0010490	0.000044	0.282811	0.000023	0.02320	0.00100	0.9	0.8	5.2
155	190827_217.FIN2	0.05140	0.00250	0.222	0.011	0.0315	0.0005	259	112	202	9	200	3	N/A	200	3	0.0004833	0.000010	0.282643	0.000024	0.01175	0.00020	-5.0	0.8	-0.6
30	190827_022.FIN2	0.05070	0.00170	0.220	0.007	0.0315	0.0004	227	77	201	6	200	2	N/A	200	2	0.0011860	0.000052	0.282785	0.000025	0.02750	0.00130	0.0	0.9	4.3
46	190827_050.FIN2	0.05050	0.00200	0.220	0.010	0.0316	0.0005	218	92	202	8	200	3	N/A	200	3	0.0004570	0.000015	0.282706	0.000020	0.00915	0.00031	-2.8	0.7	1.6
75	190827_091.FIN2	0.05010	0.00210	0.221	0.010	0.0316	0.0005	200	97	202	8	200	3	N/A	200	3	0.0006030	0.000076	0.282783	0.000021	0.01310	0.00170	-0.1	0.7	4.3
85	190827_107.FIN2	0.05070	0.00250	0.220	0.010	0.0316	0.0005	227	114	201	9	200	3	N/A	200	3	0.0009380	0.000034	0.282762	0.000033	0.02110	0.00081	-0.8	1.2	3.5
122	190827_162.FIN2	0.05050	0.00120	0.219	0.005	0.0316	0.0003	218	55	201	4	200	2	N/A	200	2	0.0013230	0.000088	0.282793	0.000020	0.02580	0.00160	0.3	0.7	4.6
130	190827_177.FIN2	0.05030	0.00230	0.220	0.011	0.0316	0.0004	209	106	200	9	200	3	N/A	200	3	0.0006240	0.000015	0.282695	0.000022	0.01424	0.00039	-3.2	0.8	1.2
36	190827_034.FIN2	0.05120	0.00210	0.220	0.009	0.0316	0.0005	250	94	201	7	201	3	N/A	201	3	0.0009080	0.000083	0.282722	0.000021	0.02050	0.00190	-2.2	0.7	2.1
76	190827_092.FIN2	0.05060	0.00200	0.220	0.009	0.0316	0.0006	223	91	201	8	201	4	N/A	201	4	0.0008340	0.000056	0.282626	0.000027	0.01890	0.00130	-5.6	1.0	-1.3
105	190827_139.FIN2	0.05200	0.00400	0.223	0.018	0.0316	0.0007	285	176	201	14	201	5	N/A	201	5	0.0006438	0.000005	0.282776	0.000022	0.01575	0.00014	-0.3	0.8	4.1
86	190827_108.FIN2	0.05040	0.00250	0.221	0.011	0.0317	0.0006	213	115	202	9	201	4	N/A	201	4	0.0011510	0.000096	0.282713	0.000028	0.02730	0.00210	-2.5	1.0	1.8
98	190827_126.FIN2	0.05080	0.00150	0.220	0.006	0.0317	0.0004	232	68	202	5	201	3	N/A	201	3	0.0011280	0.000074	0.282794	0.000030	0.02230	0.00170	0.3	1.1	4.6
127	190827_168.FIN2	0.05120	0.00270	0.222	0.012	0.0317	0.0005	250	121	203	10	201	3	N/A	201	3	0.0007890	0.000046	0.282780	0.000021	0.01704	0.00089	-0.2	0.7	4.2
26	190827_018.FIN2	0.05230	0.00290	0.227	0.011	0.0317	0.0008	299	126	208	9	201	5	N/A	201	5	0.0021500	0.000170	0.282769	0.000028	0.04310	0.00360	-0.6	1.0	3.6
24	190827_016.FIN2	0.05050	0.00160	0.221	0.008	0.0317	0.0004	218	73	202	6	201	3	N/A	201	3	0.0016230	0.000077	0.282770	0.000026	0.03500	0.00170	-0.5	0.9	3.7
59	190827_069.FIN2	0.05050	0.00200	0.221	0.009	0.0317	0.0004	218	92	201	7	201	2	N/A	201	2	0.0008980	0.000046	0.282704	0.000030	0.02200	0.00110	-2.9	1.1	1.5
93	190827_121.FIN2	0.05100	0.00270	0.222	0.012	0.0317	0.0005	241	122	203	10	201	3	N/A	201	3	0.0008530	0.000062	0.282775	0.000022	0.01990	0.00160	-0.4	0.8	4.0
114	190827_147.FIN2	0.05080	0.00310	0.218	0.014	0.0317	0.0007	232	141	202	12	201	5	N/A	201	5	0.0009080	0.000065	0.282731	0.000018	0.02040	0.00140	-1.9	0.6	2.4
146	190827_208.FIN2	0.05090	0.00190	0.220	0.008	0.0317	0.0004	236	86	201	7	201	3	N/A	201	3	0.0008080	0.000052	0.282747	0.000021	0.01770	0.00120	-1.3	0.7	3.0
4	190212_037.FIN2	0.05090	0.00450	0.225	0.021	0.0318	0.0008	236	204	204	17	202	5	N/A	202	5	0.0005930	0.000031	0.282794	0.000034	0.01267	0.00064	0.3	1.2	4.7
107	190827_140.FIN2	0.05070	0.00280	0.219	0.012	0.0318	0.0006	227	128	202	10	202	4	N/A	202	4	0.0009350	0.000021	0.282728	0.000029	0.02194	0.00043	-2.0	1.0	2.3
96	190827_124.FIN2	0.05050	0.00160	0.220	0.007	0.0318	0.0004	218	73	202	6	202	3	N/A	202	3	0.0007380	0.000036	0.282695	0.000020	0.01734	0.00092	-3.2	0.7	1.2
147	190827_209.FIN2	0.05050	0.00190	0.221	0.009	0.0319	0.0005	218	87	202	7	202	3	N/A	202	3	0.0007180	0.000094	0.282774	0.000022	0.01590	0.00200	-0.4	0.8	4.0
121	190827_161.FIN2	0.05080	0.00150	0.222	0.007	0.0319	0.0004	232	68	203	6	202	3	N/A	202	3	0.0013600	0.000140	0.282705	0.000022	0.02770	0.00300	-2.8	0.8	1.5
65	190827_075.FIN2	0.05020	0.00280	0.222	0.011	0.0319	0.0010	204	129	206	8	202	6	N/A	202	6	0.0020000	0.000140	0.282803	0.000027	0.05310	0.00400	0.6	1.0	4.9
35	190827_033.FIN2	0.05190	0.00240	0.226	0.011	0.0319	0.0005	281	106	206	9	203	3	N/A	203	3	0.0007590	0.000019	0.282779	0.000020	0.01729	0.00036	-0.2	0.7	4.2
112	190827_145.FIN2	0.05150	0.00380	0.225	0.017	0.0319	0.0007	263	169	205	14	203	4	N/A	203	4	0.0010980	0.000014	0.282765	0.000024	0.02718	0.00024	-0.7	0.8	3.6
43	190827_047.FIN2	0.05140	0.00360	0.227	0.016	0.0320	0.0006	259	161	206	13	203	4	N/A	203	4	0.0009000	0.000100	0.282922	0.000029	0.01780	0.00200	4.8	1.0	9.2
1	190212_034.FIN2	0.05140	0.00320	0.224	0.014	0.0320	0.0006	259	143	203	11	203	4	N/A	203	4	0.0007410	0.000032	0.282690	0.000025	0.01751	0.00089	-3.4	0.9	1.0
8	190212_041.FIN2	0.05140	0.00280	0.226	0.012	0.0320	0.0006	259	125	207	10	203	4	N/A	203	4									
103	190827_131.FIN2	0.05100	0.00130	0.222	0.006	0.0320	0.0003	241	59	203	5	203	2	N/A	203	2	0.0006520	0.000015	0.282723	0.000019	0.01281	0.00031	-2.2	0.7	2.2
92	190827_120.FIN2	0.05180	0.00270	0.225	0.011	0.0320	0.0005	277	119	205	9	203	3	N/A	203	3	0.0008550	0.000038	0.282766	0.000014	0.01944	0.00078	-0.7	0.5	3.7
125	190827_166.FIN2	0.05080	0.00230	0.225	0.011	0.0320	0.0004	232	105	205	9	203	3	N/A	203	3	0.0007020	0.000038	0.282340	0.000024	0.01780	0.00120	-15.7	0.9	-11.3
161	190827_230.FIN2	0.05060	0.00140	0.223	0.007	0.0320	0.0004	223	64	204	5	203	3	N/A	203	3	0.0010590	0.000051	0.282698	0.000020	0.02230	0.00110	-3.1	0.7	1.3
102	190827_130.FIN2	0.05200	0.00250	0.225	0.010	0.0320	0.0004	285	110	204	8	203	3	N/A	203	3	0.0008490	0.000062	0.282782	0.000017	0.02100	0.00190	-0.1	0.6	4.3
100	190827_128.FIN2	0.05140	0.00220	0.224	0.009	0.0321	0.0004	259	98	204	8	203	3	N/A	203	3	0.0006358	0.000005	0.282782	0.000022	0.01468	0.00011	-0.1	0.8	4.3
113	190827_146.FIN2	0.05150	0.00260	0.223	0.011	0.0321	0.0005	263	116	205	9	203	3	N/A	203	3	0.0005770	0.000049	0.282782	0.000020	0.01290	0.00120	-0.1	0.7	4.3
118	190827_158.FIN2	0.05090	0.00160	0.224	0.007	0.0321	0.0005	236	73	205	6	204	3	N/A	204	3	0.0007930	0.000020	0.282508	0.000018	0.01778	0.00027	-9.8	0.6	-5.4
156	190827_218.FIN2	0.05050	0.00150	0.223	0.007	0.0321	0.0004	218	69	204	6	204	2	N/A	204	2	0.0009120	0.000011	0.282744	0.000026	0.02002	0.00031	-1.4	0.9	3.0
134	190827_189.FIN2	0.05090	0.00180	0.224	0.008	0.0321	0.0004	236	82	204	7	204	3	N/A	204	3	0.0005020	0.000035	0.282752	0.000018	0.00983	0.00063	-1.2	0.6	3.3
131	190827_178.FIN2	0.05040	0.00150	0.224	0.007	0.0321	0.0004	213	69	204	6	204	2	N/A	204	2	0.0010840	0.000045	0.282677	0.000023	0.02366	0.00086	-3.8	0.8	0.6

U-Pb geochronology																Hf isotope geochemistry									
		Isotopic ratios						Isotopic ages									Isotopic ratios						Epsilon units		
Grain #	Spot name	$^{207}Pb/^{206}Pb$	± 2SE	$^{207}Pb/^{235}U$	± 2SE	$^{206}Pb/^{238}U$	± 2SE	$^{207}Pb/^{206}Pb$	± 2SE (Ma)	$^{207}Pb/^{235}U$	± 2SE (Ma)	$^{206}Pb/^{238}U$	± 2SE (Ma)	Conc. %	Best Age	± 2SE (Ma)	$^{176}Lu/^{177}Hf$	± 2SE	$^{176}Hf/^{177}Hf$	± 2SE	$^{176}Yb/^{177}Hf$	± 2SE	εHf_0	2SE	εHf_t
19	190827_011.FIN2	0.05150	0.00220	0.226	0.009	0.0322	0.0004	263	98	205	8	204	2	N/A	204	2	0.0004720	0.000025	0.282687	0.000016	0.01048	0.00060	-3.5	0.6	1.0
20	190827_012.FIN2	0.05170	0.00250	0.229	0.011	0.0322	0.0005	272	111	208	9	204	3	N/A	204	3	0.0009130	0.000054	0.282757	0.000021	0.02020	0.00130	-1.0	0.7	3.4
3	190212_036.FIN2	0.05050	0.00190	0.225	0.009	0.0323	0.0006	218	87	206	8	205	4	N/A	205	4	0.0008590	0.000030	0.282538	0.000029	0.01835	0.00082	-8.7	1.0	-4.3
88	190827_110.FIN2	0.05050	0.00160	0.226	0.007	0.0323	0.0004	218	73	206	6	205	3	N/A	205	3	0.0007910	0.000073	0.282744	0.000021	0.01490	0.00140	-1.4	0.7	3.0
149	190827_211.FIN2	0.05100	0.01200	0.226	0.045	0.0323	0.0019	241	542	205	38	205	12	N/A	205	12	0.0009690	0.000015	0.282696	0.000024	0.02053	0.00048	-3.1	0.8	1.3
39	190827_037.FIN2	0.05100	0.00160	0.227	0.008	0.0324	0.0005	241	72	207	6	205	3	N/A	205	3	0.0006670	0.000037	0.282521	0.000024	0.01480	0.00110	-9.3	0.8	-4.9
91	190827_119.FIN2	0.05050	0.00170	0.225	0.007	0.0324	0.0004	218	78	206	6	206	3	N/A	206	3	0.0018800	0.000120	0.282766	0.000021	0.04120	0.00240	-0.7	0.7	3.6
97	190827_125.FIN2	0.05130	0.00340	0.228	0.015	0.0325	0.0005	254	152	206	12	206	3	N/A	206	3	0.0008040	0.000018	0.282796	0.000024	0.01814	0.00049	0.4	0.8	4.9
116	190827_149.FIN2	0.05190	0.00250	0.229	0.010	0.0325	0.0007	281	110	209	9	206	4	N/A	206	4	0.0007880	0.000010	0.282743	0.000021	0.01675	0.00017	-1.5	0.7	3.0
7	190212_040.FIN2	0.05120	0.00460	0.235	0.022	0.0326	0.0008	250	207	211	18	207	5	N/A	207	5									
51	190827_055.FIN2	0.05110	0.00320	0.229	0.014	0.0326	0.0006	245	144	208	12	207	4	N/A	207	4	0.0006890	0.000015	0.282775	0.000024	0.01491	0.00032	-0.4	0.8	4.2
5	190212_038.FIN2	0.05070	0.00150	0.229	0.007	0.0327	0.0004	227	68	209	6	207	2	N/A	207	2	0.0006970	0.000046	0.282822	0.000025	0.01354	0.00084	1.3	0.9	5.8
37	190827_035.FIN2	0.05080	0.00170	0.229	0.008	0.0328	0.0003	232	77	208	6	208	2	N/A	208	2	0.0007227	0.000009	0.282772	0.000019	0.01388	0.00010	-0.5	0.7	4.1
137	190827_192.FIN2	0.05130	0.00240	0.230	0.011	0.0328	0.0005	254	108	209	9	208	3	N/A	208	3	0.0009660	0.000059	0.282762	0.000022	0.02310	0.00160	-0.8	0.8	3.7
135	190827_190.FIN2	0.05090	0.00230	0.232	0.010	0.0330	0.0005	236	104	210	9	210	3	N/A	210	3	0.0007601	0.000009	0.282746	0.000024	0.01728	0.00019	-1.4	0.8	3.2
160	190827_229.FIN2	0.05020	0.00230	0.232	0.013	0.0331	0.0009	204	106	211	10	210	6	N/A	210	6	0.0015600	0.000140	0.282776	0.000022	0.03570	0.00310	-0.3	0.8	4.1
139	190827_194.FIN2	0.05080	0.00190	0.232	0.008	0.0333	0.0006	232	86	212	7	211	3	N/A	211	3	0.0007050	0.000068	0.282928	0.000024	0.01730	0.00170	5.1	0.8	9.7
70	190827_086.FIN2	0.04940	0.00370	0.233	0.019	0.0333	0.0009	167	175	211	16	211	6	N/A	211	6	0.0009920	0.000031	0.282748	0.000021	0.02430	0.00100	-1.3	0.7	3.2
34	190827_032.FIN2	0.05220	0.00410	0.238	0.019	0.0334	0.0008	294	179	214	15	212	5	N/A	212	5	0.0006480	0.000021	0.282739	0.000021	0.01568	0.00050	-1.6	0.7	3.0
104	190827_138.FIN2	0.05130	0.00150	0.234	0.007	0.0335	0.0005	254	67	212	6	212	3	N/A	212	3	0.0011000	0.000089	0.282794	0.000027	0.02460	0.00220	0.3	1.0	4.9
140	190827_195.FIN2	0.05050	0.00170	0.235	0.008	0.0336	0.0005	218	78	214	7	213	3	N/A	213	3	0.0015300	0.000160	0.282796	0.000025	0.03770	0.00440	0.4	0.9	4.9
38	190827_036.FIN2	0.05120	0.00130	0.234	0.006	0.0337	0.0006	250	58	213	5	213	3	N/A	213	3	0.0012400	0.000150	0.282708	0.000019	0.02780	0.00360	-2.7	0.7	1.8
158	190827_227.FIN2	0.05100	0.00430	0.239	0.020	0.0339	0.0014	241	194	217	16	215	9	N/A	215	9									
152	190827_214.FIN2	0.05130	0.00210	0.237	0.010	0.0339	0.0005	254	94	216	8	215	3	N/A	215	3	0.0015700	0.000120	0.282786	0.000026	0.03670	0.00320	0.0	0.9	4.6
162	190827_231.FIN2	0.05160	0.00280	0.240	0.013	0.0340	0.0007	268	124	216	10	216	4	N/A	216	4	0.0007130	0.000012	0.282910	0.000022	0.01643	0.00057	4.4	0.8	9.1
144	190827_199.FIN2	0.05260	0.00810	0.247	0.039	0.0341	0.0013	312	350	221	32	216	8	N/A	216	8	0.0008610	0.000013	0.282729	0.000023	0.02017	0.00039	-2.0	0.8	2.7
44	190827_048.FIN2	0.05080	0.00220	0.239	0.011	0.0342	0.0005	232	100	217	9	216	3	N/A	216	3	0.0010500	0.000110	0.282978	0.000024	0.02340	0.00270	6.8	0.8	11.5
2	190212_035.FIN2	0.05240	0.00330	0.254	0.016	0.0352	0.0006	303	144	228	13	223	4	N/A	223	4	0.0007010	0.000043	0.282816	0.000022	0.01362	0.00083	1.1	0.8	5.9
82	190827_104.FIN2	0.05180	0.00660	0.318	0.040	0.0430	0.0005	277	292	280	30	271	3	N/A	271	3	0.0007250	0.000054	0.282604	0.000035	0.01700	0.00120	-6.4	1.2	-0.5
108	190827_141.FIN2	0.05340	0.00280	0.333	0.017	0.0457	0.0008	346	119	290	13	288	5	N/A	288	5	0.0004090	0.000019	0.282741	0.000023	0.00950	0.00050	-1.6	0.8	4.8
143	190827_198.FIN2	0.05300	0.00250	0.360	0.018	0.0490	0.0008	329	107	309	13	308	5	N/A	308	5	0.0010900	0.000130	0.282846	0.000025	0.02390	0.00290	2.2	0.9	8.8
41	190827_039.FIN2	0.05320	0.00260	0.361	0.018	0.0495	0.0010	337	111	312	14	311	6	N/A	311	6	0.0011990	0.000038	0.282728	0.000025	0.02567	0.00090	-2.0	0.9	4.7
128	190827_169.FIN2	0.05300	0.00120	0.362	0.009	0.0495	0.0005	329	51	313	6	312	3	N/A	312	3	0.0012620	0.000046	0.282914	0.000025	0.02970	0.00120	4.6	0.9	11.2
14	190826_253.FIN2	0.05310	0.00170	0.369	0.012	0.0504	0.0006	333	73	318	9	317	4	N/A	317	4	0.0011770	0.000048	0.282723	0.000027	0.02671	0.00096	-2.2	1.0	4.6
15	190826_254.FIN2	0.05330	0.00310	0.370	0.022	0.0506	0.0009	342	132	319	16	318	5	N/A	318	5	0.0007800	0.000020	0.282902	0.000022	0.02067	0.00062	4.1	0.8	11.1
17	190826_256.FIN2	0.05360	0.00250	0.375	0.017	0.0509	0.0009	354	105	321	13	320	5	N/A	320	5	0.0011520	0.000098	0.282672	0.000028	0.03080	0.00320	-4.0	1.0	2.9
62	190827_072.FIN2	0.05320	0.00270	0.374	0.018	0.0509	0.0009	337	115	321	14	320	5	N/A	320	5	0.0009690	0.000020	0.282901	0.000020	0.02382	0.00057	4.1	0.7	11.0
31	190827_029.FIN2	0.05350	0.00160	0.381	0.012	0.0520	0.0006	350	68	327	9	326	4	N/A	326	4	0.0022100	0.000140	0.282907	0.000029	0.05740	0.00380	4.3	1.0	11.1
16	190826_255.FIN2	0.05350	0.00280	0.386	0.021	0.0524	0.0010	350	118	330	16	329	6	N/A	329	6	0.0011820	0.000052	0.282695	0.000024	0.03260	0.00160	-3.2	0.8	3.9
83	190827_105.FIN2	0.05290	0.00150	0.394	0.013	0.0534	0.0006	325	64	336	9	336	4	N/A	336	4	0.0014750	0.000057	0.282680	0.000027	0.03240	0.00140	-3.7	1.0	3.4
117	190827_157.FIN2	0.05400	0.00150	0.394	0.011	0.0534	0.0006	371	63	336	8	336	4	N/A	336	4	0.0015080	0.000050	0.282795	0.000027	0.03460	0.00120	0.4	1.0	7.5
138	190827_193.FIN2	0.05260	0.00250	0.396	0.023	0.0535	0.0013	312	108	337	17	336	8	N/A	336	8	0.0005131	0.000008	0.282717	0.000018	0.01324	0.00025	-2.4	0.6	5.0
42	190827_040.FIN2	0.05550	0.00110	0.428	0.009	0.0564	0.0006	432	44	361	6	353	4	N/A	353	4	0.0011450	0.000011	0.282300	0.000023	0.03131	0.00047	-17.2	0.8	-9.6
132	190827_179.FIN2	0.05420	0.00180	0.426	0.014	0.0570	0.0007	379	75	358	10	357	5	N/A	357	5	0.0004925	0.000008	0.282290	0.000018	0.01282	0.00023	-17.5	0.6	-9.7
89	190827_111.FIN2	0.05360	0.00180	0.425	0.015	0.0572	0.0008	354	76	359	11	359	5	N/A	359	5	0.0006242	0.000008	0.282265	0.000023	0.01578	0.00018	-18.4	0.8	-10.6
60	190827_070.FIN2	0.08963	0.00097	3.105	0.045	0.2486	0.0035	1418	21	1432	11	1430	18	101	1418	21	0.0008240	0.000046	0.282079	0.000021	0.02130	0.00130	-25.0	0.7	6.1
157	190827_226.FIN2	0.10920	0.00130	4.761	0.072	0.3172	0.0040	1786	22	1776	13	1775	19	99	1786	22	0.0005200	0.000025	0.281568	0.000022	0.01448	0.00064	-43.0	0.8	-3.4
45	190827_049.FIN2	0.11010	0.00200	4.960	0.120	0.3240	0.0072	1801	33	1809	20	1808	35	100	1801	33	0.0004510	0.000012	0.281348	0.000027	0.01254	0.00042	-50.8	1.0	-10.8
64	190827_074.FIN2	0.11290	0.00230	5.220	0.120	0.3323	0.0055	1847	37	1852	20	1849	27	100	1847	37	0.0006740	0.000036	0.281599	0.000024	0.01950	0.00100	-41.9	0.9	-1.1
124	190827_165.FIN2	0.11390	0.00210	5.250	0.130	0.3343	0.0078	1863	33	1858	21	1856	37	100	1863	33	0.0014350	0.000034	0.281665	0.000026	0.03869	0.00080	-39.6	0.9	0.6
22	190827_014.FIN2	0.11420	0.00190	5.200	0.110	0.3307	0.0048	1867	30	1850	18	1841	23	99	1867	30	0.0007640	0.000043	0.281448	0.000023	0.02090	0.00140	-47.3	0.8	-6.1
151	190827_213.FIN2	0.11480	0.00120	5.302	0.072	0.3358	0.0042	1877	19	1866	12	1865	20	99	1877	19	0.0005740	0.000067	0.281622	0.000025	0.01570	0.00200	-41.1	0.9	0.5
99	190827_127.FIN2	0.11600	0.00190	5.350	0.120	0.3356	0.0055	1895	29	1869	19	1868	27	99	1895	29	0.0001157	0.000001	0.281363	0.000018	0.00349	0.00006	-50.3	0.6	-7.7
126	190827_167.FIN2	0.11710	0.00300	5.520	0.170	0.3413	0.0093	1912	46	1900	26	1891	44	99	1912	46	0.0015130	0.000015	0.281664	0.000029	0.04457	0.00056	-39.6	1.0	1.6
32	190827_030.FIN2	0.12290	0.00110	6.101	0.078	0.3613	0.0035	1999	16	1988	11	1987	17	99	1999	16	0.0005300	0.000020	0.281344	0.000022	0.01518	0.00055	-51.0	0.8	-6.5
33	190827_031.FIN2	0.12390	0.00160	6.120	0.100	0.3614	0.0049	2013	23	1988	14	1987	23	99	2013	23	0.0004910	0.000015	0.281427	0.000023	0.01405	0.00048	-48.0	0.8	-3.2
109	190827_142.FIN2	0.14400	0.00350	8.000	0.630	0.4110	0.0320	2276	42	2191	71	2190	140	96	2276	42	0.0009190	0.000048	0.281252	0.000023	0.02540	0.00140	-54.2	0.8	-4.1
119	190827_159.FIN2	0.17100	0.00210	11.440	0.230	0.4871	0.0087	2567	21	2557	19	2557	38	100	2567	21	0.0007170	0.000052	0.281253	0.000024	0.02030	0.00150	-54.2	0.9	2.9
23	190827_015.FIN2	0.17200	0.00370	11.340	0.220	0.4820	0.0130	2577	36	2556	21	2536	57	98	2577	36									
18	190826_257.FIN2	0.17590	0.00240	12.130	0.250	0.4980	0.0072	2615	23	2602	20	2601	31	99	2615	23	0.0002910	0.000035	0.281123	0.000029	0.00737	0.00083	-58.8	1.0	0.2
150	190827_212.FIN2	0.17600	0.00170	12.120	0.160	0.4995	0.0053	2616	16	2610	12	2609	23	100	2616	16	0.0003869	0.000004	0.281215	0.000023	0.01039	0.00012	-55.5	0.8	3.3
53	190827_057.FIN2	0.18020	0.00160	12.600	0.170	0.5079	0.0059	2655	15	2647	12	2646	25	100	2655	15	0.0011090	0.000025	0.281227	0.000024	0.02960	0.00068	-55.1	0.9	3.3
rejected analyses																									
21	190827_013.FIN2	0.11360	0.00130	4.265	0.057	0.2729	0.0031	1858	21	1686	11	1555	16	84	N/A	N/A	0.0009400	0.000027	0.281738	0.000020	0.02690	0.00110	-37.0	0.7	N/A
47	190827_051.FIN2	0.05340	0.00190	0.232	0.009	0.0311	0.0003	346	80	210	7	197	2	N/A	N/A	N/A	0.0014100	0.000028	0.282767	0.000023	0.03093	0.00059	-0.6	0.8	N/A
54	190827_058.FIN2	0.09320	0.00890	0.385	0.030	0.0310	0.0009	1492	181	327	22	197	6	13	N/A	N/A	0.0009810	0.000019	0.282810	0.000027	0.02387	0.00038	0.9	1.0	N/A
110	190827_143.FIN2	0.08440	0.00380	0.405	0.019	0.0353	0.0007	1302	87	342	13	224	5	17	N/A	N/A	0.0003490	0.000022	0.282760	0.000017	0.00703	0.00042	-0.9	0.6	N/A
115	190827_148.FIN2	0.07800	0.00590	0.351	0.027	0.0331	0.0007	1147	150	301	20	210	5	18	N/A	N/A	0.0004890	0.000034	0.282801	0.000022	0.01224	0.00090	0.6	0.8	N/A
159	190827_228.FIN2	0.06400	0.00670	0.325	0.033	0.0376	0.0014	742	221	286	27	238	9	N/A	N/A	N/A	0.0012870	0.000027	0.282685	0.000037	0.03043	0.00054	-3.5	1.3	N/A
18AW19--Faro Peak formation; (Zone 08V NAD 83, 576900 E, 6909232 N)																									
49	200928_079.FIN2	0.05140	0.00130	0.198	0.005	0.0291	0.0006	259	58	185	5	185	4	N/A	185	4	0.0019600	0.000130	0.282658	0.000022	0.04570	0.00330	-4.5	0.8	-0.6
13	200928_024.FIN2	0.05230	0.00260	0.205	0.010	0.0292	0.0008	299	113	189	9	185	5	N/A	185	5	0.0014200	0.000100	0.282711	0.000023	0.03580	0.00280	-2.6	0.8	1.3
110	200928_164.FIN2	0.05200	0.00340	0.203	0.013	0.0293	0.0006	284	75	186	11	186	4	N/A	186	4	0.0012000	0.000200	0.282785	0.000028	0.03110	0.00530	0.0	1.0	4.0
61	200928_097.FIN2	0.05190	0.00210	0.206	0.011	0.0296	0.0007	281	93	189	9	188	5	N/A	188	5	0.0017200	0.000110	0.282800	0.000037	0.03590	0.00240	0.5	1.3	4.5
15	200928_026.FIN2	0.05170	0.00290	0.205	0.011	0.0296	0.0008	272	129	189	10	188	5	N/A	188	5	0.0008740	0.000052	0.282754	0.000017	0.02110	0.00110	-1.1	0.6	3.0
43	200928_067.FIN2	0.05140	0.00240	0.210	0.010	0.0302	0.0007	259	107	194	9	192	4	N/A	192	4	0.0009080	0.000080	0.282753	0.000018	0.02160	0.00200	-1.1	0.6	3.0
68	200928_104.FIN2	0.05070	0.00150	0.209	0.006	0.0303	0.0005	227	68	192	5	192	3	N/A	192	3	0.0014700	0.000160	0.282800	0.000017	0.03440	0.00360	0.5	0.6	4.6
109	200928_163.FIN2	0.05200	0.00230	0.211	0.009	0.0303	0.0005	285	101	194	7	192	3	N/A	192	3	0.0010330	0.000041	0.282674	0.000018	0.02590	0.00110	-3.9	0.6	0.2
114	200928_168.FIN2	0.05320	0.00300	0.214	0.014	0.0303	0.0008	337	128	196	11	192	5	N/A	192	5	0.0009380	0.000027	0.282734	0.000021	0.02231	0.00072	-1.8	0.7	2.4
38	200928_061.FIN2	0.05110	0.00200	0.210	0.010	0.0304	0.0007	245	90	194	8	193	5	N/A	193	5	0.0013910	0.000098	0.282772	0.000029	0.03430	0.00240	-0.5	1.0	3.6
92	200928_140.FIN2	0.05160	0.00160	0.210	0.008	0.0304	0.0007	268	71	194	6	193	5	N/A	193	5									
72	200928_108.FIN2	0.05030	0.00140	0.215	0.007	0.0306	0.0005	209	65	198	6	194	3	N/A	194	3	0.0022070	0.000091	0.282433	0.000019	0.05560	0.00220	-12.4	0.7	-8.4
107	200928_161.FIN2	0.05050	0.00200	0.213	0.009	0.0307	0.0004	218	92	195	7	195	3	N/A	195	3	0.0009120	0.000045	0.282732	0.000018	0.02050	0.00100	-1.9	0.6	2.3
120	200925_132.FIN2	0.05170	0.00690	0.215	0.027	0.0306	0.0016	272	306	196	23	195	10	N/A	195	10	0.0008290	0.000027	0.282762	0.000020	0.02205	0.00057	-0.8	0.7	3.4
42	200928_066.FIN2	0.05070	0.00230	0.215	0.010	0.0308	0.0006	227	105	197	8	196	4	N/A	196	4	0.0011420	0.000061	0.282710	0.000015	0.02810	0.00160	-2.7	0.5	1.5
57	200928_087.FIN2	0.05110	0.00180	0.217	0.008	0.0308	0.0005	245	81	198	6	196	3	N/A	196	3	0.0012590	0.000036	0.282720	0.000022	0.03170	0.00110	-2.3	0.8	1.9
74	200928_110.FIN2	0.05230	0.00400	0.216	0.018	0.0309	0.0009	299	174	200	14	196	6	N/A	196	6	0.0014020	0.000074	0.282692	0.000019	0.03620	0.00210	-3.3	0.7	0.9
77	200928_119.FIN2	0.05190	0.00200	0.217	0.008	0.0309	0.0005	281	88	198	7	196	3	N/A	196	3	0.0010550	0.000082	0.282683	0.000017	0.02640	0.00200	-3.6	0.6	0.6
108	200928_162.FIN2	0.05100	0.00210	0.214	0.008	0.0309	0.0005	241	95	196	7	196	3	N/A	196	3	0.0010080	0.000053	0.282774	0.000017	0.02400	0.00130	-0.4	0.6	3.8
111	200928_165.FIN2	0.05080	0.00310	0.218	0.013	0.0309	0.0009	232	141	199	11	196	6	N/A	196	6	0.0012260	0.000046	0.282773	0.000022	0.03120	0.00130	-0.4	0.8	3.8
12	200928_023.FIN2	0.05060	0.00130	0.215	0.006	0.0310	0.0004	223	59	197	5	197	3	N/A	197	3	0.0009070	0.000058	0.282700	0.000019	0.02090	0.00150	-3.0	0.7	1.2
115	200928_169.FIN2	0.05220	0.00180	0.217	0.008	0.0310	0.0005	294	79	199	7	197	3	N/A	197	3	0.0009050	0.000097	0.282717	0.000017	0.02160	0.00240	-2.4	0.6	1.8
56	200928_086.FIN2	0.05040	0.00150	0.215	0.006	0.0311	0.0005	213	69	198	5	197	3	N/A	197	3	0.0014700	0.000120	0.282801	0.000026	0.03530	0.00330	0.6	0.9	4.8
91	200928_139.FIN2	0.05320	0.00260	0.221	0.011	0.0311	0.0010	337	111	202	9	197	6	N/A	197	6	0.0009200	0.000062	0.282722	0.000015	0.02210	0.00150	-2.2	0.5	2.0
116	200928_170.FIN2	0.05130	0.00170	0.218	0.008	0.0311	0.0006	254	76	199	7	197	4	N/A	197	4	0.0010240	0.000031	0.282702	0.000021	0.02341	0.00069	-2.9	0.7	1.3
53	200928_083.FIN2	0.05080	0.00120	0.217	0.006	0.0311	0.0005	232	55	199	5	198	3	N/A	198	3	0.0011450	0.000048	0.282678	0.000026	0.02650	0.00110	-3.8	0.9	0.5
95	200928_143.FIN2	0.05040	0.00120	0.217	0.006	0.0311	0.0004	213	55	198	5	198	3	N/A	198	3	0.0007470	0.000017	0.282675	0.000016	0.01713	0.00042	-3.9	0.6	0.4
113	200928_167.FIN2	0.05120	0.00150	0.218	0.007	0.0312	0.0004	250	67	199	6	198	3	N/A	198	3	0.0008310	0.000053	0.282765	0.000022	0.01890	0.00110	-0.7	0.8	3.6

U-Pb geochronology																	Hf isotope geochemistry								
		Isotopic ratios						Isotopic ages									Isotopic ratios						Epsilon units		
Grain #	Spot name	$^{207}Pb/^{206}Pb$	± 2SE	$^{207}Pb/^{235}U$	± 2SE	$^{206}Pb/^{238}U$	± 2SE	$^{207}Pb/^{206}Pb$	± 2SE (Ma)	$^{207}Pb/^{235}U$	± 2SE (Ma)	$^{206}Pb/^{238}U$	± 2SE (Ma)	Conc. %	Best Age	± 2SE (Ma)	$^{176}Lu/^{177}Hf$	± 2SE	$^{176}Hf/^{177}Hf$	± 2SE	$^{176}Yb/^{177}Hf$	± 2SE	εHf_0	2SE	εHf_t
35	200928_058.FIN2	0.05120	0.00240	0.221	0.011	0.0312	0.0007	250	108	202	9	198	4	N/A	198	4	0.0009260	0.000054	0.282687	0.000015	0.01997	0.00093	-3.5	0.5	0.8
51	200928_081.FIN2	0.05030	0.00200	0.219	0.010	0.0312	0.0006	209	92	199	8	198	4	N/A	198	4	0.0010200	0.000041	0.282769	0.000018	0.02421	0.00084	-0.6	0.6	3.7
73	200928_109.FIN2	0.05060	0.00100	0.217	0.005	0.0312	0.0004	223	46	199	4	198	3	N/A	198	3	0.0014750	0.000058	0.282718	0.000021	0.03298	0.00099	-2.4	0.7	1.8
59	200928_089.FIN2	0.05250	0.00190	0.220	0.008	0.0313	0.0006	307	82	202	7	198	4	N/A	198	4	0.0013330	0.000090	0.282757	0.000017	0.03360	0.00250	-1.0	0.6	3.2
1	200928_012.FIN2	0.05070	0.00190	0.220	0.009	0.0313	0.0006	227	87	201	8	199	4	N/A	199	4	0.0006500	0.000100	0.282762	0.000019	0.01500	0.00250	-0.8	0.7	3.5
34	200928_057.FIN2	0.05080	0.00120	0.218	0.006	0.0313	0.0005	232	55	200	5	199	3	N/A	199	3	0.0016290	0.000055	0.282786	0.000024	0.03840	0.00130	0.0	0.8	4.2
64	200928_100.FIN2	0.05070	0.00190	0.221	0.009	0.0313	0.0005	227	87	202	8	199	3	N/A	199	3	0.0007160	0.000011	0.282775	0.000018	0.01659	0.00025	-0.4	0.6	4.0
87	200928_129.FIN2	0.05130	0.00260	0.218	0.011	0.0313	0.0007	254	117	200	9	199	4	N/A	199	4	0.0012140	0.000038	0.282679	0.000019	0.02740	0.00100	-3.7	0.7	0.5
86	200928_128.FIN2	0.05060	0.00160	0.218	0.007	0.0314	0.0004	223	73	202	5	199	3	N/A	199	3	0.0007170	0.000016	0.282679	0.000017	0.01539	0.00022	-3.7	0.6	0.6
55	200928_085.FIN2	0.05080	0.00150	0.219	0.007	0.0314	0.0004	232	68	201	6	199	3	N/A	199	3	0.0007450	0.000032	0.282689	0.000018	0.01628	0.00092	-3.4	0.6	0.9
9	200928_020.FIN2	0.05050	0.00110	0.218	0.005	0.0314	0.0004	218	50	200	4	199	3	N/A	199	3	0.0015900	0.000110	0.282665	0.000021	0.03740	0.00280	-4.2	0.7	0.0
36	200928_059.FIN2	0.05470	0.00320	0.220	0.013	0.0314	0.0012	400	131	201	11	199	8	N/A	199	8	0.0008010	0.000030	0.282729	0.000017	0.01952	0.00068	-2.0	0.6	2.3
14	200928_025.FIN2	0.05110	0.00120	0.219	0.005	0.0314	0.0004	245	54	200	4	200	3	N/A	200	3	0.0011420	0.000047	0.282662	0.000017	0.02730	0.00130	-4.3	0.6	-0.1
40	200928_063.FIN2	0.05180	0.00160	0.221	0.007	0.0314	0.0005	277	71	203	6	200	3	N/A	200	3	0.0009110	0.000040	0.282654	0.000024	0.02107	0.00088	-4.6	0.8	-0.3
20	200928_037.FIN2	0.05940	0.00440	0.227	0.017	0.0315	0.0022	582	161	208	14	200	14	N/A	200	14	0.0012900	0.000080	0.282691	0.000023	0.03040	0.00180	-3.3	0.8	1.0
112	200928_166.FIN2	0.05220	0.00640	0.220	0.027	0.0314	0.0020	294	280	201	23	200	13	N/A	200	13	0.0007920	0.000053	0.282774	0.000029	0.01970	0.00120	-0.4	1.0	4.0
58	200928_088.FIN2	0.05050	0.00130	0.219	0.006	0.0316	0.0004	218	60	201	5	200	3	N/A	200	3	0.0010450	0.000041	0.282692	0.000019	0.02390	0.00120	-3.3	0.7	1.0
19	200928_036.FIN2	0.05020	0.00160	0.220	0.009	0.0316	0.0006	204	74	201	7	201	4	N/A	201	4	0.0010790	0.000032	0.282682	0.000019	0.02456	0.00043	-3.6	0.7	0.7
76	200928_118.FIN2	0.05050	0.00160	0.220	0.007	0.0317	0.0004	218	73	201	6	201	3	N/A	201	3	0.0010770	0.000055	0.282678	0.000020	0.02550	0.00130	-3.8	0.7	0.5
30	200928_047.FIN2	0.05050	0.00230	0.221	0.010	0.0317	0.0009	218	105	202	9	201	6	N/A	201	6	0.0010330	0.000049	0.282773	0.000017	0.02530	0.00110	-0.4	0.6	3.9
80	200928_122.FIN2	0.05240	0.00720	0.226	0.026	0.0317	0.0020	303	313	206	22	201	12	N/A	201	12	0.0015200	0.000093	0.282737	0.000020	0.03530	0.00230	-1.7	0.7	2.6
2	200928_013.FIN2	0.05060	0.00180	0.222	0.010	0.0318	0.0008	223	82	203	8	202	5	N/A	202	5	0.0011020	0.000047	0.282532	0.000023	0.02470	0.00130	-8.9	0.8	-4.6
4	200928_015.FIN2	0.05000	0.00120	0.221	0.005	0.0318	0.0004	195	56	203	5	202	3	N/A	202	3	0.0010890	0.000039	0.282665	0.000019	0.02530	0.00100	-4.2	0.7	0.1
83	200928_125.FIN2	0.05080	0.00130	0.221	0.006	0.0318	0.0004	232	59	202	5	202	3	N/A	202	3	0.0008200	0.000015	0.282672	0.000018	0.01804	0.00032	-4.0	0.6	0.4
48	200928_078.FIN2	0.05170	0.00240	0.226	0.010	0.0319	0.0005	272	106	205	9	202	3	N/A	202	3	0.0003760	0.000016	0.282752	0.000014	0.00724	0.00028	-1.2	0.5	3.3
7	200928_018.FIN2	0.05270	0.00350	0.226	0.015	0.0319	0.0008	316	151	206	12	203	5	N/A	203	5	0.0005250	0.000011	0.282671	0.000016	0.01381	0.00032	-4.0	0.6	0.4
66	200928_102.FIN2	0.05160	0.00170	0.223	0.009	0.0320	0.0007	268	76	204	7	203	4	N/A	203	4	0.0015370	0.000066	0.282790	0.000021	0.03320	0.00150	0.2	0.7	4.5
105	200928_153.FIN2	0.05340	0.00210	0.228	0.010	0.0320	0.0007	346	89	208	8	203	4	N/A	203	4	0.0018550	0.000077	0.282726	0.000020	0.04430	0.00170	-2.1	0.7	2.2
90	200928_132.FIN2	0.05180	0.00170	0.222	0.008	0.0319	0.0007	277	75	203	7	203	4	N/A	203	4	0.0016900	0.000310	0.282700	0.000025	0.03800	0.00810	-3.0	0.9	1.3
29	200928_046.FIN2	0.05080	0.00110	0.223	0.005	0.0320	0.0004	232	50	204	4	203	3	N/A	203	3	0.0012410	0.000051	0.282670	0.000018	0.02920	0.00140	-4.1	0.6	0.3
41	200928_064.FIN2	0.05050	0.00240	0.223	0.010	0.0321	0.0008	218	110	204	9	203	5	N/A	203	5	0.0009150	0.000023	0.282717	0.000018	0.02236	0.00061	-2.4	0.6	2.0
81	200928_123.FIN2	0.04960	0.00300	0.221	0.011	0.0321	0.0005	176	141	205	10	203	3	N/A	203	3	0.0013840	0.000043	0.282738	0.000017	0.03144	0.00098	-1.7	0.6	2.7
37	200928_060.FIN2	0.05080	0.00140	0.223	0.007	0.0321	0.0004	232	64	204	6	204	3	N/A	204	3	0.0009630	0.000043	0.282771	0.000015	0.02150	0.00077	-0.5	0.5	3.9
3	200928_014.FIN2	0.05100	0.00130	0.224	0.006	0.0321	0.0004	241	59	205	5	204	2	N/A	204	2	0.0012080	0.000045	0.282774	0.000024	0.02880	0.00100	-0.4	0.8	4.0
25	200928_042.FIN2	0.05130	0.00150	0.223	0.007	0.0321	0.0006	254	67	204	6	204	4	N/A	204	4	0.0011610	0.000022	0.282535	0.000029	0.02839	0.00060	-8.8	1.0	-4.5
46	200928_076.FIN2	0.05050	0.00130	0.223	0.006	0.0321	0.0004	218	60	204	5	204	3	N/A	204	3	0.0012780	0.000084	0.282767	0.000019	0.02920	0.00190	-0.6	0.7	3.7
70	200928_106.FIN2	0.05070	0.00180	0.224	0.008	0.0322	0.0005	227	82	205	7	204	3	N/A	204	3	0.0012480	0.000038	0.282748	0.000019	0.03016	0.00098	-1.3	0.7	3.1
60	200928_090.FIN2	0.05050	0.00130	0.224	0.007	0.0322	0.0005	218	60	205	5	204	3	N/A	204	3	0.0008050	0.000054	0.282684	0.000017	0.01960	0.00110	-3.6	0.6	0.9
17	200928_034.FIN2	0.05190	0.00180	0.224	0.009	0.0322	0.0008	281	79	205	7	205	5	N/A	205	5	0.0006630	0.000031	0.282684	0.000016	0.01633	0.00066	-3.6	0.6	0.9
88	200928_130.FIN2	0.05210	0.00250	0.225	0.011	0.0322	0.0007	290	110	206	9	205	4	N/A	205	4	0.0005730	0.000073	0.282780	0.000017	0.01260	0.00160	-0.2	0.6	4.3
94	200928_142.FIN2	0.05220	0.00170	0.226	0.008	0.0322	0.0007	294	74	206	7	205	4	N/A	205	4	0.0010730	0.000021	0.282774	0.000018	0.02453	0.00046	-0.4	0.6	4.0
33	200928_056.FIN2	0.05030	0.00120	0.224	0.006	0.0323	0.0004	209	55	205	5	205	3	N/A	205	3	0.0009840	0.000055	0.282689	0.000021	0.02180	0.00140	-3.4	0.7	1.0
27	200928_044.FIN2	0.05090	0.00110	0.225	0.005	0.0323	0.0005	236	50	205	5	205	3	N/A	205	3	0.0015620	0.000058	0.282805	0.000018	0.03540	0.00140	0.7	0.6	5.1
21	200928_038.FIN2	0.05030	0.00280	0.229	0.013	0.0323	0.0009	209	129	209	11	205	6	N/A	205	6	0.0008730	0.000014	0.282779	0.000020	0.02045	0.00027	-0.2	0.7	4.2
102	200928_150.FIN2	0.05190	0.00150	0.226	0.008	0.0324	0.0006	281	66	206	7	205	3	N/A	205	3	0.0017400	0.000068	0.282782	0.000028	0.03960	0.00190	-0.1	1.0	4.2
10	200928_021.FIN2	0.05030	0.00120	0.226	0.006	0.0325	0.0004	209	55	206	5	206	3	N/A	206	3	0.0008970	0.000038	0.282707	0.000015	0.01984	0.00078	-2.8	0.5	1.7
69	200928_105.FIN2	0.05440	0.00440	0.232	0.019	0.0326	0.0012	388	182	210	15	207	7	N/A	207	7	0.0004264	0.000009	0.282684	0.000017	0.01082	0.00018	-3.6	0.6	1.0
99	200928_147.FIN2	0.05090	0.00230	0.226	0.010	0.0326	0.0008	236	104	207	8	207	5	N/A	207	5	0.0009320	0.000057	0.282722	0.000016	0.02440	0.00140	-2.2	0.6	2.2
6	200928_017.FIN2	0.05270	0.00260	0.229	0.013	0.0326	0.0012	315	56	209	11	207	8	N/A	207	8	0.0011610	0.000074	0.282779	0.000019	0.02850	0.00190	-0.2	0.7	4.2
23	200928_040.FIN2	0.05040	0.00170	0.229	0.009	0.0329	0.0006	213	78	209	7	208	4	N/A	208	4	0.0013480	0.000065	0.282643	0.000017	0.02980	0.00150	-5.0	0.6	-0.6
82	200928_124.FIN2	0.05110	0.00270	0.234	0.013	0.0329	0.0011	245	122	213	11	209	7	N/A	209	7	0.0013190	0.000074	0.282752	0.000014	0.02900	0.00160	-1.2	0.5	3.3
98	200928_146.FIN2	0.05310	0.00280	0.230	0.014	0.0330	0.0011	333	120	210	11	209	7	N/A	209	7	0.0009310	0.000055	0.282664	0.000016	0.02120	0.00130	-4.3	0.6	0.2
32	200928_055.FIN2	0.05070	0.00160	0.231	0.008	0.0330	0.0006	227	73	210	7	209	4	N/A	209	4	0.0005710	0.000032	0.282696	0.000017	0.01363	0.00085	-3.1	0.6	1.4
67	200928_103.FIN2	0.05220	0.00350	0.232	0.015	0.0330	0.0008	294	153	210	13	209	5	N/A	209	5	0.0007990	0.000014	0.282958	0.000024	0.01942	0.00039	6.1	0.8	10.7
100	200928_148.FIN2	0.05050	0.00180	0.230	0.008	0.0330	0.0006	218	83	209	7	209	4	N/A	209	4	0.0013560	0.000044	0.282802	0.000023	0.03290	0.00120	0.6	0.8	5.1
50	200928_080.FIN2	0.05060	0.00240	0.231	0.012	0.0331	0.0007	223	110	210	10	210	4	N/A	210	4	0.0015720	0.000058	0.282729	0.000016	0.03430	0.00130	-2.0	0.6	2.5
44	200928_068.FIN2	0.05050	0.00270	0.228	0.011	0.0332	0.0009	218	124	212	10	210	5	N/A	210	5	0.0015400	0.000170	0.282939	0.000023	0.03680	0.00410	5.4	0.8	9.9
71	200928_107.FIN2	0.05130	0.00520	0.232	0.022	0.0333	0.0009	254	233	212	19	211	6	N/A	211	6	0.0006940	0.000034	0.282946	0.000020	0.01629	0.00076	5.7	0.7	10.3
96	200928_144.FIN2	0.05240	0.00180	0.234	0.009	0.0333	0.0008	303	78	213	8	211	5	N/A	211	5	0.0013220	0.000057	0.282752	0.000020	0.03420	0.00150	-1.2	0.7	3.3
45	200928_069.FIN2	0.05090	0.00140	0.233	0.007	0.0333	0.0005	236	63	212	5	211	3	N/A	211	3	0.0006450	0.000064	0.282732	0.000016	0.01350	0.00130	-1.9	0.6	2.7
5	200928_016.FIN2	0.05190	0.00220	0.234	0.010	0.0334	0.0006	281	97	213	8	212	4	N/A	212	4	0.0005470	0.000011	0.282772	0.000018	0.01346	0.00027	-0.5	0.6	4.2
26	200928_043.FIN2	0.05180	0.00210	0.237	0.010	0.0334	0.0004	277	93	215	8	212	3	N/A	212	3	0.0011300	0.000036	0.282578	0.000017	0.02249	0.00071	-7.3	0.6	-2.8
16	200928_033.FIN2	0.05120	0.00170	0.237	0.008	0.0340	0.0005	250	76	216	7	215	3	N/A	215	3	0.0007410	0.000038	0.282699	0.000019	0.01448	0.00081	-3.0	0.7	1.6
18	200928_035.FIN2	0.05140	0.00290	0.242	0.013	0.0342	0.0006	259	130	217	11	217	4	N/A	217	4	0.0004110	0.000014	0.282754	0.000017	0.00971	0.00030	-1.1	0.6	3.7
54	200928_084.FIN2	0.05100	0.00330	0.240	0.015	0.0344	0.0008	241	149	218	12	218	5	N/A	218	5	0.0015460	0.000044	0.282949	0.000021	0.03780	0.00110	5.8	0.7	10.4
62	200928_098.FIN2	0.05140	0.00160	0.241	0.007	0.0345	0.0006	259	72	219	6	219	4	N/A	219	4	0.0009810	0.000082	0.282780	0.000023	0.02370	0.00170	-0.2	0.8	4.5
22	200928_039.FIN2	0.05120	0.00140	0.241	0.007	0.0345	0.0006	250	63	219	6	219	3	N/A	219	3	0.0008370	0.000041	0.282938	0.000022	0.02000	0.00110	5.4	0.8	10.2
118	200925_130.FIN2	0.05130	0.00170	0.246	0.010	0.0346	0.0008	254	76	222	8	219	5	N/A	219	5	0.0007190	0.000044	0.282702	0.000020	0.01770	0.00100	-2.9	0.7	1.8
28	200928_045.FIN2	0.05170	0.00150	0.244	0.009	0.0347	0.0007	272	67	221	8	220	5	N/A	220	5	0.0006970	0.000064	0.282784	0.000024	0.01790	0.00120	0.0	0.8	4.7
119	200925_131.FIN2	0.05130	0.00160	0.246	0.008	0.0347	0.0005	254	72	222	6	220	3	N/A	220	3	0.0007930	0.000033	0.282802	0.000015	0.01751	0.00060	0.6	0.5	5.4
75	200928_111.FIN2	0.05330	0.00290	0.248	0.014	0.0350	0.0008	342	123	224	11	222	5	N/A	222	5	0.0013370	0.000050	0.282760	0.000016	0.03320	0.00120	-0.9	0.6	3.8
106	200928_160.FIN2	0.05310	0.00310	0.251	0.015	0.0354	0.0009	333	132	226	12	224	6	N/A	224	6	0.0004360	0.000044	0.282958	0.000017	0.00967	0.00099	6.1	0.6	11.0
39	200928_062.FIN2	0.05100	0.00650	0.261	0.040	0.0361	0.0020	241	294	232	31	229	12	N/A	229	12	0.0009580	0.000021	0.282938	0.000018	0.02187	0.00053	5.4	0.6	10.4
97	200928_145.FIN2	0.05100	0.00140	0.266	0.008	0.0379	0.0007	241	63	241	6	240	4	N/A	240	4	0.0010290	0.000029	0.282689	0.000018	0.02510	0.00130	-3.4	0.6	1.8
101	200928_149.FIN2	0.05250	0.00150	0.298	0.009	0.0411	0.0006	307	65	264	7	260	4	N/A	260	4	0.0007680	0.000061	0.282903	0.000015	0.01810	0.00140	4.2	0.5	9.8
11	200928_022.FIN2	0.05220	0.00140	0.304	0.009	0.0425	0.0005	294	61	268	7	268	3	N/A	268	3	0.0011660	0.000036	0.282917	0.000019	0.03420	0.00110	4.7	0.7	10.4
104	200928_152.FIN2	0.05380	0.00100	0.336	0.010	0.0465	0.0009	363	42	295	7	293	6	N/A	293	6	0.0023400	0.000140	0.282768	0.000026	0.06560	0.00400	-0.6	0.9	5.5
89	200928_131.FIN2	0.05780	0.00820	0.381	0.056	0.0496	0.0022	522	311	316	45	312	14	N/A	312	14	0.0010720	0.000050	0.282709	0.000023	0.02490	0.00130	-2.7	0.8	4.0
93	200928_141.FIN2	0.05750	0.00290	0.364	0.014	0.0504	0.0019	511	111	318	12	317	12	N/A	317	12	0.0014800	0.000025	0.282842	0.000018	0.03853	0.00058	2.0	0.6	8.8
103	200928_151.FIN2	0.05370	0.00170	0.379	0.018	0.0510	0.0023	358	71	326	14	321	14	N/A	321	14	0.0021400	0.000220	0.282577	0.000022	0.06250	0.00700	-7.4	0.8	-0.7
78	200928_120.FIN2	0.05280	0.00470	0.375	0.032	0.0511	0.0016	320	202	322	23	322	10	N/A	322	10	0.0013330	0.000067	0.282715	0.000023	0.03400	0.00190	-2.5	0.8	4.4
52	200928_082.FIN2	0.05400	0.00320	0.383	0.020	0.0515	0.0016	371	133	329	15	324	10	N/A	324	10	0.0015600	0.000110	0.282696	0.000026	0.04020	0.00280	-3.1	0.9	3.7
47	200928_077.FIN2	0.05450	0.00180	0.398	0.014	0.0539	0.0009	392	74	339	10	338	5	N/A	338	5	0.0012700	0.000150	0.282575	0.000016	0.02990	0.00370	-7.4	0.6	-0.2
65	200928_101.FIN2	0.05500	0.00130	0.414	0.012	0.0559	0.0011	412	53	351	8	351	7	N/A	351	7									
8	200928_019.FIN2	0.05450	0.00130	0.440	0.011	0.0587	0.0008	392	54	369	7	368	5	N/A	368	5	0.0006880	0.000023	0.282311	0.000021	0.01829	0.00067	-16.8	0.7	-8.8
31	200928_054.FIN2	0.05430	0.00250	0.477	0.026	0.0631	0.0016	384	103	398	19	395	10	N/A	395	10	0.0016800	0.000071	0.282663	0.000023	0.04540	0.00240	-4.3	0.8	4.0
24	200928_041.FIN2	0.06290	0.00410	0.978	0.056	0.1126	0.0037	705	139	691	29	688	21	N/A	688	21	0.0015310	0.000026	0.282596	0.000020	0.03894	0.00048	-6.7	0.7	8.0
84	200928_126.FIN2	0.11220	0.00280	5.010	0.170	0.3260	0.0110	1835	45	1816	28	1814	51	99	1835	45	0.0005990	0.000017	0.281541	0.000023	0.01604	0.00046	-44.0	0.8	-3.3
85	200928_127.FIN2	0.11290	0.00330	5.110	0.210	0.3290	0.0130	1847	53	1832	35	1830	62	99	1847	53	0.0002527	0.000009	0.281549	0.000016	0.00614	0.00020	-43.7	0.6	-2.4
63	200928_099.FIN2	0.12060	0.00330	5.940	0.220	0.3550	0.0100	1965	49	1957	32	1957	49	100	1965	49	0.0006230	0.000048	0.281400	0.000021	0.01840	0.00140	-49.0	0.7	-5.4
79	200928_121.FIN2	0.14480	0.00450	8.250	0.340	0.4180	0.0130	2285	53	2249	38	2247	59	98	2285	53	0.0003658	0.000008	0.281202	0.000021	0.01015	0.00024	-56.0	0.7	-4.8
rejected analyses																									
117	200925_129.FIN2	0.05780	0.00250	0.190	0.010	0.0261	0.0008	522	95	176	9	166	5	N/A	N/A	N/A	0.0013610	0.000090	0.282695	0.000023	0.03030	0.00190	-3.2	0.8	N/A

APPENDIX 2.B.1

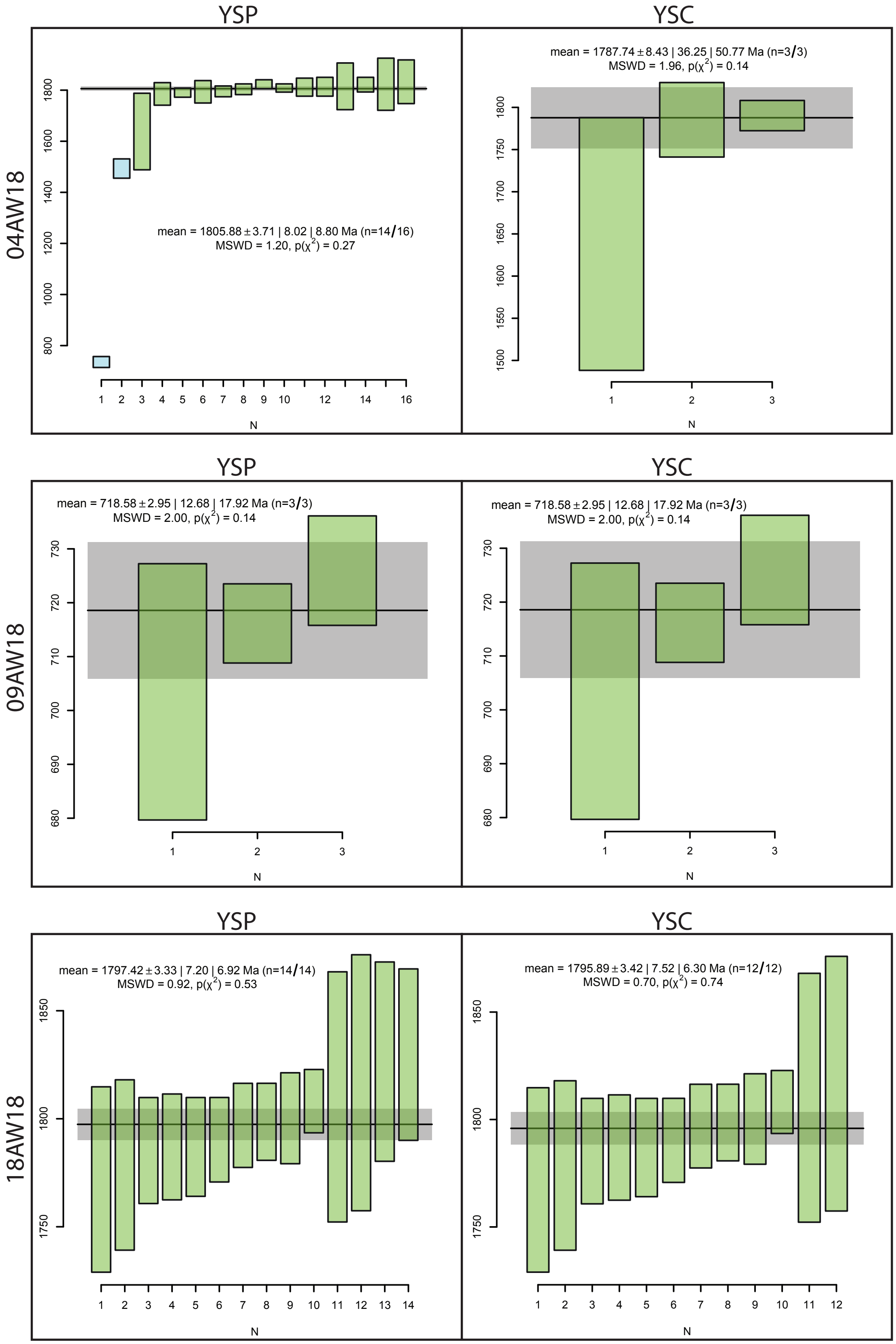

APPENDIX 2.B.2

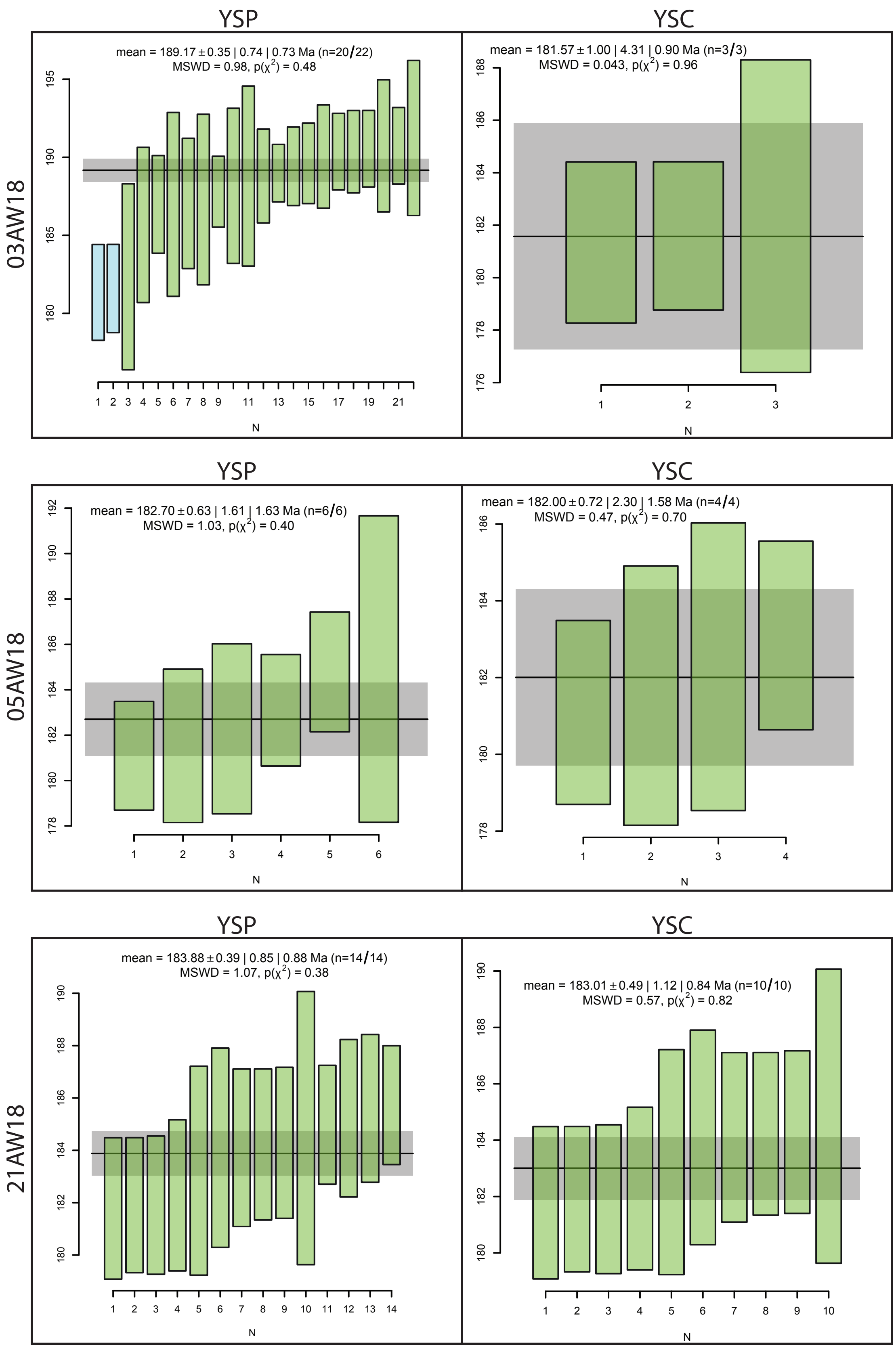

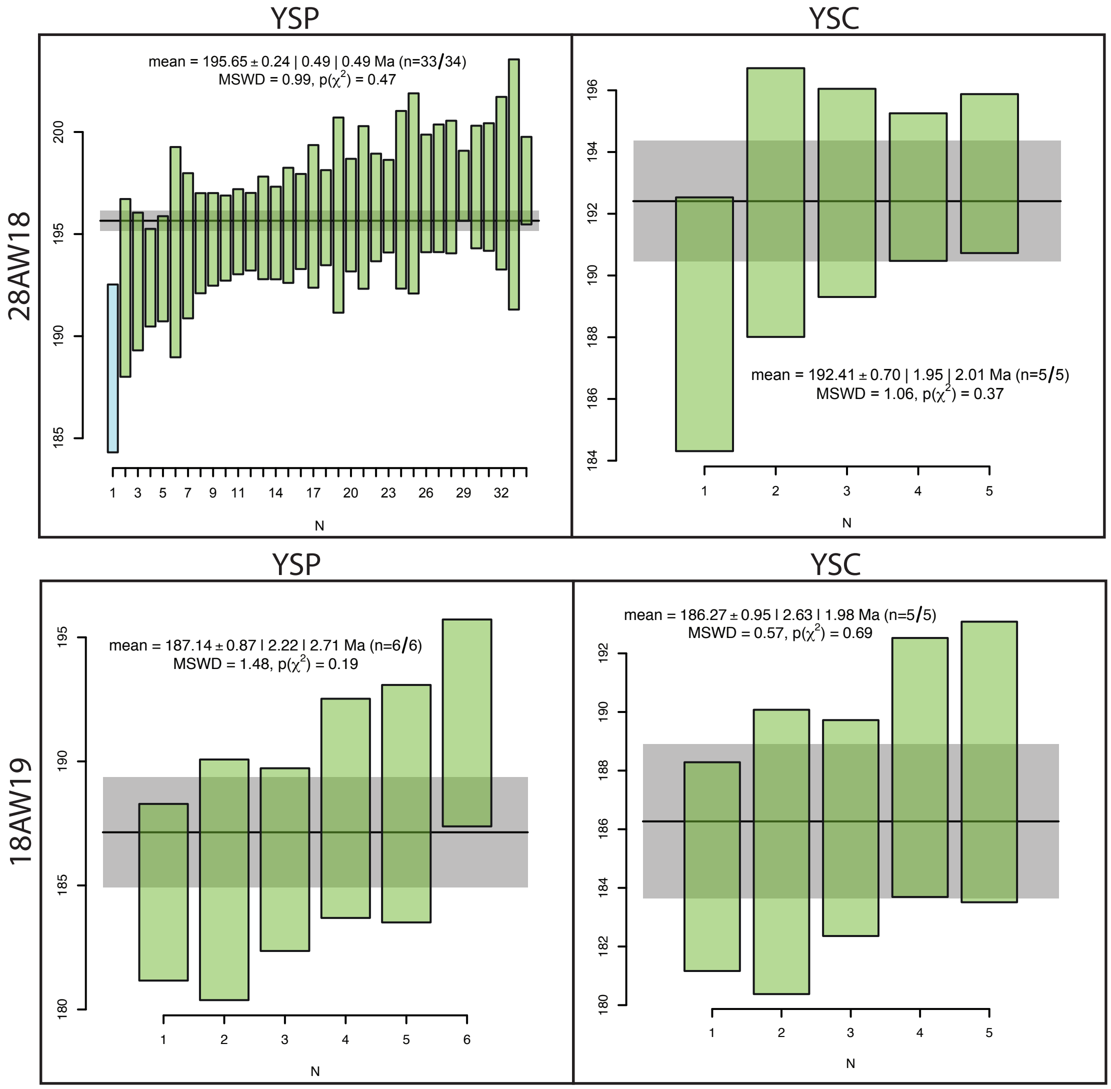

YSP
YSC
28AW18
mean = 195.65 ± 0.24 | 0.49 | 0.49 Ma (n=33/34)
MSWD = 0.99, p(χ2) = 0.47
mean = 192.41 ± 0.70 | 1.95 | 2.01 Ma (n=5/5)
MSWD = 1.06, p(χ2) = 0.37
N
YSP
YSC
18AW19
mean = 187.14 ± 0.87 | 2.22 | 2.71 Ma (n=6/6)
MSWD = 1.48, p(χ2) = 0.19
mean = 186.27 ± 0.95 | 2.63 | 1.98 Ma (n=5/5)
MSWD = 0.57, p(χ2) = 0.69
N

CHAPTER 3

Detrital zircon U-Pb geochronology and Hf isotope geochemistry of Triassic marine strata, southern Tay River map area (NTS 105K), central Yukon

This chapter is written to report data that are beyond the original scope of the thesis

3.1 INTRODUCTION

The Yukon-Tanana and Slide Mountain terranes of central Yukon (Fig. 3.1) comprise mid- to late Paleozoic arc and marginal ocean basin assemblages, respectively, that evolved along the ancient Pacific margin of North America similar to the modern Japan arc and Sea of Japan backarc basin (e.g., Creaser et al., 1997; Colpron et al., 2006a). Mid-Permian collapse of this system along the northern Cordilleran margin was the result of arc-polarity reversal and west-dipping subduction of Slide Mountain ocean lithosphere beneath the Yukon-Tanana arc (Nelson et al., 2006; Colpron et al., 2007; Beranek and Mortensen, 2011). The recognition of mid-Permian suprasubduction zone ophiolite units and the position of Slide Mountain terrane fault slices structurally above the Yukon-Tanana terrane suggest that this traditional model may be an oversimplification (e.g. van Staal et al., 2018). Part of the ambiguity in tectonic models includes late Permian (e.g. Beranek and Mortensen, 2011) to post-Middle Triassic (e.g. Parsons et al., 2019) interpretations for the timing of collision between the Yukon-Tanana terrane and western North American margin. Detrital zircon U-Pb age results of Lower to Upper Triassic sedimentary rocks from western Alaska, eastern Yukon, and northern British Columbia (Fig. 3.2) record the stratigraphic response to arc convergence, collision, and sediment recycling processes, and add constraints to these plate tectonic models (Unterschutz et al., 2002; Beranek et al., 2010b; Beranek and Mortensen, 2011).

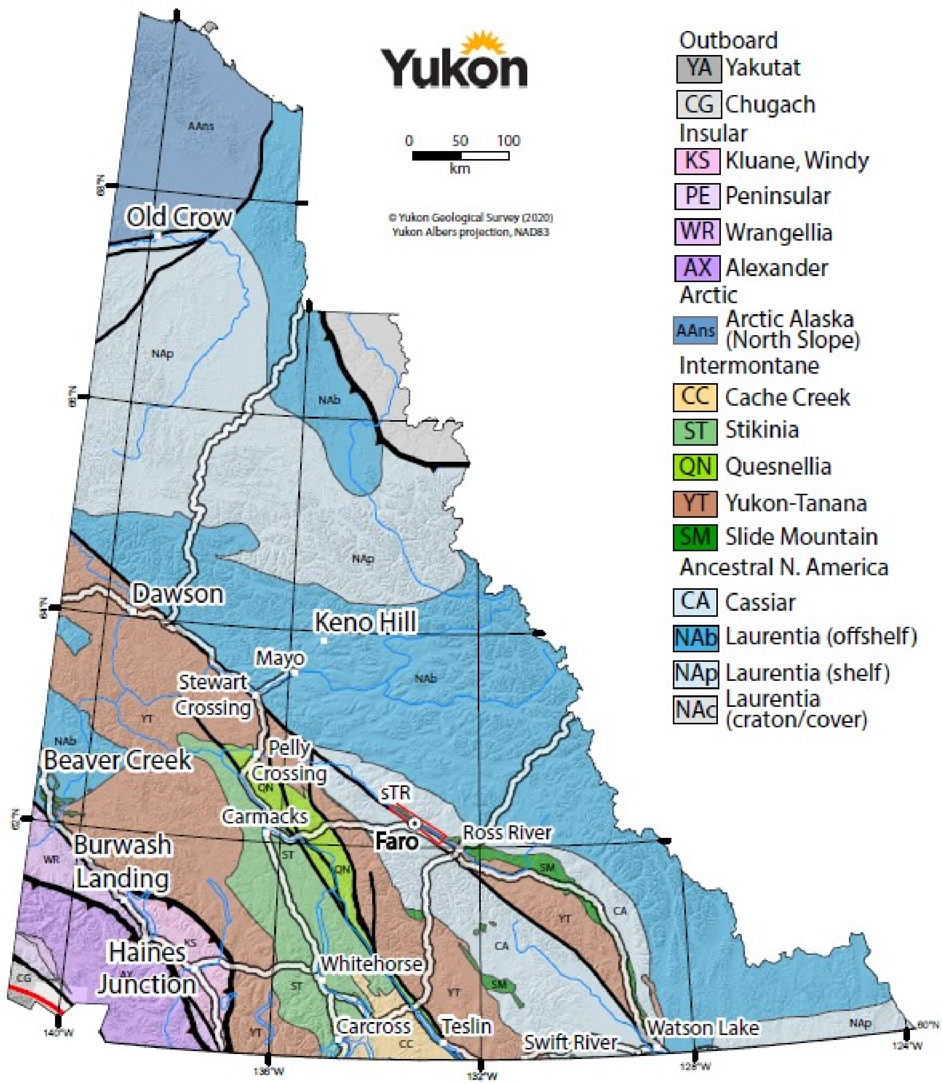

Figure 3.1 - Paleozoic to early Mesozoic bedrock terrane map of Yukon (Yukon Geological Survey, 2020). Red box outlines the southern Tay River map area shown in Fig. 3.3b.

This chapter reports and interprets a new detrital zircon laser ablation split-stream (LASS) dataset (312 U-Pb and 289 Hf isotope) from three Triassic rock samples (Table 3.1) exposed in the southern Tay River map area (105 K) of central Yukon (Fig. 3.1, 3.2, & 3.3a,b). These samples were collected as part of a two-year M.Sc. research project funded by the Geo-mapping for Energy and Minerals (GEM) program at Natural Resources Canada that investigated the stratigraphy and depositional age of the Early Jurassic Faro Peak formation (Chapter 2). These Lower Jurassic strata were originally assigned lower and upper members (e.g. Templeman-Kluit, 1972, Pigage, 2004), however, recent bedrock mapping and field stratigraphic studies indicate that lower member units are of mappable extent, lithologically distinct, and have unconformable lower and upper contacts, and should be separated from the Faro Peak formation (e.g. Wiest and Beranek, 2019; Wiest et al., 2020; Chapter 2). Triassic rock units formerly included in the lower member of the Faro Peak formation represent at least one new formation (currently unnamed) and are reported here to constrain their depositional age, provenance, and potential regional correlation with other Triassic strata of the northern Canadian Cordillera.

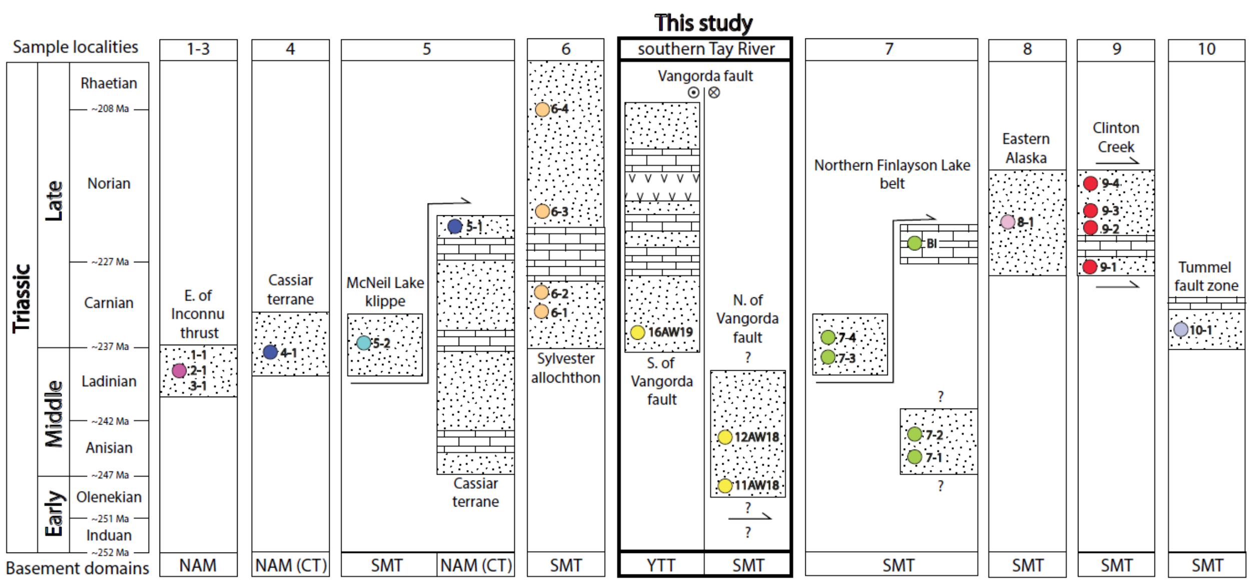

Figure 3.2 - Simplified stratigraphic locations for Triassic detrital zircon samples of this study, Beranek (2009), and Beranek and Mortensen (2011) after Beranek and Mortensen (2011).

Samples						MDA						
Sample ID	Easting	Northing	Formation	Locality	Description	YSP	error	MSWD	YSC	error	YPA	ICS chart
16AW19	577144	6909525	unnamed	Faro Peak	siltstone to fine-grained sandstone	232	2	0.54	231	2	254	Carnian
12AW18	586118	6903737	unnamed	Whiskey Mtn.	fine-grained wacke	250	0.6	0.98	244	1	253	Induan-Anisian
11AW18	586445	6909525	unnamed	Whiskey Mtn.	fine to medium-grained wacke	260	0.4	1.03	250	3	262	Capitanian-Olenekian

YSP youngest statistical peak (Coutts et al., 2019)
YSC youngest single cluster (Dickinson and Gehrels, 2009)
YPA youngest peak age (Arizona Laserchron "AgePick")

Table 3.1 - Summary of lithology, sample location, and maximum depositional ages for the unnamed Triassic samples.

3.2 GEOLOGICAL BACKGROUND

The Yukon-Tanana terrane is separated from parautochthonous North American continental margin rocks to the east by narrow, discontinuous exposures of the Slide Mountain terrane (Fig. 3.1). Together with the Stikinia, Quesnellia, and Cache Creek terranes, the Yukon-Tanana and Slide Mountain terranes are assigned to the Intermontane terranes (Colpron et al., 2006a, 2007) or Intermontane superterrane (Monger et al., 1982) and were the first Cordilleran arc-backarc elements to collide with western North America (Fig. 3.1).

Pre-Late Devonian metasedimentary and metaigneous rocks of the Snowcap assemblage comprise the exposed basement of the Yukon-Tanana terrane and represent a remnant continental fragment of western Laurentia (Piercey and Colpron, 2009; Chapter 2). The Snowcap assemblage is intruded and covered by arc-related igneous rocks of the Late Devonian to Early Mississippian Finlayson, Middle Mississippian to early Permian Klinkit, and mid- to late Permian Klondike assemblages of Yukon-Tanana terrane (Colpron et al., 2006a). The Slide Mountain terrane is characterized by Carboniferous to lower Permian sedimentary and mafic volcanic rocks and associated mafic and ultramafic plutonic rocks (Pigage, 2004; Dusel-Bacon et al., 2006; Murphy et al., 2006) that represent suprasubduction zone ophiolites in the Dunite Peak, Clinton Creek, and Midnight Dome localities of Yukon (van Staal et al., 2018; Parsons et al., 2019). During the late Permian, Snowcap assemblage units along the inboard edge of the Intermontane terranes locally underwent eclogite facies metamorphism and subsequently cooled to upper-crustal levels by Middle to Late Triassic time (Creaser et al., 1997; Erdmer et al., 1998; Philippot et al., 2001; Petrie et al., 2016). Slide Mountain terrane units escaped late Permian high P-T metamorphism, resulting in some authors questioning the west-dipping subduction model beneath the Yukon-Tanana arc and a continuous lower plate position of the Slide Mountain terrane (van Staal et al, 2018; Parsons et al., 2019).

Lower to Middle Triassic sedimentary rocks distributed along the North American continental margin contain mid- to late Paleozoic detrital muscovite and detrital zircon grains and indicate that foreland basin sedimentation related to collision of the Yukon-Tanana arc terrane began by the Olenekian (251-247 Ma) (Beranek et al., 2010b; Beranek and Mortensen, 2011). By Late Triassic time, post-accretionary overlap assemblages had blanketed parts of the Yukon-Tanana terrane, Slide Mountain terrane, and North American continental margin (Beranek and Mortensen, 2011).

3.2.1 Southern Tay River map area, central Yukon

Unnamed Triassic marine strata unconformably overlie Snowcap assemblage units to the southwest of the Vangorda fault, along the suture with Slide Mountain terrane, near the town of Faro (Fig. 3.3a,b). These Triassic strata are unconformably overlain by >800 m of Sinemurian to Toarcian conglomerate and sandstone units of the Faro Peak formation (Fig. 3.3a,b; Wiest et al., 2020; Chapter 2). Regionally, the Yukon-Tanana and Slide Mountain terranes are separated from Cassiar terrane along the Tintina fault to the southwest and parautochthonous North American continental margin strata along the Inconnu thrust to the northeast (Fig. 3.1, 3.3a,b).

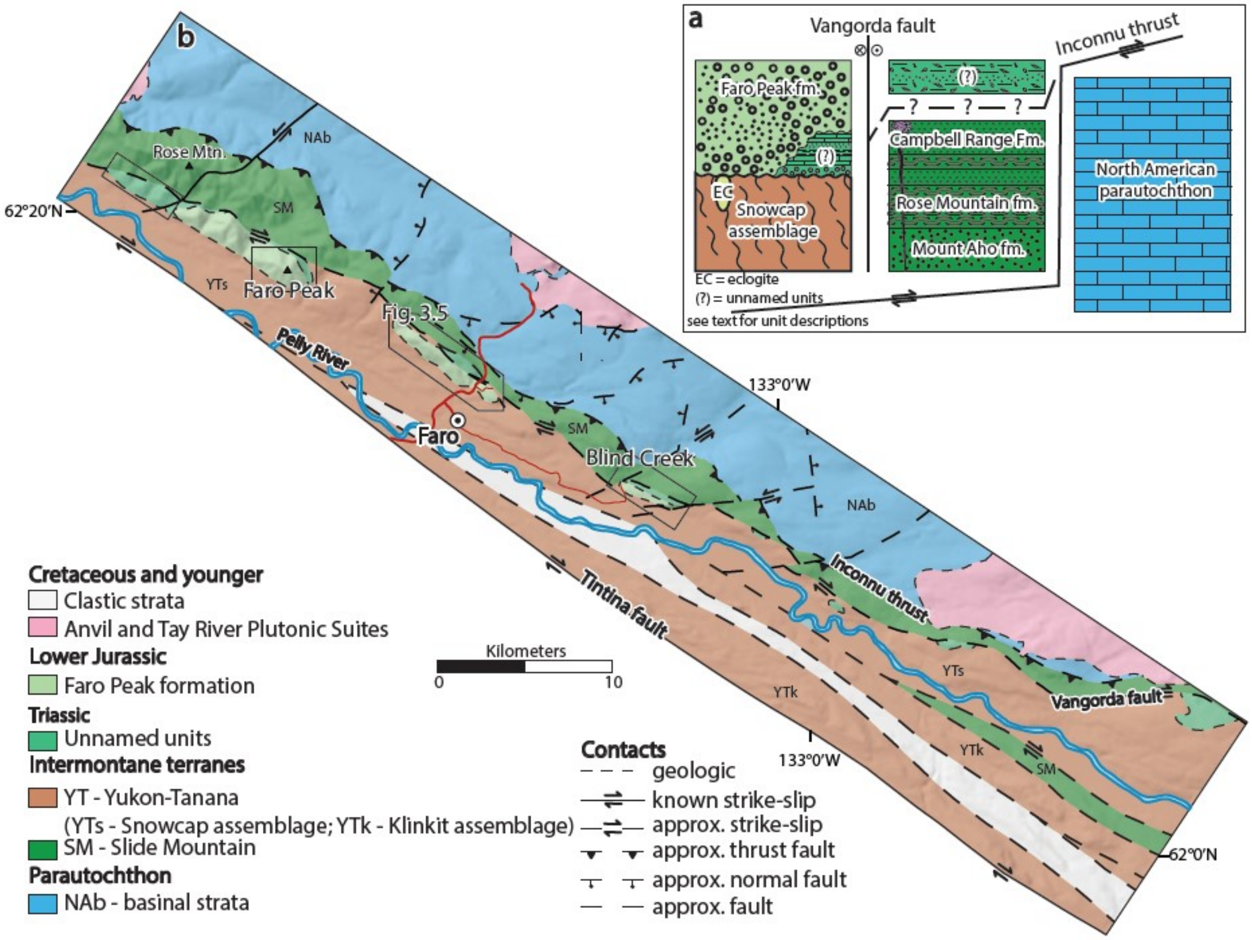

Figure 3.3 - (a) Generalized stratigraphy of the southern Tay River map area after Pigage (2004); (b) Simplified bedrock geology of the southern Tay River map area after Pigage (2004) with localities discussed in text outlined in black.

Unnamed Triassic strata are ~650 m-thick near Rose Mountain, ~20 km northwest of Faro (Fig. 3.3b). A basal conglomerate defines an unconformity with Snowcap assemblage metaclastic rocks and is overlain by interbedded tabular limestone (Fig. 3.4a), graphitic to calcareous argillite-shale (Fig. 3.4b), and basalt (Wiest et al., 2020). A Late Triassic age is assigned to these units based on late Carnian to Rhaetian conodont elements (*M. ex gr. Polygnathiformis*, *Epigondolella cf. mosheri*, *Norigondolella steinbergensis*; Pigage, 2004; Orchard, 2006) in limestone beds stratigraphically below the basalt unit. Late Triassic conodont elements (late Norian, *Epigondolella quadrata*; Pigage, 2004; Orchard, 2006) also occur in limestone units interbedded with argillite at Repeater Hill (Fig. 3.4c), ~22 km to the southeast of Rose Mountain and ~2.5 km

Figure 3.4 - Field photographs of unnamed Triassic units and their locality. (a) Thin bedded limestone, near Rose Mountain; (b) interbedded limestone and argillite, near Rose Mountain; (c) foliated argillite and siltstone, Repeater Hill; (d) thin bedded limestone, Blind Creek; (e) foliated argillite, Blind Creek; (f) micaceous argillite, Faro Peak.

northwest of Faro (Fig. 3.3b, 3.5). Interbedded limestone (Fig. 3.4d) and micaceous argillite (Fig. 3.4e) units are also exposed beneath the Faro Peak formation near Blind Creek, ~10 km southeast of Faro (Fig. 3.3b, 3.5). Near Faro Peak, ~10 km northeast of Faro, locally micaceous argillite, siltstone (Fig. 3.4f), and fine-grained feldspathic arenite units are similarly exposed unconformably below the Faro Peak formation south of the Vangorda fault (Fig. 3.3b).

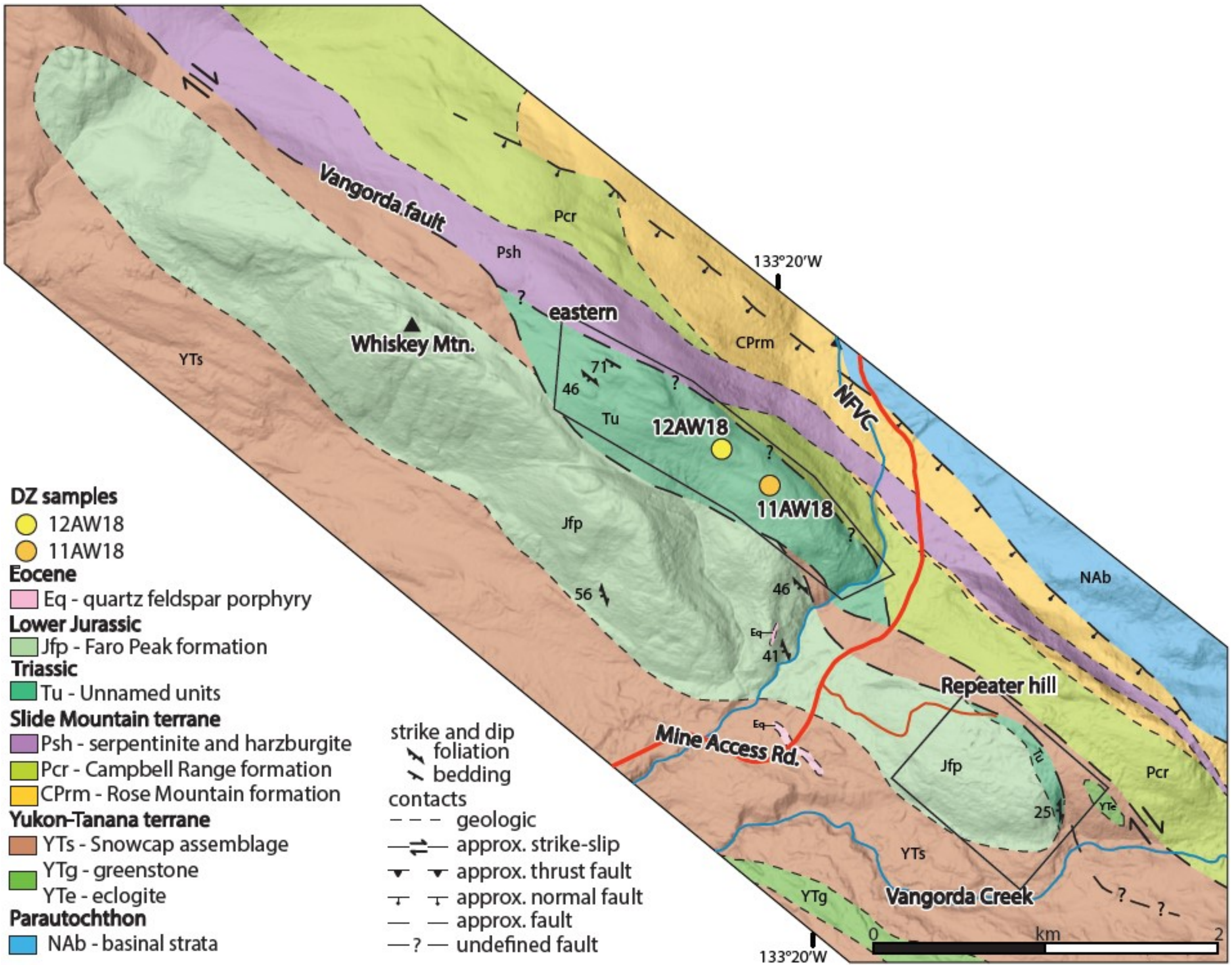

Figure 3.5 - Simplified bedrock geology of the eastern Whiskey Mountain and Repeater Hill areas modified from Pigage (2004) showing the distribution of detrital zircon samples. Basemap DEM (digital elevation model) obtained from the University of Minnesota Polar Geospatial Center (2018) and Porter et al. (2018).

Unnamed Triassic strata are exposed along the eastern ridge of Whiskey Mountain, ~3 km northeast of Faro, likely in a structural block within the Vangorda fault zone (Fig. 3.5). These units are generally more coarse-grained than exposures near Rose Mountain, Repeater Hill, Blind Creek, and Faro Peak. Lithologies include green to grey, fine to medium-grained volcanic lithic feldspathic wacke (Fig. 3.6a), medium to very coarse-grained lithic feldspathic arenite (Fig. 3.6b), and argillite (Fig. 3.6c). Thin to thick, tabular, normally graded beds are consistent with deposition by concentrated debris flows (Fig. 3.6d,e) and local convolute bedding and slump structures (Fig. 3.6f) indicate soft sediment deformation in these units.

Figure 3.6 - Field photographs of unnamed Triassic units from the eastern Whiskey Mountain area. (a) Photomicrograph of feldspathic lithic wacke (4x magnification); (b) immature coarse-grained feldspathic arenite; (c) massive green argillite; (d) tabular bedded siltstone and argillite with local scouring; (e) tabular bedded coarse-grained sandstone and siltstone; (f) slump structure in coarse-grained sandstone and argillite.

3.3 METHODS

3.3.1 Sample preparation

Rock samples (Table 3.1) were crushed and milled using standard techniques and detrital zircon grains were isolated through density separation in heavy liquids (methylene iodide). Detrital zircon grains were handpicked and mounted in epoxy, polished, and imaged with backscatter and cathodoluminescence using a JEOL JSM 7100F field emission scanning electron microscope at Memorial University of Newfoundland to determine areas with complex zoning, fractures, and inherited cores.

3.3.2 Analysis

Detrital zircon grains were analyzed using the laser ablation split-stream (LASS) method at Memorial University of Newfoundland following the methods of Fisher et al. (2014) and Beranek et al. (2020). Zircon grains were ablated with a 40 µm spot using a GeoLas 193 nm excimer laser with a frequency and fluence of 10 Hz and 5 J/cm^2. Uranium-Pb isotopes were collected using a ThermoFinnigan Element XR single-collector ICP-MS and Hf isotopes were simultaneously collected from the same ablated material with a ThermoFinnigan Neptune multi-collector ICP-MS.

3.3.3 Data reduction

Raw U-Pb results were reduced using Iolite 1.4 software (Paton et al., 2011) and the VizualAge data reduction scheme (Petrus and Kamber, 2012). U-Pb age data were calibrated with the 91500 zircon reference zircon and yielded a weighted mean $^{206}Pb/^{238}U$ age of 1063.3 ± 0.5 Ma (*n* = 149; Appendix 3.A.1) compared with a published ID-TIMS age of 1062.4 ± 1.3 Ma (Wiedenbeck et al. 1995). Hf isotope data were calibrated using the Plešovice zircon reference zircon and yielded a weighted mean $^{176}Hf/^{177}Hf$ ratio of 0.282485 ± 0.000002 (*n* = 151; Appendix 3.A.1) compared to a published weighted mean value of 0.282482 ± 0.000013 (Sláma et al. 2008).

"Best Ages" were determined for each analysis with >1000 Ma grains reporting the $^{207}Pb/^{206}Pb$ age and <1000 Ma grains reporting the $^{206}Pb/^{238}U$ ages (Appendix 3.A.2). Concordance was calculated using the $^{207}Pb/^{206}Pb$ and $^{206}Pb/^{238}U$ ages for grains >1000 Ma. Analyses with >10% discordance were removed and reverse discordance of >5% was negated manually when possible during data reduction with VizualAge. Grains <500 Ma were assessed for accuracy and removed on a grain-by-grain basis in Iolite using an evaluation of the $^{207}Pb/^{206}Pb$, $^{207}Pb/^{235}U$, and $^{206}Pb/^{238}U$ ages. Hafnium isotope data are reported in epsilon notation and are corrected for time = t ($\varepsilon_{Hf(t)}$) based on the "Best Age" (Appendix 3.A.2).

3.4 RESULTS

Medium-grained lithic feldspathic wacke collected from the eastern part of Whiskey Mountain (sample 11AW18; Fig. 3.5) yields mostly 283-245 Ma detrital zircon grains (95%) with a peak age of 262 Ma and $\varepsilon_{Hf(t)}$ values of -17.3 to +0.5 ($\bar{X}$ = -10.6) (Fig. 3.7). One mid-Permian (264 ± 4 Ma) grain yields a superchondritic $\varepsilon_{Hf(t)}$ value of +7.7. The remainder of detrital zircon grains (5%) are Precambrian in age. One Neoarchean (2749 ± 33 Ma) grain yields an $\varepsilon_{Hf(t)}$ value of +4.2. Three Paleoproterozoic (1794 ± 70, 1798 ± 65, and 2173 ± 23 Ma) grains yield $\varepsilon_{Hf(t)}$ values of +3.4, -4.1, and +2.2 respectively. Two Mesoproterozoic (1393 ± 72 Ma, 1472 ± 27 Ma) grains yield $\varepsilon_{Hf(t)}$ values of +0.2 and +2.5, respectively.

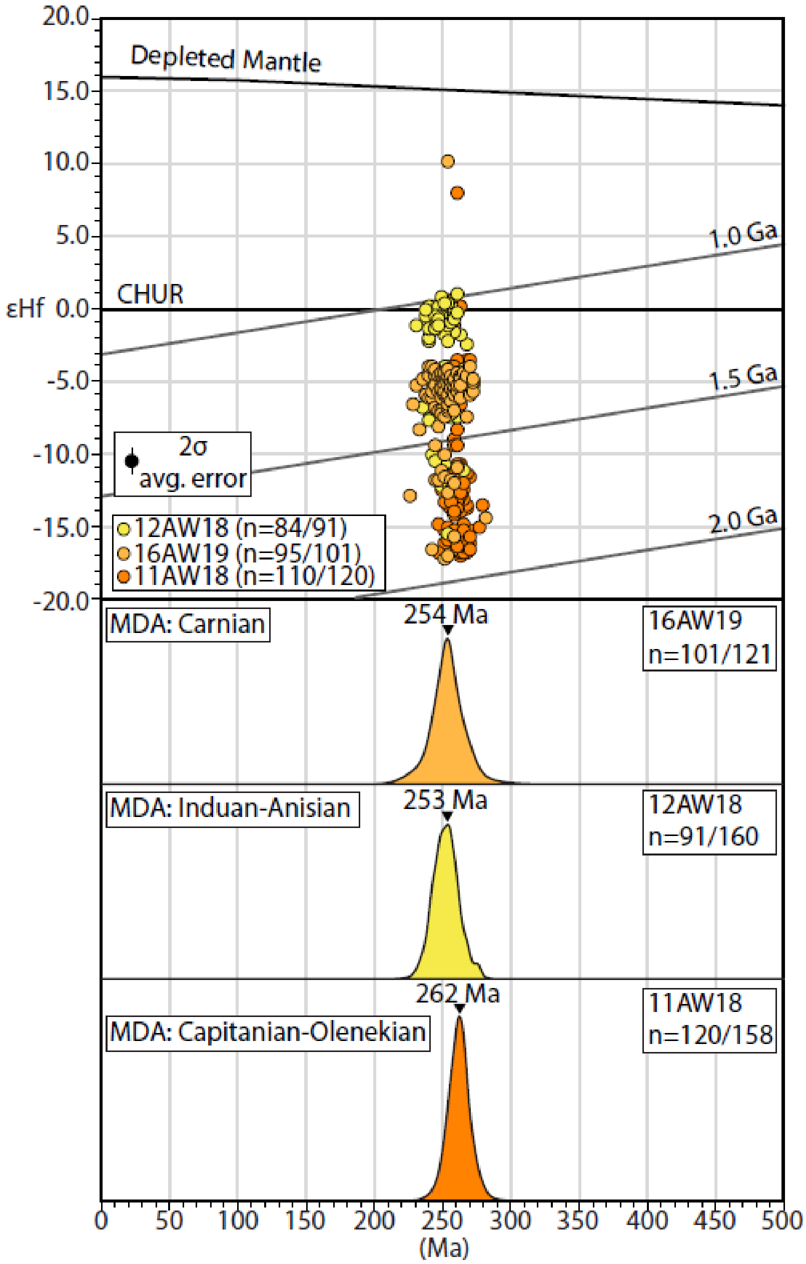

Figure 3.7 - Detrital zircon probability density U-Pb age plots versus $\varepsilon_{Hf(t)}$ values for unnamed Triassic units.

Siltstone to fine-grained feldspathic arenite from the base of Faro Peak (sample 16AW19; Fig. 3.8) yields 285-227 Ma detrital zircon grains with a peak age of 254 Ma and $\varepsilon_{Hf(t)}$ values of -17.4 to -4.2 ($\bar{X}$ = -7.0) (Fig. 3.7). One mid-Permian (256 ± 13 Ma) grain yields a superchondritic $\varepsilon_{Hf(t)}$ value of +10.0.

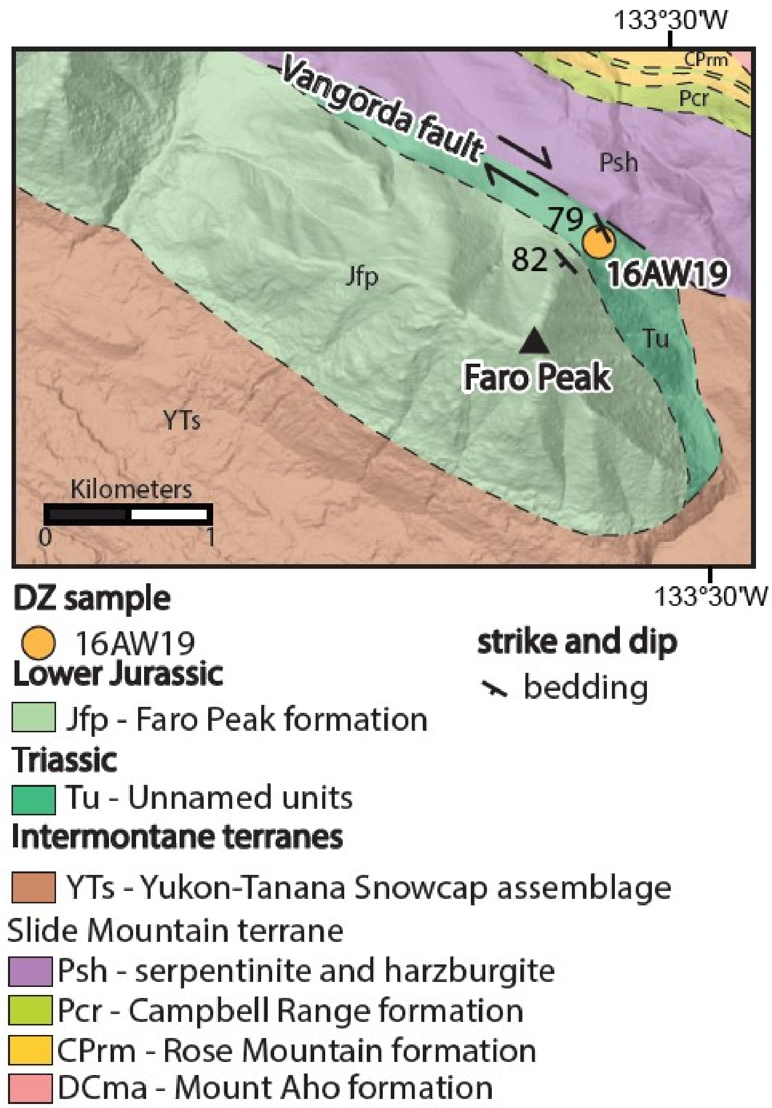

Figure 3.8 - Simplified bedrock geology of Faro Peak modified from Pigage (2004) showing the location of sample 16AW19. Contact symbols same as Figure 3.5. Basemap DEM (digital elevation model) obtained from the University of Minnesota Polar Geospatial Center (2018) and Porter et al. (2018).

Fine-grained feldspathic wacke from eastern Whiskey Mountain (sample 12AW18; Fig. 3.5) yields 276-234 Ma detrital zircon grains with a peak age of 253 Ma and $\varepsilon_{Hf(t)}$ values of -15.6 to +0.8 ($\bar{X}$ = -4.2) (Fig. 3.7).

3.5 INTERPRETATION

3.5.1 Maximum depositional age

Three techniques were employed to estimate maximum depositional ages (MDAs) for unnamed Triassic units in the Faro region:

YSP—(youngest statistical peak): weighted mean of the youngest population of 2 or more grains that yields a MSWD ≈ 1 (e.g., Coutts et al., 2019);

YSC—(youngest cluster at two sigma): weighted mean of the youngest three or more grains that overlap at 2σ (e.g., Dickinson and Gehrels, 2009);

YPA—(youngest graphical peak): youngest peak age of a probability density plot (e.g., Dickinson and Gehrels, 2009) and was determined from the "AgePick" Excel macro program from the Arizona Laserchron Center.

Maximum depositional ages for unnamed Triassic units and are summarized in Table 3.1. Maximum depositional ages are assigned a stage age from the range of YSP to YSC values using the time scale of Cohen et al. (2013) with unnamed units in the southern Tay River map area yielding Capitanian to Carnian depositional ages (Table 3.1).

3.5.2 Provenance

Unnamed units in the Faro region include a basal conglomerate unit near Rose Mountain with quartz mica schist and micaceous quartzite clasts from the underlying Snowcap assemblage, chert likely derived from the adjacent late Paleozoic rocks of the Slide Mountain terrane, and tan volcanic rocks of uncertain provenance (Wiest et al., 2020). Wacke and feldspathic arenite units near Faro Peak and along the eastern ridge of Whiskey Mountain are dominated by mid-Permian to Late Triassic detrital zircon grains that form peak ages of 262, 254, and 253 Ma with mostly subchondritic $\varepsilon_{Hf(t)}$ values.

Subsidiary Precambrian detrital zircon grains comprise two percent of the total population and include Neoarchean (ca. 2750 Ma) and Paleoproterozoic (ca. 2200 and 1800 Ma) grains that are similar in age and Hf isotope composition as those derived from quartz-mica schist and micaceous quartzite units in the Snowcap assemblage (Piercey and Colpron, 2009; Chapter 2). Mesoproterozoic (ca. 1400-1500 Ma) grains support derivation from Upper Devonian and younger units that locally cover the Intermontane terranes and northwestern Laurentian continental margin (Beranek et al., 2010a, 2010b; Beranek and Mortensen, 2011).

Mid- to late Permian felsic magmatism in the Yukon-Tanana terrane is best recognized in the Klondike assemblage of western Yukon and corresponding mafic to ultramafic magmatism is observed in the Slide Mountain terrane of northern British Columbia, Yukon, and eastern Alaska (Table 3.2). Feldspathic arenite units near Faro Peak and wacke units along the eastern ridge of Whiskey Mountain are dominated by subchondritic detrital zircon $\varepsilon_{Hf(t)}$ values that are generally consistent in age and isotopic composition to Klondike assemblage units in the Stewart River area of western Yukon (Table 3.2). Coeval to slightly older igneous rocks assigned to the Slide Mountain terrane yield superchondritic isotope values at Dunite Peak (Table 3.2; Parsons et al., 2019) and geochemical characteristics of ultramafic rocks at Clinton Creek and Midnight Dome similarly suggests juvenile magma sources (van Staal et al., 2018). Mid- to late Permian grains (264 ± 4 Ma and 256 ± 13 Ma) that yield superchondritic $\varepsilon_{Hf(t)}$ values of +7.7 and +10 are consistent with derivation from a juvenile source of the Slide Mountain terrane.

State/Province	Rock type	unit/assemblage/location	Age (Ma)	$\varepsilon Nd_{(t)}$	$\varepsilon Hf_{(t)}$*	Reference
eastern Alaska	metarhyolite porphyry or crystal tuff	Nasina assemblage (Snowcap assemblage), carbonaceous unit	~253	-	-	J.K. Mortensen, unpublished data, 2004; reported in: Dusel-Bacon et al., 2006
	metarhyolite	Nasina assemblage (Snowcap assemblage), carbonaceous unit	~267-256	-	-	
	felsic metatuff	Nasina assemblage (Snowcap assemblage), carbonaceous unit	~260	-	-	
	felsic metatuff	Klondike Schist	~255	-	-	
	metarhyolite	Klondike Schist	~256	-	-	
	granodiorite	Post-metamorphic dike into Fortymile River assemblage (Slide Mountain)	~263	-	-	J.K. Mortensen, unpublished data, 2004; reported in: Dusel-Bacon et al., 2006
Yukon	monzonite	Jim Creek	~258-253	-	-	Beranek and Mortensen, 2011
	monzonite	Sulphur Creek	~262-259	-	-	Mortensen, 1990; Beranek and Mortensen, 2011
	augen granitoid	Stewart River,Mount Burnham	~265	-11.5 to -2.9	-12.7 to -1.0	Ruks et al., 2006
	intermediate volcanics, gabbro	Glenlyon, near Ragged Lake	~267-260	-	-	Colpron et al., 2006b
	feldspar porphyry, diorite, leucogabbro, plagiogranite	Finlayson Lake	~273-255	-	-	Mortensen, 1992; Murphy et al., 2006
	leucogabbro dike	Clinton Creek	~270-257	-	-	van Staal et al., 2018
	leucogabbro dike	Midnight Dome	~271-256	-	-	
	gabbro	Dunite Peak	~265	+7.2 to +9.0	+12.7 to +15.2	Parsons et al., 2019
northern British Columbia	andesite tuff	Klinkit intra-oceanic arc, near Nasty Peak	~281	+6.7 to +7.4	+12.1 to +13.0	Roots et al., 2002; Simard et al., 2003
	pegmatite,granodiorite, monzonite	Dorsey Complex, Ram stock	~270-235	-	-	Roots et al., 2006, Nelson and Friedman, 2004

* =converted εNd to εHf (εHf=1.36(εNd)+2.95), Vervoort et al., 1999; Vervoort and Blichert-Toft, 1999

Yukon-Tanana	techtonostratigraphic setting of magmatism
Slide Mountain	

Table 3.2 - Summary of ages and isotopic compositions for potential source rocks for unnamed Triassic units.

3.6 DISCUSSION AND FUTURE WORK

Triassic sedimentary successions exposed along the Cordilleran margin from northern British Columbia to eastern Alaska represent collision-related foreland and post-collisional overlap assemblages that locally cover Paleozoic rocks of the Yukon-Tanana terrane, Slide Mountain terrane, Quesnellia, and ancestral continental North American margin (Unterschutz et al., 2002; Beranek et al., 2010b; Beranek and Mortensen, 2011). These Triassic rock units are herein assigned to two groups (Table 3.3): Group A - chert to volcanic lithic to feldspathic wacke, sandstone, and conglomerate units that have pre-Norian or no fossil age constraints, unimodal detrital zircon age distributions, and mid-Permian to Late Triassic MDAs; and Group B - micaceous to calcareous sandstone and sandy limestone units that yield Middle and Late Triassic conodont fossils, diverse detrital zircon age distributions, and Late Devonian to Late Triassic MDAs.

Sample	Location	Rock type	MDA	Fossil	Reference
16AW19	southern Tay River	siltstone to fine-grained feldspathic arenite	Carnian	-	this study
12AW18		fine to medium-grained lithic feldspathic and feldspathic wacke	Induan-Anisian	-	
11AW18			Capitanian-Olenekian	-	
1-1	east of Inconnu Thrust	fine to medium-grained micaceous to calcareous sandstone	Anisian-Ladinian	late Ladinian	Beranek and Mortensen, 2011*
2-1			Artinskian-Anisian	late Ladinian	
3-1			Capitanian	late Ladinian	
4-1	Cassiar terrane	medium to coarse-grained micaceous and calcareous sandstone	Bashkirian-Moscovian	late Ladinian-early Carnian	
5-1			Olenekian-Norian	Norian	
5-2	McNeil Lake klippe	coarse-grained volcanic lithic sandstone	Wuchiapingian-Induan	-	
6-1	Sylvester allochthon	fine to medium-grained micaceous sandstone	Changhsingian-Olenekian	Carnian-Rhaetian	
6-2			Carnian	Carnian-Rhaetian	
6-3			Carnian	Carnian-Rhaetian	
6-4			Norian	Norian	
7-1	Finlayson Lake	coarse-grained lithic to feldspathic sandstone	Induan-Olenekian	pre-Norian	
7-2			Wuchiapingian-Changhsingian	pre-Norian	
7-3		chert pebble conglomerate	Wuchiapingian-Induan	-	
7-4			Anisian-Carnian	-	
8-1	eastern Alaska	fine to medium-grained micaceous and calcareous sandstone	Visean	Carnian-Norian	
9-1	Clinton Creek		Tournaisian-Visean	early to middle Norian	
9-2			Carnian	early to middle Norian	
9-3			Carnian	early to middle Norian	
9-4			Famennian	early to middle Norian	
10-1	Tummel fault zone	fine-grained micaceous sandstone	Wuchiapingian	Anisian(?)	
BI	Finlayson Lake	sandy bioclastic limestone	Visean	late early Norian	Beranek, 2009*

* MDAs recalculated using the YSP and YSC methods

Group	
A	lithic to feldspathic wacke, sandstone, and conglomerate
B	micaceous to calcareous sandstone and sandy limestone

youngest fossil and MDA stage age period
Late Triassic
Middle Triassic
Early Triassic
late Permian
middle Permian
>Permian

Table 3.3 - Summary of samples from this study, Beranek (2009), and Beranek and Mortensen (2011), based on sample location, lithology, MDA, and biostratigraphic age.

Multidimensional scaling (MDS) techniques show that Group A rocks exposed at the McNeil Lake klippe, northern Finlayson Lake area, and units in the southern Tay River area near Faro Peak and at eastern Whiskey Mountain, share a statistically similar detrital zircon U-Pb signature (Figs. 3.9a,b, and c). Group B units with Middle to Late Triassic fossil age constraints cluster in a separate space on the MDS plot and indicating a different provenance (Figs. 3.9a,b, and c).

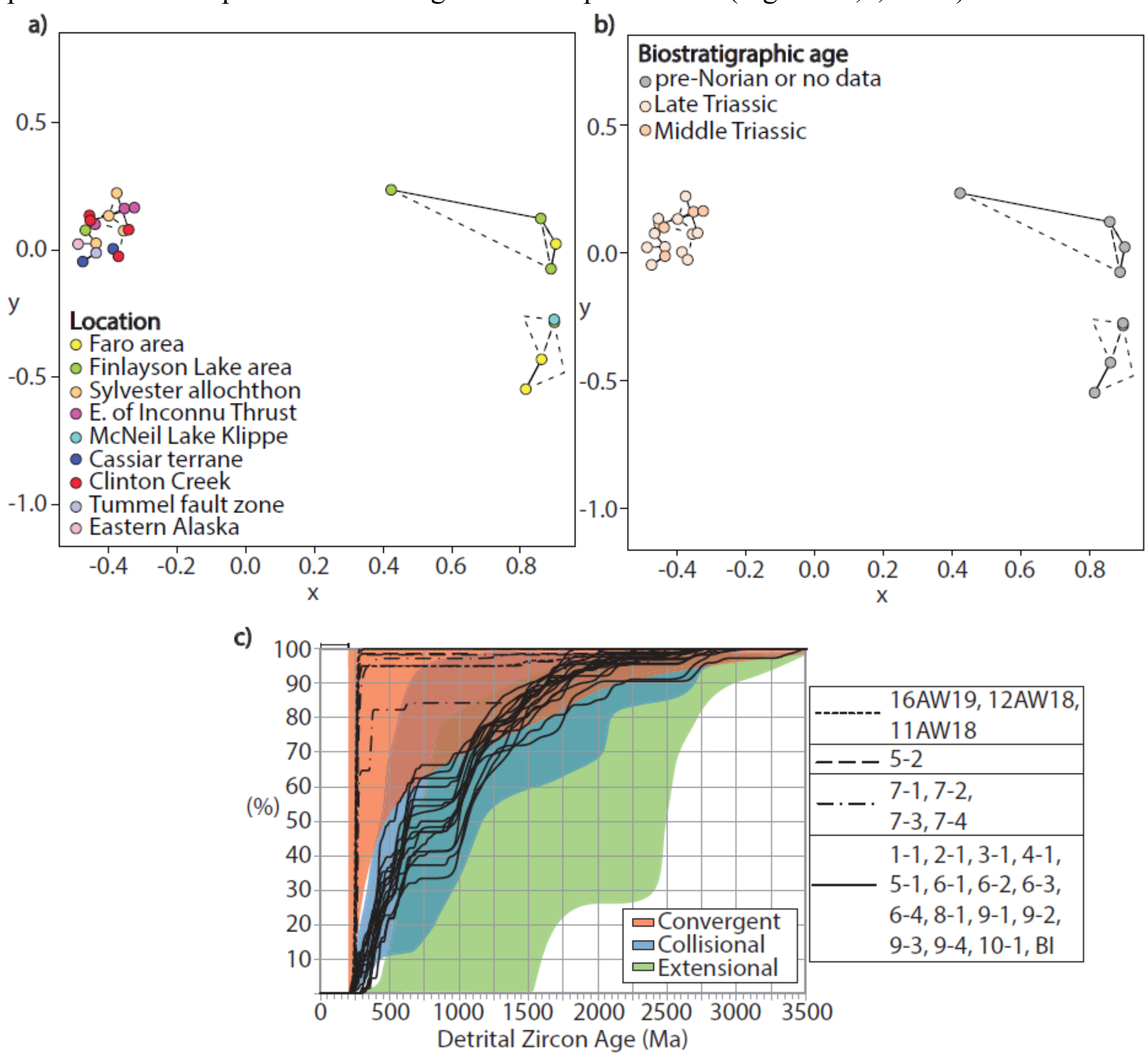

Figure 3.9 - Multidimensional scaling plots comparing unnamed Triassic units of this study and Triassic units from Beranek (2009) and Beranek and Mortensen (2011) (a) location, (b) biostratigraphic age, and (c) cumulative distribution U-Pb age plot and tectonic setting discrimination diagram (Cawood et al, 2012). Discrimination fields moved to 200 Myr to more closely match the true depositional age (c.f. Cawood et al., 2012).

The tectonic setting of sedimentary units can be assessed based on lithology (e.g., Dickinson et al., 1983) and detrital zircon age signature (e.g., Cawood et al., 2012). Triassic units exposed along the northern Cordilleran margin plot in two separate tectonic settings based on their detrital zircon U-Pb results and cluster similarly in MDS plots and lithologic groups (Fig. 3.9d). Unnamed Triassic units near Faro Peak and along the eastern ridge of Whiskey Mountain fall into Group A and the lithologic, stratigraphic, and detrital zircon data suggest primary derivation from a proximal Permian arc or its forearc basin, similar to Triassic units spatially associated with Slide Mountain terrane in the northern Finlayson Lake and the McNeil Lake klippe areas (e.g., Beranek and Mortensen, 2011). Hafnium isotope compositions suggest that the Permian arc detrital zircon source rocks were contaminated with continental crust or its supracrustal derivatives consistent with the Klondike assemblage units of the Yukon-Tanana terrane (e.g., Mortensen, 1992; Piercey et al., 2006). Evidence for Slide Mountain terrane provenance includes two Permian (264 ± 4 Ma, 256 ± 13 Ma) grains that yield superchondritic $\varepsilon_{Hf(t)}$ values in agreement with Dunite Peak and other intrusions (Midnight Dome, Clinton Creek, and undiscovered equivalents).

Upper Triassic limestone and micaceous to calcareous argillite, siltstone, and sandstone units exposed in the southern Tay River map area are lithologically similar to other Group B units in the northern Cordillera and suggest that not all unnamed units near Faro are stratigraphically correlative. Future detrital zircon U-Pb-Hf isotope studies of unnamed Triassic units in the southern Tay River map area would test this hypothesis and could assess potential stratigraphic and provenance links with other Group A and B units. Future re-sampling of Triassic units along the length of the northern Canadian Cordillera (e.g. Beranek and Mortensen, 2011) for high-*n* laser ablation detrital zircon U-Pb geochronology and Hf isotope geochemistry would provide a more robust comparison with units of the southern Tay River map area and add timing and tectonic evolution constraints to source regions and ancient sediment pathways.

3.7 REFERENCES

Beranek L.P., Mortensen, J.K., Lane, L.S., Allen, T.L., Fraser, T.A., Hadlari, T., and Zantvoort, W.G., 2010a, Detrital zircon geochronology of the western Ellesmerian clastic wedge, northwestern Canada: Insights on Arctic tectonics and the evolution of the northern Cordilleran miogeocline: Geological Society of America Bulletin, v. 112, no. 11-12, p. 1889-1911, doi: 10.1130/B30120.1.

Beranek, L.P., 2009, Provenance and paleotectonic setting of North American Triassic strata in Yukon: The sedimentary record of pericratonic terrane accretion in the northern Canadian Cordillera [PhD thesis]: Vancouver, British Columbia, Canada, The University of British Columbia, 338p.

Beranek, L.P., and Mortensen, J.K., 2011, The timing and provenance record of the Late Permian Klondike orogeny in northwestern Canada and arc-continent collision along western North America: Tectonics, v. 30, 23 p, doi: 10.1029/2010TC002849.

Beranek, L.P., Gee, D.G., and Fisher, C.M., 2020, Detrital zircon U-Pb-Hf isotope signatures of Old Red Sandstone strata constrain the Silurian to Devonian paleogeography, tectonics, and crustal evolution of the Svalbard Caledonides: Geological Society of America Bulletin, v. 132, no. 9-10, p. 1987-2003, doi: 10.1130/B35318.1.

Beranek, L.P., Mortensen, J.K., Orchard, M.J., and Ullrich, T., 2010b, Provenance of North American Triassic strata from west-central and southeastern Yukon: correlations with coeval strata in the Western Canada Sedimentary Basin and Canadian Arctic Islands: Canadian Journal of Earth Sciences, v. 47(1), p. 53-73, doi: 10.1139/E09-065.

Cawood, P.A., Hawkesworth, C.J., and Dhuime, B., 2012, Detrital zircon record and tectonic setting: Geology, v. 40, p. 875-878, doi: 10.1130/G32945.1.

Cohen, K.M., Finney, S.C., Gibbard, P.L., and Fran, J.-X., 2013;updated, The ICS International Chronostratigraphic Chart, ep. 36: 199-204, http://www.stratigraphy.org/ICSchart/ChronostratChart2021-07.pdf.

Colpron, M., Mortensen, J.K., Gehrels, G.E., and Villeneuve, M., 2006b, Basement complex, Carboniferous magmatism and Paleozoic deformation in Yukon-Tanana terrane of central Yukon: Field, geochemical and geochronological constraints from Glenlyon map area, *in* Colpron, M. and Nelson, J.L., eds., Paleozoic Evolution and Metallogeny of Pericratonic Terranes at the Ancient Pacific Margin of North America, Canadian and Alaskan Cordillera: Geological Association of Canada, Special Paper 45, p. 131-151.

Colpron, M., Nelson, J.L., and Murphy, D.C., 2006a, A tectonostratigraphic framework for the pericratonic terranes of the northern Cordillera, *in* Colpron, M. and Nelson, J.L., eds., Paleozoic Evolution and Metallogeny of Pericratonic Terranes at the Ancient Pacific Margin of North America, Canadian and Alaskan Cordillera: Geological Association of Canada, Special Paper 45, p. 1-23.

Colpron, M., Nelson, J.L., and Murphy, D.C., 2007, Northern Cordilleran terranes and their interactions through time: Geological Society of America Today, v. 17, no. 4/5, doi: 10.1130/GSAT01704-5A.1.

Coutts, D.S., Matthews, W.A., and Hubbard, S.M., 2019, Assessment of widely used methods to derive depositional ages from detrital zircon populations: Geoscience Frontiers, v. 10, no. 4, p. 1421-1435, doi: 10.1016/j.gsf.2018.11.002.

Creaser, R.A., Erdmer, P., Stevens, R.A., and Grant, S.L., 1997, Tectonic affinity of the Nisultin and Anvil assemblage strata from the Teslin tectonic zone, northern Canadian Cordillera: Constraints from neodymium isotope and geochemical evidence: Tectonics, v. 16, no. 1, p. 107-121.

Dickinson, W.R., and Gehrels, G.E., 2009, Use of U-Pb ages of detrital zircons to infer maximum depositional ages of strata: A test against a Colorado Plateau Mesozoic database: Earth and Planetary Science Letters, v. 288, p. 115-125, doi: 10.1016/j.epsl.2009.09.013.

Dusel-Bacon, C., Hopkins, M.J., Mortensen, J.K., Dashevsky, S.S., Bressler, J.R., and Day, W.C., 2006, Paleozoic tectonic and metallogenic evolution of the pericratonic rocks of east-central Alaska and adjacent Yukon, *in* Colpron, M. and Nelson, J.L., eds., Paleozoic evolution and metallogeny of pericratonic terranes at the ancient margin of North America, Canadian and Alaskan Cordillera: Geological Association of Canada, Special Paper 45, p. 25-74.

Erdmer, P., Ghent, E.D., Archibald, D.A., and Stout, M.Z., 1998, Paleozoic and Mesozoic high-pressure metamorphism at the margin of ancestral North America in central Yukon: Geological Society of America Bulletin, v. 110, no. 5, p. 615-629.

Fisher C.M., Vervoort, J.D., and DuFrane, S.A., 2014, Accurate Hf isotopic determinations of complex zircons using the “laser ablation split stream” method: Geochemistry, Geophysics, Geosystems, v. 15, p. 121-139, doi: 10.1002/2013GC004962.

Monger, J.W.H., Price, R.A., and Tempelman-Kluit, D.J., 1982, Tectonic accretion and the origin of the two major metamorphic and plutonic welts in the Canadian Cordillera: Geology, v. 10, no. 2, p. 70-75, doi: 10.1130/0091-7613(1982)10<70:TAATOO>2.0.CO;2.

Mortensen, J. K., 1990, Geology and U-Pb geochronology of the Klondike District, west-central Yukon Territory, Canadian Journal of Earth Sciences, v. 27, p. 903–914, doi:10.1139/e90-093.

Mortensen, J.K., 1992, Pre–mid-Mesozoic tectonic evolution of the Yukon-Tanana terrane, Yukon and Alaska: Tectonics, v. 11, p. 836–853, doi: 10.1029/91TC01169.

Murphy, D.C., Mortensen, J.K., Piercey, S.J., Orchard, M.J., and Gehrels, G.E., 2006, Mid-Paleozoic to early Mesozoic tectonostratigraphy evolution of Yukon-Tanana and Slide Mountain terranes and affiliated overlap assemblages, Finlayson Lake massive sulphide district, southeastern Yukon, *in* Colpron, M. and Nelson, J.L., eds., Paleozoic Evolution and Metallogeny of Pericratonic Terranes at the Ancient Pacific Margin of North America, Canadian and Alaskan Cordillera: Geological Association of Canada, Special Paper 45, p. 75-105.

Nelson, J. and Friedman, R., 2004, Superimposed Quesnel (late Paleozoic-Jurassic) and Yukon-Tanana (Devonian-Mississippian) arc assemblages, Cassiar Mountains, northern British Columbia: field, U-Pb, and igneous petrochemical evidence: Canadian Journal of Earth Sciences, v. 41, p. 1201-1235.

Nelson, J.L., Colpron, M., Piercey, S.J., Dusel-Bacon, C., Murphy, D.C., and Root, C.F., 2006, Paleozoic tectonic and metallogenic evolution of the pericrationic terranes in Yukon, northern British Columbia and eastern Alaska, *in* Colpron, M. and Nelson, J.L., eds., Paleozoic Evolution and Metallogeny of Pericratonic Terranes at the Ancient Pacific Margin of North America, Canadian and Alaskan Cordillera: Geological Association of Canada, Special Paper 45, p. 323-360.

Orchard, M.J., 2006, Late Paleozoic and Triassic conodont faunas of Yukon and northern British Columbia and implications for the evolution of the Yukon-Tanana terrane, *in* Colpron, M. and Nelson, J.L., eds., Paleozoic evolution and metallogeny of pericratonic terranes at the ancient pacific margin of North America, Canadian and Alaskan Cordillera: Geological Association of Canada, Special Paper 45, p. 229-260.

Parsons, A.J., Zagorevski, A., Ryan, J.J., McClelland, W.C., van Staal, C.R., Coleman, M.J., and Golding, M.L., 2019, Petrogenesis of the Dunite Peak ophiolite, south-central Yukon, and the distinction between upper-plate and lower-plate setting: A new hypothesis for the late Paleozoic—early Mesozoic tectonic evolution of the Northern Cordillera: Geological Society of America Bulletin, v. 131, no. 1/2, p. 74-298, doi: 10.1130/B31964.1.

Paton, C., Hellstrom, J., Paul, B., Woodhead, J., and Hergt, J., 2011, Iolite: Freeware for the visualization and processing of mass spectrometric data: Journal of Analytical Atomic Spectrometry, v. 26, p. 2508-2518, doi:10.1039/C1JA10172B.

Petrie, M.B., Massonne, H.-J., Gilotti, J.A., McClelland, W.C., and van Staal, C., 2016, The P-T path of eclogites in the St. Cyr klippe, Yukon, Canada: Permian metamorphism of a coherent high-pressure unit in an accreted terrane of the North American Cordillera:

European Journal of Mineralogy, v. 28, no. 6, p. 1111-1130, doi: 10.1127/ejm/2016/0028-2576.

Petrus, J., and Kamber, B.S., 2012, VizualAge: A Novel Approach to Laser Ablation ICP-MS U-Pb Geochronology Data Reduction: Geostandards and Geoanalytical Research, v. 36, 24 p., doi:10.1111/j.1751-908X.2012.00158.x.

Philippot, P., Blichert-Toft, J., Perchuk, A., Costa, S., Gerasimov, V., 2001, Lu-Hf and Ar-Ar chronometry supports extreme rate of subduction zone metamorphism deduced from geospeedometry: Tectonophysics, v. 342, p. 23-38.

Piercey, S.J., and Colpron, M., 2009, Composition and provenance of the Snowcap assemblage, basement to the Yukon-Tanana terrane, northern Cordillera: Implications for Cordilleran crustal growth: Geosphere, v. 5, no. 5, p. 439-464, doi: 10.1130/GS00505.1.

Piercey, S.J., Nelson, J.L., Colpron, M., Dusel-Bacon, C., Simard, R-L. and Roots, C.F., 2006, Paleozoic magmatism and crustal recycling along the ancient Pacific margin of North American, northern Canadian Cordillera, *in* Colpron, M. and Nelson, J.L., eds., Paleozoic Evolution and Metallogeny of Pericratonic Terranes at the Ancient Pacific Margin of North America, Canadian and Alaskan Cordillera: Geological Association of Canada, Special Paper 45, p. 281-322.

Pigage, L.C., 2004, Bedrock geology compilation of the Anvil District (parts of NTS 105K/2, 3, 5, 6, 7, and11), central Yukon: Yukon Geological Survey, Bulletin, v.15, p. 103.

Porter, C., Morin, P., Howat, I., Noh, M-J., Bates, B., Peterman, K., Keesey, S., Schlenk, M., Gardiner, J., Tomko, K., Willis, M., Kelleher, C., Cloutier, M., Husby, E., Foga, S., Nakamura, H., Platson, M., Wethington, M. Jr., Williamson, C., Bauer, G., Enos, J., Arnold, G., Kramer, W., Becker, P., Doshi, A., D'Souza, C., Cummens, P., Laurier, F. and Bojesen, M., 2018. ArcticDEM, https://doi.org/10.7910/DVN/OHHUKH, Harvard Dataverse, vol. 1 [accessed November, 2019].

Roots, C.F., Harms, T.A., Simard, R.-L., Orchard, M.J., and Heaman, L., 2002, Constraints on the age of the Klinkit assemblage east of Teslin Lake, northern British Columbia: Geological Survey of Canada, Current Research 2002-A7, 11p.

Roots, C.F., Nelson, J.L., Simard, R.-L., and Harms, T.A., 2006, Continental fragments, mid-Paleozoic arcs and overlapping late Paleozoic arc and Triassic sedimentary strata in the Yukon-Tanana terrane of northern British Columbia and southern Yukon, *in* Colpron, M. and Nelson, J.L., eds., Paleozoic Evolution and Metallogeny of Pericratonic Terranes at the Ancient Pacific Margin of North America, Canadian and Alaskan Cordillera: Geological Association of Canada, Special Paper 45, p. 153-177.

Ruks, T.W., Piercey, S.J., Ryan, J.J., Villeneuve, M.E., and Creaser, R.A., 2006, Mid- to late Paleozoic K-feldspar augen granitoids of the Yukon-Tanana terrane, Yukon, Canada: Implications for crustal growth and tectonic evolution of the northern Cordillera: Geological Society of America Bulletin, v. 118, no. 9/10, doi: 10.1130/B25854.1.

Simard, R.-L., Dostal, J., and Roots, C.F., 2003, Development of late Paleozoic volcanic arcs in the Canadian Cordillera: An example from the Klinkit Group, northern British Columbia and southern Yukon: Canadian Journal of Earth Sciences, v. 40, p. 907–924, doi:10.1139/e03-025.

Sláma, J., Kosler, J., Condon, D., Crowley, J.L., Gerdes, A., Hanchar, J.M, Horstwood, S.A., Morris, G.A., Nasdala, L., Norberg, N., Schaltegger, U., Schoene, B., Tubrett, M., and

Whitehouse, M.J., 2008, Plešovice zircon – A new natural reference material for U-Pb and Hf isotopic microanalysis: Chemical Geology, v. 249, p. 1-35, doi: 10.1016/j.chemgeo.2007.11.005.

Tempelman-Kluit, D.J., 1972, Geology and origin of the Faro, Vangorda, and Swim concordant zinc-lead deposits, central Yukon Territory: Geological Survey of Canada, Bulletin 208, 73 p.

Unterschutz, J.L.E., Creaser, R.A., Erdmer, P., Thompson, R.I., and Daughtry, K.L., 2002, North American margin origin of Quesnel terrane strata in the southern Canadian Cordillera: Inferences from geochemical and Nd isotopic characteristics of Triassic metasedimentary rocks: Geological Society of America Bulletin, v. 114, no. 4, p. 462-475, doi: 10.1130/0016-7606(2002)114<0462:NAMOOQ>2.0.CO;2.

van Staal, C.R., Zagorevski, A., McClelland, W.C., Escayola, M.P., Ryan, J.J., Parsons, A.J., Proenza, J., 2018, Age and setting of Permian Slide Mountain terrane ophiolitic ultramafic-mafic complexes in the Yukon: Implications for late Paleozoic-early Mesozoic tectonic models in the northern Canadian Cordillera: Tectonophysics, v. 744, p. 458-483, doi: 10.1016/j.tecto.2018.07.008.

Vervoort, J.D., and Blichert-Toft, J., 1999, Evolution of the depleted mantle: Hf isotope evidence from juvenile rocks through time: Geochemica et Cosmochimica Acta, v. 63, p. 533-556, doi: 10.1016/S0016-7037(98)00274-9.

Vervoort, J.D., Patchett, P.J., Blichert-Toft, J., and Albarède, F., 1999, Relationships between Lu-Hf and Sm-Nd isotopic systems in the global sedimentary system: Earth and Planetary Science Letters, v. 168, p. 79-99, doi: 10.1016/S0012-821X(99)00047-3.

Wiedenbeck, M., Allé, P., Corfu, F., Griffin, W.L., Meier, M., Oberli, F., Quadt, A.V., Roddick, J.C., and Spiegel, W., 1995, Three natural zircon standards for U-Th-Pb, Lu-Hf, trace element and REE analyses: Geostandards Newsletter, v. 19, p. 1-23.

Wiest, A.C. and Beranek, L.P., 2019, Stratigraphy of the Faro Peak formation, central Yukon: New field observations of Jurassic synorogenic sedimentation along the Yukon-Tanana–Slide Mountain terrane boundary, *in* Yukon Exploration and Geology 2018, K.E. MacFarlane (ed.), Yukon Geological Survey, p.127–142.

Wiest, A.C., Beranek, L.P., and Manor, M.J., 2020, Upper Triassic to Lower Jurassic stratigraphy of the Faro Peak formation, southern Tay River map area, central Yukon (NTS 105K), *in* Yukon Exploration and Geology 2019, K.E. MacFarlane (ed.), Yukon Geological Survey, p. 121-139.

Yukon Geological Survey, 2020, Yukon digital bedrock geology: Yukon Geological Survey, http://data.geology.gov.yk.ca/Compilation/3, [accessed June, 2020].

APPENDIX 3.A.1

91500
U-Pb standard

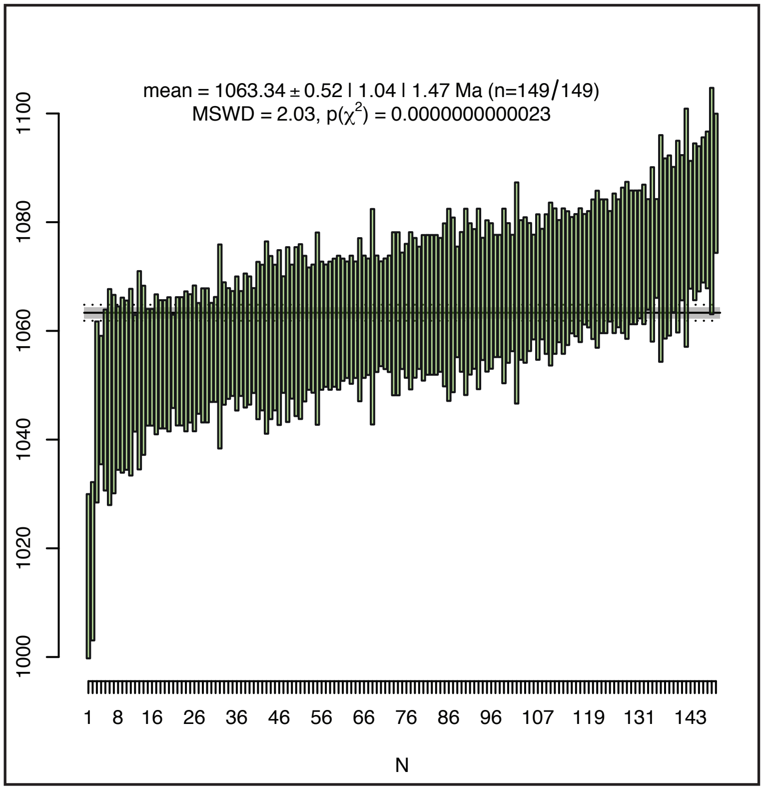

^{176}Hf/^{177}Hf
Plešovice Lu-Hf standard

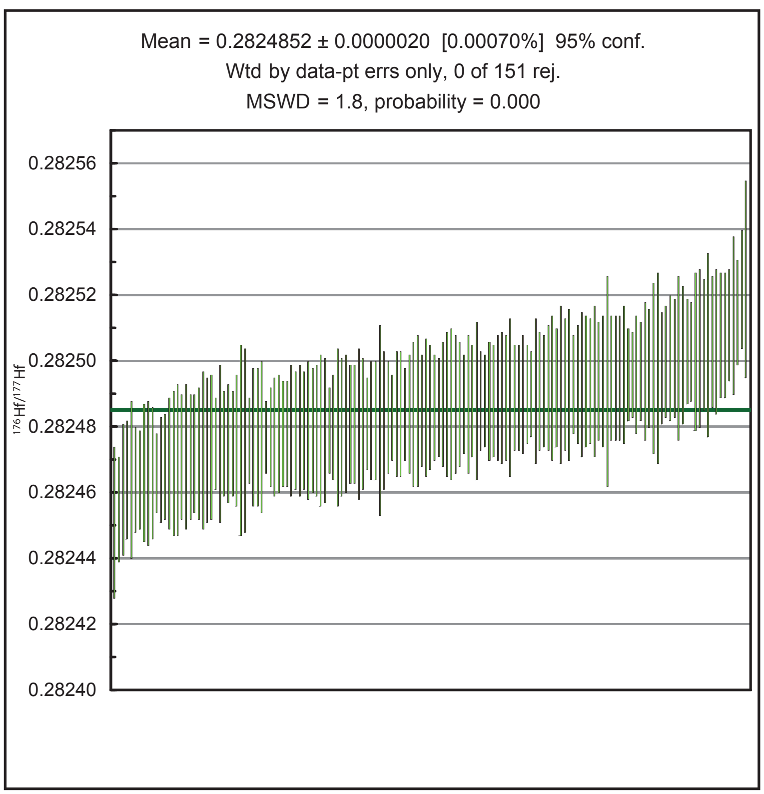

APPENDIX 3.A.2

U-Pb geochronology																	Hf isotope geochemistry								
		Isotopic ratios						Isotopic ages									Isotopic ratios						Epsilon units		
Grain #	Spot name	$^{207}Pb/^{206}Pb$	± 2SE	$^{207}Pb/^{235}U$	± 2SE	$^{206}Pb/^{238}U$	± 2SE	$^{207}Pb/^{206}Pb$	± 2SE (Ma)	$^{207}Pb/^{235}U$	± 2SE (Ma)	$^{206}Pb/^{238}U$	± 2SE (Ma)	Conc. %	Best Age	± 2SE (Ma)	$^{176}Lu/^{177}Hf$	± 2SE	$^{176}Hf/^{177}Hf$	± 2SE	$^{176}Yb/^{177}Hf$	± 2SE	εHf_0	2SE	εHf_t
11AW18--unnamed units; (Zone 08V NAD 83, 586445 E, 6903521 N)																									
13	190212_229.FIN2	0.05270	0.00230	0.2820	0.0130	0.03870	0.00110	316	99	252	10	245	7	N/A	245	7									
23	190212_245.FIN2	0.05370	0.00570	0.2920	0.0310	0.03920	0.00120	358	240	260	24	248	8	N/A	248	8									
140	190829_165.FIN2	0.05270	0.00310	0.2820	0.0140	0.03930	0.00200	316	134	252	11	249	12	N/A	249	12	0.0014900	0.0000580	0.282155	0.000034	0.04050	0.00160	-22.3	1.2	-17.0
66	190829_052.FIN2	0.05210	0.00220	0.2880	0.0150	0.03947	0.00086	290	96	256	12	250	5	N/A	250	5	0.0023600	0.0001200	0.282213	0.000033	0.06460	0.00350	-20.2	1.2	-15.1
89	190829_089.FIN2	0.05190	0.00150	0.2835	0.0099	0.03981	0.00084	281	66	253	8	252	5	N/A	252	5	0.0014690	0.0000670	0.282466	0.000031	0.03990	0.00150	-11.3	1.1	-5.9
97	190829_097.FIN2	0.05240	0.00310	0.2910	0.0170	0.03980	0.00100	303	135	258	14	252	7	N/A	252	7	0.0010940	0.0000220	0.282605	0.000031	0.03013	0.00054	-6.4	1.1	-0.9
78	190829_070.FIN2	0.05210	0.00190	0.2830	0.0110	0.03994	0.00088	290	83	254	9	252	6	N/A	252	6	0.0018920	0.0000980	0.282606	0.000029	0.05360	0.00280	-6.3	1.0	-1.0
126	190829_145.FIN2	0.05300	0.00430	0.2900	0.0230	0.04000	0.00120	329	184	257	18	253	8	N/A	253	8	0.0010930	0.0000690	0.282627	0.000035	0.02980	0.00200	-5.6	1.2	-0.1
81	190829_073.FIN2	0.05240	0.00140	0.2868	0.0079	0.04001	0.00062	303	61	256	6	253	4	N/A	253	4	0.0010770	0.0000490	0.282272	0.000028	0.02820	0.00120	-18.1	1.0	-12.7
90	190829_090.FIN2	0.05190	0.00140	0.2851	0.0076	0.04002	0.00049	281	62	255	6	253	3	N/A	253	3	0.0012800	0.0001800	0.282434	0.000027	0.03410	0.00510	-12.4	1.0	-7.0
31	190828_366.FIN2	0.05200	0.00160	0.2870	0.0090	0.04009	0.00065	285	70	256	7	253	4	N/A	253	4	0.0013000	0.0000200	0.282160	0.000024	0.03530	0.00056	-22.1	0.9	-16.7
49	190829_022.FIN2	0.05180	0.00110	0.2871	0.0074	0.04025	0.00065	277	49	256	6	254	4	N/A	254	4	0.0011190	0.0000390	0.282195	0.000021	0.02990	0.00110	-20.9	0.7	-15.4
68	190829_054.FIN2	0.05250	0.00190	0.2900	0.0130	0.04030	0.00100	307	82	258	10	255	6	N/A	255	6	0.0015420	0.0000410	0.282285	0.000036	0.04170	0.00100	-17.7	1.3	-12.3
62	190829_042.FIN2	0.05210	0.00170	0.2886	0.0099	0.04034	0.00059	290	75	257	8	255	4	N/A	255	4	0.0006589	0.0000045	0.282436	0.000023	0.01727	0.00013	-12.3	0.8	-6.8
76	190829_068.FIN2	0.05200	0.00200	0.2880	0.0120	0.04034	0.00083	285	88	257	9	255	5	N/A	255	5	0.0011919	0.0000090	0.282171	0.000030	0.03164	0.00031	-21.7	1.1	-16.3
94	190829_094.FIN2	0.05260	0.00190	0.2910	0.0100	0.04034	0.00079	312	82	259	8	255	5	N/A	255	5									
121	190829_133.FIN2	0.05220	0.00430	0.2890	0.0270	0.04030	0.00170	294	188	257	21	255	11	N/A	255	11	0.0010700	0.0001200	0.282277	0.000034	0.02880	0.00310	-18.0	1.2	-12.5
32	190828_367.FIN2	0.05230	0.00230	0.2910	0.0130	0.04039	0.00066	299	100	258	10	255	4	N/A	255	4	0.0008670	0.0000270	0.282445	0.000030	0.02345	0.00070	-12.0	1.1	-6.5
50	190829_023.FIN2	0.05200	0.00150	0.2900	0.0100	0.04040	0.00130	285	66	258	8	255	8	N/A	255	8	0.0008580	0.0000110	0.282249	0.000020	0.02178	0.00029	-19.0	0.7	-13.4
143	190829_168.FIN2	0.05240	0.00180	0.2940	0.0120	0.04050	0.00120	303	78	262	10	256	7	N/A	256	7	0.0009420	0.0000280	0.282200	0.000023	0.02408	0.00072	-20.7	0.8	-15.2
44	190829_017.FIN2	0.05160	0.00140	0.2880	0.0074	0.04056	0.00060	268	62	256	6	256	4	N/A	256	4	0.0012650	0.0000210	0.282244	0.000018	0.03361	0.00064	-19.1	0.6	-13.7
98	190829_098.FIN2	0.05180	0.00130	0.2893	0.0077	0.04057	0.00043	277	57	257	6	256	3	N/A	256	3	0.0006920	0.0000250	0.282265	0.000020	0.01807	0.00070	-18.4	0.7	-12.8
75	190829_067.FIN2	0.05310	0.00210	0.2940	0.0120	0.04059	0.00073	333	90	261	9	257	5	N/A	257	5	0.0021550	0.0000950	0.282647	0.000049	0.06030	0.00250	-4.9	1.7	0.5
100	190829_106.FIN2	0.05240	0.00220	0.2930	0.0120	0.04059	0.00075	303	96	260	9	257	5	N/A	257	5	0.0016950	0.0000760	0.282597	0.000029	0.04710	0.00230	-6.6	1.0	-1.2
8	190212_224.FIN2	0.05400	0.00450	0.3040	0.0270	0.04060	0.00150	371	188	269	21	257	10	N/A	257	10	0.0010950	0.0000290	0.282513	0.000032	0.02753	0.00069	-9.6	1.1	-4.1
73	190829_059.FIN2	0.05380	0.00240	0.3000	0.0130	0.04069	0.00096	363	101	266	10	257	6	N/A	257	6									
93	190829_093.FIN2	0.05141	0.00090	0.2889	0.0054	0.04069	0.00040	259	40	258	4	257	3	N/A	257	3	0.0018290	0.0000410	0.282177	0.000024	0.04900	0.00130	-21.5	0.9	-16.1
61	190829_041.FIN2	0.05220	0.00160	0.2913	0.0092	0.04070	0.00065	294	70	259	7	257	4	N/A	257	4	0.0013250	0.0000770	0.282435	0.000022	0.03530	0.00220	-12.4	0.8	-6.9
70	190829_056.FIN2	0.05360	0.00270	0.2990	0.0170	0.04070	0.00150	354	114	265	13	257	9	N/A	257	9	0.0008680	0.0000480	0.282277	0.000028	0.02230	0.00110	-18.0	1.0	-12.4
42	190829_015.FIN2	0.05160	0.00140	0.2908	0.0079	0.04081	0.00049	268	62	259	6	258	3	N/A	258	3	0.0009850	0.0000320	0.282579	0.000031	0.02689	0.00082	-7.3	1.1	-1.7
2	190212_212.FIN2	0.05150	0.00150	0.2900	0.0086	0.04084	0.00048	263	67	259	7	258	3	N/A	258	3	0.0006370	0.0000190	0.282442	0.000024	0.01655	0.00052	-12.1	0.8	-6.5
57	190829_037.FIN2	0.05190	0.00210	0.2930	0.0120	0.04084	0.00074	281	93	260	10	258	5	N/A	258	5									
128	190829_147.FIN2	0.05310	0.00260	0.2960	0.0160	0.04080	0.00140	333	111	263	12	258	9	N/A	258	9	0.0014160	0.0000120	0.282482	0.000039	0.03885	0.00034	-10.7	1.4	-5.2
103	190829_109.FIN2	0.05230	0.00250	0.2940	0.0140	0.04086	0.00092	299	109	261	11	258	6	N/A	258	6	0.0010080	0.0000250	0.282598	0.000027	0.02791	0.00076	-6.6	1.0	-1.0
79	190829_071.FIN2	0.05210	0.00150	0.2930	0.0088	0.04088	0.00064	290	66	260	7	258	4	N/A	258	4									
92	190829_092.FIN2	0.05300	0.00240	0.2960	0.0120	0.04092	0.00085	329	103	263	10	259	5	N/A	259	5	0.0016410	0.0000620	0.282635	0.000040	0.04520	0.00190	-5.3	1.4	0.2
47	190829_020.FIN2	0.05170	0.00110	0.2914	0.0066	0.04101	0.00053	272	49	260	5	259	3	N/A	259	3	0.0011920	0.0000410	0.282253	0.000039	0.03180	0.00110	-18.8	1.4	-13.3
34	190828_369.FIN2	0.05130	0.00300	0.2930	0.0190	0.04100	0.00120	254	134	260	15	259	7	N/A	259	7	0.0011710	0.0000470	0.282276	0.000030	0.03170	0.00120	-18.0	1.1	-12.4
65	190829_051.FIN2	0.05190	0.00160	0.2929	0.0084	0.04103	0.00051	281	71	260	7	259	3	N/A	259	3	0.0009680	0.0000280	0.282466	0.000029	0.02486	0.00070	-11.3	1.0	-5.7
60	190829_040.FIN2	0.05210	0.00150	0.2950	0.0110	0.04110	0.00079	290	66	262	9	260	5	N/A	260	5	0.0011840	0.0000310	0.282190	0.000027	0.03154	0.00087	-21.0	1.0	-15.5
138	190829_163.FIN2	0.05210	0.00170	0.2950	0.0110	0.04110	0.00066	290	75	262	9	260	4	N/A	260	4	0.0013920	0.0000580	0.282246	0.000032	0.03710	0.00160	-19.1	1.1	-13.5
48	190829_021.FIN2	0.05220	0.00180	0.2930	0.0110	0.04115	0.00075	294	79	260	9	260	5	N/A	260	5	0.0008680	0.0000300	0.282229	0.000025	0.02289	0.00086	-19.7	0.9	-14.0
27	190212_249.FIN2	0.05180	0.00460	0.2960	0.0370	0.04110	0.00360	277	203	263	29	260	22	N/A	260	22									
67	190829_053.FIN2	0.05210	0.00170	0.2933	0.0096	0.04116	0.00089	290	75	261	8	260	6	N/A	260	6	0.0018250	0.0000770	0.282428	0.000028	0.04790	0.00200	-12.6	1.0	-7.2
111	190829_123.FIN2	0.05240	0.00200	0.2950	0.0110	0.04116	0.00066	303	87	262	8	260	4	N/A	260	4	0.0015320	0.0000470	0.282624	0.000026	0.04270	0.00130	-5.7	0.9	-0.2
125	190829_144.FIN2	0.05194	0.00099	0.2938	0.0061	0.04121	0.00052	283	44	261	5	260	3	N/A	260	3	0.0013640	0.0000900	0.282299	0.000028	0.03630	0.00240	-17.2	1.0	-11.6
56	190829_036.FIN2	0.05190	0.00150	0.2960	0.0087	0.04123	0.00048	281	66	262	7	260	3	N/A	260	3	0.0011450	0.0000510	0.282441	0.000027	0.03060	0.00150	-12.2	1.0	-6.6
86	190829_078.FIN2	0.05200	0.00190	0.2970	0.0110	0.04123	0.00071	285	84	263	8	260	4	N/A	260	4	0.0013910	0.0000880	0.282355	0.000036	0.03720	0.00240	-15.2	1.3	-9.7
80	190829_072.FIN2	0.05450	0.00310	0.3080	0.0170	0.04130	0.00130	392	128	272	13	261	8	N/A	261	8	0.0009800	0.0001700	0.282175	0.000026	0.02520	0.00440	-21.6	0.9	-16.0
134	190829_153.FIN2	0.05190	0.00100	0.2949	0.0063	0.04127	0.00047	281	44	262	5	261	3	N/A	261	3	0.0013760	0.0000250	0.282219	0.000023	0.03638	0.00065	-20.0	0.8	-14.5
1	190212_211.FIN2	0.05230	0.00120	0.2972	0.0063	0.04133	0.00042	299	52	264	5	261	3	N/A	261	3	0.0009120	0.0000250	0.282187	0.000023	0.02272	0.00059	-21.1	0.8	-15.5
39	190829_012.FIN2	0.05149	0.00076	0.2945	0.0047	0.04134	0.00038	263	34	262	4	261	2	N/A	261	2	0.0008920	0.0000160	0.282369	0.000020	0.02263	0.00037	-14.7	0.7	-9.1
115	190829_127.FIN2	0.05160	0.00120	0.2948	0.0072	0.04136	0.00047	268	53	262	6	261	3	N/A	261	3	0.0014310	0.0000490	0.282614	0.000030	0.03620	0.00130	-6.0	1.1	-0.5
153	190829_184.FIN2	0.05230	0.00130	0.2948	0.0077	0.04137	0.00059	299	57	262	6	261	4	N/A	261	4	0.0009050	0.0000170	0.282178	0.000027	0.02446	0.00060	-21.5	1.0	-15.8
155	190829_186.FIN2	0.05280	0.00290	0.2990	0.0160	0.04140	0.00100	320	125	265	13	261	6	N/A	261	6	0.0007960	0.0000210	0.282442	0.000030	0.02132	0.00055	-12.1	1.1	-6.5
120	190829_132.FIN2	0.05210	0.00180	0.2960	0.0100	0.04134	0.00055	290	79	262	8	262	3	N/A	262	3	0.0013110	0.0000680	0.282592	0.000026	0.03610	0.00190	-6.8	0.9	-1.2
148	190829_179.FIN2	0.05140	0.00110	0.2962	0.0068	0.04149	0.00042	259	49	263	5	262	3	N/A	262	3	0.0008640	0.0000250	0.282189	0.000022	0.02256	0.00065	-21.1	0.8	-15.4
139	190829_164.FIN2	0.05180	0.00100	0.2967	0.0065	0.04152	0.00055	277	44	263	5	262	3	N/A	262	3	0.0019290	0.0000300	0.282185	0.000040	0.05367	0.00073	-21.2	1.4	-15.7
147	190829_178.FIN2	0.05180	0.00110	0.2967	0.0065	0.04157	0.00049	277	49	263	5	263	3	N/A	263	3	0.0009150	0.0000170	0.282225	0.000019	0.02413	0.00039	-19.8	0.7	-14.1
156	190829_187.FIN2	0.05200	0.00190	0.2970	0.0120	0.04157	0.00065	285	84	263	9	263	4	N/A	263	4	0.0007180	0.0000190	0.282506	0.000023	0.01758	0.00053	-9.9	0.8	-4.2
146	190829_171.FIN2	0.05320	0.00230	0.2980	0.0120	0.04160	0.00120	337	98	265	9	263	7	N/A	263	7	0.0014920	0.0000490	0.282388	0.000027	0.04050	0.00150	-14.0	1.0	-8.5
107	190829_113.FIN2	0.05240	0.00200	0.3000	0.0110	0.04164	0.00079	303	87	266	9	263	5	N/A	263	5	0.0013040	0.0000580	0.282267	0.000028	0.03460	0.00170	-18.3	1.0	-12.7
108	190829_114.FIN2	0.05230	0.00180	0.2980	0.0100	0.04166	0.00070	299	79	265	8	263	4	N/A	263	4	0.0008160	0.0000100	0.282284	0.000044	0.02159	0.00034	-17.7	1.6	-12.0
63	190829_049.FIN2	0.05170	0.00110	0.2973	0.0069	0.04170	0.00060	272	49	264	5	263	4	N/A	263	4	0.0009980	0.0000170	0.282242	0.000023	0.02592	0.00046	-19.2	0.8	-13.5
116	190829_128.FIN2	0.05160	0.00110	0.2966	0.0062	0.04169	0.00041	268	49	264	5	263	3	N/A	263	3	0.0007030	0.0000050	0.282230	0.000020	0.01842	0.00012	-19.6	0.7	-13.9
101	190829_107.FIN2	0.05260	0.00200	0.2980	0.0110	0.04180	0.00100	312	87	264	9	264	6	N/A	264	6	0.0012230	0.0000450	0.282424	0.000025	0.03250	0.00120	-12.8	0.9	-7.1
152	190829_183.FIN2	0.05170	0.00140	0.2976	0.0073	0.04178	0.00053	272	62	264	6	264	3	N/A	264	3	0.0008590	0.0000240	0.282484	0.000022	0.02105	0.00051	-10.6	0.8	-4.9
154	190829_185.FIN2	0.05300	0.00260	0.3040	0.0160	0.04180	0.00100	329	111	269	12	264	6	N/A	264	6	0.0012930	0.0000500	0.282353	0.000038	0.03530	0.00150	-15.3	1.3	-9.6
5	190212_215.FIN2	0.05280	0.00230	0.3050	0.0130	0.04181	0.00056	320	99	268	10	264	4	N/A	264	4	0.0010230	0.0000220	0.282842	0.000032	0.02286	0.00060	2.0	1.1	7.7
33	190828_368.FIN2	0.05183	0.00079	0.2995	0.0047	0.04186	0.00043	278	35	266	4	264	3	N/A	264	3	0.0008690	0.0000110	0.282156	0.000021	0.02345	0.00033	-22.2	0.7	-16.5
43	190829_016.FIN2	0.05230	0.00110	0.3012	0.0067	0.04186	0.00051	299	48	267	5	264	3	N/A	264	3	0.0008020	0.0000100	0.282233	0.000026	0.02137	0.00028	-19.5	0.9	-13.8
87	190829_087.FIN2	0.05230	0.00180	0.3028	0.0099	0.04185	0.00080	299	79	268	8	264	5	N/A	264	5	0.0018540	0.0000670	0.282156	0.000030	0.04960	0.00170	-22.2	1.1	-16.7
117	190829_129.FIN2	0.05220	0.00140	0.2991	0.0091	0.04186	0.00069	294	61	265	7	264	4	N/A	264	4	0.0009490	0.0000940	0.282315	0.000028	0.02540	0.00270	-16.6	1.0	-10.9
99	190829_105.FIN2	0.05260	0.00170	0.3001	0.0094	0.04187	0.00066	312	74	266	7	264	4	N/A	264	4	0.0014280	0.0000690	0.282518	0.000026	0.03770	0.00200	-9.4	0.9	-3.8
136	190829_161.FIN2	0.05250	0.00150	0.3010	0.0084	0.04182	0.00047	307	65	266	7	265	3	N/A	265	3	0.0011670	0.0000580	0.282313	0.000028	0.03070	0.00160	-16.7	1.0	-11.0
132	190829_151.FIN2	0.05200	0.00170	0.2988	0.0098	0.04191	0.00055	285	75	265	8	265	3	N/A	265	3	0.0008200	0.0000220	0.282153	0.000022	0.02048	0.00040	-22.3	0.8	-16.6
41	190829_014.FIN2	0.05153	0.00081	0.2984	0.0051	0.04194	0.00044	265	36	265	4	265	3	N/A	265	3	0.0014730	0.0000370	0.282155	0.000023	0.03839	0.00091	-22.3	0.8	-16.7
18	190212_234.FIN2	0.05172	0.00097	0.3001	0.0057	0.04202	0.00035	273	43	266	4	265	2	N/A	265	2	0.0007650	0.0000380	0.282140	0.000026	0.01990	0.00090	-22.8	0.9	-17.1
58	190829_038.FIN2	0.05171	0.00083	0.2998	0.0054	0.04202	0.00046	273	37	266	4	265	3	N/A	265	3	0.0013410	0.0000330	0.282170	0.000021	0.03499	0.00096	-21.7	0.7	-16.1
21	190212_243.FIN2	0.05220	0.00170	0.3050	0.0120	0.04212	0.00098	294	74	270	9	266	6	N/A	266	6	0.0011410	0.0000770	0.282224	0.000034	0.03040	0.00190	-19.8	1.2	-14.1
88	190829_088.FIN2	0.05290	0.00440	0.3080	0.0280	0.04210	0.00140	325	189	270	21	266	9	N/A	266	9	0.0010660	0.0000540	0.282621	0.000031	0.02890	0.00150	-5.8	1.1	-0.1
124	190829_143.FIN2	0.05350	0.00470	0.3110	0.0340	0.04210	0.00260	350	199	274	25	266	16	N/A	266	16	0.0010580	0.0000330	0.282310	0.000043	0.02894	0.00090	-16.8	1.5	-11.1
29	190212_251.FIN2	0.05290	0.00310	0.3110	0.0200	0.04210	0.00110	325	133	274	15	266	7	N/A	266	7	0.0007370	0.0000160	0.282133	0.000035	0.02056	0.00050	-23.1	1.2	-17.3
35	190828_370.FIN2	0.05170	0.00160	0.3040	0.0110	0.04217	0.00069	272	71	269	9	266	4	N/A	266	4	0.0008310	0.0000290	0.282142	0.000025	0.02211	0.00083	-22.7	0.9	-17.0
59	190829_039.FIN2	0.05130	0.00140	0.3021	0.0084	0.04220	0.00046	254	63	267	7	266	3	N/A	266	3	0.0008250	0.0000170	0.282253	0.000031	0.02055	0.00035	-18.8	1.1	-13.0
118	190829_130.FIN2	0.05220	0.00140	0.3036	0.0085	0.04219	0.00057	294	61	269	7	266	4	N/A	266	4	0.0020300	0.0002000	0.282265	0.000029	0.05590	0.00550	-18.4	1.0	-12.8
130	190829_149.FIN2	0.05186	0.00099	0.2997	0.0056	0.04215	0.00041	279	44	267	5	266	3	N/A	266	3	0.0009334	0.0000069	0.282497	0.000019	0.02320	0.00015	-10.2	0.7	-4.4
74	190829_060.FIN2	0.05270	0.00150	0.3048	0.0087	0.04221	0.00090	316	65	270	7	267	6	N/A	267	6	0.0013780	0.0000980	0.282261	0.000023	0.03710	0.00260	-18.5	0.8	-12.9
53	190829_033.FIN2	0.05290	0.00230	0.3070	0.0180	0.04220	0.00110	325	99	271	14	267	7	N/A	267	7	0.0023490	0.0000560	0.282319	0.000024	0.06490	0.00130	-16.5	0.9	-11.0
123	190829_142.FIN2	0.05200	0.00120	0.3034	0.0074	0.04224	0.00058	285	53	269	6	267	4	N/A	267	4	0.0010900	0.0001300	0.282433	0.000027	0.02910	0.00350	-12.4	1.0	-6.7
133	190829_152.FIN2	0.05230	0.00160	0.3040	0.0100	0.04237	0.00065	299	70	269	8	268	4	N/A	268	4									
106	190829_112.FIN2	0.05190	0.00110	0.3037	0.0063	0.04241	0.00041	281	49	270	5	268	3	N/A	268	3	0.0007260	0.0000170	0.282265	0.000024	0.01891	0.00051	-18.4	0.9	-12.6
110	190829_116.FIN2	0.05240	0.00150	0.3080	0.0120	0.04247	0.00092	303	65	272	9	268	6	N/A	268	6	0.0011990	0.0000540	0.282142	0.000025	0.03110	0.00130	-22.7	0.9	-17.0
45	190829_018.FIN2	0.05190	0.00160	0.3050	0.0100	0.04249	0.00062	281	71	270	8	268	4	N/A	268	4	0.0014630	0.0000300	0.282250	0.000032	0.03785	0.00083	-18.9	1.1	-13.2
144	190829_169.FIN2	0.05320	0.00210	0.3080	0.0110	0.04254	0.00063	337	89	271	8	269	4	N/A	269	4	0.0012560	0.0000710	0.282279	0.000035	0.03410	0.00200	-17.9	1.2	-12.2
150	190829_181.FIN2	0.05180	0.00100	0.3026	0.0063	0.04254	0.00045	277	44	269	5	269	3	N/A	269	3	0.0009700	0.0001300	0.282187	0.000023	0.02570	0.00370	-21.1	0.8	-15.4

U-Pb geochronology																	Hf isotope geochemistry								
		Isotopic ratios						Isotopic ages									Isotopic ratios						Epsilon units		
Grain #	Spot name	$^{207}Pb/^{206}Pb$	± 2SE	$^{207}Pb/^{235}U$	± 2SE	$^{206}Pb/^{238}U$	± 2SE	$^{207}Pb/^{206}Pb$	± 2SE (Ma)	$^{207}Pb/^{235}U$	± 2SE (Ma)	$^{206}Pb/^{238}U$	± 2SE (Ma)	Conc. %	Best Age	± 2SE (Ma)	$^{176}Lu/^{177}Hf$	± 2SE	$^{176}Hf/^{177}Hf$	± 2SE	$^{176}Yb/^{177}Hf$	± 2SE	εHf_0	2SE	εHf_t
112	190829_124.FIN2	0.05220	0.00150	0.3070	0.0110	0.04259	0.00089	294	66	271	8	269	6	N/A	269	6	0.0012090	0.0000240	0.282152	0.000026	0.03271	0.00059	-22.4	0.9	-16.6
52	190829_032.FIN2	0.05170	0.00120	0.3065	0.0078	0.04263	0.00049	272	53	271	6	269	3	N/A	269	3	0.0014200	0.0000360	0.282196	0.000031	0.03720	0.00110	-20.8	1.1	-15.1
16	190212_232.FIN2	0.05200	0.00170	0.3080	0.0097	0.04272	0.00056	285	75	272	8	270	4	N/A	270	4	0.0012400	0.0001100	0.282225	0.000026	0.03330	0.00320	-19.8	0.9	-14.0
77	190829_069.FIN2	0.05290	0.00150	0.3093	0.0097	0.04287	0.00088	325	64	273	8	271	5	N/A	271	5	0.0011530	0.0000280	0.282141	0.000025	0.02892	0.00058	-22.8	0.9	-17.0
54	190829_034.FIN2	0.05250	0.00180	0.3100	0.0120	0.04293	0.00088	307	78	274	9	271	6	N/A	271	6									
36	190828_371.FIN2	0.05200	0.00550	0.3080	0.0290	0.04300	0.00150	285	242	272	23	271	9	N/A	271	9	0.0005000	0.0000130	0.282509	0.000019	0.01273	0.00040	-9.8	0.7	-3.8
141	190829_166.FIN2	0.05150	0.00170	0.3080	0.0110	0.04299	0.00076	263	76	272	9	271	5	N/A	271	5	0.0009170	0.0000270	0.282293	0.000024	0.02249	0.00073	-17.4	0.9	-11.5
40	190829_013.FIN2	0.05210	0.00130	0.3089	0.0085	0.04302	0.00063	290	57	273	7	272	4	N/A	272	4	0.0008540	0.0000230	0.282228	0.000029	0.02242	0.00060	-19.7	1.0	-13.8
4	190212_214.FIN2	0.05170	0.00140	0.3088	0.0085	0.04306	0.00051	272	62	273	7	272	3	N/A	272	3	0.0006210	0.0000280	0.282180	0.000026	0.01575	0.00072	-21.4	0.9	-15.5
131	190829_150.FIN2	0.05250	0.00200	0.3100	0.0120	0.04314	0.00087	307	87	274	9	272	5	N/A	272	5	0.0018900	0.0001200	0.282520	0.000031	0.05070	0.00330	-9.4	1.1	-3.7
122	190829_134.FIN2	0.05300	0.00200	0.3140	0.0120	0.04330	0.00110	329	86	277	9	273	7	N/A	273	7	0.0009380	0.0000510	0.282285	0.000043	0.02580	0.00170	-17.7	1.5	-11.8
151	190829_182.FIN2	0.05310	0.00240	0.3150	0.0140	0.04329	0.00080	333	102	277	11	273	5	N/A	273	5	0.0009310	0.0000100	0.282170	0.000021	0.02419	0.00022	-21.7	0.7	-15.8
55	190829_035.FIN2	0.05210	0.00110	0.3107	0.0076	0.04338	0.00052	290	48	274	6	274	3	N/A	274	3	0.0007070	0.0000130	0.282156	0.000019	0.01838	0.00037	-22.2	0.7	-16.3
158	190829_189.FIN2	0.05160	0.00120	0.3104	0.0083	0.04338	0.00060	268	53	274	6	274	4	N/A	274	4	0.0008740	0.0000250	0.282144	0.000020	0.02264	0.00057	-22.7	0.7	-16.7
149	190829_180.FIN2	0.05270	0.00210	0.3170	0.0120	0.04377	0.00069	316	91	279	10	276	4	N/A	276	4	0.0008070	0.0000720	0.282468	0.000028	0.02160	0.00200	-11.2	1.0	-5.2
6	190212_222.FIN2	0.05310	0.00270	0.3260	0.0170	0.04407	0.00097	333	115	286	13	278	6	N/A	278	6									
25	190212_247.FIN2	0.05200	0.00140	0.3205	0.0090	0.04435	0.00057	285	62	282	7	280	4	N/A	280	4	0.0009610	0.0000390	0.282182	0.000033	0.02610	0.00120	-21.3	1.2	-15.3
127	190829_146.FIN2	0.05560	0.00390	0.3410	0.0230	0.04490	0.00140	436	156	298	18	283	9	N/A	283	9	0.0007440	0.0000430	0.282220	0.000030	0.01910	0.00120	-20.0	1.1	-13.8
95	190829_095.FIN2	0.08850	0.00330	2.8500	0.1400	0.23540	0.00990	1393	72	1366	37	1361	52	98	1393	72	0.0007837	0.0000081	0.281926	0.000028	0.02013	0.00019	-30.4	1.0	0.2
157	190829_188.FIN2	0.09220	0.00130	3.2240	0.0570	0.25420	0.00350	1472	27	1460	14	1460	18	99	1472	27	0.0012010	0.0000230	0.281952	0.000021	0.03189	0.00063	-29.5	0.7	2.5
46	190829_019.FIN2	0.10970	0.00420	4.7700	0.1800	0.31400	0.01000	1794	70	1777	32	1762	49	98	1794	70	0.0003590	0.0000300	0.281749	0.000035	0.00936	0.00090	-36.6	1.2	3.4
119	190829_131.FIN2	0.10990	0.00390	4.8200	0.2200	0.31800	0.01200	1798	65	1787	38	1782	60	99	1798	65	0.0015450	0.0000460	0.281576	0.000034	0.04140	0.00130	-42.8	1.2	-4.1
9	190212_225.FIN2	0.13570	0.00180	7.0200	0.1600	0.37150	0.00610	2173	23	2112	20	2036	29	94	2173	23	0.0008520	0.0000830	0.281492	0.000035	0.02330	0.00230	-45.7	1.2	2.2
129	190829_148.FIN2	0.19080	0.00380	13.9800	0.3900	0.53100	0.01400	2749	33	2744	27	2742	57	100	2749	33	0.0004130	0.0000190	0.281156	0.000021	0.00966	0.00031	-57.6	0.7	4.2
rejected analysis																									
3	190212_213.FIN2	0.11000	0.01000	0.6550	0.0590	0.04340	0.00140	1799	165	508	35	274	9	15	N/A	N/A	0.0009360	0.0000110	0.282472	0.000024	0.02312	0.00030	-11.1	0.8	N/A
7	190212_223.FIN2	0.06090	0.00290	0.3120	0.0130	0.03709	0.00086	636	102	276	10	235	5	N/A	N/A	N/A									
10	190212_226.FIN2	0.05480	0.00340	0.3220	0.0190	0.04240	0.00110	404	139	284	15	268	7	N/A	N/A	N/A									
11	190212_227.FIN2	0.05510	0.00150	0.3120	0.0110	0.04110	0.00150	416	61	275	8	259	9	N/A	N/A	N/A									
12	190212_228.FIN2	0.11050	0.00430	0.6600	0.0240	0.04302	0.00070	1808	71	514	15	272	4	15	N/A	N/A									
14	190212_230.FIN2	0.16900	0.01500	1.0300	0.1100	0.04360	0.00220	2548	149	713	57	275	13	11	N/A	N/A									
15	190212_231.FIN2	0.10440	0.00830	0.6610	0.0480	0.04590	0.00130	1704	146	512	28	289	8	17	N/A	N/A									
17	190212_233.FIN2	0.12800	0.01100	0.6670	0.0570	0.03770	0.00200	2071	151	516	34	239	12	12	N/A	N/A									
19	190212_235.FIN2	0.06290	0.00820	0.3530	0.0460	0.04070	0.00150	705	277	306	34	257	10	N/A	N/A	N/A									
20	190212_242.FIN2	0.08710	0.00450	0.5450	0.0270	0.04500	0.00110	1363	100	441	18	284	7	21	N/A	N/A									
22	190212_244.FIN2	0.06160	0.00230	0.3410	0.0150	0.04020	0.00150	660	80	298	11	254	10	N/A	N/A	N/A									
24	190212_246.FIN2	0.12200	0.01000	1.0730	0.0900	0.06350	0.00280	1986	146	734	45	397	17	20	N/A	N/A									
26	190212_248.FIN2	0.06550	0.00530	0.3710	0.0280	0.04100	0.00150	790	170	320	21	259	9	N/A	N/A	N/A									
28	190212_250.FIN2	0.10900	0.01300	0.5940	0.0600	0.03960	0.00180	1783	217	471	38	251	11	14	N/A	N/A									
30	190212_252.FIN2	0.12380	0.00530	4.8900	0.2400	0.28730	0.00920	2012	76	1797	43	1627	46	81	N/A	N/A									
37	190828_372.FIN2	0.20100	0.01400	1.2510	0.0990	0.04499	0.00082	2834	114	805	43	284	5	10	N/A	N/A	0.0009050	0.0000860	0.282240	0.000035	0.02550	0.00250	-19.3	1.2	N/A
38	190828_373.FIN2	0.11600	0.01100	0.6980	0.0720	0.04390	0.00100	1895	171	521	41	277	7	15	N/A	N/A	0.0006040	0.0000460	0.282796	0.000033	0.01450	0.00110	0.4	1.2	N/A
51	190829_031.FIN2	0.07030	0.00670	0.4190	0.0470	0.04230	0.00120	937	195	349	30	267	8	N/A	N/A	N/A	0.0007190	0.0000320	0.282246	0.000033	0.01881	0.00093	-19.1	1.2	N/A
64	190829_050.FIN2	0.07630	0.00300	0.5240	0.0240	0.04950	0.00120	1103	79	426	16	312	7	28	N/A	N/A	0.0012670	0.0000430	0.282358	0.000025	0.03310	0.00100	-15.1	0.9	N/A
69	190829_055.FIN2	0.06360	0.00190	0.3440	0.0120	0.03942	0.00074	728	63	300	9	249	5	N/A	N/A	N/A	0.0008200	0.0000260	0.282298	0.000030	0.02124	0.00056	-17.2	1.1	N/A
71	190829_057.FIN2	0.06650	0.00240	0.3620	0.0140	0.03973	0.00083	822	75	313	11	251	5	N/A	N/A	N/A	0.0010530	0.0000860	0.282171	0.000030	0.02830	0.00220	-21.7	1.1	N/A
72	190829_058.FIN2	0.05560	0.00150	0.2948	0.0084	0.03869	0.00084	436	60	262	7	245	5	N/A	N/A	N/A	0.0011840	0.0000710	0.282205	0.000025	0.03220	0.00210	-20.5	0.9	N/A
82	190829_074.FIN2	0.07730	0.00320	0.4290	0.0220	0.04016	0.00098	1129	82	361	16	254	6	22	N/A	N/A	0.0007488	0.0000049	0.282262	0.000040	0.01917	0.00021	-18.5	1.4	N/A
83	190829_075.FIN2	0.05480	0.00350	0.2960	0.0190	0.03950	0.00098	404	143	263	15	250	6	N/A	N/A	N/A	0.0008700	0.0001200	0.282246	0.000022	0.02320	0.00340	-19.1	0.8	N/A
84	190829_076.FIN2	0.07480	0.00300	0.4180	0.0210	0.04070	0.00110	1063	81	354	15	257	7	24	N/A	N/A	0.0013050	0.0000430	0.282431	0.000028	0.03380	0.00120	-12.5	1.0	N/A
85	190829_077.FIN2	0.05830	0.00210	0.3210	0.0110	0.04047	0.00073	541	79	282	8	256	5	N/A	N/A	N/A	0.0007950	0.0000150	0.282296	0.000024	0.02073	0.00055	-17.3	0.9	N/A
91	190829_091.FIN2	0.07910	0.00350	0.4380	0.0190	0.04043	0.00091	1175	88	368	14	256	6	22	N/A	N/A									
96	190829_096.FIN2	0.09480	0.00370	0.5120	0.0200	0.03940	0.00110	1524	74	419	13	249	7	16	N/A	N/A	0.0007300	0.0000210	0.282245	0.000030	0.01958	0.00056	-19.1	1.1	N/A
102	190829_108.FIN2	0.06060	0.00210	0.3500	0.0120	0.04239	0.00082	625	75	304	9	268	5	N/A	N/A	N/A	0.0009380	0.0000500	0.282271	0.000023	0.02500	0.00140	-18.2	0.8	N/A
104	190829_110.FIN2	0.09230	0.00360	0.5480	0.0230	0.04330	0.00089	1474	74	444	15	273	6	19	N/A	N/A	0.0010620	0.0000570	0.282251	0.000038	0.02830	0.00160	-18.9	1.3	N/A
105	190829_111.FIN2	0.06070	0.00250	0.3370	0.0150	0.04053	0.00099	629	89	295	12	256	6	N/A	N/A	N/A									
109	190829_115.FIN2	0.06310	0.00260	0.3500	0.0190	0.04020	0.00130	712	88	304	14	254	8	N/A	N/A	N/A	0.0010810	0.0000960	0.282157	0.000033	0.02790	0.00250	-22.2	1.2	N/A
113	190829_125.FIN2	0.08000	0.00390	0.4620	0.0260	0.04172	0.00083	1197	96	378	15	263	5	22	N/A	N/A	0.0005840	0.0000150	0.282552	0.000030	0.01487	0.00036	-8.2	1.1	N/A
135	190829_160.FIN2	0.05900	0.00290	0.3440	0.0160	0.04250	0.00130	567	107	300	12	268	8	N/A	N/A	N/A	0.0010200	0.0000960	0.282284	0.000021	0.02640	0.00250	-17.7	0.7	N/A
142	190829_167.FIN2	0.05740	0.00250	0.3050	0.0150	0.03876	0.00084	507	96	270	11	245	5	N/A	N/A	N/A	0.0011570	0.0000520	0.282347	0.000027	0.03020	0.00120	-15.5	1.0	N/A
12AW18--unnamed units; (Zone 08V NAD 83, 586118 E, 6903737 N)																									
103	190829_270.FIN2	0.05170	0.00150	0.2616	0.0087	0.03699	0.00056	272	67	235	7	234	4	N/A	234	4	0.0021800	0.0001800	0.282611	0.000033	0.06030	0.00500	-6.2	1.2	-1.3
126	190829_299.FIN2	0.05120	0.00230	0.2680	0.0210	0.03750	0.00200	250	103	240	17	238	13	N/A	238	13	0.0008510	0.0000940	0.282440	0.000048	0.02340	0.00290	-12.2	1.7	-7.0
102	190829_263.FIN2	0.05170	0.00190	0.2679	0.0099	0.03800	0.00110	272	84	241	8	240	7	N/A	240	7	0.0022500	0.0002500	0.282623	0.000043	0.06230	0.00730	-5.7	1.5	-0.7
141	190829_326.FIN2	0.05180	0.00210	0.2700	0.0110	0.03813	0.00069	277	93	242	9	241	4	N/A	241	4	0.0012090	0.0000700	0.282467	0.000027	0.03190	0.00200	-11.2	1.0	-6.1
93	190829_254.FIN2	0.05160	0.00220	0.2710	0.0110	0.03818	0.00075	268	98	243	9	242	5	N/A	242	5	0.0006420	0.0000200	0.282440	0.000027	0.01648	0.00054	-12.2	1.0	-6.9
107	190829_274.FIN2	0.05500	0.00630	0.2870	0.0320	0.03820	0.00160	412	256	255	25	242	10	N/A	242	10	0.0015800	0.0001100	0.282635	0.000052	0.04350	0.00330	-5.3	1.8	-0.2
73	190829_222.FIN2	0.05160	0.00140	0.2728	0.0072	0.03826	0.00045	268	62	245	6	242	3	N/A	242	3	0.0017200	0.0000540	0.282436	0.000027	0.04620	0.00140	-12.3	1.0	-7.2
74	190829_223.FIN2	0.05210	0.00310	0.2760	0.0160	0.03842	0.00085	290	136	249	13	243	5	N/A	243	5	0.0016800	0.0000480	0.282628	0.000030	0.04570	0.00140	-5.6	1.1	-0.4
105	190829_272.FIN2	0.05200	0.00170	0.2726	0.0085	0.03842	0.00057	285	75	244	7	243	4	N/A	243	4	0.0010620	0.0000670	0.282413	0.000029	0.02730	0.00180	-13.2	1.0	-7.9
65	190829_207.FIN2	0.05280	0.00300	0.2790	0.0160	0.03850	0.00068	320	129	248	13	244	4	N/A	244	4	0.0010590	0.0000720	0.282634	0.000036	0.02830	0.00200	-5.3	1.3	-0.1
96	190829_257.FIN2	0.05150	0.00270	0.2730	0.0150	0.03850	0.00086	263	120	244	12	244	5	N/A	244	5	0.0016470	0.0000610	0.282574	0.000034	0.04440	0.00170	-7.5	1.2	-2.3
137	190829_316.FIN2	0.05250	0.00290	0.2760	0.0150	0.03850	0.00120	307	126	247	12	244	7	N/A	244	7	0.0013910	0.0000230	0.282594	0.000032	0.03788	0.00072	-6.8	1.1	-1.6
75	190829_224.FIN2	0.05290	0.00450	0.2790	0.0220	0.03860	0.00170	325	193	249	17	244	11	N/A	244	11	0.0015500	0.0000910	0.282569	0.000047	0.04190	0.00250	-7.6	1.7	-2.5
97	190829_258.FIN2	0.05110	0.00180	0.2750	0.0100	0.03863	0.00049	245	81	245	8	244	3	N/A	244	3	0.0010130	0.0000330	0.282605	0.000022	0.02714	0.00085	-6.4	0.8	-1.1
98	190829_259.FIN2	0.05340	0.00370	0.2830	0.0200	0.03870	0.00110	346	157	252	16	245	7	N/A	245	7	0.0017530	0.0000590	0.282612	0.000033	0.04800	0.00180	-6.1	1.2	-1.0
87	190829_242.FIN2	0.05220	0.00220	0.2770	0.0120	0.03880	0.00110	294	96	248	9	245	7	N/A	245	7	0.0016900	0.0002100	0.282346	0.000026	0.04560	0.00590	-15.5	0.9	-10.4
142	190829_327.FIN2	0.05180	0.00190	0.2760	0.0110	0.03888	0.00065	277	84	247	9	246	4	N/A	246	4	0.0010270	0.0000470	0.282488	0.000030	0.02510	0.00130	-10.5	1.1	-5.2
82	190829_237.FIN2	0.05150	0.00160	0.2750	0.0100	0.03892	0.00077	263	71	246	8	246	5	N/A	246	5	0.0018240	0.0000760	0.282439	0.000028	0.04940	0.00210	-12.2	1.0	-7.1
67	190829_216.FIN2	0.05210	0.00260	0.2800	0.0140	0.03894	0.00076	290	114	249	11	246	5	N/A	246	5	0.0010070	0.0000910	0.282490	0.000031	0.02560	0.00220	-10.4	1.1	-5.1
99	190829_260.FIN2	0.05240	0.00190	0.2810	0.0110	0.03900	0.00120	303	83	251	9	247	7	N/A	247	7	0.0011240	0.0000200	0.282332	0.000025	0.02969	0.00062	-16.0	0.9	-10.7
143	190829_328.FIN2	0.05240	0.00500	0.2790	0.0260	0.03900	0.00120	303	218	249	20	247	7	N/A	247	7	0.0009400	0.0001200	0.282590	0.000038	0.02520	0.00330	-6.9	1.3	-1.6
95	190829_256.FIN2	0.05270	0.00310	0.2810	0.0160	0.03912	0.00085	316	134	253	14	247	5	N/A	247	5	0.0010940	0.0000350	0.282413	0.000034	0.02867	0.00070	-13.2	1.2	-7.8
64	190829_206.FIN2	0.05210	0.00310	0.2790	0.0190	0.03910	0.00140	290	136	249	15	248	9	N/A	248	9	0.0009190	0.0000320	0.282467	0.000035	0.02408	0.00088	-11.2	1.2	-5.9
135	190829_314.FIN2	0.05270	0.00530	0.2820	0.0290	0.03916	0.00091	316	229	252	23	248	6	N/A	248	6									
61	190829_203.FIN2	0.05170	0.00150	0.2789	0.0079	0.03923	0.00050	272	67	249	6	248	3	N/A	248	3	0.0012120	0.0000410	0.282427	0.000022	0.03070	0.00120	-12.7	0.8	-7.3
104	190829_271.FIN2	0.05310	0.00920	0.2850	0.0490	0.03920	0.00140	333	393	251	38	248	9	N/A	248	9	0.0013000	0.0001500	0.282613	0.000039	0.03540	0.00430	-6.1	1.4	-0.8
138	190829_317.FIN2	0.05260	0.00400	0.2820	0.0220	0.03920	0.00150	312	173	251	18	248	9	N/A	248	9	0.0010810	0.0000400	0.282593	0.000044	0.02820	0.00110	-6.8	1.6	-1.5
140	190829_325.FIN2	0.05180	0.00300	0.2810	0.0160	0.03930	0.00070	277	133	249	13	249	4	N/A	249	4	0.0015240	0.0000340	0.282590	0.000037	0.04072	0.00096	-6.9	1.3	-1.6
127	190829_306.FIN2	0.05170	0.00160	0.2797	0.0086	0.03932	0.00044	272	71	249	7	249	3	N/A	249	3	0.0014220	0.0000960	0.282598	0.000028	0.03790	0.00280	-6.6	1.0	-1.3
131	190829_310.FIN2	0.05230	0.00270	0.2810	0.0150	0.03936	0.00081	299	118	250	11	249	5	N/A	249	5	0.0013280	0.0000530	0.282609	0.000038	0.03580	0.00160	-6.2	1.3	-0.9
101	190829_262.FIN2	0.05150	0.00740	0.2860	0.0440	0.03930	0.00210	263	330	251	34	249	13	N/A	249	13	0.0009570	0.0000170	0.282616	0.000025	0.02560	0.00053	-6.0	0.9	-0.6
91	190829_252.FIN2	0.05320	0.00510	0.2840	0.0230	0.03940	0.00160	337	217	253	18	249	10	N/A	249	10	0.0012580	0.0000540	0.282631	0.000041	0.03380	0.00160	-5.4	1.5	-0.1
88	190829_243.FIN2	0.05240	0.00210	0.2830	0.0120	0.03942	0.00065	303	91	255	9	249	4	N/A	249	4	0.0016800	0.0000620	0.282636	0.000047	0.04580	0.00180	-5.3	1.7	0.0
63	190829_205.FIN2	0.05160	0.00340	0.2830	0.0240	0.03940	0.00150	268	151	252	19	249	9	N/A	249	9	0.0015900	0.0001100	0.282451	0.000025	0.04310	0.00310	-11.8	0.9	-6.5
159	190829_351.FIN2	0.05220	0.00230	0.2860	0.0140	0.03958	0.00086	294	101	255	11	250	5	N/A	250	5	0.0013590	0.0000400	0.282594	0.000039	0.03710	0.00110	-6.8	1.4	-1.4
139	190829_324.FIN2	0.05220	0.00220	0.2830	0.0130	0.03960	0.00075	294	96	252	10	250	5	N/A	250	5	0.0008912	0.0000096	0.282449	0.000043	0.02205	0.00023	-11.9	1.5	-6.5
81	190829_236.FIN2	0.05180	0.00140	0.2815	0.0083	0.03965	0.00057	277	62	251	7	251	4	N/A	251	4	0.0010350	0.0000550	0.282447	0.000024	0.02630	0.00140	-12.0	0.8	-6.6
32	190212_103.FIN2	0.05360	0.00300	0.2930	0.0150	0.03967	0.00093	354	126	261	12	251	6	N/A	251	6	0.0011990	0.0000140	0.282497	0.000036	0.03242	0.00036	-10.2	1.3	-4.8
100	190829_261.FIN2	0.05160	0.00140	0.2833	0.0082	0.03969	0.00061	268	62	252	6	251	4	N/A	251	4	0.0012370	0.0000300	0.282464	0.000028	0.03250	0.00087	-11.4	1.0	-6.0

U-Pb geochronology																	Hf isotope geochemistry								
		Isotopic ratios						Isotopic ages									Isotopic ratios						Epsilon units		
Grain #	Spot name	$^{207}Pb/^{206}Pb$	± 2SE	$^{207}Pb/^{235}U$	± 2SE	$^{206}Pb/^{238}U$	± 2SE	$^{207}Pb/^{206}Pb$	± 2SE (Ma)	$^{207}Pb/^{235}U$	± 2SE (Ma)	$^{206}Pb/^{238}U$	± 2SE (Ma)	Conc. %	Best Age	± 2SE (Ma)	$^{176}Lu/^{177}Hf$	± 2SE	$^{176}Hf/^{177}Hf$	± 2SE	$^{176}Yb/^{177}Hf$	± 2SE	εHf_0	2SE	εHf_t
36	190212_107.FIN2	0.05340	0.00430	0.2930	0.0240	0.03970	0.00140	346	182	260	19	251	9	N/A	251	9	0.0011790	0.0000200	0.282622	0.000046	0.03198	0.00065	-5.8	1.6	-0.4
122	190829_295.FIN2	0.05270	0.00320	0.2890	0.0170	0.03977	0.00094	316	138	256	13	251	6	N/A	251	6	0.0013260	0.0000520	0.282446	0.000028	0.03530	0.00150	-12.0	1.0	-6.6
6	190212_065.FIN2	0.05380	0.00600	0.2960	0.0340	0.03990	0.00150	363	252	262	27	252	9	N/A	252	9									
92	190829_253.FIN2	0.05250	0.00300	0.2870	0.0170	0.03988	0.00099	307	130	255	13	252	6	N/A	252	6	0.0009490	0.0000260	0.282432	0.000022	0.02437	0.00082	-12.5	0.8	-7.0
94	190829_255.FIN2	0.05180	0.00190	0.2830	0.0110	0.03988	0.00051	277	84	253	9	252	3	N/A	252	3	0.0010171	0.0000043	0.282609	0.000025	0.02696	0.00013	-6.2	0.9	-0.8
70	190829_219.FIN2	0.05200	0.00150	0.2847	0.0083	0.03992	0.00068	285	66	254	7	252	4	N/A	252	4	0.0005690	0.0000460	0.282432	0.000015	0.01500	0.00140	-12.5	0.5	-7.0
150	190829_335.FIN2	0.05180	0.00220	0.2830	0.0120	0.03992	0.00073	277	97	252	10	252	5	N/A	252	5	0.0014510	0.0000890	0.282648	0.000032	0.03900	0.00250	-4.8	1.1	0.5
43	190212_120.FIN2	0.05200	0.00200	0.2861	0.0096	0.04003	0.00094	285	88	255	8	253	6	N/A	253	6	0.0009660	0.0000960	0.282280	0.000032	0.02470	0.00260	-17.9	1.1	-12.4
69	190829_218.FIN2	0.05340	0.00480	0.2930	0.0280	0.04010	0.00160	346	203	260	22	253	10	N/A	253	10	0.0010400	0.0000530	0.282615	0.000031	0.02750	0.00150	-6.0	1.1	-0.6
79	190829_234.FIN2	0.05160	0.00210	0.2860	0.0120	0.04007	0.00062	268	93	254	9	253	4	N/A	253	4	0.0008610	0.0000110	0.282601	0.000027	0.02246	0.00028	-6.5	1.0	-1.0
13	190212_078.FIN2	0.05260	0.00320	0.2910	0.0190	0.04009	0.00075	312	138	258	15	253	5	N/A	253	5									
68	190829_217.FIN2	0.05270	0.00260	0.2910	0.0140	0.04016	0.00073	316	112	258	11	254	5	N/A	254	5	0.0011130	0.0000250	0.282603	0.000028	0.02984	0.00068	-6.4	1.0	-1.0
56	190829_198.FIN2	0.05290	0.00260	0.2910	0.0130	0.04028	0.00081	325	112	258	10	255	5	N/A	255	5	0.0011460	0.0000370	0.282577	0.000023	0.03080	0.00110	-7.4	0.8	-1.9
3	190212_062.FIN2	0.05230	0.00310	0.2910	0.0190	0.04029	0.00084	299	135	259	15	255	5	N/A	255	5	0.0010160	0.0000270	0.282513	0.000038	0.02639	0.00059	-9.6	1.3	-4.1
157	190829_349.FIN2	0.05360	0.00300	0.2920	0.0140	0.04036	0.00079	354	126	259	11	255	5	N/A	255	5	0.0015900	0.0001400	0.282640	0.000040	0.04420	0.00440	-5.1	1.4	0.3
84	190829_239.FIN2	0.05170	0.00130	0.2874	0.0076	0.04037	0.00042	272	58	256	6	255	3	N/A	255	3	0.0008950	0.0000250	0.282429	0.000030	0.02289	0.00060	-12.6	1.1	-7.1
8	190212_067.FIN2	0.05300	0.00490	0.2940	0.0270	0.04040	0.00120	329	210	261	21	255	8	N/A	255	8									
86	190829_241.FIN2	0.05180	0.00140	0.2879	0.0075	0.04039	0.00041	277	62	257	6	255	3	N/A	255	3	0.0012600	0.0000460	0.282447	0.000030	0.03240	0.00130	-12.0	1.1	-6.5
62	190829_204.FIN2	0.05300	0.00250	0.2940	0.0170	0.04040	0.00130	329	107	262	13	255	8	N/A	255	8	0.0018270	0.0000870	0.282323	0.000021	0.04930	0.00250	-16.3	0.7	-11.0
83	190829_238.FIN2	0.05310	0.00250	0.2950	0.0140	0.04040	0.00120	333	107	262	11	256	7	N/A	256	7	0.0016930	0.0000630	0.282470	0.000029	0.04490	0.00180	-11.1	1.0	-5.7
90	190829_245.FIN2	0.05370	0.00290	0.2960	0.0150	0.04040	0.00150	358	122	263	11	256	9	N/A	256	9	0.0007520	0.0000370	0.282558	0.000032	0.01940	0.00100	-8.0	1.1	-2.5
60	190829_202.FIN2	0.05210	0.00180	0.2900	0.0110	0.04047	0.00076	290	79	258	8	256	5	N/A	256	5	0.0015090	0.0000390	0.282190	0.000027	0.03930	0.00110	-21.0	1.0	-15.6
24	190212_089.FIN2	0.05290	0.00200	0.2930	0.0110	0.04054	0.00055	325	86	262	9	256	3	N/A	256	3	0.0008100	0.0000110	0.282459	0.000027	0.02077	0.00030	-11.5	1.0	-6.0
146	190829_331.FIN2	0.05270	0.00310	0.2930	0.0200	0.04050	0.00130	316	134	259	15	256	8	N/A	256	8	0.0010190	0.0000380	0.282588	0.000031	0.02740	0.00100	-7.0	1.1	-1.4
152	190829_344.FIN2	0.05190	0.00230	0.2880	0.0140	0.04050	0.00120	281	101	257	11	256	7	N/A	256	7	0.0007369	0.0000065	0.282284	0.000021	0.01889	0.00022	-17.7	0.7	-12.2
89	190829_244.FIN2	0.05250	0.00190	0.2930	0.0110	0.04059	0.00070	307	82	260	9	257	4	N/A	257	4	0.0015830	0.0000400	0.282461	0.000031	0.04140	0.00120	-11.5	1.1	-6.0
30	190212_101.FIN2	0.05170	0.00250	0.2890	0.0140	0.04063	0.00070	272	111	257	11	257	4	N/A	257	4	0.0011340	0.0000580	0.282598	0.000037	0.03010	0.00180	-6.6	1.3	-1.1
18	190212_083.FIN2	0.05320	0.00320	0.2970	0.0160	0.04070	0.00110	337	136	264	13	257	7	N/A	257	7	0.0016700	0.0000500	0.282458	0.000035	0.04350	0.00150	-11.6	1.2	-6.1
17	190212_082.FIN2	0.05310	0.00480	0.2990	0.0310	0.04070	0.00130	333	205	264	24	257	8	N/A	257	8	0.0009690	0.0000200	0.282568	0.000026	0.02604	0.00061	-7.7	0.9	-2.1
106	190829_273.FIN2	0.05200	0.00220	0.2910	0.0120	0.04070	0.00110	285	97	259	10	257	7	N/A	257	7	0.0021400	0.0001500	0.282637	0.000051	0.06070	0.00470	-5.2	1.8	0.1
72	190829_221.FIN2	0.05200	0.00140	0.2909	0.0087	0.04077	0.00068	285	62	259	7	258	4	N/A	258	4	0.0012050	0.0000520	0.282286	0.000027	0.03010	0.00160	-17.6	1.0	-12.1
47	190212_124.FIN2	0.05270	0.00310	0.2980	0.0180	0.04100	0.00086	316	134	264	14	259	5	N/A	259	5	0.0009610	0.0000360	0.282628	0.000030	0.02560	0.00100	-5.6	1.1	0.0
59	190829_201.FIN2	0.05240	0.00400	0.2950	0.0190	0.04110	0.00190	303	174	262	15	259	12	N/A	259	12	0.0011800	0.0001300	0.282418	0.000024	0.03180	0.00400	-13.0	0.8	-7.4
155	190829_347.FIN2	0.05370	0.00630	0.2980	0.0330	0.04090	0.00210	358	265	264	25	259	13	N/A	259	13	0.0012000	0.0001100	0.282595	0.000033	0.03220	0.00320	-6.7	1.2	-1.2
1	190212_060.FIN2	0.05230	0.00170	0.2943	0.0098	0.04109	0.00045	299	74	262	8	260	3	N/A	260	3	0.0008200	0.0000340	0.282409	0.000031	0.02071	0.00085	-13.3	1.1	-7.7
31	190212_102.FIN2	0.05210	0.00210	0.2960	0.0120	0.04117	0.00051	290	92	263	9	260	3	N/A	260	3	0.0016420	0.0000660	0.282621	0.000038	0.04500	0.00180	-5.8	1.3	-0.3
51	190212_134.FIN2	0.05170	0.00290	0.2940	0.0160	0.04120	0.00062	272	129	261	13	260	4	N/A	260	4									
49	190212_132.FIN2	0.05330	0.00490	0.3020	0.0280	0.04120	0.00120	342	208	267	22	260	8	N/A	260	8	0.0013400	0.0000730	0.282576	0.000030	0.03630	0.00210	-7.4	1.1	-1.8
85	190829_240.FIN2	0.05300	0.00310	0.3010	0.0170	0.04127	0.00096	329	133	266	14	261	6	N/A	261	6	0.0010570	0.0000960	0.282464	0.000030	0.02740	0.00260	-11.4	1.1	-5.7
11	190212_070.FIN2	0.05260	0.00340	0.2990	0.0190	0.04129	0.00080	312	147	265	15	261	5	N/A	261	5	0.0012040	0.0000660	0.282473	0.000031	0.03260	0.00190	-11.0	1.1	-5.4
54	190212_137.FIN2	0.05270	0.00480	0.3000	0.0250	0.04130	0.00140	316	207	265	20	261	9	N/A	261	9									
156	190829_348.FIN2	0.05210	0.00250	0.2980	0.0150	0.04144	0.00070	290	110	263	12	262	4	N/A	262	4	0.0009590	0.0000680	0.282597	0.000036	0.02560	0.00190	-6.6	1.3	-1.0
52	190212_135.FIN2	0.05230	0.00250	0.2970	0.0140	0.04146	0.00065	299	109	263	11	262	4	N/A	262	4	0.0008190	0.0000420	0.282464	0.000036	0.02110	0.00110	-11.4	1.3	-5.7
48	190212_125.FIN2	0.05270	0.00240	0.3010	0.0130	0.04147	0.00065	316	104	267	10	262	4	N/A	262	4									
35	190212_106.FIN2	0.05320	0.00430	0.3040	0.0270	0.04160	0.00092	337	183	268	21	263	6	N/A	263	6	0.0006820	0.0000200	0.282407	0.000025	0.01739	0.00050	-13.4	0.9	-7.6
158	190829_350.FIN2	0.05410	0.00430	0.3010	0.0230	0.04170	0.00150	375	179	266	18	263	9	N/A	263	9	0.0010710	0.0000230	0.282612	0.000028	0.02861	0.00068	-6.1	1.0	-0.4
77	190829_226.FIN2	0.05460	0.00450	0.3130	0.0280	0.04180	0.00120	396	185	276	21	264	8	N/A	264	8	0.0010440	0.0000650	0.282647	0.000029	0.02830	0.00200	-4.9	1.0	0.8
44	190212_121.FIN2	0.05220	0.00350	0.3030	0.0180	0.04210	0.00130	294	153	268	14	266	8	N/A	266	8	0.0011030	0.0000550	0.282566	0.000029	0.02920	0.00160	-7.7	1.0	-2.0
19	190212_084.FIN2	0.05260	0.00120	0.3062	0.0067	0.04259	0.00036	312	52	271	5	269	2	N/A	269	2	0.0011420	0.0000710	0.282496	0.000028	0.02730	0.00170	-10.2	1.0	-4.4
46	190212_123.FIN2	0.05260	0.00250	0.3090	0.0150	0.04260	0.00120	312	108	273	12	269	8	N/A	269	8	0.0008688	0.0000037	0.282298	0.000029	0.02211	0.00013	-17.2	1.0	-11.4
37	190212_114.FIN2	0.05390	0.00450	0.3170	0.0280	0.04279	0.00099	367	188	277	22	270	6	N/A	270	6	0.0006160	0.0000310	0.282543	0.000034	0.01600	0.00082	-8.6	1.2	-2.7
27	190212_098.FIN2	0.05220	0.00140	0.3135	0.0087	0.04375	0.00043	294	61	277	7	276	3	N/A	276	3	0.0011970	0.0000460	0.282466	0.000041	0.02980	0.00130	-11.3	1.5	-5.4
rejected analysis																									
2	190212_061.FIN2	0.06680	0.00420	0.3100	0.0220	0.03410	0.00130	832	131	274	17	216	8	N/A	N/A	N/A									
4	190212_063.FIN2	0.07160	0.00500	0.4070	0.0260	0.04159	0.00095	975	142	346	19	263	6	N/A	N/A	N/A									
5	190212_064.FIN2	0.07070	0.00520	0.3940	0.0300	0.04036	0.00081	949	151	336	22	255	5	N/A	N/A	N/A									
7	190212_066.FIN2	0.06780	0.00450	0.3850	0.0240	0.04140	0.00110	862	138	330	18	262	7	N/A	N/A	N/A									
9	190212_068.FIN2	0.06540	0.00640	0.3860	0.0380	0.04280	0.00170	787	205	330	27	270	11	N/A	N/A	N/A	0.0007870	0.0000440	0.282410	0.000041	0.02070	0.00140	-13.3	1.5	N/A
10	190212_069.FIN2	0.19400	0.01400	1.1910	0.0820	0.04450	0.00120	2776	118	791	39	281	7	10	N/A	N/A									
12	190212_071.FIN2	0.30100	0.04400	1.6800	0.2400	0.04090	0.00140	3475	226	976	86	258	9	7	N/A	N/A									
14	190212_079.FIN2	0.19000	0.01200	1.0710	0.0790	0.04090	0.00140	2742	104	736	38	259	9	9	N/A	N/A									
15	190212_080.FIN2	0.38600	0.03200	4.5900	0.4600	0.08500	0.00850	3855	125	1730	83	525	50	14	N/A	N/A									
16	190212_081.FIN2	0.08000	0.00350	0.4380	0.0170	0.03987	0.00087	1197	86	369	12	252	5	21	N/A	N/A									
20	190212_085.FIN2	0.22400	0.01400	1.1760	0.0790	0.03810	0.00120	3010	100	786	37	241	7	8	N/A	N/A									
21	190212_086.FIN2	0.37600	0.01900	2.6500	0.1500	0.05100	0.00160	3816	76	1311	42	321	10	8	N/A	N/A									
22	190212_087.FIN2	0.14900	0.01100	0.9330	0.0630	0.04580	0.00140	2334	126	666	32	288	9	12	N/A	N/A	0.0008730	0.0000150	0.282606	0.000034	0.02291	0.00050	-6.3	1.2	N/A
23	190212_088.FIN2	0.06140	0.00310	0.3280	0.0160	0.03880	0.00110	653	108	288	12	245	7	N/A	N/A	N/A									
25	190212_096.FIN2	0.07690	0.00490	0.4510	0.0260	0.04270	0.00150	1119	127	377	18	269	9	24	N/A	N/A									
26	190212_097.FIN2	0.13260	0.00830	0.8350	0.0550	0.04570	0.00130	2133	110	613	30	288	8	13	N/A	N/A									
28	190212_099.FIN2	0.14850	0.00800	0.7990	0.0470	0.03912	0.00077	2329	92	594	26	247	5	11	N/A	N/A									
29	190212_100.FIN2	0.06320	0.00410	0.3570	0.0210	0.04130	0.00100	715	138	309	16	261	6	N/A	N/A	N/A									
33	190212_104.FIN2	0.27150	0.00900	1.6040	0.0570	0.04300	0.00120	3315	52	970	22	271	8	8	N/A	N/A	0.0013240	0.0000380	0.282444	0.000043	0.03610	0.00130	-12.1	1.5	N/A
34	190212_105.FIN2	0.12600	0.00710	0.7680	0.0440	0.04420	0.00130	2043	100	577	25	279	8	14	N/A	N/A									
38	190212_115.FIN2	0.08350	0.00340	0.4720	0.0260	0.04020	0.00079	1281	79	392	18	254	5	20	N/A	N/A									
39	190212_116.FIN2	0.31400	0.01400	2.0500	0.0820	0.04770	0.00100	3541	69	1128	27	300	6	8	N/A	N/A	0.0013140	0.0000820	0.282605	0.000052	0.03610	0.00230	-6.4	1.8	N/A
40	190212_117.FIN2	0.06450	0.00540	0.3570	0.0280	0.04030	0.00150	758	177	309	21	255	9	N/A	N/A	N/A									
41	190212_118.FIN2	0.06640	0.00540	0.3720	0.0240	0.04090	0.00120	819	170	320	18	258	8	N/A	N/A	N/A									
42	190212_119.FIN2	0.08740	0.00470	0.4610	0.0220	0.03830	0.00160	1369	103	385	15	242	10	18	N/A	N/A									
45	190212_122.FIN2	0.29200	0.01600	1.8900	0.1700	0.04690	0.00210	3428	85	1082	61	295	13	9	N/A	N/A									
50	190212_133.FIN2	0.11800	0.00910	0.6530	0.0470	0.04030	0.00200	1926	138	509	29	254	13	13	N/A	N/A									
53	190212_136.FIN2	0.09570	0.00540	0.5400	0.0290	0.04090	0.00110	1542	106	438	19	258	7	17	N/A	N/A									
55	190829_197.FIN2	0.05930	0.00240	0.3210	0.0140	0.03965	0.00089	578	88	282	11	251	6	N/A	N/A	N/A	0.0007040	0.0000540	0.282392	0.000029	0.01830	0.00150	-13.9	1.0	N/A
57	190829_199.FIN2	0.07290	0.00280	0.4020	0.0160	0.04029	0.00086	1011	78	342	11	255	5	25	N/A	N/A	0.0012440	0.0000600	0.282447	0.000035	0.03240	0.00170	-12.0	1.2	N/A
58	190829_200.FIN2	0.07240	0.00660	0.3790	0.0290	0.03850	0.00130	997	185	325	21	244	8	N/A	N/A	N/A	0.0010000	0.0000180	0.282461	0.000037	0.02674	0.00045	-11.5	1.3	N/A
66	190829_208.FIN2	0.07070	0.00330	0.3550	0.0170	0.03680	0.00110	949	96	308	13	233	7	N/A	N/A	N/A									
71	190829_220.FIN2	0.06290	0.00350	0.3240	0.0160	0.03780	0.00110	705	118	285	12	239	7	N/A	N/A	N/A	0.0022500	0.0000350	0.282647	0.000032	0.06350	0.00110	-4.9	1.1	N/A
76	190829_225.FIN2	0.06320	0.00420	0.3510	0.0260	0.04010	0.00110	715	141	303	19	253	7	N/A	N/A	N/A	0.0012350	0.0000410	0.282625	0.000035	0.03390	0.00120	-5.7	1.2	N/A
78	190829_227.FIN2	0.11800	0.00510	0.5710	0.0280	0.03530	0.00083	1926	77	457	18	224	5	12	N/A	N/A									
80	190829_235.FIN2	0.06060	0.00310	0.3340	0.0160	0.04020	0.00120	625	110	292	12	254	7	N/A	N/A	N/A	0.0022200	0.0001000	0.282597	0.000043	0.06130	0.00320	-6.6	1.5	N/A
108	190829_275.FIN2	0.07670	0.00630	0.4330	0.0400	0.04090	0.00120	1113	164	363	28	258	8	23	N/A	N/A	0.0012500	0.0000920	0.282637	0.000039	0.03480	0.00290	-5.2	1.4	N/A
109	190829_276.FIN2	0.07010	0.00410	0.3960	0.0240	0.04110	0.00150	931	120	338	17	260	10	N/A	N/A	N/A	0.0015600	0.0000760	0.282590	0.000034	0.04280	0.00230	-6.9	1.2	N/A
110	190829_277.FIN2	0.08000	0.00540	0.4370	0.0300	0.04000	0.00110	1197	133	365	21	253	7	21	N/A	N/A	0.0010000	0.0000630	0.282591	0.000032	0.02650	0.00170	-6.9	1.1	N/A
111	190829_278.FIN2	0.06270	0.00350	0.3340	0.0190	0.03890	0.00120	698	119	292	14	246	7	N/A	N/A	N/A	0.0008290	0.0000700	0.282480	0.000035	0.02180	0.00190	-10.8	1.2	N/A
113	190829_280.FIN2	0.07130	0.00350	0.3910	0.0200	0.04005	0.00098	966	100	334	15	253	6	N/A	N/A	N/A	0.0010950	0.0000370	0.282591	0.000024	0.02950	0.00120	-6.9	0.8	N/A
114	190829_281.FIN2	0.07740	0.00460	0.4290	0.0260	0.04051	0.00082	1132	118	361	19	256	5	23	N/A	N/A	0.0010960	0.0000240	0.282616	0.000033	0.03002	0.00088	-6.0	1.2	N/A
115	190829_288.FIN2	0.07720	0.00380	0.4100	0.0230	0.03870	0.00130	1126	98	347	17	245	8	22	N/A	N/A	0.0008490	0.0000160	0.282478	0.000032	0.02316	0.00060	-10.9	1.1	N/A
118	190829_291.FIN2	0.07320	0.00610	0.4040	0.0330	0.04000	0.00130	1019	169	343	24	253	8	25	N/A	N/A	0.0016380	0.0000370	0.282494	0.000032	0.04450	0.00100	-10.3	1.1	N/A
129	190829_308.FIN2	0.08960	0.00790	0.4360	0.0320	0.03610	0.00100	1417	169	369	24	228	6	16	N/A	N/A	0.0016810	0.0000330	0.282612	0.000035	0.04529	0.00087	-6.1	1.2	N/A
130	190829_309.FIN2	0.06850	0.00350	0.3760	0.0200	0.04010	0.00130	884	106	324	15	254	8	N/A	N/A	N/A	0.0012810	0.0000170	0.282502	0.000032	0.03469	0.00074	-10.0	1.1	N/A
132	190829_311.FIN2	0.07580	0.00370	0.4230	0.0220	0.04080	0.00110	1090	98	357	16	258	7	24	N/A	N/A	0.0012300	0.0001100	0.282508	0.000028	0.03300	0.00290	-9.8	1.0	N/A
144	190829_329.FIN2	0.05590	0.00640	0.3000	0.0320	0.03940	0.00130	448	254	265	25	249	8	N/A	N/A	N/A									

U-Pb geochronology																Hf isotope geochemistry								
		Isotopic ratios						Isotopic ages									Isotopic ratios						Epsilon units		
Grain #	Spot name	$^{207}Pb/^{206}Pb$	± 2SE	$^{207}Pb/^{235}U$	± 2SE	$^{206}Pb/^{238}U$	± 2SE	$^{207}Pb/^{206}Pb$	± 2SE (Ma)	$^{207}Pb/^{235}U$	± 2SE (Ma)	$^{206}Pb/^{238}U$	± 2SE (Ma)	Conc. %	Best Age	± 2SE (Ma)	$^{176}Lu/^{177}Hf$	± 2SE	$^{176}Hf/^{177}Hf$	± 2SE	$^{176}Yb/^{177}Hf$	± 2SE	εHf_0	2SE	εHf_t
145	190829_330.FIN2	0.11000	0.01400	0.6200	0.0820	0.04150	0.00220	1799	232	476	52	262	14	15	N/A	N/A									
147	190829_332.FIN2	0.08070	0.00540	0.4610	0.0310	0.04178	0.00095	1214	132	383	21	264	6	22	N/A	N/A	0.0007190	0.0000160	0.282440	0.000031	0.01889	0.00049	-12.2	1.1	N/A
153	190829_345.FIN2	0.11520	0.00690	0.6660	0.0460	0.04155	0.00094	1883	108	509	27	262	6	14	N/A	N/A	0.0009970	0.0000470	0.282459	0.000030	0.02650	0.00140	-11.5	1.1	N/A
154	190829_346.FIN2	0.06830	0.00290	0.3860	0.0210	0.04120	0.00110	878	88	331	15	260	7	N/A	N/A	N/A	0.0018850	0.0000900	0.282449	0.000034	0.05160	0.00260	-11.9	1.2	N/A
160	190829_352.FIN2	0.06770	0.00410	0.3700	0.0210	0.03979	0.00074	859	126	321	16	252	5	N/A	N/A	N/A	0.0012700	0.0001300	0.282581	0.000032	0.03430	0.00380	-7.2	1.1	N/A
16AW19--unnamed units; (Zone 08V NAD 83, 577144 E, 6909525 N)																								
32	200924_195.FIN2	0.05150	0.00630	0.2510	0.0310	0.03590	0.00140	262	140	227	25	227	9	N/A	227	9									
23	200924_180.FIN2	0.05210	0.00510	0.2570	0.0210	0.03630	0.00210	289	112	232	17	230	13	N/A	230	13	0.0013360	0.0000770	0.282276	0.000025	0.03610	0.00210	-18.0	0.9	-13.1
36	200924_199.FIN2	0.05140	0.00370	0.2560	0.0200	0.03650	0.00150	258	83	231	16	231	9	N/A	231	9	0.0003215	0.0000055	0.282447	0.000025	0.01061	0.00023	-12.0	0.9	-6.9
26	200924_183.FIN2	0.05260	0.00420	0.2640	0.0200	0.03700	0.00140	311	91	238	16	234	9	N/A	234	9	0.0004100	0.0000350	0.282485	0.000016	0.01164	0.00091	-10.6	0.6	-5.5
34	200924_197.FIN2	0.05250	0.00270	0.2700	0.0130	0.03740	0.00210	306	59	243	10	236	13	N/A	236	13	0.0002630	0.0000330	0.282398	0.000013	0.00707	0.00082	-13.7	0.5	-8.5
94	200925_088.FIN2	0.05470	0.00650	0.2680	0.0230	0.03760	0.00240	399	133	241	19	238	15	N/A	238	15	0.0002840	0.0000260	0.282492	0.000022	0.00835	0.00058	-10.4	0.8	-5.1
10	200924_161.FIN2	0.05190	0.00320	0.2730	0.0220	0.03800	0.00250	281	141	245	18	241	15	N/A	241	15	0.0027440	0.0000400	0.282471	0.000034	0.07250	0.00110	-11.1	1.2	-6.2
63	200925_040.FIN2	0.05240	0.00370	0.2740	0.0210	0.03820	0.00130	303	161	245	17	242	8	N/A	242	8	0.0016650	0.0000420	0.282463	0.000023	0.04297	0.00093	-11.4	0.8	-6.3
108	200925_109.FIN2	0.05370	0.00290	0.2720	0.0140	0.03830	0.00130	358	122	244	11	242	8	N/A	242	8	0.0005390	0.0000270	0.282504	0.000032	0.01550	0.00070	-9.9	1.1	-4.6
9	200924_160.FIN2	0.05190	0.00240	0.2760	0.0120	0.03834	0.00097	281	106	247	10	243	6	N/A	243	6	0.0003680	0.0000160	0.282498	0.000029	0.01034	0.00044	-10.1	1.0	-4.8
109	200925_110.FIN2	0.05210	0.00120	0.2724	0.0073	0.03853	0.00076	290	53	244	6	244	5	N/A	244	5	0.0002750	0.0000066	0.282513	0.000023	0.00781	0.00022	-9.6	0.8	-4.2
103	200925_104.FIN2	0.05360	0.00240	0.2770	0.0130	0.03859	0.00076	354	101	248	10	244	5	N/A	244	5	0.0012950	0.0000800	0.282459	0.000025	0.03250	0.00220	-11.5	0.9	-6.3
93	200925_087.FIN2	0.05230	0.00290	0.2820	0.0230	0.03870	0.00210	299	126	252	18	245	13	N/A	245	13	0.0005490	0.0000330	0.282467	0.000024	0.01546	0.00093	-11.2	0.8	-5.9
25	200924_182.FIN2	0.05200	0.00150	0.2764	0.0099	0.03881	0.00088	285	66	247	8	245	5	N/A	245	5	0.0011050	0.0000240	0.282162	0.000016	0.02983	0.00065	-22.0	0.6	-16.8
20	200924_177.FIN2	0.05140	0.00290	0.2810	0.0190	0.03890	0.00140	259	130	250	15	246	9	N/A	246	9	0.0005420	0.0000470	0.282515	0.000030	0.01490	0.00110	-9.5	1.1	-4.2
85	200925_079.FIN2	0.05580	0.00400	0.2790	0.0190	0.03910	0.00210	443	80	249	15	247	13	N/A	247	13									
13	200924_164.FIN2	0.05170	0.00180	0.2820	0.0100	0.03920	0.00110	272	80	252	8	248	7	N/A	248	7	0.0008830	0.0000570	0.282361	0.000018	0.02320	0.00150	-15.0	0.6	-9.6
105	200925_106.FIN2	0.05310	0.00340	0.2830	0.0190	0.03920	0.00087	333	145	253	15	248	7	N/A	248	7	0.0003830	0.0000520	0.282476	0.000018	0.01080	0.00150	-10.9	0.6	-5.5
11	200924_162.FIN2	0.05160	0.00180	0.2810	0.0100	0.03920	0.00110	268	80	251	8	248	5	N/A	248	5	0.0005180	0.0000790	0.282494	0.000021	0.01370	0.00200	-10.3	0.7	-4.9
80	200925_067.FIN2	0.05330	0.00280	0.2810	0.0150	0.03920	0.00091	342	119	251	12	248	6	N/A	248	6	0.0008030	0.0000460	0.282295	0.000026	0.02220	0.00130	-17.3	0.9	-12.0
98	200925_099.FIN2	0.05190	0.00170	0.2780	0.0100	0.03921	0.00079	281	75	248	8	248	5	N/A	248	5	0.0011510	0.0000310	0.282435	0.000023	0.02940	0.00100	-12.4	0.8	-7.1
92	200925_086.FIN2	0.05230	0.00340	0.2810	0.0140	0.03920	0.00170	299	148	252	11	248	11	N/A	248	11	0.0004110	0.0000390	0.282492	0.000011	0.01170	0.00100	-10.4	0.4	-4.9
87	200925_081.FIN2	0.05420	0.00400	0.2850	0.0210	0.03930	0.00140	379	166	254	16	248	8	N/A	248	8	0.0004780	0.0000610	0.282509	0.000027	0.01300	0.00160	-9.8	1.0	-4.3
30	200924_187.FIN2	0.05040	0.00280	0.2810	0.0220	0.03930	0.00130	213	129	251	18	248	9	N/A	248	9									
81	200925_075.FIN2	0.05190	0.00190	0.2780	0.0100	0.03932	0.00086	281	84	248	8	249	5	N/A	249	5	0.0015440	0.0000100	0.282479	0.000035	0.03960	0.00021	-10.8	1.2	-5.6
29	200924_186.FIN2	0.05200	0.00160	0.2788	0.0082	0.03936	0.00063	285	70	250	7	249	4	N/A	249	4	0.0005460	0.0000350	0.282496	0.000018	0.01410	0.00088	-10.2	0.6	-4.8
95	200925_089.FIN2	0.05160	0.00510	0.2840	0.0370	0.03940	0.00210	268	227	253	29	249	13	N/A	249	13	0.0013360	0.0000330	0.282399	0.000036	0.03467	0.00091	-13.6	1.3	-8.3
97	200925_098.FIN2	0.05190	0.00220	0.2820	0.0110	0.03952	0.00082	281	97	252	9	250	5	N/A	250	5	0.0010900	0.0000370	0.282465	0.000022	0.02854	0.00081	-11.3	0.8	-5.9
106	200925_107.FIN2	0.05350	0.00360	0.2960	0.0250	0.03960	0.00220	350	152	263	20	250	13	N/A	250	13	0.0010580	0.0000410	0.282431	0.000019	0.02720	0.00140	-12.5	0.7	-7.1
117	200925_124.FIN2	0.05480	0.00270	0.2860	0.0120	0.03960	0.00130	404	110	255	10	251	8	N/A	251	8	0.0013220	0.0000380	0.282298	0.000020	0.03903	0.00096	-17.2	0.7	-11.9
72	200925_059.FIN2	0.05600	0.00320	0.2900	0.0240	0.03980	0.00200	452	127	259	19	251	23	N/A	251	23	0.0012260	0.0000240	0.282477	0.000024	0.03100	0.00091	-10.9	0.8	-5.5
33	200924_196.FIN2	0.05140	0.00180	0.2850	0.0160	0.03980	0.00370	259	80	254	13	251	12	N/A	251	12									
104	200925_105.FIN2	0.05840	0.00270	0.2990	0.0220	0.03980	0.00160	545	101	264	17	251	10	N/A	251	10	0.0016100	0.0002000	0.282315	0.000034	0.04700	0.00580	-16.6	1.2	-11.3
42	200925_012.FIN2	0.05100	0.00130	0.2805	0.0073	0.03976	0.00065	241	59	251	6	251	4	N/A	251	4	0.0011480	0.0000600	0.282469	0.000027	0.02900	0.00160	-11.2	1.0	-5.8
101	200925_102.FIN2	0.05300	0.00200	0.2870	0.0100	0.03981	0.00090	329	86	256	8	252	6	N/A	252	6	0.0002040	0.0000340	0.282491	0.000010	0.00660	0.00110	-10.4	0.3	-4.8
83	200925_077.FIN2	0.05170	0.00120	0.2818	0.0092	0.03984	0.00087	272	53	252	7	252	5	N/A	252	5	0.0003690	0.0000460	0.282498	0.000017	0.01020	0.00120	-10.1	0.6	-4.6
107	200925_108.FIN2	0.05330	0.00190	0.2859	0.0093	0.03990	0.00091	342	81	255	7	252	6	N/A	252	6	0.0002190	0.0000350	0.282494	0.000021	0.00650	0.00100	-10.3	0.7	-4.7
79	200925_066.FIN2	0.05310	0.00250	0.2830	0.0120	0.04000	0.00130	333	107	253	9	253	8	N/A	253	8	0.0010530	0.0000240	0.282471	0.000033	0.02600	0.00074	-11.1	1.2	-5.7
71	200925_058.FIN2	0.05270	0.00200	0.2890	0.0150	0.04000	0.00130	316	86	257	12	253	8	N/A	253	8	0.0021370	0.0000440	0.282435	0.000024	0.06000	0.00120	-12.4	0.8	-7.1
49	200925_019.FIN2	0.05270	0.00570	0.2940	0.0390	0.04010	0.00230	316	246	261	31	253	14	N/A	253	14	0.0010360	0.0000350	0.282461	0.000021	0.02560	0.00100	-11.5	0.7	-6.0
119	200925_126.FIN2	0.05190	0.00120	0.2844	0.0072	0.04004	0.00056	281	53	254	6	253	3	N/A	253	3	0.0006960	0.0000700	0.282471	0.000022	0.01940	0.00180	-11.1	0.8	-5.6
84	200925_078.FIN2	0.05200	0.00130	0.2855	0.0076	0.04004	0.00074	285	57	254	6	253	3	N/A	253	3	0.0012930	0.0000790	0.282424	0.000018	0.03490	0.00230	-12.8	0.6	-7.4
82	200925_076.FIN2	0.05240	0.00160	0.2845	0.0092	0.04005	0.00055	303	70	254	7	253	5	N/A	253	5	0.0012210	0.0000380	0.282499	0.000026	0.03060	0.00100	-10.1	0.9	-4.7
55	200925_025.FIN2	0.05240	0.00210	0.2890	0.0150	0.04010	0.00140	303	91	257	12	253	8	N/A	253	8	0.0012945	0.0000059	0.282453	0.000025	0.03355	0.00047	-11.7	0.9	-6.3
35	200924_198.FIN2	0.05180	0.00150	0.2849	0.0080	0.04008	0.00051	277	66	254	6	253	3	N/A	253	3	0.0013140	0.0000420	0.282139	0.000021	0.03530	0.00120	-22.8	0.7	-17.4
76	200925_063.FIN2	0.05260	0.00230	0.2880	0.0150	0.04010	0.00150	312	100	257	12	253	9	N/A	253	9	0.0003400	0.0000380	0.282492	0.000022	0.01120	0.00130	-10.4	0.8	-4.8
54	200925_024.FIN2	0.05290	0.00140	0.2860	0.0100	0.04014	0.00097	325	60	255	8	254	6	N/A	254	6	0.0014430	0.0000580	0.282344	0.000017	0.04060	0.00170	-15.6	0.6	-10.2
68	200925_055.FIN2	0.05340	0.00250	0.2860	0.0130	0.04016	0.00084	346	106	255	10	254	5	N/A	254	5	0.0009620	0.0000360	0.282455	0.000028	0.02404	0.00097	-11.7	1.0	-6.2
102	200925_103.FIN2	0.05190	0.00200	0.2930	0.0160	0.04019	0.00072	281	88	260	12	254	8	N/A	254	8	0.0013180	0.0000150	0.282298	0.000028	0.03752	0.00053	-17.2	1.0	-11.8
56	200925_033.FIN2	0.05220	0.00220	0.2850	0.0130	0.04020	0.00130	294	96	255	10	254	5	N/A	254	5	0.0012780	0.0000610	0.282474	0.000022	0.03190	0.00160	-11.0	0.8	-5.6
86	200925_080.FIN2	0.05170	0.00140	0.2866	0.0081	0.04022	0.00066	272	62	255	6	254	4	N/A	254	4	0.0011090	0.0000320	0.282456	0.000021	0.02752	0.00073	-11.6	0.7	-6.2
57	200925_034.FIN2	0.05200	0.00100	0.2865	0.0059	0.04036	0.00061	285	44	255	5	255	4	N/A	255	4	0.0015050	0.0000720	0.282415	0.000018	0.03760	0.00180	-13.1	0.6	-7.7
38	200924_201.FIN2	0.05230	0.00160	0.2888	0.0093	0.04041	0.00062	299	70	257	7	255	4	N/A	255	4	0.0007020	0.0000870	0.282499	0.000021	0.01840	0.00220	-10.1	0.7	-4.6
6	200924_157.FIN2	0.05250	0.00370	0.2900	0.0190	0.04040	0.00130	307	161	258	15	256	8	N/A	256	8	0.0011570	0.0000630	0.282463	0.000021	0.02800	0.00170	-11.4	0.7	-5.9
7	200924_158.FIN2	0.05210	0.00190	0.2920	0.0110	0.04043	0.00089	290	83	260	8	256	6	N/A	256	6	0.0003910	0.0000310	0.282498	0.000022	0.01069	0.00087	-10.1	0.8	-4.5
12	200924_163.FIN2	0.05180	0.00140	0.2900	0.0083	0.04047	0.00068	277	62	258	7	256	4	N/A	256	4	0.0004600	0.0000750	0.282491	0.000016	0.01220	0.00190	-10.4	0.6	-4.8
67	200925_054.FIN2	0.05160	0.00200	0.2900	0.0110	0.04049	0.00094	268	89	258	9	256	6	N/A	256	6	0.0008620	0.0000220	0.282505	0.000022	0.02261	0.00061	-9.9	0.8	-4.4
73	200925_060.FIN2	0.05540	0.00260	0.2930	0.0130	0.04050	0.00160	428	105	260	10	256	10	N/A	256	10	0.0013600	0.0000590	0.282428	0.000021	0.03410	0.00160	-12.6	0.7	-7.2
120	200925_127.FIN2	0.05210	0.00710	0.2910	0.0360	0.04050	0.00220	290	311	256	29	256	13	N/A	256	13	0.0016710	0.0000320	0.282915	0.000020	0.04859	0.00099	4.6	0.7	10.0
60	200925_037.FIN2	0.05210	0.00130	0.2881	0.0090	0.04054	0.00086	290	57	257	7	256	5	N/A	256	5	0.0017500	0.0001400	0.282454	0.000030	0.04410	0.00380	-11.7	1.1	-6.3
58	200925_035.FIN2	0.05230	0.00170	0.2872	0.0093	0.04053	0.00084	299	74	256	7	256	5	N/A	256	5	0.0004240	0.0000530	0.282501	0.000022	0.01130	0.00140	-10.0	0.8	-4.4
110	200925_111.FIN2	0.05210	0.00150	0.2889	0.0095	0.04060	0.00075	290	66	257	8	257	5	N/A	257	5	0.0014420	0.0000560	0.282436	0.000025	0.03700	0.00150	-12.3	0.9	-6.9
3	200924_154.FIN2	0.05170	0.00170	0.2910	0.0097	0.04060	0.00074	272	75	259	8	257	5	N/A	257	5	0.0014400	0.0000330	0.282477	0.000021	0.03636	0.00081	-10.9	0.7	-5.4
121	200925_128.FIN2	0.05890	0.00440	0.3010	0.0180	0.04070	0.00200	563	163	267	14	257	12	N/A	257	12	0.0012510	0.0000710	0.282439	0.000024	0.03260	0.00190	-12.2	0.8	-6.7
111	200925_118.FIN2	0.05100	0.00150	0.2900	0.0100	0.04070	0.00097	241	68	258	8	257	6	N/A	257	6	0.0012720	0.0000620	0.282142	0.000024	0.03600	0.00160	-22.7	0.9	-17.2
66	200925_053.FIN2	0.05410	0.00280	0.2900	0.0150	0.04070	0.00110	375	116	258	11	257	7	N/A	257	7	0.0014900	0.0001700	0.282454	0.000020	0.03790	0.00470	-11.7	0.7	-6.2
64	200925_041.FIN2	0.05420	0.00300	0.2940	0.0200	0.04080	0.00130	379	124	261	16	258	8	N/A	258	8	0.0006590	0.0000270	0.282260	0.000019	0.01745	0.00075	-18.6	0.7	-13.0
88	200925_082.FIN2	0.05210	0.00130	0.2917	0.0080	0.04078	0.00062	290	57	259	6	258	4	N/A	258	4	0.0014680	0.0000830	0.282455	0.000026	0.03720	0.00210	-11.7	0.9	-6.2
78	200925_065.FIN2	0.05290	0.00180	0.2950	0.0110	0.04080	0.00140	325	77	262	9	258	9	N/A	258	9	0.0012580	0.0000970	0.282289	0.000022	0.03480	0.00260	-17.5	0.8	-12.0
53	200925_023.FIN2	0.05170	0.00270	0.2950	0.0160	0.04090	0.00160	272	120	262	13	258	10	N/A	258	10	0.0045600	0.0001100	0.282499	0.000025	0.12630	0.00420	-10.1	0.9	-5.2
19	200924_176.FIN2	0.05280	0.00200	0.2920	0.0130	0.04090	0.00100	320	86	261	10	258	6	N/A	258	6	0.0014450	0.0000930	0.282471	0.000035	0.03610	0.00240	-11.1	1.2	-5.6
61	200925_038.FIN2	0.05230	0.00200	0.2950	0.0110	0.04095	0.00076	299	87	262	9	259	5	N/A	259	5	0.0004820	0.0000230	0.282490	0.000017	0.01306	0.00054	-10.4	0.6	-4.8
41	200925_011.FIN2	0.05210	0.00460	0.2960	0.0410	0.04100	0.00320	290	202	263	32	259	20	N/A	259	20	0.0011680	0.0000300	0.282440	0.000023	0.02899	0.00098	-12.2	0.8	-6.6
75	200925_062.FIN2	0.05230	0.00170	0.2944	0.0097	0.04114	0.00097	299	74	262	8	260	6	N/A	260	6	0.0012460	0.0000130	0.282468	0.000024	0.03066	0.00046	-11.2	0.8	-5.6
17	200924_174.FIN2	0.05150	0.00210	0.2970	0.0130	0.04128	0.00085	263	94	263	10	261	5	N/A	261	5	0.0014970	0.0000300	0.282466	0.000026	0.03666	0.00081	-11.3	0.9	-5.7
24	200924_181.FIN2	0.05220	0.00190	0.2950	0.0110	0.04130	0.00140	294	83	262	9	261	9	N/A	261	9	0.0008990	0.0000280	0.282179	0.000018	0.02437	0.00074	-21.4	0.6	-15.8
118	200925_125.FIN2	0.05170	0.00170	0.2960	0.0100	0.04133	0.00071	272	75	263	8	261	4	N/A	261	4	0.0006640	0.0000330	0.282279	0.000022	0.01902	0.00091	-17.9	0.8	-12.2
45	200925_015.FIN2	0.05190	0.00150	0.2951	0.0091	0.04130	0.00230	281	66	262	7	261	4	N/A	261	4	0.0010066	0.0000083	0.282420	0.000022	0.02472	0.00030	-12.9	0.8	-7.3
52	200925_022.FIN2	0.05220	0.00300	0.2980	0.0220	0.04132	0.00071	294	131	264	17	261	14	N/A	261	14									
22	200924_179.FIN2	0.05220	0.00160	0.2980	0.0096	0.04137	0.00069	294	70	264	8	261	4	N/A	261	4	0.0004480	0.0000470	0.282480	0.000019	0.01200	0.00120	-10.8	0.7	-5.1
46	200925_016.FIN2	0.05220	0.00240	0.2960	0.0150	0.04154	0.00089	294	105	263	11	262	6	N/A	262	6	0.0009120	0.0000120	0.282451	0.000020	0.02236	0.00034	-11.8	0.7	-6.1
62	200925_039.FIN2	0.05200	0.00260	0.3010	0.0170	0.04160	0.00140	285	114	267	13	263	8	N/A	263	8	0.0009890	0.0000510	0.282312	0.000016	0.02620	0.00120	-16.7	0.6	-11.1
70	200925_057.FIN2	0.05740	0.00570	0.3060	0.0430	0.04160	0.00410	507	218	271	33	263	25	N/A	263	25	0.0012160	0.0000400	0.282456	0.000023	0.03080	0.00100	-11.6	0.8	-6.0
96	200925_097.FIN2	0.05240	0.00470	0.3040	0.0280	0.04170	0.00210	303	204	269	22	263	13	N/A	263	13	0.0004880	0.0000640	0.282490	0.000018	0.01340	0.00170	-10.4	0.6	-4.7
100	200925_101.FIN2	0.05220	0.00170	0.3000	0.0110	0.04173	0.00094	294	74	266	9	264	6	N/A	264	6	0.0012030	0.0000250	0.282470	0.000019	0.03113	0.00073	-11.1	0.7	-5.5
2	200924_153.FIN2	0.05090	0.00630	0.2990	0.0330	0.04180	0.00190	236	286	265	25	264	11	N/A	264	11	0.0008870	0.0000360	0.282307	0.000026	0.02330	0.00100	-16.9	0.9	-11.2
65	200925_050.FIN2	0.05160	0.00260	0.3020	0.0150	0.04188	0.00096	268	116	267	12	264	6	N/A	264	6									
37	200924_200.FIN2	0.05280	0.00290	0.3050	0.0190	0.04200	0.00170	320	125	270	15	265	11	N/A	265	11	0.0005560	0.0000430	0.282487	0.000020	0.01480	0.00110	-10.5	0.7	-4.7
59	200925_036.FIN2	0.05210	0.00150	0.2997	0.0092	0.04202	0.00085	290	66	266	7	265	5	N/A	265	5	0.0004400	0.0001100	0.282477	0.000022	0.01180	0.00280	-10.9	0.8	-5.1
51	200925_021.FIN2	0.05410	0.00240	0.3050	0.0160	0.04210	0.00100	375	100	269	13	266	6	N/A	266	6	0.0002777	0.0000075	0.282477	0.000018	0.00759	0.00017	-10.9	0.6	-5.0
74	200925_061.FIN2	0.05220	0.00130	0.3010	0.0096	0.04222	0.00088	294	57	267	7	267	5	N/A	267	5	0.0015700	0.0002200	0.282447	0.000024	0.03940	0.00580	-12.0	0.8	-6.3
90	200925_084.FIN2	0.05290	0.00180	0.3060	0.0150	0.04230	0.00110	325	77	271	12	267	7	N/A	267	7	0.0016220	0.0000960	0.282469	0.000025	0.04120	0.00260	-11.2	0.9	-5.5
43	200925_013.FIN2	0.05550	0.00610	0.3170	0.0490	0.04260	0.00310	432	245	279	37	269	19	N/A	269	19	0.0012370	0.0000580	0.282495	0.000034	0.03220	0.00110	-10.3	1.2	-4.5
116	200925_123.FIN2	0.05210	0.00140	0.3070	0.0100	0.04285	0.00073	290	61	271	8	270	5	N/A	270	5	0.0011920	0.0000330	0.282484	0.000027	0.03069	0.00097	-10.6	1.0	-4.8
69	200925_056.FIN2	0.05330	0.00120	0.3081	0.0081	0.04289	0.00090	342	51	273	6	271	6	N/A	271	6	0.0001958	0.0000052	0.282402	0.000022	0.00632	0.00021	-13.5	0.8	-7.6

U-Pb geochronology																	Hf isotope geochemistry								
		Isotopic ratios						Isotopic ages									Isotopic ratios						Epsilon units		
Grain #	Spot name	$^{207}Pb/^{206}Pb$	± 2SE	$^{207}Pb/^{235}U$	± 2SE	$^{206}Pb/^{238}U$	± 2SE	$^{207}Pb/^{206}Pb$	± 2SE (Ma)	$^{207}Pb/^{235}U$	± 2SE (Ma)	$^{206}Pb/^{238}U$	± 2SE (Ma)	Conc. %	Best Age	± 2SE (Ma)	$^{176}Lu/^{177}Hf$	± 2SE	$^{176}Hf/^{177}Hf$	± 2SE	$^{176}Yb/^{177}Hf$	± 2SE	εHf_0	2SE	εHf_t
4	200924_155.FIN2	0.05090	0.00180	0.3110	0.0120	0.04313	0.00087	236	82	274	9	272	5	N/A	272	5	0.0005150	0.0000270	0.282499	0.000032	0.01366	0.00063	-10.1	1.1	-4.2
27	200924_184.FIN2	0.05270	0.00240	0.3140	0.0190	0.04330	0.00160	316	104	276	14	273	10	N/A	273	10	0.0015420	0.0000640	0.282449	0.000027	0.03770	0.00160	-11.9	1.0	-6.1
21	200924_178.FIN2	0.05250	0.00250	0.3170	0.0150	0.04349	0.00096	307	108	278	11	274	6	N/A	274	6	0.0003700	0.0000240	0.282448	0.000022	0.01096	0.00070	-11.9	0.8	-5.9
18	200924_175.FIN2	0.05210	0.00430	0.3170	0.0360	0.04370	0.00230	290	189	279	28	275	14	N/A	275	14	0.0005380	0.0000960	0.282465	0.000025	0.01500	0.00260	-11.3	0.9	-5.3
44	200925_014.FIN2	0.05210	0.00570	0.3150	0.0290	0.04360	0.00240	290	250	278	22	275	15	N/A	275	15	0.0004550	0.0000660	0.282474	0.000033	0.01290	0.00170	-11.0	1.2	-5.0
39	200924_202.FIN2	0.05300	0.00260	0.3310	0.0290	0.04530	0.00290	329	111	290	22	285	18	N/A	285	18	0.0011150	0.0000170	0.282199	0.000024	0.03016	0.00050	-20.7	0.9	-14.6
rejected analysis																									
1	200924_152.FIN2	0.05910	0.00270	0.2830	0.0200	0.03390	0.00170	571	99	253	16	215	10	N/A	N/A	N/A									
5	200924_156.FIN2	0.06460	0.00660	0.3380	0.0270	0.03730	0.00210	761	215	295	21	236	13	N/A	N/A	N/A	0.0002218	0.0000057	0.282499	0.000029	0.00690	0.00018	-10.1	1.0	N/A
8	200924_159.FIN2	0.07400	0.00640	0.4130	0.0370	0.03950	0.00140	1041	175	350	27	250	9	N/A	N/A	N/A									
14	200924_165.FIN2	0.07510	0.00500	0.4040	0.0430	0.03810	0.00240	1071	134	343	30	241	15	N/A	N/A	N/A	0.0004853	0.0000064	0.282494	0.000022	0.01274	0.00027	-10.3	0.8	N/A
15	200924_166.FIN2	0.07680	0.00450	0.4190	0.0250	0.03919	0.00089	1116	117	353	18	248	6	N/A	N/A	N/A									
16	200924_173.FIN2	0.06690	0.00270	0.3560	0.0180	0.03820	0.00100	835	84	309	14	242	6	N/A	N/A	N/A									
28	200924_185.FIN2	0.14900	0.01100	0.8940	0.0740	0.04410	0.00320	2334	126	636	40	278	20	N/A	N/A	N/A									
31	200924_194.FIN2	0.05850	0.00330	0.2990	0.0140	0.03750	0.00150	549	123	266	11	237	9	N/A	N/A	N/A	0.0016700	0.0001200	0.282471	0.000032	0.04220	0.00300	-11.1	1.1	N/A
40	200924_203.FIN2	0.05720	0.00430	0.3000	0.0290	0.03760	0.00250	499	166	265	23	238	16	N/A	N/A	N/A	0.0010880	0.0000240	0.282476	0.000027	0.02697	0.00047	-10.9	1.0	N/A
47	200925_017.FIN2	0.06230	0.00340	0.3260	0.0160	0.03770	0.00140	684	117	286	12	238	9	N/A	N/A	N/A	0.0019150	0.0000830	0.282476	0.000027	0.05190	0.00250	-10.9	1.0	N/A
48	200925_018.FIN2	0.12590	0.00570	0.7290	0.0350	0.04200	0.00100	2041	80	553	20	265	6	N/A	N/A	N/A									
50	200925_020.FIN2	0.06080	0.00320	0.3190	0.0170	0.03811	0.00095	632	113	281	13	241	6	N/A	N/A	N/A									
77	200925_064.FIN2	0.07500	0.00330	0.3980	0.0230	0.03840	0.00110	1069	88	339	16	243	7	N/A	N/A	N/A	0.0012810	0.0000300	0.282238	0.000033	0.03722	0.00084	-19.3	1.2	N/A
89	200925_083.FIN2	0.13190	0.00810	0.7630	0.0480	0.04170	0.00150	2123	108	573	28	264	9	N/A	N/A	N/A	0.0006790	0.0000820	0.282515	0.000026	0.01870	0.00190	-9.5	0.9	N/A
91	200925_085.FIN2	0.07750	0.00350	0.4050	0.0200	0.03860	0.00100	1134	90	344	15	244	7	N/A	N/A	N/A									
99	200925_100.FIN2	0.05460	0.00190	0.3040	0.0100	0.04040	0.00100	396	78	269	8	255	6	N/A	N/A	N/A	0.0011920	0.0000180	0.282285	0.000029	0.03416	0.00069	-17.7	1.0	N/A
112	200925_119.FIN2	0.07910	0.00880	0.5080	0.0560	0.04720	0.00320	1175	220	402	38	297	20	N/A	N/A	N/A	0.0016240	0.0000490	0.282919	0.000019	0.04660	0.00120	4.7	0.7	N/A
113	200925_120.FIN2	0.06090	0.00370	0.3280	0.0210	0.03960	0.00170	636	131	287	16	250	11	N/A	N/A	N/A	0.0013560	0.0000240	0.282306	0.000030	0.03845	0.00060	-16.9	1.1	N/A
114	200925_121.FIN2	0.32800	0.07200	1.9900	0.4000	0.04750	0.00820	3608	337	1100	150	299	50	N/A	N/A	N/A									
115	200925_122.FIN2	0.05910	0.00680	0.3110	0.0300	0.03860	0.00180	571	250	274	23	244	11	N/A	N/A	N/A	0.0005110	0.0000150	0.282472	0.000023	0.01402	0.00030	-11.1	0.8	N/A

APPENDIX 3.B.1

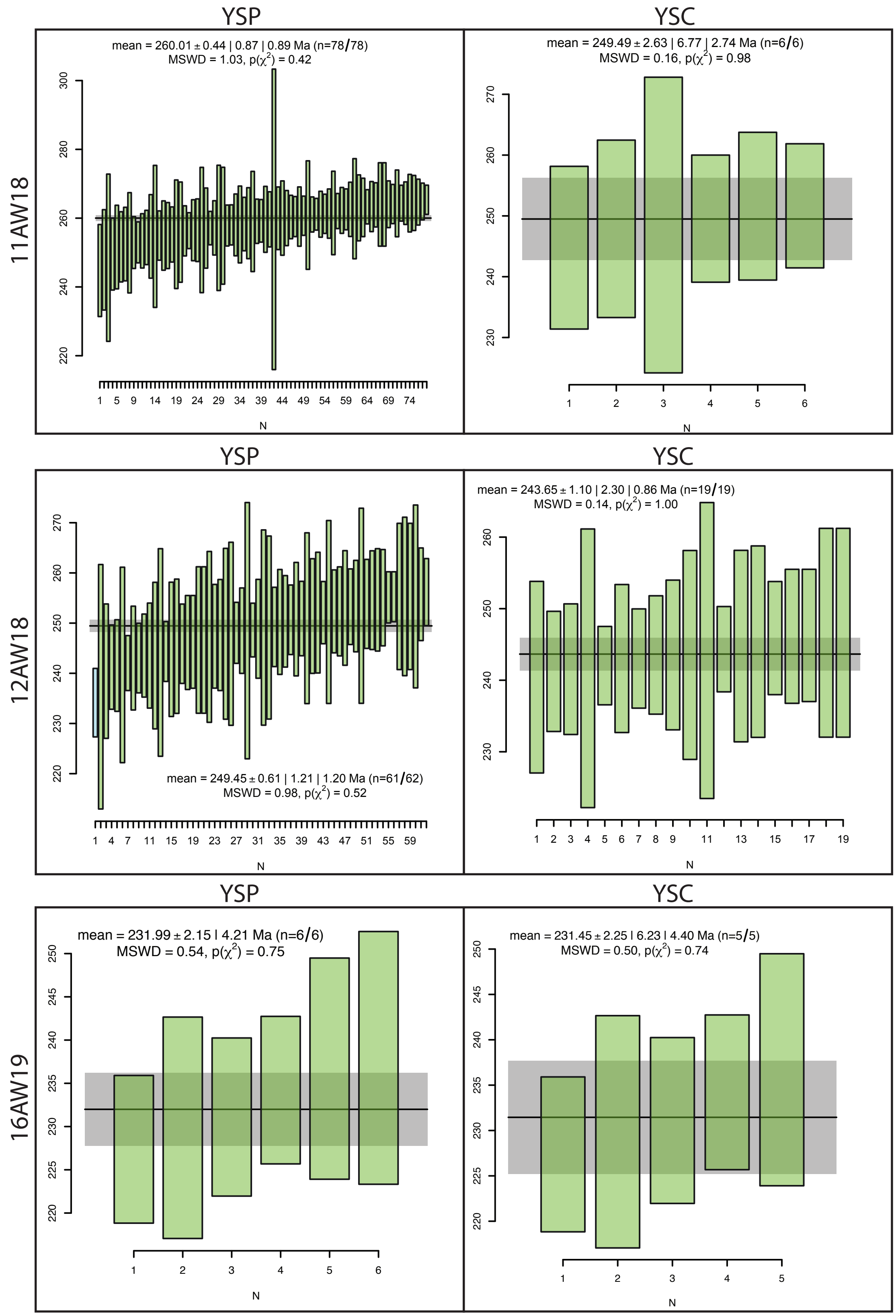

CHAPTER 4

Summary and future research

4.1 SUMMARY

Late Triassic to Early Jurassic arc collision and crustal thickening along the northern Cordilleran margin resulted in the exhumation of the Intermontane terranes and deposition of Sinemurian to Toarcian syn-tectonic units of the Faro Peak formation. In the Faro region, the Faro Peak formation is exposed along the Vangorda fault at the suture between the Yukon-Tanana and Slide Mountain terranes. Field stratigraphic and detrital zircon results indicate that Faro Peak formation sediment was sourced from both sides of the Vangorda fault, including pre-Late Devonian units of the underlying Snowcap assemblage, mid-Permian sedimentary and intrusive rocks of the Slide Mountain terrane, and Late Triassic to Early Jurassic (220-180 Ma) intrusive rocks from the Finlayson Lake and Stewart River map areas and adjacent regions of eastern Alaska.

The Faro Peak formation unconformably overlies the Snowcap assemblage and unnamed Triassic units in the Faro area and contains massively bedded sandstone and pebble to boulder conglomerate units that are consistent with deposition by mass sediment gravity flows. The Faro Peak basin was likely controlled by extensional to sinistral strike-slip faults that are interpreted to have been involved in Intermontane terrane evolution, including subsidence of the Whitehorse trough (e.g., Dickie and Hein, 1995; Berman et al., 2007; Colpron et al., 2015). Basal units of the

Faro Peak formation are dominated by sedimentary and volcanic clasts, whereas the exposed top contains a higher proportion of up to boulder-sized clasts of intrusive rock clasts indicating progressive unroofing of the source region. A basin-bounding fault, such as the proto-Vangorda fault (c.f., Tempelman-Kluit, 1972), probably facilitated rock uplift, tectonic subsidence of the Faro Peak basin, and deposition of Faro Peak formation lithofacies.

Unnamed Triassic units in the Faro region consist of limestone, argillite, basalt, wacke, and sandstone that were originally assigned to the lower Faro Peak formation (e.g., Pigage, 2004). Recent field stratigraphic results (Wiest et al., 2020) indicate that these units have unconformable lower contact relationships with the Snowcap assemblage and unconformable upper contact relationships with coarse-grained conglomerate units of the Faro Peak formation. Unnamed units are lithologically distinct, of mappable extent, and have been assigned to a new unnamed unit separate from the Faro Peak formation. Feldspathic sandstone and lithic wacke units of the unnamed Triassic units yield mostly (95-100%) mid-Permian to Late Triassic detrital zircon grains with peak ages of 262-253 Ma and mostly subchondritic $\varepsilon_{Hf(t)}$ values. Felsic igneous and pyroclastic rocks in the Klondike assemblage likely sourced the majority of zircon grains in these unnamed units. Minor similar-aged grains with superchondiritc $\varepsilon_{Hf(t)}$ values are potentially derived from comagmatic units of the Slide Mountain terrane in the Finlayson Lake map area.

Snowcap assemblage micaceous quartzite and quartz-mica schist units in the Faro area yield Cryogenian maximum depositional ages. Detrital zircon grains in the Snowcap assemblage are polycyclic and form ca. 719, 1930-1870, 2100-2000, 2300, and 2600 Ma age peaks that are consistent with Laurentian craton provenance, including its Archean core and younger Proterozoic assemblages. Analogous detrital zircon age populations from the Snowcap assemblage and some Neoproterozoic to Lower Devonian sedimentary rock strata along the northern Cordilleran margin strengthen original stratigraphic links (e.g., Piercey and Colpron, 2009) between the southeastern Yukon-northwestern British Columbia sector of northwest Laurentia and Yukon-Tanana terrane basement.

4.2 FUTURE WORK

4.2.1 Thermochronology and alternate accessory mineral study opportunities

Detrital zircon "double-dating" techniques that combine fission-track or (U-Th)/He cooling ages and U-Pb crystallization ages record the exhumation history of orogens and provide a method for reconstructing source-to-sink connections along continental margins (e.g. Enkelmann et al., 2019, 2008; Fosdick et al. 2015a; Saylor et al., 2012; Campbell et al., 2005; Carter and Bristow, 2000). Double-dating results combined with published ^{40}Ar-^{39}Ar and K-Ar mica and hornblende cooling ages from intrusive rocks in central Yukon and eastern Alaska may constrain the local exhumation rates of Intermontane basement domains.

Zircon are fertile in intermediate to felsic igneous rocks, resistant to chemical and physical weathering, and preserve their U-Pb-Hf isotope compositions during higher grade metamorphic conditions. For these reasons, the recycling of zircon grains in sedimentary systems is common and there is an inherent bias with investigating only one mineral in provenance studies. To reduce these biases, other well-characterized accessory minerals (e.g. monazite, spinel, mica, and apatite) used in conjunction with zircon can provide a more complete provenance record and increase the understanding of regional tectonic evolution.

Monazite forms under low to high grade metamorphic conditions and can record metamorphic events that are lost when strictly investigating zircon (e.g., Hietpas et al., 2010, 2011). Monazite reported in sedimentary rocks during diagenesis/low-grade burial metamorphism can also be used as a proxy for assessing the degree of detrital recycling (e.g., Moecher et al., 2019).

Spinel minerals can be used as a provenance indicator for mafic to ultramafic rocks. The composition of spinel minerals is variable and indicative of partial melt conditions (e.g., Irvine, 1967, 1974; Dick and Bullen, 1984; Barnes and Roeder, 2001) and therefore detrital spinel can be used to constrain tectonic setting (e.g., Cookenboo et al., 1997; Dare et al., 2016). Detrital spinel was identified in Faro Peak formation thin sections and could provide insight into the tectonic conditions that formed Permian(?) mafic to ultramafic rocks in the Slide Mountain terrane near Faro. Direct sampling of mafic and ultramafic rocks near Faro and comparing them to detrital spinel in the Faro Peak formation could prove or disprove that local Slide Mountain terrane rock units sourced the Faro Peak formation, as indicated from clast compositions (e.g., Wiest and Beranek, 2019; Wiest et al., 2020; Chapter 2).

Mica is ubiquitous in the Faro Peak formation and locally identified in unnamed Triassic units. Determining ^{40}Ar-^{39}Ar cooling ages on these mica minerals could identify bedrock source regions and constrain tectonic exhumation evolution models for the northern Intermontane terranes.

Snowcap assemblage units near Faro were locally metamorphosed to eclogite facies and contain late Permian white mica cooling ages (e.g., Erdmer et al., 1998) and were recycled into the overlying unnamed Triassic and Faro Peak formation units (Wiest and Beranek 2019; Wiest et al., 2020; Chapters 2,3). These dates contrast from Jurassic cooling ages typical of arc- to syn-collisional plutonic rocks in the outboard Intermontane terranes (e.g., Dusel-Bacon et al., 2002) and may be used to better understand the late Paleozoic to early Mesozoic tectonic history of the northern Canadian Cordillera.

Apatite is a common uranium-bearing accessory mineral in mafic to felsic igneous rocks (Piccoli and Candela, 2002). Apatite has different closure temperatures (i.e., ~450-500°C for U-Pb, ~120-60°C for fission-track, and ~80-60°C for [U-Th]/He) making it an important thermochronometer. These methods when combined are known as "triple-dating" and in detrital mineral studies reveal the cooling and exhumation histories of source regions and basins (e.g., Carrapa et al., 2009). Apatite also contains variable trace element compositions that can be linked to sources and used as a provenance indicator (e.g., Belousova et al., 2002; Morton and Yaxley, 2007; O'Sullivan et al., 2018). Near Faro, detrital apatite studies using all or one of these methods combined with the detrital zircon U-Pb-Hf isotope results would substantially increase the understanding of provenance, sediment transport histories, and timing and rates of tectonic exhumation. The lower temperature (U-Th)/He system in detrital apatite can be reset during burial and can add basin-scale subsidence and subsequent uplift timing constraints in active tectonic environments (e.g., Buelow et al., 2018) such as the southern Tay River map area during the Triassic to Jurassic.

4.2.2 Macauley Ridge formation and Upper Triassic units

The Macauley Ridge formation contains conglomerate and sandstone units near Beaver Creek in southwestern Yukon (Fig. 4.1). These units were originally considered to be Cretaceous or Tertiary in age (Tempelman-Kluit, 1974), however, detrital zircon U-Pb results indicate that the Macauley Ridge formation is related to Early Jurassic synorogenic sedimentation in the Intermontane terranes (Colpron et al., 2015; Chapter 2).

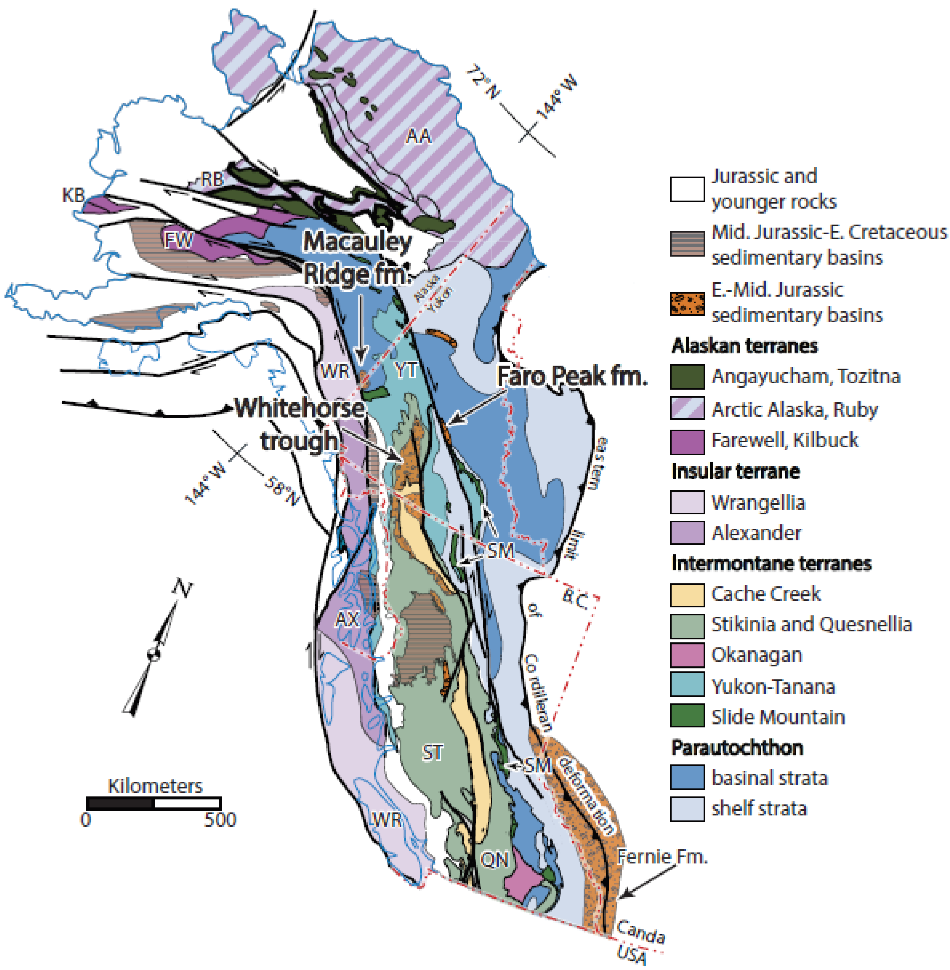

Figure 4.1 - Paleozoic to early Mesozoic terranes and Jurassic sedimentary basins of the Canadian Cordillera after Colpron et al. (2015). Terrane abbreviations: AA—Arctic Alaska; AX—Alexander; FW—Farewell; KB—Kilbuck; QN—Quesnellia; RB—Ruby; SM—Slide Mountain; ST—Stikinia; YT—Yukon-Tanana; WR—Wrangellia.

The Macauley Ridge formation is in faulted(?) contact with Triassic marine strata and Paleozoic rocks of the Slide Mountain terrane (Murphy et al., 2007, 2008) and in eastern Alaska unconformably overlies Devonian metamorphic rocks (Richter, 1976). Targeted field stratigraphic and detrital zircon U-Pb-Hf isotope studies of the Macauley Ridge formation and associated Triassic units could test hypotheses for their tectonic significance and correlation with the Laberge Group (e.g., van Drecht, 2019), Faro Peak formation (Chapter 2), and unnamed Triassic rocks near Faro (Chapter 3). Some research questions include: 1) what are the contact relationships of the Macauley Ridge formation with Triassic rocks, Slide Mountain terrane, and Devonian metamorphic rocks?; 2) how do Triassic units compare with unnamed units near Faro (Chapter 3) and other Triassic successions that overlap the Yukon-Tanana and Slide Mountain terranes from eastern Alaska to northern British Columbia (Beranek and Mortensen, 2011)?; 3) does the Macauley Ridge formation record evidence for source unroofing and local derivation from underlying and adjacent units?; 4) are Late Triassic to Early Jurassic zircon grains in the Macauley Ridge formation (Colpron et al., 2015) sourced from the same or different arc- to syn-collisional plutons that sourced the Laberge Group and Faro Peak formation?

4.2.3 Unnamed Triassic units

Unnamed Triassic units in the southern Tay River map area require detrital zircon U-Pb-Hf isotope provenance studies to test regional stratigraphic correlations and better understand Triassic sedimentation along the northern Cordilleran margin. Samples of unnamed Triassic units collected during the 2018 and 2019 field seasons (Table 4.1) provide an opportunity for a student to become familiar with sample processing, analysis, data reduction, and data interpretation methods without traveling to Yukon to do fieldwork. Whole-rock lithogeochemical investigations of Triassic basalt units that are interbedded with limestone and argillite units (03AW19 and 05AW19; Table 4.1) can constrain the Late Triassic tectonic setting of the Yukon-Tanana terrane in the Faro region.

Sample ID	Easting	Northing	Formation	Locality	Description	Method
clastic						
11AW18	586445	6903521	Unnamed	Whiskey Mtn.	fine to medium-grained sandstone	dz, t
12AW18	586118	6903737	Unnamed	Whiskey Mtn.	wackestone	dz, t
13AW18	586118	6903732	Unnamed	Whiskey Mtn.	medium-grained sandstone-wackestone	
14AW18	585849	6903136	Unnamed	Whiskey Mtn.	medium-grained sandstone	
23AW18	588084	6901667	Unnamed	Repeater Hill	micaceous argillite	t
31AW18	577103	6909497	Unnamed	Faro Peak	argillite to fine-grained sandstone	t
01AW19	567771	6913700	Unnamed (possible float)	Rose Mtn.	coarse-grained to pebble conglomerate (float?)	
04AW19	567690	6913286	Unnamed	Rose Mtn.	coarse-grained to pebble conglomerate	dz*, t
08AW19	586542	6902621	Unnamed(?) (mapped as Faro Peak fm.)	Whiskey Mtn.	siltstone to fine-grained sandstone	
10AW19	586638	6903008	Unnamed(?) (mapped as Faro Peak fm.)	Whiskey Mtn.	fine-grained sandstone	dz*, t
16AW19	577144	6909525	Unnamed	Faro Peak	siltstone to fine-grained sandstone	dz, t
20AW19	586136	6903728	Unnamed	Whiskey Mtn.	green wackestone	
21AW19	585892	6903954	Unnamed	Whiskey Mtn.	green argillite or basalt(?)	
22AW19	585830	6904076	Unnamed	Whiskey Mtn.	medium to very coarse-grained sandstone	dz*, t
25AW19	586848	6902900	Unnamed	Whiskey Mtn.	fine to medium-grained sandstone	
26AW19	587058	6902987	Unnamed	Whiskey Mtn.	fine to medium-grained sandstone	t
27AW19	587065	6902996	Unnamed	Whiskey Mtn.	argillite	
magmatic						
03AW19	567822	6913666	Unnamed	Rose Mtn.	dark grey basalt	
05AW19	568036	6913439	Unnamed	Rose Mtn.	dark grey basalt	

dz = detrital zircon U-Pb-Hf (Chapter 3)
dz* = crushed, milled, isolated, picked
t = thin section

Table 4.1 - Summary of samples from unnamed Triassic units taken during the 2018 and 2019 field seasons.

4.2.4 Permian units of the southern Tay River map area

Slide Mountain terrane units in the southern Tay River map area are up to 2300 m thick and include the Carboniferous to lower Permian Mount Aho, Rose Mountain, and Campbell Range formations that are intruded by Permian(?) mafic and ultramafic rock units (Pigage, 2004). These units are well exposed and form a complete section ~20-25 km northwest of Faro near Rose Mountain and Faro Peak. This locality represents a field area to test multiple hypothesis about the development, evolution, and closure of the Slide Mountain ocean and allow for comparison with current models derived from the study of Slide Mountain terrane units along its eastern margin overlying the Yukon-Tanana terrane (e.g., van Staal et al., 2018; Parsons et al., 2019).

The Mount Aho and Rose Mountain formations contain sandstone and conglomerate units with local detrital feldspar (e.g., Pigage, 2004) indicating they would be candidates for detrital zircon U-Pb-Hf isotope provenance studies. Due to the well exposed nature of these units near Rose Mountain and Faro Peak, systematic sampling of these units would provide insight into the extent and evolution of the Slide Mountain ocean basin. Moreover, studying these units would add to the detrital zircon reference frame for unnamed Triassic and Faro Peak formation units near Faro.

During the 2019 field season, a pegmatitic gabbro body was identified (sample 06AW19) in the Permian(?) mafic to ultramafic rock map unit and could be used to constrain the age of this unit more precisely (Table 4.2). Potentially correlative mafic to ultramafic rocks in the Finlayson Lake area are dated at ~273 Ma and provide a testable hypothesis for this gabbro unit (Mortensen, 1992; Murphy et al., 2006).

Sample ID	Easting	Northing	Formation	Locality	Description
06AW19	568378	6914926	Slide Mountain terrane mafic-ultramafic map unit	Rose Mtn.	pegmatitic gabbro
14AW19	588059	6902176	Campbell Range fm. (mapped as Snowcap assemblage)	Repeater Hill	dark green basalt
18AW19b	597514	6896218	Campbell Range fm. (mapped as Faro Peak fm.)	Blind Creek	green basalt
19AW19	597764	6895906	Campbell Range fm. (mapped as Faro Peak fm.)	Blind Creek	green basalt

Table 4.2 - Summary of igneous rock samples of taken during the 2019 field season.

Basalt samples collected during the 2019 field season include units originally mapped as Snowcap assemblage (14AW19) and Faro Peak formation (18AW19b, 19AW19) that have subsequently been included by the author in the Campbell Range formation (Table 4.2). Whole-rock lithoeochemical and Nd-Hf isotope studies of these units can provide more robust datasets from the Campbell Range formation in the southern Tay River area (e.g., Pigage, 2004) that can be compared with datasets in the Finlayson Lake area (Piercey et al., 2012).

Suprasubduction zone ophiolites (e.g., Clinton Creek, Midnight Dome, and Dunite Peak) are interpreted to overlie Yukon-Tanana terrane in Yukon and record the initial stages of closure of the Slide Mountain ocean basin (van Staal et al., 2018; Parsons et al., 2019). The study of units near Faro could test if the opposite side of the Slide Mountain terrane, which is carried eastwards over the North American continental margin along the Inconnu thrust, similarly represent a suprasubduction zone ophiolite or if other mechanisms led to their development and emplacement.

4.3 REFERENCES

Barnes, S.J. and Roeder, P.L., 2001, The range of spinel compositions in terrestrial mafic and ultramafic rocks: Journal of Petrology, v. 42, no. 12, p. 2279-2302, doi: 10.1093/petrology/42.12.2279.

Belousova, E.A., Griffin, W.L., O'Reilly, S.Y., and Fisher, N.I., 2002, Apatite as an indicator mineral for mineral exploration: trace-element compositions and their relationship to host rock type: Journal of Geochemical Exploration, v. 76, no. 1, p. 45-69, doi: 10.1016/S0375-6742(02)00204-2.

Beranek, L.P., and Mortensen, J.K., 2011, The timing and provenance record of the Late Permian Klondike orogeny in northwestern Canada and arc-continent collision along western North America: Tectonics, v. 30, 23 p, doi: 10.1029/2010TC002849.

Berman, R.G., Ryan, J.J., Gordey, S.P., and Villeneuve, M., 2007, Permian to Cretaceous polymetamorphic evolution of the Stewart River region, Yukon-Tanana terrane, Yukon, Canada: P-T evolution linked with in situ SHRIMP monazite geochronology: Journal of Metamorphic Geology, v. 25, p. 803-827, doi: 10.1111/j.1525-1314.2007.00729.x.

Buelow, E.K., Suriano, J., Mahoney, J.B., Kimbrough, D.L., Mescua, J.F., Giambiagi, L.B., and Hoke, G.D., 2018, Sedimentologic and stratigraphic evolution of the Cacheuta basin: Constraints on the development of the Miocene retroarc foreland basin, south-central Andes: Lithosphere, v. 10, no. 3, p. 366-391, doi: 10.1130/L709.1.

Campbell, I.H., Reiners, P.W., Allen, C.M., Nicolescu, S., and Upadhyay, R., 2005, He-Pb double dating of detrital zircons from the Ganges and Indus Rivers: Implication for quantifying sediment recycling and provenance studies: Earth and Planetary Science Letters, v. 237, no. 3-4, p. 402-432, doi: 10.1016/j.epsl.2005.06.043.

Carrapa, B., DeCelles, P.G., Reiners, P.W., Gehrels, G.E., and Sudo, M., 2009, Apatite triple dating and white mica $^{40}Ar/^{39}Ar$ thermochronology of syntectonic detritus in the Central Andes: A multiphase tectonothermal history: Geology, v. 37, no. 5, p. 407-410, doi: 10.1130/G25698A.1.

Carter, A., Bristow, C.S., 2000, Detrital zircon geochronology: Enhancing the quality of sedimentary source information through improved methodology and combined U-Pb and fission-track techniques: Basin Research, v. 12, p. 47-57, doi: 10.1046/j.1365-2117.2000.00112.x.

Colpron, M., Crowley, J.L., Gehrels, G., Long, D.G.F., Murphy, D.C., Beranek, L., and Bickerton, L., 2015, Birth of the northern Cordilleran orogeny, as recorded by detrital zircons in

Jurassic synorogenic strata and regional exhumation in Yukon: Lithosphere, v. 7, p. 541-562, doi: 10.1130/L451.1.

Cookenboo, H.O., Bustin, R.M., and Wilks, K.R., 1997, Detrital chromian spinel compositions used to reconstruct the tectonic setting of provenance; implications for orogeny in the Canadian Cordillera: Journal of Sedimentary Research, v. 67, no. 1, p. 116-123, doi: 10.1306/D4268509-2B26-11D7-8648000102C1865D.

Dare, M.S., Tarduno, J.A., Bono, R.K., Cottrell, R.D., Beard, J.S., and Kodama, K.P., 2016, Detrital magnetite and chromite in Jack Hills quartzite cobbles: Further evidence for the preservation of primary magnetizations and new insights into sediment provenance: Earth and Planetary Science Letters, v. 451, p. 298-314, doi: 10.1016/j.epsl.2016.05.009.

Dick, H.J.B. and Bullen, T., 1984, Chromian spinel as a petrogenetic indicator in abyssal and alpine-type peridotites and spatially associated lavas: Contributions to Mineralogy and Petrology, v. 86, p. 54-76.

Dickie, J.R., and Hein, F.J., 1995, Conglomeratic fan deltas and submarine fans of the Jurassic Laberge Group, Whitehorse trough, Yukon Territory, Canada: fore-arc sedimentation and unroofing of a volcanic island-arc complex: Sedimentary Geology, v. 98, p. 263–292, doi:10.1016/0037-0738(95)00036-8.

Dusel-Bacon, C., Lanphere, M.A., Sharp, W.D., Layer, P.W., and Hanson, V.L., 2002, Mesozoic thermal history and timing of structural events for the Yukon-Tanana Upland, east-central Alaska—$^{40}Ar/^{39}Ar$ data from metamorphic and plutonic rocks: Canadian Journal of Earth Sciences, v.39, p. 1013-1051, doi:10.1139/e02-018.

Enkelmann, E., Garver, J.I., and Pavlis, T.L., 2008, Rapid exhumation of ice covered rocks of the Chugach-St. Elias orogeny, Southeast Alaska: Geology, v. 36, no. 12, p. 915-918, doi: 10.1130/G2252A.1.

Enkelmann, E., Sanchez, S.K., and Finzel, E.S., 2019, Detrital zircon double-dating of forearc basin strata reveals magmatic, exhumational, and thermal history of sediment source areas: Geological Society of America Bulletin, v. 131, no. 7-8, p. 1364-1384, doi: 10.1130/B35043.1.

Erdmer, P., Ghent, E.D., Archibald, D.A., and Stout, M.Z., 1998, Paleozoic and Mesozoic high-pressure metamorphism at the margin of ancestral North America in central Yukon: Geological Society of America Bulletin, v. 110, no. 5, p. 615-629.

Fosdick, J.C., Grove, M., Graham, S.A., Hourigan, J.K., Lovera, O., and Romans, B.W., 2015, Detrital thermochronologic record of burial heating and sediment recycling in the Magallanes foreland basin, Patagonian Andes: Basin Research, v. 27, p. 546-572, doi: 10.1111/bre.12088.

Hietpas, J., Samson, S., and Moecher, D., 2011, A direct comparison of the ages of detrital monazite versus detrital zircon in Appalachian foreland basin sandstones: Searching for the record of Phanerozoic orogenic events, v. 310, no. 3-4, p. 488-497, doi: 10.1016/j.epsl.2011.08.033.

Hietpas, J., Samson, S., Moecher, D., and Schmitt, A.K., 2010, Recovering tectonic events from the sedimentary record: Detrital monazite plays in high fidelity: Geology, v. 38, no. 2, p. 167-170, doi: 10.1130/G30265.1.

Irvine, T.N., 1967, Chromian spinel as a petrogenetic indicator: Part 2. Petrologic applications: Canadian Journal of Earth Sciences, v. 4, p. 71-103, doi: 10.1139/e67-004.

Irvine, T.N., 1974, Petrology of the Duke Island Ultramafic Complex southeaster Alaska, Geological Society of America Memoirs, v. 138, doi: 10.1130/MEM138.

Moecher, D.P., Kelly, E.A., Hietpas, J., and Samson, S.D., 2019, Proof of recycling in clastic sedimentary systems from textural analysis and geochronology of detrital monazite: Implications for detrital mineral provenance studiets: Geological Society of America Bulletin, v. 131, no. 7-8, p. 1115-1132, doi: 10.1130/B31947.1.

Mortensen, J.K., 1992, Pre–mid-Mesozoic tectonic evolution of the Yukon-Tanana terrane, Yukon and Alaska: Tectonics, v. 11, p. 836–853, doi: 10.1029/91TC01169.

Morton, A. and Yaxley, G., 2007, Detrital apatite geochemistry and its application in provenance studies, *in* Arribas, J., Critelli, S., and Johnsson, M.J., eds., Sedimentary provenance and petrogenesis: Perspectives from petrography and geochemsitry: Geological Society of America, Special Paper 420, p. 319-344, doi: 10.1130/2006.2420(19).

Murphy, D.C., Mortensen, J.K., Piercey, S.J., Orchard, M.J., and Gehrels, G.E., 2006, Mid-Paleozoic to early Mesozoic tectonostratigraphy evolution of Yukon-Tanana and Slide Mountain terranes and affiliated overlap assemblages, Finlayson Lake massive sulphide district, southeastern Yukon, *in* Colpron, M. and Nelson, J.L., eds., Paleozoic Evolution and Metallogeny of Pericratonic Terranes at the Ancient Pacific Margin of North America, Canadian and Alaskan Cordillera: Geological Association of Canada, Special Paper 45, p. 75-105.

Murphy, D.C., van Staal, C.R., and Mortensen, J.K., 2007, Preliminary Bedrock Geology of Part of Stevenson Ridge Area (NTS 115J/3, 4, 5, 6, 7, 8, {arts of 11 and 12; 115K/1, 2, 7, 8, 9, 10, Parts of 15 and 16): Yukon Geological Survey Open-File 2007-9, scale 1:125,000.

Murphy, D.C., van Staal, C.R., and Mortensen, J.K., 2008, Windy McKinley terrane, Stevenson Ridge area (115JK), western Yukon: Composition and proposed correlations, with implications for mineral potential, *in* Emond, D.S., Blackburn, L.R., Hill, R.P., and Weston, L.H., eds., Yukon Exploration and Geology 2007: Whitehorse, Yukon, Canada, Yukon Geological Survey, p. 225–235.

O'Sullivan, G.J., Chew, D.M., Morton, C., Mark, C., and Henrichs, A., 2018, An integrated apatite geochronology and geochemistry tool for sedimentary provenance analysis: Geochemistry, Geophysics, Geosystems, v. 19, no. 4, p. 1309-1326, doi: 10.1002/2017GC007343.

Parsons, A.J., Zagorevski, A., Ryan, J.J., McClelland, W.C., van Staal, C.R., Coleman, M.J., and Golding, M.L., 2019, Petrogenesis of the Dunite Peak ophiolite, south-central Yukon, and the distinction between upper-plate and lower-plate setting: A new hypothesis for the late Paleozoic—early Mesozoic tectonic evolution of the Northern Cordillera: Geological Society of America Bulletin, v. 131, no. 1/2, p. 74-298, doi: 10.1130/B31964.1.

Piccoli, P.M. and Candela, P.A., 2002, Apatite in igneous systems: Reviews in Mineralogy and Geochemistry, v. 48, p. 255-292, doi: 10.2138/rmg.2002.48.6.

Piercey, S.J., and Colpron, M., 2009, Composition and provenance of the Snowcap assemblage, basement to the Yukon-Tanana terrane, northern Cordillera: Implications for Cordilleran crustal growth: Geosphere, v. 5, no. 5, p. 439-464, doi: 10.1130/GS00505.1.

Piercey, SJ., Murphy, D.C., and Creaser, R.A., 2012, Lithosphere-asthenosphere mixing in a transform-dominated late Paleozoic backarc basin: Implications for northern Cordilleran crustal growth and assembly: Geosphere, v. 8, no. 3, p. 716-739, doi: 10.1130/GES00757.1.

Pigage, L.C., 2004, Bedrock geology compilation of the Anvil District (parts of NTS 105K/2, 3, 5, 6, 7, and11), central Yukon: Yukon Geological Survey, Bulletin, v.15, p. 103.

Richter, D., 1976, Geologic Map of Nabesna Quadrangle, Alaska: U.S. Geological Survey, Miscellaneous Investigations Series Map-932, scale 1:250,000.

Saylor, J.E., Stockli, D.F., Horton, B.K., Nie, J., and Mora, A., 2012, Discriminating rapid exhumation from syndepositional volcanism using detrital zircon double dating: Implications for the tectonic history of the Eastern Cordillera, Colombia: Geological Society of America Bulletin, v. 124, no. 5/6, p. 762-779, doi: 10.1130/B30534.1.

Tempelman-Kluit, D.J., 1972, Geology and origin of the Faro, Vangorda, and Swim concordant zinc-lead deposits, central Yukon Territory: Geological Survey of Canada, Bulletin 208, 73 p.

Tempelman-Kluit, D.J., 1974, Reconnaissance geology of Aishihik Lake, Snag, and part of Sewart River map areas, west-central Yukon: Geological Survey of Canada Paper 73-41, 97 p.

van Staal, C.R., Zagorevski, A., McClelland, W.C., Escayola, M.P., Ryan, J.J., Parsons, A.J., Proenza, J., 2018, Age and setting of Permian Slide Mountain terrane ophiolitic ultramafic-mafic complexes in the Yukon: Implications for late Paleozoic-early Mesozoic tectonic models in the northern Canadian Cordillera: Tectonophysics, v. 744, p. 458-483, doi: 10.1016/j.tecto.2018.07.008.

Wiest, A.C. and Beranek, L.P., 2019, Stratigraphy of the Faro Peak formation, central Yukon: New field observations of Jurassic synorogenic sedimentation along the Yukon-Tanana–Slide Mountain terrane boundary, *in* Yukon Exploration and Geology 2018, K.E. MacFarlane (ed.), Yukon Geological Survey, p.127–142.

Wiest, A.C., Beranek, L.P., and Manor, M.J., 2020, Upper Triassic to Lower Jurassic stratigraphy of the Faro Peak formation, southern Tay River map area, central Yukon (NTS 105K), *in* Yukon Exploration and Geology 2019, K.E. MacFarlane (ed.), Yukon Geological Survey, p. 121-139.

COMBINED REFERENCES

Barnes, S.J. and Roeder, P.L., 2001, The range of spinel compositions in terrestrial mafic and ultramafic rocks: Journal of Petrology, v. 42, no. 12, p. 2279-2302, doi: 10.1093/petrology/42.12.2279.

Belousova, E.A., Griffin, W.L., O'Reilly, S.Y., and Fisher, N.I., 2002, Apatite as an indicator mineral for mineral exploration: trace-element compositions and their relationship to host rock type: Journal of Geochemical Exploration, v. 76, no. 1, p. 45-69, doi: 10.1016/S0375-6742(02)00204-2.

Beranek L.P., Mortensen, J.K., Lane, L.S., Allen, T.L., Fraser, T.A., Hadlari, T., and Zantvoort, W.G., 2010a, Detrital zircon geochronology of the western Ellesmerian clastic wedge, northwestern Canada: Insights on Arctic tectonics and the evolution of the northern Cordilleran miogeocline: Geological Society of America Bulletin, v. 112, no. 11-12, p. 1889-1911, doi: 10.1130/B30120.1.

Beranek, L.P., 2009, Provenance and paleotectonic setting of North American Triassic strata in Yukon: The sedimentary record of pericratonic terrane accretion in the northern Canadian Cordillera [PhD thesis]: Vancouver, British Columbia, Canada, The University of British Columbia, 338p.

Beranek, L.P., and Mortensen, J.K., 2011, The timing and provenance record of the Late Permian Klondike orogeny in northwestern Canada and arc-continent collision along western North America: Tectonics, v. 30, 23 p, doi: 10.1029/2010TC002849.

Beranek, L.P., Gee, D.G., and Fisher, C.M., 2020, Detrital zircon U-Pb-Hf isotope signatures of Old Red Sandstone strata constrain the Silurian to Devonian paleogeography, tectonics, and crustal evolution of the Svalbard Caledonides: Geological Society of America Bulletin, v. 132, no. 9-10, p. 1987-2003, doi: 10.1130/B35318.1.

Beranek, L.P., Link, P.K., and Fanning, C.M., 2016, Detrital zircon record of mid-Paleozoic convergent margin activity in the northern U.S. Rocky Mountains: Implications for the Antler orogeny and early evolution of the North American Cordillera: Lithosphere, v. 8, no. 5, p. 553-550, doi: 10.1130/L557.1.

Beranek, L.P., Mortensen, J.K., Orchard, M.J., and Ullrich, T., 2010b, Provenance of North American Triassic strata from west-central and southeastern Yukon: correlations with coeval strata in the Western Canada Sedimentary Basin and Canadian Arctic Islands: Canadian Journal of Earth Sciences, v. 47(1), p. 53-73, doi: 10.1139/E09-065.

Berman, R.G., Ryan, J.J., Gordey, S.P., and Villeneuve, M., 2007, Permian to Cretaceous polymetamorphic evolution of the Stewart River region, Yukon-Tanana terrane, Yukon, Canada: P-T evolution linked with in situ SHRIMP monazite geochronology: Journal of Metamorphic Geology, v. 25, p. 803-827, doi: 10.1111/j.1525-1314.2007.00729.x.

Bickerton, L., Colpron, M., Gibson, H.D., Thorkelson, D., and Crowley, J.L., 2020, The northern termination of the Cache Creek terrane in Yukon: Middle Triassic arc activity and Jurassic-Cretaceous structural imbrication: Canadian Journal of Earth Sciences, v. 57, no. 2, p. 227-248, doi: 10.1139/cjes-2018-0262.

Boggs, S.Jr., 2001, Principles of sedimentology and stratigraphy, 3rd edition: Prentice Hall, Englewood Cliffs, NJ, 726 p.

Brennan, D.T., Li, Z.-X., Rankenburg, K., Evans, N., Link, P.K., Nordsvan, A.R., Kirkland, C.L., Mahoney, J.B., Johnson, T., and McDonald, B.J., 2021, Recalibrating Rodinian rifting in the northwestern United States: Geology, v. 49, doi: 10.1130/G48435.1.

Buelow, E.K., Suriano, J., Mahoney, J.B., Kimbrough, D.L., Mescua, J.F., Giambiagi, L.B., and Hoke, G.D., 2018, Sedimentologic and stratigraphic evolution of the Cacheuta basin: Constraints on the development of the Miocene retroarc foreland basin, south-central Andes: Lithosphere, v. 10, no. 3, p. 366-391, doi: 10.1130/L709.1.

Campbell, I.H., Reiners, P.W., Allen, C.M., Nicolescu, S., and Upadhyay, R., 2005, He-Pb double dating of detrital zircons from the Ganges and Indus Rivers: Implication for quantifying sediment recycling and provenance studies: Earth and Planetary Science Letters, v. 237, no. 3-4, p. 402-432, doi: 10.1016/j.epsl.2005.06.043.

Campbell, R.W., Beranek, L.P., Piercey, S.J., and Friedman, R., 2019, Early Paleozoic post-breakup magmatism along the Cordilleran margin of western North America: New zircon u-Pb age and whole-rick Nd- and Hf-isotope and lithogeochemical results from the Kechika group, Yukon, Canada: Geosphere, v. 15, doi: 10.1130/GES02044.1.

Carrapa, B., DeCelles, P.G., Reiners, P.W., Gehrels, G.E., and Sudo, M., 2009, Apatite triple dating and white mica $^{40}Ar/^{39}Ar$ thermochronology of syntectonic detritus in the Central Andes: A multiphase tectonothermal history: Geology, v. 37, no. 5, p. 407-410, doi: 10.1130/G25698A.1.

Carter, A., Bristow, C.S., 2000, Detrital zircon geochronology: Enhancing the quality of sedimentary source information through improved methodology and combined U-Pb and fission-track techniques: Basin Research, v. 12, p. 47-57, doi: 10.1046/j.1365-2117.2000.00112.x.

Cawood, P.A., Hawkesworth, C.J., and Dhuime, B., 2012, Detrital zircon record and tectonic setting: Geology, v. 40, p. 875-878, doi: 10.1130/G32945.1.

Clark, A.D., 2017, Tectonometamorphic history of mid-crustal rocks at Aishihik Lake, southwest Yukon: Unpublished MSc thesis, Simon Fraser University, British Columbia, Canada, p. 153.

Cohen, K.M., Finney, S.C., Gibbard, P.L., and Fran, J.-X., 2013;updated, The ICS International Chronostratigraphic Chart, ep. 36: 199-204, http://www.stratigraphy.org/ICSchart/ChronostratChart2021-07.pdf.

Colpron, M., Crowley, J.L., Gehrels, G., Long, D.G.F., Murphy, D.C., Beranek, L., and Bickerton, L., 2015, Birth of the northern Cordilleran orogeny, as recorded by detrital zircons in Jurassic synorogenic strata and regional exhumation in Yukon: Lithosphere, v. 7, p. 541-562, doi: 10.1130/L451.1.

Colpron, M., Mortensen, J.K., Gehrels, G.E., and Villeneuve, M., 2006b, Basement complex, Carboniferous magmatism and Paleozoic deformation in Yukon-Tanana terrane of central Yukon: Field, geochemical and geochronological constraints from Glenlyon map area, *in* Colpron, M. and Nelson, J.L., eds., Paleozoic Evolution and Metallogeny of Pericratonic Terranes at the Ancient Pacific Margin of North America, Canadian and Alaskan Cordillera: Geological Association of Canada, Special Paper 45, p. 131-151.

Colpron, M., Nelson, J.L., and Murphy, D.C., 2006a, A tectonostratigraphic framework for the pericratonic terranes of the northern Cordillera, *in* Colpron, M. and Nelson, J.L., eds., Paleozoic Evolution and Metallogeny of Pericratonic Terranes at the Ancient Pacific Margin of North America, Canadian and Alaskan Cordillera: Geological Association of Canada, Special Paper 45, p. 1-23.

Colpron, M., Nelson, J.L., and Murphy, D.C., 2007, Northern Cordilleran terranes and their interactions through time: Geological Society of America Today, v. 17, no. 4/5, doi: 10.1130/GSAT01704-5A.1.

Cookenboo, H.O., Bustin, R.M., and Wilks, K.R., 1997, Detrital chromian spinel compositions used to reconstruct the tectonic setting of provenance; implications for orogeny in the Canadian Cordillera: Journal of Sedimentary Research, v. 67, no. 1, p. 116-123, doi: 10.1306/D4268509-2B26-11D7-8648000102C1865D.

Corfu, F., and Davis, D.W., 1992, A U-Pb geochronological framework for the western Superior Province, Ontario: *in* Geology of Ontario, Ontario Geological Survey, special v. 4, part 2, p. 1335-1346.

Corfu, F., Stott, G.M., and Breaks, F.W., 1995, U-Pb geochronology and evolution of the English River Subprovince, an Archean low P-high T metasedimentary belt in the Superior Province: Tectonics, v. 14, no. 5, p. 1220-1233, doi: 10.1029/95TC01452.

Corrigan, D., Pehrsson, S., Wodicka, N., and de Kemp, E., 2009, The Paleoproterozoic Trans-Hudson Orogen: a prototype of modern accretionary processes: Geological Society of London, Special Publications 327, p. 457-479, doi: 10.1144/SP327.19.

Coutts, D.S., Matthews, W.A., and Hubbard, S.M., 2019, Assessment of widely used methods to derive depositional ages from detrital zircon populations: Geoscience Frontiers, v. 10, no. 4, p. 1421-1435, doi: 10.1016/j.gsf.2018.11.002.

Creaser, R.A., Erdmer, P., Stevens, R.A., and Grant, S.L., 1997, Tectonic affinity of the Nisultin and Anvil assemblage strata from the Teslin tectonic zone, northern Canadian Cordillera: Constraints from neodymium isotope and geochemical evidence: Tectonics, v. 16, no. 1, p. 107-121.

Cushing, G.W., 1984, The tectonic evolution of the eastern Yukon-Tanana Upland [M.S. thesis]: Albany, State University of New York, 235 p.

Dare, M.S., Tarduno, J.A., Bono, R.K., Cottrell, R.D., Beard, J.S., and Kodama, K.P., 2016, Detrital magnetite and chromite in Jack Hills quartzite cobbles: Further evidence for the preservation of primary magnetizations and new insights into sediment provenance: Earth and Planetary Science Letters, v. 451, p. 298-314, doi: 10.1016/j.epsl.2016.05.009.

Day, W.C., Aleinikoff, J.N., and Gamble, B., 2002, Geochemistry and age constraints on metamorphism and deformation in the Fortymile River area, eastern Yukon-Tanana Upland, Alaska, *in* Wilson, F.H., and Galloway, J.P., eds., Studies by the U.S. Geological Survey in Alaska, 2000: U.S. Geological Survey Professional Paper 1662, p. 5–18.

de Keijzer, M., Mihalynuk, M.G., and Johnston, S.T., 2000, Structural investigation of an exposure of the Teslin fault, northwestern British Columbia: Geological Survey of Canada, Current Research 2000-A5, 10 pp.

DeGraff-Surpless, K., Graham, S.A., Wooden, J.L., and McWilliams, M.O., 2002, Detrital zircon provenance analysis of the Great Valley group, California: Evolution of an arc-forearc system: Geological Society of America Bulletin, v. 114, no. 12, p. 1564-1580, doi: 10.1130/0016-7606(2002)114<1564:DZPAOT>2.0.CO;2.

DeGraff-Surpless, K., Mahoney, J.B., Wooden, J.L., and McWilliams, M.O., 2003, Lithofacies control in detrital zircon provenance studies: Insights from the Cretaceous Methow basin, southern Canadian Cordillera: Geological Society of America Bulletin, v. 115, no. 8, p. 899-915, doi: 10.1130/B25267.1.

Dick, H.J.B. and Bullen, T., 1984, Chromian spinel as a petrogenetic indicator in abyssal and alpine-type peridotites and spatially associated lavas: Contributions to Mineralogy and Petrology, v. 86, p. 54-76.

Dickie, J.R., and Hein, F.J., 1995, Conglomeratic fan deltas and submarine fans of the Jurassic Laberge Group, Whitehorse trough, Yukon Territory, Canada: fore-arc sedimentation and unroofing of a volcanic island-arc complex: Sedimentary Geology, v. 98, p. 263–292, doi:10.1016/0037-0738(95)00036-8.

Dickinson, W.R., and Gehrels, G.E., 2009, Use of U-Pb ages of detrital zircons to infer maximum depositional ages of strata: A test against a Colorado Plateau Mesozoic database: Earth and Planetary Science Letters, v. 288, p. 115-125, doi: 10.1016/j.epsl.2009.09.013.

Dickinson, W.R., and Suczek, C.A., 1979, Plate tectonics and sandstone compositions: American Association of Petroleum Geologists Bulletin, v. 63, p. 2164-2182, doi: 10.1306/2F9188FB-16CE-11D7-8645000102C1865D.

Dickinson, W.R., Beard, L.S., Brakenridge, G.R., Erjavec, J.L., Ferguson, R.C., Inman, K.F., Knepp, R.A., Lindberg, F.A., and Ryberg, P.T., 1983, Provenance of North American Phanerozoic sandstones in relation to tectonic setting: Geological Society of America Bulletin, v. 94, p. 222-235.

Dostal, J., Keppie, J.D., and Ferri, F., 2009, Extrusion of high-pressure Cache Creek rocks into the Triassic Stikinia-Quesnellia arc of the Canadian Cordillera: Implications for terrane analysis of ancient orogens and palaeogeography, *in* Murphy, J.B., Keppie, J.D., and Hynes, A.J., eds., Ancient Orogens and Modern Analogues: Geological Society of London Special Publication 327, p.71-87.

Dusel-Bacon, C., Aleinikoff, J.N., Day, W.C., and Mortensen, J.K., 2015, Mesozoic magmatism and timing of epigenetic Pb-Zn-Ag mineralization in the western Fortymile mining district, east-central Alaska: Zircon U-Pb geochronology, whole-rock geo-chemistry, and Pb isotopes: Geosphere, v. 11, no. 3, p. 786-822, doi:10.1130/GES01092.

Dusel-Bacon, C., Hansen, V.L., 1992, High-pressure amphibolite-facies metamorphism and deformation within the Yukon-Tanana and Taylor Mountain terranes, eastern Alaska, *in* Geologic Studies in Alaska, US Geological Survey, 1991, Bradley, D.C. and Dusel-Bacon, C. (eds), US Geological Survey Bulletin 2041, p. 140-159.

Dusel-Bacon, C., Hansen, V.L., and Scala, J.A., 1995, High-pressure amphibolite facies dynamic metamorphism and the Mesozoic tectonic evolution of an ancient continental margin, east-central Alaska: Journal of Metamorphic Geology, v.13, p. 9-24, doi:10.1111/j.1525-1314.1995.tb00202.x.

Dusel-Bacon, C., Hopkins, M.J., Mortensen, J.K., Dashevsky, S.S., Bressler, J.R., and Day, W.C., 2006, Paleozoic tectonic and metallogenic evolution of the pericratonic rocks of east-central Alaska and adjacent Yukon, *in* Colpron, M. and Nelson, J.L., eds., Paleozoic evolution and metallogeny of pericratonic terranes at the ancient margin of North America, Canadian and Alaskan Cordillera: Geological Association of Canada, Special Paper 45, p. 25-74.

Dusel-Bacon, C., Lanphere, M.A., Sharp, W.D., Layer, P.W., and Hanson, V.L., 2002, Mesozoic thermal history and timing of structural events for the Yukon-Tanana Upland, east-central Alaska—$^{40}Ar/^{39}Ar$ data from metamorphic and plutonic rocks: Canadian Journal of Earth Sciences, v.39, p. 1013-1051, doi:10.1139/e02-018.

Dusel-Bacon, C., Slack, J.F., Aleinikoff, J.N., and Mortensen, J.K., 2009, Mesozoic magmatism and basemetal mineralization in the Fortymile mining district, eastern Alaska—Initial results of petrographic, geochemical, and isotopic studies in the Mount Veta area, *in* Haeussler, P.J., and Galloway, J.P., eds., Studies by the U.S. Geological Survey in Alaska, 2007: U.S. Geological Survey Professional Paper 1760-A, 42 p.

Einsele, G., 1992, Sedimentary Basins: Evolution, Facies, and Sediment Budget: Springer-Verlag, Berlin, 628 p.

Enkelmann, E., Garver, J.I., and Pavlis, T.L., 2008, Rapid exhumation of ice covered rocks of the Chugach-St. Elias orogeny, Southeast Alaska: Geology, v. 36, no. 12, p. 915-918, doi: 10.1130/G2252A.1.

Enkelmann, E., Sanchez, S.K., and Finzel, E.S., 2019, Detrital zircon double-dating of forearc basin strata reveals magmatic, exhumational, and thermal history of sediment source areas: Geological Society of America Bulletin, v. 131, no. 7-8, p. 1364-1384, doi: 10.1130/B35043.1.

Erdmer, P., Ghent, E.D., Archibald, D.A., and Stout, M.Z., 1998, Paleozoic and Mesozoic high-pressure metamorphism at the margin of ancestral North America in central Yukon: Geological Society of America Bulletin, v. 110, no. 5, p. 615-629.

Fisher C.M., Vervoort, J.D., and DuFrane, S.A., 2014, Accurate Hf isotopic determinations of complex zircons using the "laser ablation split stream" method: Geochemistry, Geophysics, Geosystems, v. 15, p. 121-139, doi: 10.1002/2013GC004962.

Fosdick, J.C., Grove, M., Graham, S.A., Hourigan, J.K., Lovera, O., and Romans, B.W., 2015, Detrital thermochronologic record of burial heating and sediment recycling in the Magallanes foreland basin, Patagonian Andes: Basin Research, v. 27, p. 546-572, doi: 10.1111/bre.12088.

Foster, H.L., 1992, Geologic map of the eastern Yukon-Tanana region, Alaska: US Geological Survey, Open-File Report 92-313, scale 1:50,000.

Foster, H.L., Donato, M.M., and Yount, M.E., 1978, Petrographic and chemical data on Mesozoic granitic rocks of the Eagle quadrangle, Alaska: U.S. Geological Survey Open-File Report 78-253, 29 p., 2 maps, scale 1:250,000.

Foster, H.L., Keith, T.E.C., and Menzie, W.D., 1994, Geology of the Yukon-Tanana area of east-central Alaska, *in* Plafker, G. and Berg, H.C., (eds.), The geology of Alaska: Geological Society of America, G-1, p. 197-217.

Furlanetto, F., Thorkelson, D.J., Rainbird, R.H., Davis, W.J., Gibson, H.D., and Marshall, D.D., 2016, The Paleoproterozoic Wernecke Supergroup of Yukon, Canada: Relationships to orogeny in northwestern Laurentia and basins in North America, East Australia, and China: Gondwana Research, v. 39, p. 14-40, doi: 10.1016/j.gr.2016.06.007.

Gabrielse, H., Murphy, D.C., and Mortensen, J.K., 2006, Cretaceous and Cenozoic dextral orogeny-parallel displacements, magmatism, and paleogeography, north-central Canadian Cordillera, *in* Haggart, J.W., Enkin, R.J. and Monger, J.W.H., eds., Paleogeography of the North American Cordillera: Evidence for and Against Large-Scale Displacements: Geological Association of Canada Special Paper 46, p. 255-276.

Gaidies, F., Morneau, Y.E., Petts, D.C., Jackson, S.E., Zagorevski, A. and Ryan, J.J., 2021, Major and trace element mapping of garnet: Unravelling the conditions, timing and rates of metamorphism of the Snowcap assemblage, west-central Yukon: Journal of metamorphic Geology, v. 39, p. 133-164, doi: 10.1111/jmg.12562.

Gehrels, G. and Pecha, M., 2014, Detrital zircon U-Pb geochronology and Hf isotope geochemistry of Paleozoic and Triassic passive margin strata of western North America: Geosphere, v. 10, no. 1, p. 49-65, doi: 10.1130/GES00889.1.

Gehrels, G., 2012, Detrital zircon U-Pb geochronology: Current methods and new opportunities, *in* Busby, C. and Azor Pérez, A., eds., Tectonics of sedimentary basins: Recent advances, p. 45-62, doi: 10.1002/9781444347166.ch2

Gehrels, G., 2014, Detrital zircon U-Pb geochronology applied to tectonics: Annual Review of Earth and Planetary Sciences, v. 42, p. 127-149.

Gehrels, G.E. and Ross, G.M., 1998, Detrital zircon geochronology of Neoproterozoic to Permian miogeoclinal strata in British Columbia and Alberta: Canadian Journal of Earth Sciences, v. 35, p. 1380-1401, doi: 10.1139/e98-071.

Golding, M.L., Mortensen, J.K., Ferri, F., Zonneveld, J.-P., and Orchard, M.J., 2016, Determining the provenance of Triassic sedimentary rocks in northeastern British Columbia and western

Alberta using detrital zircon geochronology, with implications for regional tectonics. Canadian Journal of Earth Sciences, vol. 53, p. 140-155, doi: 10.1139/cjes-2015-0082.

Goodfellow, W.D., Cecile, M.P., and Leybourne, M.I., 1995, Geochemistry, petrogenesis, and tectonic setting of lower Paleozoic alkalic and potassic volcanic rocks, Northern Canadian Cor-dilleran Miogeocline: Canadian Journal of Earth Sciences, v. 32, p. 1236-1254, doi: 10.1139/e95-101.

Gordey, S.P., McNicoll, V.J., and Mortensen, J.K., 1998, New U-Pb ages from the Teslin area, southern Yukon, and their bearing on terrane evolution in the northern Cordillera, *in* Current Research 1998-F: Geological Survey of Canada, p.129-148.

Grunsky, E.C., 2010, The interpretation of geochemical survey data: Geochemistry, Exploration, Environmental Analysis, v. 10, no. 1 p. 27-74, doi: 10.1144/1467-7873/09-210.

Hadlari, T., Davis, W.J., Dewing, K., Heaman, L.M., Lemieux, Y., Ootes, L., Pratt, B.R., and Pyle, L.J., 2012, Two detrital zircon signatures for the Cambrian passive margin of northern Laurentia highlighted by new U-Pb results from northern Canada: Geological Society of America Bulletin, v. 124, p. 1155–1168, doi: 10.1130 /B30530.1.

Hansen, V.L., and Dusel-Bacon, C., 1998, Structural and kinematic evolution of the Yukon-Tanana Upland tectonites, east-central Alaska: A record of late Paleozoic to Mesozoic crustal assembly: Geological Society of America Bulletin, v. 110, p. 211–230, doi:10.1130/0016-7606(1998)110<0211 :SAKEOT >2.3.CO;2.

Hansen, V.L., Heizler, M.T., and Harrison, T.M., 1991, Mesozoic thermal evolution of the Yukon-Tanana composite terrane—New evidence from ^{40}Ar/^{39}Ar data: Tectonics, v. 10, p. 51–76, doi:10.1029/90TC01930.

Hart, C.J.R., 1997, A Transect across Northern Stikinia: Geology of the Northern Whitehorse Map Area, Southern Yukon Territory (105D/13–16): Exploration and Geological Services Division, Yukon Region, Indian and Northern Affairs Canada, Bulletin 8, p. 112.

Hart, C.J.R., Dickie, J.R., Ghosh, D.K., and Armstrong, R.L., 1995, Provenance constraints for Whitehorse trough conglomerate: U-Pb zircon dates and initial Sr ratios of granitic clasts in Jurassic Laberge Group, Yukon Territory, *in* Miller, D.M., and Busby, C., eds., Jurassic Magmatism and Tectonics of the North American Cordillera: Geological Society of America Special Paper 299, p. 47–63.

Hempton, M., Dunne, L., 1984, Sedimentation in pull-apart basins: Active examples in Eastern Turkey: The Journal of Geology, v. 92, no. 5, p. 513-530.

Herriott, T.M., Crowley, J.L., Schmitz, M.D., Wartes, M.A., and Gillis, R.J., 2019, Exploring the law of detrital zircon: LA-ICP-MS and CA-TIMS geochronology of Jurassic forearc strata, Cook Inlet, Alaska, USA: Geology, v. 47, no. 11, p. 1044-1048, doi: 10.1130/G46312.1.

Hietpas, J., Samson, S., and Moecher, D., 2011, A direct comparison of the ages of detrital monazite versus detrital zircon in Appalachian foreland basin sandstones: Searching for the record of Phanerozoic orogenic events, v. 310, no. 3-4, p. 488-497, doi: 10.1016/j.epsl.2011.08.033.

Hietpas, J., Samson, S., Moecher, D., and Schmitt, A.K., 2010, Recovering tectonic events from the sedimentary record: Detrital monazite plays in high fidelity: Geology, v. 38, no. 2, p. 167-170, doi: 10.1130/G30265.1.

Hoffman, P.F., 1989, Precambrian geology and tectonic history of North America, *in* Bally, A.W., and Palmer, A.R., eds., The Geology of North America: An Overview: Boulder, Colorado, Geological Society of America, The Geology of North America, v. A, p. 447–512.

Hunt, P.A. and Roddick, J.C., 1987, A compilation of K-Ar ages, report 17, *in* Radiogenic age and isotopic studies: Report 1, Geological Survey of Canada Paper 87-2, p. 203.

Hunt, P.A. and Roddick, J.C., 1991, A compilation of K-Ar ages: report 20, *in* Radiogenic age and isotopic studies: Report 4, Geological Survey of Canada Paper no. 90-2, p.113-143, doi: 10.4095/131943.

Hunt, P.A. and Roddick, J.C., 1992, A compilation of K-Ar and ^{40}Ar-^{39}Ar ages, report 22, *in* Radiogenic age and isotopic studies: Report 6, Geological Survey of Canada Paper 92-2, p. 179–226.

Ingersoll, R.V., 1988, Tectonics of sedimentary basins: Geological Society of America Bulletin, b. 100, p. 1704-1719, doi: 10.1130/0016-7606(1988)100<1704:TOSB>2.3.CO;2

Ingersoll, R.V., 2012, Tectonics of sedimentary basins, with revised nomenclature, *in* Busby, C. and Azor Pérez, A., eds., Tectonics of sedimentary basins: Recent advances: Blackwell Publishing Ltd., 656 p.

Irvine, T.N., 1967, Chromian spinel as a petrogenetic indicator: Part 2. Petrologic applications: Canadian Journal of Earth Sciences, v. 4, p. 71-103, doi: 10.1139/e67-004.

Irvine, T.N., 1974, Petrology of the Duke Island Ultramafic Complex southeaster Alaska, Geological Society of America Memoirs, v. 138, doi: 10.1130/MEM138.

Johannson, G.G., Smith, P.L., and Gordey, S.P., 1997, Early Jurassic evolution of the northern Stikinian arc: evidence from the Laberge Group, northwestern British Columbia: Canadian Journal of Earth Science, v. 34, p. 1030-1057.

Johnsson, M. J., 1993, The system controlling the composition of clastic sediments, *in* Johnsson, M J., and Basu, A., eds., Processes Controlling the Composition of Clastic Sediments: Geological Society of America Special Paper 284, p. 1-19.

Johnston, S.T., Mortensen, J.K., and Erdmer, P., 1996, Igneous and metaigneous age constraints for the Aishihik metamorphic suite, southwest Yukon: Canadian Journal of Earth Sciences, v. 33, p. 1543-1555.

Joyce, N.L., Ryan, J.J., Colpron, M., Hart, C.J.R., and Murphy, D.C., 2015, A compilation of 40Ar/39Ar age determinations for igneous and metamorphic rocks, and mineral occurrences from central and southeast Yukon: Geological Survey of Canada Open-File 7924, 229 p., doi: 10.4095/297446.

Kellett, D.A. and Zagorevski, A., 2021, Overlap assemblages: Laberge Group of the Whitehorse trough, northern Canadian Cordillera, Yukon–British Columbia, *in* Ryan, J.J. and Zagorevski, A., eds., Northern Cordillera geology: a synthesis of research from the Geo-mapping for Energy and Minerals program, British Columbia and Yukon: Geological Survey of Canada, Bulletin 610, p. 1-22.

Kellett, D.A., Weller, O.M., Zagorevski, A., and Regis, D., 2018, A petrochronological approach for the detrital record: Tracking mm-sized eclogite clasts in the northern Canadian Cordillera: Earth and Planetary Science Letters, v. 494, p. 23-31, doi:10.1016/j.epsl.2018.04.036.

Kemp, A.I.S., Hawkesworth, C.J., Paterson, B.A., and Kinny, P.D., 2006, Episodic growth of the Gondwana supercontinent from hafnium and oxygen isotopes in zircon: Nature, v. 439, p. 580-583.

Knight, E., Schneider, D.A., and Ryan, J., 2013, Thermochronology of the Yukon-Tanana Terrane, West-Central Yukon: Evidence for Jurassic Extension and Exhumation in the Northern Canadian Cordillera: The Journal of Geology, v. 121, p. 371-400, doi: 10.1086/670721.

Lane, L.S. and Gehrels, G.E., 2014, Detrital zircon lineages of late Neoproterozoic and Cambrian strata, NW Laurentia: Geological Society of America Bulletin, v. 126, no. 3/4, p. 398-414, doi: 10.1130/B30848.1.

Leslie, C.D., 2009, Detrital zircon geochronology and rift-related magmatism: central Mackenzie Mountains, Northwest Territories [M.Sc. thesis]: Vancouver, British Columbia, The University of British Columbia, 224 p.

Lowey, G.W., 2004, Preliminary lithostratigraphy of the Laberge Group (Jurassic), south-central Yukon: Implications concerning the petroleum potential of the Whitehorse trough, *in* Emond, D.S., and Lewis, L.L., eds., Yukon Exploration and Geology 2003: Whitehorse, Yukon, Canada, Yukon Geological Survey, p.129–142.

Lowey, G.W., 2008, Summary of the stratigraphy, sedimentology, and hydrocarbon potential of the Laberge Group (Lower–Middle Jurassic), Whitehorse trough, Yukon, *in* Emond, D.S., Blackburn, L.R., Hill, R.P., and Weston, L.H., eds., Yukon Exploration and Geology 2007: Whitehorse, Yukon, Canada, Yukon Geological Survey, p.179–197.

Matthews, W., Guest, B., and Madronich, L., 2018, Latest Neoproterozoic to Cambrian detrital zircon facies of western Laurentia: Geosphere, v. 14, no. 1, p. 243-264, doi: 10.1130/GES01544.1.

McCausland, P.J.A., Symons, D.T.A., Hart, C.J.R., and Blackburn, W.H., 2002, Paleomagnetism and geobarometry of the Granite Mountain batholith, Yukon: Minimal geotectonic motion of the Yukon-Tanana Terrane relative to North America, *in* Yukon Exploration and Geology, 2001, D.S. Emond, L.H. Weston and L.L. Lewis (eds.), Exploration and Geological Services Division, Yukon, Indian and Northern Affairs Canada, p. 163-177.

McMechan, M., Currie, L., Ferri, F., Matthews, W., O'Sullivan, P., 2017, Cambrian detrital zircon signatures of the northern Cordillera passive margin, Liard area, Canada: evidence of sediment recycling, non-Laurentian ultimate sources, and basement denudation: Canadian Journal of Earth Sciences, v. 54, p. 609-621, doi: 10.1139/cjes-2016-0127.

Metcalfe, P., 1981, Petrogenesis of the Klondike formation, Yukon Territory [MS.c. thesis], University of Manitoba, Winnipeg, M.B., 305 p.

Mihalynuk, M.G., Erdmer, P., Ghent, E.D., Cordey, F., Archibald, D.A., Friedman, R.M., and Johannson, G.G., 2004, Coherent French Range blueschist: Subduction to exhumation in<2.5m.y.?: Geological Society of America Bulletin, v.116, p.910–922, doi: 10.1130/B25393.1.

Mihalynuk, M.G., Nelson, J.A., and Diakow, L.J., 1994, Cache Creek terrane entrapment: Oroclinal paradox within the Canadian Cordillera: Tectonics, v. 13, p. 575-595.

Moecher, D.P., Kelly, E.A., Hietpas, J., and Samson, S.D., 2019, Proof of recycling in clastic sedimentary systems from textural analysis and geochronology of detrital monazite:

Implications for detrital mineral provenance studiets: Geological Society of America Bulletin, v. 131, no. 7-8, p. 1115-1132, doi: 10.1130/B31947.1.

Monger, J., and Price, R., 2002, The Canadian Cordillera: Geology and Tectonic Evolution: Canadian Society of Exploration Geophysicists Recorder, v. 27, p. 17-36.

Monger, J.W.H., Price, R.A., and Tempelman-Kluit, D.J., 1982, Tectonic accretion and the origin of the two major metamorphic and plutonic welts in the Canadian Cordillera: Geology, v. 10, no. 2, p. 70-75, doi: 10.1130/0091-7613(1982)10<70:TAATOO>2.0.CO;2.

Mortensen, J. K., 1990, Geology and U-Pb geochronology of the Klondike District, west-central Yukon Territory, Canadian Journal of Earth Sciences, v. 27, p. 903–914, doi:10.1139/e90-093.

Mortensen, J.K., 1992, Pre–mid-Mesozoic tectonic evolution of the Yukon-Tanana terrane, Yukon and Alaska: Tectonics, v. 11, p. 836–853, doi: 10.1029/91TC01169.

Morton, A. and Yaxley, G., 2007, Detrital apatite geochemistry and its application in provenance studies, *in* Arribas, J., Critelli, S., and Johnsson, M.J., eds., Sedimentary provenance and petrogenesis: Perspectives from petrography and geochemsitry: Geological Society of America, Special Paper 420, p. 319-344, doi: 10.1130/2006.2420(19).

Murphy, D.C., Mortensen, J.K., Piercey, S.J., Orchard, M.J., and Gehrels, G.E., 2006, Mid-Paleozoic to early Mesozoic tectonostratigraphy evolution of Yukon-Tanana and Slide Mountain terranes and affiliated overlap assemblages, Finlayson Lake massive sulphide district, southeastern Yukon, *in* Colpron, M. and Nelson, J.L., eds., Paleozoic Evolution and Metallogeny of Pericratonic Terranes at the Ancient Pacific Margin of North America, Canadian and Alaskan Cordillera: Geological Association of Canada, Special Paper 45, p. 75-105.

Murphy, D.C., van Staal, C.R., and Mortensen, J.K., 2007, Preliminary Bedrock Geology of Part of Stevenson Ridge Area (NTS 115J/3, 4, 5, 6, 7, 8, {arts of 11 and 12; 115K/1, 2, 7, 8, 9, 10, Parts of 15 and 16): Yukon Geological Survey Open-File 2007-9, scale 1:125,000.

Murphy, D.C., van Staal, C.R., and Mortensen, J.K., 2008, Windy McKinley terrane, Stevenson Ridge area (115JK), western Yukon: Composition and proposed correlations, with implications for mineral potential, *in* Emond, D.S., Blackburn, L.R., Hill, R.P., and Weston, L.H., eds., Yukon Exploration and Geology 2007: Whitehorse, Yukon, Canada, Yukon Geological Survey, p. 225–235.

Nelson, J. and Friedman, R., 2004, Superimposed Quesnel (late Paleozoic-Jurassic) and Yukon-Tanana (Devonian-Mississippian) arc assemblages, Cassiar Mountains, northern British Columbia: field, U-Pb, and igneous petrochemical evidence: Canadian Journal of Earth Sciences, v. 41, p. 1201-1235.

Nelson, J.L., Colpron, M., Piercey, S.J., Dusel-Bacon, C., Murphy, D.C., and Root, C.F., 2006, Paleozoic tectonic and metallogenic evolution of the pericrationic terranes in Yukon, northern British Columbia and eastern Alaska, *in* Colpron, M. and Nelson, J.L., eds., Paleozoic Evolution and Metallogeny of Pericratonic Terranes at the Ancient Pacific Margin of North America, Canadian and Alaskan Cordillera: Geological Association of Canada, Special Paper 45, p. 323-360.

Newberry, R.J., Layer, P.W., Burleigh, R.E., and Solie, D.N., 1998, New $^{40}Ar/^{39}Ar$ dates for intrusions and mineral prospects in the eastern Yukon-Tanana terrane—Regional patterns and significance, Alaska, *in* Gray, J.E., and Riehle, J.R., eds., Geologic studies in Alaska by the United States Geological Survey, 1996: U.S. Geological Survey Professional Paper 1595, p.131–159.

O'Sullivan, G.J., Chew, D.M., Morton, C., Mark, C., and Henrichs, A., 2018, An integrated apatite geochronology and geochemistry tool for sedimentary provenance analysis: Geochemistry, Geophysics, Geosystems, v. 19, no. 4, p. 1309-1326, doi: 10.1002/2017GC007343.

Orchard, M.J., 2006, Late Paleozoic and Triassic conodont faunas of Yukon and northern British Columbia and implications for the evolution of the Yukon-Tanana terrane, *in* Colpron, M. and Nelson, J.L., eds., Paleozoic evolution and metallogeny of pericratonic terranes at the ancient pacific margin of North America, Canadian and Alaskan Cordillera: Geological Association of Canada, Special Paper 45, p. 229-260.

Parsons, A.J., Coleman, M.J., Ryan, J.J., Zagorevski, A., Joyce, N.L., Gibson, H.D., and Larson, K.P., 2018, Structural evolution of a crustal-scale shear zone through a decreasing temperature regime: The Yukon River shear zone, Yukon-Tanana terrane, northern Cordillera: Lithosphere, v. 10, p. 760-782, doi: 10.1130/L724.1.

Parsons, A.J., Zagorevski, A., Ryan, J.J., McClelland, W.C., van Staal, C.R., Coleman, M.J., and Golding, M.L., 2019, Petrogenesis of the Dunite Peak ophiolite, south-central Yukon, and the distinction between upper-plate and lower-plate setting: A new hypothesis for the late Paleozoic—early Mesozoic tectonic evolution of the Northern Cordillera: Geological Society of America Bulletin, v. 131, no. 1/2, p. 74-298, doi: 10.1130/B31964.1.

Paton, C., Hellstrom, J., Paul, B., Woodhead, J., and Hergt, J., 2011, Iolite: Freeware for the visualization and processing of mass spectrometric data: Journal of Analytical Atomic Spectrometry, v. 26, p. 2508-2518, doi:10.1039/C1JA10172B.

Petrie, M.B., Massonne, H.-J., Gilotti, J.A., McClelland, W.C., and van Staal, C., 2016, The P-T path of eclogites in the St. Cyr klippe, Yukon, Canada: Permian metamorphism of a coherent high-pressure unit in an accreted terrane of the North American Cordillera: European Journal of Mineralogy, v. 28, no. 6, p. 1111-1130, doi: 10.1127/ejm/2016/0028-2576.

Petrus, J., and Kamber, B.S., 2012, VizualAge: A Novel Approach to Laser Ablation ICP-MS U-Pb Geochronology Data Reduction: Geostandards and Geoanalytical Research, v. 36, 24 p., doi:10.1111/j.1751-908X.2012.00158.x.

Pettit, B.S., Blum, M., Pecha, M., McLean, N., Bartschi, N.C., and Saylor, J.E., 2019, Detrital-zircon U-Pb paleodrainage reconstruction and geochronology of the Campanian Blackhawk-Castlegate succession, Wasatch plateau and Brooks Cliffs, Utah, U.S.A.: Journal of Sedimentary Research, v. 89, p. 273-292, doi: 10.2110/jsr.2019.18.

Philippot, P., Blichert-Toft, J., Perchuk, A., Costa, S., Gerasimov, V., 2001, Lu-Hf and Ar-Ar chronometry supports extreme rate of subduction zone metamorphism deduced from geospeedometry: Tectonophysics, v. 342, p. 23-38.

Piccoli, P.M. and Candela, P.A., 2002, Apatite in igneous systems: Reviews in Mineralogy and Geochemistry, v. 48, p. 255-292, doi: 10.2138/rmg.2002.48.6.

Piercey, S.J., and Colpron, M., 2009, Composition and provenance of the Snowcap assemblage, basement to the Yukon-Tanana terrane, northern Cordillera: Implications for Cordilleran crustal growth: Geosphere, v. 5, no. 5, p. 439-464, doi: 10.1130/GS00505.1.

Piercey, S.J., Mortensen, J.K. and Creaser, R.A., 2003, Neodymium isotope geochemistry of felsic volcanic and intrusive rocks from the Yukon-Tanana terrane in the Finlayson Lake region, Yukon, Canada: Canadian Journal of Earth Sciences, v. 40, p. 77-97.

Piercey, S.J., Nelson, J.L., Colpron, M., Dusel-Bacon, C., Simard, R-L. and Roots, C.F., 2006, Paleozoic magmatism and crustal recycling along the ancient Pacific margin of North American, northern Canadian Cordillera, *in* Colpron, M. and Nelson, J.L., eds., Paleozoic Evolution and Metallogeny of Pericratonic Terranes at the Ancient Pacific Margin of North America, Canadian and Alaskan Cordillera: Geological Association of Canada, Special Paper 45, p. 281-322.

Piercey, SJ., Murphy, D.C., and Creaser, R.A., 2012, Lithosphere-asthenosphere mixing in a transform-dominated late Paleozoic backarc basin: Implications for northern Cordilleran crustal growth and assembly: Geosphere, v. 8, no. 3, p. 716-739, doi: 10.1130/GES00757.1.

Pigage, L.C., 2004, Bedrock geology compilation of the Anvil District (parts of NTS 105K/2, 3, 5, 6, 7, and11), central Yukon: Yukon Geological Survey, Bulletin, v.15, p. 103.

Pigage, L.C., 2009, Bedrock geology of NTS 95C/5 (Pool Creek) and NTS 95D/8 map sheets, southeast Yukon: Yukon Geological Survey, Bulletin 16, 150 p.

Pigage, L.C., Roots, C.F., and Abbott, J.G. 2015. Regional bedrock geology for Coal River map area (NTS 95D), southeast Yukon: Yukon Geological Survey, Bulletin 17, 155 p.

Porter, C., Morin, P., Howat, I., Noh, M-J., Bates, B., Peterman, K., Keesey, S., Schlenk, M., Gardiner, J., Tomko, K., Willis, M., Kelleher, C., Cloutier, M., Husby, E., Foga, S., Nakamura, H., Platson, M., Wethington, M. Jr., Williamson, C., Bauer, G., Enos, J., Arnold, G., Kramer, W., Becker, P., Doshi, A., D'Souza, C., Cummens, P., Laurier, F. and Bojesen, M., 2018. ArcticDEM, https://doi.org/10.7910/DVN/OHHUKH, Harvard Dataverse, vol. 1 [accessed November, 2019].

Rainbird, R., Cawood, P., and Gehrels, G., 2012, The great Grenvillian sedimentation episode: Record of supercontinent Rodinia's assembly, *in* Busby, C., and Azor,A., eds., Tectonics of Sedimentary Basins: Recent Advances: Chichester, West Sussex, UK, Wiley-Black-well Publishing, p. 583-601.

Rainbird, R.H., Heaman, L.M., and Young, G., 1992, Sampling Laurentia: Detrital zircon geochronology offers evidence for an extensive Neoproterozoic river system originating from the Grenville orogen: Geology, v. 20, p. 351-354, doi: 10.1130/0091-7613(1992)020<0351:SLDZGO>2.3.CO;2.

Richter, D., 1976, Geologic Map of Nabesna Quadrangle, Alaska: U.S. Geological Survey, Miscellaneous Investigations Series Map-932, scale 1:250,000.

Roots, C.F., Harms, T.A., Simard, R.-L., Orchard, M.J., and Heaman, L., 2002, Constraints on the age of the Klinkit assemblage east of Teslin Lake, northern British Columbia: Geological Survey of Canada, Current Research 2002-A7, 11p.

Roots, C.F., Nelson, J.L., Simard, R.-L., and Harms, T.A., 2006, Continental fragments, mid-Paleozoic arcs and overlapping late Paleozoic arc and Triassic sedimentary strata in the Yukon-Tanana terrane of northern British Columbia and southern Yukon, *in* Colpron, M.

and Nelson, J.L., eds., Paleozoic Evolution and Metallogeny of Pericratonic Terranes at the Ancient Pacific Margin of North America, Canadian and Alaskan Cordillera: Geological Association of Canada, Special Paper 45, p. 153-177.

Ross, G.M., 1990, Deep crust and basement structure of the Peace River Arch region: constraints on mechanisms of formation: Bulletin of Canadian Petroleum Geology, v. 38A, p. 25-35, doi: 10.35767/gscpgbull.38a.1.025.

Ross, G.M., Villeneuve, M.E., and Theriault, R.J., 2001, Isotopic provenance of the lower Muskwa assemblage (Mesoproterozoic, Rocky Mountains, British Columbia): new clues to correlation and source areas: Precambrian Research, v. 111, p. 57-77, doi: 10.1016/S0301-9268(01)00156-5.

Ruks, T.W., Piercey, S.J., Ryan, J.J., Villeneuve, M.E., and Creaser, R.A., 2006, Mid- to late Paleozoic K-feldspar augen granitoids of the Yukon-Tanana terrane, Yukon, Canada: Implications for crustal growth and tectonic evolution of the northern Cordillera: Geological Society of America Bulletin, v. 118, no. 9/10, doi: 10.1130/B25854.1.

Sack, P.J., Colpron, M., Crowley, J.L., Ryan, J.J., Allan, M.M. Beranek, L.P., Joyce, N.L., 2020, Atlas of Late Triassic to Jurassic plutons in the Intermontane terranes of Yukon: Yukon Geological Survey, Open File 2020-1, p. 365.

Sauer, K.B., Gordon, S.M., Miller, R.B., Vervoort, J.D., and Fisher, C.M., 2017, Evolution of the Jura-Cretaceous North American Cordilleran margin: Insights from detrital-zircon U-Pb and Hf isotopes of sedimentary units of the North Cascades Range, Washington: Geosphere, v. 13, no. 6, p. 2094-2118, doi: 10.1130/GES01501.1.

Saylor, J.E., Stockli, D.F., Horton, B.K., Nie, J., and Mora, A., 2012, Discriminating rapid exhumation from syndepositional volcanism using detrital zircon double dating: Implications for the tectonic history of the Eastern Cordillera, Colombia: Geological Society of America Bulletin, v. 124, no. 5/6, p. 762-779, doi: 10.1130/B30534.1.

Shirmohammad, F., Smith, P.L., Anderson, R.G., and McNicoll, V.J., 2011, The Jurassic succession at Lisadale Lake (Tulsequah map area, British Columbia, Canada) and its bearing on the tectonic evolution of the Stikine terrane: Volumnia Jurassica, v. 9, p. 43-60.

Simard, R.-L., Dostal, J., and Roots, C.F., 2003, Development of late Paleozoic volcanic arcs in the Canadian Cordillera: An example from the Klinkit Group, northern British Columbia and southern Yukon: Canadian Journal of Earth Sciences, v. 40, p. 907–924, doi:10.1139/e03-025.

Sircombe, K.N. and Stern, R.A., 2002, An investigation of artificial biasing in detrital zircon U-Pb geochronology due to magnetic separation in sample preparation: Geochemica et Cosmochimica Acta, v. 66, no. 13, p. 2379-2397, doi: 10.1016/S0016-7037(02)00839-6.

Skulski, T., Corkery, M.T., Stone, D., Whalen, J.B., Stern, R.A., 2000, Geological and geochronological investigations in the Stull Lake-Edmund Lake greenstone belt and granitoid rocks of the northwestern Superior Province: *in* Report of Activities 2000, Manitoba Industry, Trade and Mines, Manitoba Geological Survey, p. 117-128.

Sláma, J., Kosler, J., Condon, D., Crowley, J.L., Gerdes, A., Hanchar, J.M, Horstwood, S.A., Morris, G.A., Nasdala, L., Norberg, N., Schaltegger, U., Schoene, B., Tubrett, M., and Whitehouse, M.J., 2008, Plešovice zircon – A new natural reference material for U-Pb and

Hf isotopic microanalysis: Chemical Geology, v. 249, p. 1-35, doi: 10.1016/j.chemgeo.2007.11.005.

Sloss, L.L., 1988, Tectonic evolution of the craton in Phanerozoic time, *in* Sloss, L.L., ed., Sedimentary Cover—North American Craton: Boulder, Colorado, Geological Society of America, The Geology of North America, v. D-2, p. 25–51.

Sloss, L.L., 1988, Tectonic evolution of the craton in Phanerozoic time, *in* Sloss, L.L., ed., Sedimentary Cover—North American Craton: Boulder, Colorado, Geological Society of America, The Geology of North America, v. D-2, p. 25–51.

Stevens, R.D., DeLabio, R.N., and LaChance, G.R., 1982, Age determinations and geological studies, K-Ar isotopic ages: Geological Survey of Canada, Report 15, p. 74.

Symons, D.T.A., Williams, P.R., McCausland, P.J.A., Harris, M.J., Hart, C.J.R., and Blackburn, W.H., 2000, Paleomagnetism and geobarometry of the Big Creek Batholith suggests that Yukon-Tanana Terrane has been a parautochthon since Early Jurassic: Tectonophysics, v. 326, p. 57-72.

Szumigala, D.J., Newberry, R.J., Werdon, M.B., Finseth, B.A., Pinney, D.S., and Flynn, R.L., 2000, Major-oxide, minor-oxide, trace-element, and geochemical data from rocks collected in a portion of the Fortymile Mining District, Alaska: State of Alaska Division of Geological and Geophysical Surveys Raw-Data File 2000-1, 24 p., scale 1:63,360.

Tafti, R., 2005, Nature and Origin of the Early Jurassic Copper (-Gold) Deposits at Minto and Williams Creek, Carmacks Copper Belt, Western Yukon: Examples of Deformed Porphyry Deposits [M.Sc. thesis]: Vancouver, British Columbia, Canada, University of British Columbia, 213 p.

Tempelman-Kluit, D.J., 1972, Geology and origin of the Faro, Vangorda, and Swim concordant zinc-lead deposits, central Yukon Territory: Geological Survey of Canada, Bulletin 208, 73 p.

Tempelman-Kluit, D.J., 1974, Reconnaissance geology of Aishihik Lake, Snag, and part of Sewart River map areas, west-central Yukon: Geological Survey of Canada Paper 73-41, 97 p.

Tempelman-Kluit, D.J., 1984, Geology, Laberge (105E) and Carmacks (105I), Yukon Territory: Geological Survey of Canada Open-File 1101, scale 1:250,000.

Tempelman-Kluit, D.J., 2009, Geology of Carmacks and Laberge Map Areas, Central Yukon: Incomplete Draft Manuscript on Stratigraphy, Structure and its Early Interpretation(ca.1986): Geological Survey of Canada Open-File 5982, 399 p.

Thomas, W.A., Gehrels, G.E., Sundell, K.E., Greb, S.F., Finzel, E.Z., Clark, R.J., Malone, D.H., Hampton, B.A., and Romero, M.C., 2020, Detrital zircons and sediment dispersal in the eastern Midcontinent of North America: Geosphere, v. 16, doi: 10.1130/GES02152.1.

Topham, M.J., Allan, M.M., Mortensen, J.K., Hart, C.J.R., Colpron, M., and Sack, P.J., 2016, Crustal depth of emplacement of the Early Jurassic Aishihik and Tatchun batholiths, west-central Yukon, *in* Yukon Exploration and Geology 2015, K.E. MacFarlane (ed.), Yukon Geological Survey, p. 233–251.

Tyler, S.A., Marsden, R.W., Grout, F.F., and Thiel, G.A., 1940, Studies of the Lake Superior Precambrian by accessory-mineral methods: Geological Society of America Bulletin, v. 51, p. 1429-1538.

University of Minnesota, 2018, Polar Geospatial Center, https://www.pgc.umn.edu, [accessed November, 2019].

Unterschutz, J.L.E., Creaser, R.A., Erdmer, P., Thompson, R.I., and Daughtry, K.L., 2002, North American margin origin of Quesnel terrane strata in the southern Canadian Cordillera: Inferences from geochemical and Nd isotopic characteristics of Triassic metasedimentary rocks: Geological Society of America Bulletin, v. 114, no. 4, p. 462-475, doi: 10.1130/0016-7606(2002)114<0462:NAMOOQ>2.0.CO;2.

van Drecht, L.H., 2019, Detrital zircon U-Pb geochronology and Hf isotope geochemistry of the Laberge Group: synorogenic siliciclastic record of early Mesozoic crustal thickening and tectonic evolution of the Whitehorse trough in the northern Canadian Cordillera [M.Sc. thesis]: St. John's, Newfoundland, Canada, Memorial University of Newfoundland, 351 p.

van Staal, C.R., Zagorevski, A., McClelland, W.C., Escayola, M.P., Ryan, J.J., Parsons, A.J., Proenza, J., 2018, Age and setting of Permian Slide Mountain terrane ophiolitic ultramafic-mafic complexes in the Yukon: Implications for late Paleozoic-early Mesozoic tectonic models in the northern Canadian Cordillera: Tectonophysics, v. 744, p. 458-483, doi: 10.1016/j.tecto.2018.07.008.

Vermeesch, P., 2013, Multi-sample comparison of detrital age distributions: Chemical Geology, v. 341, p. 140-146, doi: 10.1016/j.chemgeo.2013.01.010.

Vermeesch, P., Garzanti, E., 2015, Making geological sense of 'Big Data' in sedimentary provenance analysis: Chemical Geology, g. 409, p. 20-27, doi: 10.1016/j.chemgeo.2015.05.004.

Vermeesch, P., Resentini, A., and Garzanti, E., 2016, An R package for statistical provenance analysis: Sedimentary Geology, v. 336, no. 1, p. 14-25, doi: 10.1016/j.sedgeo.2016.01.009.

Vervoort, J.D., and Blichert-Toft, J., 1999, Evolution of the depleted mantle: Hf isotope evidence from juvenile rocks through time: Geochemica et Cosmochimica Acta, v. 63, p. 533-556, doi: 10.1016/S0016-7037(98)00274-9.

Vervoort, J.D., Patchett, P.J., Blichert-Toft, J., and Albarède, F., 1999, Relationships between Lu-Hf and Sm-Nd isotopic systems in the global sedimentary system: Earth and Planetary Science Letters, v. 168, p. 79-99, doi: 10.1016/S0012-821X(99)00047-3.

Vinyoles, A., López-Blanco, M., Garcés, M., Arbués, P., Valero, L., Beamud, E., Oliva-Urcia, B., and Cabello, P., 2020, 10 Myr evolution of sedimentation rates in a deep marine to non-marine foreland basin system: Tectonic and sedimentary controls (Eocene, Tremp—Jaca Basin, Southern Pyrenees, NE Spain): Basin Research, v. 33, p. 447-477, doi: 10.1111/bre.12481.

Werdon, M.B., Newberry, R.J., and Szumigala, D.J., 2001, Bedrock geologic map of the Eagle A-2 quadrangle, Fortymile mining district, Alaska: Alaska Division of Geological and Geophysical Surveys Preliminary Interpretive Report 2001–3b, scale: 1:63,360.

Wernicke, B., and Klepacki, D.W., 1988, Escape hypothesis for the Stikine block: Geology, v. 16, p. 461-464, doi:10.1130/0091-7613(1988)016<0461:EHFTSB>2.3.CO;2.

White, D., Colpron, M., and Buffett, G., 2012, Seismic and geological constraints on the structure of the northern Whitehorse trough, Yukon, Canada: Bulletin of Canadian Petroleum Geology, v. 60, p.239-255, https://doi.org/10.2113/gscpgbull.60.4.239.

Wiedenbeck, M., Allé, P., Corfu, F., Griffin, W.L., Meier, M., Oberli, F., Quadt, A.V., Roddick, J.C., and Spiegel, W., 1995, Three natural zircon standards for U-Th-Pb, Lu-Hf, trace element and REE analyses: Geostandards Newsletter, v. 19, p. 1-23.

Wiest, A.C. and Beranek, L.P., 2019, Stratigraphy of the Faro Peak formation, central Yukon: New field observations of Jurassic synorogenic sedimentation along the Yukon-Tanana–Slide Mountain terrane boundary, *in* Yukon Exploration and Geology 2018, K.E. MacFarlane (ed.), Yukon Geological Survey, p.127–142.

Wiest, A.C., Beranek, L.P., and Manor, M.J., 2020, Upper Triassic to Lower Jurassic stratigraphy of the Faro Peak formation, southern Tay River map area, central Yukon (NTS 105K), *in* Yukon Exploration and Geology 2019, K.E. MacFarlane (ed.), Yukon Geological Survey, p. 121-139.

Xie, X., Heller, P.L., 2009, Plate tectonics and basin subsidence history: Geological Society of America Bulletin, v. 121, no. 1/2, p. 55-64, doi: 10.1130/B26398 .1.

Yukon Geological Survey, 2020, Yukon digital bedrock geology: Yukon Geological Survey, http: //data.geology.gov.yk.ca/Compilation/3, [accessed June, 2020].